Molecular Mechanisms Underlying the Enhancement of Cardiac Contraction by Modifications of Troponin

by

Sandra Elizabeth Pineda Sanabria

A thesis submitted in partial fulfillment of the requirements for the degree of

Doctor of Philosophy

Department of Biochemistry

University of Alberta

Abstract

A fine balance between contraction and relaxation is crucial for the heart to function properly. But often the heart cannot contract with enough force to meet the demands of the body. This condition, called systolic heart failure, is the leading cause of death in the modern society. A common treatment consists in the administration of positive inotropes, which induce more forceful contractions. However, traditional inotropes carry serious adverse effects in the long term. An emerging group of therapeutics, called calcium sensitizers, also enhance contraction but without posing the risks associated with traditional inotropes. Thus, calcium sensitizers are a promising alternative in the search for better therapies for the treatment of heart failure.

Calcium sensitizers act directly on the contractile proteins of the heart muscle. One of these proteins, troponin, regulates contraction in a calcium-dependent manner in cardiac and skeletal muscle. Troponin is composed of C, I, and T subunits. Troponin C and troponin I associate in the presence of calcium to form the regulatory complex that triggers contraction. Modifications to troponin, such as mutations, phosphorylation, and its interaction with small molecules, have an impact on the relaxation-contraction equilibrium of the heart. It is clear that the interaction of troponin with calcium sensitizers favors cardiac contraction. Another modification to troponin that favors contractility is the A162H mutation. However, their mechanisms of action are not fully understood. Thus, the general purpose of this thesis is to provide insight into the molecular mechanism of enhancement of cardiac contraction by these two changes on troponin.

To accomplish this objective I mainly used nuclear magnetic resonance (NMR) spectroscopy to characterize the effect of the A162H substitution on cardiac troponin, and the interaction of cardiac troponin with several calcium sensitizers. I determined the biochemical and structural details of the cardiac troponin C-troponin I (A162H) interaction using NMR spectroscopy. I also investigated these details in skeletal troponin I as a means of comparison. In addition, I designed a troponin C-troponin I chimera to better study their interaction with small molecules. I screened potential drugs that target

the troponin C-I interface using that chimera. I designed and synthesized a covalent calcium sensitizer (i9) that binds to troponin C. I carried out the reaction of i9 with troponin in a variety of conditions to verify the mechanism by which small molecules sensitize troponin. I also resorted to muscle fibers to study its physiologic effect. And because structure dictates function, I determined two independent NMR structures of troponin C bound to calcium sensitizers to correlate with the data already gathered.

The main findings of this work indicate that the mechanism of action of the A162H substitution consists of an increase in the affinity of troponin I for troponin C, as well as a conformational change of troponin I that favors contraction in the context of the thin filament. Another major conclusion of this thesis is that effective calcium-sensitizers primarily stabilize of the open conformation of the N-domain of troponin C, having an increase in affinity of troponin I for troponin C as a secondary but desirable effect. The elucidation of these mechanisms may aid the design of effective therapies that target troponin to enhance contraction and bring balance back to the diseased heart.

Preface

Most of the research conducted for this thesis is the result of teamwork. The literature review in Chapter 1, the final conclusions in Chapter 11, and the ideas for future work in Appendix B are my original work. Most of the remaining chapters have been published previously, as detailed in the first paragraph of each chapter. The exceptions are Chapter 7 and Chapter 10, which contain unpublished data. All the work is presented in the order that attains the best readability of this thesis; thus, published material is not in chronological order. In the following paragraphs I detail the author's contributions to each chapter.

In preparing Chapter 2, I was responsible for data collection and result analysis as well as manuscript writing including the preparation of figures. Ian M. Robertson, Monica X. Li, and Brian D. Sykes were involved in discussion of results and manuscript editing. Brian D. Sykes led the research.

For Chapter 3, I had a major role in the discussion and interpretation of the results. I was also involved in manuscript editing. Ian M. Robertson and Peter C. Holmes collected and analyzed the data. Ian M. Robertson wrote the manuscript. Olga K. Baryshnikova and Brian D. Sykes developed the pulse sequence for the ^{1}H, ^{13}C HCBCGCO NMR experiment (Baryshnikova, O. K. (2008). *Cardiomyopathy mutations in cardiac troponin C: functional and structural consequences* (Doctoral thesis) University of Alberta, Edmonton. Canada). Brian D. Sykes led the project. All authors were involved in manuscript editing.

In developing Chapter 4, I performed all of the experiments involving the peptide cTnI(A162H)$_{144-170}$ and had a major role in interpretation of results. Ian M. Robertson and Peter C. Holmes collected the rest of the data. Ian M. Robertson and I prepared the manuscript and figures. Brian D. Sykes directed the research. All authors were involved in manuscript editing.

I performed all of the experiments reported in Chapter 5. I was also responsible for analysis and interpretation of the results as well as preparation of the manuscript and figures. Ian M. Roberson was involved in troubleshooting during structure determination and discussion of the results. Brian D. Sykes guided the research. All three authors helped review and edit the manuscript.

I helped design the cChimera construct reported in Chapter 6. I also performed all the experiments, analyzed the results, and wrote the manuscript. Olivier Julien and Brian D. Sykes conceived the project and were involved in experimental design, discussion of the results, and manuscript editing.

Chapter 7 contains unpublished data. Brian D. Sykes and I designed the i9 molecule. Brian D. Sykes and I also synthesized i9 with advice from John Corrie. I initially labeled all the proteins with i9 and determined the structure of cChimera-i9. Esther Joo-Young Lee also assisted in protein labeling with i9 and NMR sample preparation. In the laboratory of our collaborator, Dr. Malcom Irving at King's College London, Ian M. Robertson reconstituted the cTnC(C35S)-i9 protein into rat ventricular trabeculae and performed Ca^{2+} titrations. I analyzed the results, and composed the manuscript. Ian M. Robertson also helped in manuscript composition. Brian D. Sykes led the research and helped review the manuscript.

For Chapter 8 and Chapter 9, Ian M. Robertson and I collected and processed the data, analyzed the results, and wrote the manuscript. Brian D. Sykes led the project and was also involved in manuscript editing.

The work reported in Chapter 10 has not been published and is the result of a collaboration with Drs. Peter M. Hwang at the University of Alberta, Andrew McCammon at the University of California San Diego, and Dr. Maurizio Pellecchia at the Sanford-Burnham Medical Research Institute. I performed all the experiments reported and analyzed the data. Peter M. Hwang suggested five compounds to titrate into cChimera. Steffen Lindert performed *in silico* screening of the NCI library. Lloyd Slivka and Ziming Zhang performed initial NMR screening of the compound library at the laboratory of Dr. Pellecchia.

For the work presented in Appendix A, I helped to develop the fluorescence assays used for assessing Ca^{2+} binding with the assistance of summer students Eric Chan and Cathy Qin. Peter M. Hwang acquired and interpreted the NMR data, analyzed the results, and prepared the manuscript. Fangze Cai performed the Ca^{2+} titrations. David Corson purified the proteins used in this work. Brian D. Sykes led the project.

With love to Sam and Yasmi,

my inspiration for life.

Acknowledgments

On the road to achievement one never travels alone. There is always a vast number of people who with their words and actions impact the direction we take. No matter how close or how distant, they are there. That is why this page is dedicated to express my gratitude to those who were there.

First, I would like to thank my supervisor, Dr. Brian Sykes, for providing honest invaluable advice throughout all the stages of my PhD program. His leadership, patience, and kind nature undoubtedly made my stay in his laboratory a fruitful and pleasant experience. I also want to thank the members of my supervisory committee, Dr. Joanne Lemieux and Dr. Leonidas Spyracopoulos, for their time, guidance, and useful suggestions that helped shape this project into success. In addition, I thank Dr. Alexander Clanachan from the Department of Pharmacology at the University of Alberta, and Dr. Gary Shaw from the Department of Biochemistry at the University of Western Ontario, for serving as examiners in my PhD defense.

Thanks to my colleagues and friends Ian Robertson, Monica Li, Olivier Julien, Marta Oleszczuk, Robert Boyko, Peter Hwang, and Dave Corson for sharing their knowledge and experiences with me to make this road less bumpy and more successful. It was a pleasure to have met and worked with them.

I am deeply grateful to my family for their unconditional support all along this project and always. Thanks to my husband Samuel Hernández Anzaldo for being so loving, understanding, and reassuring. To my daughter Yasmi for being a well behaved embryo and fetus during the last and busiest stages of my PhD. To my parents Mili Sanabria Cortés and Jorge Pineda Jiménez for giving me the great gift of education in the first place, and to my brothers Jorge Pineda Sanabria and Ulises Hernández Anzaldo and my sister Ivette Rojas for being so caring and supportive.

Thanks to my amazing friends Jessy Martínez P., Brad Young, Nata Lifshitz G-B., Edgar Pérez, Dey Valdéz, Lucio Gutiérrez, Adriana Bustos C., Paco Arguelles V., and Aruna Augustine who made me feel at home and helped make this a truly wonderful and fun experience even after six winters in this frozen city of Edmonton.

I want to acknowledge summer students Eric Chan, Cathy Qin, Brett Orr, Fangze Cai, and Esther Joo-Young Lee for their contributions to the lab; it was a pleasure to work with them.

Lastly, I also want to acknowledge the funding provided by Alberta Innovates Health Solutions during the last four years of my PhD program that allowed me to focus on doing what I really enjoy: science.

Table of Contents

CHAPTER 8. Structure of trans-resveratrol in complex with the cardiac regulatory protein troponin C

CHAPTER 9. Approaches to protein-ligand structure determination by NMR spectroscopy: applications in drug binding to the cardiac regulatory protein troponin C 229

CHAPTER 10. Drug binding to the regulatory troponin C-troponin I complex 245

CHAPTER 11. Conclusions 267

Bibliography 274

Appendix A. The intrinsically disordered cardiac-specific N-terminal region of troponin I positions the regulatory domain of troponin C 299

List of Tables

Tables

Supplementary Tables

List of Figures

Figures

Supplementary Figures

CHAPTER 1

Introduction

The finest balance must exist between relaxation and contraction of the heart to guarantee healthy heartbeat dynamics. But often the heart is unable to relax or contract properly, a condition called diastolic or systolic heart failure, respectively. Thus the failing heart cannot pump enough blood to meet the oxygen and nutrient demands of the body. Heart failure remains the leading cause of death in the world. Various disorders, such as ischemic heart disease and dilated cardiomyopathy, can progress to a failing heart. A current treatment to overcome the contractile dysfunction characteristic of systolic heart failure consists of the administration of medications (called inotropic agents) that induce forceful contractions. But far from real benefits, adverse effects and increased mortality have been observed from their use. This reflects the need for better therapies to treat heart failure.

After more than twenty years of remarkable research the molecular mechanism of contraction in the cardiac muscle is now better understood. Amongst the multiple players, troponin plays a key role in the regulation of muscle contraction. Troponin is a protein complex found on the thin filament that leads to contraction in response to a high concentration of ionic calcium (Ca^{2+}) inside the muscle cell or cardiomyocyte. Because of its regulatory role, it seems logical to directly target troponin with drugs in order to alleviate contractile dysfunction. Instead, all traditional inotropes induce an increase of Ca^{2+} inside the cardiomyocyte. This stimulates troponin indirectly but at the expense of favoring the development of arrhythmias and cell death due to Ca^{2+} overload. Only the novel therapy of Ca^{2+} sensitization has troponin as a central target. Yet, the benefits of the best clinically characterized Ca^{2+} sensitizer, levosimendan, remain controversial since a decrease in mortality was observed in one but not confirmed in two subsequent clinical trials.

Structural biology plays an essential role in the investigation of protein-drug interactions. However, there is a limited amount of structures of troponin in complex with Ca^{2+} sensitizers. Although these structures shed light into the mechanism of action of Ca^{2+} sensitizers, there is no single effect on troponin that consistently explains sensitization. For example, the binding site on troponin is different for different sensitizers. While some seem to rely on enhancing intersubunit interactions in troponin, some others weaken those same interactions. The case of levosimendan is even more uncertain since the structure of a troponin-levosimendan complex remains elusive. Thus, a unifying principle for Ca^{2+} sensitization is needed to truly take advantage of structural biology in rational drug design.

Despite extensive study of cardiac contraction, our scientific community has not found an effective way to enhance the contractility of the failing heart. But perhaps the answer lies on the

understanding of the diseased heart. In this regard, the study of ischemic heart disease has brought to the attention of health researchers a natural modification on troponin that favors contraction. This key change consists of a histidine residue in the skeletal and fetal cardiac isoforms of troponin that maintains contraction during myocardial acidosis. The histidine is swapped to an alanine in the adult cardiac isoform to favor relaxation and ensure proper diastole. Introducing the histidine in the cardiac isoform (A162H substitution) offers tremendous benefits for the diseased heart including retention of contraction under acidic conditions. This opens new avenues for potential treatments of contractile dysfunction, such as the design of small molecules that mimic the effect of A162H substitution and gene therapy that targets troponin.

The development of new therapies to enhance cardiac contraction is in an early stage, ideal for introducing innovative alternatives. However the mechanisms of action of the A162H substitution or Ca^{2+} sensitization are not fully understood. This thesis aims to aid both predicaments by providing a detailed structural assessment of two modifications of troponin that favor contraction. First, the A162H substitution will be examined in order to explain its unique effect on enhancing cardiac performance. Then the interaction of troponin with a pair of small molecules will be assessed in order to shed light into the mechanism of Ca^{2+} sensitization. This new knowledge can hopefully be used as a starting point for the rational design of small molecules that target troponin to enhance cardiac contraction in the diseased heart. It may also provide evidence to support troponin as a target for gene therapy.

To accomplish the purpose of this document the present chapter continues with a brief review of troponin (Tn) as a modulator of contraction in response to Ca^{2+} and Ca^{2+} sensitizers and lands on the research questions to be addressed here. Most of the following chapters have been previously published. Chapter 2 to Chapter 5 are dedicated to the biochemical and structural characterization of the A162H substitution by NMR spectroscopy. This includes the NMR structure of a cardiac troponin complex containing the A162H substitution that provided the final pieces to propose a model of contraction enhancement by this particular modification. A more focused view of troponin as a drug target is presented in Chapter 6 to Chapter 10. In Chapter 6, I report on the design and characterization of cChimera, a hybrid troponin system that provides more information about the mechanism of Ca^{2+} sensitization and serves as a stable target for NMR-based drug screening. Chapter 7 and Chapter 8, each report on the structure of a drug molecule bound to troponin. Chapter 9 deals with the methodology involved in structure determination of protein-ligand complexes by NMR. The penultimate Chapter 10 extensively demonstrates the applicability of cChimera in drug screening. Finally in Chapter 11, I provide an overarching conclusion that incorporates all of the individual publications. Appendix A contains the full versions of other publications in which I have made a contribution, and Appendix B contains original ideas for future work.

The molecular mechanism of muscle contraction

The muscle is a highly organized tissue with a repeating bundle-in-bundle structure that allows the contraction and relaxation of every moving part of the organism. Muscles are formed by fascicles, which are bundles of muscle cells or myofibers surrounded by connective tissue. At the same time, each myofiber is formed by bundles of myofibrils that contain the contractile proteins. Inside the myofibrils, the contractile proteins are organized into sarcomeres, the contractile unit of the muscle cell. This repeating arrangement of sarcomeres is what gives skeletal and cardiac muscles their striated appearance. The sarcomeres of skeletal muscle are regular and parallel, while those of cardiac muscle are branched at irregular angles. However, the structure of the sarcomere and the general mechanism of contraction is the same in these muscle types[1]. Each sarcomere is formed by regular arrangements of protein filaments; the thin filaments are mostly composed of actin and attached to the Z-line on each side of the sarcomere, the thick filaments are mainly formed by myosin and are attached to the middle M-line of the sarcomere (Figure 1.1 A). This arrangement allows the shortening of the sarcomere to occur from both sides toward the center when the thin filaments slide past the thick filaments[1,2].

The thick filament contains the motor protein myosin that interacts with the thin filament to form strong cross-bridges and produce contraction. Myosin is formed by two heavy chains, two essential light chains (ELC), and two regulatory light chains (RLC). The heavy chains of myosin constitute the backbone of the thick filament as they form a coiled-coil along most of their length. The N-terminal globular heads of myosin, named subfragment 1 (S1), protrude out of the thick filament at regular intervals of 14.3 nm. The S1 heads interact with adjacent actin filaments to generate force. In the center of the thick filament, by the M-line, the myosin molecules interact head-to-tail to form a bipolar polymer. In this bipolar configuration, the thick filament is competent for shortening of the sarcomere from both sides (Figure 1.1 B). The thick filament also contains scaffolding C-, X-, and H-proteins that hold the myosin bundles together. In addition, the M-protein connects the thick filaments together in the M-line, while titin contributes to the elasticity and stability of the sarcomere[1,2].

The thin filament is formed by actin, tropomyosin and troponin (Figure 1.1 C), and is the major site of regulation of muscle contraction by Ca^{2+}. The backbone of the thin filament is formed by actin monomers (globular actin) polymerized into filamentous actin (F-actin) with a double-stranded helical structure. Each actin monomer in F-actin has two sub-domains exposed to the solvent available to bind myosin. Wrapped around the F-actin helix lays tropomyosin (Tm); a long α-helical protein that forms a coiled-coil dimer. Each Tm spans seven actin monomers on each side of the F-actin helix. Adjacent Tm molecules interact in a head-to-tail configuration along the entire F-actin filament. The overlapping regions between contiguous Tm molecules have been shown to be important for binding of Tm and of

S1 to actin[1-3]. The position of Tm on the actin filament changes during the contraction cycle, at low cytoplasmic Ca^{2+} concentrations Tm blocks the myosin-binding sites on actin. Binding of Ca^{2+} to Tn induces a cascade of events that result in the movement of Tm deep in the F-actin groove to expose the actin sub-domains that bind myosin and allow cross-bridge formation[3]. One troponin (Tn) heterotrimer binds on the Tm-Tm overlap region and functions as the Ca^{2+} sensor. Tn regulates the association of F-actin to myosin in response to Ca^{2+} and will be the focus of our discussion in the following section.

A

Z disc   M line   Z disc

Thin filament   Thick filament

B   S1

C   Actin Filament

Tropomyosin (Tm)   Troponin complex (Tn)
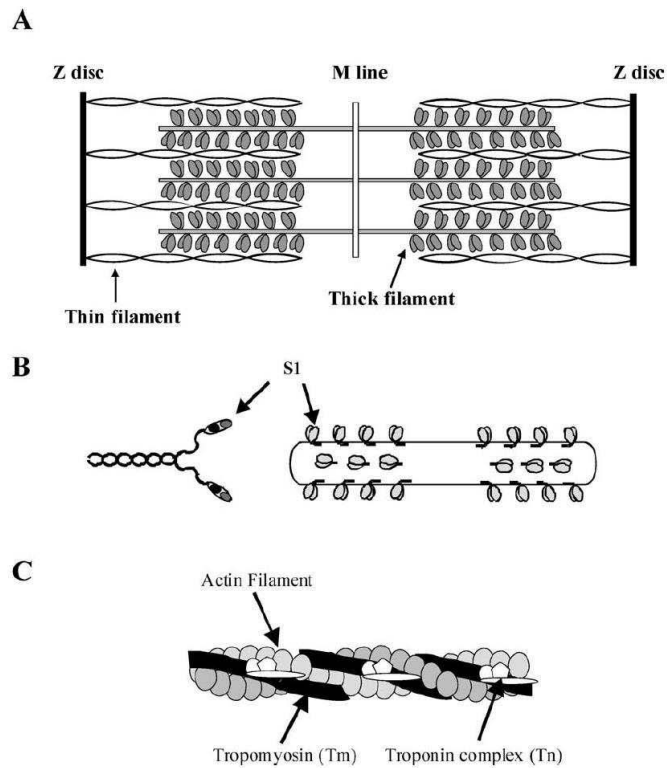
Figure 1.1. Schematic representation of the sarcomere.
A: relative position of thin and thick filaments in the structure of a sarcomere. B: the structure of the thick filament showing the coiled-coil structure of myosin (left) and the bipolar configuration of a myofilament polymer (right). C: relative localization of tropomyosin and troponin along F-actin in the thin filament. (From Sorsa *et al*. 2004[1]).

In the sliding filament mechanism ATP provides the energy for the cross-bridges to produce force. The cross-bridge cycle (Equation 1-1) involves the rapid binding of ATP to actomyosin followed by rapid dissociation of actin from myosin·ATP. Binding of ATP also induces the myosin heads to move further along the actin filament. Next, ATP is hydrolyzed to ADP and inorganic phosphate (Pi) that remain bound to the myosin head. The myosin head then binds weakly to actin and a small

conformational change occurs in myosin that leads to strong actin binding, release of Pi, and the power stroke that pulls the actin filament. It has been suggested that the release of Pi constitutes a separate step in the cycle that stabilizes the force-generating conformation of AM·ADP. However, the change from weak to strong actomyosin binding is the force generating step that drives the power stroke. Finally, ADP is released from actomyosin and the complex is available for another round of contraction[2]. Note that in this mechanism actin must be available to bind myosin, a condition regulated by Ca^{2+}.

$$AM + ATP \longleftrightarrow AM \cdot ATP \longleftrightarrow A + M \cdot ATP \longleftrightarrow M \cdot ADP \cdot P_i \overset{\textit{force generation}}{\underset{\textit{weak} \qquad\qquad \textit{strong}}{\longleftrightarrow} A\text{-}M \cdot ADP \cdot P_i \longleftrightarrow} AM \cdot ADP + P_i \longleftrightarrow AM + ADP$$
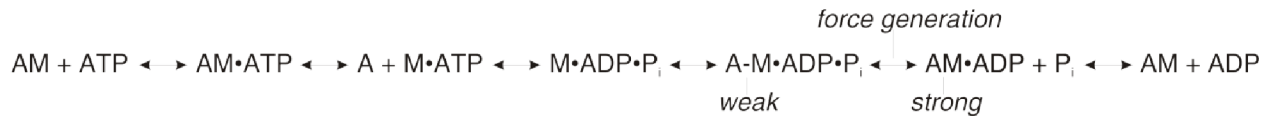
Equation 1-1. The cross-bridge cycle (modified from Gordon _et al._ 2002).

A current molecular model for the Ca^{2+} activation of the thin filament includes blocked (B-state), closed (C-state), and myosin (M-state) states. In this model, the B-state corresponds to low cytosolic Ca^{2+} and steric block of cross-bridges by Tm. The C-state is reached after Ca^{2+} activation and consists of weakly bound cross-bridges that do not generate force but are primed to enter the force-generating step. In the M-state cross-bridges are strongly bound and generate force to contract the muscle[4]. In cardiac muscle in the absence of Ca^{2+} only 10% of thin filaments are in the M-state, whereas in the presence of Ca^{2+} this proportion increases to 75%. Thus, the role of Ca^{2+} is to change the equilibrium between these states[3] and it does so by binding to Tn.

The structure of troponin

Ca^{2+} activation of the thin filament occurs through its binding to Tn with some differences between skeletal and cardiac muscle. Throughout almost 30 years structural biologists have elucidated the structure of a variety of relevant Tn complexes. This excellent work has revealed the molecular details of the Tn -intersubunit and -Ca^{2+} interactions to understand the process of Ca^{2+} activation in skeletal and cardiac muscle. Although the structures of both Tn isoforms are similar, some important differences exist. In this section I point to the relevant differences as necessary, as well as to the missing pieces of the Tn structure.

Tn is a complex composed of C (TnC), I (TnI), and T (TnT) subunits. TnC (~18KDa) is the Ca^{2+} binding subunit and is formed by two globular domains named N (NTnC) and C (CTnC). Each domain is formed by two EF-hand motifs that bind a divalent metal ion. The helices, from N- to C- termini, are named A through H. However, in the cardiac isoform the N-terminal domain (cNTnC) contains one extra

helix (helix N) making it larger than the C-terminal domain (cCTnC). The ion-binding sites are named I through IV. Sites I and II in the N-domain (NTnC) are Ca^{2+} specific; however, in the cardiac isoform only site II is competent for binding Ca^{2+} due to several amino acid mutations in site I. Site II shows a low Ca^{2+} affinity that allows the exchange rate to be fast enough to occur within a heartbeat thus being responsible for its regulation. Sites III and IV in the C-domain are high affinity Ca^{2+} or Mg^{2+} sites and they remain saturated most of the time[4,5]. All the known high resolution structures of cardiac and skeletal TnC observe the general configuration described above. However, discrepancies exist in the structure of the linker between the N and C domains. Whereas in the x-ray crystal structures of sTnC[6-8] the linker itself is a helix continuing helices D and E, in the NMR solution structure[9] the linker remains unstructured. For cTnC, the D-E linker is observed as unstructured in both the NMR and x-ray structures[10,11] (Figure 1.2).
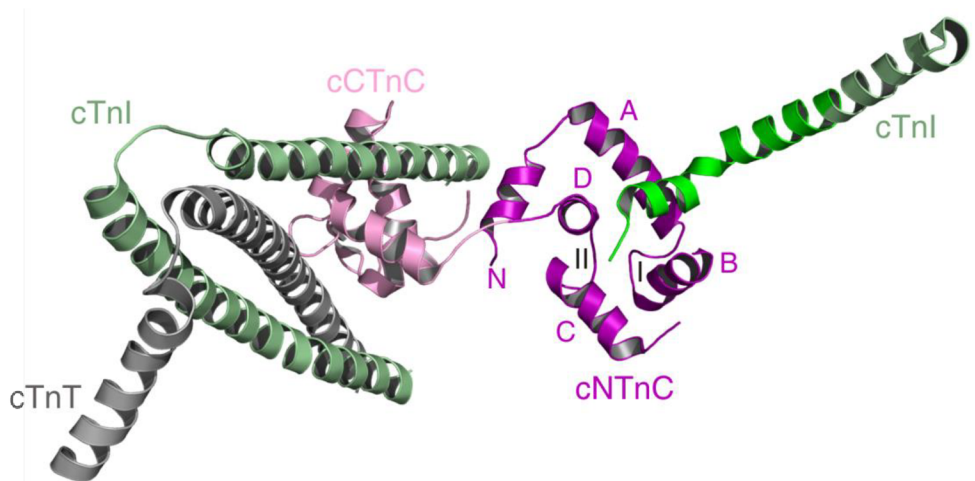
Figure 1.2. X-ray structure of the core domain of cTn.
One of the two molecules on the asymmetric unit of the crystal showing a long helix for the C-terminal region of cTnI (next to region bound to cNTnC). The helices of cNTnC are labeled N, and A through D, as well as its metal binding sites I and II.

TnI is the inhibitory subunit of the Tn complex. It is a large, mainly helical protein that inhibits the actomyosin ATPase activity. The cardiac isoform (cTnI, ~24 KDa) is bigger than the skeletal (sTnI, ~21 KDa) due to an N-terminal extension of 31 residues on cTnI. At least six regions are recognized in TnI according to their function and interaction with other proteins. Starting by the N-terminus, the cardiac-specific N-terminal extension contains two PKA-dependent phosphorylation sites and plays an important role in regulation by adrenergic stimulation. Two structural regions that anchor the Tn complex to the thin filament: the N-terminal region, which forms a long helix that binds to CTnC, and the TnT-binding region which forms a coiled-coil with the C-terminal region of TnT. It follows the

inhibitory region, a stretch of basic amino acids that can bind TnC in the presence of Ca^{2+}, or actin-tropomyosin in the absence of Ca^{2+} to inhibit myosin ATPase activity. The switch region forms a helix that binds to NTnC during Ca^{2+} activation and thus has a central role in regulation. Finally, the C-terminal region contains a second actin-binding site necessary for full inhibition of myosin ATPase by TnI[5]. Recently, the pH-sensitive region within TnI is being recognized. This region comprises a few residues (159-164) in between the switch and C-terminal regions. It is important for regulation of contraction in response to intracellular pH changes and will be a major point of focus in this thesis.
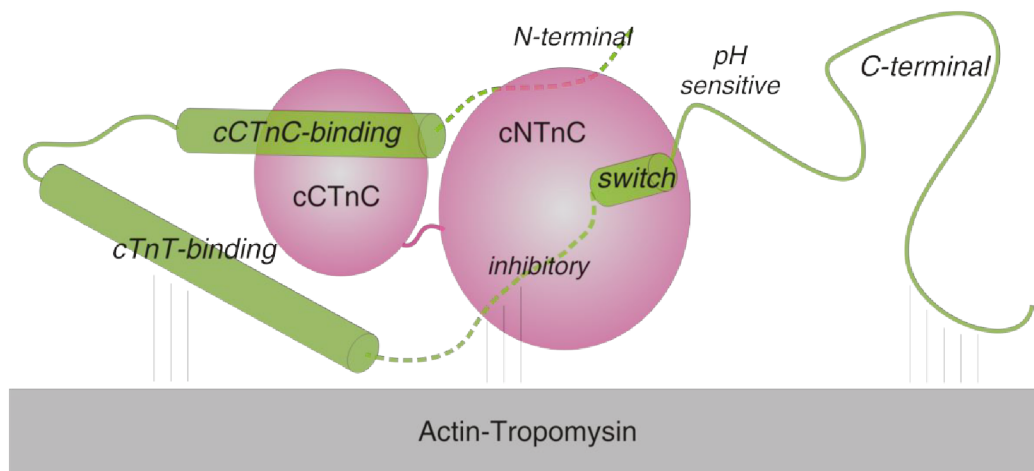
Figure 1.3. Schematic of cTn structure and interactions.
Representation of the cTn complex based on the x-ray structure by Takeda *et al*. cTnC and cTnI are shown in pink and green, respectively. Cilinders represent α-helices, dashed lines represent regions of cTnI missing in the crystal structure, and vertical lines represent intermolecular interactions. Labels in italics indicate cTnI regions. The C-terminal region of cTnI is shown as unstructured based on experimental evidence (see text). TnT was not included for clarity.

The structure of most of these regions is known and consistent among different studies with exception of the N-terminal extension of cTnI, the inhibitory, and the C-terminal regions (Figure 1.3). The x-ray structure of the core domain of cTn[11] displays the disposition of most cTnI regions. However, neither the N-terminal extension nor the inhibitory region are present. In addition the C-terminal region is different in the two molecules composing the asymmetric unit. The N-terminal region has been suggested to form a helix spanning residues 25-30 that extends to residues 21-30 upon phosphorylation of S22 and S23[12]. However, as detailed in the Appendix, our NMR studies indicate that the N-terminal extension remains unstructured. Residues 19-37 are weakly bound to cNTnC by electrostatic interactions that are disrupted by phosphorylation of S22 and S23[13]. The structure of the inhibitory region has been solved but different structural studies are not consistent. Whereas the NMR

structure of cCTnC·cTnI[14] (residues 128-147) shows a helix spanning residues 134-139 that interacts with helices E and H of cCTnC, an extended conformation[15] and a ß–hairpin[16] have also been suggested for sTnI by other groups. However, a growing number of evidence supports a helical structure for this region in sTnI[17,18] and cTnI.[14,19,20] Finally, the C-terminal region of cTnI is shown as unstructured in the NMR structure of cNTnC·cTnI (residues 147-163)[21] and one molecule of the asymmetric unit in the x-ray structure of the cTn core domain[11], but in the other molecule, this region forms a long helix. Fluorescence anisotropy data indicates that this region remains flexible in solution[22] suggesting that the helix observed in the x-ray structure may be an artifact of crystal packing.

TnT is the largest (31-36 KDa) subunit of Tn and makes the most diverse interactions as it binds to TnI, TnC, and Tm. Alternate splicing around the N-terminal site of TnT yields multiple isoforms that vary during development. Two fragments named T1 and T2 are distinguished based on digestion by chymotrypsin. T1 is the N-terminal fragment and it binds the Tm-Tm overlap regions to confer cooperative binding of the myosin heads to the thin filament. T2 is the C-terminal fragment included in the x-ray structure of the core domain of cTn where it shows two helices that interact with cTnC and cTnI. Helix 1 interacts with the cTnT-binding region of cTnI. Helix 2 makes a coiled-coil interaction with the C-terminal side of the cCTnC-binding helix of cTnI, but also interacts with cCTnC[4,23].

Troponin as a regulator of contraction

Tn is subject to regulation by Ca^{2+} binding to TnC and phosphorylation at different sites of the TnI and TnT subunits. For the purpose of this document, we will focus mainly on Ca^{2+} binding to TnC. This process is very similar for the skeletal and cardiac muscle but the differences will be clearly specified. Its understanding will prepare the reader to appreciate the mechanism of action of Ca^{2+} sensitizers. Another focus point will be phosphorylation on the cardiac specific N-terminal extension of cTnC. Regulation by phosphorylation in this region is one of the mechanisms that the heart has evolved to favor relaxation and guarantee proper heartbeat dynamics.

The overall structure of the Tn complex remains relatively constant during Ca^{2+} activation; however, the inter-subunit interactions change substantially. Upon Ca^{2+} release from the sarcoplasmic reticulum, the cytosolic concentration of Ca^{2+} increases by ten-fold. Ca^{2+} then binds to the regulatory N-domain of TnC and promotes the binding of the switch region of TnI to NTnC. However, this process occurs in a different manner for cardiac and skeletal muscle. Comparing the structures of sTnC in the absence and presence of Ca^{2+} [24] it is clear that Ca^{2+} induces a conformational change on sNTnC. Upon Ca^{2+} binding to sites I and II, the B and C helices of sTnC shift away from the N, A, and D helices towards an open conformation that exposes a hydrophobic patch to where the switch region of sTnI can readily bind. In contrast, in cTnC Ca^{2+} binding to cNTnC does not induce such a closed-to-open

transition as observed in the NMR structure of cNTnC and cNTnC·Ca^{2+} [25]. Instead, Ca^{2+} shifts the typical equilibrium between the closed and open conformations of cNTnC to favor the open conformation[26,27]. This increase in the sampling of the open conformation increases the chance for the switch region of cTnI to bind. Once the ternary cNTnC·Ca^{2+}·cTnI complex is formed the open conformation is fully stabilized[21]. As a consequence of this association the inhibitory region of TnI is pulled off actin releasing the inhibition of ATPase activity that powers myosin movement and contraction (Figure 1.4). The formation cNTnC·Ca^{2+}·cTnI complex also induces a conformational change in Tm that shifts to expose the myosin binding sites on actin. This corresponds to the transition from the B-state to the C-state of the thin filament. Then we can see that association of the switch region to NTnC in skeletal and cardiac muscle is a crucial step in the mechanism of muscle contraction.
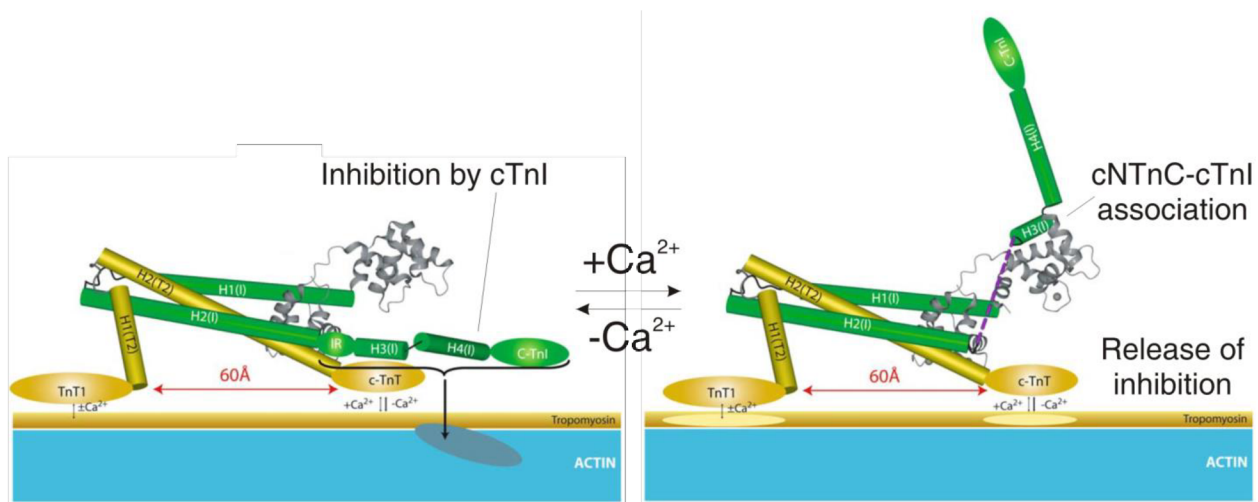
Figure 1.4. Thin filament activation by Ca^{2+}.
Schematic representation of the structural changes on Tn induced by Ca^{2+} (based on the x-ray structure of the core domain of cTnC). cTnC, cTnI, and cTnT are shown in gray, green, and yellow, respectively. Upon Ca^{2+} binding to cNTnC, the switch region of cTnI associates to cNTnC and pulls the inhibitory region away from actin-tropomyosin. Modified from Li *et al*. 2004[18].

Another site of regulation of contraction specific for cardiac muscle lies on the N-terminal extension of cTnI which can be phosphorylated to reduce Ca^{2+} sensitivity. Recall that this region is only present in the cardiac isoform. Residues S22 and S23 can be phosphorylated by several protein kinases such as PKA, PKC, and PKD[28]. It has been shown that in the absence of phosphorylation the region C-terminal to the S22 and S23 of cTnI interacts with cNTnC[29,30]. This interaction is disrupted upon phosphorylation of S22 and S23 resulting in a decrease of Ca^{2+} sensitivity of the myofiber[31,32]. Although this region is not observed in the structure of the core domain of cTn, a model has been proposed for its function. In this model cTnI forms a helix from residues 25-30 that extends to 21-30 upon

biphosphorylation of S22/S23. It is proposed that the expansion of this helix stabilizes the N-terminal extension to weaken interactions with cNTnC[12].

Ischemic heart disease

Ischemic heart disease is currently the number one cause of death in the world and it is expected to remain this way by 2030[33]. Myocardial ischemia is characterized by reduced or absent blood flow to an area of the heart and is usually related to atherosclerotic disease of the arteries. In the acute phase, the rupture of the atheromatous plaque leads to the formation of a platelet plug in a major vessel. The obstruction deprives the cardiac cells of blood and oxygen which alters the metabolism of the myofiber. The obstruction also impedes the washout function of blood and causes accumulation of acidic products of metabolism and protons. This intracellular acidosis is the strongest determinant of life-threatening ventricular arrhythmias and is directly correlated with contractile failure[34-36]. The reduction in force development during myocardial ischemia is a direct result of reduced Ca^{2+} sensitivity of cTnC in the cardiac myocyte observed when the intracellular pH drops from 7.4 to as low as 6.2[37,38].

In contrast, neonatal hearts and skeletal muscle are not sensitive to acidosis. From the early 70's it had been known that the mechanical properties of adult and neonatal hearts were different, including a remarkable resistance to hypoxia in the immature hearts. In 1986 Solaro *et al.* suggested that such differences may be due to variations in the thin filament structure that occur during development, specifically in TnI or TnT[39]. In fact, the sTnI isoform characteristic of adult slow skeletal muscle is expressed in the fetal and neonatal hearts and later replaced by cTnI[40]. Solaro and coworkers also proposed a role for these variations on the pH sensitivity of the thin filament while studying the effect of hypercapnic[1] acidosis in adult and neonatal rat hearts[41]. This established a relation between pH-sensitivity and Tn developmental isoforms.

It was later demonstrated that TnI plays a major role in determining the pH sensitivity of the muscle fiber. Metzger and collaborators reported that incorporation of sTnI in adult rat cardiac myocytes enhances Ca^{2+}-dependent contractility under physiological and acidic (pH 6.2) conditions[42]. Both the Solaro and Metzger groups demonstrated that the region of sTnI that confers resistance to acidosis localizes to the C-terminus by incorporating specific cTnI-sTnI chimeras into adult rat cardiac myocytes and mouse cardiac fibers[43,44]. According to the differences in the sequences of sTnI and cTnI at the C-terminal region the Smillie group at the University of Alberta reported that an alanine to histidine substitution at position 162 of cTnI (the A162H substitution) prevents the drop in Ca^{2+} sensitivity of cTnC at low pH in ATPase assays[38]. They also showed that the reverse mutation in sTnI

---

[1] Hypercapnia refers to the accumulation of CO_2 and is observed during myocardial ischemia.

(H130A) turns the sTn system pH sensitive (Figure 1.5). This identified H162 of sTnI as the single-residue determinant of pH sensitivity in the muscle, but raised the question of its underlying mechanism that I intend to address in this document.
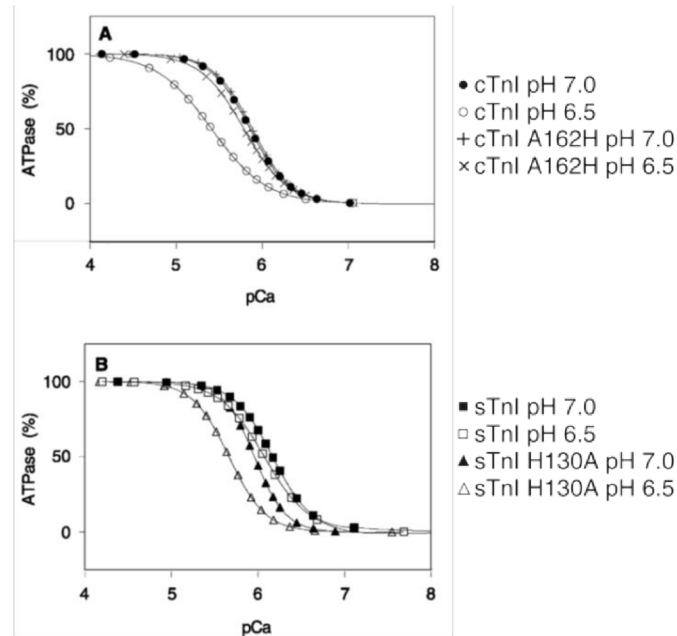
Figure 1.5. Effect of histidine mutations on ATPase activity.
A. In a reconstituted Tn-Tm-actomyosin system, cTnI displays a shift to the left on the pCa curve when the pH is lowered from 7 to 6.5. When cTnI is mutated to A162H this shift is no longer observed. B. sTnI does not display the shift to the left until the reverse mutation H130A is introduced. Modified from Dargis *et al.* 2002[20].

The A162H substitution

Remarkably, the A162H substitution improves cardiac performance under hypoxic and ischemic challenges *in vivo*. In a comprehensive study by Day and Westfall, they showed that adult rat cardiac myocytes expressing cTnI A164H (rat numbering) had increased Ca^{2+}-activated tension at pH 7 and 6.2. They also showed that mice expressing cTnI A164H developed smaller hearts but had the same heart rates as the controls without the mutation. At basal conditions the hearts and myocytes of these mice showed enhanced systolic function but no consistent change in diastolic performance. After exposure to acidic solutions myocytes and hearts retained contractility and improved diastolic function. In the whole-animal model, A164H mice showed more resistance to hypoxic and ischemic challenges, maintaining contractility and improving survival compared with the control group. Basal diastolic performance was variable but improved throughout acidosis; however, basal phosphorylation of S22

and S23 was higher in the hearts of mice expressing cTnI A162H[45]. This could counteract the effect of A162H since phosphorylation of S22 and S23 is known to reduce Ca^{2+} sensitivity. Note that mice expressing sTnI show diastolic dysfunction[46] as sTnI lacks the N-terminal extension containing the phosphorylation sites. However, it was later shown that baseline diastolic function of A164H mice is not different from the control group in a model of adrenergic blockade using esmolol as ß–blocker[47].

Although the A162H substitution has been shown to improve cardiac performance in ischemic conditions *in vitro*[38]*, ex vivo* and *in vivo*[45], the underlying mechanism is not fully understood. Dargis suggested that the more positively charged histidine at low pH may stabilize the cNTnC-cTnI interface by interacting with glutamate(s) or aspartate(s) residues in cNTnC[38]. Day *et al.*[45] added that this positive charge could weaken interactions with lysine or arginine residues in actin. In support of the first suggestion, the high resolution structure of the sTnC-sTnI complex[18] shows close proximity between E20 of sTnC and H130 of sTnI (Figure 1.6 A) which suggests that these residues interact in skeletal muscle to stabilize the complex at low pH. In contrast, the structures of the cNTnC-cTnI complex[18,19] show that the homologous residues E19 and A162 are far from each other, with A162 being on a presumably flexible region of cTnI (Figure 1.6 B). However, the lack of a high resolution structure involving cTnI A162H prevents a full understanding of the benefits of the A162H substitution for the failing heart. Elucidation of this structure and the mechanism of contraction enhancement by A162H is a major objective of this thesis as it constitutes a first step in the development of new therapies that mimic the A162H effect to restore contractile function.
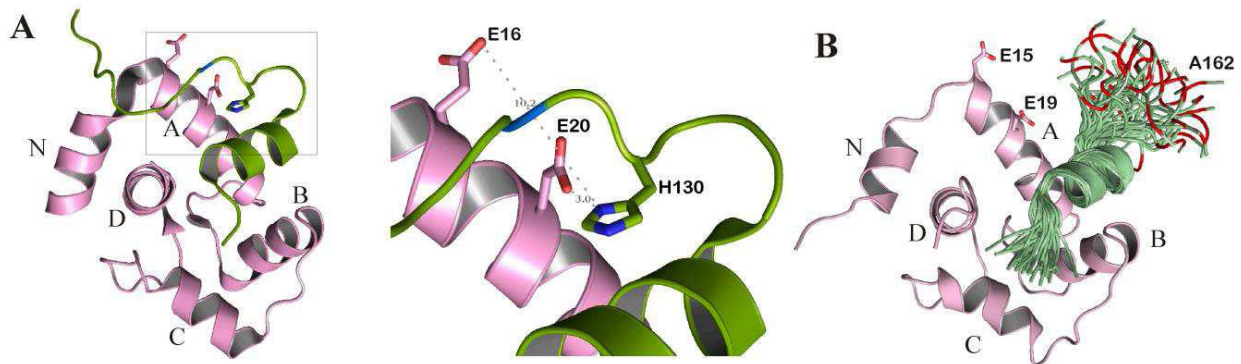
Figure 1.6. Relative position of H130 and A162 in sTnI and cTnI.
A: Structure of sNTnC•Ca^{2+}•sTnI (residues 115-131) (PDB ID: 1YTZ) showing the positions of E16, E20 and H130, the expansion depicts the distances from E16 and E20 to H130. B: The structure of cNTnC•Ca^{2+}•cTnI (residues 147-163) (PDB ID: 1MXL) shows the positions of the homologue residues E15 and E19, the ensemble is shown for the switch peptide and the position of A162 is in red.

Inotropic therapy

Inotropic agents constitute a group of medications that increase the strength of muscular contractions. Currently the first choice of treatment for patients with heart failure (enalapril), as well as its novel competitor (LCZ696), act by inhibiting the angiotensin-converting enzyme, which causes vasodilation[48]. Nonetheless, according to the European Society of Cardiology and the American Heart Association, inotropic therapy is indicated for patients with reduced cardiac output and low blood pressure. Patients with such characteristics represent 10-15% of all patients admitted for heart failure and present severe systolic and diastolic dysfunction. Inotropic therapy is currently the only treatment that can improve systolic function in those patients in the short-term. However, most inotropic agents are associated with long-term cardiac damage. This highlights the need for improved therapies that can offer higher benefit-to-risk ratios[49].

Traditional inotropic agents

The adverse effects observed at long term are directly related to the mechanism of action of traditional inotropic agents. Arrhythmias, myocardial ischemia and necrosis are the most common harmful effects of inotropic therapy[50]. Phosphodiesterase 3 (PDE3) inhibitors and β-agonists increase cyclic adenosine monophosphate (cAMP) and induce PKA-dependent phosphorylation of Ca^{2+} handling proteins including phospholamban. Phosphorylation of phospholamban activates the sarcoendoplasmic reticulum Ca^{2+}-ATPase (SERCA) that pumps Ca^{2+} into the sarcoplasmic reticulum (SR). This in turn can result in Ca^{2+} overload of the SR and spontaneous release of Ca^{2+} into the cytoplasm that trigger arrhythmias. Inhibitors of the Na^+/K^+-ATPase also result in an increase of the concentration of intracellular Ca^{2+} [51,52]. Thus, all of these positive inotropes pose a risk of Ca^{2+} toxicity to the mitochondria and consequently of cell death. In addition, they all show no improvement in mortality[51]. Therefore, medications that act by a different mechanism to enhance cardiac muscle contraction are necessary.

Alternative inotropes that are currently under investigation act by a variety of different mechanisms. These include SERCA2a activators, ryonidine recepetor (RyR) stabilizers, and Na^+/K^+-ATPase inhibitors which still are Ca^{2+} mobilizers. However, they alter Ca^{2+} homeostasis in a more balanced manner; for example, istaroxime has a dual mechanism of action: while it inhibits the Na^+/K^+-ATPase to increase intracellular Ca^{2+} and improve systolic function, it also inhibits PDE3 which stimulates Ca^{2+} uptake by SERCA to improve relaxation. However, their effects on mortality are still to be determined[49,51]. Other novel groups of inotropes under investigation are cardiac myosin activators and Ca^{2+} sensitizers which do not influence Ca^{2+} mobility.

Ca^{2+} sensitizers induce positive inotropy by acting directly on cTnC in the thin filament of the sarcomere. This type of inotropes overcomes the disadvantages of the traditional ones since they do not increase intracellular Ca^{2+} levels. They may also be superior to other novel inotropic agents as Ca^{2+} sensitizers induce no Ca^{2+} mobilization. However, one potential disadvantage of their use could be the impairment of relaxation that may lead to diastolic dysfunction. Structural studies of a few Ca^{2+} sensitizers bound to cTnC (Figure 1.7) have provided insights into the mechanism of Ca^{2+} sensitization. We will review the characteristics of the interaction between cTnC and four Ca^{2+} sensitizers (bepridil, dfbp-o, levosimendan, and EMD-57033). We will also look at one Ca^{2+} desensitizer which has the effect of decreasing Ca^{2+} sensitivity of skeletal and cardiac muscle fibers.
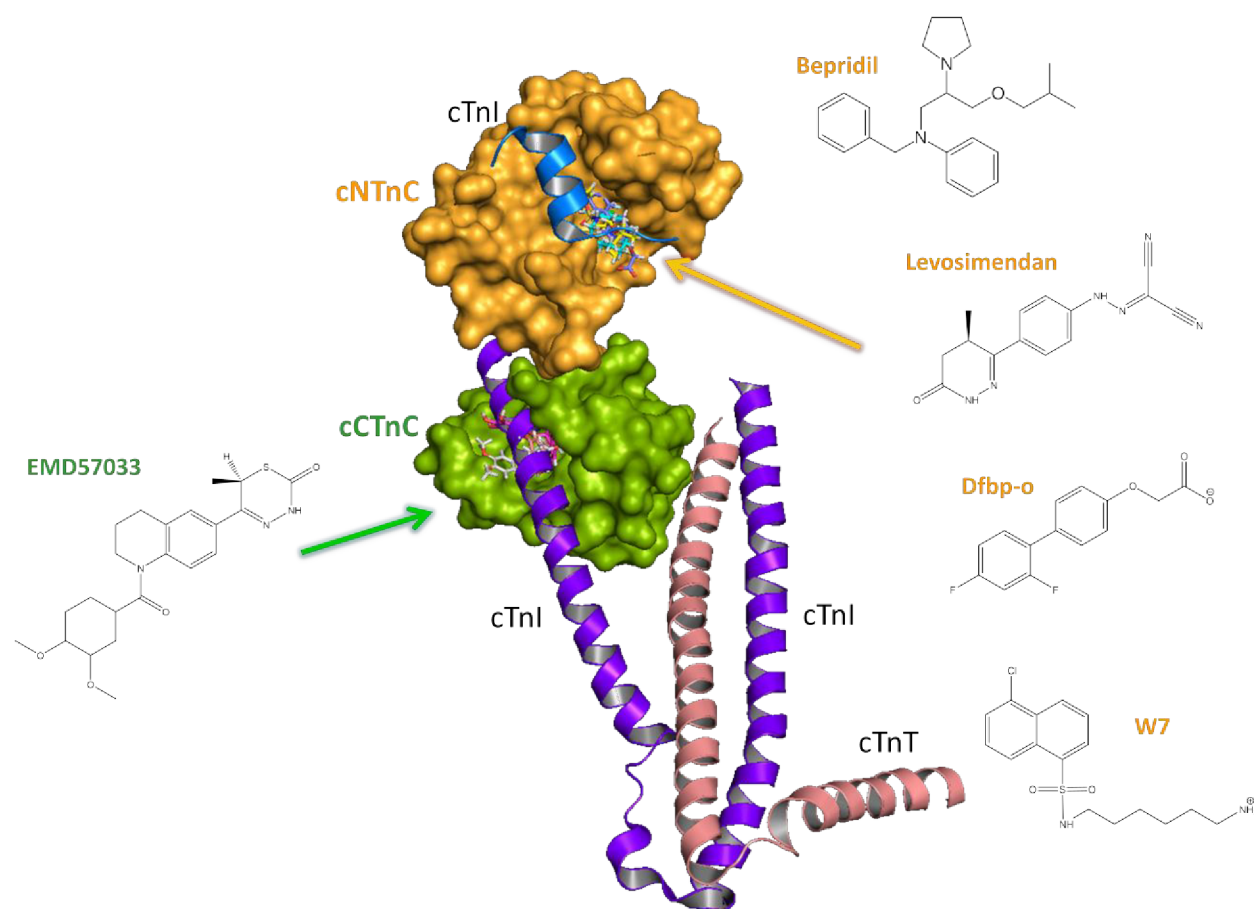
Figure 1.7. Drug binding sites on cTnC.
The structure of the Ca^{2+} sensitizers bepridil, levosimendan, dfbp-o, and EMD-57033, and of the Ca^{2+} desensitizer W7. All compounds on the right bind to the regulatory N-domain of cTnC. Only EMD-57033 on the left binds to the C-domain.

Bepridil has been shown to enhance Ca^{2+} binding to cNTnC in skinned muscle fibers[53]. In the absence of cTnI three bepridil molecules can bind cTnC[54]. In the x-ray structure of cTnC bound to bepridil[55] there are three bepridil molecules. The structure has both domains of cTnC bound to each other by their hydrophobic cavities with the bepridil molecules in between the domains. Two of the bepridil molecules seem to be more superficial on the cNTnC-cCTnC interface. The third molecule is bound deeper into the hydrophobic cleft of cNTnC which is in the open conformation. However, in the presence of cTnI only one molecule binds to cNTnC with an estimated affinity of ~140 μM[56]. This indicates that cTnI blocks the other two bepridil binding sites. The NMR structure of cNTnC bound to the switch region of cTnI (residues 147-163) and bepridil[57] shows one bepridil molecule bound deep in cNTnC. In this structure cNTnC is also in the open conformation; however, cTnI is slightly shifted away from the hydrophobic cleft compared to the cNTnC·cTnI complex[21]. This is correlated with a decrease in the binding affinity of cTnI to cNTnC from 154 ± 30 μM to 550 ± 50 μM in the presence of bepridil. The affinity of bepridil for cNTnC is also decreased in the presence of cTnI from 23 ± 5 μM to 80 ± 15 μM[57]. Thus, bepridil increases Ca^{2+} binding by stabilizing the open conformation of cNTnC despite reducing cTnI binding.

Levosimendan is the best characterized Ca^{2+} sensitizer clinically but not structurally. It is a Ca^{2+} sensitizer approved for clinical use in Europe, Asia, South America and Australia[58]. Unlike other inotropes, levosimendan enhances cardiac contractility without increasing oxygen consumption, intracellular cAMP, or cytosolic Ca^{2+} concentrations at clinically relevant doses[58,59]. Administration of levosimendan also presents vasodilator, anti-ischemic, and cardioprotective effects[58,60]. At high concentrations levosimendan inhibits PDE3, but its positive inotropic effect is mainly due to its interaction with cTnC[61]. In the absence of cTnI, levosimendan has been shown to bind both domains of cTnC[62,63]. Nevertheless, in the presence of the cCTnC and cNTnC binding regions of cTnI, levosimendan binds only to the N-domain with an estimated affinity of 200 μM[64]. To date there is no three-dimensional structure of levosimendan in complex with cNTnC and cTnI due to the short lifetime of this complex. Instead structural studies using x-ray scattering estimate that the binding site is close to the D/E linker between the domains of cTnC[1]. In addition, it has been found that cysteine 84 of cNTnC is essential for levosimendan binding since mutation of this residue to serine abolishes their interaction[65]. Binding of levosimendan to cNTnC does not affect the affinity for Ca^{2+} but stabilizes the cNTnC·Ca^{2+} complex that initiates contraction[66].

Dfbp-o is an analogue of levosimendan that also induces Ca^{2+} sensitization on rat cardiac trabeculae. Dfbp-o binds to cNTnC with an affinity of 820 ± 190 μM which is increased to 380 ± 80 μM in the presence of the switch region of cTnI (residues 147-163). Importantly, dfbp-o enhances the binding of cTnI to cNTnC from 130 ± 10 μM to 60 ± 10 μM. In the NMR structure of cNTnC bound to cTnI (residues 147-163) and dfbp-o, cNTnC is in the open conformation[67]. The position and orientation of

cTnI is not changed compared to cNTnC·cTnI on the structure of the core domain of cTnC[11]. This is an important difference with the structure of bepridil which has cTnI shifted away. Dfbp-o localizes to the hydrophobic cleft of cNTnC with the biphenyl moiety making multiple hydrophobic contacts with residues deeper in the cleft. The more hydrophobic part of dfbp-o contains an ether and a carboxylate group that make electrostatic interaction with solvent exposed residues toward the surface of cNTnC. Indeed the interaction between the negative carboxylate group of dfbp-o and arginine 147 of cTnI was proposed to be responsible for the enhanced binding of cTnI to cNTnC[67]. Thus the Ca^{2+} sensitizing effects of dfbp-o rely on stabilization of the open conformation of cNTnC and favorable interactions between cTnI and dfbp-o.

EMD-57033 increases the Ca^{2+} sensitivity of force development in skinned muscle fibers without altering Ca^{2+} mobilization[68,69]. Its Ca^{2+} sensitizing effect is stereospecific. EMD-57033 is the (+) enantiomer of a racemate. The (-) enantiomer, EMD-57439, has only PDE-3 inhibitory effects but no Ca^{2+} sensitizing activity. In contrast to bepridil, levosimendan, or dfbp-o, EMD-57033 binds to the C-domain of cTnC with a K_D of ~10 μM. The NMR structure of EMD-57033 bound to cCTnC[70] shows key interactions between the chiral methyl group of the drug and cCTnC that explain the stereospecificity of its binding. EMD-57003 is displaced completely by the cCTnC-binding region of cTnI (residues 34-71) but not by the inhibitory region (residues 128-147) since a stable cCTnC·cTnI(128-147)·EMD-57033 ternary complex can be formed[71,70]. It has been suggested that EMD-57033 weakens the interaction of cTnI (residues 34-71) with cCTnC to enhance the binding of the C-terminal region and enhance the apparent Ca^{2+} sensitivity[72]. Then, EMD-57033 has a different mechanism of action compared to other Ca^{2+} sensitizers but it is more probable that this involves an effect on the myosin-actin interface than direct binding to cTnC.

W7 is a calmodulin antagonist that inhibits the maximum ATPase activity and Ca^{2+} sensitivity of skeletal and cardiac muscle fibers[73]. It was shown to bind specifically to cTnC and not to tropomomyosin, actin or myosin[74]. In the absence of cTnI, W7 can bind to both domains of cTnC as shown by widespread chemical shift perturbations in NMR titrations[75]. But in the presence of the cCTnC-binding, inhibitory, and switch regions of cTnI it can only bind to the N-domain with a K_D of ~500 μM[75]. However, W7 causes a ~13-fold decrease in the binding affinity of cTnI (residues 147-163) for cNTnC from 154 ± 30 μM to 2000 ± 50 μM. The NMR structure of the cNTnC·cTnI·W7 complex[76] shows W7 binding in the hydrophobic groove of cNTnC in a similar way to other drug molecules that bind cNTnC. cNTnC is also in the open conformation accommodating both the drug and cTnI. In the structure cTnI is shifted away from cNTnC compared to the orientation observed in the x-ray structure of the core domain of cTnC. The naphthalene ring of W7 accommodates deeper into cNTnC than the aminohexyl tail which points to the solvent. From the structure, a repulsive interaction between the positively charged NH^{3+} group of W7 and arginine 147 of cTnI was correlated with the decrease in cTnI binding by

W7. This is similar to the effect of bepridil, which also decreased cTnI binding, but is contrary to the effect of dfpb-o, which increased cTnI binding due to attractive electrostatic interactions. Then W7 may decrease Ca^{2+} sensitivity by perturbing the association of the switch region of cTnI to cNTnC.

The reader can now appreciate that stabilization of the cTnC states that promote contraction are the main effects of Ca^{2+} sensitizers. The cNTnC•Ca^{2+} complex, the open state of cNTnC, and binding of the switch region of cTnI, all promote contraction. However, no single combination of such events seems to be definitive to cause sensitization. In all cases, even for the desensitizer W7, the open conformation of cNTnC is observed in the ternary structure of the drug bound to cNTnC•cTnI (switch region), except for levosimendan for which no structure is available. But, whereas Ca^{2+} binding is directly increased by bepridil, it is not by levosimendan. In addition, enhanced binding of cTnI is promoted by dfbp-o, and decreased by bepridil and W7, but the latest causes desensitization. Therefore, this thesis aims to provide more information to clarify the mechanism of action by which this group of drugs act on troponin.

References

1. Sorsa, T., Pollesello, P., and Solaro, R. J. (2004) The contractile apparatus as a target for drugs against heart failure: Interaction of levosimendan, a calcium sensitiser, with cardiac troponin c. *Molecular and Cellular Biochemistry. 266*, 87-107.

2. Gordon, A. M., Homsher, E., and Regnier, M. (2000) Regulation of contraction in striated muscle. *Physiol. Rev. 80*, 853-924.

3. Kobayashi, T., Jin, L., and de Tombe, P. (2008) Cardiac thin filament regulation. *Pflügers Arch. 457*, 37-46.

4. Kobayashi, T., and Solaro, R. J. (2005) Calcium, thin filaments, and the integrative biology of cardiac contractility. *Annu. Rev. Physiol. 67*, 39-67.

5. Li, M., Wang, X., and Sykes, B. (2004) Structural based insights into the role of troponin in cardiac muscle pathophysiology. *J. Muscle Res. Cell Motil. 25*, 559-579.

6. Satyshur, K. A., Rao, S. T., Pyzalska, D., Drendel, W., Greaser, M., and Sundaralingam, M. (1988) Refined structure of chicken skeletal muscle troponin C in the two-calcium state at 2-A resolution. *J. Biol. Chem. 263*, 1628-1647.

7. Herzberg, O., and James, M. N. (1988) Refined crystal structure of troponin C from turkey skeletal muscle at 2.0 A resolution. *J. Mol. Biol. 203*, 761-779.

8. Houdusse, A., Love, M. L., Dominguez, R., Grabarek, Z., and Cohen, C. (1997) Structures of four Ca^{2+}-bound troponin C at 2.0 A resolution: Further insights into the Ca^{2+}-switch in the calmodulin superfamily. *Structure. 5*, 1695-1711.

9. Slupsky, C. M., Reinach, F. C., Smillie, L. B., and Sykes, B. D. (1995) Solution secondary structure of calcium-saturated troponin C monomer determined by multidimensional heteronuclear NMR spectroscopy. *Protein Sci. 4*, 1279-1290.

10. Sia, S. K., Li, M. X., Spyracopoulos, L., Gagné, S. M., Liu, W., Putkey, J. A., and Sykes, B. D. (1997) Structure of cardiac muscle troponin C unexpectedly reveals a closed regulatory domain. *J. Biol. Chem. 272*, 18216-18221.

11. Takeda, S., Yamashita, A., Maeda, K., and Maeda, Y. (2003) Structure of the core domain of human cardiac troponin in the Ca^{2+}-saturated form. *Nature. 424*, 35-41.

12. Howarth, J. W., Meller, J., Solaro, R. J., Trewhella, J., and Rosevear, P. R. (2007) Phosphorylation-dependent conformational transition of the cardiac specific N-extension of troponin I in cardiac troponin. *J. Mol. Biol. 373*, 706-722.

13. Hwang, P. M., Cai, F., Pineda-Sanabria, S. E., Corson, D. C., and Sykes, B. D. (2014) The cardiac-specific N-terminal region of troponin I positions the regulatory domain of troponin C. *Proceedings of the National Academy of Sciences. 111*, 14412-14417.

14. Lindhout, D. A., and Sykes, B. D. (2003) Structure and dynamics of the C-domain of human cardiac troponin C in complex with the inhibitory region of human cardiac troponin I. *Journal of Biological Chemistry. 278*, 27024-27034.

15. Hernández, G., Blumenthal, D. K., Kennedy, M. A., Unkefer, C. J., and Trewhella, J. (1999) Troponin I inhibitory peptide (96-115) has an extended conformation when bound to skeletal muscle troponin C. *Biochemistry (N. Y.). 38*, 6911-6917.

16. Tung, C. S., Wall, M. E., Gallagher, S. C., and Trewhella, J. (2000) A model of troponin-I in complex with troponin-C using hybrid experimental data: The inhibitory region is a beta-hairpin. *Protein Sci. 9*, 1312-1326.

17. Campbell, A. P., and Sykes, B. D. (1991) Interaction of troponin I and troponin C: Use of the two-dimensional nuclear magnetic resonance transferred nuclear Overhauser effect to determine the structure of the inhibitory troponin I peptide when bound to skeletal troponin C. *J. Mol. Biol. 222*, 405-421.

18. Vinogradova, M. V., Stone, D. B., Malanina, G. G., Karatzaferi, C., Cooke, R., Mendelson, R. A., and Fletterick, R. J. (2005) Ca^{2+}-regulated structural changes in troponin. *Proceedings of the National Academy of Sciences of the United States of America. 102*, 5038-5043.

19. Campbell, A. P., Van Eyk, J. E., Hodges, R. S., and Sykes, B. D. (1992) Interaction of troponin I and troponin C: Use of the two-dimensional transferred nuclear overhauser effect to determine the structure of a gly-110 inhibitory troponin I peptide analog when bound to cardiac troponin C. *Biochim. Biophys. Acta. 1160*, 35-54.

20. Brown, L. J., Sale, K. L., Hills, R., Rouviere, C., Song, L., Zhang, X., and Fajer, P. G. (2002) Structure of the inhibitory region of troponin by site directed spin labeling electron paramagnetic resonance. *Proceedings of the National Academy of Sciences. 99*, 12765-12770.

21. Li, M. X., Spyracopoulos, L., and Sykes, B. D. (1999) Binding of cardiac troponin-I147-163 induces a structural opening in human cardiac troponin-C. *Biochemistry (N. Y.). 38*, 8289-8298.

22. Zhou, Z., Li, K., Rieck, D., Ouyang, Y., Chandra, M., and Dong, W. (2012) Structural dynamics of C-domain of cardiac troponin I protein in reconstituted thin filament. *Journal of Biological Chemistry. 287*, 7661-7674.

23. Ohtsuki, I. (2007) Troponin: Structure, Function and Dysfunction, in (S. Ebashi, and I. Ohtsuki, Eds.) pp 21-36, Springer Japan.

24. Gagne, S. M., Tsuda, S., Li, M. X., Smillie, L. B., and Sykes, B. D. (1995) Structures of the troponin C regulatory domains in the apo and calcium-saturated states. *Nat. Struct. Biol. 2*, 784-789.

25. Spyracopoulos, L., Li, M. X., Sia, S. K., Gagné, S. M., Chandra, M., Solaro, R. J., and Sykes, B. D. (1997) Calcium-induced structural transition in the regulatory domain of human cardiac troponin C. *Biochemistry (N. Y.). 36*, 12138-12146.

26. Robinson, J. M., Cheung, H. C., and Dong, W. (2008) The cardiac Ca^{2+}-sensitive regulatory switch, a system in dynamic equilibrium. *Biophys. J. 95*, 4772-4789.

27. Lindert, S., Kekenes-Huskey, P., Huber, G., Pierce, L., and McCammon, J. A. (2012) Dynamics and calcium association to the N-terminal regulatory domain of human cardiac troponin C: A multiscale computational study. *J PhysChem B. 116*, 8449-8459.

28. Solaro, R. J., Henze, M., and Kobayashi, T. (2013) Integration of troponin I phosphorylation with cardiac regulatory networks. *Circulation Research. 112*, 355-366.

29. Abbott, M. B., Dong, W., Dvoretsky, A., DaGue, B., Caprioli, R. M., Cheung, H. C., and Rosevear, P. R. (2001) Modulation of cardiac troponin Câˆ'Cardiac troponin I regulatory interactions by the amino-terminus of cardiac troponin Iâ€ . *Biochemistry (N. Y.). 40*, 5992-6001.

30. Ward, D. G., Brewer, S. M., Calvert, M. J., Gallon, C. E., Gao, Y., and Trayer, I. P. (2004) Characterization of the interaction between the N-terminal extension of human cardiac troponin I and troponin C. *Biochemistry. 43*, 4020-4027.

31. Robertson, S. P., Johnson, J. D., Holroyde, M. J., Kranias, E. G., Potter, J. D., and Solaro, R. J. (1982) The effect of troponin I phosphorylation on the Ca^{2+}-binding properties of the Ca^{2+}-regulatory site of bovine cardiac troponin. *Journal of Biological Chemistry. 257*, 260-263.

32. Solaro, R. J., Moir, A. J., and Perry, S. V. (1976) Phosphorylation of troponin I and the inotropic effect of adrenaline in the perfused rabbit heart. *Nature. 262*, 615-617.

33. World Health Organization 2012 www.who.int/mediacentre/factsheets/fs310/en/

34. Lee, J. A., and Allen, D. G. (1991) Mechanisms of acute ischemic contractile failure of the heart. role of intracellular calcium. *J. Clin. Invest. 88*, 361-367.

35. Jennings, R., and Reimer, K. (1991) The cell biology of acute myocardial-ischemia. *Annu. Rev. Med. 42*, 225-246.

36. Niwano, S., and Tojo, T. (2010) Systemic acidosis in acute myocardial ischemia; – cause or result of life-threatening ventricular arrhythmia? –. *Circulation Journal. 74*, 1794-1795.

37. Metzger, J. M., and Westfall, M. V. (2004) Covalent and noncovalent modification of thin filament action. *Circulation Research. 94*, 146-158.

38. Dargis, R., Pearlstone, J. R., Barrette-Ng, I., Edwards, H., and Smillie, L. B. (2002) Single mutation (A162H) in human cardiac troponin I corrects acid pH sensitivity of Ca^{2+}-regulated actomyosin S1 ATPase. *J. Biol. Chem. 277*, 34662-34665.

39. Solaro, R. J., Kumar, P., Blanchard, E. M., and Martin, A. F. (1986) Differential effects of pH on calcium activation of myofilaments of adult and perinatal dog hearts. Evidence for developmental differences in thin filament regulation. *Circ. Res. 58*, 721-729.

40. Reiser, P. J., Westfall, M. V., Schiaffino, S., and Solaro, R. J. (1994) Tension production and thin-filament protein isoforms in developing rat myocardium. *American Journal of Physiology - Heart and Circulatory Physiology. 267*, H1589-H1596.

41. Solaro, R. J., Lee, J. A., Kentish, J. C., and Allen, D. G. (1988) Effects of acidosis on ventricular muscle from adult and neonatal rats. *Circulation Research. 63*, 779-787.

42. Westfall, M. V., Rust, E. M., and Metzger, J. M. (1997) Slow skeletal troponin I gene transfer, expression, and myofilament incorporation enhances adult cardiac myocyte contractile function. *Proceedings of the National Academy of Sciences. 94*, 5444-5449.

43. Westfall, M. V., Albayya, F. P., Turner, I. I., and Metzger, J. M. (2000) Chimera analysis of troponin I domains that influence Ca^{2+}-activated myofilament tension in adult cardiac myocytes. *Circulation Research. 86*, 470-477.

44. Li, G., Martin, A. F., and Solaro, J. R. (2001) Localization of regions of troponin I important in deactivation of cardiac myofilaments by acidic pH.*J. Mol. Cell. Cardiol. 33*, 1309-1320.

45. Day, S. M., Westfall, M. V., Fomicheva, E. V., Hoyer, K., Yasuda, S., Cross, N. C. L., D'Alecy, L.,G., Ingwall, J. S., and Metzger, J. M. (2006) Histidine button engineered into cardiac troponin I protects the ischemic and failing heart. *Nat. Med. 12*, 181-189.

46. Fentzke, R. C., Buck, S. H., Patel, J. R., Lin, H., Wolska, B. M., Stojanovic, M. O., Martin, A. F., Solaro, R. J., Moss, R. L., and Leiden, J. M. (1999) Impaired cardiomyocyte relaxation and diastolic function in transgenic mice expressing slow skeletal troponin I in the heart. *J. Physiol. (Lond.). 517*, 143-157.

47. Palpant, N. J., D'Alecy, L. G., and Metzger, J. M. (2009) Single histidine button in cardiac troponin I sustains heart performance in response to severe hypercapnic respiratory acidosis in vivo. *The FASEB Journal. 23*, 1529-1540.

48. McMurray, J. J. V., Packer, M., Desai, A. S., Gong, M. P. H., Lefkowitz, M. P., Rizkala, A. R., …, Zile, M. R. (2014) Angiotensin-neprilysin inhibition versus enalapril in heart failure. *N Engl J Med. 371*, 993-1004.

49. Metra, M., Bettari, L., Carubelli, V., and Cas, L. D. (2011) Old and new intravenous inotropic agents in the treatment of advanced heart failure. *Prog. Cardiovasc. Dis. 54*, 97-106.

50. Metra, M., Bettari, L., Carubelli, V., Bugatti, S., Dei Cas, A., Del Magro, F., Lazzarini, V., Lombardi, C., and Dei Cas, L. (2011) Use of inotropic agents in patients with advanced heart failure. *Drugs. 71*, 515-525.

51. Goldhaber, J. I., and Hamilton, M. A. (2010) Role of inotropic agents in the treatment of heart failure. *Circulation. 121*, 1655-1660.

52. McCann, P., and Hauptman, P. J. (2012) Inotropic therapy: An important role in the treatment of advanced symptomatic heart failure. *Med. Clin. North Am. 96*, 943-954.

53. Solaro, R. J., Bousquet, P., and Johnson, J. D. (1986) Stimulation of cardiac myofilament force, ATPase activity and troponin C ca++ binding by bepridil. *Journal of Pharmacology and Experimental Therapeutics. 238*, 502-507.

54. Kleerekoper, Q., Liu, W., Choi, D., and Putkey, J. A. (1998) Identification of binding sites for bepridil and trifluoperazine on cardiac troponin C. *Journal of Biological Chemistry. 273*, 8153-8160.

55. Li, Y., Love, M. L., Putkey, J. A., and Cohen, C. (2000) Bepridil opens the regulatory N-terminal lobe of cardiac troponin C. *Proceedings of the National Academy of Sciences. 97*, 5140-5145.

56. Abusamhadneh, E., Abbott, M. B., Dvoretsky, A., Finley, N., Sasi, S., and Rosevear, P. R. (2001) Interaction of bepridil with the cardiac troponin C/troponin I complex. *FEBS Lett. 506*, 51-54.

57. Wang, X., Li, M. X., and Sykes, B. D. (2002) Structure of the regulatory N-domain of human cardiac troponin C in complex with human cardiac troponin I$_{147\text{-}163}$ and bepridil. *J. Biol. Chem. 277*, 31124-31133.

58. Pathak, A., Lebrin, M., Vaccaro, A., Senard, J. M., and Despas, F. (2013) Pharmacology of levosimendan: Inotropic, vasodilatory and cardioprotective effects. *J. Clin. Pharm. Ther. 38*, 341-349.

59. Moreno, N., Tavares-Silva, M., Lourenco, A. P., Oliveira-Pinto, J., Henriques-Coelho, T., and Leite-Moreira, A. F. (2014) Levosimendan: The current situation and new prospects. *Rev. Port. Cardiol. 33*, 795-800.

60. Pierrakos, C., Velissaris, D., Franchi, F., Muzzi, L., Karanikolas, M., and Scolletta, S. (2013) Levosimendan in critical illness: A literature review. *Journal of Clinical Medicine Research. 6*, 75-85.

61. Deschodt-Arsac, V., Calmettes, G., Raffard, G., Massot, P., Franconi, J., Pollesello, P., and Diolez, P. (2010) Absence of mitochondrial activation during levosimendan inotropic action in perfused paced guinea pig hearts as demonstrated by modular control analysis. *American Journal of Physiology - Regulatory, Integrative and Comparative Physiology. 299*, R786-R792.

62. Haikala, H., Kaivola, J., Nissinen, E., Wall, P., Levijoki, J., and Lindén, I. (1995) Cardiac troponin C as a target protein for a novel calcium sensitizing drug, levosimendan. *J. Mol. Cell. Cardiol. 27*, 1859-1866.

63. Sorsa, T., Heikkinen, S., Abbott, M. B., Abusamhadneh, E., Laakso, T., Tilgmann, C., Serimaa, R., Annila, A., Rosevear, P. R., Drakenberg, T., Pollesello, P., and Kilpeläinen, I. (2001) Binding of levosimendan, a calcium sensitizer, to cardiac troponin C. *J. Biol. Chem. 276*, 9337-9343.

64. Sorsa, T., Pollesello, P., Permi, P., Drakenberg, T., and Kilpeläinen, I. (2003) Interaction of levosimendan with cardiac troponin C in the presence of cardiac troponin I peptides. *J. Mol. Cell. Cardiol. 35*, 1055-1061.

65. Levijoki, J., Pollesello, P., Kaivola, J., Tilgmann, C., Sorsa, T., Annila, A., Kilpeläinen, I., and Haikala, H. (2000) Further evidence for the cardiac troponin C mediated calcium sensitization by levosimendan: Structure-response and binding analysis with analogs of levosimendan. *J. Mol. Cell. Cardiol. 32*, 479-491.

66. Endoh, M. (2008) Cardiac Ca^{2+} signaling and Ca^{2+} sensitizers. *Circ. J. 72*, 1915-1925.

67. Robertson, I. M., Sun, Y., Li, M. X., and Sykes, B. D. (2010) A structural and functional perspective into the mechanism of Ca^{2+}-sensitizers that target the cardiac troponin complex. *J. Mol. Cell. Cardiol. 49*, 1031-1041.

68. Solaro, R. J., Gambassi, G., Warshaw, D. M., Keller, M. R., Spurgeon, H. A., Beier, N., and Lakatta, E. G. (1993) Stereoselective actions of thiadiazinones on canine cardiac myocytes and myofilaments. *Circulation Research. 73*, 981-990.

69. Senzaki, H., Isoda, T., Paolocci, N., Ekelund, U., Hare, J. M., and Kass, D. A. (2000) Improved mechanoenergetics and cardiac rest and reserve function of in vivo failing heart by calcium sensitizer EMD-57033. *Circulation. 101*, 1040-1048.

70. Wang, X., Li, M. X., Spyracopoulos, L., Beier, N., Chandra, M., Solaro, R. J., and Sykes, B. D. (2001) Structure of the C-domain of human cardiac troponin C in complex with the Ca^{2+} sensitizing drug EMD 57033. *Journal of Biological Chemistry. 276*, 25456-25466.

71. Li, M. X., Spyracopoulos, L., Beier, N., Putkey, J. A., and Sykes, B. D. (2000) Interaction of cardiac troponin C with Ca^{2+} sensitizer EMD 57033 and cardiac troponin I inhibitory peptideâ€ . *Biochemistry (N. Y.). 39*, 8782-8790.

72. Li, M. X., Robertson, I. M., and Sykes, B. D. (2008) Interaction of cardiac troponin with cardiotonic drugs: A structural perspective. *Biochem. Biophys. Res. Commun. 369*, 88-99.

73. Adhikari, B. B., and Wang, K. (2003) Interplay of troponin- and myosin-based pathways of calcium activation in skeletal and cardiac muscle: The use of W7 as an inhibitor of thin filament activation. *Biophys. J. 86*, 359-370.

74. Hidaka, H., Yamaki, T., Naka, M., Tanaka, T., Hayashi, H., and Kobayashi, R. (1980) Calcium-regulated modulator protein interacting agents inhibit smooth muscle calcium-stimulated protein kinase and ATPase. *Mol. Pharmacol. 17*, 66-72.

75. Li, M. X., Hoffman, R. M. B., and Sykes, B. D. (2006) Interaction of cardiac troponin C and troponin I with W7 in the presence of three functional regions of cardiac troponin Iâ€ . *Biochemistry (N. Y.). 45*, 9833-9840.

76. Oleszczuk, M., Robertson, I. M., Li, M. X., and Sykes, B. D. (2010) Solution structure of the regulatory domain of human cardiac troponin C in complex with the switch region of cardiac troponin I and W7: The basis of W7 as an inhibitor of cardiac muscle contraction. *J. Mol. Cell. Cardiol. 48*, 925-933.

CHAPTER 2

Interaction between the regulatory domain of cardiac troponin C and the acidosis resistant cardiac troponin I A162H

Sandra E. Pineda-Sanabria[1], Ian M. Robertson[2], Monica X. Li[1] and Brian D. Sykes[1]

[1]Department of Biochemistry, School of Translational Medicine, Faculty of Medicine and Dentistry, University of Alberta, Edmonton, Alberta, Canada T6G 2H7. [2]Current address: Randall Division of Cell and Molecular Biophysics, New Hunt's House, Guy's Campus, King's College London, London, UK, SE1 1UL.

This chapter begins the journey of discovering the mechanism behind the A162H substitution. It describes the interaction between the relevant troponin subunits C and I in the presence of A162H — namely, the pH dependence of the strength of binding and the determination of the acid dissociation constant (pK_a) of A162H by NMR spectroscopy. Finally, these factors interconnect to reveal electrostatic interactions facilitated by protonated H162. A version of this chapter has been previously published: Pineda-Sanabria *et al*. (2013) *Cardiovascular Research*. 97: 481-489.

Introduction

Ischemic heart disease accounts for almost half of the deaths caused by cardiovascular diseases worldwide, which is the number one cause of death[1]. Ischemia results from reduced blood flow to the cardiac cells that deprives them of oxygen and causes accumulation of ions and products of metabolism; this results in the reduction of force, the increase of arrhythmias and ultimately cell death. The fall in force during myocardial ischemia is caused by the reduced Ca^{2+} sensitivity of the contractile protein troponin C[2] (cTnC), as the pH in the heart muscle falls from normal values of 7.4 to values of 6.2 or lower[3]. In contrast to cardiac muscle, the force development of skeletal muscle is not compromised in an acidic environment. The explanation of this difference in sensitivity to acidosis has been the object of investigation in a number of studies[4-7] and it was found that the thin filament protein, troponin I (TnI), plays a major role in the underlying mechanism.

TnI forms part of the troponin complex, which regulates contraction in a Ca^{2+} dependent manner. In the cardiac system, the switch region of TnI comprising residues 147 to 163 interacts with the N terminal, Ca^{2+} binding domain of troponin C (cNTnC); this association causes the dissociation of cTnI from actin and the movement of tropomyosin that exposes the myosin binding sites on actin leading to cross bridge formation and generation of force[7,8]. Amongst the differences in sequences

between skeletal and cardiac troponin I isoforms (sTnI and cTnI, respectively), a single residue was identified[9] to be responsible for the change in sensitivity under acidic environment: H130 in the slow (ssTnI) and fast skeletal isoforms. ssTnI is the major isoform in fetal and neonatal hearts, but it is replaced by adult cTnI shortly after birth[7]; it is also present in adults in slow-twitch muscles like the soleus muscles.

The A162H substitution in the adult isoform of cTnI has been studied at different levels of biological organization to probe its effects on cardiac performance. It has been shown that the A162H substitution restores the Ca^{2+}-sensitivity at pH 6.5 to that at pH 7 in a reconstituted human cardiac troponin-tropomyosin actomyosin system, and that the reverse mutation, H130A, in sTnI reduces Ca^{2+}-sensitivity to that of the cardiac system at low pH[9]. Using a transgenic mouse model, it was demonstrated *ex vivo* that the histidine substitution A164H, corresponding to human A162H, causes retention of contractility after exposure to ischemia mimetic solution in membrane intact adult cardiac myocytes and improves diastolic performance of isolated hearts after perfusion with acidic buffer. In an *in vivo* animal model, transgenic A164H mice showed more resistance to hypoxic and ischemic challenges maintaining contractility and improving survival compared to non-transgenic mice[10, 11].

Different molecular mechanisms have been proposed for the improvement in myocardial performance by the cTnI A162H substitution. One suggests that the increased positive charge of the histidine during intracellular acidosis leads to stronger interaction with glutamate or aspartate residues in cTnC[9], or to weaker interactions with arginine or lysine residues in actin, or a combination. The other proposes the direct enhancement of sarcomeric Ca^{2+} activation as basal and peak Ca^{2+} levels are lower in A164H transgenic myocytes[10]. The interaction of cNTnC with sTnI, naturally containing H130, has been studied by nuclear magnetic resonance (NMR) spectroscopy. It was shown that H130 makes electrostatic interactions with cNTnC at low pH[12] and computational analysis predicted that the electrostatic interaction between cTnC and sTnI is four times stronger than the interaction with cTnI[13].

This study examines the underlying interactions in the cardiac cTnC-cTnI interface that dictate myocardial improvement by the A162H substitution. We use NMR spectroscopy to study the interaction of Ca^{2+}-saturated cNTnC with the switch peptide region of cTnI containing the A162H substitution under normal and acidic conditions, and a longer version containing the native histidine at position 171, downstream from H162. Our results show that the presence of H162 increases the affinity of cTnI for cNTnC at pH 7 and the increase is further enhanced at pH 6. To determine the interactions responsible, we determined the acid dissociation constant (pK_a) for glutamate residues in cNTnC. The results show that E15 and E19 exhibit deviations in their pK_a profiles, E15 has a shifted pK_a and E19 shows biphasic pK_a curves, and both residues display a common high pK_a value that indicates an electrostatic

interaction with H162. H171 does not have the same effect as H162, because H171 is too far away to form salt bridges with E15 or E19.

Experimental procedures

Materials and sample conditions

Human [^{15}N]-cNTnC and [^{15}N, ^{13}C]-cNTnC proteins were purified from *Escherichia coli* strains as previously described[14]. Two switch cTnI peptides were independently titrated into cNTnC•Ca^{2+} at both normal (pH 7) and acidic (pH 6) conditions: 1) the mutated peptide (cTnI$_{144-170}$ A162H) and 2) the native peptide (cTnI$_{144-173}$). Both synthetic peptides were obtained from GL Biochem Ltd. (Shanghai, China); the sequences are shown in Table 3.1. In the present study we used a version placing H162 in a middle position to avoid having A162H in a highly flexible C-terminal region.

All the NMR samples were 500 µL in volume and consisted of 100 mM KCl, 10 mM imidazole, 10 mM CaCl$_2$, 10 mM DTT and 0.25 mM 2,2-dimethyl-2-silapentane-5-sulfonate-d$_6$ sodium salt (DSS-d$_6$) as NMR internal reference. The initial concentration of cNTnC for each titration was determined by NMR spectral integration[15]. All the NMR experiments were acquired in a 500 or 600 MHz Varian Inova spectrometers at 30 °C. The 1D spectra were processed using VNMRJ v.2.21B (Varian Inc.) and the 2D spectra were processed with the NMRPipe[16] suite and analyzed with NMRViewJ[17].

cTnI titrations into cNTnC•Ca^{2+}

For all titrations, [^{15}N]-cNTnC was Ca^{2+} saturated and a stock solution of the cTnI peptide of interest was prepared fresh in deuterated dimethyl sulfoxide (DMSO-d$_6$); by the end of each titration, the addition of DMSO-d$_6$ did not exceed 10% of the sample volume. The concentration of each cTnI stock solution was determined by NMR spectral integration analysis relative to the DSS-d$_6$ standard. The pH was kept constant and adjusted with 1M NaOH or 1M HCl as needed.

For the titration of mutated cTnI peptide into cNTnC at pH 7, a 5.79 mM stock solution of cTnI$_{144-170}$ A162H was added in aliquots into a 72 µM cNTnC sample. The concentration of cTnI$_{144-170}$ A162H at each titration point was 0, 12, 103, 158, 212, 317, 418 and 656 µM. For the titration at pH 6, the initial cNTnC concentration was 126 µM, the cTnI$_{144-170}$ A162H stock concentration was 3.7 mM, and the concentration of mutated peptide at each point was 0, 7, 22, 44, 65, 100, 149, 215 and 342 µM.

For the titration of the native cTnI peptide, the initial concentrations of cNTnC at pH 7 and pH 6 were 146 and 160 µM, respectively; the cTnI$_{144-173}$ stock concentrations were 4.83 mM and 3.77 mM,

respectively; the cTnI concentrations at each point were 0, 10, 29, 57, 104, 149, 194, 281, 365 and 485 μM (pH 7); and 0, 15, 37, 74, 145, 213, 279 and 373 μM (pH 6).

All the titrations were followed by 1D ^{1}H and 2D ^{1}H, ^{15}N correlation NMR spectra at each titration point. The total chemical shift perturbations (CSP) were calculated using the following equation:

$$\Delta\delta = \sqrt{\left(\Delta\delta_H\right)^2 + \frac{\left(\Delta\delta_N\right)^2}{25}}$$

where $\Delta\delta_H$ and $\Delta\delta_N$ are the individual hydrogen and nitrogen CSP, respectively. Dilution of cNTnC by addition of cTnI peptide stock was taken into consideration. The total CSPs were plotted against the $[cTnI]_{total}:[cNTnC]_{total}$ concentration ratio and fit using the xcrvfit global fitting protocol (http://www.bionmr.ualberta.ca/bds/software/xcrvfit/index.html) to obtain the dissociation constant (K_D) that best matches all the data[18]. The standard error (SE = σ/n) was calculated from the standard deviation reported by xcrvfit for the global fit and using n = 20, 21 or 22 depending on the number of residues used for the global K_D determination.

pH titrations of cNTnC•Ca^{2+}•cTnI$_{144-170}$ A162H, cNTnC•Ca^{2+}•cTnI$_{144-173}$ and of the peptides alone.

For the cNTnC•Ca^{2+}•cTnI$_{144-170}$ A162H complex, an NMR sample containing 0.2 mM [^{15}N, ^{13}C]-cNTnC•Ca^{2+} and 0.8 mM cTnI$_{144-170}$ A162H peptide was used to perform a pH titration. The pH was progressively changed by adding aliquots of 1M NaOH or 1M HCl directly to the NMR tube to cover a range from 4.1 to 8.8. For this titration 4 mM piperazine was added to the original buffer since the value of pH at each titration point was confirmed by the chemical shift of the NMR proton signals of imidazole or piperazine as previously described[19]. 1D ^{1}H, 2D ^{1}H, ^{15}N correlation spectra and 2D carboxyl ^{1}H, ^{13}C correlation spectra[20,21] were acquired at each titration point. The same procedure was followed for the cNTnC•Ca^{2+}•cTnI$_{144-173}$ complex using concentrations of 0.3 mM and 1.2 mM for protein and peptide, respectively.

A series of 1D ^{1}H NMR spectra recorded during the pH titration of the cNTnC•Ca^{2+}•cTnI$_{144-170}$ A162H complex was used to determine the pK$_a$ of H162 in the mutated peptide by monitoring the resonances of its H2 and H5 aromatic hydrogen atoms (see Figure 2.5C for numbering). A separate pH titration was performed for free cTnI$_{144-170}$ A162H in solution ranging from 4.3 to 8.9 for the pK$_a$ determination of H162 when the mutated peptide is not in the bound form. In a similar fashion, the pK$_a$ of H171 in the native peptide cTnI$_{144-173}$ was determined. The determination of the pK$_a$ values was made

by using xcrvfit for monophasic curves and Wolfram Mathematica for biphasic curves as previously described[12]. The spread of the mean indicates the standard deviation (SD) of the fit.

Results

pH dependent affinities of cTnI$_{144-170}$ A162H and cTnI$_{144-173}$ for cNTnC•Ca^{2+}

The sequence comparison of the two peptides used in this study is shown in Table 2.1. The first peptide is the wild-type cardiac sequence with a naturally occurring histidine at position 171; the second a slightly shorter version without H171 but, with alanine 162 mutated to histidine. In order to determine the affinities of the peptides for cNTnC, and to map the changes in binding under acidosis, we performed titrations of each into Ca^{2+} saturated cNTnC at pH 7 and pH 6 and monitored these titrations using 2D ^{1}H, ^{15}N correlation NMR spectroscopy. We used calcium saturating conditions since calcium association to cNTnC is necessary for cTnI$_{147-163}$ switch peptide binding[21]. At low Ca^{2+} conditions, resembling diastole, weak or no binding at all is expected for the switch peptide.

Table 2.1. K$_D$ ± SE for the binding of the native and mutated cTnI peptides. Residues corresponding to the switch region of TnI are underlined and residues under investigation are bold.

Peptide	Sequence		K$_D$ (µM)	
			pH 7	pH 6
	144 154 162 171			
cTnI$_{144-173}$	RRVRISADAMMQALLGAR**A**K ESLDLRA**H**LK		200 ± 24	395 ± 39
cTnI$_{144-170}$ A162H	RRVRISADAM MQALLGAR**H**K ESLDLRA		40 ± 11	10 ± 3
	144 154 162 170			

Figure 2.1A depicts the NMR CSP for a selected group of backbone NHs of cNTnC upon binding of cTnI$_{144-170}$ A162H under normal and acidic conditions; the spectra showing all of the backbone NHs are shown in the supplementary material (Supplementary Figure 2.1). The chemical shift assignments are as reported previously[22]. The peptide-induced spectral changes are virtually identical under the two sets of conditions. We have used an extended version of the cardiac switch peptide in this study; however the residues experiencing CSP in cNTnC and the direction of such changes are the typical for switch peptide binding and consistent with those observed for shorter versions[22,23]; for example, large perturbations for residues L29, G34, G42, E66, G68, T71 and D73 were observed. These large changes were expected since these amino acids are located in the hinge regions of cNTnC which are responsible for the closed to open structural transition[24]. The linear fashion of the perturbations is characteristic of a one-to-one binding stoichiometry.
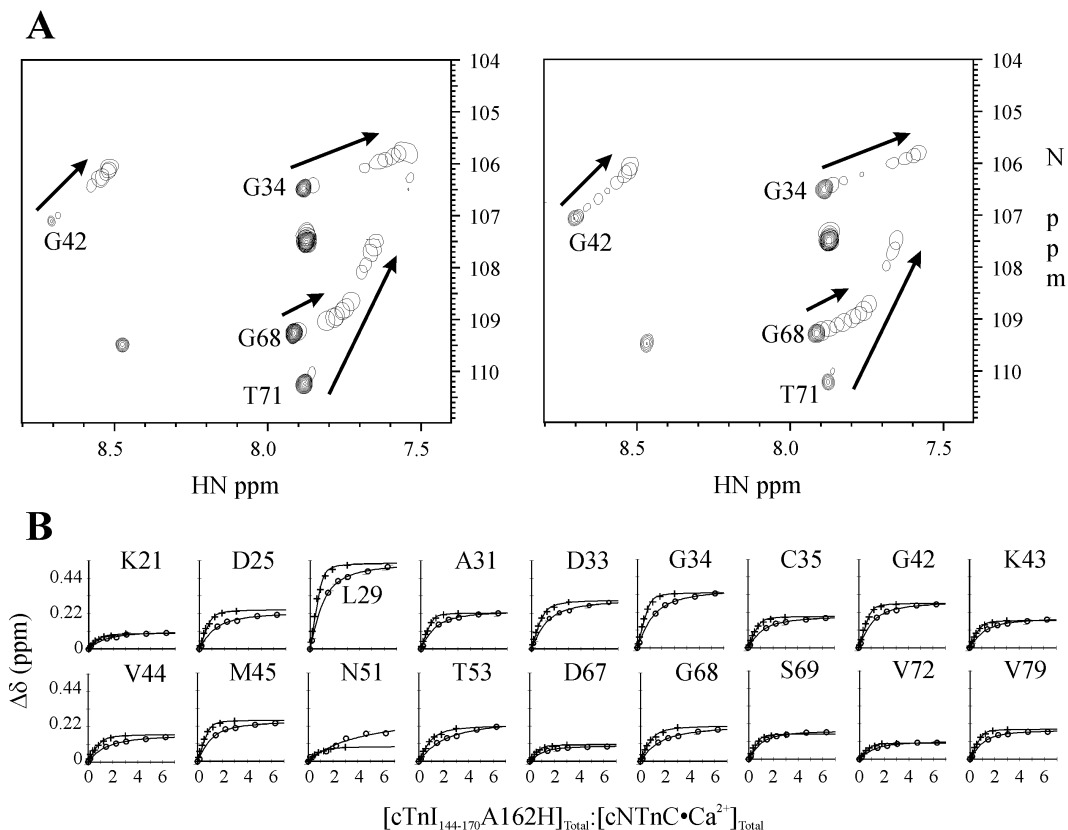
Figure 2.1. Titration of cTnI$_{144\text{-}170}$ A162H into cNTnC at different pH values.
A: An expanded region of the overlay of 2D ^{1}H,^{15}N correlation NMR spectra of cNTnC•Ca^{2+} acquired during the titration of cTnI$_{144\text{-}170}$ A162H at pH 7 (left) and 6 (right). The first point of the titration is represented with multiple contours and consequent additions of peptide by single contours. Arrows indicate the direction of the CSP. **B**: Global fitting for residues of cNTnC that experienced large CSP upon addition of cTnI$_{144\text{-}170}$ A162H at pH 7 (circles) and 6 (crosses).

Global fitting of the most perturbed residues (Figure 2.1B) results in a dissociation constant of 40 ± 11 µM for binding of cTnI$_{144\text{-}170}$ A162H under normal conditions and 10 ± 3 µM for binding under acidic conditions. The results indicate that the presence of H162 in cTnI stabilizes the cTnC-cTnI interaction by a factor of 4. In order to investigate if the naturally occurring H171 plays a similar role in stabilizing this interaction, we determined the dissociation constants for the binding of a slightly longer, native cardiac switch peptide (cTnI$_{144\text{-}173}$) at the two different pH values. The CSP of the amide NHs for these titrations are shown in Supplementary Figure 2.2 along with their respective fitting curves and the results are summarized in Table 2.1. The affinity of the native cardiac peptide at pH 6 is roughly half of its affinity at pH 7. Thus the presence of H162 in the mutated peptide makes binding at pH 7 tighter than that of native peptide at pH 7 by a factor of 5 and 20 times tighter than that of native peptide in acidic conditions. These observations are in agreement with those made at cellular

and organ level for the cTnI A164H studies performed in transgenic mice, where the beneficial effects of the substitution are evident at both normal and acidic conditions, but much more at acidic pH[10]. An acidic environment improves binding of the mutated peptide by a factor of 4, this is comparable to a 3.6 improvement on binding for the skeletal isoform in acidic conditions[12].

Determination of pK$_a$ of aspartate and glutamate residues of cNTnC•Ca^{2+}

The observed pH-dependent change in affinity of the mutated peptide suggests that protonation of H162 at the lower pH is important to the binding affinity. To investigate whether residues on cNTnC•Ca^{2+} are involved in electrostatic interactions with this histidine, we used three NMR experiments (1D ^{1}H, 2D ^{1}H, ^{15}N correlation, and the 2D carboxyl ^{1}H, ^{13}C correlation) to determine the pK$_a$ of aspartate and glutamate residues of cNTnC•Ca^{2+} in the cNTnC•Ca^{2+}•cTnI$_{144-170}$ A162H and the cNTnC•Ca^{2+}•cTnI$_{144-173}$ complexes. In both cases, cNTnC was Ca^{2+} saturated and excess peptide was used to assure saturation of the cNTnC•Ca^{2+}. pK$_a$'s can be obtained from 2D ^{1}H, ^{15}N correlation spectra by tracking the CSP of the amide NHs as a function of the pH; backbone hydrogen atoms located in non-titratable residues can be sensitive to and indicative of intramolecular hydrogen bonding between carboxylate groups and backbone amide protons[25,26]. However, the carboxyl group chemical shift is a more direct indicator of the pK$_a$ because it is the group that is being ionized (or protonated). The 2D carboxyl ^{1}H, ^{13}C spectrum correlates the aliphatic protons with the carboxyl carbon of glutamate and aspartate residues of cNTnC. The distribution of glutamate and aspartate residues in cNTnC is depicted in Supplementary Figure 2.3. We focused on E19 and E15, as they are the closest negatively charged residues (<3 and <10 Å, respectively) to H130 in the homologous sTnI structure, and E55 as a control since it is far away.

Figure 2.2 shows the CSP of the backbone NH's of E19 and E55 (panels A and B) and the carboxyl groups (panel C) of E15, E19 and E55 in cNTnC•Ca^{2+} when bound to cTnI$_{144-170}$ A162H. The ^{1}H and ^{15}N resonances of E55 show a linear behavior of CSP typical for a single dissociation event. E19, on the other hand, shows an unusual curved change in the amide proton shift as the pH changes (Figure 2.2B), which indicates a dependence on two different acid dissociation events. E15 is located in a highly overlapping region in the ^{1}H, ^{15}N correlation spectra, and cannot be reliably tracked (Figure 2.2A). In the 2D carboxyl ^{1}H, ^{13}C spectra (Figure 2.2C) the indication of two dissociation events is not obvious for E19 but is revealed in the fitting of the data (see below). One of the gamma hydrogen atoms of E15 moves earlier in the titration, reflecting a higher pK$_a$ than the typical for a glutamate residue (see fitting below). E55 shows linear CSP with the pH variations characteristic of a single dissociation event.
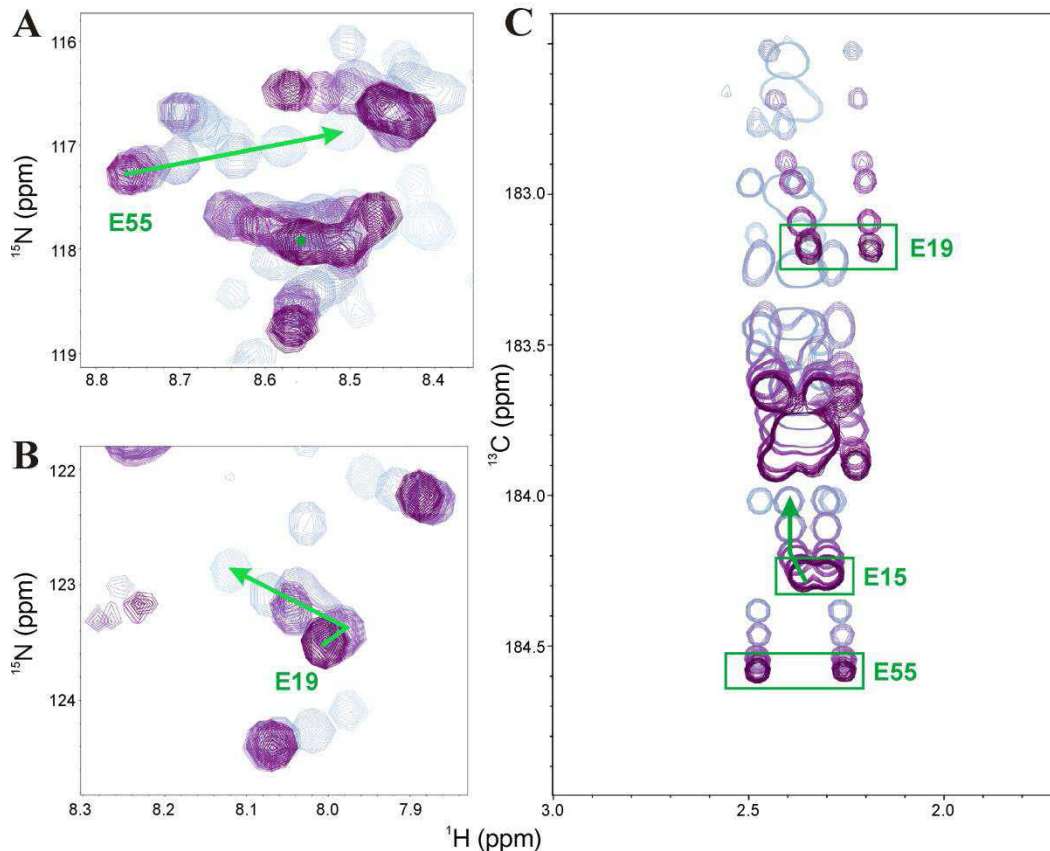
Figure 2.2. pH titration of cNTnC•Ca²⁺•cTnI₁₄₄₋₁₇₀ A162H.
Overlay of regions from the 2D ¹H,¹⁵N correlation (**A**, **B**) and 2D carboxyl¹H,¹³C correlation (**C**) NMR spectra acquired during the pH titration of the cNTnC•Ca²⁺•cTnI₁₄₄₋₁₇₀ A162H complex. Arrows indicate the direction of CSP as the pH decreases from dark to light purple. Residues E15, E19 and E55 are labeled. E15 in the 2D ¹H, ¹⁵N correlation spectra is located in a highly overlapping region (green dot in **A**).

The same sets of experiments were repeated for the native complex, cNTnC•Ca²⁺•cTnI₁₄₄₋₁₇₃. In this case, E15, E19 and E55 all show linear CSP on their proton, nitrogen and carbon resonances (Supplementary Figure 2.4) indicative of single protonation events for each of these residues. These results imply that the unusual behavior of E19 and E15 in the A162H complex are directly linked to the presence of H162, and provide evidence for an interaction being formed between H162 and E15 and E19. In order to address this possibility further, the pKₐ values of each residue were calculated.

The ¹H, ¹⁵N, and ¹³C NMR chemical shifts of the NH, CH₂, and CO atoms in the 2D spectra were fitted to monophasic or biphasic pKₐ curves, depending on whether one or two titration events were observed. The results for the native and A162H complexes are shown in Figure 2.3. Reference pKₐ

values for glutamate residues are estimated to range from 4.3 to 4.5 in oligopeptides and from 4.1 to 4.6 in proteins[27]. The observed pK_a for E55 in this study was typical, always fit with a single pK_a, and remained constant in the presence or absence of H162 (4.6 ± 0.04 versus 4.5 ± 0.14). The pK_a of E15 was also always fit with a single pK_a, and not significantly altered (from 4.10 ± 0.38 to 4.55 ± 0.30)[1] by the presence of H162. However, the $H^{\gamma 2}$ resonance of E15 showed a pK_a value of 3.8 ± 0.38 in the wild-type complex, but a much higher pK_a value of 6.8 ± 0.31 in the complex with the A162H peptide. The curves for all of the resonances of E19 in the wild-type complex showed a single pK_a values with an average pK_a of 5.3 ± 0.2. In contrast, four of the E19 resonances showed biphasic curves in the presence of the mutated $cTnI_{144-170}$ A162H peptide; for these an average pK_a value of 4.7 ± 0.11 is observed corresponding to the protonation of the carboxyl group in addition to an average higher pK_a value of 6.83 ± 0.25. The lower pK_a is decreased from that observed in the absence of H162. Therefore both E15 and E19 are sensing the protonation of a residue with a pK_a of ~6.8, and given the amino acid sequence of the peptides of interest and that this effect is only observed in the presence of the mutated peptide, this residue is most likely H162.
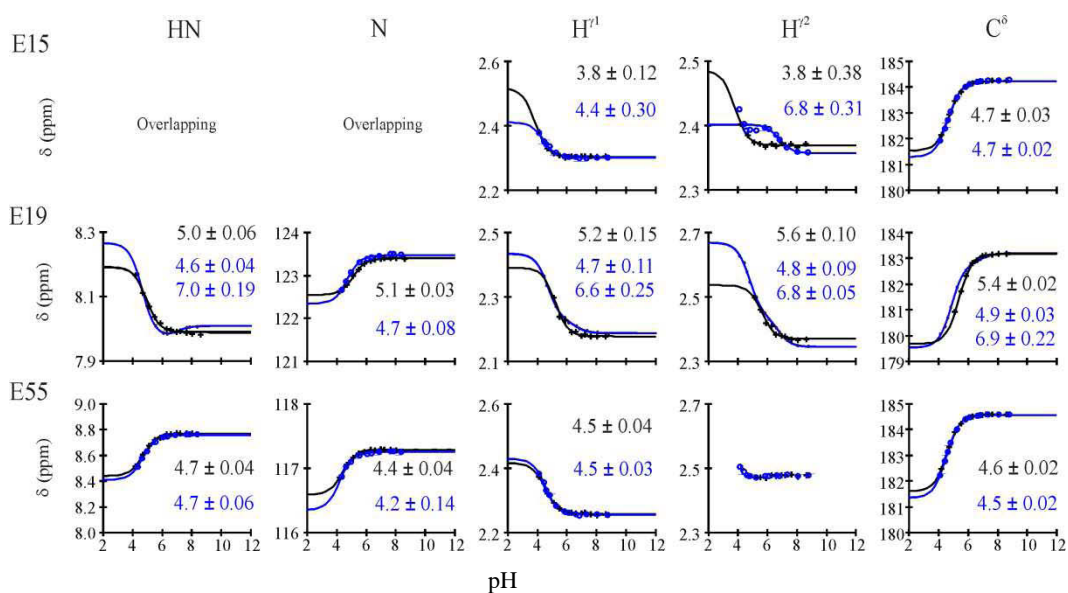
Figure 2.3. The effect of A162H in the pK_a of glutamate residues of cNTnC.
CSP of amide hydrogen, amide nitrogen, hydrogen gamma 1, hydrogen gamma 2 and carbon delta for E15, E19 and E55 as a function of pH for the cNTnC•Ca^{2+} in the presence of $cTnI_{144-173}$(black) and $cTnI_{144-170}$ A162H (blue). The pK_a values are shown for each curve with their respective SD. The Hill coefficient for all curves was set to 1.

---

[1] The fitting errors are the largest for E15, because it has the lowest pK_a and we were unable to go below pH 4.1 in our titrations because of the solubility of cTnC.

The pH-dependent CSP of aspartate residues D2, D3, D25, D33, D87 and D88 of cNTnC when bound to the mutated and native peptide were also followed. Because the typical pK_a value for aspartate residues is low (3.8 - 4.1[27]), determination of their pK_a values was difficult due to poor solubility of troponin below pH 4.1. The data is shown in Supplementary Figure 2.5, in all cases the overlap between pairs of data points indicates identical titrations, and differences are only observed in the lower pH region of the fitting curves. D3 displays a biphasic curve in both complexes with the second pK_a higher than typical for a histidine residue. The second protonation event is attributed to the NH^{3+} at the N-terminus. D25 and D33 do not yet display significant CSP at the lowest pH tested, this indicates that they have even lower pK_a values. None of the aspartate residues are in close proximity to the site of interest (Supplementary Figure 2.3).

Determination of the pK_a for H162 and H171

To determine whether the higher pK_a value associated to E15 and E19 corresponds to that of H162, we determined the pK_a for this residue in the $cTnI_{144-170}$ A162H peptide in the absence and presence of a 0.25 molar ratio of cNTnC•Ca^{2+}. We collected 1D ^1H experiments during the pH titration (4.1 to 8.9) of the complex. The changes in the aromatic region of the 1D ^1H spectrum, where the H162 signals are found, in the absence and presence of cNTnC•Ca^{2+} are shown in Figure 2.4A and B, respectively. The signals corresponding to hydrogens H2 and H5 of H162 are indicated, the large pair of signals seen in both sets of experiments corresponds to hydrogens H4 and H5 (large upfield signal) and H2 (large downfield signal) of imidazole used to measure the pH of the sample at each titration point. Signals from the amide hydrogens of the protein and the peptide can also be seen in the aromatic region. In the spectra corresponding to the cNTnC•$cTnI_{144-170}$ A162H complex, this set of signals become more intense and better resolved as the pH decreases as a result of reduced chemical exchange of the amide hydrogen atoms[28].

Fitting of the CSP of the hydrogen atoms H2 and H5 of H162 as a function of pH in the absence (Figure 2.4A) and presence (Figure 2.4B) of cNTnC, results in average pK_a values of 6.28 ± 0.02 in the free form and 6.34 ± 0.03 in the 25% bound form. The pK_a value of the fully bound form can be extrapolated since the observed NMR signals of protons H2 and H5 are in fast exchange and represent a weighted average signal with contributions from the bound and the excessive free forms. Furthermore, since the binding of $cTnI_{144-170}$ A162H is sufficiently tight at both acidic and alkaline pH values (Table 3.1), the fraction bound doesn't substantially change during the pH titration. The extrapolated value for the fully bound form is 6.52 ± 0.24, which is consistent with the additional value observed for E15 and E19, within the range of error (6.80 ± 0.31 and 6.83 ± 0.25, respectively).
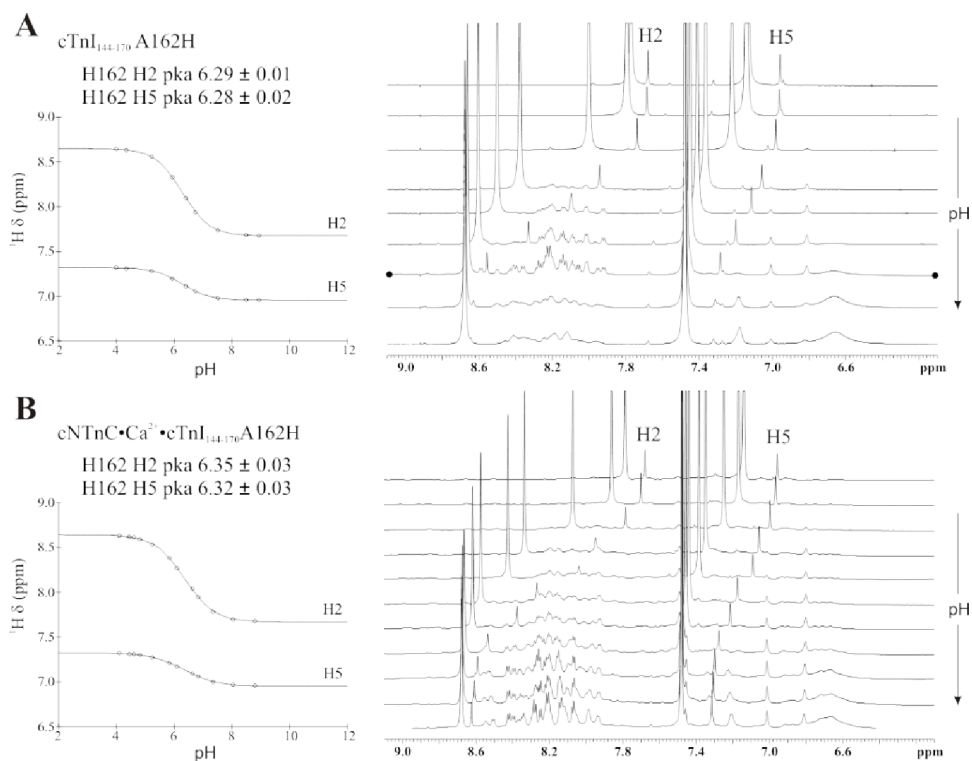
Figure 2.4. pK$_a$ values for A162H in the free and cNTnC-bound forms.
CSP of hydrogens H2 and H5 of H162 in the absence (**A**) and presence (**B**) of cNTnC•Ca^{2+} as a function of pH tracked by 1D ^{1}H NMR. Fitting curves and pK$_a$ values for both ring hydrogen atoms of H162 are shown on the side of each titration, the Hill coefficient was set to 1 for all curves.

The same procedure was followed to determine the pK$_a$ of H171 in the native peptide in the free state. For the bound form the dependence of K$_D$ on the pH was taken into account as previously described[12]. The results (Supplementary Figure 2.6) indicate a pK$_a$ range of 6.43 to 6.46 for the bound form, which is not sensed by any other glutamate (Figure 2.3, black) or aspartate (Supplementary Figure 2.5) residue in cNTnC.

Discussion

In the structure of the Ca^{2+} saturated cardiac troponin core complex[29], the switch helix of cTnI that makes contact with cNTnC stretches from residues 144 to 160; residue A162 is in a linker region which connects to a C-terminal α helix that has been shown to be intrinsically disordered in solution[30]. In the NMR structure of cNTnC•Ca^{2+}•cTnI$_{147-163}$[22], residue A162 extends out of the hydrophobic pocket of cNTnC. In the structure of the Ca^{2+} saturated skeletal troponin complex[31], the switch helix of sTnI is bound in a similar fashion except that residue H130 (corresponding to A162 in cTnI) makes contact with E20 in sNTnC•2Ca^{2+}; and flexibility on that region starts at approximately residue 137 as shown by NMR

relaxation studies[32,33]. These structures are shown in Figure 2.5. Our recent study of sTnI$_{115\text{-}131}$ bound to cNTnC•Ca^{2+} showed that an electrostatic interaction was formed between H130 of sTnI and E19 of cNTnC[12]. In this work, we used a mutant of cTnI switch peptide, cTnI$_{144\text{-}170}$ A162H to test if this single mutation is solely responsible for a stronger interaction between cTnI and cTnC, and whether the naturally occurring H171 could play a similar role. The present data indicate an electrostatic interaction between E15 and E19 with H162 in cTnI whereas H171, downstream from A162, makes no observable interaction with cNTnC•Ca^{2+}.
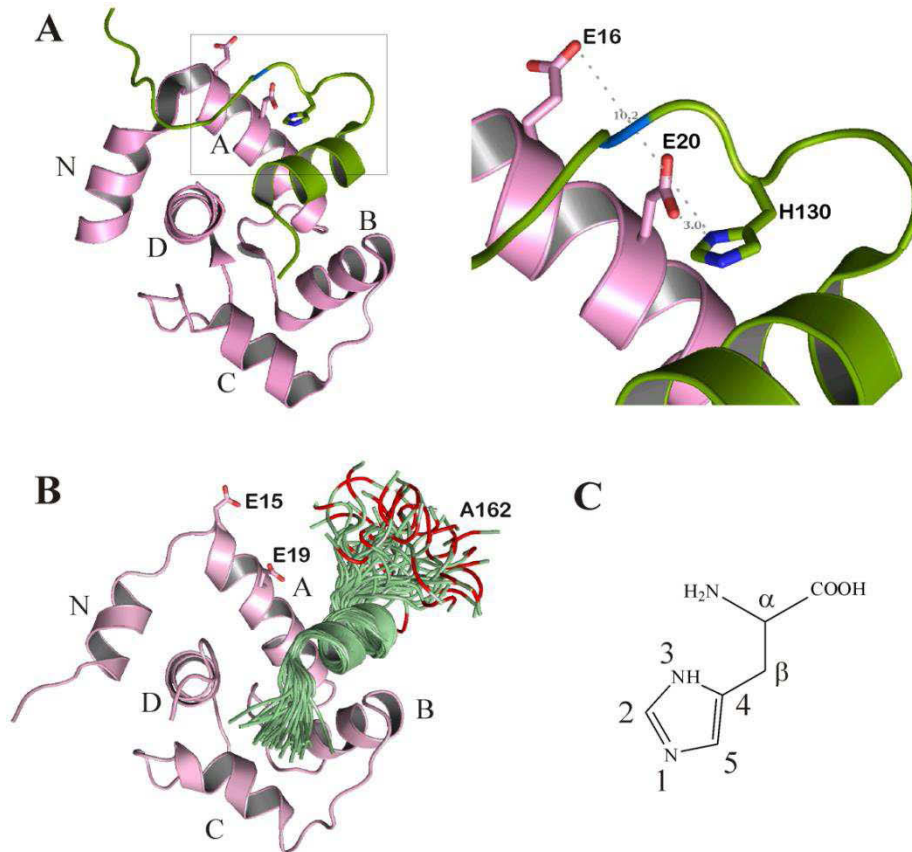
Figure 2.5. Position of A162 (H130) relative to E15 (E16) and E19 (E20) in the structure of cNTnC (sNTnC).
A: Structure of sNTnC•Ca^{2+}•sTnI$_{115\text{-}131}$(PDB ID: 1YTZ) showing the positions of E16, E20 and H130, the expansion depicts the distances from E16 and E20 to H130. V132 is in light blue (see text). **B:** The structure of cNTnC•Ca^{2+}•cTnI$_{147\text{-}163}$ (PDB ID: 1MXL) shows the positions of the homologue residues E15 and E19, the ensemble is shown for the switch peptide and the position of A162 is in red. Helices are named in both structures with letters N and A through D. **C:** Nomenclature of the imidazole ring in the amino acid histidine.

We demonstrated that H162 in the $cTnI_{144-170}$ A162H peptide is in close proximity of the two glutamate residues in cNTnC, E15 and E19, since both are sensitive to the protonation of H162 and exhibit deviations in their pK_a profiles displaying a high pK_a value of ~ 6.8. We observed biphasic pK_a curves for most of E19 resonances; the same profile of biphasic curves was seen for the gamma proton of E19, but not for E15, when $cNTnC \cdot Ca^{2+}$ is bound to $sTnI_{115-131}$[12], in this case the X-ray structure for the skeletal structure[31] (Figure 2.5A) confirms the close proximity (3Å) of nitrogen 3 in H130 with oxygen ε of E20 (analogues of H162 and E19, respectively); in the same structure E16 (analogue of E15 in cTnC) is too far away from H130 (>10Å).

Determination of the pK_a of H162 when $cTnI_{144-170}$ A162H is fully bound to cNTnC (6.5 ± 0.24) provides evidence that the protonation event sensed by E15 and E19 corresponds to H162 in the mutated peptide and confirms the electrostatic interaction between them. This was verified by investigating the pK_a values for the native complex $cNTnC \cdot Ca^{2+} \cdot cTnI_{144-173}$, which show monophasic curves for all the resonances of E15, E19, and E55 with no indication of close proximity to another titratable residue despite the presence of H171 in the native switch peptide. This observation, along with the weak binding observed for the native peptide, also indicates that H171 does not play any role in the isoform-dependent pH sensitivity of the cardiac thin filament. The fact that E19 experiences a drop in pK_a with the presence of H162 further confirmed their electrostatic interaction. Neutralization of the negative charge of E19 by interaction with the positive charge of H162 would cause an increase in its electrostatic potential for which a lower pK_a is expected according to the trend of decreasing pK_a values with increasing electrostatic potential observed for aspartate and glutamate residues in proteins[27]. This shift of a pK_a to a more acidic value was also observed for the $cNTnC \cdot Ca^{2+} \cdot sTnI_{115-131}$ complex and confirms the electrostatic interaction between E19 and H162.

Regarding the possibility of salt bridge formation, we considered protonation of N1 in the skeletal structure (Figure 2.5A and C) which would render a H3-Oε distance of ~2Å since the N-H bond length for N3 in the cationic state of histidine is 1.09 ± 0.01[34]; this is sufficient for N⁺-H⋯O hydrogen bond formation at low pH. To investigate the energy associated to the salt bridge formation in our $cNTnC \cdot Ca^{2+} \cdot cTnI_{147-170}$ A162H complex, we calculated the difference in free energy of binding (ΔΔG) of $cTnI_{144-170}$ A162H and $cTnI_{144-173}$ at different pH values using the equation:

$$\Delta G = RT \ln K_D$$

where R is the gas constant (8.314 $Jmol^{-1}K^{-1}$) and T is the absolute temperature. The results are summarized in Supplementary Table 2.1. ΔΔG between the mutated and native peptides at pH 7 (-0.9 Kcal/mol) corresponds to an estimate of the stabilization energy of the hydrogen-bond component contributed by the proton donor H162 in the neutral state. ΔΔG for binding of the mutated peptide to cNTnC between pH 6 and 7 (-0.9 Kcal/mol) corresponds to additional stabilization energy from the charge-charge interaction between E15/E19 and H162 once the pH drops. This explains the

observations done at the molecular level in the present study, and at cellular and organ levels shown previously, that the A162H mutation shows improvement from basal conditions that is further enhanced under acidosis.

We estimate that the contribution of the salt bridge made by H162 at low pH is ~2.2 Kcal/mol. This value is not identical to the sum of the individual components of the salt bridge (hydrogen bond + charge-charge = -1.8 Kcal/mol) because of the length difference between the mutated and native peptides that may affect the binding affinity.

Our hypothesis is consistent with the reported $\Delta\Delta G$ of -0.9 Kcal/mol[12] for sTnI binding to cNTnC•Ca^{2+} at pH 6.1 and 7.5; and with computational alanine scanning performed for the cTnC•ssTnI complex, where the $\Delta\Delta G$ caused by alanine substitution was calculated for residues at the cTnC•ssTnI interface. The study calculated a $\Delta\Delta G$ of 0.91 Kcal/mol for E19A cTnC when binding to sTnI and 2.46 Kcal/mol for H132A ssTnI when it binds to cTnC[13]. Thus, we speculate that the E19A substitution leads to a smaller destabilizing effect because the presence of E15 that may make weak electrostatic interactions with H162, E19A may introduce new hydrophobic stabilizing contacts with the aromatic ring of H162, and/or the H132A substitution may interrupt interactions with D121 that stabilize the proper conformation of ssTnI.

Regarding the role of other residues in TnI isoform dependence of myofilament function, it has been shown that N141 and V134 in ssTnI (H171 and E164 in human cTnI) partially influence the isoform-specific contractile function in rat cardiac myocytes expressing ssTnI, and are involved in modulating the Ca^{2+} sensitivity at physiological and acidic pH, respectively[35]. When the N141H substitution is introduced to ssTnI, the Ca^{2+} sensitivity of the myofilaments becomes comparable to that of cTnI but the pH sensitivity remains similar to that of ssTnI. Considering that our present results show no role of H171 in regulating pH sensitivity, this implies that N141 is responsible for the Ca^{2+} sensitivity difference between cTnI and ssTnI at physiological pH, and that H132 is solely responsible for the reduced pH sensitivity observed for ssTnI N141H. We predict that the reverse substitution introduced in the cardiac isoform (cTnI H171N) would show increased Ca^{2+} sensitivity at physiological pH but would still be sensitive to acidosis. For V134, if H162 of mutated cTnI in the present study is located close to E15 and E19 in cNTnC, and H130 close to E19/E20[12,31], mutation to the cardiac analogous (V134E) introduces unfavorable interactions with cNTnC since V134E would also be in the vicinity of the same negatively charged glutamate residues (Figure 2.5A). Therefore, V134 may have shown a role in modulating Ca^{2+} sensitivity by reducing unfavorable interactions between ssTnI and cNTnC. In cardiac muscle, the absence of H162 in cTnI and the consequent increased local flexibility prevents close cTnI-cNTnC interactions in that region such that the effect of the reverse mutation (cTnI E164V) in pH sensitivity would either be small or negligible.

The estimated stabilizing effect of A162H on the cTnI-cNTnC interaction (-2.2 Kcal/mol) is close to the destabilizing effect of low pH in Ca^{2+} binding (2.4 Kcal/mol) [36]. This supports our previous theory that Ca^{2+} binding to cNTnC at low pH is partially compensated by stronger binding of the cTnI switch peptide. However the stabilizing effect of H162 is still much larger than the stabilization induced by the calcium sensitizer, dfbp-o (-0.5 Kcal/mol) [15], which highlights the necessity for the development of more potent cardiotonic agents to treat heart failure.

Unlike other fetal contractile proteins, ssTnI with constitutive H130 (corresponding to residue 162 in cTnI) is not re-expressed in the failing heart. Activation of the fetal cardiac gene program is a hallmark of hypertrophy and heart failure; the expression of the fetal isoform of the contractile proteins skeletal α-actin and ß-myosin heavy chain is re-induced[37, 38], but not that of ssTnI as shown for hypertrophic rat hearts and end-stage failing human hearts[39,39]. This study could be useful for the design of novel therapeutic agents for the treatment of myocardial ischemia and heart failure as it reveals the location and nature of the additional cTnI-cNTnC interactions promoted by H162 and an estimation of the energy required to stabilize the cTnI-cNTnC interface during acidosis.

Acknowledgments
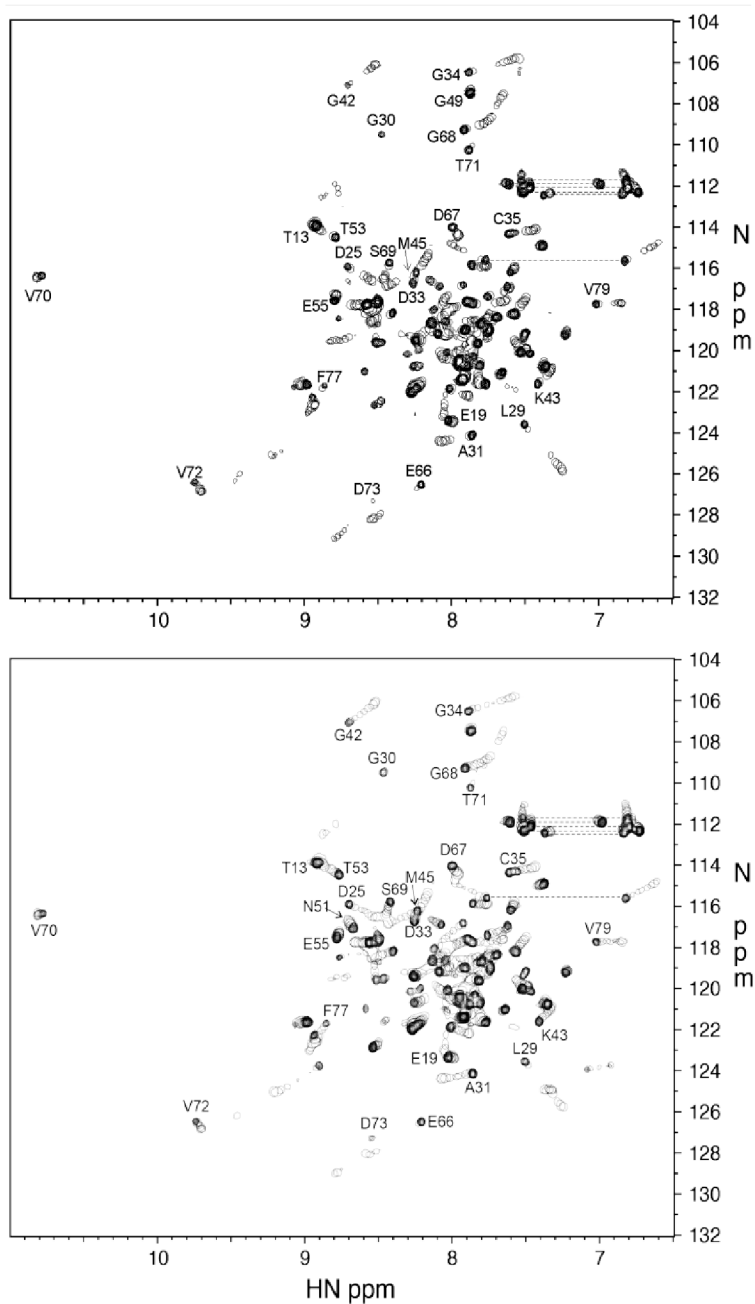
Supplementary Figure 2.1. Titration of cTnI$_{144-170}$ A162H into cNTnC under normal and acidic conditions.

Overlay of 2D ^{1}H, ^{15}N correlation NMR spectra of cNTnC acquired during the titration of the mutated peptide cTnI$_{144-170}$ A162H at pH 7 (top) and 6 (bottom). The first point is represented with multiple contours and consequent additions of peptide are represented by single contours. Residues that experienced large chemical shift changes are labeled.
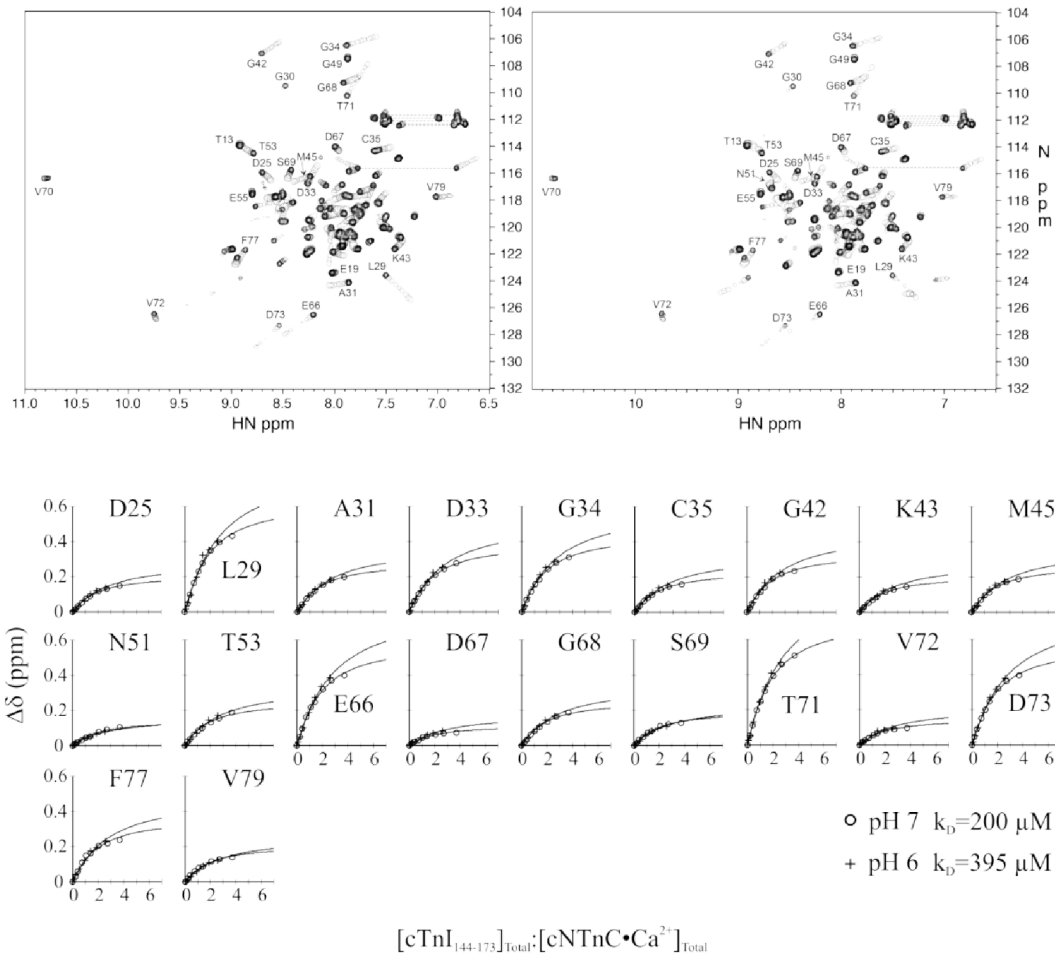
Supplementary Figure 2.2. Titration of cTnI$_{144\text{-}173}$ into cNTnC under normal and acidic conditions. Amide chemical shift perturbations of cNTnC•Ca^{2+} upon binding of wild-type cTnI$_{144\text{-}173}$ peptide and global fitting of perturbed residues at pH 7 (left, circles) and pH 6 (right, crosses).
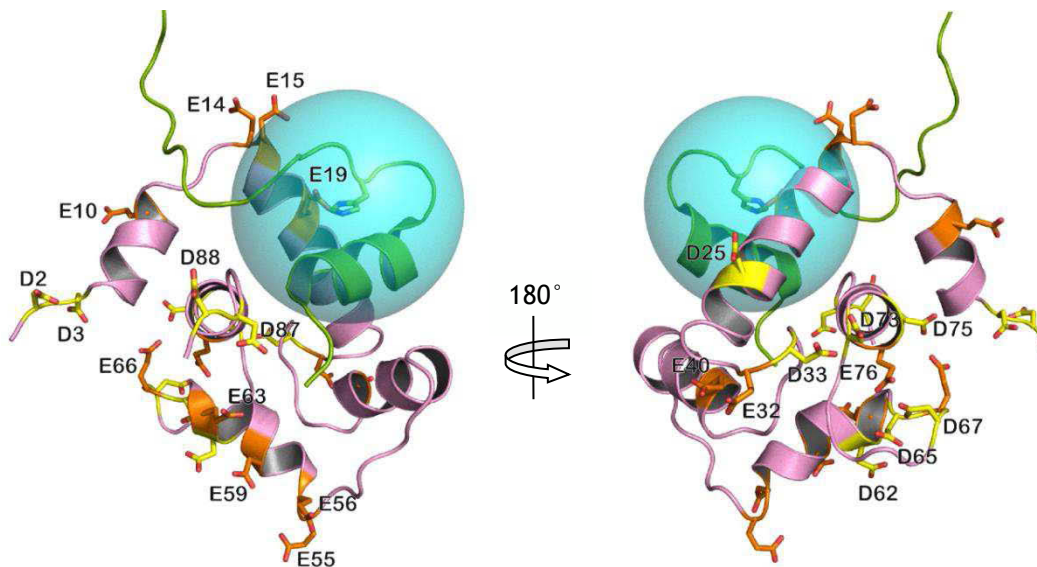
Supplementary Figure 2.3. Location of acidic residues in cNTnC.

Distribution of glutamate (orange) and aspartate (yellow) residues in cNTnC (PDB ID: 1MXL). The switch peptide corresponds to sTnI (PDB ID: 1YTZ). The 10 Å-radius cyan sphere is centered at the imidazole ring of H130 to show the position of glutamates and aspartates relative to the site of study. Residues E15 and E19 are within the sphere radius.
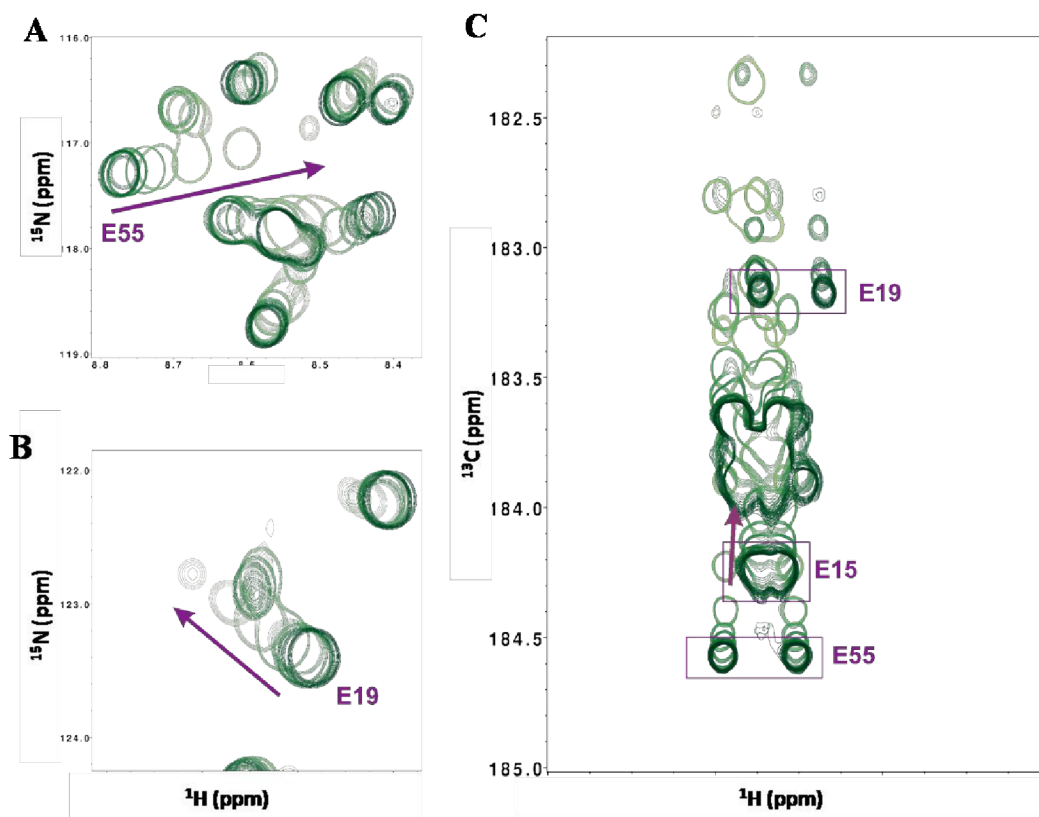
Supplementary Figure 2.4. pH titration of cNTnC•Ca²⁺•cTnI₁₄₄₋₁₇₃.

Overlay of regions from the 2D ¹H,¹⁵N correlation(**A**, **B**) and 2D carboxyl ¹H,¹³C correlation (**C**) NMR spectra acquired during the pH titration of the native cNTnC•Ca²⁺•cTnI₁₄₄₋₁₇₃ complex. The pH decreases from dark to light green and the direction of chemical shift perturbation is indicated by arrows. The same labeling scheme as in Figure 3.2 is used.
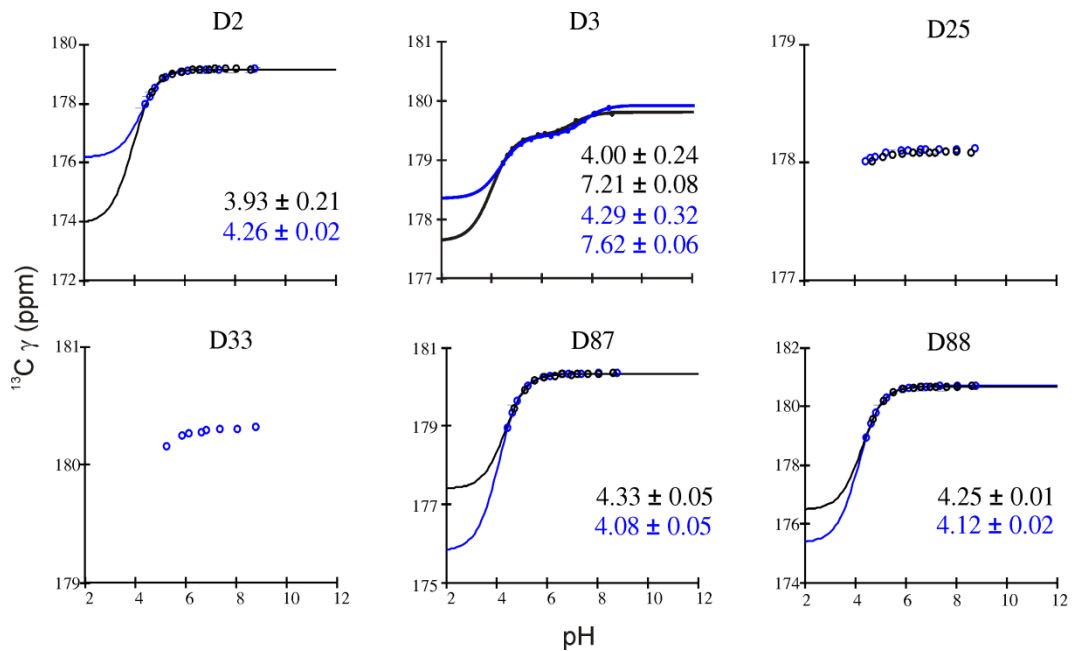
Supplementary Figure 2.5. The effect of A162H in the pK$_a$ of aspartate residues of cNTnC.
Acid dissociation curves for aspartate residues in cNTnC•Ca^{2+} in complex with cTnI$_{144-173}$ (black) and cTnI$_{144-170}$ A162H (blue) according to their ^{13}C chemical shift in the 2D carboxyl ^{1}H, ^{13}C correlation spectra. D3 displays biphasic curves for both complexes; the second pK$_a$ value was attributed to the NH^{3+} group at the N-terminus of cNTnC. D33 was only reliably tracked in the A162H complex.
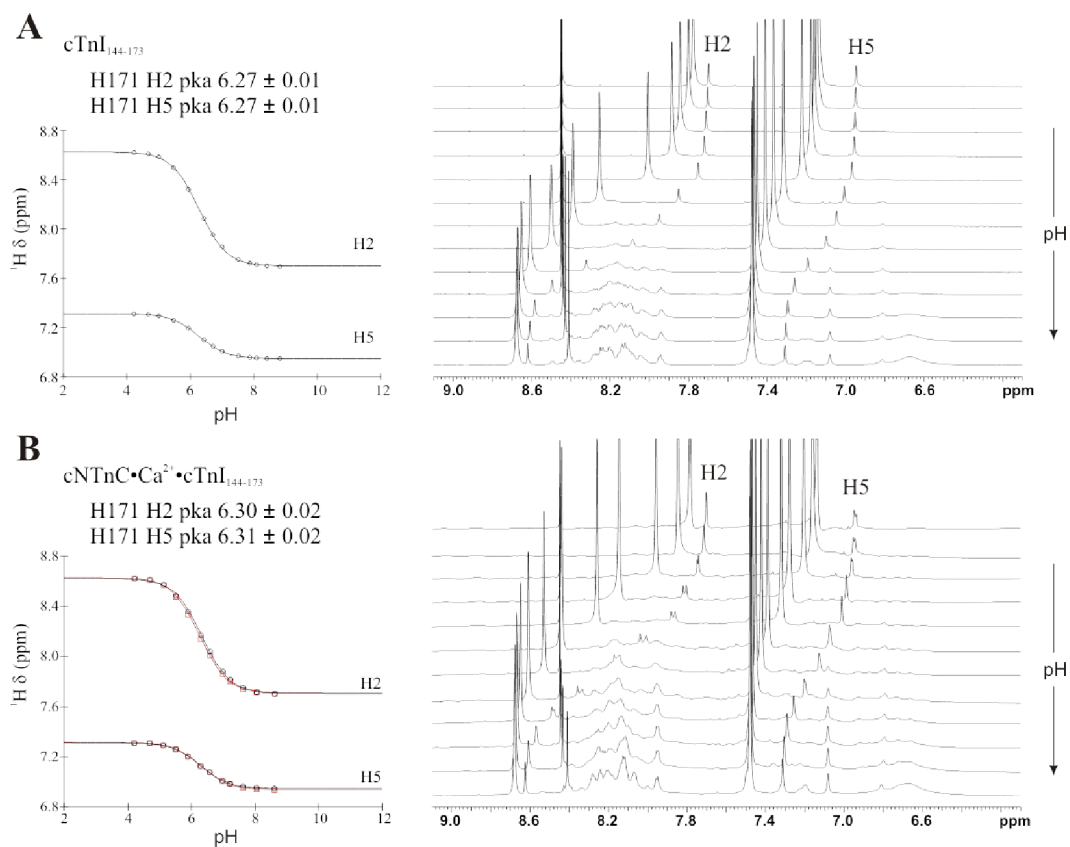
Supplementary Figure 2.6. pK$_a$ values for A162H in the free and cNTnC-bound forms.

pK$_a$ curves for H171 of the native cTnI$_{144-173}$ in the absence (**A**) and presence (**B**) of cNTnC•Ca^{2+} as a function of pH followed by 1D ^{1}H NMR. The Hill coefficient was set to 1 for all curves. The pK$_a$ values presented for the bound form correspond to the average value for the downfield (black) and upfield (red) resonances observed for each proton signal: H2 downfield 6.33 ± 0.02, upfield 6.26 ± 0.01; H5 downfield 6.29 ± 0.01, upfield 6.32 ± 0.02.

Supplementary Table 2.1. ΔG and ΔΔG for cTnI$_{144-173}$ and cTnI$_{144-170}$ A162H binding to cNTnC under normal and acidic conditions.

Free energy (ΔG) for the binding of native and mutated cTnI peptides at normal and acidic pH and their differences (ΔΔG). ΔΔG of each row corresponds to energy changes caused by a decrease in pH (from 7 to 6) for each cTnI peptide. Values of ΔΔG of each column correspond to an estimation of the effect of H162 in cTnI at a specific pH.

Peptide binding to cNTnC•Ca^{2+}	ΔG at pH 7 (Kcal/mol)	ΔG at pH 6 (Kcal/mol)	ΔΔG (Kcal/mol)
cTnI$_{144-173}$	-5.1	-4.7	0.4
cTnI$_{144-170}$ A162H	-6.0	-6.9	-0.9
ΔΔG (Kcal/mol)	-0.9	-2.2	

45

References

1. Causes of death 2008, World Health Organization, Geneva, http://www.who.int/healthinfo/ global_burden_disease/ cod_2008_sources_methods.pdf.

2. Lee, J. A., & Allen, D. G. (1991) Mechanisms of acute ischemic contractile failure of the heart. Role of intracellular calcium. *J Clin Invest*. 88, 361-367.

3. Metzger, J. M., & Westfall, M. V. (2004) Covalent and noncovalent modification of thin filament action. *Cardiovasc Res* 94, 146-158.

4. Li, G., Martin, A. F., & Solaro, J. R. (2001) Localization of regions of troponin I important in deactivation of cardiac myofilaments by acidic pH. *J Mol Cell Cardiol* 33, 1309-1320.

5. Westfall, M. V., & Metzger, J. M. (2001) Troponin I isoforms and chimeras: Tuning the molecular switch of cardiac contraction. *Physiology* 16, 278-281.

6. Wolska, B. M., Vijayan, K., Arteaga, G. M., Konhilas, J. P., Phillips, R. M., Kim, R. *et al*. (2001) Expression of slow skeletal troponin I in adult transgenic mouse heart muscle reduces the force decline observed during acidic conditions. *J Physiol* 536, 863-870.

7. Li, M., Wang, X., & Sykes, B. (2004) Structural based insights into the role of troponin in cardiac muscle pathophysiology. *J Muscle Res Cell Motil* 25, 559-579.

8. Kobayashi, T., Jin, L., & de Tombe, P. Cardiac thin filament regulation. *Eur J Physiol* 2008457, 37-46.

9. Dargis, R., Pearlstone, J. R., Barrette-Ng, I., Edwards, H., & Smillie, L. B. (2002) Single mutation (A162H) in human cardiac troponin I corrects acid pH sensitivity of Ca^{2+}-regulated actomyosin S1 ATPase. *J Biol Chem* 277, 34662-34665.

10. Day, S. M., Westfall, M. V., Fomicheva, E. V., Hoyer, K., Yasuda, S., Cross, N. C. L. *et al*. (2006) Histidine button engineered into cardiac troponin I protects the ischemic and failing heart. *Nature Med* 12, 181-189.

11. Day, S., Westfall, M., & Metzger, J. (2007) Tuning cardiac performance in ischemic heart disease and failure by modulating myofilament function. *J Mol Med* 85, 911-921.

12. Robertson, I. M., Holmes, P. C., Li, M. X., Pineda-Sanabria, S. E., Baryshnikova, O. K., & Sykes, B. D. (2012) Elucidation of isoform-dependent pH sensitivity of troponin I by NMR spectroscopy. *J Biol Chem* 287, 4996-5007.

13. Palpant, N. J., Houang, E. M., Delport, W., Hastings, K. E. M., Onufriev, A. V., Sham, Y. Y. *et al*. (2010) Pathogenic peptide deviations support a model of adaptive evolution of chordate cardiac performance by troponin mutations. *Physiol Genomics* 42, 287-299.

14. Li, M., Saude, E., Wang, X., Pearlstone, J., Smillie, L., & Sykes, B. (2002) Kinetic studies of calcium and cardiac troponin I peptide binding to human cardiac troponin C using NMR spectroscopy. *Eur Biophys J* 31, 245-256.

15. Robertson, I. M., Sun, Y., Li, M. X., & Sykes, B. D. (2010) A structural and functional perspective into the mechanism of Ca^{2+}-sensitizers that target the cardiac troponin complex. *J Mol Cell Cardiol* 49, 1031-1041

16. Delaglio, F., Grzesiek, S., Vuister, G. W., Zhu, G., Pfeifer, J., & Bax, A. (1995) NMRPipe, A multidimensional spectral processing system based on UNIX pipes. *J Biomol NMR* 6, 277-293.

17. Johnson, B. A., & Blevins, R. A. (1994) NMR view, A computer program for the visualization and analysis of NMR data. *J Biomol NMR* 4, 603-614.

18. Hoffman, R. M. B., Li, M. X., & Sykes, B. D. (2005) The binding of W7, an inhibitor of striated muscle contraction, to cardiac troponin C. *Biochemistry* 44, 15750-15759.

19. Baryshnikova, O., Williams, T., & Sykes, B. (2008) Internal pH indicators for biomolecular NMR. *J Biomol NMR* 41, 5-7.

20. Baryshnikova, O. K. Cardiomyopathy mutations in cardiac troponin C, Functional and structural consequences. Edmonton, Alberta, University of Alberta. 2008 (Thesis).

21. Yamazaki, T., Yoshida, M., & Nagayama, K. (1993) Complete assignments of magnetic resonances of ribonuclease H from *Escherichia* coli by double- and triple-resonance 2D and 3D NMR spectroscopies. *Biochemistry* 32, 5656-5669.

22. Li, M. X., Spyracopoulos, L., & Sykes, B. D. (1999) Binding of cardiac troponin-$I_{147-163}$ induces a structural opening in human cardiac troponin-C. *Biochemistry* 38, 8289-8298.

23. Robertson, I. M., Baryshnikova, O. K., Li, M. X., & Sykes, B. D. (2008) Defining the binding site of levosimendan and its analogues in a regulatory cardiac troponin C-troponin I complex. *Biochemistry* 47, 7485-7495.

24. Robertson, I. M., Boyko, R., & Sykes, B. D. (2011) Visualizing the principal component of ^{1}H, ^{15}N-HSQC NMR spectral changes that reflect protein structural or functional properties, application to troponin C. *J Biomol NMR* 51, 115-122

25. Bundi, A., & Wüthrich, K. (1979) Use of amide ^{1}H-NMR titration shifts for studies of polypeptide conformation. *Biopolymers* 18, 299-311.

26. Mayer, R., Lancelot, G., & Spach, G. (1979) Side chain-backbone hydrogen bonds in peptides containing glutamic acid residues. *Biopolymers* 18, 1293-1296.

27. Forsyth, W. R., Antosiewicz, J. M., & Robertson, A. D. (2002) Empirical relationships between protein structure and carboxyl pK_a values in proteins. *PROTEINS* 48, 388-403.

28. Wüthrich, K. NMR of Proteins and Nucleic Acids. USA, Wiley Interscience, 1986.

29. Takeda, S., Yamashita, A., Maeda, K., & Maeda, Y. (2003) Structure of the core domain of human cardiac troponin in the Ca^{2+}-saturated form. *Nature* 424, 35-41.

30. Lassalle, M. W. (2010) Defective dynamic properties of human cardiac troponin mutations. *Biosci Biotechnol Biochem* 74, 82-91.

31. Vinogradova, M. V., Stone, D. B., Malanina, G. G., Karatzaferi, C., Cooke, R., Mendelson, R. A., & Fletterick, R. J. (2005) Ca^{2+}-regulated structural changes in troponin. *PNAS* 102, 5038-5043.

32. Blumenschein, T. M. A., Stone, D. B., Fletterick, R. J., Mendelson, R. A., & Sykes, B. D. (2006) Dynamics of the C-terminal region of TnI in the troponin complex in solution. *Biophys J* 90, 2436-2444.

33. McKay, R. T., Tripet, B. P., Pearlstone, J. R., Smillie, L. B., & Sykes, B. D. (1999) Defining the region of troponin-I that binds to troponin-C. *Biochemistry* 38, 5478-5489.

34. Li, S., & Hong, M. (2011) Protonation, tautomerization, and rotameric structure of histidine, A comprehensive study by magic-angle-spinning solid-state NMR. *JACS* 133, 1534-1544.

35. Westfall, M. V., & Metzger, J. M. (2007) Single amino acid substitutions define isoform-specific effects of troponin I on myofilament Ca^{2+} and pH sensitivity. *J Mol Cell Cardiol* 43, 107-118.

36. Liou, Y. M., & Chang, J. C. H. (2004) Differential pH effect on calcium-induced conformational changes of cardiac troponin C complexed with cardiac and fast skeletal isoforms of troponin I and troponin T. *J Biochem* 136, 683-692.

37. Kuwahara, K., Nishikimi, T., & Nakao, K. (2012) Transcriptional regulation of the fetal cardiac gene program. *J Pharmacol Sci* 119, 198-203.

38. Huang, X., Lee, K. J., Beth, R., Zhang, C., Lemanski, L. F., & Walker, J. W. (2000) Thyroid hormone regulates slow skeletal troponin I gene inactivation in cardiac troponin I null mouse hearts. *J Mol Cell Cardiol* 32,2221-2228.

39. Cumming, D. V. E., Seymour, A. M. L., Rix, L. K., Kellett, R., Dhoo, G. K., Yacoub, M. H. *et al*. (1995) Troponin I and T protein expression in experimental cardiac hyperthophy. *Cardioscience* 6, 65-70.

40. Sasse, S., Brand, N. J., Kyprianou, P., Dhoot, G. K., Wade, R. Arai, M. *et al*. (1993) Troponin I gene expression during human cardiac development and in end-stage heart failure. *Circ Res* 72, 932-938.

CHAPTER 3

Elucidation of isoform-dependent pH sensitivity
of troponin I by NMR spectroscopy

Ian M. Robertson, Peter C. Holmes, Monica X. Li, Sandra E. Pineda-Sanabria,
Olga K. Baryshnikova, and Brian D. Sykes

Department of Biochemistry, Faculty of Medicine and Dentistry,
University of Alberta, Edmonton, Alberta, Canada T6G 2H7.

This chapter focuses on the interaction of cardiac troponin C and skeletal troponin I which contains the key histidine residue we are interested in. As a means of comparing the interaction of cardiac troponin C with cardiac troponin I containing the A162H substitution, this work reports the pK_a of H130 of skeletal troponin I, as well as the strength and nature of binding of skeletal troponin I to cardiac troponin C. The correlation demonstrates the role of electrostatics in the troponin C-I interaction promoted by H130. A version of this chapter has been previously published: Robertson *et al.* (2012) *JBC* 287:4996-5007.

Introduction

In myocardial ischemia, cardiomyocytes do not receive adequate oxygen supply, which culminates in a significant drop in intracellular pH (≤6.5). This acidosis is coupled with a dramatic reduction in the Ca^{2+} sensitivity and force of muscle contraction[1, 2]. Ca^{2+} entering the cytosol following muscle cell excitation triggers a series of thin and thick filament protein-protein interactions that lead to the force-generating actomyosin ATPase activity. The thin filament is composed of three proteins, actin, tropomyosin, and the Ca^{2+}-binding molecule troponin. Troponin is a heterotrimeric protein complex with three subunits as follows: cardiac troponin C (cTnC), responsible for binding Ca^{2+}; cardiac troponin I (cTnI), the inhibitory subunit; and cardiac troponin T, the subunit that attaches troponin to the thin filament via interactions with troponin I and tropomyosin. During muscle relaxation (diastole), the "inhibitory" and C-terminal regions of cTnI interact with actin preventing contraction. The association of Ca^{2+} with the N-terminal domain of cTnC (cNTnC) leads to the binding of the "switch" region of cTnI (cTnI(147–163)) to cNTnC. This interaction prompts the dissociation of the inhibitory and C-terminal regions of cTnI from actin, resulting in contraction (for reviews see Refs. 3–5).

The negative inotropic effect (decrease in contractility) of acidosis is due, in part, to a decrease in the Ca^{2+} [6-8] and cTnI[9] affinity for cTnC. Cardiomyocytes of neonatal rats are less sensitive to

low pH than adult heart cells[10], and Westfall *et al.*[11] noticed that the pH sensitivity of cardiac muscle cells is dramatically reduced by the substitution of cTnI with the neonatal troponin I (also termed slow skeletal TnI (ssTnI)). Likewise, the fast skeletal isoform of TnI (sTnI) has been shown to make the myofilament less sensitive to acidic conditions[8, 12, 13]. The regions of ssTnI and sTnI that are responsible for the isoform-specific response to pH were initially localized to the C-terminal region[12, 14]. It was later determined that the difference in pH sensitivity between TnI isoforms largely arises from a single histidine in the switch region of sTnI and ssTnI, which is replaced by an alanine in cTnI[13, 15]. For a comparison of the sequences of the switch regions of cTnI, sTnI, and ssTnI, see Figure 3.1. Smillie and co-workers[13] found that when this alanine of cTnI (Ala-162) was replaced by a histidine, a dramatic reduction in pH sensitivity was observed. Furthermore, when His-130 of sTnI was replaced by an alanine (the numbering is different between the isoforms, because cTnI has an extra 32 residues at its N terminus not present in sTnI and ssTnI), the pH sensitivity of muscle containing sTnI was similar to cTnI. Recently, this alanine to histidine substitution (dubbed the "histidine button") has been shown to partially blunt the adverse effects of acidosis in intact myocytes, isolated hearts, and whole mice[15].

$cTnI_{147-163}$ 147- R I S A D A M M Q A L L G A R A K -163
            | * | | | | | * * | | | | * |
$sTnI_{115-131}$ 115- R M S A D A M L K A L L G S K H K -131
            | * | | | | | * * | | | | * |
$ssTnI_{116-132}$ 116- R V S A D A M L R A L L G S K H K -132
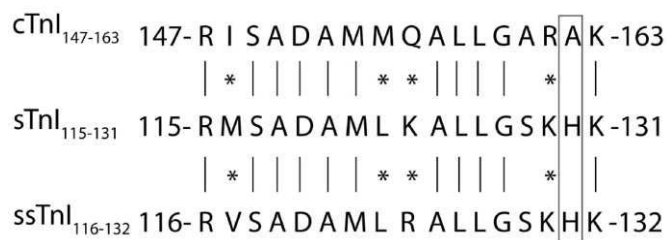
Figure 3.1. Peptide sequences of sTnI(115-131) and cTnI(147-163).
The alanine and histidine are indicated by the box.

The enhanced pH resistance of sTnI has been suggested to stem from interactions with the side chain of histidine; it is the only amino acid that can be either neutral or positively charged in the physiological pH range. Thus, if the imidazole group of histidine is protonated during acidosis, its positive charge may interact with the abundant negatively charged side chains of cNTnC. This may increase the affinity of sTnI for cNTnC and could explain how replacing cTnI with sTnI partially restores myocardial sensitivity at low pH[13]. In the skeletal x-ray crystal structure, His-130 of sTnI forms a salt bridge with Glu-20 of sNTnC (4.1 Å between Nδ1 of His-130 and Cδ of Glu-20), amino acid numbering is taken from the deposited x-ray crystal structure[16]. Solution NMR relaxation[17] and chemical shift[18] data of sTnI in complex with sTnC confirm that this region of sTnI is rigid, consistent with the formation of this salt bridge in solution. The x-ray and NMR structures of cardiac troponin indicate that the corresponding glutamate in cTnC, Glu-19, does not make a homologous interaction with cTnI[19, 20].

The focus of this study was to use NMR spectroscopy to define the molecular basis for the reduced depression of myofilament Ca^{2+} sensitivity at low pH caused by this single histidine residue of

sTnI. The nuclear Overhauser enhancement (NOE) is a fundamental measurement utilized by NMR spectroscopists to determine the atomic resolution structure of proteins. NOE spectroscopy (NOESY) provides structural information of a molecule by relying on short proton-proton distances (≤5 Å) [21]. Because the closest distances between the imidazole protons of His-130 and the side chain protons of Glu-20 are 5.4 and 5.6 Å (Hβ1 and Hβ2) in the skeletal x-ray structure[16], NOEs between these residues would be too weak to observe. However, if these groups make an electrostatic interaction, knowledge of their acid dissociation constants could provide clues as to whether the same interaction occurs when sTnI is bound to cNTnC. Palpant et $al.$[22] used computational methods to predict that the pK_a of His-130 in sTnI would be shifted upward when in complex with cTnC, an indication of the formation of a salt bridge with a negatively charged moiety[23]. We used NMR spectroscopy to investigate the role of electrostatic interactions between sTnI and cNTnC because it is a particularly well suited technique to monitor amino acid pK_a values of individual residues in a protein[24 -26].

The pK_a values of glutamate residues on cNTnC were determined for four different states of cNTnC as follows: Ca^{2+}-free (apo), Ca^{2+}-bound, Ca^{2+}- and cTnI(147–163)-bound, and the complex of cNTnC bound to Ca^{2+} and the switch region of sTnI (sTnI(115-131)). The pK_a of His-130 of sTnI(115–131) was also monitored in both free and bound states. The pK_a of Glu-19 was depressed when in complex with sTnI(115–131), and a second ionization event was observed (from the protonation of the imidazole of His-130). The pK_a of His-130 increased when sTnI(115–131) was bound to cNTnC. Both the increase in His-130 pK_a and the decrease in the pK_a of Glu-19 are consistent with the formation of an electrostatic interaction between these two residues. The affinity of cNTnC for sTnI(115–131) was also measured at two pH values (6.1 and 7.5), and it was found that sTnI(115–131) bound with a tighter affinity at pH 6.1. The pH-dependent differences in the affinity of sTnI(115–131) for cNTnC revealed that the ionization state of His-130 fine-tunes the affinity of sTnI(115–131) for cNTnC. These results provide structural insights into the mechanism by which a single histidine on troponin I can reverse the decrease in myofilament Ca^{2+} sensitivity during acidosis.

Experimental procedures

Sample preparation

For the recombinant human cNTnC (residues 1–89, C84S/C35S, a-Cys form) the engineering of the vector and the expression of ^{15}N- and ^{13}C, ^{15}N-labeled proteins in *Escherichia coli* were as described previously[27]. GL Biochem Ltd. (Shanghai, China) synthesized cTnI(147–163) (acetyl-RISADAMMQALLGARAK-amide) and Alberta Peptide Institute (API) synthesized sTnI(115-131) (acetyl-RMSADAMLKALLGSKHK-amide). HPLC and mass spectrometry (ESI and MALDI) were employed to verify peptide quality and purity. All NMR samples were prepared in 5-mm NMR tubes and had a volume of

500 μL. Protein samples were prepared in an NMR buffer composed of 90% H_2O, 10% D_2O, 100 mM KCl, 10 mM imidazole, 5–10 mM $CaCl_2$ (Fluka), and 0.5 mM 2,2-dimethyl-2-silapentane-5-sulfonate-d_6 sodium salt (DSS) (Chenomx Inc.). The NMR sample prepared for measuring the pK_a value of residues on cNTnC contained excess sTnI ([cNTnC] = 0.25 mM and [sTnI(115–131)] = 0.83 mM). The sample prepared for measuring the pK_a of His-130 on sTnI(115–131) contained excess cNTnC ([cNTnC] = 0.41 mM and [sTnI(115–131)] = 0.07 mM).

NMR spectroscopy

All NMR experiments were run on either a Varian Inova 500 MHz or Unity 600 MHz NMR spectrometers at 30°C. Prior to each multidimensional experiment, one-dimensional ^1H and two-dimensional ^1H,^{15}N HSQC NMR spectra were acquired. The three-dimensional CBCA(CO)NNH, three-dimensional HNCACB, and three-dimensional HCCONH NMR experiments were acquired for backbone and side chain assignments (Figure 3.2) of ^{13}C,^{15}N-cNTnC (apo) and ^{13}C,^{15}N-cNTnC-sTnI(115–131). The two-dimensional ^1H,^{13}C HCBCGCO NMR experiment[28] was acquired to follow glutamate carboxylate $^{13}C\delta$ and $^1H\gamma$ signals of ^{13}C,^{15}N-cNTnC(apo), ^{13}C,^{15}N-cNTnC-Ca^{2+}, ^{13}C,^{15}N-cNTnC-Ca^{2+}-cTnI(147–163), and ^{13}C,^{15}N-cNTnC-Ca^{2+}-sTnI(115–131) during the pH titrations. The chemical shifts of ^1H signals from sTnI(115–131) were monitored at different pH values by the one-dimensional ^1H and the one-dimensional ^{13}C,^{15}N-filtered ^1H,^1H-NOESY (mixing time = 100 ms) [29-31] NMR experiments. The assignment of signals from sTnI(115–131) in complex with ^{13}C,^{15}N-cNTnC-Ca^{2+} was done with the two-dimensional ^{13}C,^{15}N-filtered ^1H,^1HNOESY (mixing time = 200 ms) and two-dimensional ^{13}C,^{15}N filtered ^1H,^1H-TOCSY (mixing time = 60 ms) NMR experiments[29-32]. Spectral processing was accomplished with the programs VNMRJ (Version 2.21B, Varian Inc.) and NMRPipe[33] and referenced to DSS according to the IUPAC conventions. Processed NMR spectra were analyzed using NMRViewJ[34]. The backbone resonances of ^{13}C,^{15}N-cNTnC(apo) and ^{13}C,^{15}N-cNTnC-sTnI(115–131) were assigned with the program SmartNotebook[35].

pH titrations

The pH was gradually adjusted by adding aliquots of 1 M NaOH or 1 M HCl covering a range from ~3.5 to 8.5. The pH at each titration point was verified by the chemical shift of Tris, imidazole, piperazine, or formate in the NMR buffer (36). At each titration point, one-dimensional ^1H, two dimensional ^1H, ^{15}N HSQC and two-dimensional ^1H,^{13}C HCBCGCO NMR spectra were recorded.
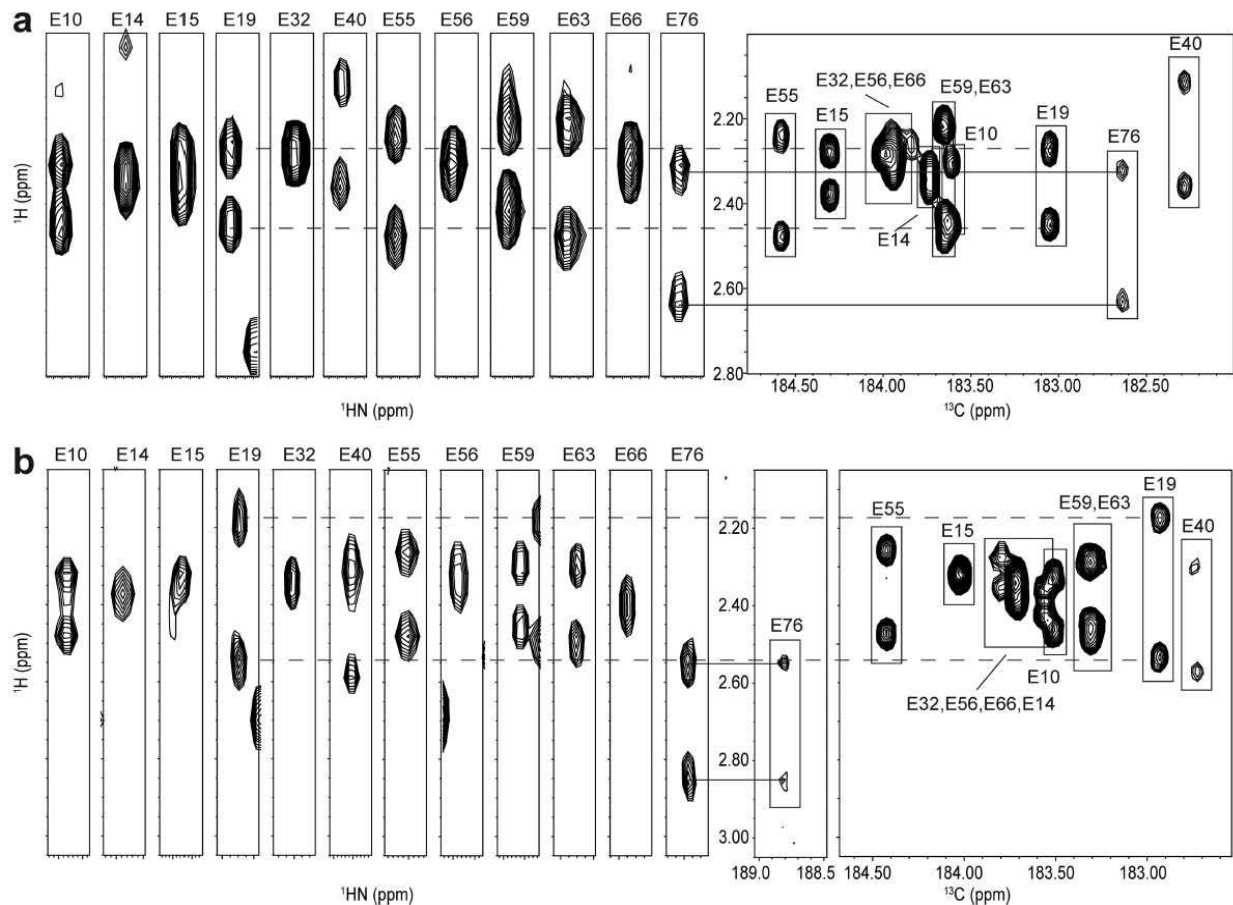
Figure 3.2. Assignment of glutamate carboxyl carbons of cNTnC(apo) and cNTnC-sTnI(115–131).
The glutamate region of the two-dimensional ^{1}H,^{13}C HCBCGCO spectrum of cNTnC is shown on the right. Slices from the three-dimensional HCCONH NMR experiment are shown on the left. The carboxyl carbon chemical shifts were assigned by matching the γ proton chemical shifts.

The monophasic pH titration data were analyzed using the programs xcrvfit and Wolfram Mathematica. Datasets showing a pK_a were fit to Equation 1,

$$\delta_{obs} = \delta_{HA} + \frac{\Delta\delta}{1 + 10^{n(pK_a - pH)}}$$

(Eq. 1)

where δ_{obs} is the observed chemical shift at a given pH; δ_{HA} is the chemical shift for the protonated form; $\Delta\delta$ is the total shift from deprotonated to protonated forms, and n is the Hill parameter (held constant at 1 unless otherwise indicated). The biphasic pK_a datasets were fitted in xcrvfit and Wolfram Mathematica to Equation 2 [24],

$$\delta_{obs} = \delta_{HA} + \frac{\Delta\delta1}{1 + 10^{n(pK_{a}1 - pH)}} + \frac{\Delta\delta2}{1 + 10^{n(pK_{a}2 - pH)}}$$

(Eq. 2)

Where δ_{obs} is the observed chemical shift at a given pH; δ_{HA} is the chemical shift for the protonated form, $\Delta\delta1$ and $\Delta\delta2$ are the total shifts from deprotonated to protonated forms, and n is the Hill parameter (held constant at 1 unless otherwise indicated).

The fraction sTnI(115-131) bound (f_{bs}) to cNTnC and fraction cNTnC bound (f_{bc}) with sTnI(115-131) were determined using Equations 3 and 4,

$$f_{b}^{s} = \frac{K_{D} + [\text{sTnI}] + [\text{cNTnC}] - \sqrt{(K_{D} + [\text{sTnI}] + [\text{cNTnC}])^{2} - 4[\text{sTnI}][\text{cNTnC}]}}{2[\text{sTnI}]}$$

(Eq. 3)

$$f_{b}^{c} = \frac{K_{D} + [\text{sTnI}] + [\text{cNTnC}] - \sqrt{(K_{D} + [\text{sTnI}] + [\text{cNTnC}])^{2} - 4[\text{sTnI}][\text{cNTnC}]}}{2[\text{cNTnC}]}$$

(Eq. 4)

[sTnI] and [cNTnC] are the concentrations of sTnI(115-131) and cNTnC, respectively. K_{D} is the dissociation constant of sTnI(115-131) (see below). The pK_{a} of His-130 for bound sTnI(115-131) was calculated by extrapolating the pK_{a} values versus fraction bound to the 1:1 complex ratio using SigmaPlot.

sTnI(115-131) titrations at pH 6.1 and pH 7.5

The titrations with sTnI(115-131) were performed at two different pH values (6.1 and 7.5). For both titrations, fresh stocks of sTnI(115-131) were prepared in NMR buffer. The sTnI(115–131) stock solution concentrations were determined by preparing an NMR sample containing 5 μL of sTnI(115-131) stock in 500 μL of NMR buffer in 99.9% D_2O and 25 μL of 4.963 mM DSS in 98% D_2O. One-dimensional ^{1}H NMR spectra were acquired with an acquisition time of 8 s, and a relaxation delay of 4 s, thus providing time for DSS and sTnI(115-131) to return to equilibrium in between transients. The concentration of sTnI(115-131) was then calculated by comparing the signal integral from the methyl protons of sTnI(115-131) to the integral of DSS protons. To determine the concentration of cNTnC, the intensity of the ^{1}H,^{15}N HSQC spectrum was compared with that of another sample of cNTnC for which amino acid analysis was used to determine concentration[37]. Any subtle variations in pH during the titrations were corrected for by adding aliquots of 1 M HCl or 1 M NaOH. At each aliquot, two-dimensional ^{1}H,^{15}N HSQC spectra were acquired, and the amide chemical shift changes (Δδ) were calculated by Equation 5,

$$\Delta\delta = \sqrt{(\Delta\delta_H)^2 + \frac{1}{25}(\Delta\delta_N)^2}$$

<div align="right">(Eq. 5)</div>

$\Delta\delta_H$ and $\Delta\delta_N$ are the change in proton and nitrogen chemical shifts, respectively, for each titration point. The dissociation constants of sTnI(115-131) binding to cNTnC were fit to a 1:1 stoichiometry to Reaction 1, where P is free protein and L is free ligand, and PL is the protein-ligand complex. Concentrations of sTnI(115-131) and cNTnC were corrected for dilution during the titration. The dissociation constants were determined by using the global fitting protocol in xcrvfit[37]. Rather than fitting NMR chemical shift data to each individual residue and then averaging the individual dissociation constants, the global fitting method works by fitting all chemical shift data to one dissociation constant that best represents the ensemble of titration curves (i.e. had the lowest sum of squared error). Residues used in the global fit were those that underwent large chemical shift perturbations and did not significantly overlap with other signals.

$$P + L \leftrightarrow PL$$

<div align="right">(Reaction 1)</div>

Results

cNTnC glutamate pK$_a$ values as a function of structure

The acid dissociation constants for ionizable residues can provide insight into the molecular interactions within a protein complex. The shift in pK$_a$ of an ionizable residue can signify the formation of an electrostatic interaction or hydrogen bond[23]. To investigate the electrostatic forces between cNTnC and cTnI or sTnI, we measured the pK$_a$ values of the glutamates of cNTnC for a variety of troponin complexes. Two-dimensional ^{1}H,^{15}N HSQC and two-dimensional ^{1}H,^{13}C HCBCGCO NMR spectra were acquired over a range of pH values for four different complexes of cNTnC as follows: cNTnC(apo), cNTnC-Ca^{2+} [1], cNTnC-cTnI(147-163), and cNTnC-sTnI(115-131). To ensure that cNTnC was mostly in their complexed states, excess Ca^{2+}, cTnI(147-163), and sTnI(115-131) were used. The ^{1}H,^{15}N HSQC NMR experiment correlates backbone amide protons with ^{15}N nuclei so that each signal in the ^{1}H,^{15}N HSQC spectrum belongs to a single residue in the ^{15}N-labeled protein. The two-dimensional ^{1}H,^{13}C HCBCGCO NMR experiment[28] correlates the aliphatic protons of a residue with its side chain ^{13}C carboxyl (or ^{13}C-carbonyl) nucleus. The glutamates of cNTnC(apo) and cNTnC-sTnI(115-131) were assigned in this work (the assignments of cNTnC and cNTnC-cTnI(147-163) have been previously published [20, 38, 39]). The

---

[1] Unless otherwise stated, cNTnC will be assumed to be Ca$_2$-saturated, and therefore the Ca$_2$ will be omitted when discussing the different states of cNTnC.

assignments of the two-dimensional ^{1}H,^{13}C HCBCGCO NMR spectra of cNTnC(apo) and cNTnC-sTnI(115–131) are shown in Figure 3.2; some glutamates could not be resolved in the two-dimensional ^{1}H, ^{13}C HCBCGCO spectrum due to signal overlap. Surprisingly, the pattern of chemical shifts in the two-dimensional ^{1}H,^{13}C HCBCGCO spectrum were consistent in the four states of cNTnC (Figure 3.2 and Figure 3.3). The only exception was Glu-76, which had its carboxyl ^{13}C shifted from 182.7 ppm in cNTnC(apo) to 188.8 ppm in the other states of cNTnC (Figure 3.2). This large downfield shift is expected for a bidentate ligand of Ca^{2+} [40, 41], such as Glu-76.

At low pH, the cNTnC solutions were not stable. In the case of the Ca^{2+}-bound complexes, precipitation was observed below pH 4.25, and the NMR spectra resembled the apo-form, suggesting Ca^{2+} had dissociated. Because it was not possible to measure the glutamate chemical shifts at pH values below 4.25, in most instances the pK_a values reported are approximate. Furthermore, given that the pK_a of aspartates are typically even lower than that of glutamates[42], it was not possible to determine their acid dissociation constants with confidence.

Many of the pK_a values obtained from the ^{1}H,^{15}N HSQC spectra were difficult to interpret because the change in amide chemical shifts can stem from several phenomena, such as intraresidue ionization, pH-dependent conformational changes, or the ionization of nearby residues[24]. An expanded region of the ^{1}H,^{15}N HSQC NMR spectrum acquired during each pH titration is shown for all four states of cNTnC in Supplementary Figure 3.1.

Given the difficulty associated with interpreting ^{1}H,^{15}N HSQC NMR chemical shifts, we turned to the two-dimensional ^{1}H,^{13}C HCBCGCO NMR experiment to track the pH-dependent chemical shift perturbations of the carboxyl carbons and the aliphatic γ protons of the glutamate residues (Figure 3.3). Because the two-dimensional ^{1}H,^{13}C HCBCGCO NMR experiment directly monitors the chemical shift of each carboxyl group, the pK_a values obtained from this experiment will likely arise primarily from intraresidue ionization. As the pH was reduced, the carboxylate ^{13}C nuclei shifted to a lower value, and the methylene γ protons shifted toward higher chemical shifts. These chemical shift trends are consistent with the protonation of a carboxylate moiety[43, 44]. Titration data for three residues, Glu-55 (a residue removed from the binding site of TnI), Glu-19 (a residue possibly interacting with His-130, based on the crystal structure of the skeletal complex), and Glu-15 (a residue in close proximity to His-130 in the skeletal crystal structure, and may interact with His-130), are highlighted in Figure 3.3.
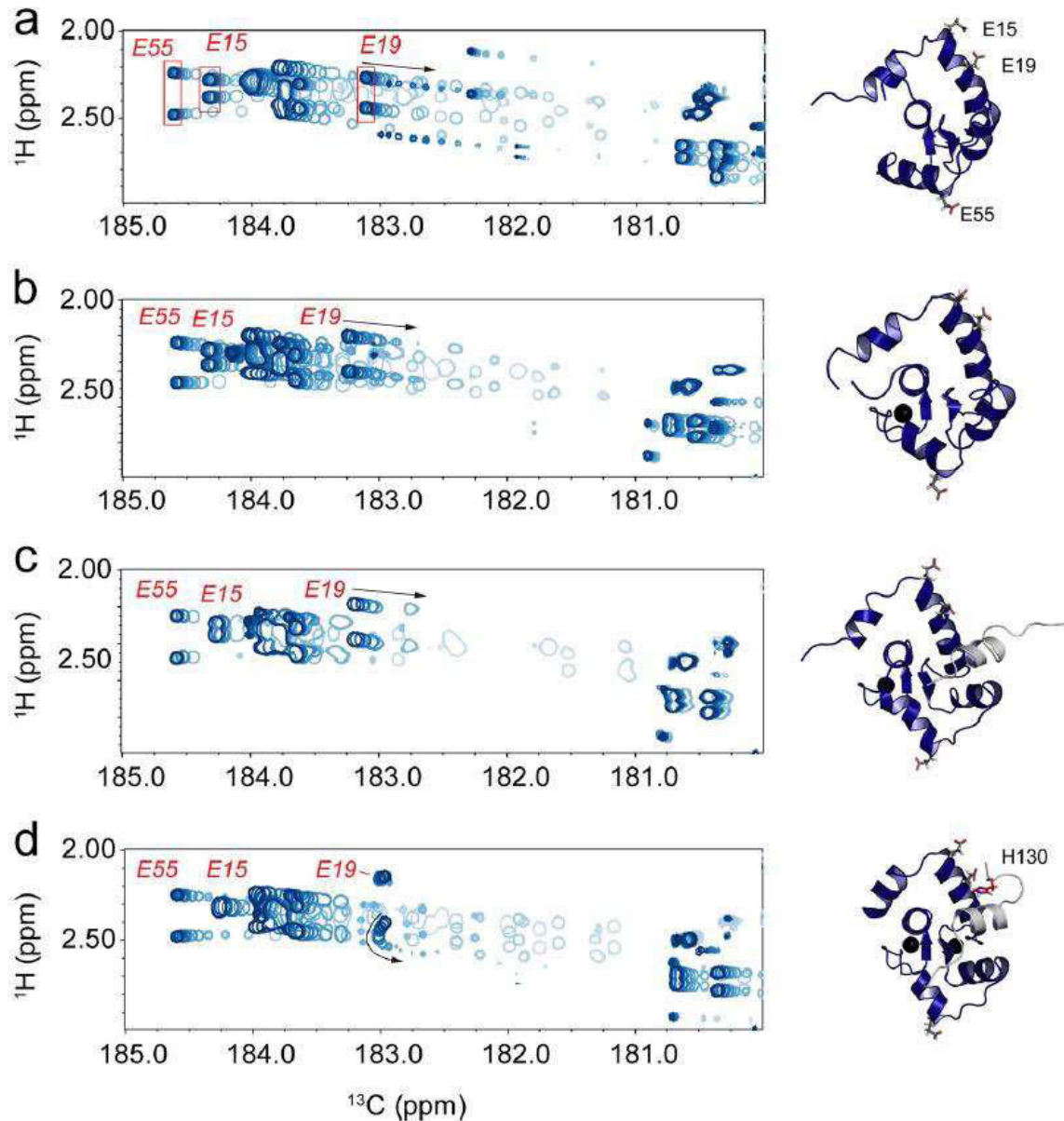
Figure 3.3. Superimposed two-dimensional ^{1}H,^{13}C HCBCGCO NMR spectra acquired throughout the pH titration of cNTnC(apo), cNTnC, cNTnC-cTnI(147-163), and cNTnC-sTnI(115-131).

As the pH decreases, the peak contour color changes from dark blue to light blue contours. See Fig. 4 for pK$_a$ fits of Glu-15, Glu-19, and Glu-55 and Table 1 and supplemental Tables 1 and 2 for pK$_a$ values. The resonances of three glutamates are labeled in red. Residues Glu-15, Glu-19, and Glu-55 are depicted in stick representation and are labeled in a. The structure beside the pH titration of cNTnC-sTnI(115–131) is from the x-ray structure of the skeletal troponin complex[16], and His-130 is shown in stick representation and is labeled.

The results for the pK$_a$ values calculated using the ^{1}H,^{15}N HSQC and ^{1}H,^{13}C HCBCGCO NMR data for all cNTnC glutamates are listed in Supplementary Table 3.1 and Supplementary Table 3.2, respectively. Residues with missing pK$_a$ values either had overlapping signals or did not titrate over the pH range examined. The pK$_a$ curve fitting data for Glu-55, Glu-15, and Glu-19 from the two-dimensional ^{1}H,^{13}C HCBCGCO and two-dimensional ^{1}H,^{15}N HSQC experiments are shown in Figure 3.4 for the cTnI(147–163)-and sTnI(115–131)-bound complexes. The pK$_a$ values for all three residues in the four different states of cNTnC monitored are listed in Table 3.1. The ionization of a side chain is most accurately portrayed by monitoring the carboxyl chemical shift due to its large chemical shift perturbation and proximity to the protonation site when compared with the amide or ^{1}Hγ nuclei[25, 45]. Therefore, pK$_a$ values derived from the ^{13}C chemical shifts will be referred to for the majority of the discussion.

The pK$_a$ values of Glu-55 and Glu-15 are not significantly perturbed across the four different states of cNTnC. The titration curves of Glu-19 are monophasic in the apo-, Ca^{2+}-bound, and cTnI(147–163)-bound complexes; however, it is distinctly biphasic when sTnI(115–131) is bound (Figure 3.4c). The pK$_a$ of Glu-19 is 5.06 ± 0.03 in the apo-state, 5.06 ± 0.02 in the Ca^{2+}-bound state, and 5.23 ± 0.01 when cTnI(147–163) is bound. The two measured pK$_a$ values for Glu-19 when sTnI(115–131) is bound are 4. $\pm$ 0.01 and 6.73 ± 0.17 (the elevated pK$_a$ represents an average from the five nuclei monitored). The large ^{13}C perturbation corresponds to ionization of the carboxyl of Glu-19 (pK$_a$ 4.70 ± 0.01), and the smaller chemical shift change was assigned to a neighboring residue.

Because the major difference between cTnI(147–163) and sTnI(115–131) is the presence of a histidine in sTnI(115–131) (Fig. 1), it is likely that the pK$_a$ of 6.73 ± 0.17 is from His-130 of sTnI(115–131). In addition, it has been shown that the direction of the ^{13}C-carbonyl chemical shift is correlated to hydrogen bonding[46, 47]. Hydrogen bonding to the carbonyl results in an increase in the polarity of the carbonyl bond, which causes a decrease in the shielding of the ^{13}C-carboxyl nucleus and an increase in its chemical shift. Close inspection of Figure 3.3d reveals an initial increase in the ^{13}C chemical shift of Glu-19 as the pH was decreased from 8.5 to 6.5, consistent with the formation of an electrostatic interaction with a neighboring residue that is becoming protonated. The pK$_a$ of Glu-19 decreases from 5.06 ± 0.02 when Ca^{2+} is bound to 4.70 ± 0.01 when sTnI(115– 131) is bound (a difference of 0.36 ± 0.03). The reduction in the pK$_a$ of Glu-19 is more evidence that Glu-19 is involved in the formation of an electrostatic interaction.
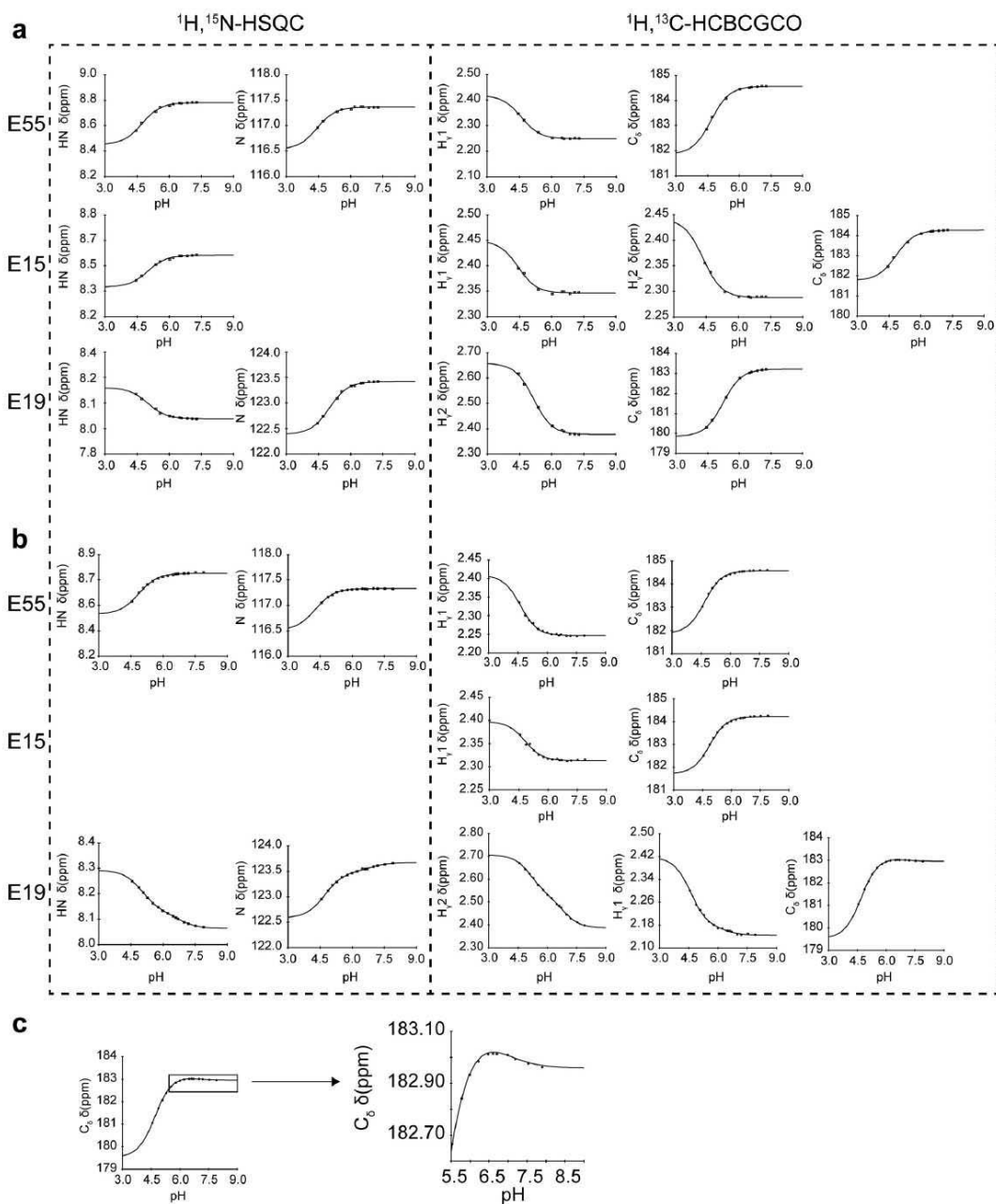
Figure 3.4. pH dependence of glutamate resonances of cNTnC bound to cTnI peptides.

[1]HN, ^{15}N, [13]Cδ, and [1]Hγ resonances of Glu-15, Glu-19, and Glu-55 of cNTnC when bound to cTnI(147–163) (a) and sTnI(115–131) (b). The pK_a curves of the amide resonances from the two-dimensional ^{1}H,^{15}N HSQC experiment are shown on the left, and the aliphatic proton and carboxylate carbon resonances from the two-dimensional ^{1}H,[13]C HCBCGCO experiment are shown on the right. Peaks that were overlapped with other signals or that did not titrate were omitted. All five pK_a curves of Glu-19 in the sTnI(115–131) bound state were fitted to Equation 2. c, second inflection of the ^{13}C chemical shift of Glu-19 is expanded. For the pK_a values refer to Table 3.1 and Supplementary Table 3.1 and 3.2.

Table 3.1. pKa* values determined for Glu-15, Glu-19, and Glu-55.

cNTnC	Glu-15						Glu-19						Glu-55					
	^{1}HN	^{15}N	^{1}Hγ1	^{1}Hγ2	^{13}Cδ	Ave.	^{1}HN	^{15}N	^{1}Hγ$_1$	^{1}Hγ2	^{13}Cδ	Ave.	^{1}HN	^{15}N	^{1}Hγ1	^{1}Hγ2	^{13}Cδ	Ave.
Apo	5.09	5.22	4.49	4.88	4.88	4.92	5.08	5.14	5.06	5.09	5.06	5.09	4.67	4.13	4.58		4.75	4.53
Ca^{2+}	5.03		4.37	4.84	4.84	4.75	4.82	5.22		5.17	5.06	5.07	4.64	4.64	4.60		4.63	4.63
cTnI(147–163)	5.00		4.36	4.43	4.83	4.66	5.00	5.00		5.15	5.23	5.10	4.73	4.43	4.58		4.66	4.60
sTnI(115–131)				4.83	4.87	4.85	5.03	4.72	4.60	5.15	4.70	4.84	4.86	4.28	4.62		4.68	4.61
							6.77	6.87	6.44	6.80	6.78	6.73						

*as determined from the Cδ chemical shift two-dimensional ^{1}H,^{13}C HCBCGCO NMR experiments. Data were fitted using Equations 1 or 2, setting the Hill coefficient to 1. Ave. means average.

sTnI(115–131) histidine pK$_a$ values as a function of structure

The results above suggest that Glu-19 interacts with His-130 on sTnI(115-131); to further investigate this possibility, the pK$_a$ of His-130 was measured for sTnI(115–131) in the absence and presence of cNTnC. The stacked one-dimensional ^{1}H NMR spectra for the pH titrations are shown in Figure 3.5. The pK$_a$ of His-130 in free sTnI(115–131), using the histidine aromatic protons H2 and H5, was determined to be 6.11 ± 0.01 and 6.14 ± 0.03, respectively (Figure 3.5a). Because fitting the pK$_a$ curves for His-130 in the presence of cNTnC required fitting the Hill parameter (see below), this coefficient was also fitted for free sTnI(115-131). As expected, the Hill coefficient was close to unity for both H2 and H5 (0.96 and 1.07, respectively).

The pK$_a$ of His-130 was then measured in the presence of cNTnC. The pH titration of sTnI(115–131) with excess cNTnC (ratio ~6:1) is shown in Figure 3.5b. Because cNTnC signals overlapped H2 and H5, we employed a ^{13}C,^{15}N-filtered ^{1}H,^{1}HNOESY NMR experiment (29-31) to monitor the sTnI(115–131) signals (Figure 3.5b). The pK$_a$ derived from proton H2 was 6.33 ± 0.02 (the chemical shift of the protonated state was fixed at 8.70 ppm), and the pK$_a$ shift of H5 was 6.39 ± 0.04. The pK$_a$ values were determined by also fitting the Hill coefficient, because the pK$_a$ curves did not fit the simple pK$_a$ model. Low Hill coefficients fitted for H2 (n = 0.63) and H5 (n = 0.58) indicated that His-130 is most likely interacting with other ionizable group(s). For example, as a nearby residue is deprotonated, the protonated form of His-130 is stabilized; this will result in a flattened pK$_a$ curve (n < 1). For a summary of the pK$_a$ values measured for His-130 see Table 3.2. The pK$_a$ curves of H2 and H5 are overlaid in Figure 3.6, and the rightward shifts in the pK$_a$ curves clearly illustrate an increase in the stability of the positively charged species of His-130 when in the presence of cNTnC.
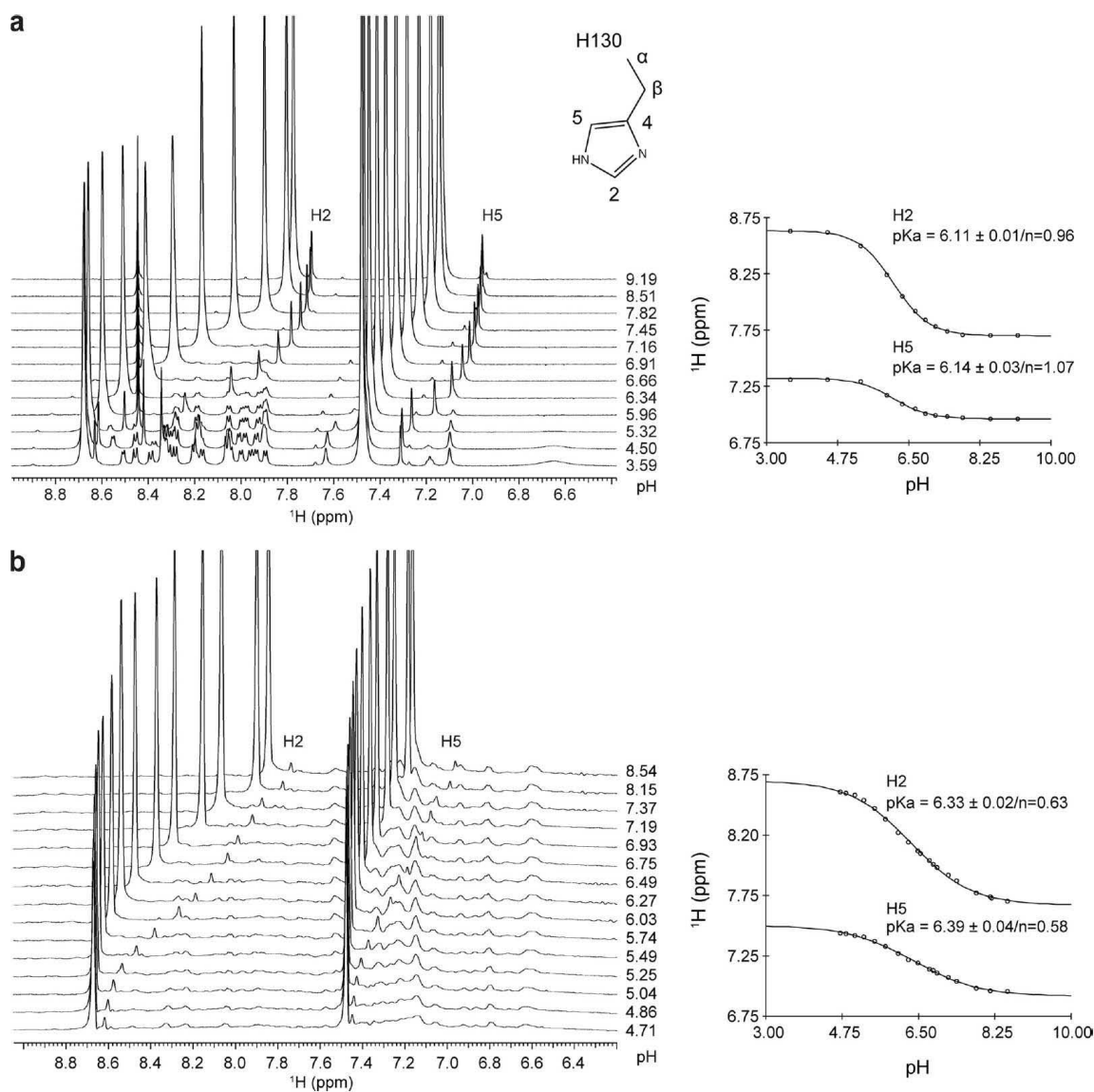
Figure 3.5. pH titrations of His-130 of sTnI(115-131) when free (*a*) and in 6-fold excess cNTnC (*b*). One-dimensional ^{1}H NMR spectra are shown on the left with histidine aromatic protons assigned. The pK_a curves for H2 and H5 in the free and bound states are shown on the right.

Table 3.2. pKa values determined for His-130 using one-dimensional NMR experiments.

	H2		H5		Average (σ)	
Fraction bound[a]	pK_a	*n*	pK_a	*n*	pK_a	*n*
0	6.11 (0.01)	0.96 (0.02)	6.14 (0.03)	1.07 (0.08)	6.13 (0.02)	1.02 (0.08)
0.51–0.78	6.33 (0.02)	0.63 (0.02)	6.39 (0.04)	0.58 (0.04)	6.36 (0.04)	0.61 (0.04)

Data were fitted using Equations 1 or 2; errors are shown in parentheses. [a] Fraction bound was calculated using Equation 3; the lower value was calculated using the K_D determined at pH 7.5 (360 µM), and the higher value was calculated using the K_D determined at pH 6.1 (100 µM).
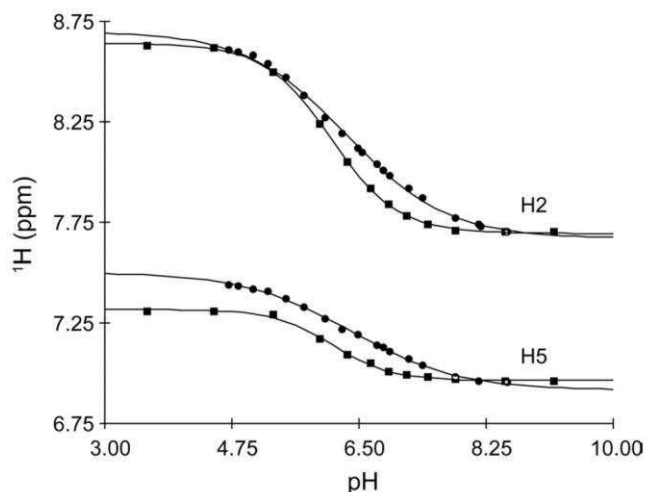
Figure 3.6. pH dependence of the pKa values of His-130 (H2 and H5) as a function of fraction sTnI(115–131) bound.
Squares correspond to data points for free sTnI(115–131); circles correspond to excess cNTnC (mostly bound).

There were minor peaks next to H2 and H5 noted in samples containing excess sTnI(115–131). The pK_a values of these secondary peaks were near the values for free sTnI(115–131) and probably represent a second bound conformation of sTnI(115–131) in slow exchange with the major conformation[48]. Similar observations have been made for histidine residues in neurophysin II[49] and staphylococcal nuclease[50]. In line with this conclusion, sTnI has been shown by NMR experiments to be in two conformations when bound to sNTnC[18]. These peaks are presumably not from impurities because HPLC and mass spectrometry indicated that peptide was pure. Moreover, these minor peaks were not witnessed in the free sTnI(115–131) experiments. To ensure the second minor peak was indeed from histidine on sTnI(115–131), the $^{13}C,^{15}N$-filtered $^{1}H,^{1}H$TOCSY NMR experiment was run[29-32]. The TOCSY spectrum shows the presence of signals attributable to two separate histidine conformations (Supplementary Figure 3.2).

The pK_a values of H2 and H5 from His-130 are shifted upward but is not shifted to the value measured from the Glu-19 pK_a curves (pK_a = 6.73 ± 0.17). This can be explained by the fact that even though the concentration of cNTnC is ~6:1 sTnI(115–131), the fraction-bound sTnI(115–131) may not be one. As mentioned earlier, a Hill coefficient different from unity may indicate an interaction with another titrating species. Another potential cause of the altered Hill coefficient may be that the fraction of sTnI(115–131)-bound changes as a function of pH, for example if sTnI(115–131) binds with different affinity at low and high pH values. The dissociation constant was determined at two pH values to assess this possible pH dependence.

sTnI(115-131) was titrated into cNTnC at two pH values (6.1 and 7.5). At each aliquot of sTnI(115-131), two-dimensional ^{1}H,^{15}N HSQC spectra were acquired. The global dissociation constant (K_D) was determined to be 100 µM (sum of squared error = 0.066) at pH 6.1 and K_D = 360 µM (sum of squared error = 0.076) at pH 7.5 (for an overlay of fits at the two pH values, residue Thr-71 is shown in Figure 3.7a, and the global fits are shown in Supplementary Figure 3.3 and Supplementary Figure 3.4).
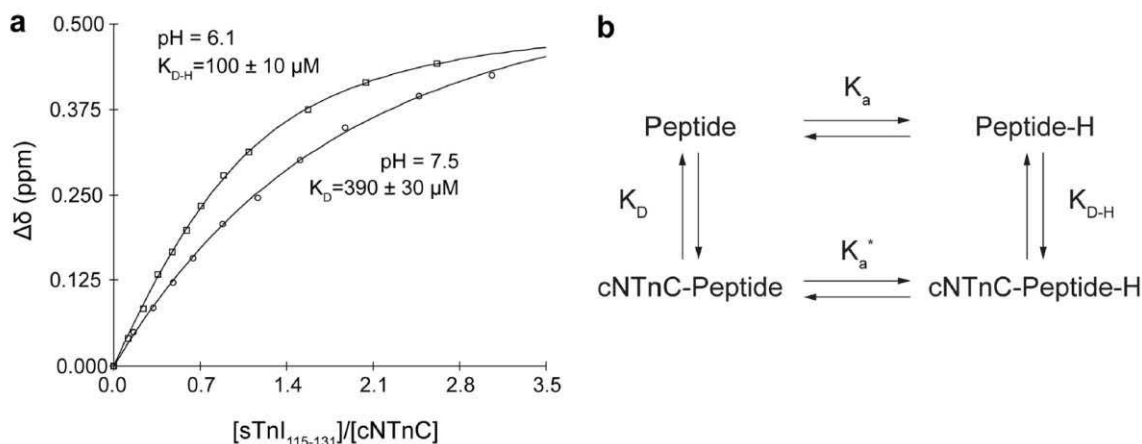
Figure 3.7. Titration of sTnI(115–131) into cNTnC at two different pH values.
a, dissociation curves fit to the amide ^{1}H NMR chemical shift data of Thr-71. sTnI(115–131) binds to cNTnC with a significantly higher affinity at the lower pH. *b,* scheme that was fit to model the pH dependence of sTnI(115–131) binding to cNTnC.

The change in affinity as a consequence of pH indicates that the fraction bound will change over the course of the pH titrations. Using Equation 3, the fraction bound goes from 0.51 to 0.78 as the pH goes from 7.5 to 6.1. Typically, one could calculate fraction bound and extrapolate to the bound species to calculate the pK_a value of the bound species; however, with the varying K_D values as a function of pH, this was difficult. We did two extrapolations using averaged pK_a values of H2 and H5, one assuming fraction bound of 0.78 and another assuming fraction bound of 0.52; the extrapolated pK_a values for the bound species ranged from 6.43 to 6.58. The pK_a of 6.58 is close to the pK_a monitored by Glu-19 (6.73 ± 0.17).

If the pH-dependent change in the affinity of sTnI(115–131) for cNTnC is solely related to the protonation state of His-130, then this should be reflected in the acid dissociation constant of His-130. We fitted the dissociation data to the simple model shown in the scheme in Figure 3.7b to investigate whether the pK_a shifts of His-130 are directly correlated to the modulation of the K_D value of sTnI(115–

131). Protonation constants are represented by K_a (free) and K_a^* (bound), and the peptide dissociation constants are indicated by K_D (deprotonated peptide) and K_{D-H} (protonated peptide). We used the pK_a value for His-130 monitored from Glu-19 due to the uncertainty of the bound pK_a of His-130 by monitoring His-130 directly as already mentioned. The same model has been previously fitted to characterize the pH dependence of a peptide binding to calmodulin[51]. For His-130, $K_a = 7.410 \times 10^{-7}$ M ($pK_a = 6.13$, an average of H2 and H5) and $K_a^* = 1.9 \times 10^{-7}$ M ($pK_a = 6.73$). $K_D = 3.9 \times 10^{-4}$ M and $K_{D-H} = 1.0 \times 10^{-4}$ M. $K_a/K_a^*(3.9)$ is equal to K_D/K_{D-H} (3.9), which is consistent with the scheme in Figure 3.7b. This result implies that the protonation state of His-130 directly tunes the pH-dependent affinity of sTnI(115–131).

Discussion

Impairment of coronary blood flow results in ischemia, which is characterized by a decline of oxygen and substrate supply to the cardiomyocytes. The decrease in blood supply leads to a buildup of ions and metabolic products, whose accumulation culminates with intracellular acidosis and a concomitant reduction in the force and Ca^{2+} sensitivity of muscle contraction[1, 2]. This decrease in contractility occurs despite an elevation of the Ca^{2+} transient during acidosis[52]. Instead, the increase of adenosine diphosphate, inorganic phosphate, and proton concentrations may inhibit actomyosin-ATPase activity[53, 54], and the increased [H^+] may decrease Ca^{2+} sensitivity by lowering the affinity of troponin for Ca^{2+} [6-8].

Interestingly, slow and fast skeletal muscles are less sensitive to acidic conditions than cardiac muscle[10, 12]. These differences in pH sensitivity have been localized to the C-terminal region of TnI[12, 14], specifically in its switch region[13]. The sequence comparison of the switch regions of cTnI, sTnI, and ssTnI (Figure 3.1) reveals that both sTnI and ssTnI have a histidine in place of the alanine present in cTnI. *In vitro*[13] and *in vivo*[15] functional studies have verified that this histidine is the chief source of the reduced pH sensitivity of sTnI and ssTnI. The data presented here provide a structural understanding for how the sTnI isoform is less sensitive to the decline in pH associated with acidosis.

In the crystal structure of the skeletal complex[16], an electrostatic interaction between Glu-20 of sTnC and His-130 of sTnI is observed, and the data presented herein suggest that an analogous interface is formed between Glu-19 and His-130 in the cNTnC-sTnI(115–131) complex. In the crystal structure, the imidazole N3 of His-130 is only 4.1 Å away from the carboxylate carbon of Glu-20, and assuming this interaction also occurs in the cNTnC-sTnI(115–131) complex, a change in the pK_a values of both Glu-19 and His-130 should be observed. To investigate this possibility, we measured the pK_a values of Glu-19 and His-130. The pK_a value of His-130 shifted from 6.13 ± 0.02 to 6.73 ± 0.17 (using data obtained from Glu-19) or 6.54 to 6.4 (using data obtained by extrapolating from His-130 data). Glu-19

also experienced a pK_a perturbation of 0.36 (5.06 ± 0.03/0.02 to 4.70 ± 0.01) and 0.53 units (5.23 ± 0.01 to 4.70 ± 0.01) when compared with apo/Ca^{2+}- and cTnI(147– 163)-bound states, respectively. The elevated pK_a of Glu-19 when cNTnC is in complex with cTnI(147–163) may be the result of its proximity to the carboxyl group of Asp-152 from cTnI(147–163) (Cδ-Cγ distance: 7.3 Å, Protein Data Bank code 1j1e, and 10.6 ± 1.7 Å, Protein Data Bank code 1mxl).

If the interaction between Glu-19 and His-130 was solely responsible for the elevated pK_a of His-130, then their ΔpK_a values should be identical. Differences in the pK_a shifts of His- 130 and Glu-19 can be explained by several phenomena. First, the pK_a of Glu-19 was measured at a [cNTnC]/[sTnI(115– 131)] ratio of ~4:1; using Equation 4 the fraction of cNTnC bound to sTnI(115-131) ranges from 0.65 at pH 7.5 to 0.86 at pH 6.1. Therefore, at a fraction bound of one the pK_a would be expected to be lower than what was actually measured. Extrapolation of Glu-19 in a similar manner as described for His-130 yielded a pK_a range for bound of 4.64 to 4.51 (ΔpK_a of 0.42 and 0.55, respectively, close to that determined for His-130, ~0.6). Second, the carboxylate of Asp-119 on sTnI in the x-ray structure is only 3.7 Å from N4 of His-130. If this interaction occurs when sTnI(115-131) is bound to cNTnC, then it will also contribute to an increase in the pK_a of His-130. Glu-16 is also near His-130 (10.1 Å), and it may be involved in driving sTnI binding to sTnC, because electrostatic forces can span distances ~10 Å [55-59]. Conversely, in the NMR and x-ray structures of cardiac troponin, these interactions do not occur, presumably because the histidine is replaced by an alanine[19, 20]. Comparison of the crystal structures of the cardiac and skeletal troponin complexes in Figure 3.8 illustrates that in the cardiac system Ala-162 is much further from Glu-15 and Glu-19 (11.8 and 16.4 Å, respectively). Thus, it is likely that when sTnI(115-131) binds to cNTnC, it adopts a conformation more similar to the skeletal complex.

The observed pH dependence of sTnI(115–131) binding is directly related to the ionization state of His-130, which can be explained in part by an interaction made between Glu-19 of cNTnC and His-130 of sTnI(115-131). At first glance, this result seems to imply that muscle with sTnI would have enhanced Ca^{2+}sensitivity at low pH. However, functional studies of cardiac myofilaments replaced with sTnI demonstrate that although the negative inotropic effects of acidosis are partially suppressed, the Ca^{2+} sensitivity is not enhanced when compared with values at neutral pH[12, 13]. Given that we were explicitly interested in probing the role His-130 played in dictating sTnI(115–131) binding to cNTnC, and as it is well established that the Ca^{2+} binding to cTnC is reduced as pH is lowered[6-8], we worked with excess Ca^{2+} to ensure Ca^{2+} saturation, even at the lower pH values. Moreover, the increased affinity of sTnI(115–131) measured at low pH in this report is not large enough to fully compensate for the reduced Ca^{2+} affinity at low pH. To illustrate this, we calculated the free energies of Ca^{2+} and sTnI(115–
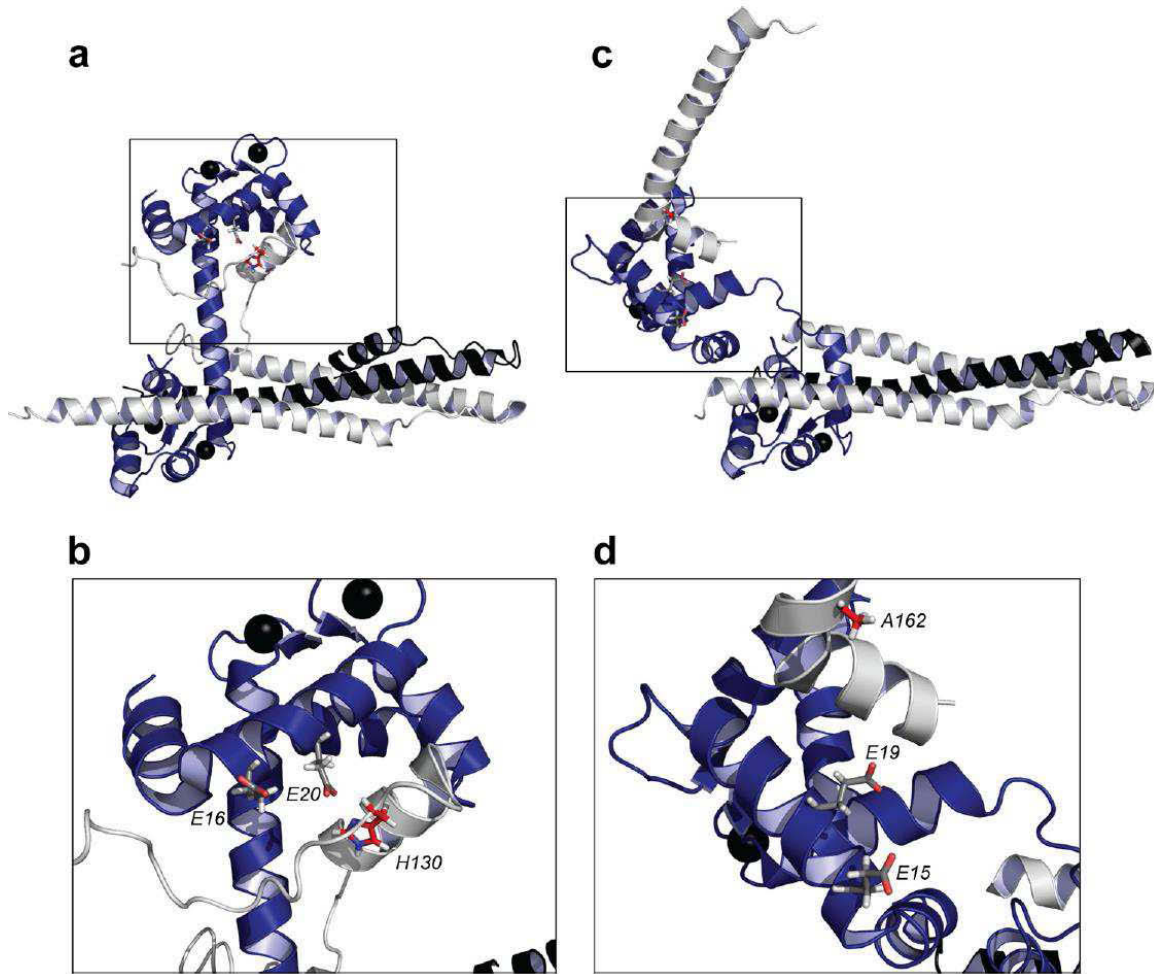
Figure 3.8. Schematic representations of the core skeletal troponin complex (a and b: PDB ID: 1ytz) and core cardiac troponin complex (c and d: PDB ID: 1j1e)

In both structures, TnC is shown in dark blue, TnI in light gray, and TnT in black, and Ca^{2+} ions are depicted as black spheres. Glu-16, Glu-20, and His-130 (Glu-15, Glu-19, and Ala-162 in the cardiac system) are shown in stick representation. Expanded regions of a and c are shown in b and d, respectively.

131) binding to cNTnC. The free energy (ΔG) of sTnI(115–131) binding to cNTnC can be determined as shown in Equation 6,

$$\Delta G = RT\ln K_D$$

(Eq. 6)

where R is the ideal gas constant, and T is the temperature in Kelvin. Using this equation, the ΔG of sTnI(115-131) binding at pH 6.1 is approximately -5.6 kcal/mol and at pH 7.5 is approximately -4.7

kcal/mol, corresponding to a $\Delta\Delta G$ of 0.9 kcal/mol. Using the values for Ca^{2+} binding to cNTnC at pH 7 and pH 6 as reported by Liou and Chang[8], Ca^{2+} binding is ~2.4 kcal/mol less favorable at pH 6 than pH 7. Therefore, the enhanced binding of sTnI(115–131) at low pH would not entirely offset the reduced binding of Ca^{2+} to cNTnC. We propose that the reduction in Ca^{2+} affinity of cNTnC at low pH would be only partially compensated for by the concomitant enhancement in the affinity of sTnI for cTnC. This interpretation is consistent with findings that sTnI enhances the Ca^{2+} affinity of cTnC at low pH values by its enhanced affinity for cTnC[8].

In this study, we show that the histidine of sTnI makes an interaction with cNTnC, and it is likely that cTnI(A162H) forms a similar interaction. It is worth mentioning that there may be some detrimental effects of increasing Ca^{2+} sensitivity during acidosis. Transgenic mice containing the hypertrophic cardiomyopathy mutation, E180G, in tropomyosin (Tm-E180G) do not experience a substantial decline of Ca^{2+} sensitivity during acidosis[60]. Although it might be expected that the reduced pH sensitivity of Tm-E180G would be beneficial because heart failure would be reversed, the increased muscle contractility seems to contribute to a worsening of heart disease[60]. Therefore, although it seems to be intuitive that one would want to enhance contractility in a weakened heart, this may not always be the case. However, *in vivo* studies done on transgenic mice expressing cTnI(A162H), which also have a reduced decrease in Ca^{2+} sensitivity during acidosis, do not have the same deleterious effects as Tm-E180G. The ability of cTnI(A162H) to be down-regulated by phosphorylation may help explain why this mutation has less severe consequences than Tm-E180G[15].

The fact that the interaction between His-130 and Glu-19 is important in stabilizing the interaction between sTnI(115– 131) and cTnC has implications not only for explaining why the neonatal heart contractility is less sensitive to low pH but also for the development of pharmaceuticals. The design of molecules that become charged at low pH and then stabilize the interaction between cTnI and cNTnC could be beneficial for the treatment of ischemic heart failure. Finally, although the protonation state of His-130 modifies the affinity of sTnI(115– 131) for cNTnC, it is also possible that its charge state may have other functional effects in an intact muscle fiber. For example, the protonation may both enhance the interaction between sTnI and cTnC and diminish sTnI binding to actin as has also been proposed[15].

Acknowledgments
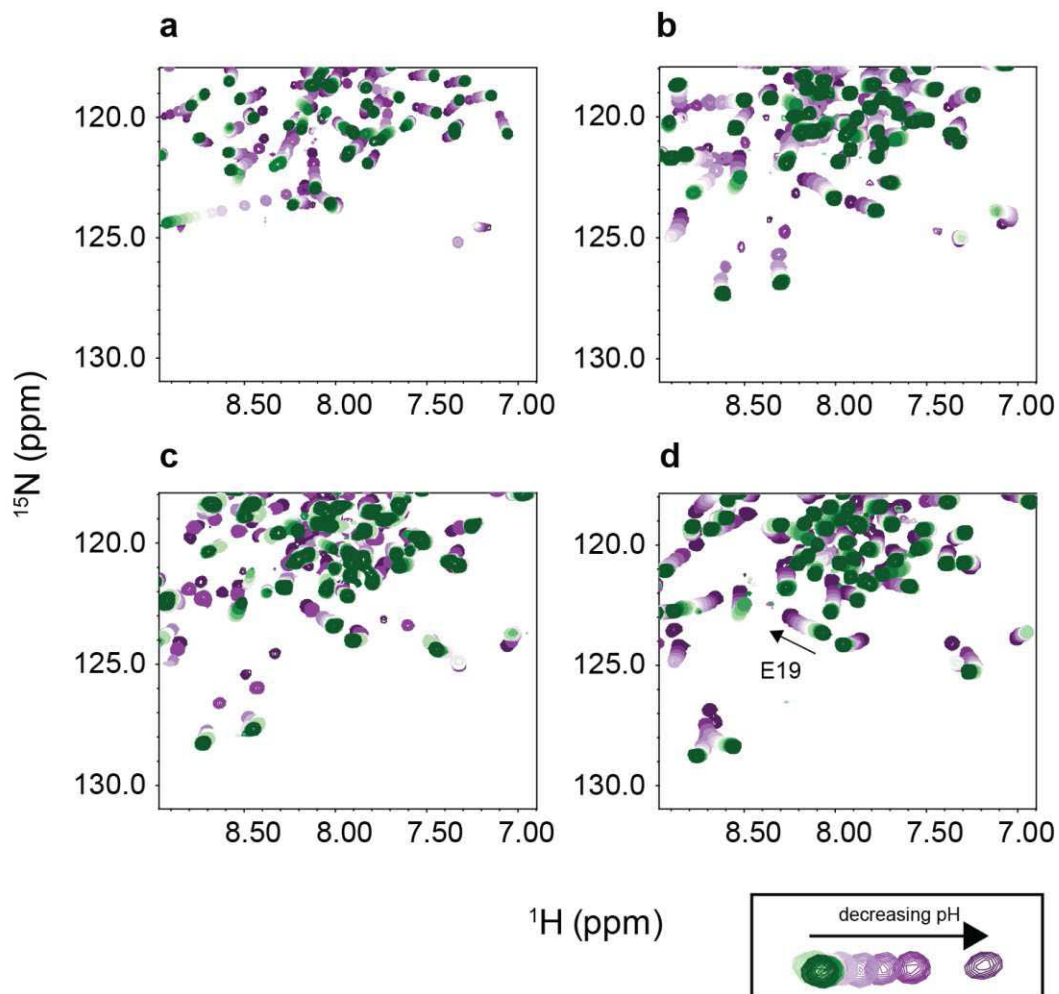
Supplementary Figure 3.1. Superimposed 2D ^{1}H,^{15}N-HSQC NMR spectra acquired throughout the pH titration of a. cNTnC(apo), b. cNTnC, c. cNTnC-cTnI$_{147-163}$, and d. cNTnC-sTnI$_{115-131}$.
As the pH decreases the peak contour color changes from dark green to purple. See table S1 for pK_a values. The resonance of E19 is labeled in cNTnC-sTnI$_{115-131}$.
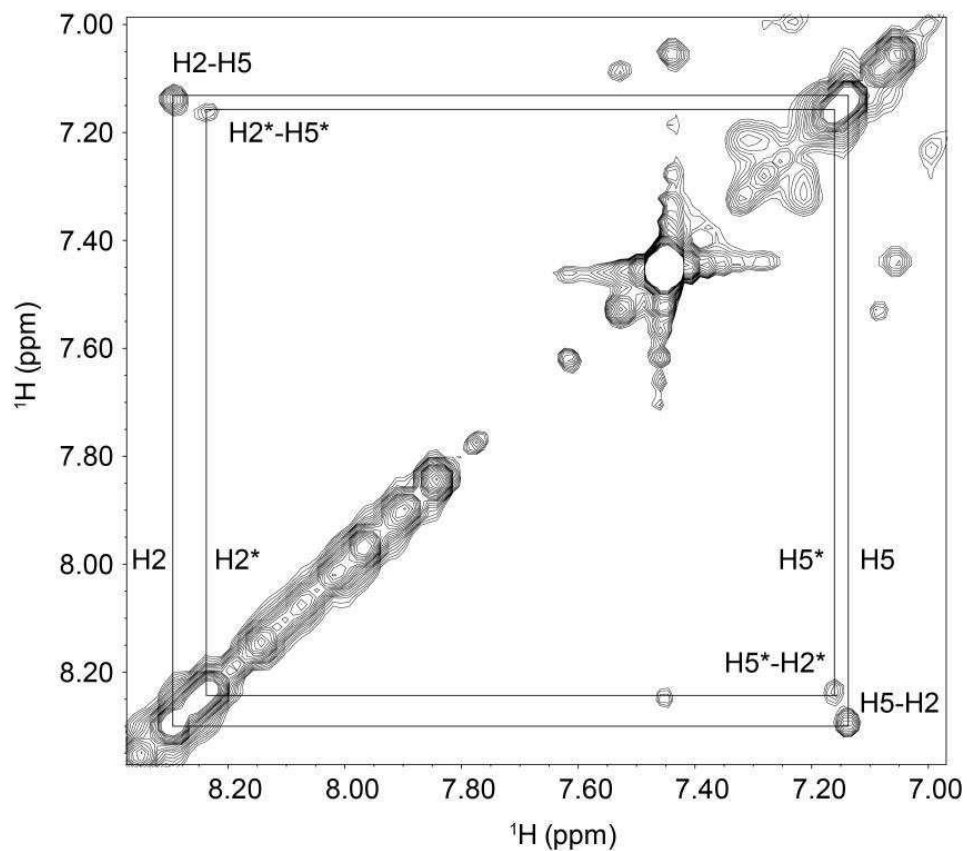
Supplementary Figure 3.2. 2D ^{13}C,^{15}N-filtered TOCSY NMR spectrum of ^{13}C,^{15}N-labeled cNTnC in complex with unlabeled sTnI(115-131).

The spectrum was acquired at pH 5.90 and with mixing time = 60 ms. The spectrum clearly indicates the presence of a major and minor (*) conformation of H130.
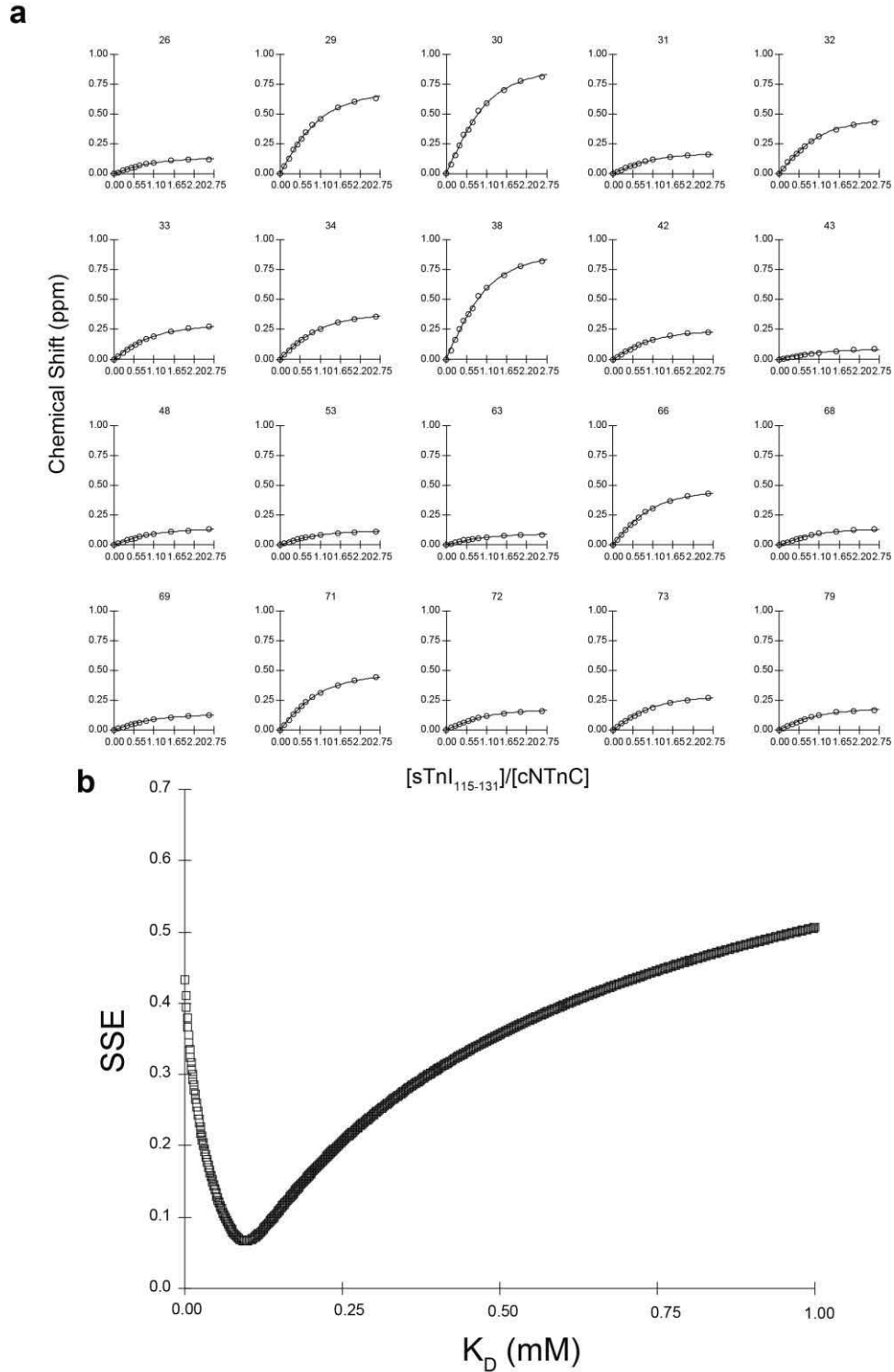
Supplementary Figure 3.3.

a. Global fit of the amide chemical shift changes of cNTnC when sTnI$_{115-131}$ is titrated to cNTnC at pH 6.1. **b.** The minimum SSE for the global fit in **a.** is at K$_D$= 100 μM (SSE = 0.066).
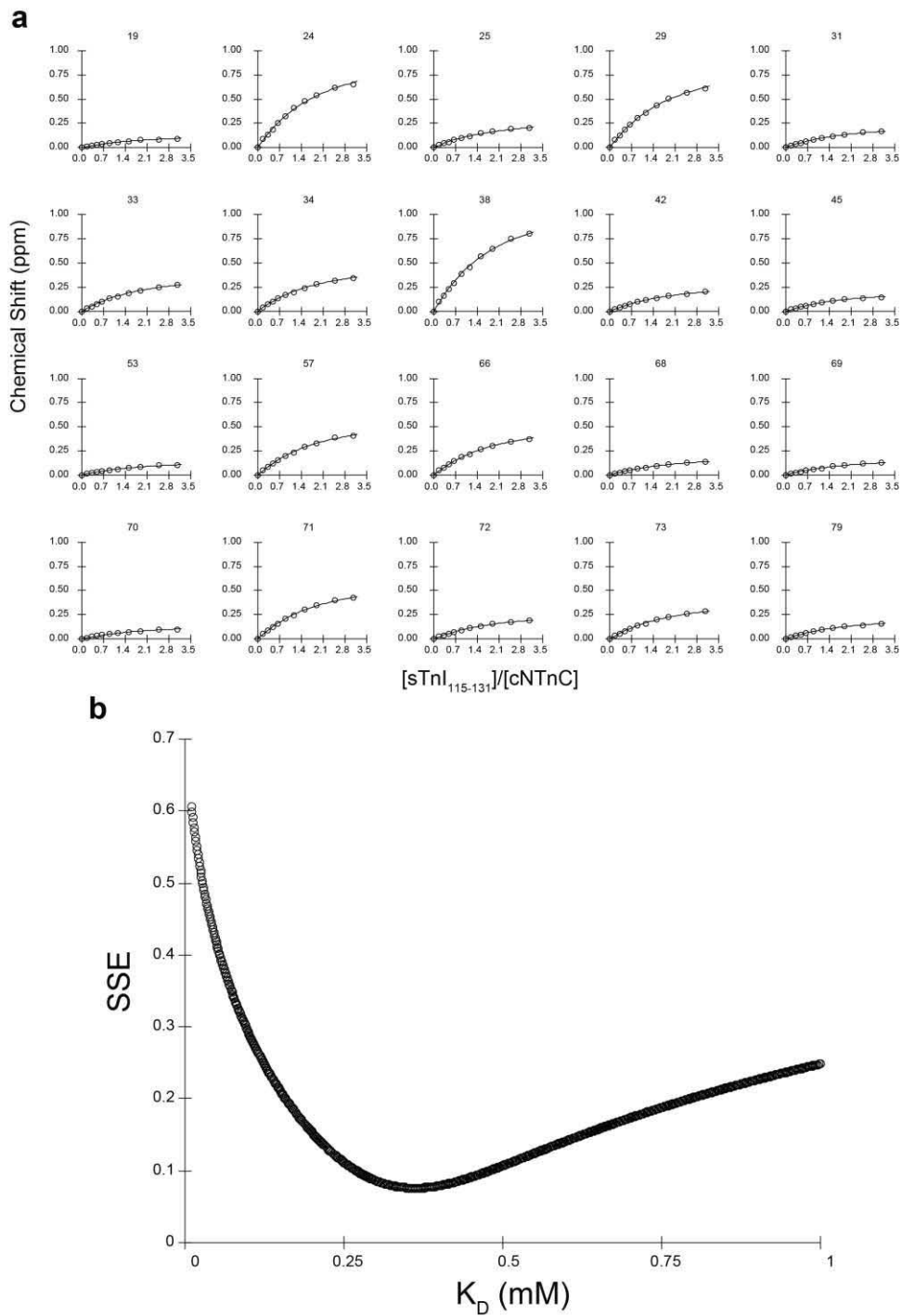
Supplementary Figure 3.4.

a. Global fit of the amide chemical shift changes of cNTnC when sTnI$_{115-131}$ is titrated to cNTnC at pH 7.5. **b.** The minimum SSE for the global fit in **a.** is at K$_D$= 360 μM (SSE = 0.076).

Supplementary Table 3.1. Three-parameter or four-parameter fits of titration data for glutamate residues using 2D ^{1}H,^{15}N-HSQC NMR spectra[a].

Residue	Apo		Ca^{2+}		cTnI$_{147-163}$		sTnI$_{115-131}$	
	HN	N	HN	N	HN	N	HN	N
E10	4.57 (0.18)	4.93 (0.09)	-	4.89 (0.09)	-	4.92 (0.1)	4.15 (0.09) 8.65(6.14)	3.92 (0.17)
E14	-	4.67 (0.32)	-	-	-	-	-	-
E15	5.09 (0.04)	5.22 (0.03)	5.03 (0.03)	-	5.00 (0.05)	-	-	-
E19	5.08 (0.05)	5.14 (0.06)	4.82 (0.03)	5.22 (0.02)	5.00 (0.04)	5.00 (0.03)	5.03 (0.02) 6.77 (0.04)	4.72 (0.05) 6.87 (0.11)
E32	4.28 (0.11)	4.68 (0.08) 6.29 (0.11)	4.32 (0.06)	4.22 (0.04)	3.64 (0.56)	3.16 (1.16)	3.69 (0.19)	-
E40	4.13 (0.18)	-	-	3.29 (0.45) 5.10 (0.06)	-	-	5.74 (0.1)	4.65 (0.11)
E55	4.67 (0.06)	4.13 (0.19)	4.64 (0.04)	4.64 (0.02)	4.73 (0.06)	4.43 (0.12)	4.86 (0.04)	4.28 (0.06)
E56	4.85 (0.08)	-	-	4.51 (0.02)	-	4.3 (0.03)	4.77 (0.06)	4.25 (0.07)
E59	4.89 (0.03)	5.63 (0.11)	4.63 (0.05)	-	-	-	-	-
E63	5.31 (0.06)	4.06 (0.16) 6.53 (0.08)	4.05 (0.19) 8.04 (0.25)	2.98 (1.0) 5.29 (0.08)	-	-	4.85 (0.07) 6.49 (0.09)	-
E66	4.49 (0.33)	4.86 (0.06)	-	-	-	-	5.93 (0.08)	4.37 (0.045)
E76	4.57 (0.08)	4.98 (0.09) 6.77 (0.11)	4.38 (0.03)	4.57 (0.06)	4.92 (0.07)	4.63 (0.09)	4.97 (0.05)	4.93 (0.03) 7.13(0.18)

[a]Data were fitted to equation 1 or 2, setting the hill coefficient to 1.

Supplementary Table 3.2. Three-parameter or four-parameter fits of titration data for glutamate residues using 2D ^{1}H,^{13}C-HCBCGCO spectra[a].

Residue	Apo			Ca^{2+}			cTnI$_{147-163}$			sTnI$_{115-131}$		
	Hγ1	Hγ2	Cδ	Hγ1	Hγ2	Cδ	Hγ1	Hγ2	Cδ	Hγ1	Hγ2	Cδ
E10	-	4.58 (0.18)	4.66 (0.03)	4.73 (0.06)	4.88 (0.09)	4.62 (0.02)	4.74 (0.03)	4.83 (0.16)	4.67 (0.03)	-	-	-
E14	-	-	-	-	-	-	-	-	-	-	-	-
E15	4.49 (0.09)	-	4.88 (0.03)	4.37 (0.05)	-	4.84 (0.03)	4.36 (0.10)	4.43 (0.22)	4.83 (0.06)	-	4.83 (0.09)	4.87 (0.03)
E19	5.06 (0.04)	5.09 (0.03)	5.06 (0.03)	-	5.17 (0.03)	5.06 (0.02)	-	5.15 (0.05)	5.23 (0.01)	4.60 (0.11) 6.44 (0.32)	5.15 (0.05) 6.8 (0.05)	4.70 (0.01) 6.78 (0.05)
E32	-	-	-	-	-	-	-	-	-	-	-	-
E40	4.85 (0.06)	-	4.57 (0.03)	-	-	-	-	-	-	-	-	4.07 (0.22)
E55	4.58 (0.07)	-	4.75 (0.04)	4.60 (0.05)	-	4.63 (0.04)	4.58 (0.06)	-	4.66 (0.06)	4.62 (0.05)	-	4.68 (0.03)
E56	-	-	-	-	-	-	-	-	-	-	-	-
E59	5.44 (0.05)	5.15 (0.08)	5.43 (0.05)	5.38 (0.03)	4.97 (0.05)	5.31 (0.03)	5.40 (0.02)	5.02 (0.09)	5.38 (0.04)	5.43 (0.03)	5.21 (0.06)	5.37 (0.02)
E63	5.40 (0.06)	5.64 (0.06)	5.26 (0.05)	5.42 (0.05)	5.71 (0.08)	5.34 (0.03)	5.29 (0.13)	5.71 (0.09)	5.19 (0.04)	5.22 (0.05)	5.55 (0.04)	5.05 (0.03)
E66	-	-	-	-	-	-	4.96 (0.03)	5.40 (0.06)	4.97 (0.02)	-	-	-
E76	-	6.35 (0.06)	6.06 (0.07)	-	-	-	-	-	-	-	-	-

[a]Data were fitted to equation 1 or 2, setting the hill coefficient to 1.

References

1. Donaldson, S. K., Hermansen, L., and Bolles, L. (1978) Differential, direct effects of H^+ on Ca^{2+} activated force of skinned fibers from the soleus, cardiac, and adductor magnus muscles of rabbits. *Pflugers Arch.* 376, 55–65

2. Fabiato, A., and Fabiato, F. (1978) Effects of pH on the myofilaments and the sarcoplasmic reticulum of skinned cells from cardiac and skeletal muscles. *J. Physiol.* 276, 233–255

3. Gordon, A. M., Homsher, E., and Regnier, M. (2000) Regulation of contraction in striated muscle. *Physiol. Rev.* 80, 853–924

4. Kobayashi, T., Jin, L., and de Tombe, P. P. (2008) Cardiac thin filament regulation. *Pflugers Arch.* 457, 37–46

5. Li, M. X., Wang, X., and Sykes, B. D. (2004) Structural based insights into the role of troponin in cardiac muscle pathophysiology. *J. Muscle Res. Cell Motil.* 25, 559–579

6. Blanchard, E. M., and Solaro, R. J. (1984) Inhibition of the activation and troponin calcium binding of dog cardiac myofibrils by acidic pH. *Circ. Res.* 55, 382–391

7. Parsons, B., Szczesna, D., Zhao, J., Van Slooten, G., Kerrick, W. G., Putkey, J. A., and Potter, J. D. (1997) The effect of pH on the Ca2_ affinity of the Ca2_ regulatory sites of skeletal and cardiac troponin C in skinned muscle fibers. *J. Muscle Res. Cell Motil.* 18, 599–609

8. Liou, Y. M., and Chang, J. C. (2004) Differential pH effect on calciuminduced conformational changes of cardiac troponin C complexed with cardiac and fast skeletal isoforms of troponin I and troponin T. *J. Biochem.* 136, 683–692

9. el-Saleh, S. C., and Solaro, R. J. (1988) Troponin I enhances acidic pHinduced depression of Ca2_ binding to the regulatory sites in skeletal troponin C. *J. Biol. Chem.* 263, 3274–3278

10. Solaro, R. J., Lee, J. A., Kentish, J. C., and Allen, D. G. (1988) Effects of acidosis on ventricular muscle from adult and neonatal rats. *Circ. Res.* 63, 779–787 11. Westfall, M. V., Rust, E. M., and Metzger, J. M. (1997) Slow skeletal troponin I gene transfer, expression, and myofilament incorporation enhances adult cardiac myocyte contractile function. *Proc. Natl. Acad. Sci. U.S.A.* 94, 5444–5449

11. Li, G., Martin, A. F., and Solaro, J. R. (2001) Localization of regions of troponin I important in deactivation of cardiac myofilaments by acidic pH. *J. Mol. Cell. Cardiol.* 33, 1309–1320

12. Dargis, R., Pearlstone, J. R., Barrette-Ng, I., Edwards, H., and Smillie, L. B. (2002) Single mutation (A162H) in human cardiac troponin I corrects acid pH sensitivity of Ca2_-regulated actomyosin S1 ATPase. *J. Biol. Chem.* 277, 34662–34665

13. Westfall, M. V., Albayya, F. P., Turner, I. I., and Metzger, J. M. (2000) Chimera analysis of troponin I domains that influence Ca(2_)-activated myofilament tension in adult cardiac myocytes. *Circ. Res.* 86, 470–477

14. Day, S. M., Westfall, M. V., Fomicheva, E. V., Hoyer, K., Yasuda, S., La Cross, N. C., D'Alecy, L. G., Ingwall, J. S., and Metzger, J. M. (2006) Histidine button engineered into cardiac troponin I protects the ischemic and failing heart. *Nat. Med.* 12, 181–189

15. Vinogradova, M. V., Stone, D. B., Malanina, G. G., Karatzaferi, C., Cooke, R., Mendelson, R. A., and Fletterick, R. J. (2005) Ca(2_)-regulated structural changes in troponin. *Proc. Natl. Acad. Sci. U.S.A.* 102, 5038–5043

16. Julien, O., Mercier, P., Allen, C. N., Fisette, O., Ramos, C. H., Lague, P., Blumenschein, T. M., and Sykes, B. D. (2011) Is there nascent structure in the intrinsically disordered region of troponin I? *Proteins Struct. Funct. Bioinformatics* 79, 1240–1250

17. McKay, R. T., Tripet, B. P., Pearlstone, J. R., Smillie, L. B., and Sykes, B. D. (1999) Defining the region of troponin-I that binds to troponin-C. *Biochemistry* 38, 5478–5489

18. Takeda, S., Yamashita, A., Maeda, K., and Mae´da, Y. (2003) Structure of the core domain of human cardiac troponin in the Ca(2_)-saturated form. *Nature* 424, 35–41

19. Li, M. X., Spyracopoulos, L., and Sykes, B. D. (1999) Binding of cardiac troponin-I147–163 induces a structural opening in human cardiac troponin- C. *Biochemistry* 38, 8289–8298

20. Wuthrich, K. (1986) *NMR of Proteins and Nucleic Acids*, pp. 1–292, John Wiley & Sons, Inc., New York

21. Palpant, N. J., Houang, E. M., Delport, W., Hastings, K. E., Onufriev, A. V., Sham, Y. Y., and Metzger, J. M. (2010) Pathogenic peptide deviations support a model of adaptive evolution of chordate cardiac performance by troponin mutations. *Physiol. Genomics* 42, 287–299

22. Russell, S. T., and Warshel, A. (1985) Calculations of electrostatic energies in proteins. The energetics of ionized groups in bovine pancreatic trypsin inhibitor. *J. Mol. Biol.* 185, 389–404

23. Farrell, D., Miranda, E. S., Webb, H., Georgi, N., Crowley, P. B., McIntosh, L. P., and Nielsen, J. E. (2010) Titration_DB. Storage and analysis of NMR monitored protein pH titration curves. *Proteins* 78, 843–857

24. Forsyth, W. R., Antosiewicz, J. M., and Robertson, A. D. (2002) Empirical relationships between protein structure and carboxyl p*Ka* values in proteins. *Proteins Struct. Funct. Genet.* 48, 388–403

25. Szaka´cs, Z., Kraszni, M., and Nosza´l, B. (2004) Determination of microscopic acid-base parameters from NMR-pH titrations. *Anal. Bioanal. Chem.* 378, 1428–1448

26. Li, M. X., Saude, E. J., Wang, X., Pearlstone, J. R., Smillie, L. B., and Sykes, B. D. (2002) Kinetic studies of calcium and cardiac troponin I peptide binding to human cardiac troponin C using NMR spectroscopy. *Eur. Biophys. J.* 31, 245–256

27. Yamazaki, T., Yoshida, M., and Nagayama, K. (1993) Complete assignments of magnetic resonances of ribonuclease H from *Escherichia coli* by double- and triple-resonance two- and three-dimensionalNMRspectroscopies. *Biochemistry* 32, 5656–5669

28. Gemmecker, G., Olejniczak, E. T., and Fesik, S. W. (1992) An improved method for selectively observing protons attached to C-12 in the presence of H-1-C-13 spin pairs. *J. Magn. Reson.* 96, 199–204

29. Ogura, K., Terasawa, H., and Inagaki, F. (1996) An improved double-tuned and isotope-filtered pulse scheme based on a pulsed field gradient and a wide-band inversion shaped pulse. *J. Biomol. NMR* 8, 492–498

30. Ikura, M., and Bax, A. (1992) Isotope-filtered 2DNMRof a protein peptide complex-study of a skeletal-muscle myosin light chain kinase fragment bound to calmodulin. *J. Am. Chem. Soc.* 114, 2433–2440

31. Robertson, I. M., Spyracopoulos, L., and Sykes, B. D. (2009) *Biophysics and the Challenges of Emerging Threats,* NATOScience for Peace and Security Series B: Physics and Biophysics (Puglisi, J. D., ed) pp. 101–119, IOS Press, Amsterdam

32. Delaglio, F., Grzesiek, S., Vuister, G. W., Zhu, G., Pfeifer, J., and Bax, A. (1995) NMRPipe. A multidimensional spectral processing system based on UNIX pipes. *J. Biomol. NMR* 6, 277–293

33. Johnson, B. A., and Blevins, R. A. (1994) NMRView–a computer-program for the visualization and analysis ofNMRdata. *J. Biomol.NMR*4, 603–614

34. Slupsky, C. M., Boyko, R. F., Booth, V. K., and Sykes, B. D. (2003) Smart-Notebook. A semi-automated approach to protein sequential NMR resonance assignments. *J. Biomol. NMR* 27, 313–321

35. Baryshnikova, O. K., Williams, T. C., and Sykes, B. D. (2008) Internal pH indicators for biomolecular NMR. *J. Biomol. NMR* 41, 5–7

36. Hoffman, R. M., Li, M. X., and Sykes, B. D. (2005) The binding of W7, an inhibitor of striated muscle contraction, to cardiac troponin C. *Biochemistry* 44, 15750–15759

37. Sia, S. K., Li, M. X., Spyracopoulos, L., Gagne´, S. M., Liu, W., Putkey, J. A., and Sykes, B. D. (1997) Structure of cardiac muscle troponin C unexpectedly reveals a closed regulatory domain. *J. Biol. Chem.* 272, 18216–18221

38. Spyracopoulos, L., Li, M. X., Sia, S. K., Gagne´, S. M., Chandra, M., Solaro, R. J., and Sykes, B. D. (1997) Calcium-induced structural transition in the regulatory domain of human cardiac troponin C. *Biochemistry* 36, 12138–12146

39. Bjornson, M. E., Corson, D. C., and Sykes, B. D. (1985) 13Cand 113Cd NMR studies of the chelation of metal ions by the calcium-binding protein parvalbumin. *J. Inorg. Biochem.* 25, 141–149

40. Nelson, D. J., Theoharides, A. D., Nieburgs, A. C., Murray, R. K., GonzalezFernandez, F., and Brenner, D. S. (1979) C-13 magnetic-resonance study of lanthanide-substituted muscle calcium-binding parvalbumins. *Int. J. Quantum Chem.* 16, 159–174

41. Bundi, A., and Wuthrich, K. (1979) H-1-NMR parameters of the common amino-acid residues measured in aqueous-solutions of the linear tetrapeptides H-Gly-Gly-X-L-Ala-OH. *Biopolymers* 18, 285–297

42. Hagen, R., and Roberts, J. D. (1969) Nuclear magnetic resonance spectroscopy–13C spectra of aliphatic carboxylic acids and carboxylate anions. *J. Am. Chem. Soc.* 91, 4504-4506

43. Horsley, W. J., and Sternlicht, H. (1968) Carbon-13 magnetic resonance studies of amino acids and peptides. *J. Am. Chem. Soc.* 90, 3738–3748

44. Oda, Y., Yamazaki, T., Nagayama, K., Kanaya, S., Kuroda, Y., and Nakamura, H. (1994) Individual ionization constants of all the carboxyl groups in ribonuclease HI from *Escherichia coli* determined by NMR. *Biochemistry* 33, 5275–5284

45. Maciel, G. E., and Natterstad, J. J. (1965) Carbon-13 chemical shifts of carbonyl group. III. Solvent effects. *J. Chem. Phys.* 42, 2752–2759

46. Maciel, G. E., and Traficante, D. D. (1966) Carbon-13 chemical shifts of carbonyl group. IV. Dilution curves for acetic acid in representative solvents. *J. Am. Chem. Soc.* 88, 220–223

47. Markley, J. L. (1975) Observation of histidine residues in proteins by means of nuclear magnetic-resonance spectroscopy. *Acc. Chem. Res.* 8, 70–80

48. Cohen, P., Griffin, J. H., Camier, M., Caizergues, M., Fromageot, P., and Cohen, J. S. (1972) Hormonal interactions at the molecular level. A high resolution proton magnetic resonance study of bovine neurophysins and their interactions with oxytocin. *FEBS Lett.* 25, 282–286

49. Markley, J. L., Williams, M. N., and Jardetzky, O. (1970) Nuclear magnetic resonance studies of the structure and binding sites of enzymes. XII. A conformational equilibrium in staphylococcal nuclease involving a histidine residue. *Proc. Natl. Acad. Sci. U.S.A.* 65, 645–651

50. Martin, S. R., Biekofsky, R. R., Skinner, M. A., Guerrini, R., Salvadori, S., Feeney, J., and Bayley, P. M. (2004) Interaction of calmodulin with the phosphofructokinase target sequence. *FEBS Lett.* 577, 284–288

51. Lee, J. A., and Allen, D. G. (1991) Mechanisms of acute ischemic contractile failure of the heart. Role of intracellular calcium. *J. Clin. Invest.* 88, 361–367

52. Tran, K., Smith, N. P., Loiselle, D. S., and Crampin, E. J. (2010) A metabolite-sensitive, thermodynamically constrained model of cardiac crossbridge cycling. Implications for force development during ischemia. *Biophys. J.* 98, 267–276

53. Allen, D. G., and Orchard, C. H. (1987) Myocardial contractile function during ischemia and hypoxia. *Circ. Res.* 60, 153–168

54. Rees, D. C. (1980) Experimental evaluation of the effective dielectric constant of proteins. *J. Mol. Biol.* 141, 323–326

55. Russell, A. J., Thomas, P. G., and Fersht, A. R. (1987) Electrostatic effects on modification of charged groups in the active site cleft of subtilisin by protein engineering. *J. Mol. Biol.* 193, 803–813

56. Sternberg, M. J., Hayes, F. R., Russell, A. J., Thomas, P. G., and Fersht, A. R. (1987) Prediction of electrostatic effects of engineering of protein charges. *Nature* 330, 86–88

57. Jackson, S. E., and Fersht, A. R. (1993) Contribution of long range electrostatic interactions to the stabilization of the catalytic transition state of the serine protease subtilisin BPN. *Biochemistry* 32, 13909–13916

58. Cederholm, M. T., Stuckey, J. A., Doscher, M. S., and Lee, L. (1991) Histidine p*Ka* shifts accompanying the inactivating Asp-121. Asn substitution in a semisynthetic bovine pancreatic ribonuclease. *Proc. Natl. Acad. Sci. U.S.A.* 88, 8116–8120

59. Sheehan, K. A., Arteaga, G. M., Hinken, A. C., Dias, F. A., Ribeiro, C., Wieczorek, D. F., Solaro, R. J., and Wolska, B. M. (2011) Functional effects of a tropomyosin mutation linked to FHC contribute to maladaptation during acidosis. *J. Mol. Cell. Cardiol.* 50, 442–450

CHAPTER 4

Conformation of the critical pH sensitive region of troponin depends upon a single residue in troponin I

Ian M. Robertson[1,2], Sandra E. Pineda-Sanabria[1],

Peter C. Holmes[1,3], and Brian D. Sykes[1]

[1]Department of Biochemistry, University of Alberta, Edmonton, Alberta, Canada, T6G 2H7. [2]Current Address: Randall Division of Cell and Molecular Biophysics, Guy's Campus, King's College London, London, UK, SE1 1UL. [3]Current Address: Department of Biochemistry, University of Oxford, South Parks Road, Oxford OX1 3QU

To continue unraveling the effects of A162H in the cardiac muscle, this chapter presents the structure of skeletal troponin I bound to cardiac troponin C. The insights gained by examining this structure allow us to unequivocally declare that the conformation of troponin I is independent of the troponin C isoform. It also allow us to propose a model that explains the isoform change of troponin I in the development, and the histidine-to-alanine swap in the evolution, of the heart muscle. A version of this chapter has been previously published: Robertson *et al.* (2014) *Archives of Biochemistry and Biophysics* 552-553:40-49.

Introduction

Muscle contraction is triggered by the thin filament protein complex troponin. Ca^{2+} binding to the "low-affinity" site (site II) of troponin C (TnC) leads to the association of the "switch" domain of troponin I (TnI) with the N-domain of TnC (NTnC) and the removal of the "inhibitory" and C-terminal "mobile" domains of TnI from actin. As TnI dissociates from actin, the orientation of tropomyosin on the actin filament changes, exposing myosin binding sites. Myosin-actin cross-bridges subsequently form and contraction ensues. Muscle relaxation begins with a decrease in cytosolic Ca^{2+} concentration, which leads to the dissociation of Ca^{2+} and the switch region of TnI from NTnC and the inhibitory and mobile domains of TnI binding actin. Subsequent rearrangement of tropomyosin blocks the myosin binding interface and the myosin heads release from actin[1-5].

Structural biology has been instrumental in elucidating the molecular mechanism of contraction regulation by troponin[2]. There have been a large number of structures published on the skeletal and cardiac systems using both Nuclear Magnetic Resonance (NMR) spectroscopy and X-ray crystallography. The first structure of troponin C was of the skeletal variant (sTnC), and it featured a dumbbell shape,

composed of two globular EF-hand domains connected by a helical linker[6]. sTnC has been shown to undergo a large closed-to-open conformational change when Ca^{2+} binds to the N-domain (sNTnC)[7]. The central helical linker of sTnC has been shown to be flexible in solution[8]. The NMR structure of a rhodamine-labelled sNTnC bound to Ca^{2+} and to the switch region of sTnI (sTnI$_{115-131}$) indicated that no major change in sNTnC occurred upon binding sTnI[9]. In the cardiac system, there have also been a number of structures solved. The first structure of Ca^{2+} saturated cardiac troponin C (cTnC) showed that, similar to sTnC, the central linker between the N- and C- domains of cTnC is flexible; however, in contrast with sTnC, the N-domain of cTnC (cNTnC) remains essentially closed in the presence of Ca^{2+} [10, 11]. It was later shown that cNTnC must bind the switch region of TnI (cTnI$_{147-163}$)[1] as well as Ca^{2+} before going through the closed-to-open transition[12], emphasizing the significance of the cNTnC-cTnI$_{147-163}$ interaction in the thermodynamic and kinetic balance that regulates cardiac muscle contraction.

There have been two X-ray crystal structures of the "core" troponin complex published. While the structures are generally similar, they differ in two distinct ways: the conformation of the central helix of TnC (and thus the relative orientations of the sNTnC-sTnI$_{115-131}$ and cNTnC-cTnI$_{147-163}$ regulatory regions), and the conformation of the C-terminus of TnI, a region that is important in regulation[13-17]. In the core structure of the cardiac troponin complex (cTn)[18] the central helix is bent, and for one of the molecules in the asymmetric unit of the crystal, cTnI adopted a long helix beyond the switch region that extended away from cTnC (Figure 4.1a). Although cTnI adopts a helix in the crystal, fluorescence anisotropy has indicated that this region is highly mobile and most likely unstructured[19]. The bent orientation of cNTnC has been used to build a model of the interaction of cNTnC with the cardiac specific N-terminal region of cTnI[20, 21] – a segment that regulates myofilament Ca^{2+}-sensitivity through its phosphorylation by protein kinase A (PKA)[4]. In the crystal structure of the skeletal complex (sTn)[22], the central helix is straight; however, in a different structure of a sTnC-sTnI complex the central helix in sTnC is bent[23], akin to cTnC in the cardiac complex, bringing up the question of whether the quaternary structural differences are real or an artifact of crystal packing. Indeed, *in vitro* NMR dynamics[24, 25] and *in situ* fluorescence studies of sTnC indicate that this central helix is flexible[26, 27]. Moreover, unlike the extended conformation adopted by cTnI, the residues C-terminal to the switch region of sTnI make several contacts with the A-helix of sTnC (Figure 4.1b and e). This difference in conformations has been attributed to H130 of sTnI (A162 in cTnI), which appears to form a salt-bridge with the side chain carboxylate of E20 on sNTnC (E19 in cNTnC). The presence of an interaction between H130 and E20 has been further supported by NMR relaxation and molecular dynamics that have indicated that sTnI does not become flexible until after residue H130 [28, 29].

---

[1] The numbering differences between the cardiac and skeletal isoforms of troponin I is the result of an initial 32 residue segment of cardiac troponin I, not present in either fast or slow skeletal troponin I.
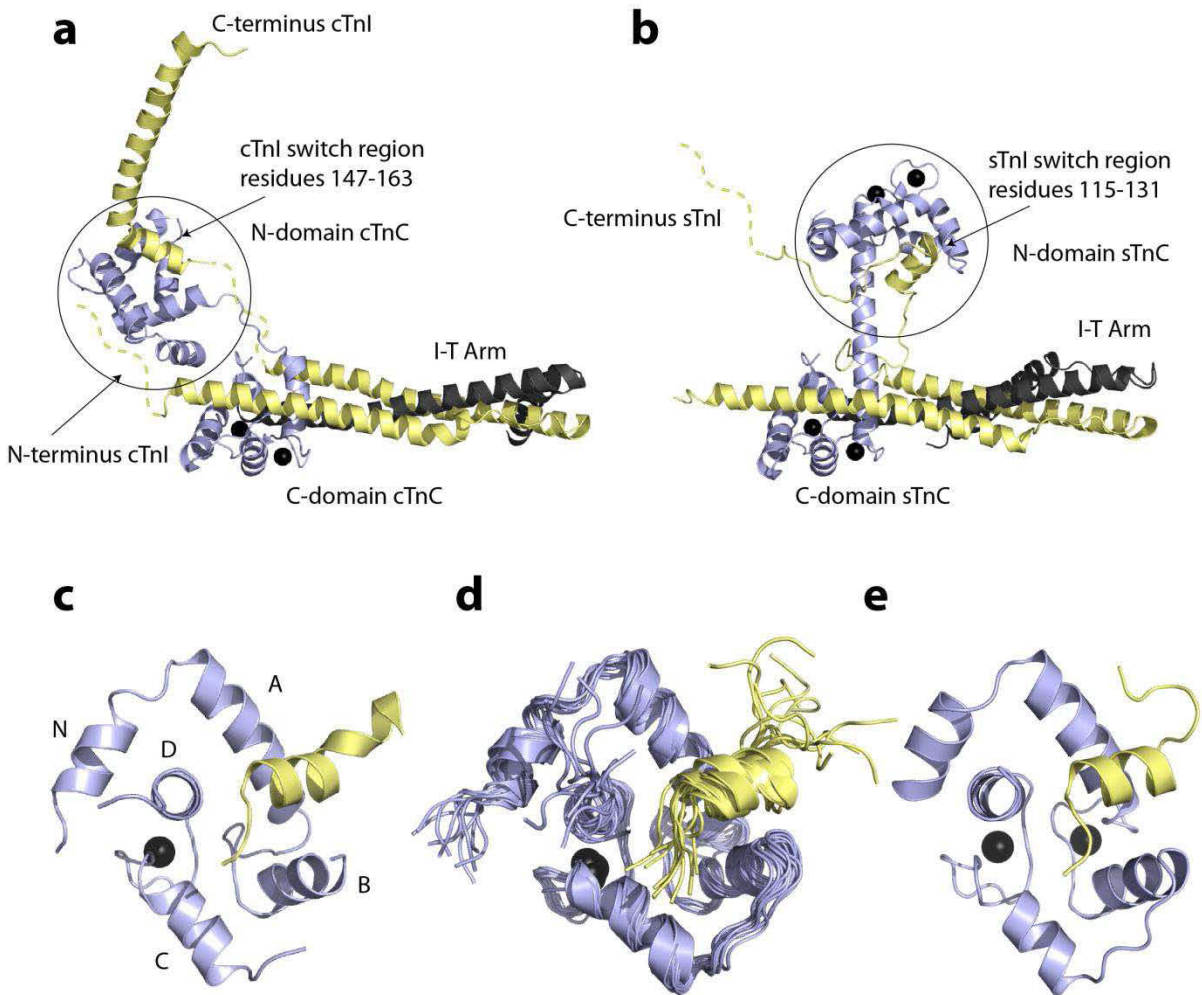
Figure 4.1. Structures of the cardiac and skeletal troponin complexes.

TnC is coloured in light blue, TnI in pale yellow, TnT in dark grey, and Ca^{2+} is represented as black spheres. Dashed lines represent regions of TnI that are either missing in the structure due to motion, or because they were truncated to aid in the crystallization. **a.** The X-ray structure of the core cardiac troponin complex (PDB: 1J1E). **b.** The X-ray structure of the core skeletal troponin complex (PDB: 1YTZ). The regulatory N-domain of TnC and the switch-region of TnI are encircled. **c-e.** The N-domain of TnC and the switch region of TnI looking towards the TnC-TnI interface. **c.** The cNTnC-cTnI$_{147-163}$ complex from the X-ray structure in **a**. The missing structural information of the loop connecting helices B and C were due to motion. **d.** The NMR ensemble (10 lowest energy structures) of cNTnC-cTnI$_{147-163}$ (PDB: 1MXL). **e.** The sNTnC-sTnI$_{115-131}$ complex from the X-ray structure in **b**. The five helices of NTnC (N,A,B,C,D) are labelled in **c**.

During myocardial ischemia, intracellular accumulation of H^+ and other metabolic products due to reduced or absent blood flow to the tissue can produce acidosis. Acidic pH reduces the Ca^{2+} sensitivity of cNTnC, which diminishes the force developed, and is reflected in defective contractions in the first few seconds after occlusion[30, 31]. It has been shown that replacing cTnI with sTnI[32] or slow-skeletal TnI (ssTnI)[33, 34] reduces the ischemic-induced drop in Ca^{2+}-sensitivity. Moreover, if just the C-terminal domain of cTnI (residues 150-211) is replaced by the residues from sTnI (residues 118-182) most of this protection can be accounted for[32]. More recent studies have identified H130 as the principal source of this protection[35, 36]. NMR studies have shown that H130 of sTnI[37] and H162 from cTnI(A162H)[38] form electrostatic interactions with E19 of cNTnC at low pH, which enhances TnI binding. These results suggested that sTnI and cTnI(A162H) bind in a similar fashion; consistent with how sTnI binds sTnC in the X-ray structure of sTn.

In this study we used solution NMR spectroscopy to solve the structure of the sTnI, and model the structure of cTnI(A162H) bound to cNTnC at pH 6. The structure of sTnI is remarkably similar to its structure in sTn. This indicates that the conformation of sTnI is independent of the TnC isoform. NMR structural restraints for cTnI(A162H) also predict a structure more like the structure of sTnI than cTnI. These results add to the structural evidence for an electrostatic interaction made between sTnI or cTnI(A162H) and cNTnC. Taken in unison, the data presented herein indicate that a single residue change can cause TnI to undergo a substantial conformational change when bound to the NTnC. The role of the conformation of cTnI and sTnI is discussed in the context of the differences in regulation of muscle contraction by the different isoforms of TnI.

Experimental procedures

Protein Preparation

Human ^{15}N- and $^{13}C,^{15}N$-cNTnC (wild type) and ^{15}N- and $^{13}C,^{15}N$-cNTnC C35S,C84S proteins were expressed on *E. coli* and purified as described previously[39]. The unlabelled synthetic peptides N-acetyl-RMSADAMLKALLGSKHK-amide (sTnI$_{115-131}$) and N-acetyl-RRVRISADAMMQALLGARHKESLDLRA-amide (cTnI(A162H)$_{144-170}$) were obtained from GL Biochem LTD. Lyophilized protein and sTnI$_{115-131}$ peptide were dissolved in a 1:4 ratio in 100 mM KCl, 10 mM imidazole, 10 mM $CaCl_2$, 0.25 mM 4,4-dimethyl-4-silapentane-1-sulfonate-d_6 sodium salt as an internal NMR standard and 5% D_2O; lyophilized wild type protein and cTnI$_{144-170}$ peptide were dissolved in a 1:4 ratio in the same buffer with an additional 10 mM dithiothreitol to prevent cysteine oxidation. The pH of the NMR samples were set to ~ 6 (using HCl and NaOH). The pH was determined using the ^1H chemical shift of imidazole as an indicator[40].

NMR spectroscopy

All NMR data were collected on either a Varian Inova 500 MHz or Unity 600 MHz spectrometers at 30 °C. The structure of Ca^{2+}-saturated cNTnC-sTnI$_{115-131}$[2] was solved using data collected from the ^{13}C-edited-filtered HMQCNOESY (mixing time = 150 ms) and $^{13}C,^{15}N$-filtered NOESY/TOCSY (mixing time = 200 ms and 60 ms, respectively) experiments[41-43]. The residues on $^{13}C,^{15}N$-cNTnC that made intermolecular NOEs with sTnI$_{115-131}$ were assigned using the CBCACONNH, HNCACB, HCCONH, and CCONH experiments. The processing of all the experiments were done with NMRPipe[44] and assigned using NMRViewJ[45]. ORBplus[46] was used to predict the tertiary structure of cNTnC when bound to sTnI$_{115-131}$ based on the amide chemical shifts of residues from site I (27-40) and site II (64-74).

Structure Calculation

Xplor-NIH was used to calculate the structure of cNTnC-sTnI$_{115-131}$[47, 48]. The protocol followed was modified from [49] to only use NOEs in the structure calculation. Initially, the structures of sTnI$_{115-131}$ were calculated using a simulated annealing protocol. The temperature was slowly cooled from 1000 to 100 K; 24000 high temperature steps and 3000 cooling steps were used. The intramolecular sTnI$_{115-131}$ NOEs were calibrated using the bin method (strong, 2.8 Å; medium, 3.4 Å; and weak, 5.0 Å) with the NOE module in NMRViewJ. The averaging method selected was sum with a soft potential. Dihedral restraints for sTnI$_{115-131}$ were set to helical (ϕ = -60 ± 25°; ψ = -30 ± 25°) using the chemical shift index[50]. The k_{noe} was 50 kcal•mol^{-1}•Å^{-2} and k_{dihed} was 200 kcal•mol^{-1}•rad^{-2}. The lowest energy structure was saved for the rigid docking protocol.

Following the calculation of the structure of sTnI$_{115-131}$ when bound to cNTnC, independent of cNTnC, a rigid minimization of the cNTnC-sTnI$_{115-131}$ complex was done. The structure of cNTnC was from the cNTnC-cTnI$_{147-163}$ structure (with cTnI$_{147-163}$ removed from the structure) PDB: 1MXL[12]. The model with the least number of restraint violations from the ensemble was selected for the rigid docking. In this calculation, intermolecular NOEs between sTnI$_{115-131}$ and cNTnC were used to drive the docking. The NOEs were also calibrated using the bin method (strong, 2.8 Å; medium, 3.4 Å; and weak, 5.0 Å). Because sTnI$_{115-131}$ is expected to bind deep into the hydrophobic groove of cNTnC (as cTnI does), 22 of the intermolecular NOEs were violated (> 0.5 A). This is presumably because the side-chains at the interface were not allowed to rotate. Therefore, following the rigid-docking, a semi-rigid simulated annealing protocol was used[49]. The backbone atoms for cNTnC were kept rigid during the calculation, but the side chains were permitted to rotate. A conformational database potential was used for the side-chain dihedral angles[51]. Since sTnI$_{115-131}$ is relatively flexible and its conformation may change when the intermolecular NOEs with cNTnC were introduced, none of the peptide atoms were

---

[2] Unless otherwise stated, all protein complexes discussed in this study were Ca^{2+}-saturated.

kept rigid. The intraresidue NOEs from the initial structure calculation of $sTnI_{115-131}$ were reintroduced, in addition to the $cNTnC$-$sTnI_{115-131}$ intermolecular NOEs, and the structure of $sTnI_{115-131}$ was recalculated in the presence of cNTnC. The packing of the protein complex was improved by including a potential for the expected radius of gyration for the complex[52]. The final k_{noe} was 60 kcal•mol^{-1}•Å^{-2} and k_{dihed} was 200 kcal•mol^{-1}•rad^{-2}. The ensemble presented in this study represents the 10 lowest energy structures, and none of the models had any NOE violations >0.5 Å nor dihedral violations > 5°. For a detailed description on the semi-rigid annealing calculation see Clore, 2000[49].

Theoretical acid dissociation constant calculation

The webserver H++ [53] was used to predict the pK_a of H130 for the structure of $cNTnC$-$sTnI_{115-131}$. The H130-E19 interaction is at the surface of the protein complex, so a protein dielectric of 10 was chosen for the calculation[53]. The surrounding solvent was given the high dielectric constant of 80. The ionic strength was set to 0.1 M. The pK_a for H130 was calculated for both the lowest energy structure in the ensemble and across the 10 structures in the ensemble. Errors in the pK_a calculation and distance measurements are reported as standard deviations.

Preparation of final model

The structure of the thin filament in the Ca^{2+}-activated state was prepared based on the electron microscopy-based reconstitution[54] of actin[55] and tropomyosin[56]. The orientation of the X-ray structure of the cardiac troponin complex[18] on the thin filament is based on the orientation of the C-domain of sTnC from Knowles *et al.*[27]. The C-terminal extension of TnI was added in PyMOL (http://www.pymol.org/) and its orientation relative the switch region of TnI was randomized using Xplor-NIH[47, 48]. The ensemble of structures for the C-terminal extension generated by Xplor-NIH are meant to indicate its flexibility as shown by NMR and fluorescence anisotropy[19, 28, 29]. The residues that were considered to be flexible were residues 160-211 in the case of the cardiac model and residues 144-182 in the case of the cardiac-skeletal hybrid model. The NMR structure of the N-terminus of cTnI[20] was docked on the X-ray structure of the core troponin complex.

Results

Structure of $sTnI_{115-131}$ when bound to cNTnC

We have previously shown that when $sTnI_{115-131}$ is bound to cNTnC, the pK_a of H130 in $sTnI_{115-131}$ is increased and the pK_a of E19 in cNTnC is reduced, which suggested that the two residues form a salt-bridge[37]. We also found that when H130 is protonated (pH~ 6), $sTnI_{115-131}$ bound tighter to cNTnC than

when it was deprotonated (pH ~ 7.5) – presumably the result of an electrostatic interaction between E19 and H130. In this study, we employed NMR spectroscopy to solve the high-resolution solution structure of sTnI$_{115-131}$ bound to cNTnC at pH 6 to provide structural evidence of this interaction.

The principal experiment used to solve three-dimension structures by NMR spectroscopy is the Nuclear Overhauser Enhancement (NOE) Spectroscopy (NOESY) experiment. The NOE is a correlation made between two protons close in space (<6 Å). Most NOEs observed in a NOESY experiment arise from ^{1}H-^{1}H correlations from the same residue (i, i) or from sequential residues (i, i ± 1). These short-range correlations are useful in assigning the chemical shifts of residues. The observation of longer range NOEs are essential in characterizing the secondary and tertiary structure of proteins[57].

The two-dimensional ^{13}C,^{15}N-filtered ^{1}H-^{1}H NOESY experiment[41, 43] was used to solve the structure of sTnI$_{115-131}$ when bound to ^{13}C,^{15}N-cNTnC. The filtered experiment is designed to remove all ^{1}H-^{1}H NOEs that are either within ^{13}C,^{15}N-cNTnC or between ^{13}C,^{15}N-cNTnC and sTnI$_{115-131}$, thereby measuring only distance contacts within sTnI$_{115-131}$. The assignment of the NOESY was done in tandem with the two-dimensional ^{13}C,^{15}N-filtered ^{1}H-^{1}H total correlation spectroscopy (TOCSY) experiment [41, 43] which only contains intraresidue ^{1}H-^{1}H correlations. With the exception of the histidine imidazole ring protons, none of the other assignments presented in this paper were stereo-specifically assigned; however, for clarity (i.e. for distinguishing between the two terminal δ methyls of a leucine) when presenting the NOES, we labeled them as uniquely assigned. Methyl group protons are labelled with a '#' symbol to indicate that the three protons are indistinguishable.

The region of the ^{13}C,^{15}N-filtered ^{1}H-^{1}H NOESY spectrum shown in figure 2a is especially useful in characterizing the secondary structure of a polypeptide. This so-called "fingerprint" region shows NOEs involving the backbone amide ^{1}H nuclei. The expanded region in figure 2b highlights NOEs that are consistent with an α-helical structure[57], such as those made between the HN of A124 and the Hα of A120 or between the HN of K123 and the Hα nuclei of D119 and A120 (Figure 4.2b,c). The overall ^{1}H-^{1}H NOE patterns observed in sTnI$_{115-131}$ are summarized in Supplementary Figure 4.1, and in general, support an α-helical structure from residues D119 to L125. Another indicator of protein conformation is the chemical shift index, which uses the chemical shifts to predict secondary structure[58, 59]. The Hα NMR chemical shift index[50] for sTnI$_{115-131}$ at 30° C and pH 6 predicted a central α-helix (residues S117-A124). The presence of this α-helix is consistent with the other structures of sTnI$_{115-131}$ bound to sNTnC[9, 22].
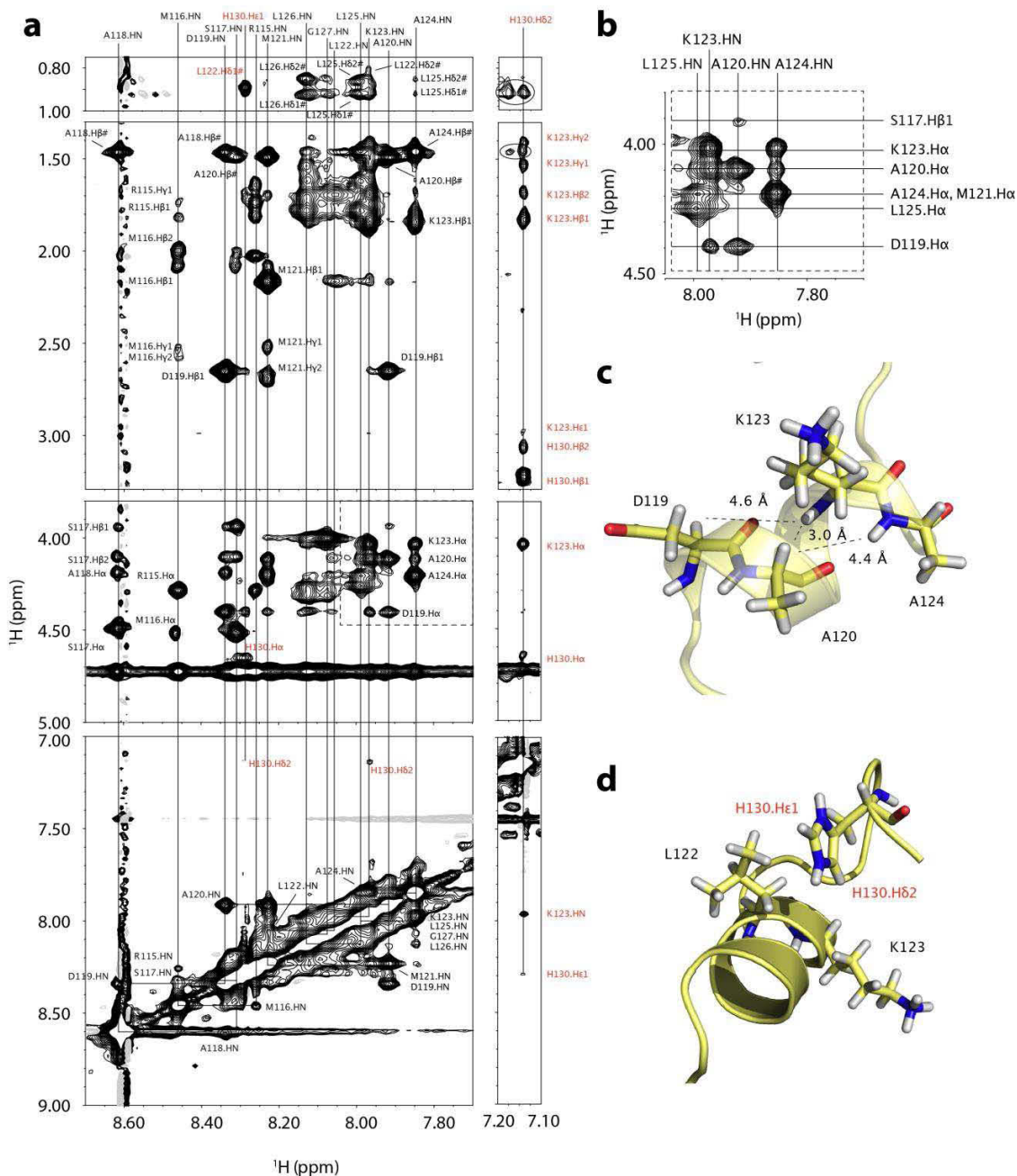
Figure 4.2. Conformation of sTnI$_{115-131}$ when bound to cNTnC.

a. Several sections of the 2D filtered ^{1}H-^{1}H NOESY spectrum of sTnI$_{115-131}$. Peaks that correspond to contacts involving H130 are labelled in red. The signals circled indicate artifacts in the spectrum. **b.** A close up of the region of the NOESY that is boxed off in **a**. **c.** A segment of the structure of sTnI$_{115-131}$ (shown in cartoon and stick representation) highlighting several of the residues that make the NOEs shown in **b**. The helix was made transparent for clarity. **d.** A segment of the structure of sTnI$_{115-131}$ (shown in cartoon and stick representation) depicting the orientation of the imidazole ring of H130, which is determined based on NOEs it makes with L122 and K123 shown in **a**.

The tertiary structure of sTnI$_{115-131}$ was also solved using the ^{13}C,^{15}N-filtered ^{1}H-^{1}H NOESY experiment. In addition to the central α-helix, there were several long-range NOEs between the imidazole ^{1}H signals of H130 and the side-chains of K123 and L122 that indicate a bend in sTnI$_{115-131}$ that brings H130 back over the center of the peptide. Strong NOEs made between Hδ2 and the entire side chain of K123 as well as NOEs between Hε1 of H130 and one of the terminal methyls from L122 position the imidazole ring of H130 in-between both residues (Figure 4.2d). This bent conformation adopted by sTnI$_{115-131}$ is starkly different than both the NMR and X-ray structures of cTnI$_{147-163}$ bound to cNTnC, both of which show A162 sticking out into solution. On the other hand, in the skeletal complex of troponin sTnI makes a very similar type bend just C-terminal to the α-helix that binds the N-domain of sTnC (Figure 4.1e).

Structure of the cNTnC-sTnI$_{115-131}$ complex

We next determined the structure of the cNTnC-sTnI$_{115-131}$ complex to see if we could discern any interaction between H130 and E19 of cNTnC as has been previously postulated[37, 60, 61]. The structure of cNTnC has been determined in a variety of ligand bound states[12, 18, 62-66] and in all of the structures, the conformation of cNTnC remains essentially unchanged[46]. We have recently described a program called ORBplus[46], which compares the backbone ^{1}H,^{15}N chemical shifts of a protein with a database of structures and associated chemical shifts to predict its structure. We assigned the backbone amide chemical shifts of cNTnC bound to sTnI$_{115-131}$ and used ORBplus to contrast its predicted structure to the conformation of cNTnC when bound to cTnI$_{147-163}$.

The global conformation of cNTnC can be described by the interhelical angles between the helices that flank their Ca^{2+}-binding loops (see Figure 4.1c for the labelling of cNTnC helices). ORBplus predicted that the interhelical angle between the A and B helices (AB) is 102.7° and the C helix - D helix (CD) interhelical angle is 93.1°. For the AB prediction, chemical shifts from residues 27-40 were used and for the CD calculation residues 64-74 were chosen, since these residues are indicative of the global conformation of cNTnC[46]. The interhelical angles predicted by ORBplus were very close to those seen in the ensemble of structure of cNTnC-cTnI$_{147-163}$: AB = 102 ± 4° and CD = 95 ± 6°. The interhelical angles were calculated for cNTnC-cTnI$_{147-163}$ with the program interhlx (K. Yap, University of Toronto). We therefore concluded that the structure of cNTnC bound with sTnI$_{115-131}$ is not significantly altered from the cTnI$_{147-163}$ bound state and focused on solving the orientation of sTnI$_{115-131}$ with respect to cNTnC by measuring NOEs between the two molecules.

The NMR experiment used to measure NOEs between an unlabelled ligand, such as sTnI$_{115-131}$ and a labelled target protein, such as ^{13}C,^{15}N-labelled cNTnC, is called the ^{13}C-edited/filtered HMQCNOESY experiment[41, 42]. The only signals observed in the ^{13}C-edited/filtered HMQCNOESY arise

from intermolecular NOEs between an unlabelled ligand and a ^{13}C,^{15}N-labelled protein. A few representative NOEs are shown in Figure 4.3. In total, 54 intermolecular NOEs were assigned between sTnI$_{115-131}$ and cNTnC, a large number of which were between methyl groups. Strong NOEs are observed between the terminal methyl protons of A22 from cNTnC and L126 of sTnI$_{115-131}$ as well as between V44 of cNTnC and L125 and M116 from sTnI$_{115-131}$.
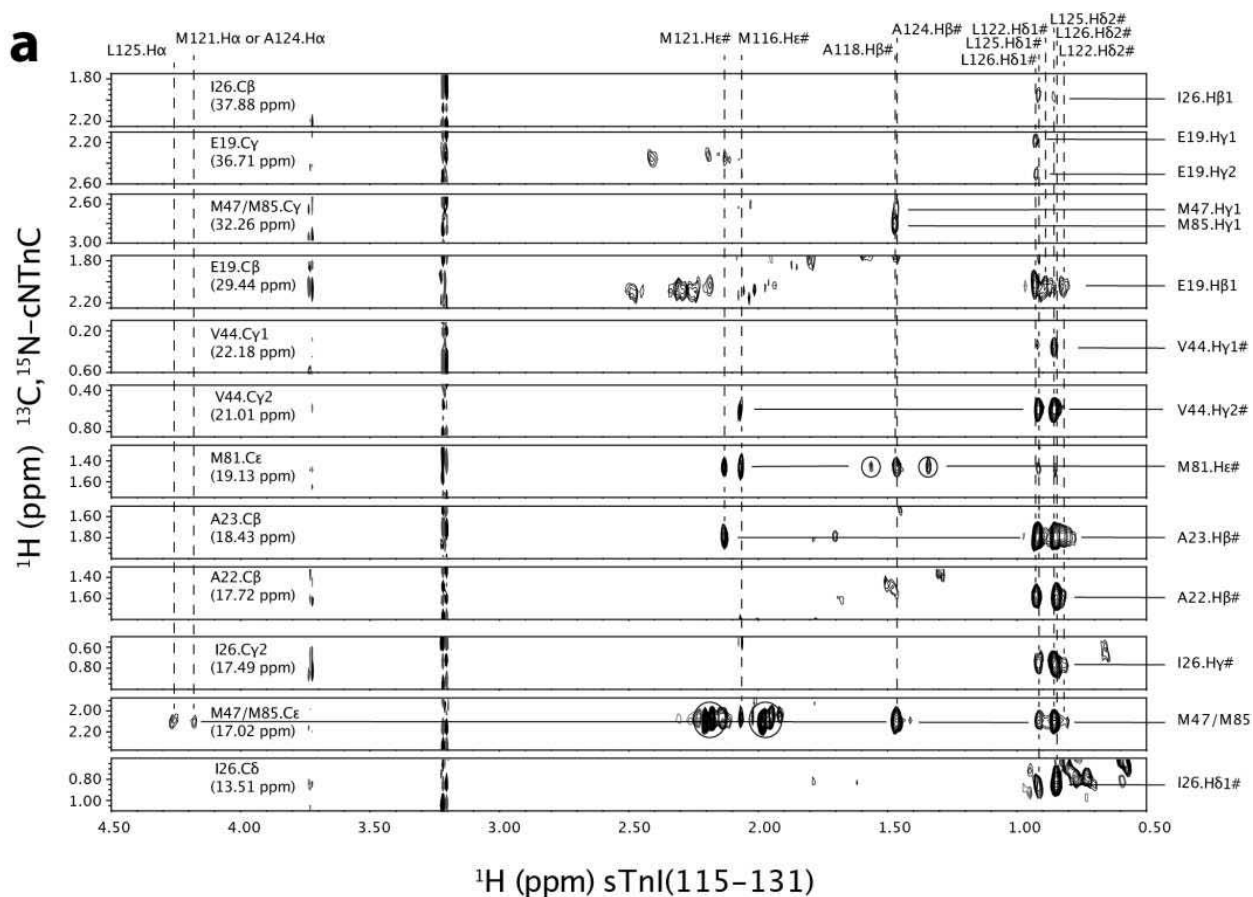
Figure 4.3. Intermolecular NOEs between sTnI$_{115-131}$ and cNTnC.
A selection of intermolecular NOEs made between sTnI$_{115-131}$ and ^{13}C,^{15}N-cNTnC. The ^{13}C planes are labelled on the left and the proton chemical shifts belonging to ^{1}H atoms attached to the ^{13}C nuclei are identified on the right. The assignments from residues on sTnI$_{115-131}$ are listed at the top of the spectra.

To solve the structure of the complex, we performed a semi-rigid docking[49] of sTnI$_{115-131}$ onto cNTnC, where the backbone of cNTnC was kept rigid and its side chains were allowed to rotate. Initially, just the structure of sTnI$_{115-131}$ was solved using the intramolecular NOEs within sTnI$_{115-131}$. Next, the cTnI$_{147-163}$ peptide was removed from the coordinates of the deposited structure of the cNTnC-cTnI$_{147-163}$ complex (PDB: 1MXL) and the structure of sTnI$_{115-131}$ was docked to cNTnC using solely

the intermolecular NOEs between cNTnC and $sTnI_{115-131}$. At this stage, the backbone atoms of both cNTnC and $sTnI_{115-131}$ were kept rigid. Following the rigid docking, a simulated-annealing protocol was performed wherein only the backbone atoms of cNTnC were kept rigid and the structure of $sTnI_{115-131}$ was solved using intramolecular NOEs, intermolecular NOEs between cNTnC and $sTnI_{115-131}$, and dihedral restraints for $sTnI_{115-131}$ from the chemical shift index[50].

The ensemble of the 10 lowest energy structures for the $cNTnC$-$sTnI_{115-131}$ complex is shown in Figure 4.4a. No NOE violations greater than 0.5 Å and no dihedral angles greater than 5° were observed in the ensemble of the 10 lowest energy structures (Supplementary Table 4.1). The ensemble was well-defined with an rmsd of 0.55 ± 0.15 Å for Cα atoms of residues 118-126 and 1.54 ± 0.19 Å for all heavy atoms for resides 118-126. The general orientation of $sTnI_{115-131}$ is unchanged from $cTnI_{147-163}$ (Figure 4.4b,c); however, unlike $cTnI_{147-163}$, the C-terminal end of $sTnI_{115-131}$ turns back on itself, making specific contacts with residues on cNTnC and other residues on $sTnI_{115-131}$. As previously mentioned, this unique feature is more similar to what was observed for sTnI when its bound to sNTnC in the skeletal complex (Figure 4.4d).
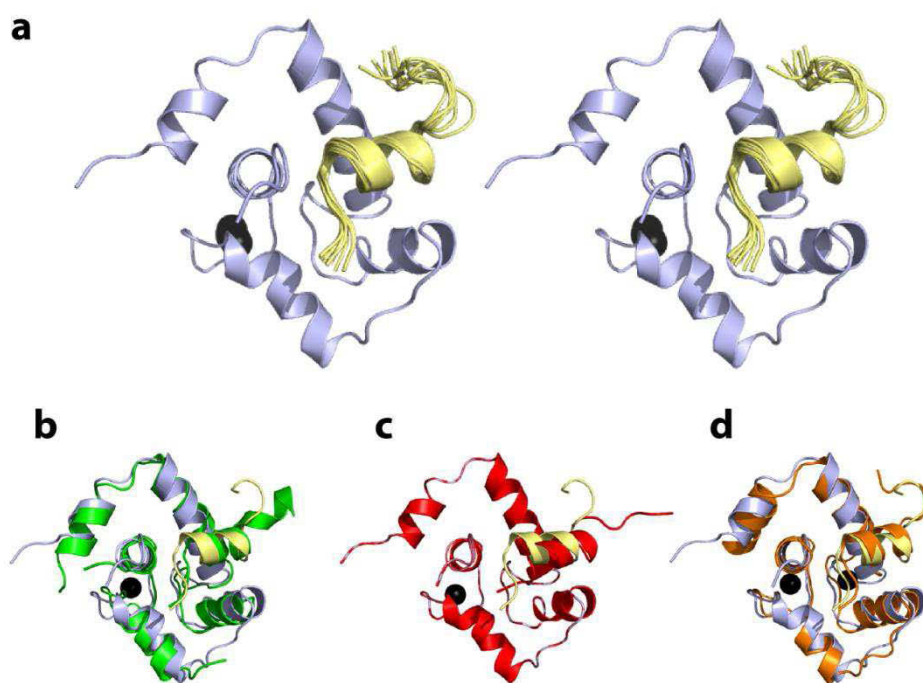
Figure 4.4. Structural comparison of the switch region of TnI in different NTnC-TnI complexes.
a. Stereo-view of the ensemble of 10 lowest energy structures of cNTnC (light blue) bound to $sTnI_{115-131}$ (pale yellow) and Ca^{2+} (black spheres). Overlays of the lowest energy structure of $cNTnC$-$sTnI_{115-131}$ with **b,** $cNTnC$-$cTnI_{147-163}$ (PDB: 1J1E; green), **c,** the lowest energy structure of $cNTnC$-$cTnI_{147-163}$ (PDB: 1MXL; red), and **d** $sNTnC$-$sTnI_{115-131}$ (PDB: 1YTZ; orange).

We also compared the structure of cNTnC-sTnI$_{115-131}$ with the solution structure of the rhodamine labelled sNTnC-sTnI$_{115-131}$[9]. In that structure, the bent conformation of sTnI$_{115-131}$ was not observed (Supplementary Figure 4.2). There are several explanations for this discrepancy: first, the pH at which the sNTnC-sTnI$_{115-131}$ complex structure was solved was 6.8 instead of 6.0 as in our study. Assuming the pK$_a$ of H130 is approximately the same in both the sNTnC-sTnI$_{115-131}$ and cNTnC-sTnI$_{115-131}$ complexes, then roughly only half of the histidine imidazole side chains would be protonated in the sNTnC-sTnI$_{115-131}$ complex[37]. Second, the salt concentration was much higher in sNTnC-sTnI$_{115-131}$ (320 mM KCl) *versus* cNTnC-sTnI$_{115-131}$ (100 mM KCl), which will significantly disrupt the formation of electrostatic interactions[67].

Interaction between H130 and E19 in the cNTnC-sTnI$_{115-131}$ complex

The increase in the acid dissociation constant of H130 from 6.13 ± 0.02 to 6.73 ± 0.17 when sTnI$_{115-131}$ is bound to cNTnC is most likely the result of the formation of a salt-bridge[37]. To provide a structural basis for this observation, the distances between H130 and E19 in the solution structure of the cNTnC-sTnI$_{115-131}$ complex were measured. In the X-ray structure of sTn, the distance between the centre of the carboxyl group of E20 (E19 in cNTnC) of sTnC and the centre of the imidazole ring from H130 of sTnI is 4.9 Å (Figure 4.5a), indicating the potential for an electrostatic interaction between these two residues in solution. On the other hand, in the NMR structure of cNTnC-cTnI$_{147-163}$ (PDB: 1MXL) the Cβ of A162 is 18.8 Å away from E19 (Figure 4.5b) and in the X-ray structure (PDB: 1J1D) it is 11.7 Å away. In the NMR structure of cNTnC-sTnI$_{115-131}$, H130 is 5.8 Å away from E19 (5.1 ± 0.8 Å for the ensemble) (Figure 4.5c). We used the webserver H++ [53] to predict the pK$_a$ of H130 for the structure of cNTnC-sTnI$_{115-131}$. H++ predicted the pK$_a$ of H130 as 6.8 (for the lowest energy structure) and 6.53 ± 1.09 (for the ensemble), which are consistent with the experimental values (6.73 ± 0.17)[37]. This result indicates that as previously hypothesized, the altered pK$_a$ of H130 is due to the formation of a salt-bridge with E19.
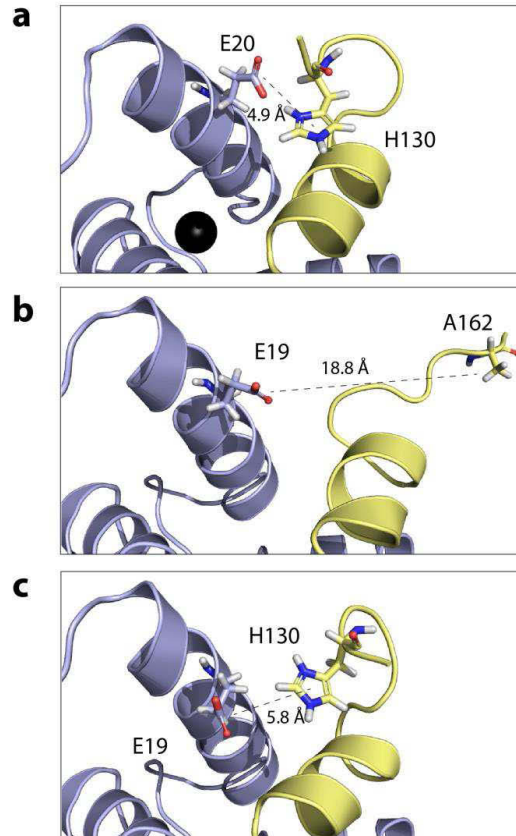
Figure 4.5. Structures of TnC-TnI complexes highlighting the distance between E19/E20 and H130/A162.

TnC is coloured in light blue, TnI in pale yellow and Ca^{2+} is represented as black spheres. **a.** The structure of sTnI$_{115-131}$ bound to sNTnC (PDB: 1YTZ). **b.** The NMR structure of cTnI$_{147-163}$ bound to cNTnC (PDB: 1MXL). **c.** The structure of sTnI$_{115-131}$ bound to cNTnC from this study.

Comparison of the NOEs formed by sTnI$_{115-131}$ and cTnI(A162H)$_{144-170}$

The structure of sTnI$_{115-131}$ bound to cNTnC indicates that the conformation of sTnI$_{115-131}$ is very similar to its structure in the skeletal troponin complex. To investigate whether this is the result of the presence of H130 or the additive effect of a number of amino acid substitutions when compared to cTnI (Figure 4.6a), we measured NOEs for the mutant peptide, cTnI(A162H)$_{144-170}$, bound to cNTnC and contrasted them with the data collected for the sTnI$_{115-131}$-cNTnC complex. It has been shown that mutating A162 to H162 in cTnI prevents the effects of acidosis[36]. We also showed that the pK$_a$ changes for E19 of cNTnC and H162 of cTnI(A162H)$_{144-170}$ indicated an electrostatic interaction between them in a similar way to the skeletal system[38]. By comparing the NOE data for the two complexes containing H130 or H162, the effect of a single amino acid change on TnI's tertiary structure was gauged.

92
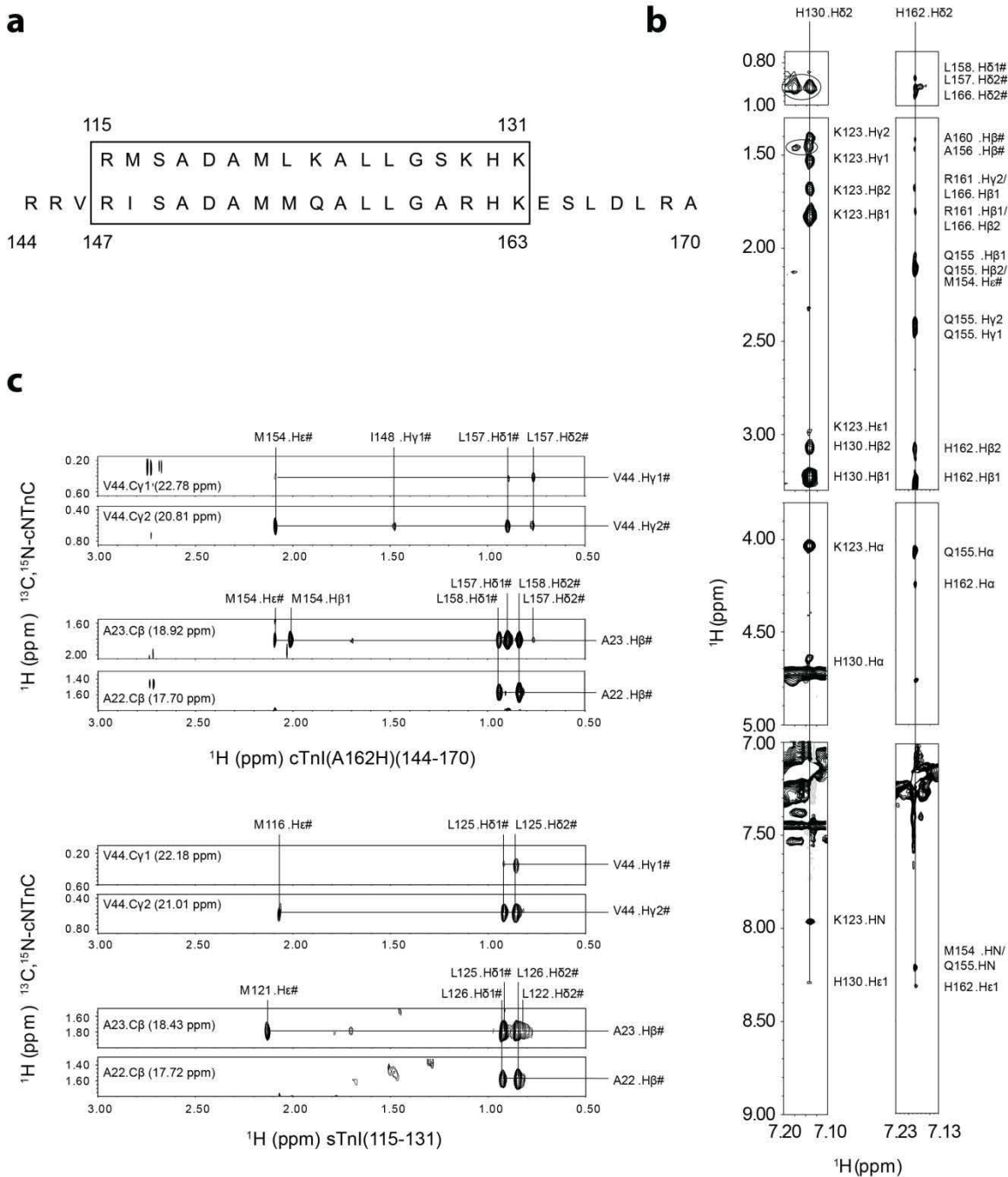
Figure 4.6. Comparison of sequences and intermolecular NOEs for sTnI$_{115-131}$ and cTnI(A162H)$_{144-170}$.
a. The sequences of sTnI$_{115-131}$ and cTnI(A162H)$_{144-170}$. The switch region of TnI is bounded by a box. **b.** A comparison of the intramolecular NOEs made by H130 Hδ2 of sTnI$_{115-131}$ and H162 Hδ2 of cTnI(A162H)$_{144-170}$. Assignments that are ambiguous are separated by a slash. **c.** A selection of the intermolecular NOEs made between cTnI(A162H)$_{144-170}$ and cNTnC (top) or sTnI$_{115-131}$ and cNTnC (bottom).

The chemical shifts of cTnI(A162H)$_{144-170}$ were assigned in the absence and presence of cNTnC to identify key residues that are involved in the interaction with cNTnC. The Hα and HN chemical shifts of the mutant peptide are substantially different in the free and bound states with the largest differences observed in the middle region of the peptide and for Hα of H162 (Supplementary Figure 4.3). The large perturbations at these residues suggest they are in direct contact with cNTnC, or undergo a significant structural change upon binding cNTnC, or both. The Hα NMR chemical shift index[50] for the bound peptide at 30° C and pH 6 predicted the presence of a helix comprising residues S149 to L157. In contrast, the Hα chemical shift index of the free peptide does not display any secondary structure under the same conditions. The central α-helix in cTnI(A162H)$_{144-170}$ is analogous to other cNTnC-cTnI structures[12, 18, 65, 66]. Although the intramolecular NOEs for the bound form of cTnI(A162H)$_{144-170}$ were assigned, only a few contacts characteristic of helical secondary structure were observed due to exchange broadening and the high degree of overlap in the "fingerprint" region of the NMR spectra.

The orientation of H130 in sTnI$_{115-131}$ when bound to cNTnC was largely characterized by NOEs formed between its imidazole ring and the side-chains of L122 and K123. In Figure 4.6b the region of the ^{13}C,^{15}N-filtered NOESY spectrum highlighting NOEs made by Hδ2 is shown. Note that, much like H130 Hδ2, H162 Hδ2 makes a series of long-range NOEs with the side-chain of residue Q155 (K123 in sTnI$_{115-131}$, see Figure 4.6a). It is evident that in order for H162 to make contacts with Q155, the conformation of cTnI(A162H)$_{144-170}$ must be very similar to sTnI$_{115-131}$. Other interresidue contacts with H162 Hδ2 were ambiguously assigned to the neighboring residue R161 Hγ2 and Hβ1 or L166 Hβ1 and Hβ2, L166 Hδ2# or L168 Hδ2#; and unambiguously assigned to L157 Hδ2# and L158 Hδ1#. The Hε1 ring proton of H162 also makes NOEs to L157 Hδ2# and L158 Hδ1# and to L166 or L168 Hγ. In previously published structures of cTnI$_{147-163}$ bound to cNTnC, A162 does not make these same intramolecular NOEs[12, 65, 66] and therefore these data imply that cTnI(A162H)$_{144-170}$ adopts a conformation analogous to sTnI in the skeletal troponin complex[22] or as shown in this work.

We next compared a few of the intermolecular NOEs made between cTnI(A162H)$_{144-170}$ and cNTnC with those made between sTnI$_{115-131}$ and cNTnC (Figure 4.6c). The cNTnC residues V44 (on the B helix), A22 and A23 (both on the A helix) lie in the hydrophobic pocket where TnI binds and therefore NOEs they make are highly indicative of the orientation of TnI. In the complex of cNTnC-cTnI(A162H)$_{144-170}$, V44 Hγ1# makes NOEs with L157 Hδ1# and L157 Hδ2#, and V44 Hγ2# makes NOEs with L157 Hδ1#, L157 Hδ2#, M154 Hε#, and I148 Hγ1#. When compared with sTnI$_{115-131}$ we note analogous NOEs: L125 Hδ1#, L125 Hδ2# (L157 in cTnI) and M116 Hε# (I148 in cTnI). No NOEs between L122 Hδ1# or Hδ2# and V44 Hγ2# were observed, which would be analogous to the NOE made with M154 Hε#. This is not surprising since the side chain of a methionine can easily adopt a different conformation than a leucine. A22 Hβ# and A23 Hβ# from cNTnC make analogous NOEs with cTnI(A162H)$_{144-170}$ and sTnI$_{115-131}$. Some distinct intermolecular NOEs were observed that are not consistent with X-ray structure of

cardiac troponin. Residues S165, L166 and L168 at the C-terminal region of cTnI(A162H)$_{144-170}$ contacted residues T13 and E19 on the N-terminal side of helix A, and M85 on helix D of cNTnC. These NOEs would position the post-helical part of cTnI(A162H)$_{144-170}$ in the space between the switch peptide helix and the A helix of cNTnC, and in combination with the other intermolecular NOEs indicate cTnI(A162H)$_{144-170}$ is in a similar orientation as sTnI is in the skeletal complex.

It was previously shown that the substitution of A162 with H162 in the cardiac switch peptide causes a substantial increase in affinity for cNTnC at pH 6 due to the formation of a new salt bridge between H162 and E19 or E15 in cNTnC[38], for this reason a curved conformation for the mutant switch peptide was expected but not confirmed since electrostatic interactions may span long distances. The introduction of H162 in the cardiac switch peptide may drive the switch peptide towards E15 and E19 by electrostatic attraction, positioning other residues in a favorable orientation to interact with residues in helix A and D of cNTnC stabilizing the mutant switch peptide in the curved conformation observed for sTnI$_{115-131}$.

Discussion

In this study, the structure of sTnI$_{115-131}$ bound to cNTnC at pH 6 has been solved by NMR spectroscopy. Overall, the structure of sTnI$_{115-131}$ was not different than either the cardiac switch region[12, 18] or the switch region in other skeletal structures[9, 22]. Analogous to the other structures, sTnI$_{115-131}$ contained a central α-helix and was found to bind in the hydrophobic cleft of cNTnC. In the cardiac troponin structures the C-terminal region of cTnI is unstructured immediately following the switch helix[12, 19], or in the case of one of the molecules in the asymmetric unit of the crystal structure, adopts long helix that extends away from cTnC[18]. In contrast to the extended, unstructured, conformation of cTnI, the C-terminus of sTnI bends back over the switch helix and makes a series of contacts with itself and with the A helix of sTnC before extending into solution[22]. In the structure presented in this study, residues 126-131 of sTnI$_{115-131}$ adopted a conformation much more similar to that observed in the crystal structure of sTn. The consistency in the structure of sTnI between the X-ray structure of sTn and the NMR structure in this study suggests that the unique conformation of sTnI is not dependent on the isoform of TnC.

Cytosolic acidosis occurs during myocardial ischemia, and leads to a decrease in Ca^{2+}-sensitivity. The replacement of cTnI with either sTnI or ssTnI leads to a reversal in the decreased sensitivity at low pH[32-34]. This reversal in Ca^{2+}-sensitivity has been localized to the C-terminus of sTnI[32], specifically at H130[35, 36]. In a recent NMR study[37], we showed that when sTnI$_{115-131}$ is bound to cNTnC the pK$_a$ of H130 is elevated which is indicative of the formation of a salt-bridge. In the X-ray structure of sTn, H130 comes in close contact with E20 on sTnC (4.9 Å between the center of the histidine ring

and the center of the carboxyl group), and this suggests that the change in pK_a of H130 in the study with $sTnI_{115-131}$ bound to cNTnC is the result of a similar interaction with E19 on cTnC. Indeed, in the structure of $cNTnC-sTnI_{115-131}$, we found that the average distance between H130 and E19 was 5.1 ± 0.8 Å. Furthermore, the theoretical predication of the pK_a of H130 (6.8 for the lowest energy structure and 6.53 ± 1.09 over the ensemble of structures) is within the range measured by NMR (6.73 ± 0.17).

The structure of $sTnI_{115-131}$ bound to cNTnC suggests that the bent structure it adopts is the result of the salt-bridge between E19 and H130. In order to further investigate the role of this histidine in TnI, we also measured structural restraints for cTnI(A162H). Palpant *et al.*[61] used molecular dynamics to assess the structural effect of replacing A162 with a protonated histidine. They found that in one of the five simulations they ran, H162 was close enough to E19 to form a salt-bridge. They did not see the same effect with the wild-type cTnI or with a deprotonated histidine. They also predicted the pK_a of H162 to be increased in the presence of cNTnC. In a more recent study[38], the pK_a of H162 on cTnI(A162H) was measured experimentally by NMR spectroscopy and indeed was found to be increased in the presence of cNTnC. The pK_a of E19 was also perturbed by H162, which suggests that it is the primary residue involved in forming an electrostatic interaction with H162. The consistent structural data between $cTnI(A162H)_{144-170}$ and $sTnI_{115-131}$observed in this study strongly suggests that both peptides bind cNTnC in a similar manner and that their binding mode is primarily the result of a salt-bridge formed between E19 and H162 or H130, respectively.

Given the beneficial nature of the histidine in the switch region of TnI in protection against acidosis, it is odd that the cardiac isoform of TnI would have evolved to lose this residue. Shaffer and Gillis[68] noted that cellular acidosis is only present in adult cardiac tissue under extreme conditions such as ischemia, and that the histidine-containing isoforms of TnI are indeed expressed in muscle prone to acidic conditions (for example, in skeletal muscle sTnI is expressed and in neonatal hearts[69] ssTnI is expressed instead of cTnI[33]). In this section, we rationalize the replacement of the histidine with alanine, the concomitant increase in the mobility of the C-terminus of the switch region, and the 'bent' conformation of cNTnC and its interaction with N-terminus of cTnI, all in the context of the topology of the mobile domain of cTnI and its role in regulation.

Over the course of the evolution of cTnI, a number of major modifications occurred. First, the ability to regulate muscle contraction by phosphorylation at residues S22 and S23 in the N-terminus of cTnI[70] appeared after the divergence of the fishes, but before that of amphibians[68]. Phylogenetic analyses of TnI[60, 68, 71] also indicated that another major change in cTnI was the replacement of H162 with alanine in all eutherian mammals. Two other amino acids, valine and asparagine, were replaced by glutamate (residue 164) and a histidine (residue 172) in cTnI. These residues have also been implicated in the reduction of cardiac myofilament Ca^{2+}-sensitivity[72]. Given that phosphorylation at S22

and S23 is also known to decrease Ca^{2+}-sensitivity, it is likely that in addition to a greater control over contractility, a reduction in Ca^{2+}-sensitivity were the aim with these modifications. It has been postulated that phosphorylation of cTnI regulates the Ca^{2+}-sensitivity of contraction through its interaction with cNTnC[20, 21, 73-75]. In order for the N-terminus of cTnI to interact with cNTnC, the central helix between the two domains of cTnC must be bent – akin to that observed in the crystal structure of cTn (Figure 4.1a). Recently, the structure and orientation of sTnC in muscle fibers has been determined by fluorescence for *in situ* structure determination (FISS)[27]. We have aligned the C-terminus of the crystal structure of cTn with C-terminus of sTn as determined by FISS (Figure 4.7) to investigate how a change in the orientation of the C-terminus of cTnI from the cardiac to the skeletal conformation would affect the location of the mobile domain with respect to the thin filament.
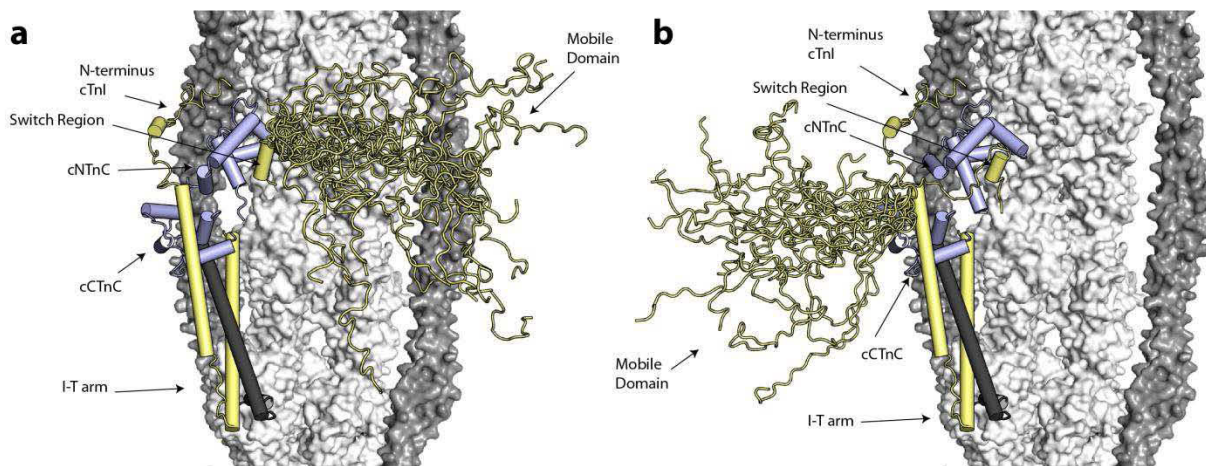
Figure 4.7. Model of the orientation of the C-terminus of TnI as a function of the conformation of the switch-region.

Comparison of the orientation of the C-terminus of TnI in the troponin complex relative to the actin (white surface)-tropomyosin (grey surface) thin filament when the conformation of the switch region of cTnI is **a.** the same as in the X-ray structure of the cardiac complex (PDB: 1J1D) or **b.** in the orientation observed for sTnI or cTnI(A164H). For the orientation in b, the I-T arm and the C-domain of cTnC are from the core cardiac troponin complex, whereas sNTnC and the C-domain of sTnI are from the core skeletal troponin complex (PDB: 1YTZ) where sNTnC is aligned to cNTnC. In order to convey the flexibility of the C-terminal mobile domain, it is represented as an ensemble of 20 structures. To simplify the diagram, helices are shown as cylinders, otherwise the layout and coloring scheme for troponin is the same as in Figure 4.1.

The C-terminus of TnI is required for its full inhibitory effect on muscle contraction[13-16]. This inhibition of contraction involves the interaction of the mobile domain of TnI with actin. Since NMR, molecular dynamics, and fluorescence anisotropy experiments have indicated that the mobile domain

is dynamic in the Ca^{2+}-activated state[19, 28, 29], and therefore may use a fly-casting mechanism as a means of binding with actin and thereby regulating contraction[24], we have depicted it as a flexible extension in Figure 4.7. When the N-terminus of cTnC is in an orientation so that it can interact with the N-terminus of cTnI, the C-terminus of cTnI is in a conformation making it possible to interact with actin. However, if the C-terminus of TnI is in the same conformation as observed in this study for sTnI and cTnI(A162H), the C-terminus is no longer in an orientation primed for an interaction with actin. Therefore, when TnI contains a protonated histidine in place of A162, in addition to the enhanced binding of cTnI to cNTnC through the formation of an electrostatic interaction with E19, the *in vivo* Ca^{2+}-sensitization observed for A162H may be the result of a movement of the mobile domain further from actin. It is important to emphasize, that it is known that in addition to the mobility of TnI, TnC is also known to be flexible[8, 10, 29], and therefore the conformation of cTnC depicted in Figure 4.7 most likely represents only one conformation it adopts in the fiber.

Acknowledgements

Supplementary figures and tables
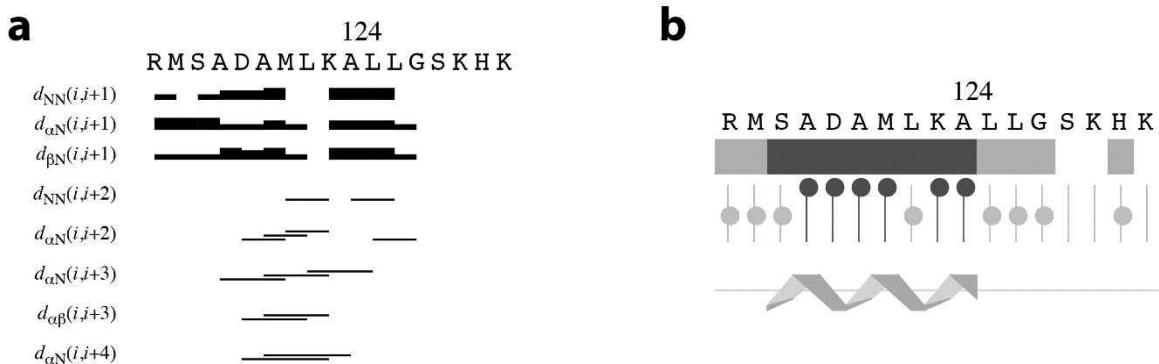
Supplementary Figure 4.1. Secondary structure of sTnI$_{115-131}$.
a. The ^{1}H-^{1}H NOEs made within sTnI$_{115-131}$. The bar charts represent strength of NOEs between nuclei according to how they were binned (2.8 Å, tallest; 3.4 Å, medium height; and 5 Å, shortest). Furthermore, the d$_{\alpha N}$(i, i+3), d$_{\alpha N}$(i, i+4), and d$_{\alpha\beta}$(i, i+3) NOEs in the center of the sequence (*ca.* residues A118-L125) are indicative of an α-helical structure. **b.** The secondary structure predicted using the chemical shift index.
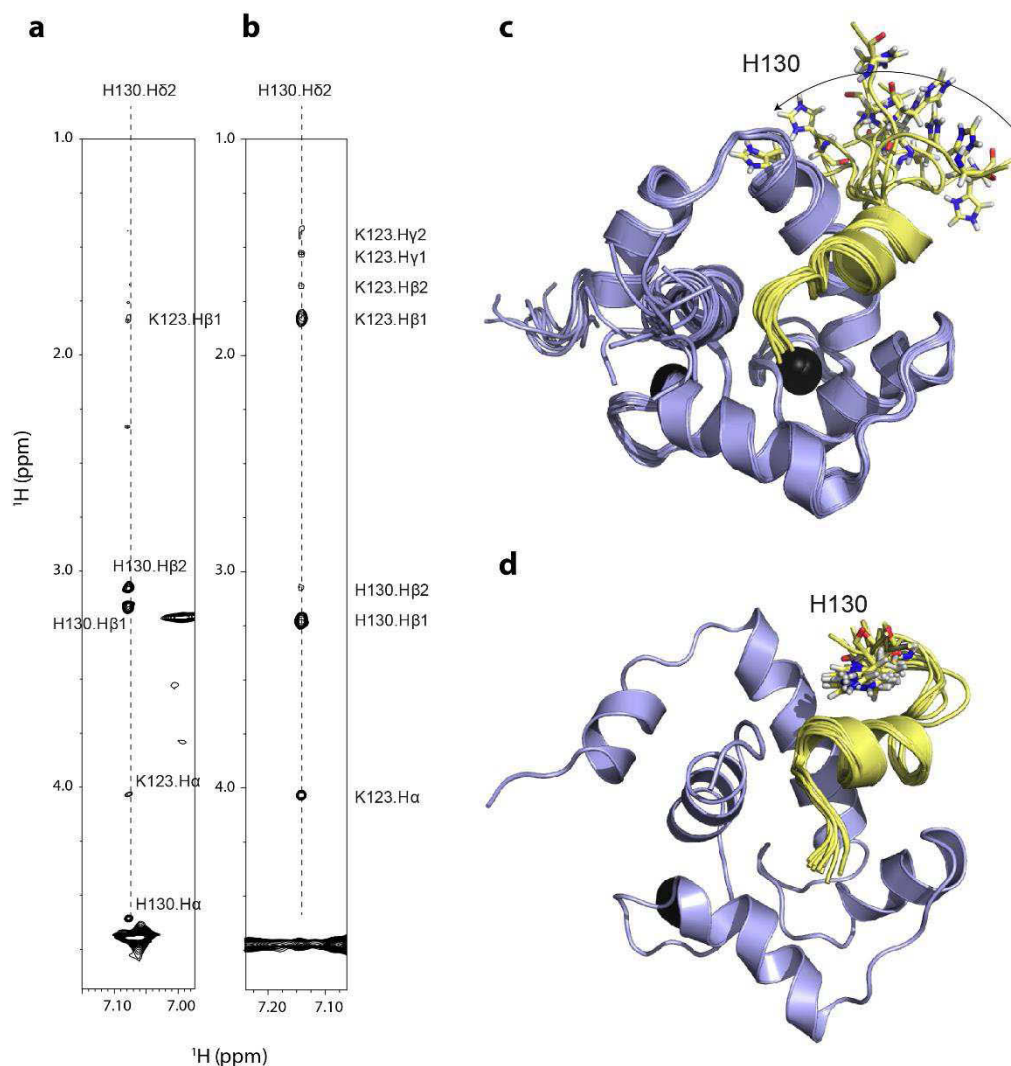
Supplementary Figure 4.2. Comparison of the NOEs and structures of sNTnC-sTnI$_{115-131}$ and cNTnC-sTnI$_{115-131}$.

a. NOEs made by H130 Hδ2 of sTnI$_{115-131}$ when in complex with sNTnC[9]. **b.** NOEs made by H130 Hδ2 of sTnI$_{115-131}$ when in complex with cNTnC (this work). Cartoon representations of the ensembles of 10 lowest energy structures of **c.** sNTnC-sTnI$_{115-131}$ (PDB: 1NPQ) and **d.** cNTnC-sTnI$_{115-131}$. The side chain of H130 is shown in stick representation to highlight the differences in its flexibility between the two complexes. H130 is much more disordered in sNTnC-sTnI$_{115-131}$ than in cNTnC-sTnI$_{115-131}$; a result of the lack of intramolecular NOEs. The disorder difference between the structures at H130 is also evidenced by the differences in intraresidue NOEs. In the sNTnC-sTnI$_{115-131}$ complex (**a**), the equally intense Hδ2-Hβ1 and Hδ2-Hβ2 NOEs means that both ß-protons are an equal distance from Hδ2, which is consistent with a flexible imidazole ring. The different intensities observed for the same intraresidue NOEs in the cNTnC-sTnI$_{115-131}$ complex (**b**) indicates that the imidazole ring is fixed in a position such that one of its ß-protons is closer than the other to Hδ2. Color scheme is the same as Figure 4.1
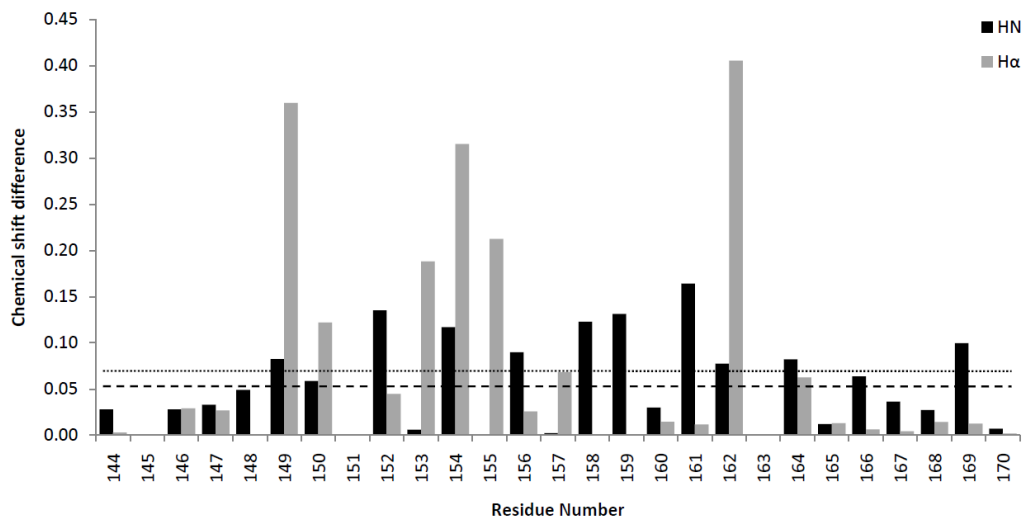
Supplementary Figure 4.3. Chemical shift perturbation of the HN and Hα resonances of the cTnI$_{144-170}$ A162H upon binding to cNTnC.

The average perturbation in ppm for the HN and Hα resonances are indicated with a dashed and dotted line respectively.

Supplementary Table 4.1. Restraints and statistics for the structure calculation of cNTnC·sTnI$_{115-131}$

Distance restraints	274
Total intramolecular sTnI$_{115-131}$ NOEs	220
intra residue (j-i = 0)	99
sequential (j-i = 1)	65
medium range (j-i = 2)	9
medium range (j-i = 3)	17
medium range (j-i = 4)	16
long range (j-i >= 5)	14
total intermolecular NOEs	54
Dihedrals restraints (ψ,ϕ)	13
Restraint violations	
distance > 0.5 Å	0
dihedral > 5°	0
RMSD (Å)[1]	
Cα atoms	0.55 ± 0.15
heavy atoms	1.54 ± 0.19
(ψ,ϕ) in most favoured regions[2]	98%
(ψ,ϕ) in less favoured regions[2]	2%
(ψ,ϕ) in disallowed regions[2]	0%

[1]Residues 118-126 in the α-helix. Structures were aligned to the backbone of cNTnC and then rmsd was measured for the α-helix of sTnI$_{115-131}$ as compared to the lowest energy structure in the ensemble.
[2]PROCHECK[76] was used to characterize the backbone dihedral angle distribution. Distribution calculated for the ordered residues (residues 116-125) as identified by the protein structure validation suite (PSVS) (http://psvs-1_4-dev.nesg.org/).

References

1. Gordon, A. M., Homsher, E., and Regnier, M. (2000) Regulation of contraction in striated muscle, *Physiol. Rev.80*, 853-924.
2. Li, M. X., Wang, X., and Sykes, B. D. (2004) Structural based insights into the role of troponin in cardiac muscle pathophysiology, *J. Muscle Res. Cell Motil.25*, 559-579.
3. Parmacek, M. S., and Solaro, R. J. (2004) Biology of the troponin complex in cardiac myocytes, *Prog. Cardiovasc. Dis.47*, 159-176.
4. Solaro, R. J., and Kobayashi, T. (2011) Protein phosphorylation and signal transduction in cardiac thin filaments, *J. Biol. Chem.286*, 9935-9940.
5. Kobayashi, T., Jin, L., and de Tombe, P. P. (2008) Cardiac thin filament regulation, *Pflugers Archiv-European Journal of Physiology457*, 37-46.
6. Herzberg, O., and James, M. N. G. (1985) Structure of the Calcium Regulatory Muscle Protein Troponin-C at 2.8-a Resolution, *Nature313*, 653-659.
7. Gagne, S. M., Tsuda, S., Li, M. X., Smillie, L. B., and Sykes, B. D. (1995) Structures of the troponin C regulatory domains in the apo and calcium-saturated states, *Nat. Struct. Biol.2*, 784-789.
8. Slupsky, C. M., Boyko, R. F., Booth, V. K., and Sykes, B. D. (2003) Smartnotebook: A semi-automated approach to protein sequential NMR resonance assignments, *J. Biomol. NMR27*, 313-321.
9. Mercier, P., Ferguson, R. E., Irving, M., Corrie, J. E. T., Trentham, D. R., and Sykes, B. D. (2003) NMR structure of a bifunctional rhodamine labeled N-domain of troponin C complexed with the regulatory "switch" peptide from troponin I: Implications for in situ fluorescence studies in muscle fibers, *Biochemistry42*, 4333-4348.
10. Sia, S. K., Li, M. X., Spyracopoulos, L., Gagne, S. M., Liu, W., Putkey, J. A., and Sykes, B. D. (1997) Structure of cardiac muscle troponin C unexpectedly reveals a closed regulatory domain, *J. Biol. Chem.272*, 18216-18221.
11. Spyracopoulos, L., Li, M. X., Sia, S. K., Gagne, S. M., Chandra, M., Solaro, R. J., and Sykes, B. D. (1997) Calcium-induced structural transition in the regulatory domain of human cardiac troponin C, *Biochemistry36*, 12138-12146.
12. Li, M. X., Spyracopoulos, L., and Sykes, B. D. (1999) Binding of cardiac troponin-I147-163 induces a structural opening in human cardiac troponin-C, *Biochemistry38*, 8289-8298.
13. Farah, C. S., Miyamoto, C. A., Ramos, C. H. I., Dasilva, A. C. R., Quaggio, R. B., Fujimori, K., Smillie, L. B., and Reinach, F. C. (1994) Structural and Regulatory Functions of the Nh2- and Cooh-Terminal Regions of Skeletal-Muscle Troponin-I, *J. Biol. Chem.269*, 5230-5240.
14. Ramos, C. H. I. (1999) Mapping subdomains in the C-terminal region of troponin I involved in its binding to troponin C and to thin filament, *J. Biol. Chem.274*, 18189-18195.

15. Rarick, H. M., Tu, X. H., Solaro, R. J., and Martin, A. F. (1997) The C terminus of cardiac troponin I is essential for full inhibitory activity and Ca2+ sensitivity of rat myofibrils, *J. Biol. Chem.272*, 26887-26892.

16. Tripet, B., VanEyk, J. E., and Hodges, R. S. (1997) Mapping of a second actin tropomyosin and a second troponin C binding site within the C terminus of troponin I, and their importance in the Ca2+-dependent regulation of muscle contraction, *J. Mol. Biol.271*, 728-750.

17. Galinska, A., Hatch, V., Craig, R., Murphy, A. M., Van Eyk, J. E., Wang, C. L. A., Lehman, W., and Foster, D. B. (2010) The C Terminus of Cardiac Troponin I Stabilizes the Ca2+-Activated State of Tropomyosin on Actin Filaments, *Circ. Res.106*, 705-U148.

18. Takeda, S., Yamashita, A., Maeda, K., and Maeda, Y. (2003) Structure of the core domain of human cardiac troponin in the Ca(2+)-saturated form, *Nature424*, 35-41.

19. Zhou, Z. Q., Li, K. L., Rieck, D., Ouyang, Y. X., Chandra, M., and Dong, W. J. (2012) Structural Dynamics of C-domain of Cardiac Troponin I Protein in Reconstituted Thin Filament, *J. Biol. Chem.287*, 7661-7674.

20. Howarth, J. W., Meller, J., Solaro, R. J., Trewhella, J., and Rosevear, P. R. (2007) Phosphorylation-dependent conformational transition of the cardiac specific N-extension of troponin I in cardiac troponin, *J. Mol. Biol.373*, 706-722.

21. Warren, C. M., Kobayashi, T., and Solaro, R. J. (2009) Sites of Intra- and Intermolecular Cross-linking of the N-terminal Extension of Troponin I in Human Cardiac Whole Troponin Complex, *J. Biol. Chem.284*, 14258-14266.

22. Vinogradova, M. V., Stone, D. B., Malanina, G. G., Karatzaferi, C., Cooke, R., Mendelson, R. A., and Fletterick, R. J. (2005) Ca(2+)-regulated structural changes in troponin, *Proc. Natl. Acad. Sci. U. S. A.102*, 5038-5043.

23. Vassylyev, D. G., Takeda, S., Wakatsuki, S., Maeda, K., and Maeda, Y. (1998) Crystal structure of troponin C in complex with troponin I fragment at 2.3-angstrom resolution, *Proc. Natl. Acad. Sci. U. S. A.95*, 4847-4852.

24. Hoffman, R. M., Blumenschein, T. M., and Sykes, B. D. (2006) An interplay between protein disorder and structure confers the Ca2+ regulation of striated muscle, *J. Mol. Biol.361*, 625-633.

25. Blumenschein, T. M., Stone, D. B., Fletterick, R. J., Mendelson, R. A., and Sykes, B. D. (2005) Calcium-dependent changes in the flexibility of the regulatory domain of troponin C in the troponin complex, *J. Biol. Chem.280*, 21924-21932.

26. Ferguson, R. E., Sun, Y. B., Mercier, P., Brack, A. S., Sykes, B. D., Corrie, J. E. T., Trentham, D. R., and Irving, M. (2003) In situ orientations of protein domains: Troponin C in skeletal muscle fibers, *Mol. Cell11*, 865-874.

27. Knowles, A. C., Irving, M., and Sun, Y. B. (2012) Conformation of the troponin core complex in the thin filaments of skeletal muscle during relaxation and active contraction, *J. Mol. Biol.421*, 125-137.

28. Julien, O., Mercier, P., Allen, C. N., Fisette, O., Ramos, C. H. I., Lague, P., Blumenschein, T. M. A., and Sykes, B. D. (2011) Is there nascent structure in the intrinsically disordered region of troponin I?, *Proteins-Structure Function and Bioinformatics79*, 1240-1250.

29. Blumenschein, T. M. A., Stone, D. B., Fletterick, R. J., Mendelson, R. A., and Sykes, B. D. (2006) Dynamics of the C-terminal region of TnI in the troponin complex in solution, *Biophys. J.90*, 2436-2444.

30. Lee, J. A., and Allen, D. G. (1991) Mechanisms of Acute Ischemic Contractile Failure of the Heart - Role of Intracellular Calcium, *J. Clin. Invest.88*, 361-367.

31. Jennings, R. B., and Reimer, K. A. (1991) The Cell Biology of Acute Myocardial-Ischemia, *Annu. Rev. Med.42*, 225-246.

32. Li, G., Martin, A. F., and Solaro, J. R. (2001) Localization of regions of troponin I important in deactivation of cardiac myofilaments by acidic pH, *J. Mol. Cell. Cardiol.33*, 1309-1320.

33. Westfall, M. V., Rust, E. M., and Metzger, J. M. (1997) Slow skeletal troponin I gene transfer, expression, and myofilament incorporation enhances adult cardiac myocyte contractile function, *Proc. Natl. Acad. Sci. U. S. A.94*, 5444-5449.

34. Wolska, B. M., Vijayan, K., Arteaga, G. M., Konhilas, J. P., Phillips, R. M., Kim, R., Naya, T., Leiden, J. M., Martin, A. F., de Tombe, P. P., and Solaro, R. J. (2001) Expression of slow skeletal troponin I in adult transgenic mouse heart muscle reduces the force decline observed during acidic conditions, *Journal of Physiology-London536*, 863-870.

35. Dargis, R., Pearlstone, J. R., Barrette-Ng, I., Edwards, H., and Smillie, L. B. (2002) Single mutation (A162H) in human cardiac troponin I corrects acid pH sensitivity of Ca2+-regulated actomyosin S1 ATPase, *J. Biol. Chem.277*, 34662-34665.

36. Day, S. M., Westfall, M. V., Fomicheva, E. V., Hoyer, K., Yasuda, S., La Cross, N. C., D'Alecy, L. G., Ingwall, J. S., and Metzger, J. M. (2006) Histidine button engineered into cardiac troponin I protects the ischemic and failing heart, *Nat. Med.12*, 181-189.

37. Robertson, I. M., Holmes, P. C., Li, M. X., Pineda-Sanabria, S. E., Baryshnikova, O. K., and Sykes, B. D. (2012) Elucidation of Isoform-dependent pH Sensitivity of Troponin I by NMR Spectroscopy, *J. Biol. Chem.287*, 4996-5007.

38. Pineda-Sanabria, S. E., Robertson, I. M., Li, M. X., and Sykes, B. D. (2013) Interaction between the regulatory domain of cardiac troponin C and the acidosis-resistant cardiac troponin I A162H, *Cardiovasc. Res.97*, 481-489.

39. Li, M. X., Saude, E. J., Wang, X., Pearlstone, J. R., Smillie, L. B., and Sykes, B. D. (2002) Kinetic studies of calcium and cardiac troponin I peptide binding to human cardiac troponin C using NMR spectroscopy, *European Biophysics Journal with Biophysics Letters31*, 245-256.

40. Baryshnikova, O. K., Williams, T. C., and Sykes, B. D. (2008) Internal pH indicators for biomolecular NMR, *J. Biomol. NMR41*, 5-7.

41. Robertson, I. M., Spyracopoulos, L., and Sykes, B. D. (2009) The Evaluation of Isotope Editing and Filtering for Protein-Ligand Interaction Elucidation by Nmr, *Biophysics and the Challenges of Emerging Threats*, 101-119.

42. Lee, W., Revington, M. J., Arrowsmith, C., and Kay, L. E. (1994) A Pulsed-Field Gradient Isotope-Filtered 3d C-13 Hmqc-Noesy Experiment for Extracting Intermolecular Noe Contacts in Molecular-Complexes, *FEBS Lett.350*, 87-90.

43. Ikura, M., and Bax, A. (1992) Isotope-Filtered 2d Nmr of a Protein Peptide Complex - Study of a Skeletal-Muscle Myosin Light Chain Kinase Fragment Bound to Calmodulin, *J. Am. Chem. Soc.114*, 2433-2440.

44. Delaglio, F., Grzesiek, S., Vuister, G. W., Zhu, G., Pfeifer, J., and Bax, A. (1995) Nmrpipe - a Multidimensional Spectral Processing System Based on Unix Pipes, *J. Biomol. NMR6*, 277-293.

45. Johnson, B. A., and Blevins, R. A. (1994) Nmr View - a Computer-Program for the Visualization and Analysis of Nmr Data, *J. Biomol. NMR4*, 603-614.

46. Robertson, I. M., Boyko, R. F., and Sykes, B. D. (2011) Visualizing the principal component of (1)H, (1)N-HSQC NMR spectral changes that reflect protein structural or functional properties: application to troponin C, *J. Biomol. NMR51*, 115-122.

47. Schwieters, C. D., Kuszewski, J. J., and Clore, G. M. (2006) Using Xplor-NIH for NMR molecular structure determination, *Prog. Nucl. Magn. Reson. Spectrosc.48*, 47-62.

48. Schwieters, C. D., Kuszewski, J. J., Tjandra, N., and Clore, G. M. (2003) The Xplor-NIH NMR molecular structure determination package, *J. Magn. Reson.160*, 65-73.

49. Clore, G. M. (2000) Accurate and rapid docking of protein-protein complexes on the basis of intermolecular nuclear Overhauser enhancement data and dipolar couplings by rigid body minimization, *Proc. Natl. Acad. Sci. U. S. A.97*, 9021-9025.

50. Wishart, D. S., and Sykes, B. D. (1994) Chemical-Shifts as a Tool for Structure Determination, *Method Enzymol239*, 363-392.

51. Kuszewski, J., Gronenborn, A. M., and Clore, G. M. (1997) Improvements and extensions in the conformational database potential for the refinement of NMR and X-ray structures of proteins and nucleic acids, *J. Magn. Reson.125*, 171-177.

52. Kuszewski, J., Gronenborn, A. M., and Clore, G. M. (1999) Improving the packing and accuracy of NMR structures with a pseudopotential for the radius of gyration, *J. Am. Chem. Soc.121*, 2337-2338.

53. Anandakrishnan, R., Aguilar, B., and Onufriev, A. V. (2012) H++3.0: automating pK prediction and the preparation of biomolecular structures for atomistic molecular modeling and simulations, *Nucleic Acids Res.40*, W537-W541.

54. Pirani, A., Vinogradova, M. V., Curmi, P. M., King, W. A., Fletterick, R. J., Craig, R., Tobacman, L. S., Xu, C., Hatch, V., and Lehman, W. (2006) An atomic model of the thin filament in the relaxed and Ca2+-activated states, *J. Mol. Biol.357*, 707-717.

55. Holmes, K. C., Angert, I., Kull, F. J., Jahn, W., and Schroder, R. R. (2003) Electron cryo-microscopy shows how strong binding of myosin to actin releases nucleotide, *Nature425*, 423-427.

56. Whitby, F. G., and Phillips, G. N., Jr. (2000) Crystal structure of tropomyosin at 7 Angstroms resolution, *Proteins38*, 49-59.

57. Wuthrich, K. (1986) *NMR of proteins and Nucleic Acids*, John Wiley & Sons, Inc.

58. Wishart, D. S., Sykes, B. D., and Richards, F. M. (1991) Relationship between Nuclear-Magnetic-Resonance Chemical-Shift and Protein Secondary Structure, *J. Mol. Biol.222*, 311-333.

59. Wishart, D. S., Sykes, B. D., and Richards, F. M. (1992) The Chemical-Shift Index - a Fast and Simple Method for the Assignment of Protein Secondary Structure through Nmr-Spectroscopy, *Biochemistry31*, 1647-1651.

60. Palpant, N. J., Houang, E. M., Delport, W., Hastings, K. E., Onufriev, A. V., Sham, Y. Y., and Metzger, J. M. (2010) Pathogenic peptide deviations support a model of adaptive evolution of chordate cardiac performance by troponin mutations, *Physiol. Genomics42*, 287-299.

61. Palpant, N. J., Houang, E. M., Sham, Y. Y., and Metzger, J. M. (2012) pH-responsive titratable inotropic performance of histidine-modified cardiac troponin I, *Biophys. J.102*, 1570-1579.

62. Hoffman, R. M. B., and Sykes, B. D. (2009) Structure of the Inhibitor W7 Bound to the Regulatory Domain of Cardiac Troponin C, *Biochemistry48*, 5541-5552.

63. Li, Y., Love, M. L., Putkey, J. A., and Cohen, C. (2000) Bepridil opens the regulatory N-terminal lobe of cardiac troponin C, *Proc. Natl. Acad. Sci. U. S. A.97*, 5140-5145.

64. Oleszczuk, M., Robertson, I. M., Li, M. X., and Sykes, B. D. (2010) Solution structure of the regulatory domain of human cardiac troponin C in complex with the switch region of cardiac troponin I and W7: The basis of W7 as an inhibitor of cardiac muscle contraction, *J. Mol. Cell. Cardiol.48*, 925-933.

65. Robertson, I. M., Sun, Y. B., Li, M. X., and Sykes, B. D. (2010) A structural and functional perspective into the mechanism of Ca2+-sensitizers that target the cardiac troponin complex, *J. Mol. Cell. Cardiol.49*, 1031-1041.

66. Wang, X., Li, M. X., and Sykes, B. D. (2002) Structure of the regulatory N-domain of human cardiac troponin C in complex with human cardiac troponin I147-163 and bepridil, *J. Biol. Chem.277*, 31124-31133.

67. Tanford, C. (1961) *Physical Chemistry of Macromolecules*, John Wiley, New York.

68. Shaffer, J. F., and Gillis, T. E. (2010) Evolution of the regulatory control of vertebrate striated muscle: the roles of troponin I and myosin binding protein-C, *Physiol. Genomics42*, 406-419.

69. Makinde, A. O., Kantor, P. F., and Lopaschuk, G. D. (1998) Maturation of fatty acid and carbohydrate metabolism in the newborn heart, *Mol. Cell. Biochem.188*, 49-56.

70. Robertson, S. P., Johnson, J. D., Holroyde, M. J., Kranias, E. G., Potter, J. D., and Solaro, R. J. (1982) The effect of troponin I phosphorylation on the Ca2+-binding properties of the Ca2+-regulatory site of bovine cardiac troponin, *J. Biol. Chem.257*, 260-263.

71. Kirkpatrick, K. P., Robertson, A. S., Klaiman, J. M., and Gillis, T. E. (2011) The influence of trout cardiac troponin I and PKA phosphorylation on the Ca2+ affinity of the cardiac troponin complex, *J. Exp. Biol.214*, 1981-1988.

72. Westfall, M. V., and Metzger, J. M. (2007) Single amino acid substitutions define isoform-specific effects of troponin I on myofilament Ca2+ and pH sensitivity, *J. Mol. Cell. Cardiol.43*, 107-118.

73. Ward, D. G., Brewer, S. M., Comes, M. P., and Trayer, I. P. (2003) A cross-linking study of the N-terminal extension of human cardiac troponin I, *Biochemistry42*, 10324-10332.

74. Ward, D. G., Brewer, S. M., Calvert, M. J., Gallon, C. E., Gao, Y., and Trayer, I. P. (2004) Characterization of the interaction between the N-terminal extension of human cardiac troponin I and troponin C, *Biochemistry 43*, 4020-4027.

75. Finley, N., Abbott, M. B., Abusamhadneh, E., Gaponenko, V., Dong, W. J., Gasmi-Seabrook, G., Howarth, J. W., Rance, M., Solaro, R. J., Cheung, H. C., and Rosevear, P. R. (1999) NMR analysis of cardiac troponin C-troponin I complexes: effects of phosphorylation, *FEBS Lett.453*, 107-112.

76. Laskowski, R. A., Rullmann, J. A. C., MacArthur, M. W., Kaptein, R., and Thornton, J. M. (1996) AQUA and PROCHECK-NMR: Programs for checking the quality of protein structures solved by NMR, *J. Biomol. NMR 8*, 477-486.

CHAPTER 5

Structure and dynamics of the acidosis-resistant
A162H mutant of the switch region of troponin I
bound to the regulatory domain of troponin C

Sandra E. Pineda-Sanabria[1], Ian M. Robertson[2], and Brian D. Sykes[1]

[1] Department of Biochemistry, Faculty of Medicine & Dentistry, University of Alberta, Edmonton AB Canada, T6G 2H7. [2] Department of Pediatrics, Faculty of Medicine & Dentistry, University of Alberta, Edmonton AB Canada, T6G 2H7.

This is the concluding chapter in the investigation of the enhancement of contraction by the A162H substitution. It presents the NMR structure of the relevant troponin C-troponin I A162H complex that provides the final details that enable us to propose a model of "degrees of stabilization" for the mechanism of action. The change in dynamics upon protonation of A162H is also reported here in support of this model. This may serve the health research community in the development of cardiotonic agents by providing a specific effect to target during design and optimization. A version of this chapter has been published: Pineda-Sanabria *et al*. (2015) *Biochemistry* 54: 3583-3593.

Introduction

In contrast to skeletal muscle, acidosis in the heart significantly diminishes the force of contraction of cardiac muscle and the overall capacity of the heart to pump blood. It has been shown that the change of a single residue from histidine (H130) in the skeletal isoform of troponin I (sTnI) to alanine (A162) in the cardiac isoform of troponin I (cTnI) is responsible for the observed differential sensitivity to acidosis[1-3]. Introducing the histidine into cTnI by mutagenesis in *in vitro* assays[1], by gene transfer into failing human cardiomyocytes *ex vivo*[2], or using transgenic mice *in vivo*[3], reverts the phenotype to that of skeletal muscle, conferring resistance to acidosis.

TnI is part of the heterotrimeric troponin (Tn) complex that regulates muscle contraction in response to intracellular Ca^{2+}. The Tn complex in cardiac and skeletal muscle is composed of TnT, TnI, and TnC subunits that orchestrate muscle contraction in response to Ca^{2+}. TnT is a long helical protein that interacts with TnI, tropomyosin, and actin to anchor the complex onto the thin filament. TnC contains two globular domains with two EF-hand motifs in each domain; the C-domain binds two Ca^{2+} or Mg^{2+} ions with high affinity and low specificity, and interacts with TnI; the regulatory N-domain (NTnC) binds one Ca^{2+} ion with low affinity and high specificity and interacts with TnI only in the presence of

Ca^{2+}. TnI is a long multi-helical protein that interacts with TnT as well as both domains of TnC, and it inhibits contraction through its interaction with actin. When Ca^{2+} binds to NTnC the switch region of TnI (switch-TnI) associates with NTnC, stabilizing the 'open' conformation of NTnC, and drags the inhibitory region of cTnI off actin resulting in movement of tropomyosin, exposure of the myosin binding sites on actin, and contraction[4, 5]. This detailed description of the muscle architecture and the mechanism of contraction have been enabled largely by structural studies.

Based on the structures of skeletal and cardiac NTnC (sNTnC and cNTnC) bound to their respective switch regions of TnI (switch-sTnI and switch-cTnI), it was proposed that the introduction of A162H in the cardiac isoform induces electrostatic interactions with glutamate residues in cNTnC. The x-ray structure of the core skeletal complex[6] (1YTZ) shows the switch region of sTnI bound to sNTnC via a helix that interacts with the hydrophobic core of sNTnC followed by a curved region that contains H130 and interacts with helix A, possibly involving electrostatics with E20 of sNTnC. For the cardiac isoform there are three structures that show switch-cTnI bound to cNTnC in the presence of Ca^{2+} (1MXL, 1J1E)[7,8] which all show that switch-cTnI forms a helix that interacts with the hydrophobic core of cNTnC just like in the skeletal isoform. The NMR structure (1MXL) and one molecule of the asymmetric unit form the x-ray structure (1J1E) show the region immediately following switch-cTnI in a random coil configuration that contains A162 and does not interact with cNTnC; in contrast, this region in the other molecule in the asymmetric unit forms a bent helix that extends to the C-terminus of switch-cTnI and does not interact with cNTnC. Zhou and collaborators showed that this region remains unstructured in solution using fluorescence anisotropy[9], suggesting that the bent helix is probably an artifact of crystallization[8]. Investigation of acid dissociation constants (pK$_a$) on glutamate residues on cNTnC when bound to switch-sTnI, switch-cTnI, and switch-cTnI$_{A162H}$ confirmed electrostatic interactions between switch-sTnI and switch-cTnI$_{A162H}$, but not switch-cTnI, with E19 on cNTnC through H130 and H162, respectively[10, 11].

The mechanism of resistance to acidosis conferred by the A162H substitution has also been studied from a structural perspective. We recently published the structure of switch-sTnI bound to cNTnC at pH 6 [12]. As predicted, the structure shows sTnI in the same conformation as sTnI when bound to sNTnC, with H130 in close proximity to E19. Because binding of the C-terminal region of cTnI to actin is necessary to achieve full inhibition, based on this structure and the orientation of sTnC in muscle fibers[13] we proposed that introducing A162H in switch-cTnI increases Ca^{2+} sensitivity by increasing the affinity of switch-cTnI$_{A162H}$ for cNTnC via the additional H162-E19 interaction which stabilizes the open conformation of cNTnC[11] and changes the orientation of the C-terminal region of cTnI away from actin[12], the cNTnC and cTnI states that favor contraction. However, the structural studies using switch-sTnI do not take into account other residues besides H130 that differ in switch-

cTnI some of which have been suggested to have a role in the mechanism of resistance to acidosis[14] and their impact on the structure of the switch-cTnI$_{A162H}$ mutant remains unclear.

In this work we have determined the structure of switch-cTnI$_{A162H}$ bound to cNTnC at pH 6 by NMR. The structure addresses the structural changes induced by A162H in the presence of the other native switch-cTnI residues. The results indicate that protonation of H162 induces a small positive potential in the pH-sensitive region due to the countering effect of the native cardiac residue E164. This change, however, is sufficient to transiently change the conformation of switch-cTnI to one similar but not identical to that of switch-sTnI and to stabilize its interaction with cNTnC. We also evaluated the change in dynamics of the pH sensitive region of cTnI$_{A162H}$ upon protonation of H162 to distinguish motion from structural heterogeneity. Our work explains the effect of a variety of previously studied TnI mutants along with the physiological effects of the A162H substitution on improving cardiac performance on the face of acidosis without causing diastolic dysfunction.

Experimental procedures

Materials and sample conditions

For structure determination, the recombinant human proteins ^{15}N-cNTnC and ^{15}N, ^{13}C-cNTnC (residues 1-89) were expressed in *E. coli* and purified as previously described[15], and the synthetic peptide cTnI$_{A162H}$ (residues 144-170) containing the A162H substitution was obtained from GL Biochem Ltd (Shanghai, China). To study backbone dynamics upon protonation of H162 we used a stable hybrid system that represents the cNTnC·switch-cTnI interaction during systole (cChimera)[16] to introduce the A162H substitution by site-directed mutagenesis of the original cChimera plasmid using the protocol described by Zheng[17]. The incorporation of the A162H substitution was confirmed by DNA sequencing, mass spectrometry, and NMR spectroscopy.

In the NMR experiments, all samples consisted of 500-600 µL of 100 mM KCl, 10 mM imidazole or imidazole-d$_4$, 10 mM CaCl$_2$, 10 mM dithiothreitol (DTT), and 0.25 mM 2,2-dimethyl-2-silapentane-5-sulfonate-d$_6$ sodium salt (DSS-d$_6$) as an internal standard. For structure determination, the sample contained 0.8-1 mM ^{15}N-cNTnC or ^{15}N, ^{13}C-cNTnC, a 4:1 molar excess of cTnI$_{A162H}$ to ensure saturation of cNTnC, and the pH was set to 6.1. For backbone dynamics experiments, the sample contained 0.8 mM ^{15}N-cChimera$_{A162H}$ and the pH was set to 6.4 or 7.4 accordingly. For the pH titration of cChimera$_{A162H}$ the sample contained 0.7 mM ^{15}N-cChimera$_{A162H}$, and 2 mM piperazine to accurately determine pH values below 6 [18].

NMR spectroscopy

All the NMR experiments were acquired in Varian spectrometers of 500, 600, or 800 MHz at 30°C. One-dimensional spectra were processed with VnmrJ v.3.2 (Varian, Inc), multidimensional spectra were processed with NMRPipe[19] and analyzed with NmrViewJ[20]. Spectral assignments for the cNTnC-cTnI$_{A162H}$ complex were obtained by acquiring two- and three dimensional experiments as detailed in Supplementary Table 5.1. Note that two independent ^{13}C,^{15}N -filtered noesy NMR spectra were acquired, one at pH 6.1 and the other at pH 7.4, for assessment of conformational changes (* in Supplementary Table 5.1). Assignments for cChimera$_{A162H}$ were guided by the assignment of wild type cChimera[16], homonuclear assignment of the cTnI$_{A162H}$ peptide (residues 144-173) bound to cNTnC, and the titration of unlabelled cNTnC into ^{15}N-cTnI$_{A162H}$ (Supplementary Figure 5.1). All the ^{15}N relaxation experiments were done at 600 MHz and acquired in random order with variable relaxation delays of 10, 100, 200, 500, 750, and 1000 ms for T_1 and 10, 30, 50, 70, 90, 110, and 150 ms for T_2. The data was fit to a two-parameter exponential decay curve using the Rate Analysis module of NMRViewJ with the noise level as an estimation of the standard deviation of the signal intensities.

Structure determination

All the experiments used to obtain distance restrains are detailed in Supplementary Table 5.1. Intramolecular NOEs for cNTnC were calibrated in NMRViewJ with the median method. Intramolecular NOEs for cTnI$_{A162H}$ and intermolecular NOEs between cNTnC and cTnI$_{A162H}$ were classified as weak (1.8-6.0 Å). Intermolecular NOEs between cNTnC and Ca^{2+} were derived from crystallographic data. Dihedral angle restraints for cNTnC were determined using the TALOS+ server[21] (available at http://spin.niddk.nih.gov/bax/nmrserver/talos/) based on the chemical shifts of backbone atoms. For cTnI$_{A162H}$, -60° ± 25° and -30° ± 25° were used for φ and ψ dihedral angles, respectively, for residues for which the chemical shift index and random coil index indicated helical values according to their backbone ^{1}H chemical shifts. The distance and dihedrals experimental constraints were used in the simulated annealing module of Xplor-NIH version 2.35[22], to improve the quality of backbone and side chain conformations we used the statistical torsion angle potential[23] of Xplor-NIH based on a database of over a million residues from high quality crystal structures, we also used the gyration volume potential term to restraint the volume associated with the gyration tensor also based on values observed in the Protein Data Bank (PDB). Initially 100 structures were calculated from which the lowest energy structure was used as the starting point for refinement. The final ensemble consisted of the 20 lowest energy structures from the refinement step with no NOE or dihedral violations greater than 0.5 Å and 5 degrees, respectively, and was validated with Procheck using the Protein Structure Validation Suite (PSVS 1.5) server available at http://psvs-1_5-dev.nesg.org/.

Results

Structure of cNTnC-cTnI$_{A162H}$

      The overall conformation of the cNTnC-cTnI$_{A162H}$ complex has structural elements of the cardiac and skeletal wild type complexes (Figure 5.1A). The number and type of restraints used in the structure determination are shown in Supplementary Table 5.2 along with scores from the structure validation. The structure coordinates have been deposited in the PDB under the ID 2MZP, and the NMR data for this system in the BMRB under the ID 25495. The root mean square deviation (rmsd) of alpha carbons for all residues with the x-ray structure of the cardiac (1J1E) and skeletal (1YTZ) Tn complexes are 2.02 Å and 1.58 Å, respectively; and for helical components the rmsd values are 1.70 Å and 1.19 Å, indicating higher similarity with the structure of the skeletal isoform of the complex (Figure 5.1B) mostly due to the differences in the C-terminus of the cTnI$_{A162H}$ peptide.
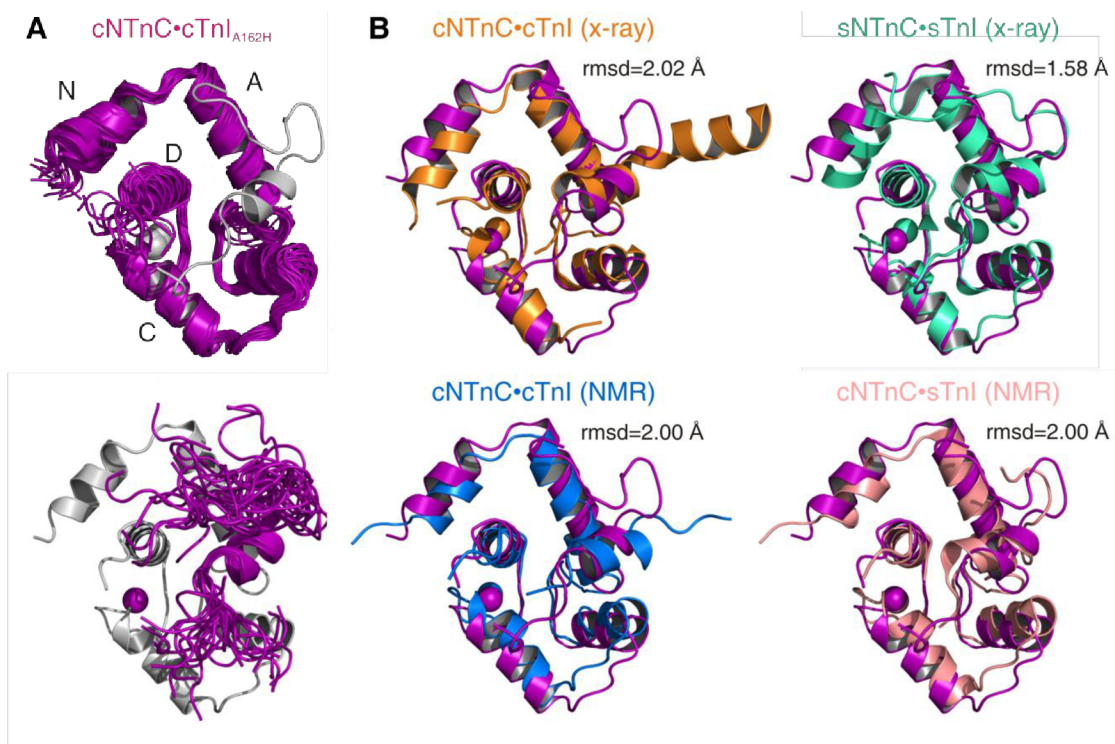
Figure 5.1. Structure of cNTnC•cTnI$_{A162H}$ compared with homologous complexes.
A. The ensemble of twenty structures is shown independently for cNTnC (top) and cTnI$_{A162H}$ (bottom) for clarity. The helices of cNTnC are labeled N, and A through D. **B.** Alignment and corresponding rmsd values for alpha carbons for all residues (1-89 and 144-170) for the present structure of cNTnC·cTnI$_{A162H}$ (purple) and the x-ray structures of cNTnC·cTnI (orange) and sNTnC·sTnI (green), and the NMR structures of cNTnC·cTnI (blue) and cNTnC·sTnI (pink). The Ca^{2+} atoms are displayed as spheres.

Structure of cNTnC in the cNTnC-cTnI$_{A162H}$ complex

The conformation of cNTnC when bound to cTnI$_{A162H}$ is not significantly changed by the A162H substitution. Three-dimensional noesyNhsqc and noesyChsqc NMR spectra were used to obtain the intramolecular distance information for cNTnC. A total of 1108 NOE and 157 dihedral restraints were used in the annealing and refinement protocols of Xplor-NIH[22] for this subunit of the complex. The structure displays five α-helices, N and A through D, of which the A-D helices are well defined and the N-helix is more variable between models. There is also a short anti-parallel β-sheet like in all other cTnI-bound structures of cNTnC. Comparing NTnC domains only, the rmsd of alpha carbons with the x-ray cardiac structure (1J1E) is 1.60 Å for all residues, and 1.46 Å for residues in helical regions; compared to the x-ray skeletal structure (1YTZ) the rmsd for all residues is 1.58 Å and for residues in helical regions is 1.19 Å.

Structure of cTnI$_{A162H}$ in the cNTnC-cTnI$_{A162H}$ complex

The experimental data localizes cTnI$_{A162H}$ on the hydrophobic patch of cNTnC and dictates a curved conformation similar to that of sTnI. The two-dimensional ^{13}C,^{15}N -filtered noesy NMR spectrum was used to obtain the intramolecular distance restraints for the cTnI$_{A162H}$ peptide (Figure 5.2), whereas the three-dimensional edited ^{13}C -filtered Chmqcnoesy NMR spectrum provided the intermolecular distance restraints for the cNTnC-cTnI$_{A162H}$ interaction (Figure 5.3). A total of 140 intramolecular and 34 intermolecular NOEs, and 13 dihedral restraints were used in the structure determination. The intramolecular NOEs between H162 and residues M154 and Q155 on the switch helix are consistent with the curved conformation of the switch peptide. When the pH was raised to 7.4 (blue dotted line in Figure 5.2A) only strong intra-residue NOEs are observed for the δ2 proton of H162; the lack of additional inter-residue contacts indicates an extended conformation for this region at physiological pH when H162 is not protonated. The intermolecular NOEs position cTnI$_{A162H}$ between helices A, B, and D of cNTnC. Residues V146 and I148 on the N-terminal region of cTnI$_{A162H}$ contact M60 on the C-helix, and L48 and Q50 on helix B of cNTnC, respectively, localizing this region towards helix C. The NOEs from the switch helix can be divided into two groups, one group formed by A150, M154, L157, and L158 defines one side of the helix and contacts residues A22 and A23 on helix A of cNTnC, and M81, C84, and M85 on helix D. The other group, formed by residues A152 and A156, lies on the opposite side of the helix and contacts residues V44, M47, and L48 on the B helix of cNTnC, positioning the switch helix on the hydrophobic groove of cNTnC. Following the helical region, residues L166 and A170 contact residue M85 on helix D of cNTnC, thereby restricting the C-terminal side of the cTnI$_{A162H}$ peptide and contributing to its curved conformation. The pH sensitive region (residues 161-164) is less constrained than the switch helix with the distance from protons δ2 and ε1 of H162 to β of E19 varying from 8.2 Å to 14.7 Å, and to the γ protons from 8.5 Å to 16.2 Å, within the final ensemble.

Figure 5.2. Intramolecular NOEs for cTnI$_{A162H}$.

A. Strip plots of the ^{13}C, ^{15}N-filtered noesy NMR spectrum showing the intramolecular contacts used in the structure calculation at pH 6.1. The resonances of the δ2 and ε1 protons of H162 are indicated by the red dashed lines. Ambiguous assignments are separated by a slash. The strip on the far right corresponds to the δ2 proton of H162 at pH 7.4 (blue dotted line). **B.** Schematic of the contacts made by H162 within cTnI$_{A162H}$. Interatomic distances represented by dashed lines are in Å.

Figure 5.3. Intermolecular NOEs for cNTnC•cTnI$_{A162H}$.

Strip plots from the ^{13}C-filtered Chmqcnoesy NMR spectrum showing the intermolecular NOEs used in the structure calculation. The schematics on the right illustrate from top to bottom contacts involving the N-terminal, helical, and post-helical regions of cTnI$_{A162H}$. Dashed lines indicate interatomic distances in Å.

Comparing the TnI segments only with the cardiac (1J1E) and x-ray skeletal (1YTZ) structures, the respective rmsd values based on alpha carbons are 12.98 Å and 3.70 Å for all residues, 0.19 Å and 0.25 Å for residues on the switch helix only (150-157), and 17.95 Å and 4.08 Å for residues after the switch helix (158-170) indicating higher resemblance to sTnI; however, and despite the closer sequence similarity with sTnI introduced by H162 (Figure 5.4A), a consistent difference in the pH sensitive region is observed. In all models, H162 on the pH sensitive region lies farther away from helix A compared to

116

sTnI and in the model where H162 is in a similar position to H130 of sTnI, helix A and E19 are pushed away (Figure 5.4B, C). To investigate if these differences are genuine or are a consequence of structural heterogeneity, we studied the backbone dynamics of the pH sensitive region in different protonation states of H162.

A

human cTnI$_{A162H}$	144	RRVRISADAM MQALLGAR**H**K ESLDLRA 170
human sTnI	112	RRVRMSADAM LKALLGSKHK VCMDLRA 138
mouse cTnI	146	RRVRISADAM MQALLGTRAK ESLDLRA 172
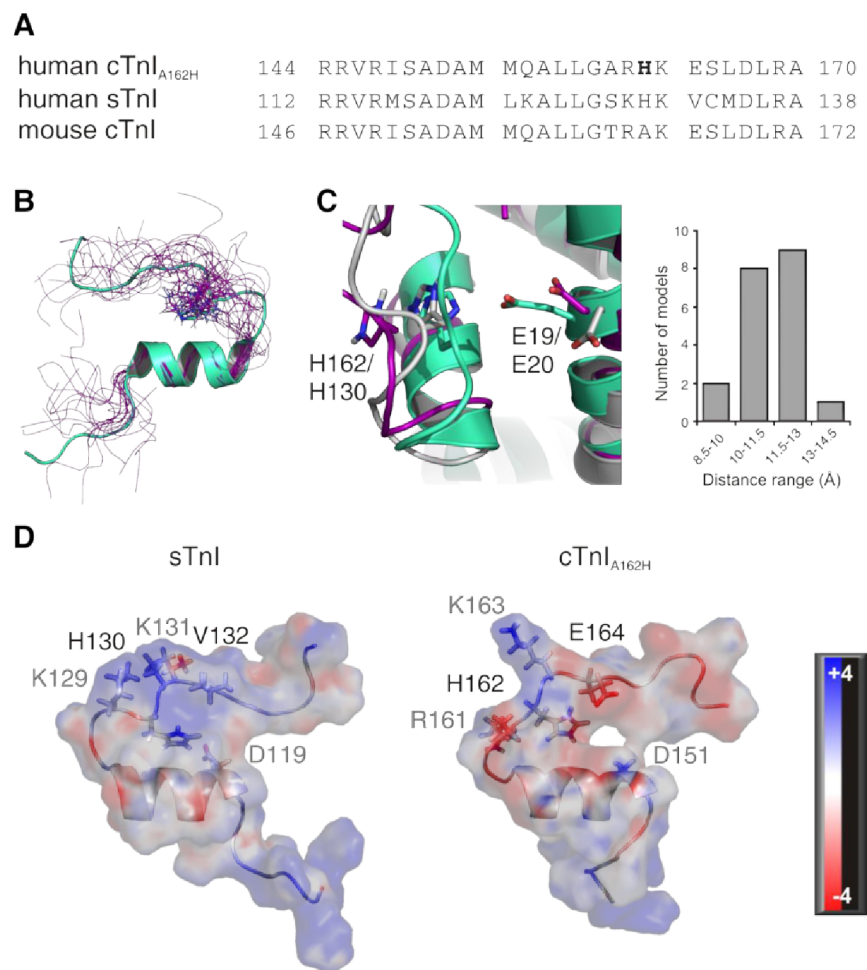
Figure 5.4. Comparisons of cTnI$_{A162H}$ and sTnI.
A. Sequence alignment of cTnI$_{A162H}$ with the homologous regions of sTnI, and mouse cTnI for reference, the site of mutation is in bold. **B.** The structure alignment of the switch helix of cTnI$_{A162H}$ (purple, residues 150-157) and sTnI (green, residues 118-125) from the x-ray structure (1YTZ) shows similar peptide conformation. **C.** An expansion of the pH-sensitive region shows variable location of H162 of cTnI$_{A162H}$ (purple and grey) compared to sTnI. The histogram displays the distribution of average distances between the δ2/ε1 protons of H162 and the ß/γ protons of E19 within the 20 lowest energy structures. **D.** Electrostatic potential mapped on the surface of sTnI and cTnI$_{A162H}$; residues labeled in black are on the side of TnI that faces cNTnC whereas those in grey are on the other side that faces the solvent.

For the measurement of the dynamics of the pH sensitive region of TnI$_{A162H}$ as a function of the protonation state of H162 we used a cTnC-cTnI chimera containing the A162H substitution (cChimera$_{A162H}$) based on the wild type cChimera which reliably represents the cNTnC·switch-cTnI complex but offers superior stability, solubility, and 1:1 stoichiometry[16]. cChimera consists of cNTnC attached to cTnI (residues 144-173) by a flexible cleavable linker; it preserves the structural features of the original cNTnC·cTnI$_{144-173}$ complex corresponding to the systolic state of the heart due to a high apparent concentration of switch-cTnI. Because this is a more soluble and stable system that allows us to directly observe the ^{1}H and ^{15}N resonances of residues in cTnI once it is bound to cNTnC, it is ideally suitable for the focused investigation of the protonation of H162 and the dynamics of the pH sensitive region of cTnI$_{A162H}$.
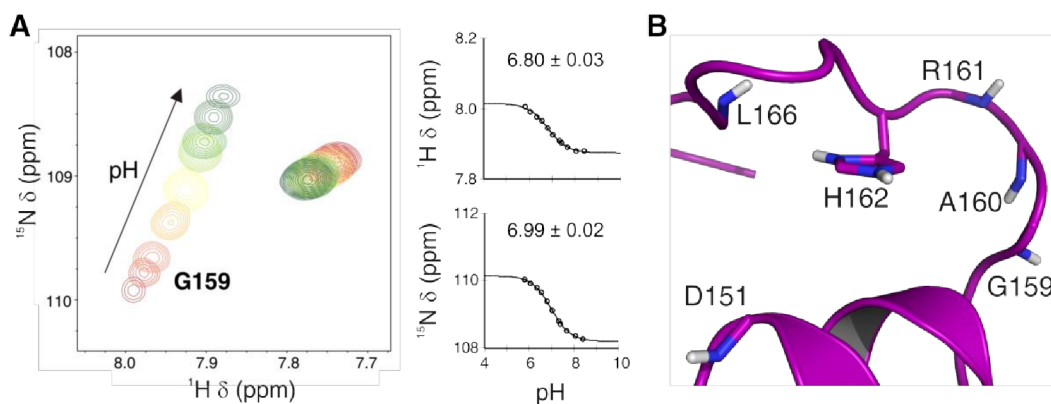
Figure 5.5. Determination of pK$_a$ for H162 in cChimera$_{A162H}$.
A. Overlap of a section of the ^{1}H, ^{15}N correlation spectra of cChimera$_{A162H}$ for the pH range from 5.81-8.40 (red to green), curve fitting, and pK$_a^{app}$ for residue G159. The error indicates the standard deviation of the fit. **B.** Location of residue G159 relative to H162 in the present structure.

We performed a pH titration of cChimera$_{A162H}$ monitored by ^{1}H, ^{15}N -HSQC NMR experiments at each titration point to investigate the pK$_a$ of H162 in this system. The pK$_a$ of a specific residue can be determined by plotting the chemical shift change as a function of the pH. In the pH titration, the backbone ^{1}H and ^{15}N amide resonances of titratable residues and some non-titratable residues of cChimera$_{A162H}$ were pH sensitive especially around the site of the mutation (Figure 5.5 and Supplementary Figure 5.2). Although H162 displays a very weak signal located in a crowded region of the spectrum, making direct pK$_a$ determination difficult and inaccurate, its pK$_a$ could be determined indirectly by analyzing nearby residues for which a pK$_a$ is not expected (non-titratable) but where an apparent pK$_a$ (pK$_a^{app}$) was observed, as well as from residues for which the observed pK$_a$ value is far

from the expected, as previously done for other related complexes[10,11]. According to the conformation observed in our structure of cNTnC-cTnI$_{A162H}$, the residues closest to H162 that displayed large chemical shift changes are G159, A160, R161, and L166; in addition D151 at the beginning of the switch helix was also analyzed to investigate intermolecular interactions within the cTnI$_{A162H}$ region. Based on their ^{1}H resonances the pK$_a$ of H162 in cChimera$_{A162H}$ expressed as the average ± the standard deviation is 6.82 ± 0.06, based on their ^{15}N resonances the value is 6.78 ± 0.06; yielding a combined average of 6.80 ± 0.06, the same as determined previously in the cNTnC·switch-cTnI$_{A162H}$ complex (6.82 ± 0.28)[11]. Knowing the pK$_a$ we can determine the protonation state of H162 in cChimera$_{A162H}$ at different pH values in order to choose representative but physiological conditions. According to the Henderson-Hasselbach equation H162 is 20% and 72% protonated at pH 7.4 and 6.4, respectively; values that have physiological relevance and represent different protonation states of H162 for the dynamics analysis.

Dynamics of cTnI$_{A162H}$

To evaluate changes in the dynamics of cTnI$_{A162H}$ upon protonation of H162 we determined the T$_1$ and T$_2$ relaxation times for the backbone amide NH pairs of cChimera$_{A162H}$ at pH 7.4 and 6.4 (Figure 5.6A). The data has been deposited in the BMRB under the ID 25511. Average T$_1$ and T$_2$ values are listed in Table 5.1 for the different regions of cChimera$_{A162H}$. The T$_1$ profile was very similar at the two pH values tested. The T$_2$ profiles at the two pH values were very similar but consistently lower for the cNTnC region due to a slight tendency to aggregation as the pH lowers closer to 6 [24]. The T$_2$ data indicates that the most pH-sensitive region corresponds to cTnI residue 157 to prior 164 with the highest significant difference between the different pH values (Table 5.1). The cTnI$_{A162H}$ region also displays a plateau from residue 164 to 170 at both pH values.

Table 5.1. T1 and T2 values for various regions of cChimeraA162H.

cChimera$_{A162H}$ region (residues)	T$_1$ (ms ± se)		T$_2$ (ms ± se)	
	pH 7.4	pH 6.4	pH 7.4	pH 6.4
Full cChimera$_{A162H}$	588 ± 26	579 ± 39	78 ± 3	65 ± 7
cNTnC (1-89)	597 ± 27	585 ± 31	72 ± 2	54 ± 7
cTnI$_{A162H}$ helix (150-157)	580 ± 33	552 ± 37	61 ± 3	48 ± 6
cTnI$_{A162H}$ C-terminus (158-170)	534 ± 23	522 ± 44	92 ± 4	82 ± 4
cTnI$_{A162H}$ pH-sensitive (157-163)	554 ± 29	538 ± 42	68 ± 2	38 ± 4
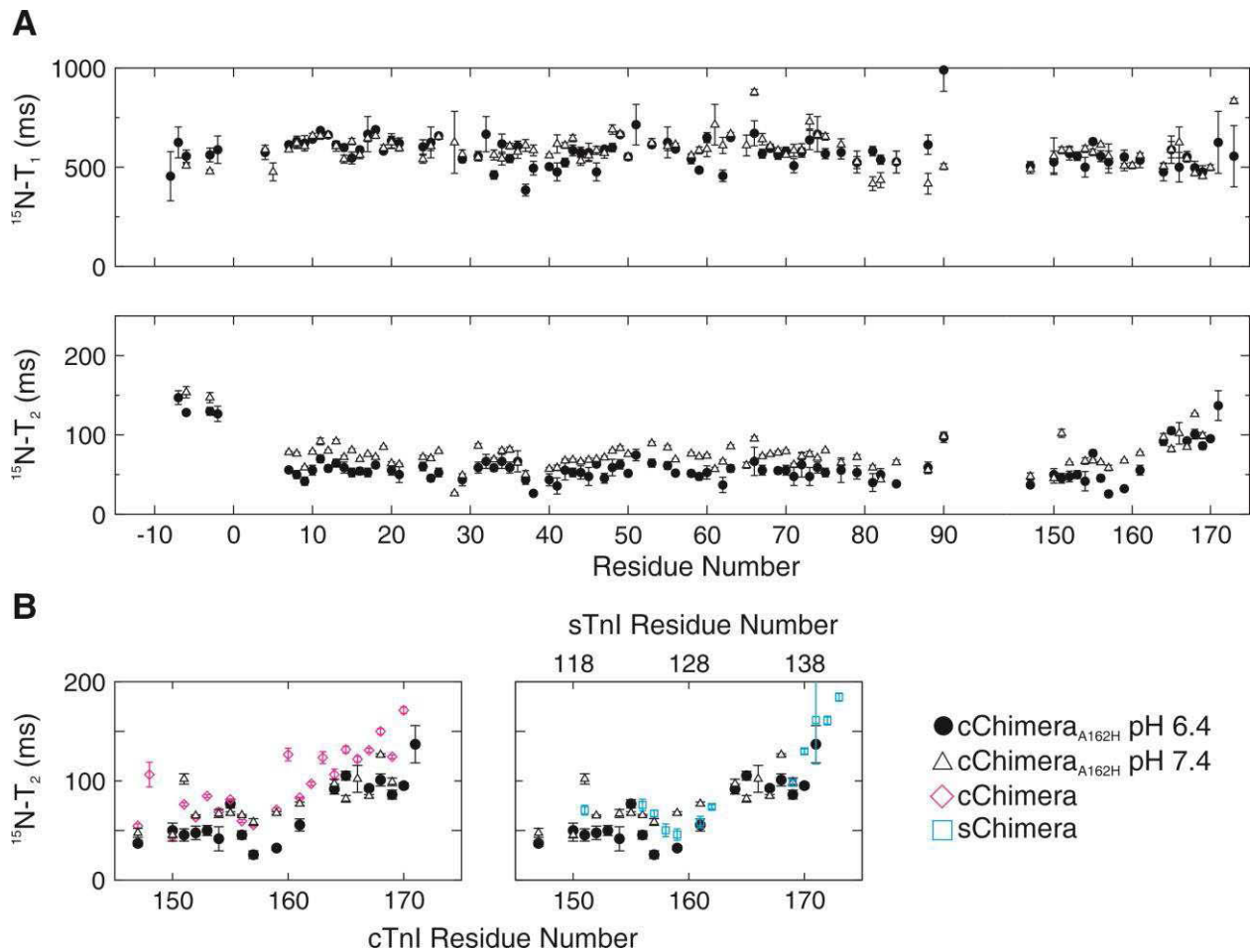
Figure 5.6. Dynamics of cChimera$_{A162H}$.
A. ^{15}N-T$_1$ and ^{15}N-T$_2$ relaxation times for the backbone NH pairs of cChimera$_{A162H}$ when H162 is protonated (filled circles) and deprotonated (empty triangles). **B.** Comparison of ^{15}N-T$_2$ profiles for the TnI region of protonated and deprotonated cChimera$_{A162H}$ with cChimera (left), and sChimera (right).

Discussion

Myocardial contraction is a vital process that requires fine regulation of the contraction-relaxation equilibrium to ensure the survival of the organism and the species. Several mechanisms control cardiac performance, but one of the most intrinsic levels of regulation is the sensitivity of cTnC for Ca^{2+}. Two modulators of Ca^{2+} sensitivity that favor relaxation have evolved in cardiac muscle: phosphorylation and pH-dependent sensitivity. Only the cardiac isoform of TnI contains an N-terminal extension that can be phosphorylated at residues S22 and S23 by PKA and disrupt interactions of the N-terminal extension with cNTnC resulting in a decrease in Ca^{2+} sensitivity on the thin filament in

response to adrenergic stimulation[25-27]. The other mechanism is the replacement of H130 in sTnI for A162 in the analogous position of cTnI which, according to an evolutionary model[28], lowered the Ca^{2+} sensitivity of the cardiac thin filament in higher order chordates in response to less demanding environmental conditions compared to cold water fish and amphibians[28], but made the heart muscle vulnerable to low pH conditions such as hypoxia and myocardial ischemia. Placing the histidine in cTnI, as the A162H mutant, produces a gain-of-function phenotype at pH ~6 protecting the heart from intracellular acidosis.

In this study we determined the structure and dynamics of the cNTnC·cTnI$_{A162H}$ complex to address the effect of the A162H substitution in the presence of other native cTnI residues. When comparing the present structure of cNTnC·cTnI$_{A162H}$ with homologous complexes, the NTnC subunit is unchanged overall and the differences are mostly in the TnI subunit (Figure 5.1B). The cTnI subunits of all these complexes display the switch helix interacting with the hydrophobic patch of cNTnC; however two different conformations can be distinguished for the pH sensitive region (residues 161-164 for cardiac or residues 129-132 for skeletal). One conformation is extended with the pH sensitive region pointing away the switch helix and is observed in the x-ray and NMR structures of cNTnC·cTnI. The other conformation is curved with the pH sensitive region parallel to the switch helix and is observed in the structures of sTnI bound to sNTnC or cNTnC, and in the present structure as the result of electrostatic interactions between the positively charged H130/H162 of sTnI/cTnIA162H and E20 of sNTnC or E19 of cNTnC, as shown previously[11, 12]. Importantly, the lack of intramolecular NOEs between H162 and other cTnI residues at pH 7.4 in our present study (Figure 5.2A) indicates that cTnI$_{A162H}$ adopts the extended conformation when bound to cNTnC at physiological pH. We previously proposed that the extended conformation favors relaxation in cardiac muscle by positioning the C-terminal region of cTnI, necessary for its full inhibitory activity, close to actin in the thin filament whereas the curved conformation of sTnI positions the C-terminal region away from actin favoring contraction[12].

The conformation observed for cTnI$_{A162H}$ in this study is curved, similar to that observed for sTnI when bound to either sNTnC or cNTnC, but the location of the pH sensitive region is slightly different (Figure 5.4B, C). Previous data point to a curved conformation for cTnI$_{A162H}$, such as the demonstration of electrostatic interactions between H162 and E19 and E15 of cNTnC, the preservation of the curved conformation of sTnI when binding to cNTnC, and the great similarity of intramolecular NOE contacts for sTnI and cTnI$_{A162H}$ when bound to cNTnC[11, 12]. While the intermolecular NOEs that dictate the localization of the peptides are very similar between sTnI and cTnI$_{A162H}$ when bound to cNTnC, the actual localization of their pH-sensitive regions is slightly different with H162 positioned further from cNTnC compared to H130.

One explanation for the different localization of cTnI$_{A162H}$ and sTnI is that the electrostatic potential of cTnI$_{A162H}$ on the pH-sensitive region is more negative and therefore may shift it further from E19 of cNTnC compared to sTnI via electrostatic repulsion. We previously showed that the position of the pH sensitive region of sTnI bound to sNTnC and cNTnC was the same[12], which indicates that the difference observed in the present cTnI$_{A162H}$ structure results from other residues within the cTnI$_{A162H}$ peptide. From the residues neighboring H162/H130 the most significant difference in the sequence corresponds to E164 in cTnI$_{A162H}$ substituted for V132 in sTnI introducing an extra negative charge in cTnI$_{A162H}$. To investigate how E164 impacts peptide electrostatics we used the Delphi web server[29, 30] (available at http://compbio.clemson.edu/delphi_webserver/) to calculate the electrostatic potential of the cTnI$_{A162H}$, cTnI, and sTnI peptides using a linear solver for the Poisson-Boltzmann equation. Figure 5.4D shows the potential mapped onto each TnI peptide; although cTnI$_{A162H}$ and sTnI have three consecutive positively charged residues, in the structure two of them lie on the side of TnI that faces the solvent and only one (H162/H130) faces cNTnC along with V132 in sTnI which is neutral or E164 of cTnI$_{A162H}$ which displays a strong negative potential. Then in sTnI the mostly positive potential generated by H130 favors interactions with E19, whereas in cTnI$_{A162H}$ the negative potential prevents closer interactions. In fact, the average distance from the δ2 and ε1 protons of H162 to the β protons of E19 is 11.2 Å and to the γ protons is 12.0 Å, which constitutes a larger separation compared to 7.2 Å and 7.6 Å for H130-E19 and H130-E20, respectively[12]. Despite the repulsive effect of E164, the presence of the small positive potential of H162 is enough to produce a positive inotropic effect in the hearts and myocytes of transgenic mice expressing cTnI$_{A164H}$ (mouse numbering, Figure 5.4A), and in myocytes from failing human hearts transduced with cTnI$_{A164H}$2, which underlines the significance of electrostatics in the mechanism of contraction enhancement by the A162H substitution.

Stabilization and a conformational change of switch-cTnI$_{A162H}$ upon protonation of H162 are also supported by our backbone dynamics. The drop in T$_2$ observed for residues 157-160 (pH sensitive loop) immediately following the switch helix indicates increased rigidity or exchange broadening in that region upon protonation of H162. Increased rigidity can correlate with stabilization of the pH sensitive loop in a curved conformation via the H162-E19 interaction; this also correlates with the increased affinity of switch-cTnI$_{A162H}$ for cNTnC at pH 6 observed previously[11]. Stabilization of the curved conformation could also be mediated by intramolecular interactions between H162 and D151 on the switch helix as D151 displayed an average pK$_a$^{app} of 6.86 ± 0.08 corresponding to H162 of cTnI$_{A162H}$; however, its pK$_a$ could not be determined due to precipitation of cChimera$_{A162H}$ under pH 5.5. Exchange broadening is an indication of different conformations that interconvert with each other; in this case protonation of H162 may induce transient interactions with E19 that cause the loop to change its conformation. Another feature of the T$_2$ profile at both pH conditions is the presence of a plateau, which indicates that residues 164-170 tumble together in solution as a single unit. The dynamics of protonated and deprotonated cTnI$_{A162H}$ approximate the dynamics of the homologous regions of sTnI

and cTnI, respectively. The relaxation parameters of the TnI regions for skeletal and cardiac isoforms have been studied before using hybrid proteins. We compared the T_2 profiles at 600 MHz of the TnI region of cChimera$_{A162H}$ at pH 6.4 and 7.4 (this work), with the TnI regions of cChimera at pH 6.9[16] (Fig 6 B, left), and of sChimera at pH 6.8[31] (Fig 6 B, right). There is a large degree of overlap between cChimera$_{A162H}$ at pH 7.4 and cChimera up to residue 164, where the T_2 plateau starts; this indicates that in that region cTnI$_{A162H}$ resembles native cTnI when H162 is uncharged. On the other hand, although there are some data points missing for sChimera, cChimera$_{A162H}$ at pH 6.4 is closer to sChimera than to cChimera, indicating that the pH sensitive region of cTnI$_{A162H}$ when H162 is protonated is similar, but not identical to, the corresponding region of sTnI.

We propose that in the thin filament, small changes in charge complementarity between the pH sensitive region of TnI and helix A of cNTnC dictate the inclination of the contraction-relaxation equilibrium. The effects of charge substitutions in TnI have been studied in the past using different mutants of sTnI and cTnI[1, 2, 14, 32]. For example, the sTnI$_{V134E}$ (sTnI$_{V132E}$) [1] mutant was shown to decrease Ca^{2+} sensitivity to cardiac levels in myocytes but only at pH 6.2[14]; however the reverse mutant cTnI$_{Q155R/E164V}$ did not show any increase in Ca^{2+} sensitivity in an actomyosin ATPase assay[1]. Also the cTnI$_{Q155R/A162H/E164V}$ mutant displayed improved Ca^{2+} sensitivity at pH 6.5 in the ATPase assay[1]. This can be explained by our present findings. The presence of a positive residue at position 162/130 on the side facing cNTnC will enhance contraction by inducing a curved conformation of TnI and positioning the C-terminal region away from actin; however, the stability of the curved conformation will be dictated by the amount of positive potential on the side that faces cNTnC (Figure 5.7); at the same time the pH and the charge of the neighboring residues on that side can alter the amount of positive potential. Thus, low intracellular pH will stabilize the curved conformation by increasing the fraction of protonated H162/130 and the positive potential. In addition, along with H162/130 the simultaneous presence of neutral residues like V132 have no effect, while acidic residues like E164 counteract the positive potential producing only a transient curved conformation which stills enhances contraction but allows efficient conversion to the extended conformation that facilitates relaxation, as in the case of the sTnI$_{V134E}$ (sTnI$_{V132E}$) and cTnI$_{A164H}$ (cTnI$_{A162H}$) mutants, which do not cause diastolic failure[14,33]. According to this model, introducing basic residues at position 164/132 (cardiac/skeletal numbering) may further enhance contraction at the cost of impairing relaxation. On the other hand, in the absence of H162/130 the conformation of TnI in the pH sensitive region is extended keeping the C-terminal region of TnI close to actin to favor relaxation despite residue 164/132 being negative or neutral. This is the case for the cTnI$_{Q155R/E164V}$ mutant which, despite containing the reverse sTnI$_{V134E}$ Ca^{2+}-desensitizing substitution, still shows the cardiac phenotype[1]. This model of "degrees of stabilization"

---

[1] The numbering for the mouse protein used in the original publications is given in the text with the homologous human numbering in parenthesis. The sequence of mouse cTnI is shown in Figure 4A. Only human protein numbering is used in Figure 7 for clarity.

also agrees with previous dynamics simulation data that show large structural variation for protonated cTnI$_{A164H}$ (cTnI$_{A162H}$) and more consistency for the constitutively charged cTnI$_{A164R}$ (cTnI$_{A162R}$) mutant on
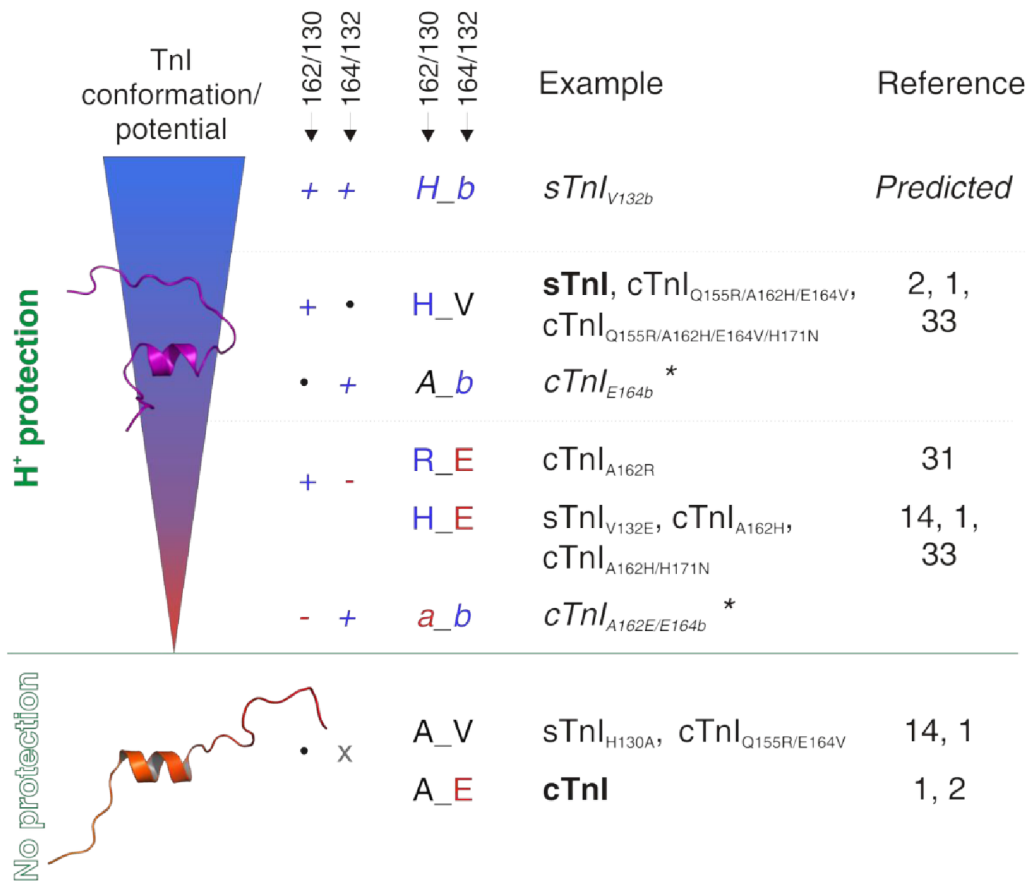
Figure 5.7. Model of H$^+$-protection.

The stability of the curved conformation of the pH-sensitive region of cTnI that confers protection against acidosis depends on the amount of positive electrostatic potential of the side of cTnI that faces cNTnC determined first by the residue type found at position 162/130 (cardiac/skeletal numbering) and then by the residue type present at position 164/132 in a gradual pH-dependent manner. The curved conformation and H$^+$ protection are lost once residue 162/130 becomes a non-charged residue. Different TnI mutants are localized in their corresponding levels on the electrostatic potential gradient, or in the no-protection zone, and the residues present at their 162/130 and 164/132 positions are specified. Native cTnI and sTnI are shown in bold. The + sign indicates a positively charged residue, -, a negatively charged residue, •, a hydrophobic residue, x, a negatively or non-charged residue, a, an acidic residue, and b, a basic residue. Blue and red indicate positive and negative potentials, respectively. Predicted cases are in italics and unknown cases are marked *

the formation of salt bridge with E19 of cNTnC[32]. Other mutants can also be explained by this model, such as the sTnI$_{H132A}$ (sTnI$_{H130A}$) mutant which adopted the cardiac phenotype[14], and the cTnI$_{A164R}$ (cTnI$_{A162R}$) mutant which displayed enhanced contraction in transduced rat cardiomyocytes at acidic and baseline conditions due to a sustained positive charge at position 162[32]. The cTnI$_{Q157R/A164H/E166V/H173N}$ (cTnI$_{Q155R/A162H/E164V/H171N}$) and cTnI$_{A164H/H173N}$ (cTnI$_{A162H/H171N}$) mutants showed increased contractility in transduced rat cardiomyocytes at acidic conditions[34], which fits in our model, but also at baseline conditions despite the lack of a sustained positive charge at position 162 which suggests a role of residue N171 of sTnI (not studied yet independently) on enhancing contraction beyond the scope of our model. Finally, mutants that carry a positive charge at position 164/132 have not been reported and raise the question of the specificity of localization of the positive potential that induces the curved conformation (* in Figure 5.7).

Taken together, we conclude that the A162H substitution induces transient interactions of the partially positive pH sensitive region with helix A of cNTnC to enhance contraction without impairing relaxation. The pK$_a$ of the histidine residue and the consequent variability of its degrees of protonation make it optimal for maintaining muscle contraction in response to changing intracellular proton concentrations in the diseased heart. The understanding of this mechanism may aid in the pharmacological development of pH-sensitive agents that temporarily enhance the cTnI-cNTnC interaction to induce myocardial contraction without inducing diastolic dysfunction.

Acknowledgements
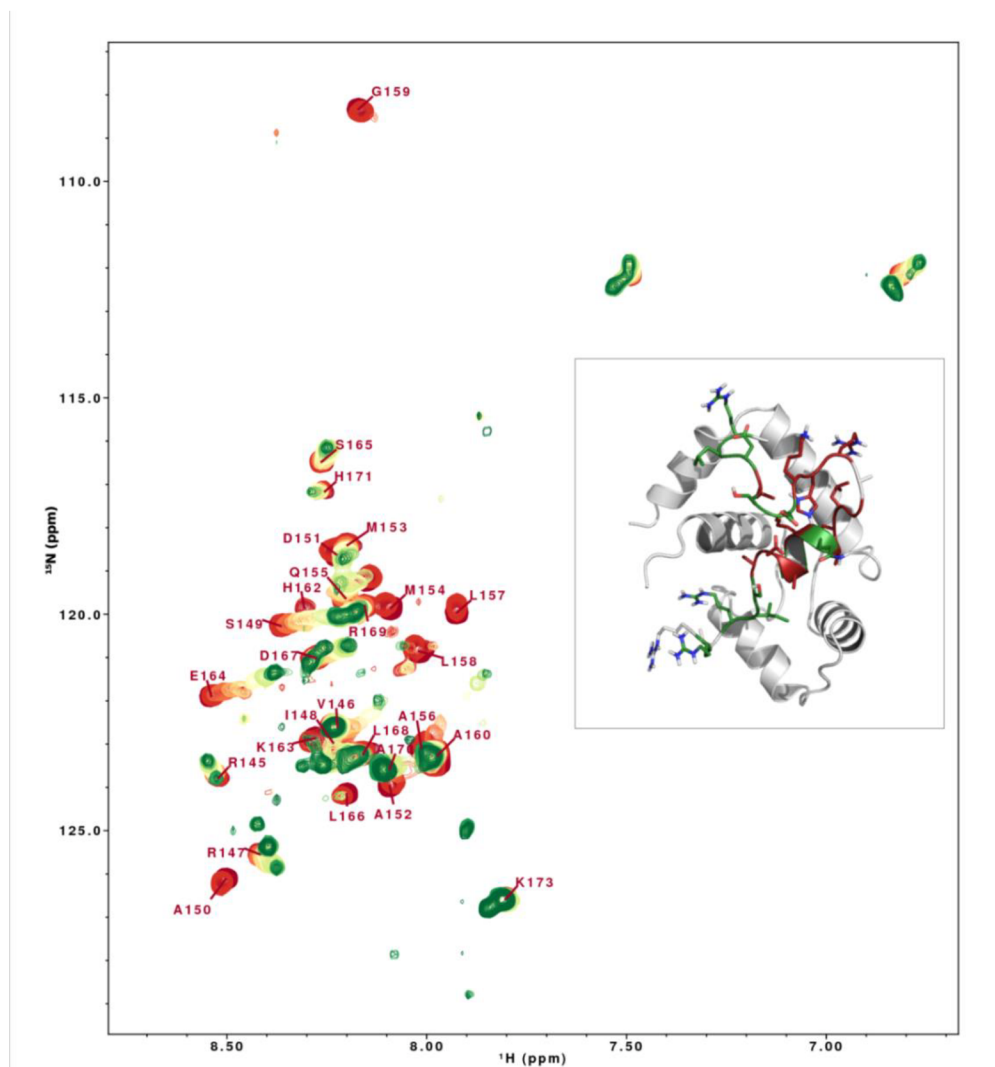
Supplementary Figure 5.1. Titration of cNTnC into ^{15}N-cTnI$_{A162H}$.

Overlap of ^{1}H, ^{15}N correlation spectra for the addition (maroon to green) of unlabelled cNTnC to ^{15}N-cTnI$_{A162H}$ (residues 144-173) used to aid the assignment of cChimera$_{A162H}$. The insert shows chemical shift mapping of cTnI residues that did not experienced significant chemical shift changes (146, 170, 171, 173) or underwent fast exchange (145, 147, 148, 149, 153, 155, 160, 165, 167, 168, 169) or intermediate exchange (164) in green, and those that underwent slow exchange (150, 151, 152, 154, 156, 157, 158, 159, 161, 162, 163, 166) in maroon.
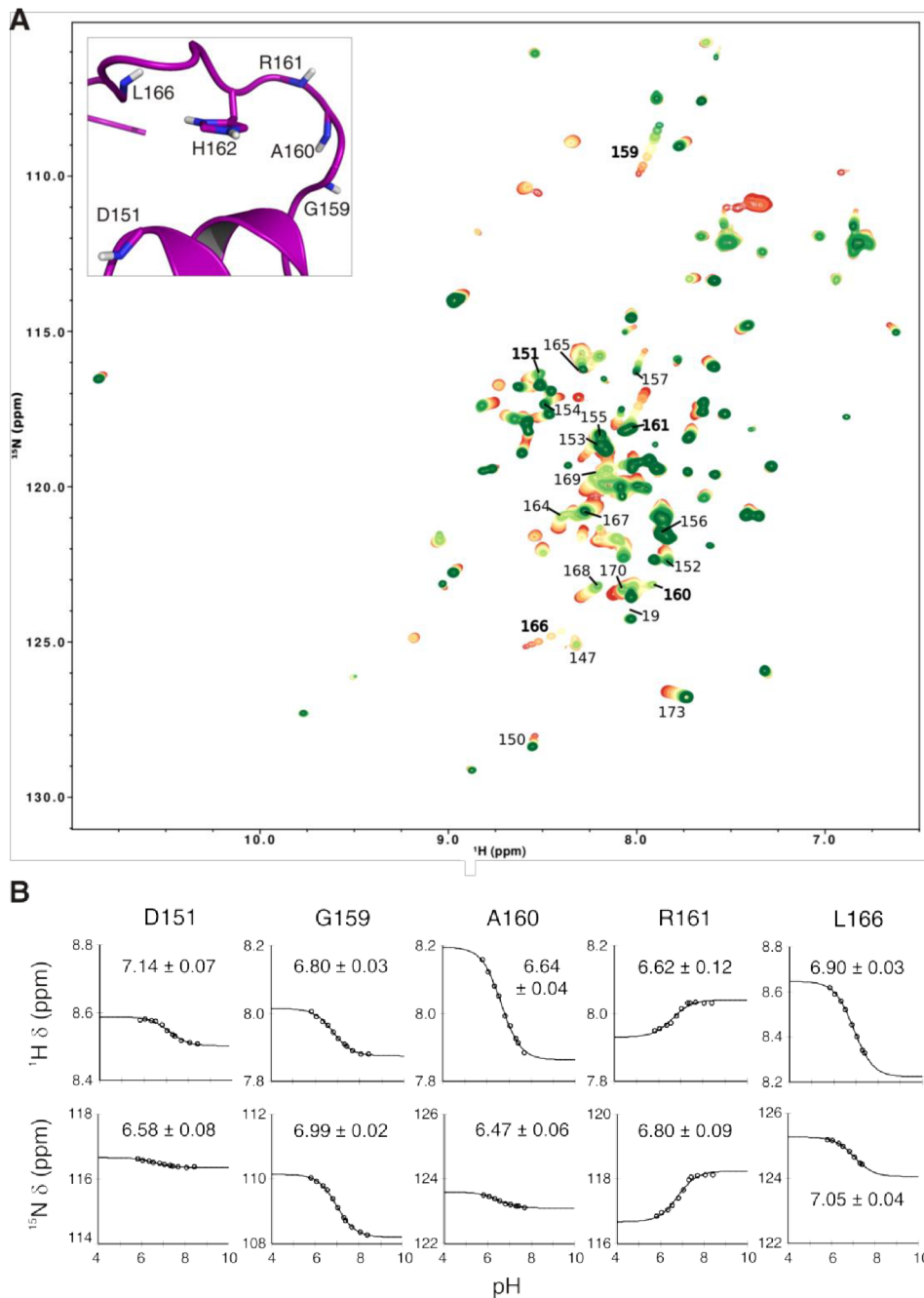
Supplementary Figure 5.2. Determination of pK$_a$ for H162 in cChimera$_{A162H}$

A. Overlap of ^{1}H, ^{15}N correlation spectra of cChimera$_{A162H}$ for the pH range from 5.81-8.40 (red to green), residues in the cTnI$_{A162H}$ region close to H162 that experienced large chemical shift perturbations are labeled in bold, the insert shows the location of those residues in the present structure. **B.** Curve fitting, pK$_a$, and pK$_a$^{app} values for the residues labeled bold in **A**, the error indicates the standard deviation of the fit.

Supplementary Table 5.1. Parameters of the NMR spectra acquired for the assignment of cNTnC•cTnI$_{A162H}$.

Experiment name (Varian)	Solvent	Nucleus in x/y/z dimension	^{1}H frequency (MHz)	nt[a]	x-points[b]	y-points[b]	z-points[b]	x-sw[c]	y-sw[c]	z-sw[c]	Mixing time (ms)
gNhsqc	H$_2$O	^{1}H/^{15}N	500	4	512	128		8398	2432		
ghn_cacb	H$_2$O	^{1}H/^{13}C/^{15}N	500	16	512	59	32	8385	10056	2026	
gcbca_co_nh	H$_2$O	^{1}H/^{13}C/^{15}N	500	16	512	59	32	8385	10056	2026	
gChsqc	H$_2$O	^{1}H/^{13}C	500	4	512	192		8398	12066		
ghc_co_nh	H$_2$O	^{1}H/^{1}H/^{15}N	500	16	512	72	32	8385	8385	2026	
gc_co_nh	H$_2$O	^{1}H/^{13}C/^{15}N	500	16	512	64	32	8385	10056	2026	
ghnha	H$_2$O	^{1}H/^{1}H/^{15}N	600	8	512	128	32	8398	7198	1823	
gnoesyChsqc	D$_2$O	^{1}H/^{1}H/^{13}C	600	16	512	64	64	8398	5999	4525	100
gnoesyNhsqc	H$_2$O	^{1}H/^{1}H/^{15}N	600	8	512	128	48	8398	7198	1823	100
tndqcosy	D$_2$O	^{1}H/^{1}H	600	64	2048	512		8398	5999		
tnnoesy	D$_2$O	^{1}H/^{1}H	600	32	2048	512		8398	8398		100
zdpsitocsy	D$_2$O	^{1}H/^{1}H	600	32	2048	512		8398	8398		60
CNfiltocsy	H$_2$O	^{1}H/^{1}H	800	128	4096	256		11990	11998		60
CNfilnoesy	H$_2$O	^{1}H/^{1}H	800	128	4096	512		11990	11998		150
CNfilnoesy*	H$_2$O	^{1}H/^{1}H	800	128	4096	512		11990	11998		150
gChmqcnoesy_Cfilt	D$_2$O	^{1}H/^{1}H/^{13}C	800	16	2048	72	40	11990	7998	4022	150

[a] Number of scans, [b] number of complex points, [c] spectral width (Hz), * acquired at pH 7.4.

Supplementary Table 5.2. Structural statistics for final ensemble of 20 structures.

NOE restraints	
Total	1282
Intramolecular for cNTnC·Ca^{2+}	
Short range (|i-j|≤1)	858
Medium range (2≤|i-j|≤4)	167
Long range (|i-j|≥5)	83
Intramolecular for cTnI$_{A162H}$	140
Intermolecular between cNTnC and cTnI$_{A162H}$	34
intermolecular between cNTnC and Ca^{2+}	8
Dihedral restraints	
For cNTnC	157
For cTnI$_{A162H}$	13
PROCHECK validation	
RMSD from average (backbone atoms N, CA, C, O)	2.1 Å [a], 0.9 Å [b]
φ, ψ in allowed regions of Ramachandran plot	98.7 % [a], 100% [b]
Z-score[c] (all)	0.12 [a], 2.90 [b]
Z-score[c] (φ, ψ)	0.90 [a], 3.82 [b]

[a] For all residues, [b] for ordered residues: 3-11, 14-27, 38-48, 54-64, 74-85, 150-157, [c] with respect to mean and standard deviation for a set of 252 x-ray structures < 500 residues, resolution ≤ 1.80 Å, R-factor ≤ 0.25, and R-free ≤ 0.28; a positive value indicates a "better" score.

References

1. Dargis, R., Pearlstone, J. R., Barrette-Ng, I., Edwards, H., and Smillie, L. B. (2002) Single mutation (A162H) in human cardiac troponin I corrects acid pH sensitivity of Ca^{2+}-regulated actomyosin S1 ATPase. *J. Biol. Chem. 277*, 34662-34665.

2. Day, S. M., Westfall, M. V., Fomicheva, E. V., Hoyer, K., Yasuda, S., Cross, N. C. L., D'Alecy, L.,G., Ingwall, J. S., and Metzger, J. M. (2006) Histidine button engineered into cardiac troponin I protects the ischemic and failing heart. *Nat. Med. 12*, 181-189.

3. Palpant, N. J., Day, S. M., Herron, T. J., Converso, K. L., and Metzger, J. M. (2008) Single histidine-substituted cardiac troponin I confers protection from age-related systolic and diastolic dysfunction. Cardiovasc. Res. 80, 209-218

4. Kobayashi, T., Jin, L., and de Tombe, P. (2008) Cardiac thin filament regulation. *Pflügers Arch. 457*, 37-46.

5. Li, M., Wang, X., and Sykes, B. (2004) Structural based insights into the role of troponin in cardiac muscle pathophysiology. *J. Muscle Res. Cell Motil. 25*, 559-579.

6. Vinogradova, M. V., Stone, D. B., Malanina, G. G., Karatzaferi, C., Cooke, R., Mendelson, R. A., and Fletterick, R. J. (2005) Ca^{2+}-regulated structural changes in troponin. *Proceedings of the National Academy of Sciences of the United States of America. 102*, 5038-5043.

7. Li, M. X., Spyracopoulos, L., and Sykes, B. D. (1999) Binding of cardiac troponin-I147-163 induces a structural opening in human cardiac troponin-C. *Biochemistry (N. Y.). 38*, 8289-8298.

8. Takeda, S., Yamashita, A., Maeda, K., and Maeda, Y. (2003) Structure of the core domain of human cardiac troponin in the Ca^{2+}-saturated form. *Nature. 424*, 35-41.

9. Zhou, Z., Li, K., Rieck, D., Ouyang, Y., Chandra, M., and Dong, W. (2012) Structural dynamics of C-domain of cardiac troponin I protein in reconstituted thin filament. *Journal of Biological Chemistry. 287*, 7661-7674.

10. Robertson, I. M., Holmes, P. C., Li, M. X., Pineda-Sanabria, S. E., Baryshnikova, O. K., and Sykes, B. D. (2012) Elucidation of isoform-dependent pH sensitivity of troponin I by NMR spectroscopy. *J. Biol. Chem. 287*, 4996-5007.

11. Pineda-Sanabria, S. E., Robertson, I. M., Li, M. X., and Sykes, B. D. (2013) Interaction between the regulatory domain of cardiac troponin C and the acidosis-resistant cardiac troponin I A162H. *Cardiovasc. Res. 97*, 481-489.

12. Robertson, I. M., Pineda-Sanabria, S. E., Holmes, P. C., and Sykes, B. D. (2014) Conformation of the critical pH sensitive region of troponin depends upon a single residue in troponin I. *Arch. Biochem. Biophys. 552-553*, 40-49.

13. Knowles, A. C., Irving, M., and Sun, Y. (2012) Conformation of the troponin core complex in the thin filaments of skeletal muscle during relaxation and active contraction. *J. Mol. Biol. 421*, 125-137.

14. Westfall, M. V., and Metzger, J. M. (2007) Single amino acid substitutions define isoform-specific effects of troponin I on myofilament Ca^{2+} and pH sensitivity. *J. Mol. Cell. Cardiol. 43*, 107-118.

15. Li, M., Saude, E., Wang, X., Pearlstone, J., Smillie, L., and Sykes, B. (2002) Kinetic studies of calcium and cardiac troponin I peptide binding to human cardiac troponin C using NMR spectroscopy. *E. B. J. 31*, 245-256.

16. Pineda-Sanabria, S., Julien, O., and Sykes, B. D. (2014) Versatile cardiac troponin chimera for muscle protein structural biology and drug discovery. *ACS Chem. Biol. 9*, 2121-2130.

17. Zheng, L., Baumann, U., and Reymond, J. (2004) An efficient one-step site-directed and site-saturation mutagenesis protocol. *Nucleic Acids Research. 32*, e115-e115.

18. Baryshnikova, O., Williams, T., and Sykes, B. (2008) Internal pH indicators for biomolecular NMR. *Journal of Biomolecular NMR. 41*, 5-7.

19. Delaglio, F., Grzesiek, S., Vuister, G. W., Zhu, G., Pfeifer, J., and Bax, A. (1995) NMRPipe: A multidimensional spectral processing system based on UNIX pipes. *Journal of Biomolecular NMR. 6*, 277-293.

20. Johnson, B. A., and Blevins, R. A. (1994) NMR view: A computer program for the visualization and analysis of NMR data. *Journal of Biomolecular NMR. 4*, 603-614.

21. Shen, Y., Delaglio, F., Cornilescu, G., and Bax, A. (2009) TALOS+: A hybrid method for predicting protein backbone torsion angles from NMR chemical shifts. *J. Biomol. NMR. 44*, 213-223.

22. Schwieters, C. D., Kuszewski, J. J., and Marius Clore, G. (2006) Using Xplor–NIH for NMR molecular structure determination. *Prog. Nucl. Magn. Reson. Spectrosc. 48*, 47-62.

23. Bermejo, G. A., Clore, G. M., and Schwieters, C. D. (2012) Smooth statistical torsion angle potential derived from a large conformational database via adaptive kernel density estimation improves the quality of NMR protein structures. *Protein Science. 21*, 1824-1836.

24. Spyracopoulos, L., Gagné, S. M., Li, M. X., and Sykes, B. D. (1998) Dynamics and thermodynamics of the regulatory domain of human cardiac troponin C in the apo- and calcium-saturated states. *Biochemistry. 37*, 18032-18044.

25. Robertson, S. P., Johnson, J. D., Holroyde, M. J., Kranias, E. G., Potter, J. D., and Solaro, R. J. (1982) The effect of troponin I phosphorylation on the Ca^{2+}-binding properties of the Ca^{2+}-regulatory site of bovine cardiac troponin. *J. Biol. Chem. 257*, 260-263.

26. Solaro, R. J., Rosevear, P., and Kobayashi, T. (2008) The unique functions of cardiac troponin I in the control of cardiac muscle contraction and relaxation. *Biochem. Biophys. Res. Commun. 369*, 82-87.

27. Hwang, P. M., Cai, F., Pineda-Sanabria, S. E., Corson, D. C., and Sykes, B. D. (2014) The cardiac-specific N-terminal region of troponin I positions the regulatory domain of troponin C. *Proceedings of the National Academy of Sciences. 111*, 14412-14417.

28. Palpant, N. J., Houang, E. M., Delport, W., Hastings, K. E. M., Onufriev, A. V., Sham, Y. Y., and Metzger, J. M. (2010) Pathogenic peptide deviations support a model of adaptive evolution of chordate cardiac performance by troponin mutations. Physiological Genomics. 42, 287-299.

29. Smith, N., Witham, S., Sarkar, S., Zhang, J., Li, L., Li, C., and Alexov, E. (2012) DelPhi web server v2: Incorporating atomic-style geometrical figures into the computational protocol. *Bioinformatics*. *28*, 1655-1657.

30. Sarkar, S., Witham, S., Zhang, J., Zhenirovskyy, M., Rocchia, W., and Alexov, E. (2012) DelPhi web server: A comprehensive online suite for electrostatic calculations of biological macromolecules and their complexes. *Communications in computational physics. 13*, 269-284.

31. Julien, O., Mercier, P., Allen, C. N., Fisette, O., Ramos, C. H. I., Lagüe, P., Blumenschein, T. M. A., and Sykes, B. D. (2011) Is there nascent structure in the intrinsically disordered region of troponin I? *Proteins. 79*, 1240-1250.

32. Palpant, N. J., Houang, E. M., Sham, Y. Y., and Metzger, J. M. (2012) pH-responsive titratable inotropic performance of histidine-modified cardiac troponin I. *Biophys. J. 102*, 1570-1579.

33. Palpant, N. J., D'Alecy, L. G., and Metzger, J. M. (2009) Single histidine button in cardiac troponin I sustains heart performance in response to severe hypercapnic respiratory acidosis in vivo. *The FASEB Journal. 23*, 1529-1540.

34. Thompson, B., Houang, E., Sham, Y., and Metzger, J. (2014) Molecular determinants of cardiac myocyte performance as conferred by isoform-specific TnI residues. *Biophys. J.* 106, 2105-2114.

CHAPTER 6

Versatile cardiac troponin chimera for muscle protein structural biology and drug discovery

Sandra E. Pineda-Sanabria[1], Olivier Julien[2], and Brian D. Sykes[1]

[1]Department of Biochemistry, University of Alberta, Edmonton, Alberta, Canada T6G 2H7. [2]Current address: Department of Pharmaceutical Chemistry, University of California - San Francisco, CA 94158, U.S.A.

Beginning in this chapter, the focus of the thesis turns to troponin as a drug target to help alleviate contractile failure. Here I introduce cChimera as a novel biochemical tool to study the regulatory troponin C-troponin I interaction with drug molecules. The analysis of this system includes its Ca^{2+} affinity, saturation state, and drug binding properties. These characteristics are compared to those of the original troponin complex that cChimera aims to represent. Our design of cChimera has also inspired other constructs that are currently being used in NMR-based drug screening. A version of this chapter has been previously published: Pineda-Sanabria *et al*. (2014) *ACS Chem. Biol.* 9: 2121-2130.

Introduction

Like most biological processes, contraction of cardiac muscle is regulated by finely orchestrated protein-protein interactions within and between thin and thick filaments of the cardiac myofibril. In the thin filament, cardiac troponin C (cTnC) and troponin I (cTnI) toggle between bound and unbound states to regulate contraction in response to intracellular Ca^{2+} concentrations. cTnC consists of two globular domains that contain two Ca^{2+} binding sites each; the regulatory N-domain (cNTnC) has only one functional Ca^{2+} binding site of high specificity and low affinity; the C-domain (cCTnC) binds two Ca^{2+} or Mg^{2+} ions with high affinity and has a structural role. cTnI is a long largely helical protein that holds the troponin complex together by interacting with cCTnC, troponin T (cTnT), and actin in the thin filament and transmits the Ca^{2+}-induced structural changes in cTnC to trigger contraction. cTnT is also a long helical protein that interacts with cTnI and anchors the complex to actin-tropomyosin in the thin filament[1-3] (Figure 6.1 in page 135).

The cNTnC-cTnI interaction is a key step in regulation of muscle contraction that has been extensively studied. Association of the switch region of TnI (switch-cTnI, residues 147 to 163) to cNTnC drags the inhibitory region of cTnI off actin releasing the inhibition of the actomyosin ATPase and

allowing contraction. The crystal structure of the core domain of cTnC in the presence of Ca[2+ 4], and the NMR structure of the cNTnC•Ca^{2+}•switch-cTnI complex[5] show cNTnC in an open conformation compared to apo-cNTnC[6] with switch-cTnI bound to a hydrophobic surface and forming a helix from residues 150 to 156. In the X-ray structure, residues following 156 form a long helix that extends to the C-terminus; however, in the NMR structure those residues lack any secondary structure. Backbone dynamics studies of cTnI[7] and skeletal TnI (sTnI)[8,9] show that the C-terminal region of both isoforms is flexible and a fly-casting mechanism has been proposed as a key regulatory event; however, the lack of relaxation data for residues prior to 176 of cTnI obscures the dynamic properties of switch-cTnI and the residues following 156. An important site of interaction on switch-TnI is the pH sensitive region; in sTnI it contains a histidine at position 130 that interacts with glutamate 20 of sNTnC at low pH and stabilizes the bound state and the open conformation of sNTnC[10]. In contrast, cTnI has an alanine in the homologous position 162 which is incapable of making this interaction resulting in decreased calcium sensitivity under acidic conditions. An A162H mutant was shown to counteract Ca^{2+}-desensitization rescuing the phenotype to that of sTnC[11-13].

Troponin has been recognized as a drug target since the early 90s[14] and the study of the cNTnC•switch-cTnI interaction in the presence of cardiotonic drugs has advanced our understanding of the mechanism of action of drugs that target this interface. Unlike conventional cardiotonic agents for the treatment of heart failure that act by increasing intracellular Ca^{2+}, a novel group of therapeutics known as Ca^{2+} sensitizers, act by increasing the sensitivity of the myofilament for Ca^{2+} and lack the risks of cardiac arrhythmias and cell death associated with Ca^{2+} overload[15]. Levosimendan, bepridil, and the levosimendan analog dfbp-o are examples of Ca^{2+} sensitizers that bind the regulatory cNTnC•switch-cTnI interface. Analysis of the structures of bepridil and dfbp-o bound to the cNTnC•switch-cTnI complex suggests that these drugs act by stabilizing the open conformation of cNTnC[16,17]. Although a high resolution structure for the complex of cNTnC•switch-cTnI with levosimendan is not available, multiple studies indicate a similar binding site as bepridil and dfbp-o, as well as similar mechanism of action[18-20]. W7 also binds the cNTnC•switch-cTnI interface but induces a desensitization effect instead[21]. For some of this drugs, additional binding sites on the surface of cTnC have been found *in vitro*; however, for all cases the relevant physiological conformation targeted is the cNTnC•switch-cTnI interface.

The *in vitro* structural studies commonly use isolated cNTnC, the relevant cTnI peptide, and the small molecule, all in solution. However, the use of excess cTnI peptide to saturate cNTnC obligated by the weak cTnI-cNTnC interaction, its low solubility, and the difficulty of producing isotope labeled peptides, present the main disadvantages of this setting. In addition, such conditions do not necessarily reflect the *in situ* environment of the myofibril since cNTnC and switch-cTnI are spatially confined in the thin filament by being attached to cTnT through cCTnC and cTnT-binding region of

cTnI, respectively. The intact ternary troponin complex is less soluble, prone to aggregation, unstable in solution, and less advantageous for structural studies by NMR and X-ray crystallography due to its large molecular weight and higher flexibility.
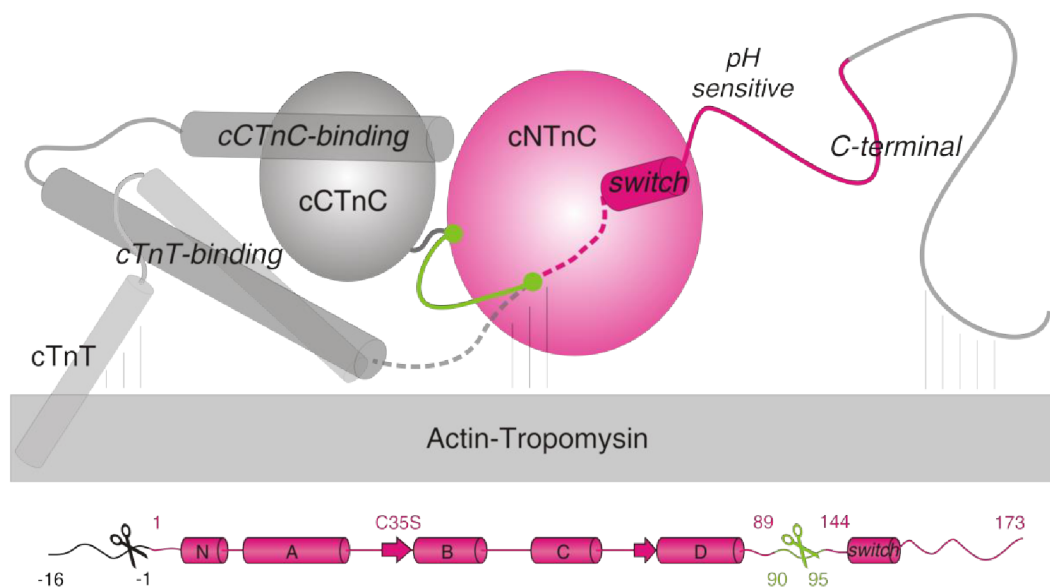
Figure 6.1. Design of cChimera.

A schematic representation of the core domain of cTnC in the thin filament according to the X-ray structure[4] (PDB ID: 1J1E). The regions of cTnC and cTnI used in cChimera are shown in pink, green elements represent the linker tethering cNTnC to switch-cTnI, cylinders represent α-helices, and arrows represent β-strands. Labels in italics refer to functional cTnI regions, the inhibitory region (not visible in the crystal structure) is represented as a dashed line; the vertical lines represent intermolecular interactions. The original numbering of cNTnC and switch-cTnI is maintained in cChimera and is shown in the extended scheme at the bottom.

Hybrid proteins have been used before to study biochemical processes involving protein-protein interfaces, and to produce peptides difficult to isolate[9,22-24]. In this study, we designed and characterized a cardiac chimeric protein (cChimera), consisting of cNTnC and switch-cTnI attached by a thrombin-protease cleavable linker that stabilizes their originally weak interaction and represents the systolic cNTnC•switch-cTnI complex (Figure 6.1), to overcome the disadvantages mentioned, and facilitate structural and biochemical studies, and drug screening. Characterization by NMR spectroscopy and fluorescence spectroscopy shows that the Ca^{2+} affinity and the effective concentration of switch-cTnI are greatly increased in cChimera; these properties promote stabilization of the open state of cNTnC and the bound state of switch-cTnI providing experimental support to theoretical considerations about the thermodynamics of tethered protein domains[25]. Investigation of

drug binding to cChimera allowed us to corroborate and augment the theory of Ca^{2+}-sensitization by small molecules that target the cNTnC•switch-cTnI interface. We proved the utility of cChimera by using it as a tool to explore the differential backbone dynamics of switch-cTnI compared to switch-sTnI, and to aid the production of switch-cTnI peptides from bacterial cultures followed by protease cleavage. Finally, cChimera can be a valuable tool in drug screening programs aimed to find molecules that target the cNTnC•switch-cTnI interface as it provides a stable representation of the relevant conformation to be targeted. Since most protein-protein interactions are relatively weak, this approach can be used in any other system for which enhanced binding is desired; for example, structure determination of other weak protein-protein complexes, regulation of processes controlled by receptor-ligand interactions, antibody engineering, and design of high-affinity DNA-binding proteins.

Experimental procedures

Protein design and purification

To represent the cNTnC•switch-cTnI complex during systole, allow for the production of isotope-labeled switch-cTnI peptides, decrease inter and intra molecular disulphide bridge formation, and facilitate the purification process; the cChimera design consisted of an N-terminal histidine tag, the tobacco etch virus (TEV) protease recognition site ENLYFQG, cNTnC C35S (residues 1 to 89), the thrombin protease recognition site LVPRGS, and switch-cTnI (residues 144 to 173) resulting in a 141-residue protein (15.9 KDa). Throughout this manuscript we maintain the numbering of the original components such that the his-tag and TEV cleavage site upstream from cNTnC were numbered –16 to –1, cNTnC 1 to 89, the thrombin-cleavable linker 90 to 95, and switch-cTnI 144 to 173. Another version with the cleavage sites exchanged was also studied, and referred to as cChimeraX.

[^{15}N]-, and [^{15}N, ^{13}C]-cChimera and [^{15}N]-cChimeraX were expressed in *Escherichia coli* as described previously[26]. The expression plasmids were obtained from Clear View Biostructures Inc. A Ni-NTA column was used to purify cChimera from the cell lysate followed by gel filtration chromatography and lyophilization. Protein identity and purity was assessed by gel electrophoresis, mass spectrometry, and confirmed by the NMR sequential assignment.

Sample preparation

All NMR samples were prepared in 10 mM KCl, 100 mM imidazole, 2 mM $CaCl_2$ (except for Ca^{2+} titrations), and 10 mM DTT at pH 6.9 with 0.25 mM 2,2-dimethyl-2-silapentane-5-sulfonate-d$_6$ sodium salt (DSS-d$_6$) or 1 mM trifluoroacetic acid as NMR internal references. Full, uncleaved cChimera or cChimeraX were used for all experiments. For NMR assignments, the sample contained 0.5 to 0.8 mM

cChimera. For TEV protease cleavage, the sample contained 0.2 mM cChimeraX, 2mM EDTA, and the pH was 8. For thrombin cleavage the sample contained 0.4 mM cChimera. Both cleavage reactions were monitored by 2D NMR spectroscopy after TEV or thrombin protease was added to the sample in the NMR tube and until changes in the amide NH signals were no longer observed; at this point cleavage was verified by SDS-polyacrylamide gel electrophoresis. For the competitive Ca^{2+} binding assays, 0.55 or 0.90 mM 5,5'-dimethyl BAPTA or 5,5'-difluoro BAPTA in the absence and presence of 0.13 or 0.17 mM cChimera were used in 100% D_2O. For all drug titrations, 0.2 to 0.4 mM cChimera was used in 95/5% H2O/D_2O and 10 mM $CaCl_2$ was added to saturate cChimera. N-(6-aminohexyl)-5-chloro-1-naphthalenesulfinamide (W7), 2',4'-difluoro(1,1'-biphenyl)-4-yloxy acetic acid (dfbp-o), and N-benzyl-N-[3-(2-methylpropoxy)-2-(pyrrolidin-1-yl)propyl]aniline (bepridil) were purchased from Sigma-Aldrich and their purity and identity confirmed by NMR spectroscopy. Stock solutions of 10 to 50 mM of W7, dfbp-o, and bepridil were prepared in DMSO-d_6 and added independently in aliquots to the protein sample until large chemical shift changes were no longer observed.

NMR Spectroscopy

All NMR experiments were acquired in 500 or 800 MHz Varian Inova spectrometers at 30°C (see Supplementary Table 6.1). One-dimensional spectra were processed using VNMRJ v.3.2 (Varian, Inc.) and two-dimensional spectra were processed with NMRPipe[28] and analyzed with NMRViewJ[29]. For the ^{15}N T_1 and T_2 relaxation experiments, we randomly acquired a series of ^1H,^{15}N-HSQC experiments with variable relaxation delays of 10, 100, 200, 500, 750, and 1000 ms for T_1, and of 10, 30, 50, 70, 90, 110, and 150 ms for T_2. We used the Rate Analysis module of NMRViewJ to fit the decay of signal intensities to a two-parameter exponential decay function to determine T_1 and T_2 relaxation times. For the $\{^1H\}^{15}N$-NOE data we used the HetNOE Analysis module of NMRViewJ to determine the ratio and the error of the signal intensities from ^1H,^{15}N-HSQC experiments with and without ^1H saturation. The noise level of the spectra was used as an estimation of the standard deviation of the signal intensities.

Competition binding assays

The chelators 5,5'-difluoro BAPTA and 5,5'-dimethyl BAPTA with K_D for Ca^{2+} of 250 and 150 nm[30], respectively, were used to perform two independent Ca^{2+} titrations, first into the chelator, and then into the same chelator in the presence of a known concentration of cChimera while monitored by ^1H NMR spectroscopy. The Ca^{2+} free protein was obtained by incubation with EDTA followed by size exclusion chromatography[27]. The Ca^{2+} free buffer was obtained by incubation with chelex100 resin (BioRad). All solutions were handled in plastic containers and the NMR tube used for titrations was acid-washed to avoid contamination by metals. The absence of a signal corresponding to the bound form of each chelator in the first titration point verified the absence of Ca^{2+} in the starting solutions.

The concentrations of the chelator and the protein were determined by ^{1}H NMR integration and amino acid analysis respectively. The fraction of chelator bound to Ca^{2+} was determined by NMR integration of the bound signal at each titration point, plotted against Ca^{2+}:chelator ratio and fit using a numerical model as previously described[31].

Fluorescence spectroscopy

cChimeraX was reacted with the environmentally sensitive label 2-(4'-(iodoacetamido)anilino)naphthalene-6-sulfonic acid (IAANS) at C84, as described previously[32]. A 2 mL sample of 200 mM MOPS, 150 mM KCl, 2 mM EGTA, 1 mM DTT, 3 mM MgCl$_2$, and 0.02% Tween 20 containing 2μM IAANS-labeled cChimeraX was excited at 330 nm and monitored at 450 nm while aliquots of 50 mM CaCl$_2$ were added with constant stirring. The concentration of free Ca^{2+} was calculated using the Maxchelator server available at http://maxchelator.stanford.edu/downloads.htm. Fluorescence values were plotted against pCa, and fit using xcrvfit available at http://www.bionmr.ualberta.ca/bds/software/xcrvfit/.

Production of switch-cTnI peptide from cChimera

A solution of ~1mg/mL of cChimeraX in 20 mM TRIS, 2 mM EDTA, 1 mM DTT, pH 8 was treated with TEV protease at room temperature. The completion of the reaction was verified by polyacrylamide gel electrophoresis and the solution was lyophilized. The dry products were redissolved in 2% trifluoroacetic acid, from where switch-cTnI was purified by HPLC to ~99%. The purity of the switch-cTnI peptide obtained was verified by MS and NMR spectroscopy.

Preparation of a model of cChimera

We built a model of the three-dimensional structure of cChimera using MODELLER 9.13[33]. We used the structure of cNTnC•switch-cTnI in the presence of Ca^{2+} as determined by NMR (PDB ID: 1MXL), and by X-ray crystallography (PDB ID: 1J1E, chains A and C) as the initial templates to generate 10 homology models of cChimera. The quality of the ten models was assessed using the discrete optimized protein energy (DOPE) method included in MODELLER (Supplementary Figure 6.1). We chose the model with the lowest energy for the loop between helices B and C of cNTnC, and for the linker region of cChimera, which is where the highest energy variation among models was observed.

Results and Discussion

Conformation of cChimera

Full cChimera was examined by NMR spectroscopy to investigate if the structural characteristics of the original cNTnC•switch-cTnI complex are retained before and after cleavage; especially the structure and disposition of the tethered switch-cTnI subdomain[4,5,25]. Heteronuclear[1]H,^{15}N HSQC, CBCA(CO)NNH, and HNCACB 2D and 3D NMR spectra were acquired to assign the backbone nuclei of cChimera in the presence of Ca^{2+}. Chemical shift assignments are deposited in the Biological Magnetic Resonance Bank database with the ID # 25034. The ^{1}H, ^{15}N HSQC 2D NMR spectra of cChimera before (pink) and after (green) cleavage were overlaid on top of a titration of switch-cTnI into cNTnC (black) to compare their chemical shifts (Figure 6.2, Supplementary Figure 6.2). The cChimera spectra showed well dispersed signals, characteristic of folded proteins, with resonance positions very similar to those of cNTnC when bound to switch-cTnI[13] indicating that its conformation in cChimera is similar to the original. The last point of the titration (last black single contour) corresponds to a switch-cTnI:cNTnC ratio of 3.7:1. Signals for cChimera lie beyond the last point of the titration along the same path analogous to a switch-cTnI:cNTnC ratio higher than 3.7:1; signals from the cleaved form of cChimera lie closer on the path of the titration comparable to a switch-cTnI:cNTnC ratio lower than 3.7:1. In the NMR fast-exchange limit, the observed chemical shift is a weighted average of the chemical shifts of the free and bound species; as the ligand concentration increases, the bound species predominates. Then, the chemical shift differences observed reflect the effective concentration of switch-cTnI in cChimera[26] (see below). Although a saturation state where only the 100% bound species contributes to the chemical shift is typically impossible to verify[36,37], cChimera approaches this state.
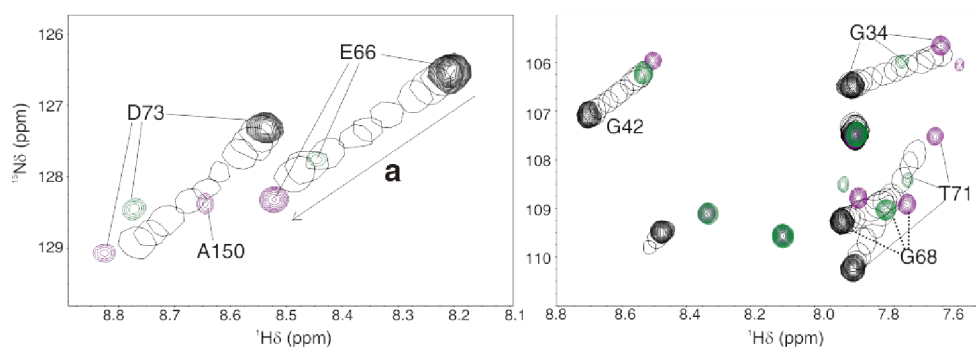
Figure 6.2. Chemical shift comparison of cChimera and cNTnC•switch-cTnI.
Overlay of expanded sections of the ^{1}H, ^{15}N-HSQC NMR spectra of cNTnC upon titration of switch-cTnI (black, with filled contours for the free cNTnC), and of cChimera before (pink) and after (green) cleavage to release the switch-cTnI peptide. Several of the most conformation-sensitive residues are labeled.

In the design of hybrid proteins it is common to incorporate glycine residues in the linkers between the target protein and its ligand to ensure flexibility and retain native intermolecular interactions; however, the incorporation of protease cleavage sites[24] could be more advantageous for some systems. Our design of cChimera contains cNTnC and switch-cTnI attached by a flexible cleavable linker that did not compromise the structural or dynamic features of the cNTnC•switch-cTnI complex. Another version containing a tobacco etch virus cleavage site on the linker was also studied (cChimeraX) and also showed conservation of the cNTnC conformation (Supplementary Figure 6.3).

Production of labeled switch-cTnI peptide

[^{15}N]-cChimera and [^{15}N]-cChimeraX were cleaved with TEV and thrombin protease, respectively, and the cleaved switch-cTnI peptide purified by HPLC. Mass spectrometry of the pure products indicated that only the reaction with TEV protease yielded a homogeneous peptide product. The resonances of the backbone nuclei of the switch-cTnI peptide were assigned using typical heteronuclear^{1}H,^{15}N HSQC, CBCA(CO)NNH, and HNCACB spectra. The ^{1}H,^{15}N HSQC of the [^{15}N]-switch-cTnI peptide (Supplementary Figure 6.4) shows all backbone HN signals grouped in a narrow range of ^{1}H resonances (7.8 to 8.6 ppm) typical of unstructured proteins as expected for the disordered free form of the switch-cTnI peptide. This proves cChimera as a useful tool to produce isotope enriched switch-cTnI peptide using bacterial cultures, a task that had been difficult in the past, providing a fast and easy way of obtaining enough ^{15}N and/or ^{13}C labeled peptides for use in NMR studies.

Effective concentration of switch-cTnI in cChimera

The effective concentration of switch-cTnI in cChimera can be estimated experimentally from the switch-cTnI titration into cNTnC. This is illustrated in Supplementary Table 6.2 where the effective concentration of switch-cTnI in cChimera is predicted using a global K_D of 200 ± 24 μM[13] and assuming a 1:1 binary complex for the cNTnC switch-cTnI titration. Using the 18 most shifted residues during the titration, which include the most conformation-sensitive residues L29, A31, G34, E66, G68, T71, D73, and F77[38], the effective switch-cTnI concentration in cChimera is 1.04 ± 0.21 mM, equivalent to a 8:1 switch-cTnI:cNTnC ratio in the titration.

Intramolecular binding theory states that tethering a ligand to its target molecule by a flexible linker has the effect of increasing the ligand concentration to ~1 mM and can also increase the stability of a folded protein[26]. Our results indicate that the effective concentration of switch-cTnI in cChimera is enough to stabilize the bound form due to decreased translational entropy corroborating this hypothesis experimentally. According to the relation between intra- and inter-molecular binding developed by Zhou[39], our experimental values of effective concentration and of K_D for cNTnC•switch-

cTnI binding (200 ± 24 μM)[13] can be used to calculate an intramolecular binding constant (K_i) of 5.2 ± 1.2. Since K_i does not depend on the concentration of the target-linker-ligand molecule, but on the ratio of probabilities of the tethered ligand being in the bound or unbound conformations, a value of 1 indicates equally populated conformations. For cChimera the high K_i value found confirms that the most populated conformation corresponds to switch-cTnI bound to cNTnC.

The bound cNTnC•switch-cTnI complex corresponds to the 'on' state of cardiac troponin during systole, and the cChimera chemical shifts correspond to this bound state. This is shown in Figure 6.3 where the extrapolated chemical shift change from free to switch-cTnI bound cNTnC is plotted against the change from free cNTnC to the cChimera (example vector **a** in Figure 6.2) using the most conformation-sensitive residues[29] (plus E19 and V79). The data points have an excellent linear correlation (R^2=0.91) with a slope corresponding to a 74% bound state for cChimera. Thus cChimera is a faithful representation of the systolic form of the cNTnC•switch-cTnI complex.
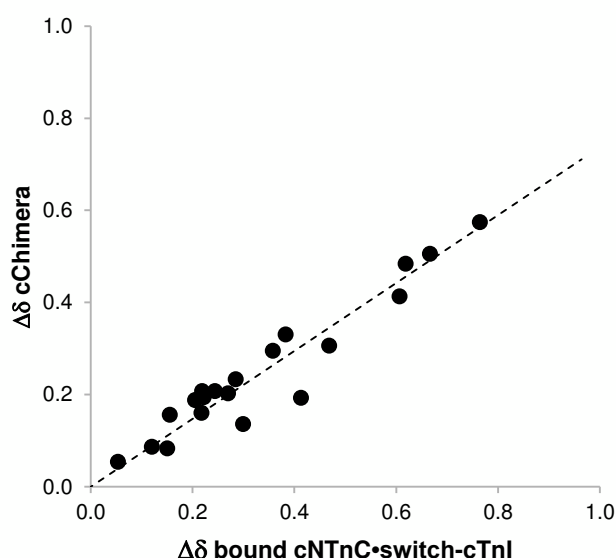
Figure 6.3. Saturation state of cChimera.

Chemical shift change $\Delta\delta$ of cNTnC resonances from the free state to the extrapolated 100% switch-cTnI bound state (x-axis, from titration) versus $\Delta\delta$ from free cNTnC to the observed cChimera resonances (y-axis). $\Delta\delta$ corresponds to total (^{1}H and ^{15}N) chemical shift change calculated as $\Delta\delta = \sqrt{\delta_H^2 + (\delta_N/5)^2}$. The resonances presented are those that are the most sensitive to switch-cTnI binding. For the dashed trend line the coefficient R^2 is 0.91, the slope is 0.74, and the x-intercept was set to zero.

The affinity of cChimera for Ca^{2+} was investigated by competition binding assays (see methods) monitored using ^1H and ^{19}F NMR spectroscopy. For the titration of Ca^{2+} to 5,5'-difluoro BAPTA in the presence of cChimera (Figure 6.4a), in the absence of Ca^{2+} (bottom spectrum) a singlet at -45.1 ppm is observed corresponding to the equivalent fluorine atoms present in the free form. The disappearance of the free form and proportional appearance of the Ca^{2+}-bound form singlet at -39.4ppm indicates that the binding is in the NMR slow exchange limit. The normalized fraction of chelator bound to Ca^{2+} was determined by spectral integration and plotted against the Ca^{2+}:chelator ratio (Figure 6.4b); note that the presence of cChimera causes a shift to the right on the Ca^{2+} binding curve of 5,5'-difluoroBAPTA. The data was then fit to obtain the K_D for the cChimera-Ca^{2+} interaction. In the same manner 5,5'-dimethyl BAPTA was used to investigate the Ca^{2+} affinity of cChimera by ^1H NMR spectroscopy (Supplementary Figure 6.5 a and b). Fluorescence spectroscopy was used to determine the Ca^{2+} affinity of IAANS-labeled cChimeraX (Supplementary Figure 6.5 c). Dissociation constants for cChimera and cChimeraX were 150 ± 50 nM and 98 ± 3 nM, respectively, indicating a higher affinity compared to the values reported for cNTnC *in vitro*[40] and in skinned cardiac muscle fibers[41-44] which are in the low micromolar range.
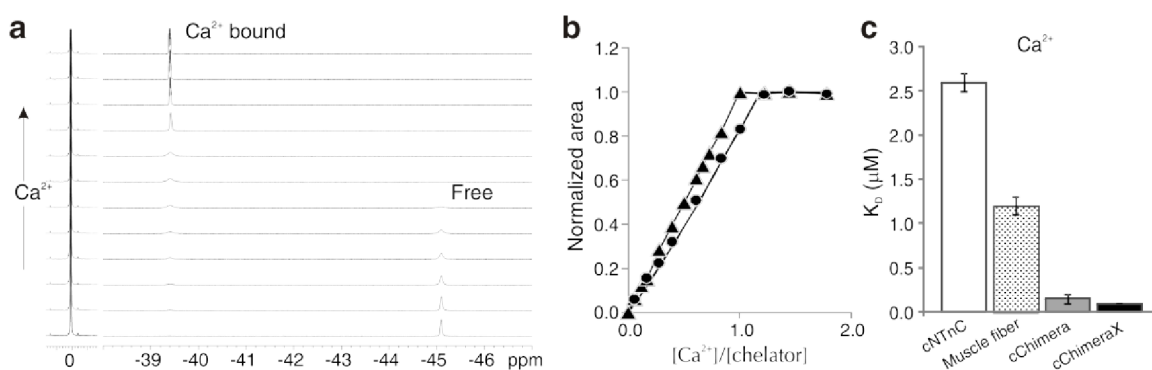
Figure 6.4. Ca²⁺ binding to cChimera.
a. ^{19}F NMR spectra monitoring the Ca^{2+} titration into 5,5'-difluoro BAPTA in the presence of cChimera.
b. Titration curves for Ca^{2+} binding to 5,5'-difluoro BAPTA alone (triangles) and in the presence of cChimera (circles). **c.** Comparison of K_D for Ca^{2+} binding to cNTnC[40], muscle fibers[41-43], cChimera and cChimeraX. Values are the mean of n=2 for cChimera and n=4 for cChimeraX ± s.e.

In the absence of a linker the formation of the cNTnC•Ca^{2+}•switch-cTnI•drug complex follows the equilibrium shown in the black box in equation (1) where cNTnC is in an equilibrium of closed and open conformations. Binding of Ca^{2+} to cNTnC induces only small structural changes in cNTnC which remains in a predominantly closed conformation (red), with sampling of the open conformation[45,46].

Binding of switch-cTnI or a suitable drug to the Ca^{2+}-bound form of cNTnC induces a large opening of cNTnC that shifts the equilibrium to a predominantly open conformation (green) and corresponds to the release of inhibition of the actomyosin ATPase. Binding of switch-cTnI to Ca^{2+}-free cNTnC has not been detected *in vitro* (grey), but given that Ca^{2+} alone does not cause the mainly-closed to mainly-open transition, this could mean that binding occurs with lower affinity than the concentration range previously tested5. In cChimera (green box) this limitation is overcome with the increase in effective concentration of switch-cTnI. The high Ca^{2+} affinity observed in cChimera suggests an already open conformation of Ca^{2+}-free cNTnC to which Ca^{2+} binds preferentially. This supports the mechanism of Ca^{2+}-sensitization wherein the binding of cardiotonic drugs help stabilize the open conformation of cNTnC to enhance Ca^{2+} binding.

$$\begin{array}{ccccc}
cNTnC + Ca^{2+} & \rightleftharpoons & cNTnC \bullet Ca^{2+} + drug & \rightleftharpoons & cNTnC \bullet Ca^{2+} \bullet drug \\
+ & & + & & + \\
cTnI & & cTnI & & cTnI \\
\updownarrow & & \updownarrow & & \updownarrow \\
cNTnC \bullet cTnI + Ca^{2+} & \rightleftharpoons & cNTnC \bullet Ca^{2+} \bullet cTnI + drug & \rightleftharpoons & cNTnC \bullet Ca^{2+} \bullet cTnI \bullet drug
\end{array} \qquad (1)$$
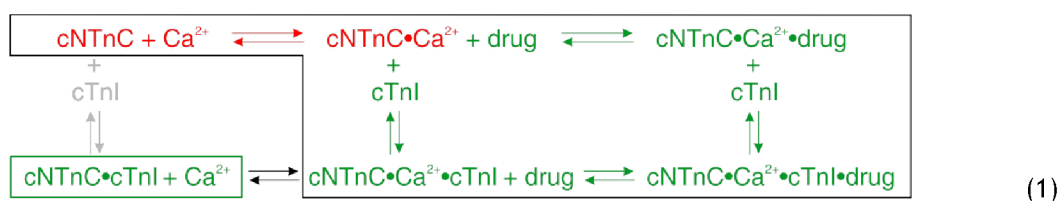
Drug binding to cChimera

To assess drug binding to cChimera, we used three different compounds for which the interaction with cNTnC and switch-cTnI had been characterized previously. The calcium desensitizer W7, and the calcium sensitizers bepridil and dfbp-o were titrated into cChimera and followed by acquiring a ^1H, ^{15}N HSQC 2D NMR spectrum at each titration point. For the titration of W7 (Figure 6.5 a and Supplementary Figure 6.6) several residues undergo large chemical shift perturbations upon binding of W7 including F24, I36, S37, T53, I61, V64, D65, E66, D67, G70, D73, F77, and C84, located on the cNTnC region of cChimera, and R147, A150, D151, L157, and G159 on the switch-cTnI region. The same direction and magnitude of chemical shift changes for the cNTnC HN resonances was observed previously when W7 was titrated into whole cTnC in the presence of two unlabeled cTnI peptides that included the switch-cTnI region[47]. The HN resonances corresponding to switch-cTnI were followed for the first time and contain valuable information; for example, the curved trace of the chemical shift perturbation (G159 and A150 in Figure 6.5a) indicates the presence of two titration events. It was shown that the mechanism of W7 as a calcium desensitizer involves decreasing the binding affinity of switch-cTnI for cNTnC by ~13-fold due to the insertion of W7 deep in the hydrophobic pocket of cNTnC, the electrostatic repulsion between the positively charged NH_3^+ moiety of W7 and the N-terminal R147 of switch-cTnI, and the consequent reorientation of switch-cTnI relative to cNTnC[21]. The two titration events correspond to the binding of W7 and either the subsequent displacement of the switch-cTnI region or the binding of a second W7 molecule of less affinity. Global fitting of the mostly perturbed residues resulted in a K_D of 230 ± 17 μM for cChimera and 167 ± 19 μM for cChimeraX (Supplementary

Figure 6.6 and Supplementary Figure 6.7), these are comparable to the affinity of W7 for cNTnC alone, but significantly higher than in the presence of switch-cTnI (Figure 6.5c).
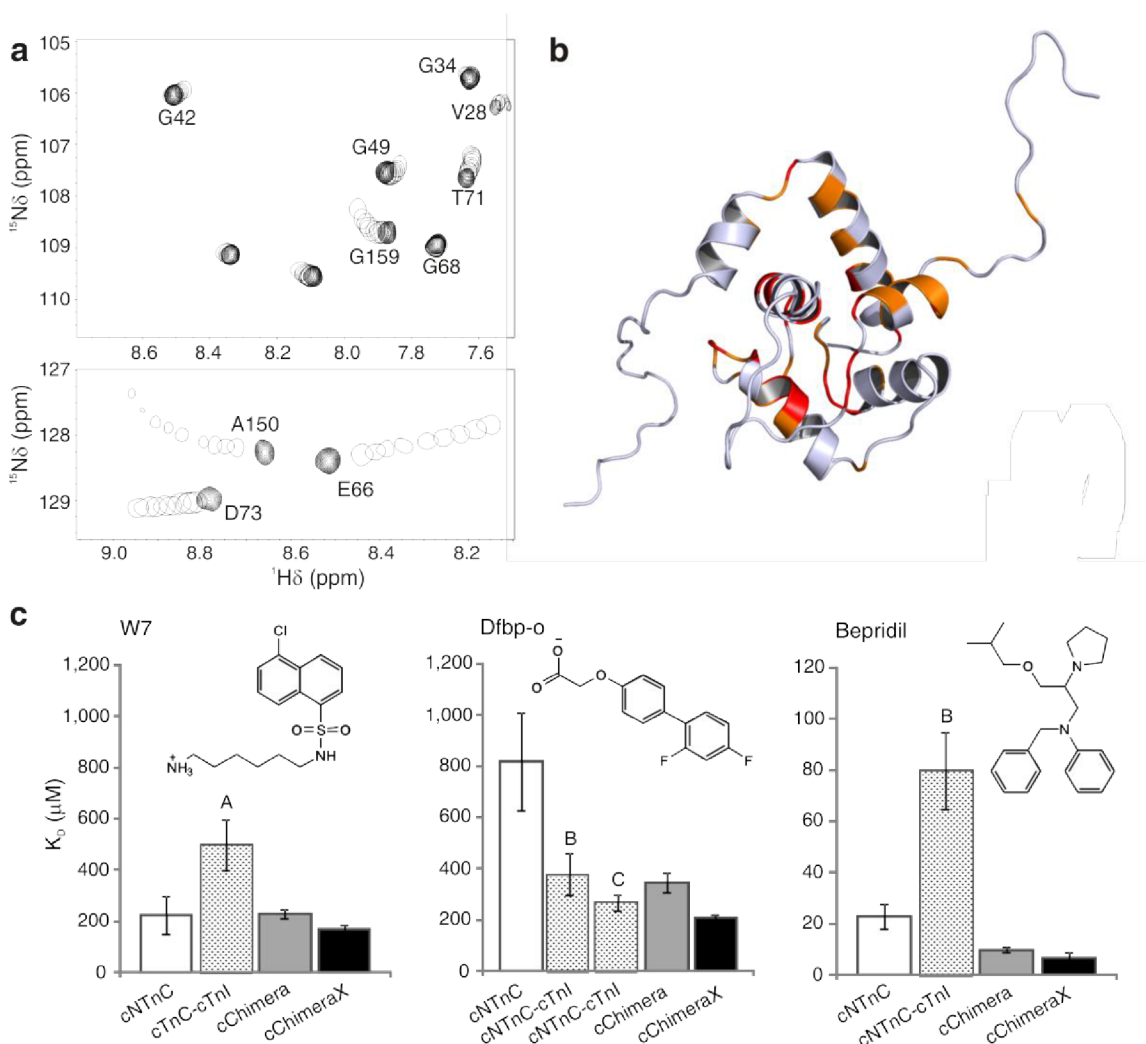
Figure 6.5. Drug binding to cChimera.
a. Overlays of expanded sections of the ^{1}H, ^{15}N-HSQC NMR spectra for the titration of W7 into cChimera, the initial state is shown in multiple contours. **b.** Chemical shift mapping of the binding of W7 on a structural model of cChimera (see Methods). Residues that shifted more than the average chemical shift perturbation (≥ 0.072 ppm) are colored orange, and those that shifted more than the average plus one standard deviation (≥ 0.141 ppm) are red. **c.** Comparison of dissociation constants of W7, dfbp-o and bepridil upon binding to cNTnC[16,17,34], cNTnC•cTnI complexes (A: cTnI$_{128-163}$ and cTnI$_{34-71}$[47], B: cTnI$_{147-163}$[16], C: cTnI$_{144-163}$[16]), cChimera, and cChimeraX. Values are of best fit ± s.e. for cChimera and cChimeraX.

In a similar way, we assessed the binding of dfbp-o and bepridil (Supplementary Figure 6.8 – 6.11). For dfbp-o we found a K_D of 345 ± 38 μM for cChimera and 206 ± 15 μM for cChimeraX; these are comparable to the affinity of dfbp-o for cNTnC in the presence of two versions of switch-cTnI peptides, but significantly higher than the affinity for cNTnC alone. The affinity of bepridil for cChimera and cChimeraX, with K_D's of 10 ± 1 μM and 7 ± 2 μM respectively, is significantly higher than the affinity of bepridil for cNTnC and cNTnC in the presence of switch-cTnI (Figure 6.5c). The direction and magnitude of the chemical shift perturbations caused by dfbp-o and bepridil on cChimera was also extremely similar to their respective titration into the cNTnC•switch-cTnI complex.

Differential perturbation observed for the first time on the switch-cTnI region indicates that modulation of the strength of cNTnC•switch-cTnI interaction is essential for the mechanism of Ca^{2+} sensitization. Chemical shift mapping of the perturbations caused by the binding of a ligand to a target can be used to localize the ligand's binding site. We used a model of cChimera to estimate the localization of the binding site of W7 (Figure 6.5b), dfbp-o, and bepridil (Supplementary Figure 6.12). Residues in the hydrophobic pocket of cNTnC are the most perturbed by all ligands, this agrees with the localization of each ligand in the structure of the corresponding cNTnC•switch-cTnI•drug complex and indicates conservation of ligand binding in cChimera. However, the degree of perturbation on the switch-cTnI region was different for all ligands: W7>>bepridil>dfbp-o. This can be correlated with the effect of each drug on the cNTnC•switch-cTnI interaction; whereas W7 and bepridil weaken the cNTnC•switch-cTnI interaction due to steric clash and electrostatic repulsions respectively[17,21], dfbp-o enhances their binding affinity.

The cNTnC-cTnI interaction poses a very particular challenge to drug discovery, which is the search for small molecules that conjunctively bind the weak cNTnC•switch-cTnI complex since this is the systolic conformation that needs to be targeted. Protein-protein interactions are increasingly gaining interest as targets for drug discovery. As opposed to enzyme-receptor interactions that commonly contain small defined pockets, protein-protein interactions pose more difficulties to rational design of small molecule inhibitors in part due to the large surface areas they comprise and their inherent flexibility[48]. The use of NMR-based screenings as well as computational methods for this purpose are common strategies that have proven to be successful in several cases[49,50,51]. We propose cChimera as a tool for rational drug design of interaction modulators and as an optimized target system for drug screening as it was shown to reproduce the features of drug binding to the original cNTnC•switch-cTnI complex in terms of chemical shift perturbation and localization of the binding site, with equal or higher affinity. Given that switch-cTnI binding and the open state of cNTnC are stabilized in cChimera, so that binding of dfbp-o matches the affinity observed for the original complex, cChimera can be particularly useful for the study of agonists that target the cNTnC•switch-cTnI

interface. However, cChimera could not be used to assess calcium sensitization by drug candidates due to the predominantly open state of cNTnC in cChimera and the suggested predisposition to bind Ca^{2+}.

cChimera dynamics

We determined the NMR relaxation parameters T_1, T_2, and heteronuclear $\{^1H\}$ ^{15}N-NOE at 500 and 600 MHz for the backbone NH pairs of cChimera (Supplementary Figure 6.13) and cChimeraX (Figure 6.6) to compare the dynamic properties of their different regions. Average T_1 values (in ms ± average standard error) for whole cChimera (cChimeraX) at 500 MHz and 600 MHz were 514 ± 8 (509 ± 8), and 627 ± 8 (625 ± 8); for residues 1 to 89 corresponding to cNTnC were 517 ± 8 (514 ± 8), and 632 ± 8 (641 ± 8); and for residues 144 to 170 corresponding to switch-cTnI[1] were 483 ± 9 (479 ± 8), and 587 ± 8 (577 ± 8), respectively. The pattern of T_1 values were similar for both fields and the values determined at 600 MHz were constantly higher for most residues in the protein as expected for a rigid globular protein; however, this difference is decreased for residues –7 to –2 in the his-tag of the protein and residues 160 to 173 in switch-cTnI, which correlates with flexible regions. Also, T_1 for the switch-cTnI region was lower than for the cNTnC region indicating additional internal motions for this region. Average T_2 values (in ms ± average standard error) for whole cChimera (cChimeraX) at 500 MHz and 600 MHz were 96 ± 2 (93 ± 1), and 89 ± 1 (86 ± 1); for the cNTnC region were 88 ± 2 (80 ± 1), and 81 ± 1 (74 ± 1); and for the switch-cTnI region were 102 ± 2 (104 ± 1), and 91 ± 1 (97 ± 1), respectively. The T_2 patterns were also verysimilar for the two fields tested and higher values were observed for the N- and C-terminal residues as expected; nevertheless, for the switch-cTnI component a gradual increase of T_2 was observed startingfrom residue 159 which indicates increasing flexibility on this region. NOE average values ± average standard error for cChimera (cChimeraX) at 500 MHz and 600 MHz were 0.69 ± 19 (0.66 ± 0.13), and 0.78 ± 0.15 (0.74 ± 0.15); for the cNTnC region were 0.74 ± 0.20 (0.73 ± 0.14), and 0.84 ± 0.15 (0.80 ± 0.16); and for the switch-cTnI region were 0.61 ± 0.19 (0.53 ± 0.12), and 0.71 ± 0.14 (0.62 ± 0.15). The NOE data for cChimera remains high (>0.65) and constant for most residues, but lowers rapidly for the his-tag region and gradually from residue 157 in the switch-cTnI region, again indicating higher mobility in this parts. In general, similar relaxation parameters were obtained for cChimera and cChimeraX which implies the residues forming the linker do not interfere with the mobility of the components.

---

[1] In cChimera residues 144 to 173 correspond to switch-cTnI; however, the calculation of the NMR relaxation parameters for the switch-cTnI region included only residues 144 to 170 to omit the intrinsically flexible terminal residues and to avoid bias.
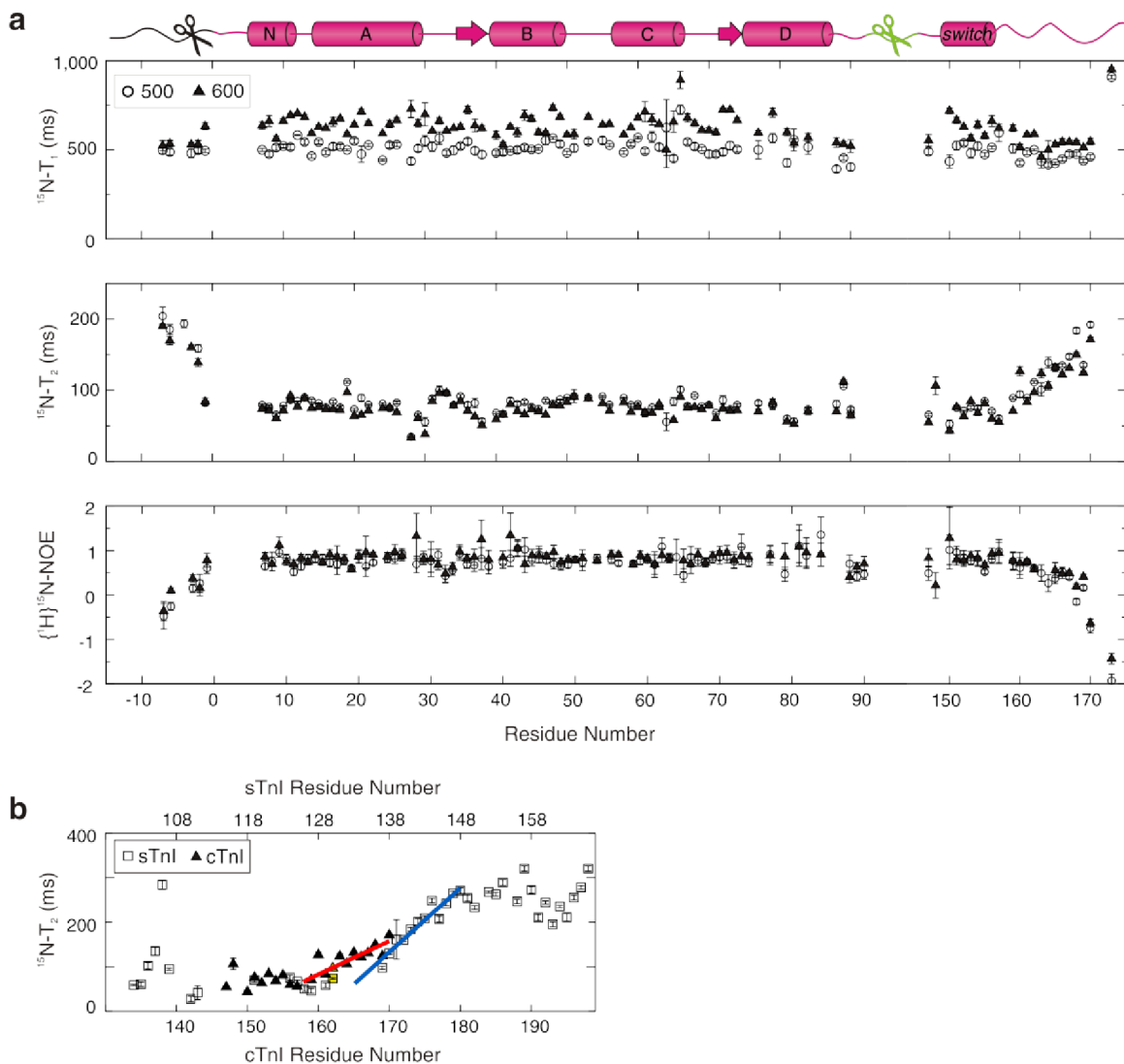
Figure 6.6. Dynamics of cChimeraX.

a. ^{15}N-T_1, ^{15}N-T_2 and heteronuclear {^{1}H}^{15}N-NOE NMR relaxation data for backbone amide NH pairs of cChimeraX at 500 (open circles) and 600 (closed triangles) MHz. **b.** Comparison of ^{15}N-T_2 relaxation times at 600 MHz for a homologous region of sTnI (squares) and cTnI (triangles, this work). The scale on the top indicates the corresponding residue numbering for the homologous region of sTnI. Yellow symbols mark the position of the cardiac and skeletal pH sensitive residues A162 and H130, respectively. The extrapolation of red and blue lines shows where the mobility begins in the cardiac and skeletal Chimeras, respectively. All error bars correspond to s.e.

To contrast the dynamic properties of the switch-TnI region between the cardiac (this work) and skeletal[9] isoforms, T_2 values at 600 MHz of residues 159 and 161 to 170 of cTnI and of residues 169 to 180 of sTnI were independently fit to straight lines by linear regression and extrapolated up to the

T_2 value of the rigid region (Figure 6.6b). The slope values of the trend lines for the homologous cardiac and skeletal TnI regions are 7.5 and 14.4, respectively, and the last residue on the rigid region according to the extrapolation of the trend lines are 158 and 133, respectively. Typically, the ratio of T_1/T_2 is independent of internal motions when the correspondent NOE is > 0.60 at 500 MHz or > 0.65 at 600 MHz, and can be used as an estimate of the correlation time for the molecule which at the same time correlates with the molecular weight. Excluding residues for which NOE < 0.60 or < 0.65, T_1/T_2 ratios for cChimera (cChimeraX) at 500 and 600 MHz were 512 ± 8 (513 ± 8) and 625 ±8 (635 ± 9), respectively; which corresponds roughly to a molecular weight of 13 KDa and correlates well with our < 16 KDa protein. The R_2 relaxation rate (1/ T_2) also correlates well with the expected molecular weight according to determinations done previously in the laboratory for similar protein systems of different mass under similar experimental conditions[52].

The relaxation data presented here indicates that cChimera is well folded and does not form intermolecular interactions, aggregation, or dimers, and was used to reveal isoform-specific muscle dynamics. Our results indicate that the switch-cTnI region is immobilized and tumbles together with the cNTnC region as a rigid domain, but with a gradual increase of internal motions from residue 158. This correlates well with the structure of cNTnC•switch-cTnI, where switch-cTnI forms a helix from residues 150 to 156 that binds cNTnC. A previous study on the skeletal isoform of a sNTnC•sTnI complex showed that residues 124 to 130 of sTnI are as rigid as sNTnC, and that residues 140 to 170 are flexible[9]. Although switch-sTnI also forms a helix (117–127) that binds sNTnC, comparison of the relaxation data for both isoforms (Figure 6.6b) indicates that mobility of the switch-TnI region is different between isoforms; whereas in sTnI rigidity spans the switch helix and several residues beyond up to residue 133, in cTnI rigidity ceases shortly after the last residue of the switch helix. This supports the "histidine-button" theory for which an electrostatic interaction between H130 of sTnI (located beyond the switch helix) and E20 of sNTnC was demonstrated to stabilize their association in the face of acidosis[10]. This is not the case for the cardiac system in which the analogous residue of H130 is A162 incapable of promoting electrostatic interactions, consistent with the extended increased flexibility that we observed for this region. For an A162H mutant of cTnI that diminishes pH sensitivity we anticipate the relaxation parameters to be more similar to those of sTnI than cTnI.

In conclusion, our design of cChimera provides a reliable representation of the cNTnC•switch-cTnI complex at systole that offers several advantages over using the separate components including perfect 1:1 stoichiometry, improved solubility and ease of isotope labeling. cChimera allowed us to test the thermodynamic considerations relative to the effective concentration, structure, and dynamics of a tethered domain[25,38], and to get molecular level insight into differential muscle dynamics. We anticipate that our work can be applied to the design of other hybrid protein systems for the study of protein-protein interactions, drug design, and the production of labile peptides. In the endeavor of

accelerating the drug discovery process, stabilization of protein-protein interfaces as shown here, could be used to create optimized targets for drug screening that reduce the number of hits by restricting the binding space to that of the relevant physiological conformation. In addition to serve in the traditional search for inhibitors, our approach may be useful to search for protein-protein interaction enhancers, an important task currently much less pursued.

Acknowledgments
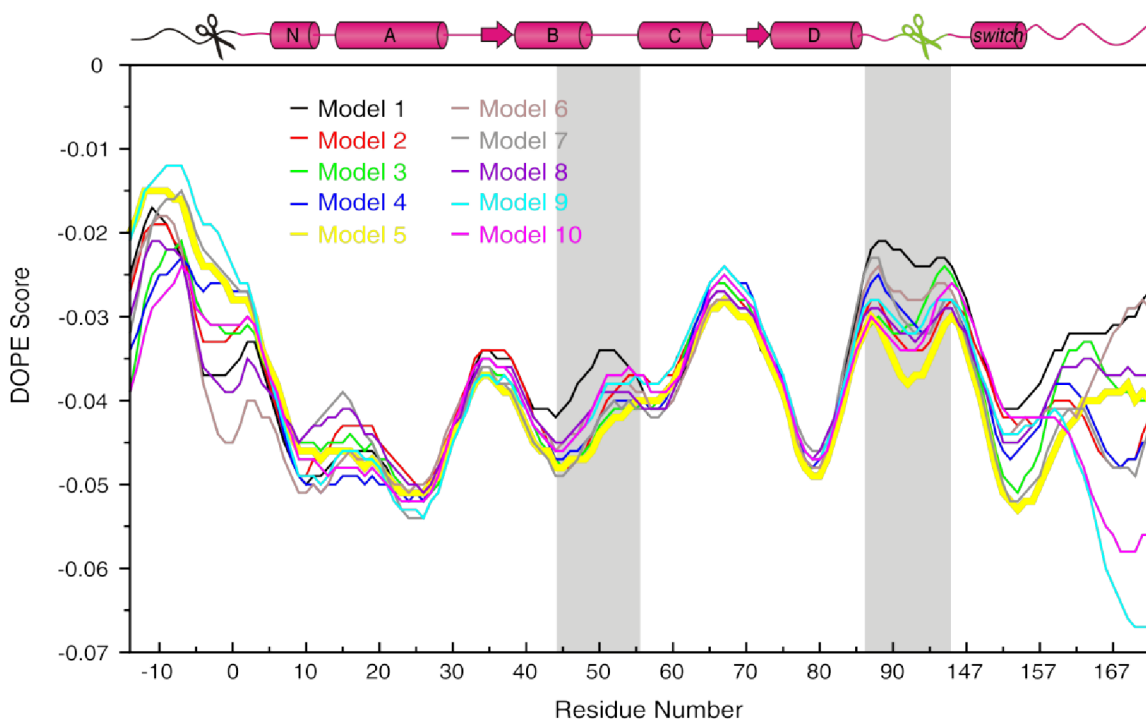
Supplementary Figure 6.1. Preparation of the cChimera model.

DOPE score by residue number for ten models of cChimera generated by MODELLER. The schematic for the cChimera structural elements is shown at the top. Grey boxes indicate zones of high energy variability among models. The thick yellow line corresponds to model 5 which showed the lowest energy in the BC loop and the cleavable linker between cNTnC and switch-cTnI.
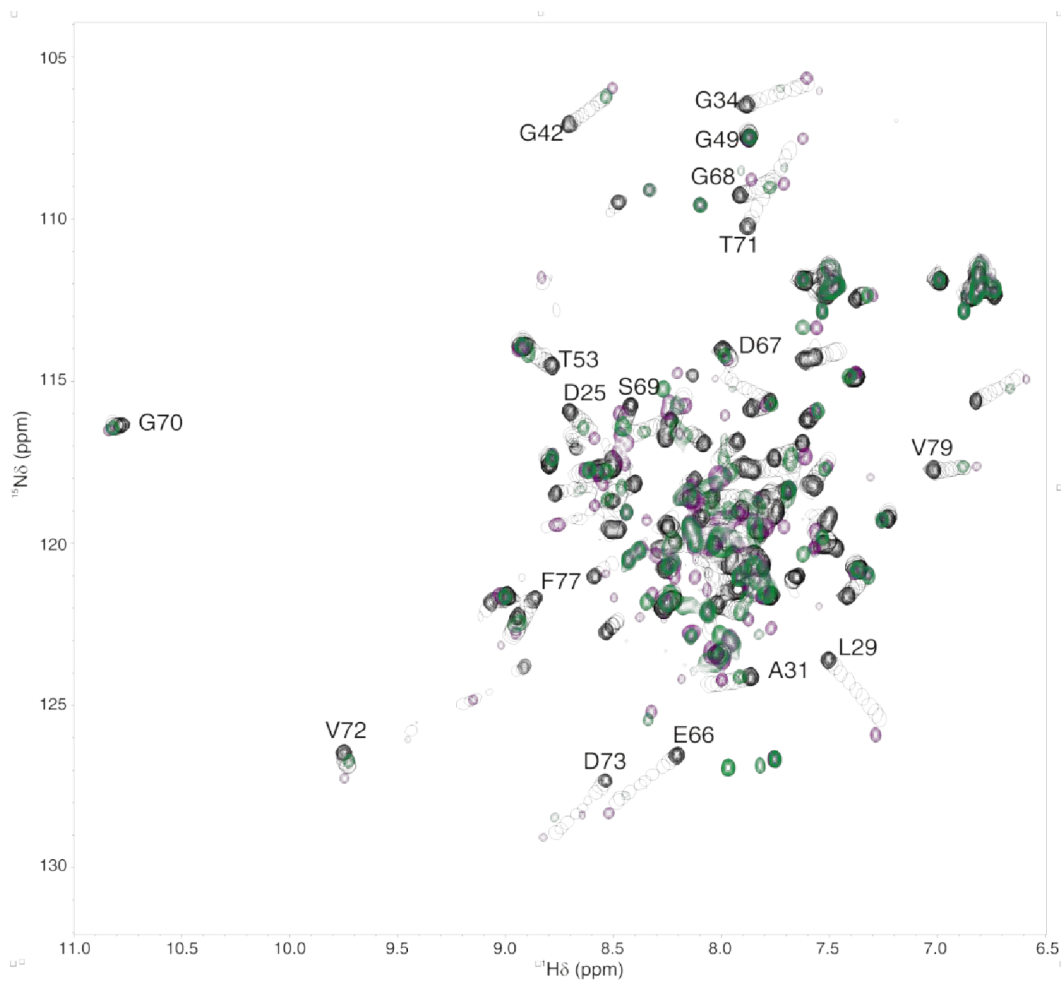
Supplementary Figure 6.2. Chemical shift comparison of cChimera and cNTnC•switch-cTnI.

Overlay of full ^{1}H, ^{15}N-HSQC NMR spectra of cNTnC upon titration of switch-cTnI (black, with filled contours for the free cNTnC), and of cChimera before (pink) and after (green) cleavage to release the switch-cTnI peptide. Signals corresponding to the most conformation-sensitive residues are labeled.
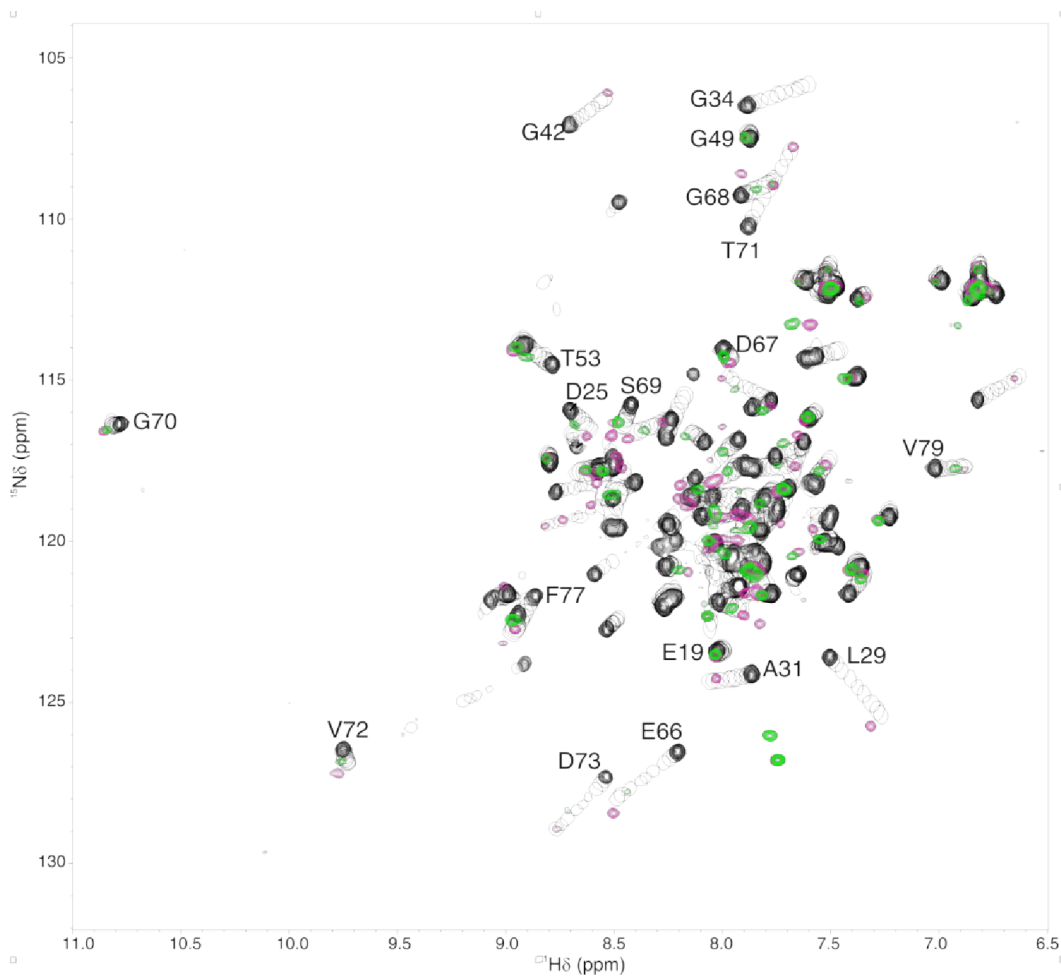
Supplementary Figure 6.3. Chemical shift comparison of cChimeraX and cNTnC•switch-cTnI.

Overlay of full ¹H, ¹⁵N-HSQC NMR spectra of cNTnC upon titration of switch-cTnI (black, with filled contours for the free cNTnC), and of cChimeraX before (pink) and after (green) cleavage to release the switch-cTnI peptide. Signals corresponding to the most conformation-sensitive residues are labeled.
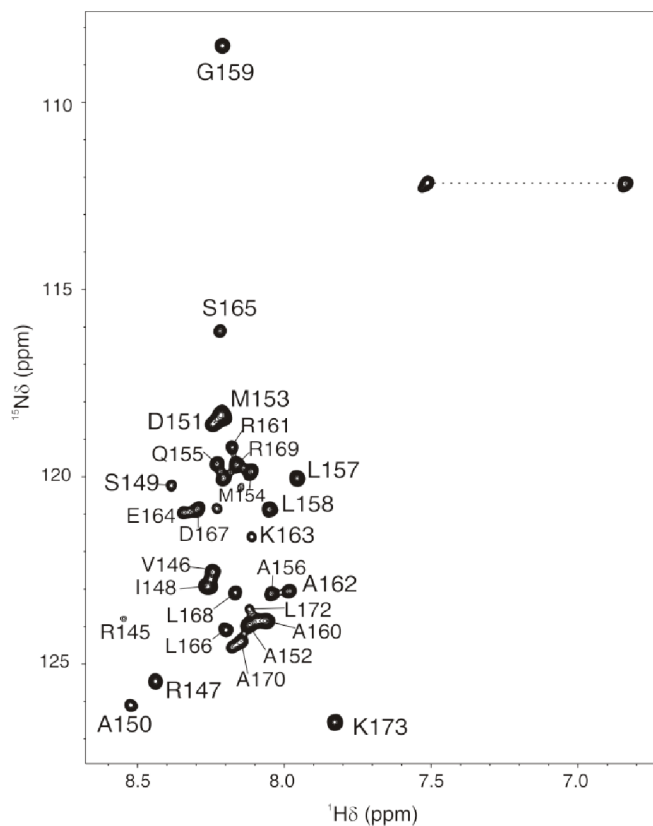
Supplementary Figure 6.4. ^{15}N-labeled switch-cTnI purified from cChimeraX.

^{1}H, ^{15}N HSQC NMR spectrum of the switch-cTnI peptide purified after TEV cleavage of cChimeraX. All assigned residues are labeled. The resonances connected through a dashed line correspond to side chain NH$_2$ groups.
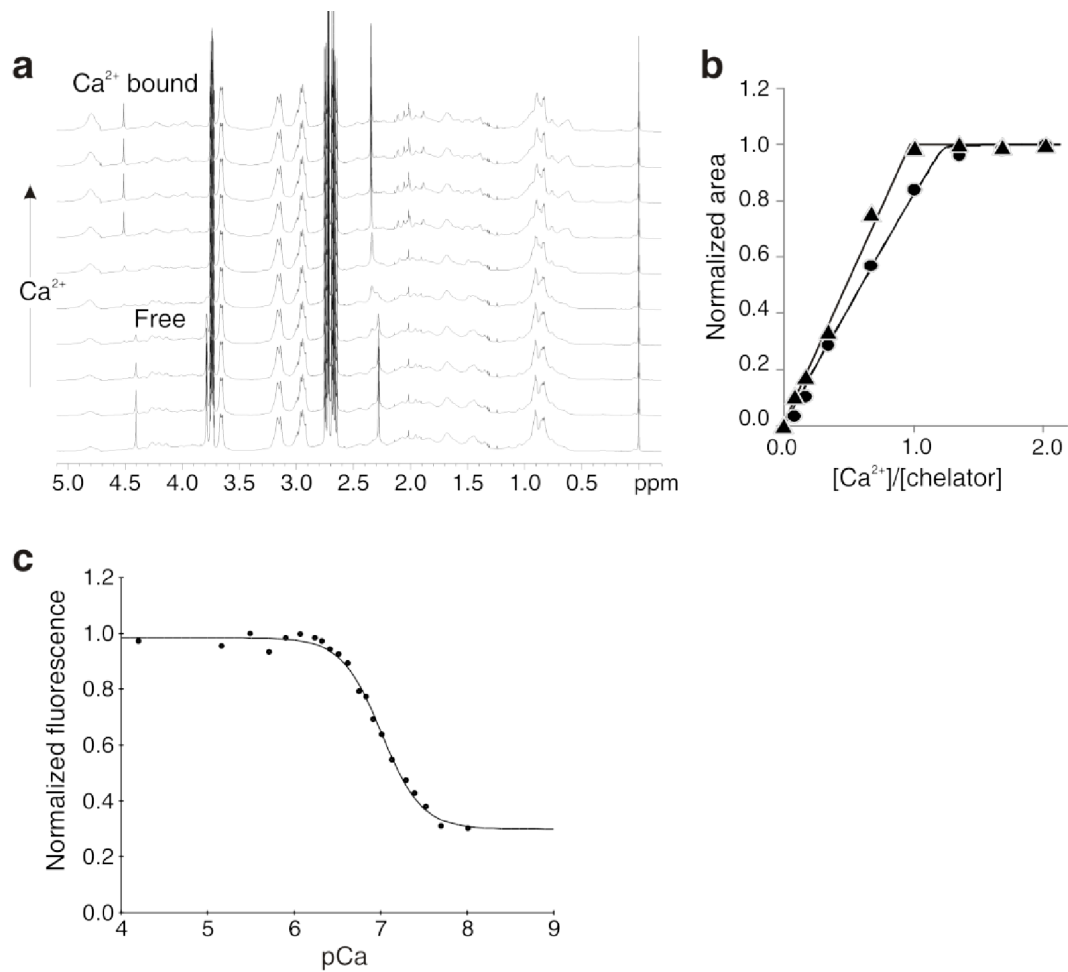
Supplementary Figure 6.5. Ca²⁺ binding to cChimera and cChimeraX.

a.¹H NMR spectral stack for the titration of Ca²⁺ into 5,5'-dimethyl BAPTA in the presence of cChimera.

b. Fit curves for Ca²⁺ binding to 5,5'-dimethyl BAPTA alone (triangles) and in the presence of cChimera (circles). **c.** Fluorescence change of cChimeraX-IAANS as a function of pCa.
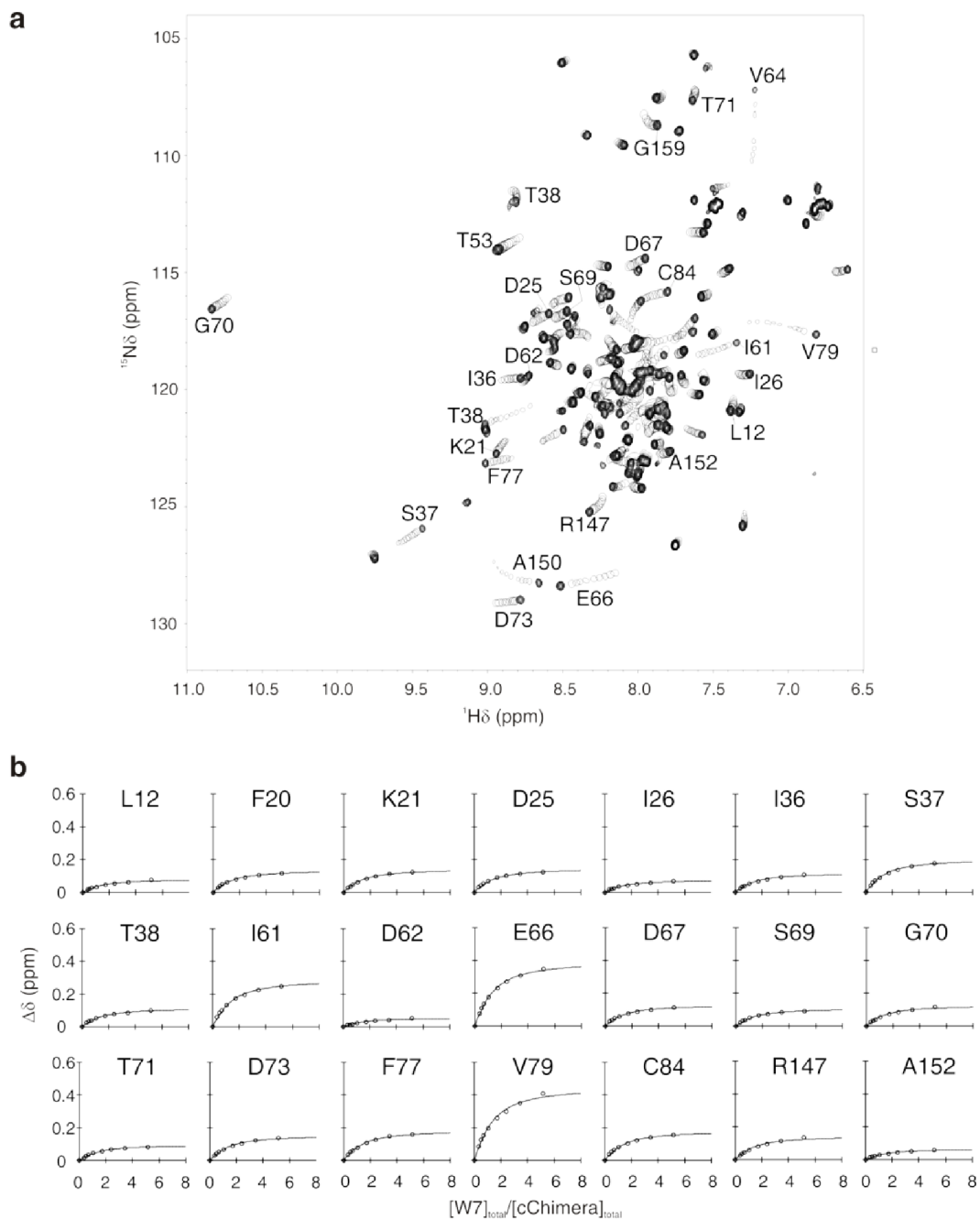
Supplementary Figure 6.6. W7 binding to cChimera.

a. ^{1}H, ^{15}N HSQC spectral stack and **b.** representative global fit curves for the titration of W7 into cChimera, the first point of the titration is represented in multiple contours. Residues experiencing large chemical shift perturbations are labeled. Non-linear points at latter stages of titration were not used.
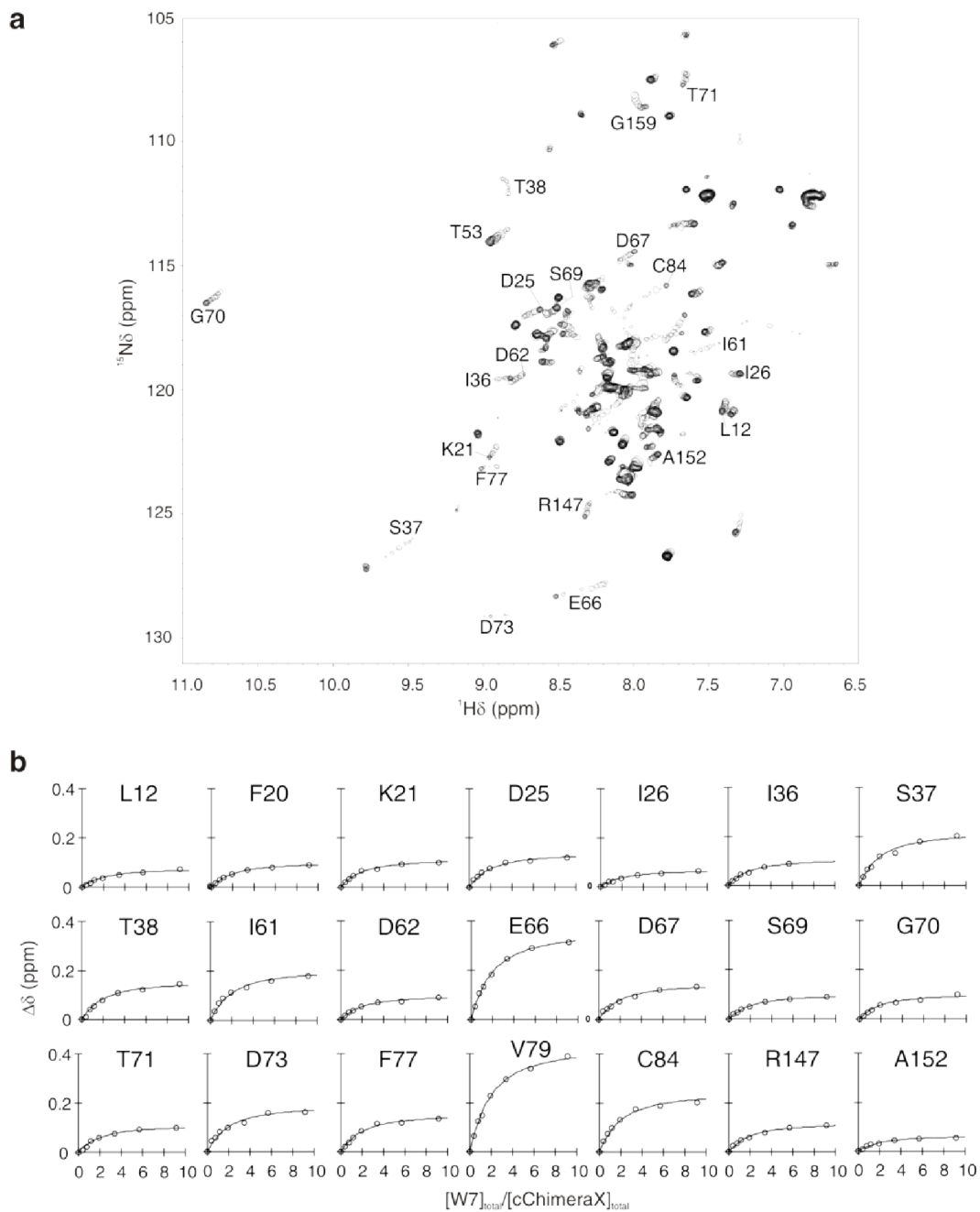
Supplementary Figure 6.7. W7 titration to cChimeraX.

^{1}H, ^{15}N HSQC spectral stack (**a**) and representative global fit curves (**b**) for the titration of W7 into cChimeraX, the first point of the titration is represented in multiple contours. Residues experiencing large chemical shift perturbations are labeled
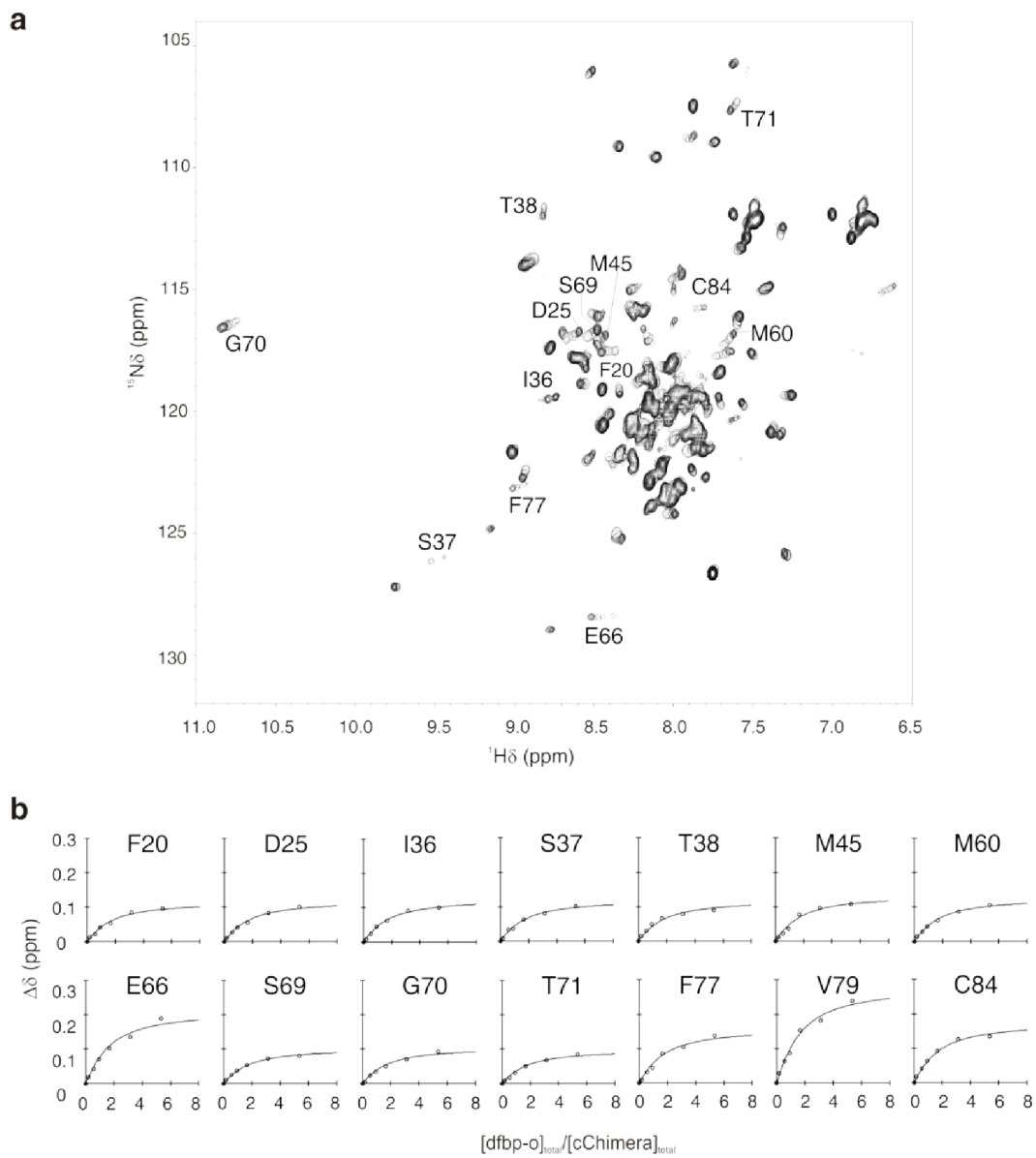
Supplementary Figure 6.8. Dfbp-o binding to cChimera.

^{1}H, ^{15}N HSQC spectral stack (**a**) and representative global fit curves (**b**) for the titration of dfbp-o into cChimera, the first point of the titration is represented in multiple contours. Residues experiencing large chemical shift perturbations are labeled.
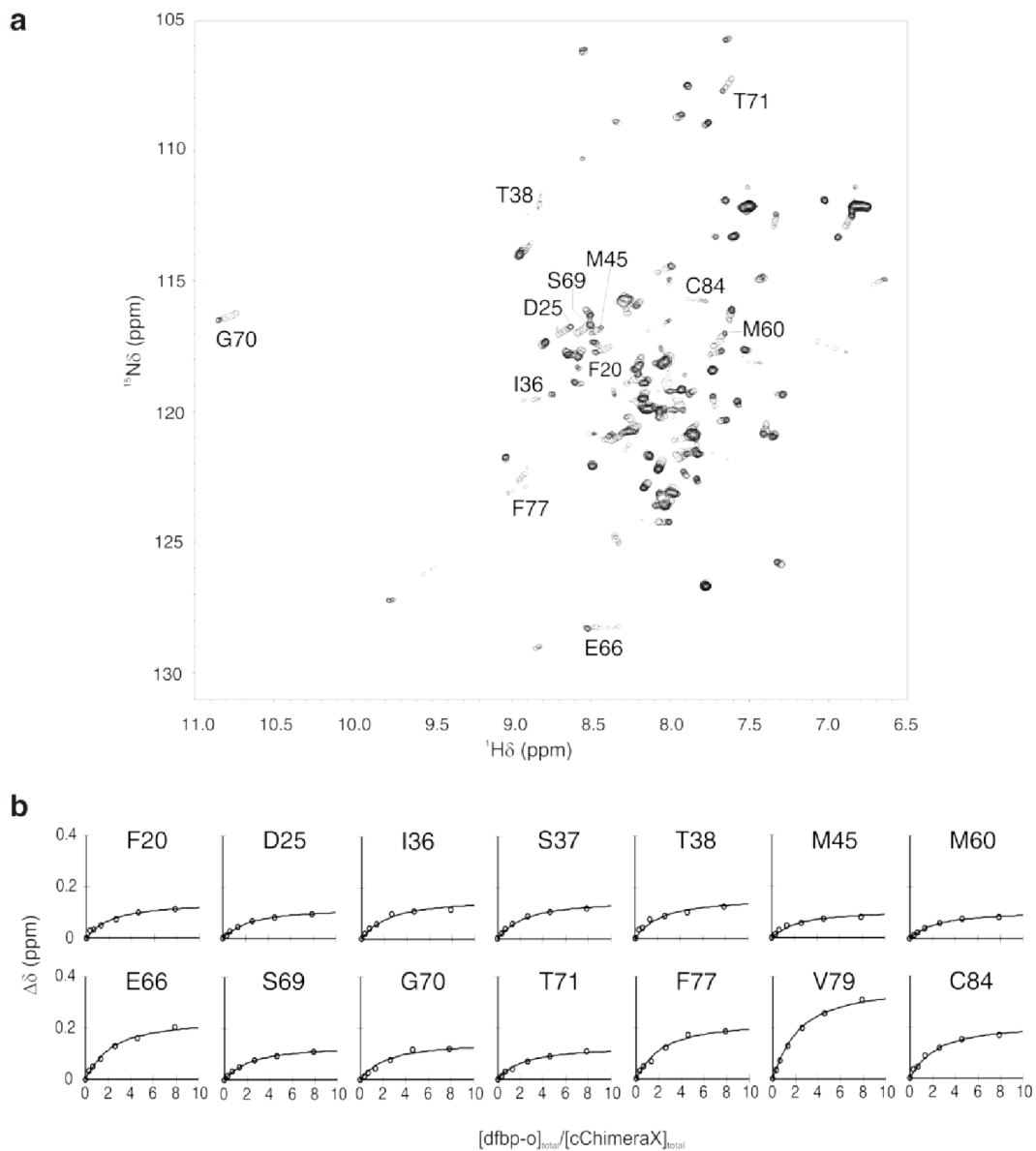
Supplementary Figure 6.9. Dfbp-o binding to cChimeraX.

¹H, ¹⁵N HSQC spectral stack (a) and representative global fit curves (b) for the titration of dfbp-o into cChimeraX, the first point of the titration is represented in multiple contours. Residues experiencing large chemical shift perturbations are labeled.
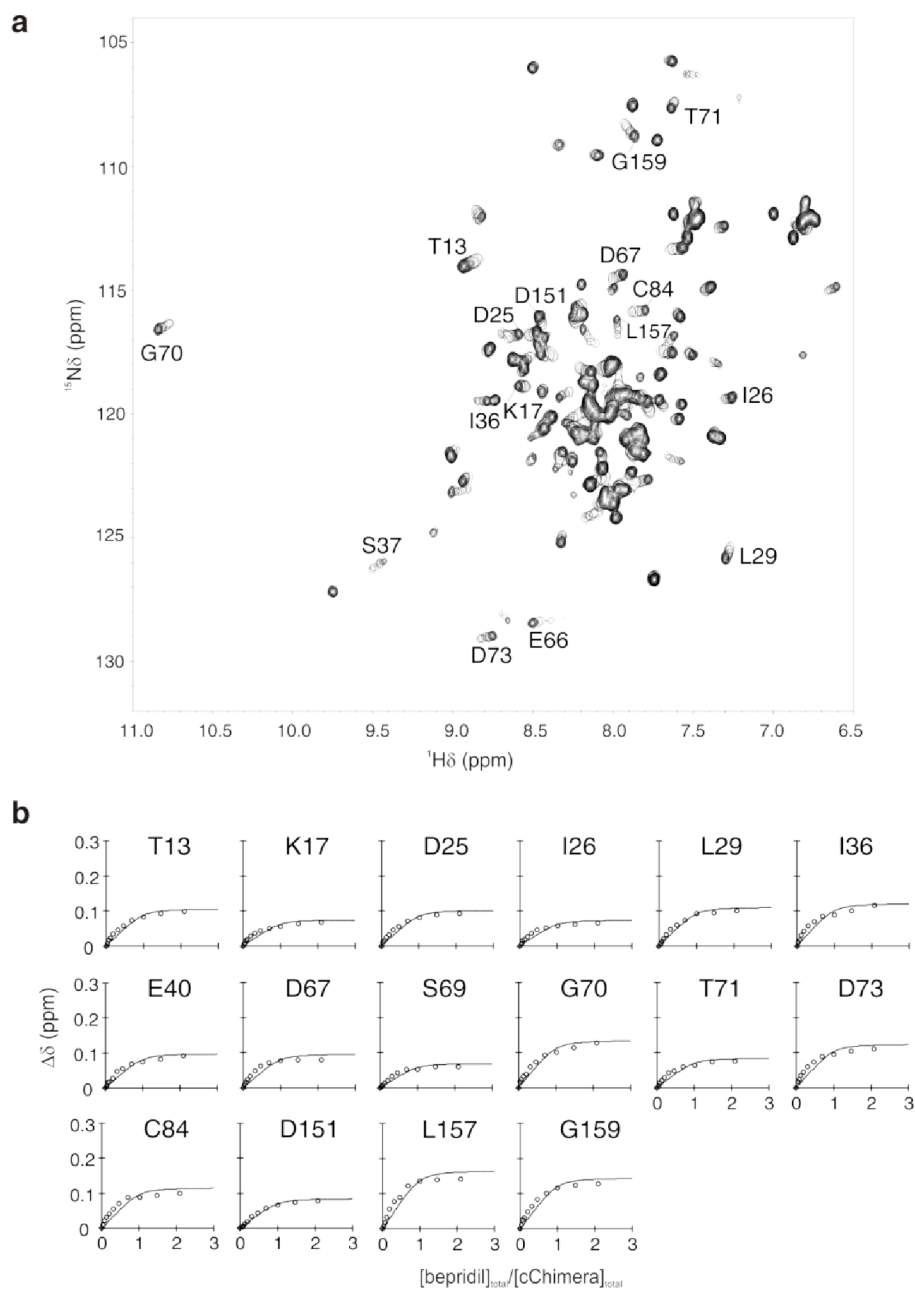
Supplementary Figure 6.10. Bepridil binding to cChimera.

^{1}H, ^{15}N HSQC spectral stack (a) and representative global fit curves (b) for the titration of bepridil into cChimera, the first point of the titration is represented in multiple contours. Residues experiencing large chemical shift perturbations are labeled.
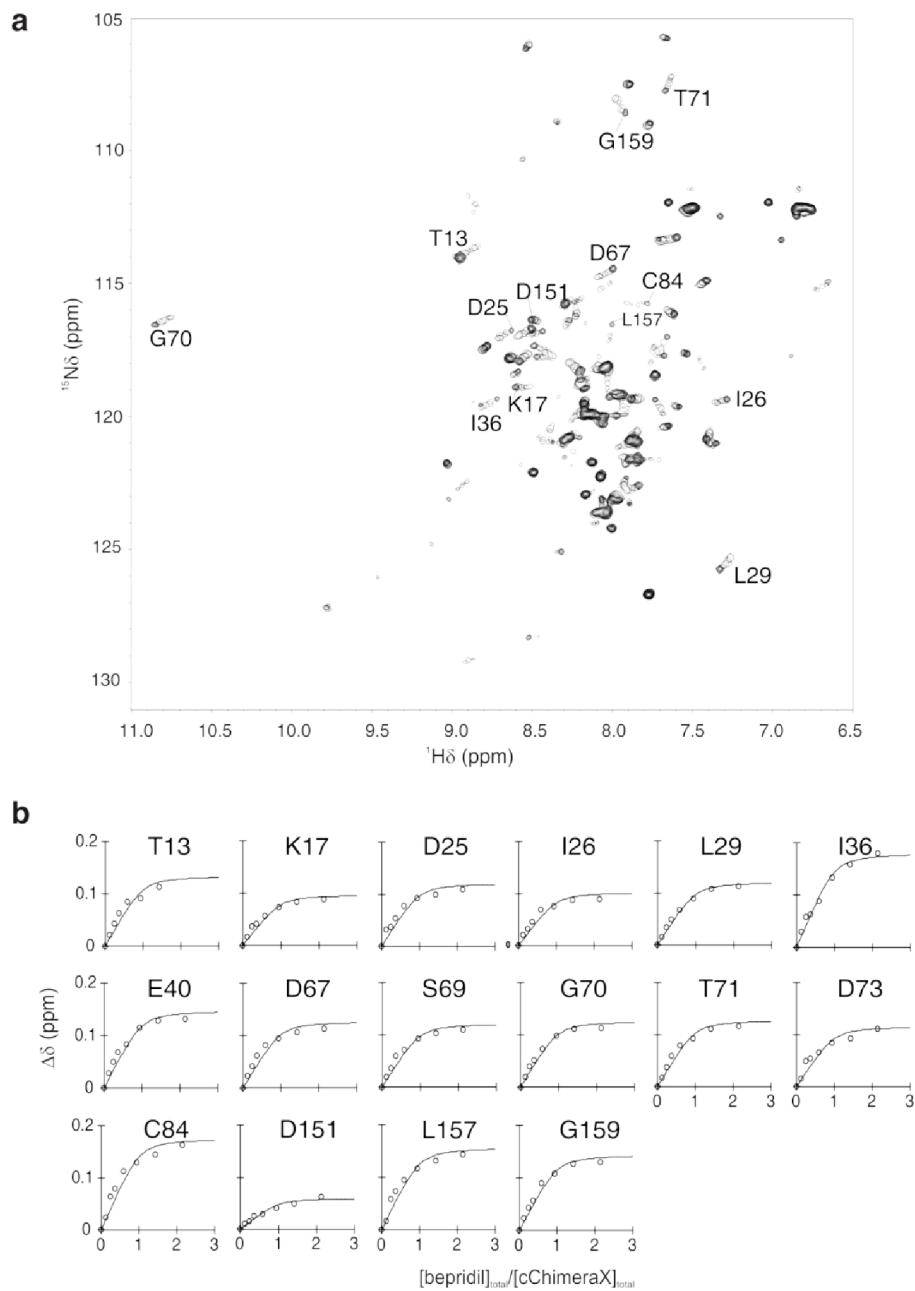
Supplementary Figure 6.11. Bepridil binding to cChimeraX.

^{1}H, ^{15}N HSQC spectral stack (a) and representative global fit curves (b) for the titration of bepridil into cChimeraX, the first point of the titration is represented in multiple contours. Residues experiencing large chemical shift perturbations are labeled.
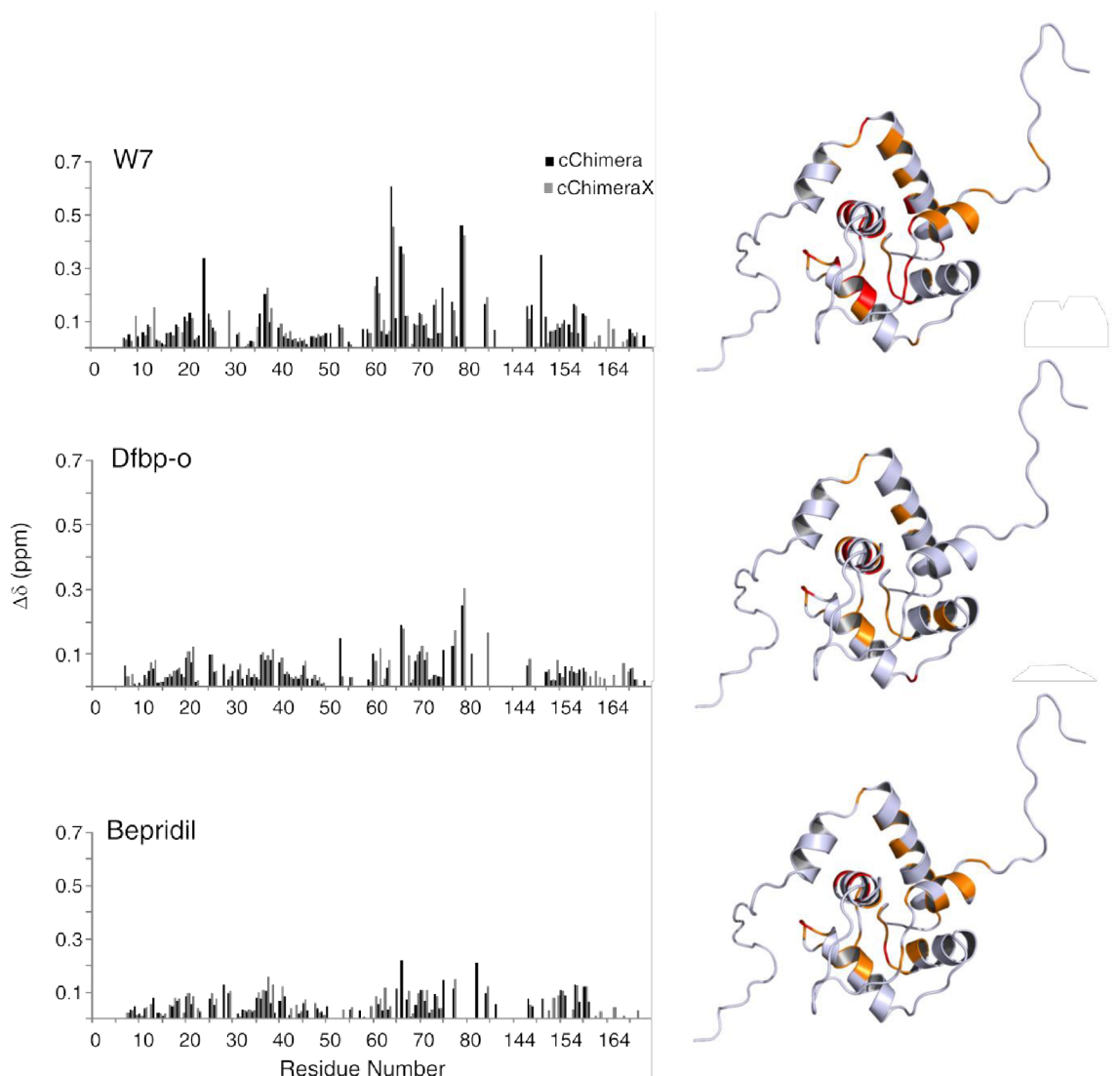
Supplementary Figure 6.12. Summary of drug binding to cChimera and cChimeraX.

Left, magnitude of chemical shift perturbations (Δδ) upon binding of W7, dfbp-o, and bepridil to cChimera, and cChimeraX. Right, chemical shift mapping of the binding of each compound on a structural model of cChimera. Residues that shifted more than the average chemical shift perturbation (≥ 0.072 ppm) are colored orange, and those that shifted more than the average plus one standard deviation (≥ 0.141 ppm) are red.
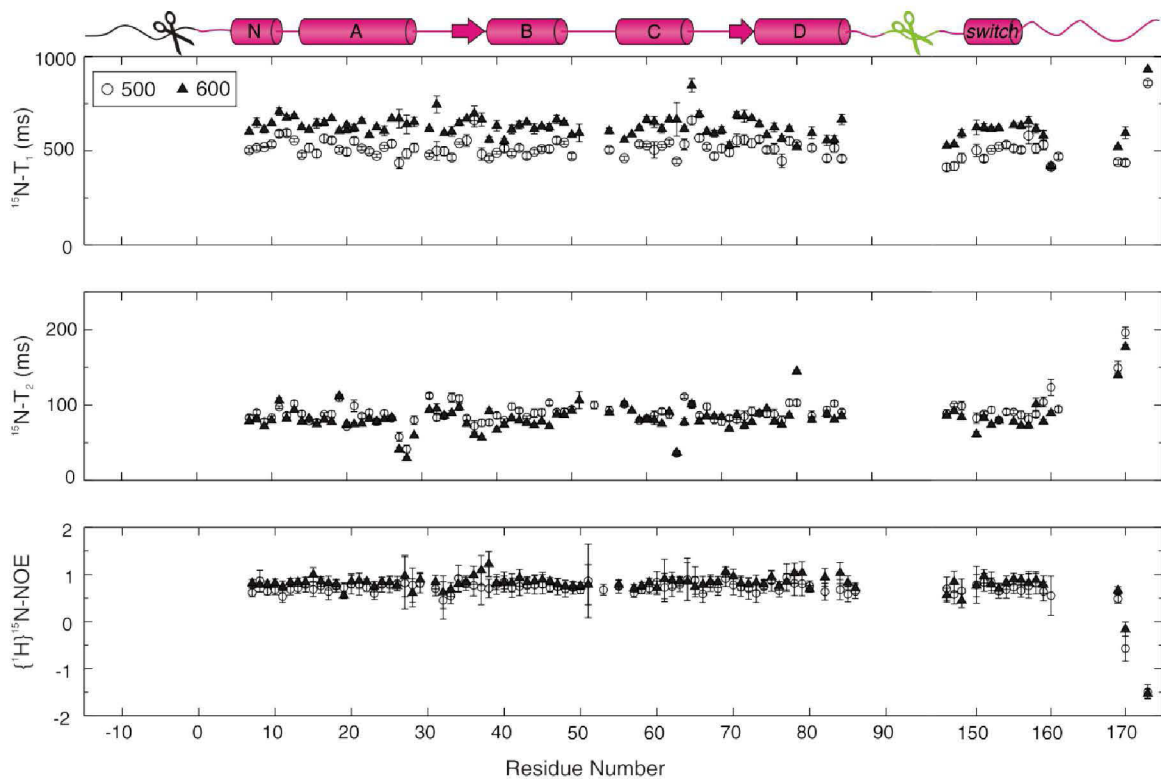
Supplementary Figure 6.13. Dynamics of cChimera.

^{15}N-T_1, ^{15}N-T_2 and heteronuclear $\{^1H\}^{15}N$-NOE NMR relaxation data for backbone amide NH pairs of cChimeraX at 500 and 600 MHz. The color scheme is as in Figure 1.

Supplementary Table 6.1. Parameters of the NMR spectra acquired for the assignment of cChimera, cChimeraX, and switch-cTnI.

Protein	Experiment name (Varian)	Nucleus in x/y/z dimension	^1H frequency (MHz)	nt^a	x-points^b	y-points^b	z-points^b	x-sw^c	y-sw^c	z-sw^c	Mixing time (ms)
cChimera	gNhsqc	$^1H/^{15}N$	800	8	2048	128		11990	3242		
	gnoesyNhsqc	$^1H/^1H/^{15}N$	800	8	2048	144	36	11990	9598	3242	80
	gtocsyNhsqc	$^1H/^1H/^{15}N$	800	8	2048	144	36	11990	9597	3242	60
	ghnha	$^1H/^1H/^{15}N$	800	8	1024	144	36	11990	6398	3242	
cChimeraX	gNhsqc	$^1H/^{15}N$	500	4	1024	128		8385	1317		
	gChsqc	$^1H/^{13}C$	500	4	1024	128		8385	8798		
	ghn_cacb	$^1H/^{13}C/^{15}N$	500	16	1024	59	36	8385	10057	2023	
	gcbca_co_nh	$^1H/^{13}C/^{15}N$	500	16	1024	59	36	8385	10057	2026	
Switch-cTnI	gNhsqc	$^1H/^{15}N$	500	8	1024	128		8385	2026		
	gChsqc	$^1H/^{13}C$	500	8	1024	237		8385	8798	2200	
	ghn_cacb	$^1H/^{13}C/^{15}N$	500	16	1024	59	36	8385	10056	1317	
	gcbca_co_nh	$^1H/^{13}C/^{15}N$	500	16	1024	59	36	8385	10056	1317	

^{a} Number of scans, ^{b} number of complex points, ^{c} spectral width.

Supplementary Table 6.2. Concentration of switch-cTnI in cChimera calculated from cNTnC switch-cTnI titration.

Residue number	Expected Δδ to saturation (ppm)	Observed Δδ to cChimera (ppm)	Normalized Δδ to cChimera	Calculated [cTnI] in cChimera (μM)
D25	0.22180	0.19461	0.88	1546
L29	0.66607	0.50564	0.76	730
A31	0.29901	0.13608	0.46	227
D33	0.41261	0.19314	0.47	237
G34	0.46804	0.30669	0.66	466
C35	0.24397	0.20763	0.85	1254
G42	0.35785	0.29501	0.82	1047
K43	0.21764	0.16067	0.74	661
M45	0.28437	0.23361	0.82	1028
N51	0.15003	0.08347	0.56	324
E66	0.61859	0.48446	0.78	825
D67	0.11996	0.08679	0.72	618
G68	0.26951	0.20268	0.75	705
S69	0.20457	0.18818	0.92	2416
T71	0.76443	0.57479	0.75	705
D73	0.60663	0.41358	0.68	518
F77	0.38280	0.33067	0.86	1382
V79	0.21868	0.20779	0.95	3940
			0.75 ± 0.03	**1035 ± 213**

Values in bold are average ± se.

References

1. Gordon, A. M., Homsher, E., and Regnier, M. (2000) Regulation of contraction in striated muscle. *Physiol. Rev. 80*, 853–924.

2. Kobayashi, T., Jin, L., and de Tombe, P. (2008) Cardiac thin filament regulation. *Pflügers Arch. 457*, 37–46.

3. Li, M., Wang, X., and Sykes, B. (2004) Structural based insights into the role of troponin in cardiac muscle pathophysiology. *J. Muscle Res. Cell Motil. 25*, 559–579.

4. Takeda, S., Yamashita, A., Maeda, K., and Maeda, Y. (2003) Structure of the core domain of human cardiac troponin in the Ca^{2+}-saturated form. *Nature. 424*, 35–41.

5. Li, M. X., Spyracopoulos, L., and Sykes, B. D. (1999) Binding of cardiac troponin-$I_{147-163}$ induces a structural opening in human cardiac troponin-C. *Biochemistry 38*, 8289–8298.

6. Spyracopoulos, L., Li, M. X., Sia, S. K., Gagné, S. M., Chandra, M., Solaro, R. J., and Sykes, B. D. (1997) Calcium-induced structural transition in the regulatory domain of human cardiac troponin C. *Biochemistry 36*, 12138–12146.

7. Lassalle, M. W. (2010) Defective dynamic properties of human cardiac troponin mutations. *Biosci. Biotechnol. Biochem. 74*, 82–91.

8. Blumenschein, T. M. A., Stone, D. B., Fletterick, R. J., Mendelson, R. A., and Sykes, B. D. (2006) Dynamics of the C-terminal region of TnI in the troponin complex in solution. *Biophys. J. 90*, 2436–2444.

9. Julien, O., Mercier, P., Allen, C. N., Fisette, O., Ramos, C. H. I., Lagüe, P., Blumenschein, T. M. A., and Sykes, B. D. (2011) Is there nascent structure in the intrinsically disordered region of troponin I? *Proteins. 79*, 1240–1250.

10. Robertson, I. M., Holmes, P. C., Li, M. X., Pineda-Sanabria, S. E., Baryshnikova, O. K., and Sykes, B. D. (2012) Elucidation of isoform-dependent pH sensitivity of troponin I by NMR spectroscopy. *J. Biol. Chem. 287*, 4996–5007.

11. Dargis, R., Pearlstone, J. R., Barrette-Ng, I., Edwards, H., and Smillie, L. B. (2002) Single mutation (A162H) in human cardiac troponin I corrects acid pH sensitivity of Ca^{2+}-regulated actomyosin S1 ATPase. *J. Biol. Chem. 277*, 34662–34665.

12. Day, S. M., Westfall, M. V., Fomicheva, E. V., Hoyer, K., Yasuda, S., Cross, N. C. L., D'Alecy, L.,G., Ingwall, J. S., and Metzger, J. M. (2006) Histidine button engineered into cardiac troponin I protects the ischemic and failing heart. *Nat. Med. 12*, 181–189.

13. Pineda-Sanabria, S. E., Robertson, I. M., Li, M. X., and Sykes, B. D. (2013) Interaction between the regulatory domain of cardiac troponin C and the acidosis-resistant cardiac troponin I A162H. *Cardiovasc. Res. 97*, 481–489.

14. Overington, J. P., Al-Lazikani, B., and Hopkins, A. L. (2006) How many drug targets are there? *Nat Rev Drug Discov. 5*, 993–996.

15. Endoh, M. (2008) Cardiac Ca^{2+} signaling and Ca^{2+} sensitizers. *Circ. J. 72*, 1915–1925.

16. Robertson, I. M., Sun, Y., Li, M. X., and Sykes, B. D. (2010) A structural and functional perspective into the mechanism of Ca^{2+}-sensitizers that target the cardiac troponin complex. *J. Mol. Cell. Cardiol. 49*, 1031–1041.

17. Wang, X., Li, M. X., and Sykes, B. D. (2002) Structure of the regulatory N-domain of human cardiac troponin C in complex with human cardiac troponin $I_{147-163}$ and bepridil. *J. Biol. Chem. 277*, 31124–31133.

18. Haikala, H., Kaivola, J., Nissinen, E., Wall, P., Levijoki, J., and Lindén, I. (1995) Cardiac troponin C as a target protein for a novel calcium sensitizing drug, levosimendan. *J. Mol. Cell. Cardiol. 27*, 1859–1866.

19. Sorsa, T., Heikkinen, S., Abbott, M. B., Abusamhadneh, E., Laakso, T., Tilgmann, C., Serimaa, R., Annila, A., Rosevear, P. R., Drakenberg, T., Pollesello, P., and Kilpeläinen, I. (2001) Binding of levosimendan, a calcium sensitizer, to cardiac troponin C. *J. Biol. Chem. 276*, 9337–9343.

20. Papp, Z., Édes, I., Fruhwald, S., De Hert, S. G., Salmenperä, M., Leppikangas, H., Mebazaa, A., Landoni, G., Grossini, E., Caimmi, P., Morelli, A., Guarracino, F., Schwinger, R. H. G., Meyer, S., Algotsson, L., Wikström, B. G., Jörgensen, K., Filippatos, G., Parissis, J. T., González, M. J. G., Parkhomenko, A., Yilmaz, M. B., Kivikko, M., Pollesello, P., and Follath, F. (2012) Levosimendan: Molecular mechanisms and clinical implications: Consensus of experts on the mechanisms of action of levosimendan. *Int. J. Cardiol. 159*, 82–87.

21. Oleszczuk, M., Robertson, I. M., Li, M. X., and Sykes, B. D. (2010) Solution structure of the regulatory domain of human cardiac troponin C in complex with the switch region of cardiac troponin I and W7: The basis of W7 as an inhibitor of cardiac muscle contraction. *J. Mol. Cell. Cardiol. 48*, 925–933.

22. Porumb, T., Yau, P., Harvey, T. S., and Ikura, M. (1994) A calmodulin-target peptide hybrid molecule with unique calcium-binding properties. *Protein Eng. 7*, 109–115.

23. Westfall, M. V., and Metzger, J. M. (2001) Troponin I isoforms and chimeras: Tuning the molecular switch of cardiac contraction. *Physiology. 16*, 278–281.

24. Rezvanpour, A., Phillips, J. M., and Shaw, G. S. (2009) Design of high-affinity S100-target hybrid proteins. *Protein Sci. 18*, 2528–2536.

25. Zhou, H., and Gilson, M. K. (2009) Theory of free energy and entropy in noncovalent binding. *Chem. Rev. 109*, 4092–4107.

26. Li, M., Saude, E., Wang, X., Pearlstone, J., Smillie, L., and Sykes, B. (2002) Kinetic studies of calcium and cardiac troponin I peptide binding to human cardiac troponin C using NMR spectroscopy. *E. B. J. 31*, 245–256.

27. Li, M. X., Gagne, S. M., Tsuda, S., Kay, C. M., Smillie, L. B., and Sykes, B. D. (1995) Calcium binding to the regulatory N-domain of skeletal muscle troponin C occurs in a stepwise manner. *Biochemistry. 34*, 8330–8340.

28. Delaglio, F., Grzesiek, S., Vuister, G. W., Zhu, G., Pfeifer, J., and Bax, A. (1995) NMRPipe: A multidimensional spectral processing system based on UNIX pipes. *J. Biomol. NMR 6*, 277–293.

29. Johnson, B. A., and Blevins, R. A. (1994) NMR view: A computer program for the visualization and analysis of NMR data. *J. Biomol. NMR 4*, 603–614.

30. Pierson, E. S., Miller, D. D., Callaham, D. A., Shipley, A. M., Rivers, B. A., Cresti, M., and Hepler, P. K. (1994) Pollen tube growth is coupled to the extracellular calcium ion flux and the intracellular calcium gradient: Effect of BAPTA-type buffers and hypertonic media. *Plant Cell. 6*, 1815–1828.

31. Linse, S., Helmersson, A., and Forsén, S. (1991) Calcium binding to calmodulin and its globular domains. *J. Biol. Chem. 266*, 8050–8054.

32. Davis, J. P., Norman, C., Kobayashi, T., Solaro, R. J., Swartz, D. R., and Tikunova, S. B. (2007) Effects of thin and thick filament proteins on calcium binding and exchange with cardiac troponin C. *Biophys. J. 92*, 3195–3206.

33. Marti-Renom, M. A., Stuart, A. C., Fiser, A., Sanchez, R., Melo, F., and Sali, A. (2000) Comparative protein structure modeling of genes and genomes. Annu. Rev. Biophys. Biomol. Struct. 29, 291–325.

34. Hoffman, R. M. B., Li, M. X., and Sykes, B. D. (2005) The binding of W7, an inhibitor of striated muscle contraction, to cardiac troponin C. *Biochemistry 44*, 15750–15759.

35. Zhou, H. (2001) The affinity-enhancing roles of flexible linkers in two-domain DNA-binding proteins. *Biochemistry 40*, 15069–15073.

36. Fielding, L. (2007) NMR methods for the determination of protein-ligand dissociation constants. *Prog. Nucl. Magn. Reson. Spectrosc. 51*, 219–242.

37. Macomber, R. S. (1992) An introduction to NMR titration for studying rapid reversible complexation. *J. Chem. Educ. 69*, 375.

38. Robertson, I., Boyko, R., and Sykes, B. (2011) Visualizing the principal component of 1H,15N-HSQC NMR spectral changes that reflect protein structural or functional properties: Application to troponin C. *J. Biomol. NMR. 51*, 115-122.

39. Zhou, H. (2006) Quantitative relation between intermolecular and intramolecular binding of pro-rich peptides to SH3 domains. *Biophys. J. 91*, 3170–3181.

40. Li, M. X., Gagné, S. M., Spyracopoulos, L., Kloks, C. P. A. M., Audette, G., Chandra, M., Solaro, R. J., Smillie, L. B., and Sykes, B. D. (1997) NMR studies of Ca^{2+} binding to the regulatory domains of cardiac and E41A skeletal muscle troponin C reveal the importance of site I to energetics of the induced structural changes. Biochemistry 36, 12519–12525.

41. Pan, B. S., and Solaro, R. J. (1987) Calcium-binding properties of troponin C in detergent-skinned heart muscle fibers. *J. Biol. Chem. 262*, 7839–7849.

42. Wang, Y. P., and Fuchs, F. (1994) Length, force, and Ca(2+)-troponin C affinity in cardiac and slow skeletal muscle. *Am. J. Physiol. 266*, C1077–82.

43. Wolska, B. M., Keller, R. S., Evans, C. C., Palmiter, K. A., Phillips, R. M., Muthuchamy, M., Oehlenschlager, J., Wieczorek, D. F., de Tombe, P. P., and Solaro, R. J. (1999) Correlation between myofilament response to Ca^{2+} and altered dynamics of contraction and relaxation in transgenic cardiac cells that express ß-tropomyosin. *Circ. Res. 84*, 745–751.

44. Kischel, P., Bastide, B., Potter, J. D., and Mounier, Y. (2000) The role of the Ca($^{2+}$) regulatory sites of skeletal troponin C in modulating muscle fibre reactivity to the Ca($^{2+}$) sensitizer bepridil. *Br. J. Pharmacol. 131*, 1496–1502.

45. Lindert, S., Kekenes-Huskey, P., Huber, G., Pierce, L., and McCammon, J. A. (2012) Dynamics and calcium association to the N-terminal regulatory domain of human cardiac troponin C: A multiscale computational study. *J PhysChem B. 116*, 8449-8459.

46. Robinson, J. M., Cheung, H. C., and Dong, W. (2008) The cardiac Ca^{2+}-sensitive regulatory switch, a system in dynamic equilibrium. *Biophys. J. 95*, 4772-4789.

47. Li, M. X., Hoffman, R. M. B., and Sykes, B. D. (2006) Interaction of cardiac troponin C and troponin I with W7 in the presence of three functional regions of cardiac troponin I. *Biochemistry 45*, 9833–9840.

48. Voet, A., Banwell, E. F., Sahu, K. K., Heddle, J. G., and Zhang, K. Y. (2013) Protein interface pharmacophore mapping tools for small molecule protein: Protein interaction inhibitor discovery. *Curr. Top. Med. Chem. 13*, 989–1001.

49. Barile, E., and Pellecchia, M. (2014) NMR-based approaches for the identification and optimization of inhibitors of protein-protein interactions. *Chem. Rev. 114*, 4749-4763.

50. Gonzalez-Ruiz, D., and Gohlke, H. (2006) Targeting protein-protein interactions with small molecules: Challenges and perspectives for computational binding epitope detection and ligand finding. *Curr. Med. Chem. 13*, 2607–2625.

51. Morelli, X., Bourgeas, R., and Roche, P. (2011) Chemical and structural lessons from recent successes in protein–protein interaction inhibition (2P2I). *Curr. Opin. Chem. Biol. 15*, 475–481.

52. Blumenschein, T. M. A., Stone, D. B., Fletterick, R. J., Mendelson, R. A., and Sykes, B. D. (2005) Calcium-dependent changes in the flexibility of the regulatory domain of troponin C in the troponin complex. *J. Biol. Chem. 280*, 21924–21932.

CHAPTER 7

Covalent binding of the levosimendan analog i9 to cardiac troponin C induces contraction in muscle fibers

The reader will find here an examination of the interaction between troponin and a powerful covalent calcium sensitizer (i9). The chapter starts by probing potential covalent binding for the Ca^{2+} sensitizer levosimendan, for which no structure bound to troponin is available. It continues by presenting the design of i9, the structure of i9 bound to cChimera, and the physiological effects of i9 in muscle fibers. The use of a covalent Ca^{2+} sensitizer allows us to unequivocally ascribe physiological effects in muscle tissue to the i9-troponin interaction. With these findings we confirm the mechanism of calcium sensitization of the thin filament and suggest troponin as amenable to the design of covalent sensitizers. (Unpublished).

Introduction

Decreased contractility is a characteristic of a variety of heart diseases including heart failure. One approach to treating this condition is to administer positive inotropic agents that increase cardiac muscle contraction by increasing intracellular Ca^{2+} concentrations. However, this can lead to the development of arrhythmias and myocyte death due to Ca^{2+} overload. An emerging alternative is the administration of Ca^{2+} sensitizers, which also cause positive inotropy but act directly on the contractile proteins of the cardiac muscle to enhance contractility[1]. The best characterized Ca^{2+} sensitizer is levosimendan; however, its mechanism of action is still not fully understood. This work aims to provide insight into the molecular mechanism behind Ca^{2+} sensitization of levosimendan by characterizing the structure and effect on contraction of a levosimendan analog (i9) that binds covalently to cNTnC.

Contraction is regulated in the heart muscle by troponin (cTn) in a Ca^{2+} dependent manner. cTn is a heterotrimeric complex composed of C, I and T subunits (cTnC, cTnI, and cTnT, respectively) localized to the thin filament of the sarcomere. cTnC contains two globular domains, the regulatory N-domain (cNTnC) that acts as the Ca^{2+} sensor, and the structural C-domain that binds to cTnI and holds cTnC on the thin filament. cNTnC is formed by five helices (named N, and A through D), whereas the smaller cCTnC contains four helices (named E through H). During systole, when the cytosolic concentration of Ca^{2+} increases, Ca^{2+} binds to cNTnC and increases the prevalence of the open conformation of cNTnC[2,3]. Following this shift towards the open state of cNTnC, the switch region of cTnI (switch-cTnI) binds to cNTnC and drags the inhibitory region of cTnI away from actin. This causes a conformational change in tropomyosin and a subsequent exposure of the myosin binding sites on actin to allow the formation of the force-producing cross-bridges. During diastole, the intracellular

concentration of Ca^{2+} decreases, cNTnC returns to a mostly closed conformation, and cTnI binds actin and blocks the actin-myosin cross-bridges to allow for muscle relaxation[4,5].

The mechanism by which levosimendan enhances cardiac muscle contraction is its Ca^{2+} sensitization effect on cTnC; however, the molecular details of this interaction are not entirely clear. Besides a sensitizer effect, levosimendan has also been shown to have important vasodilator, anti-inflammatory, and anti-apoptotic effects[6, 7]. Although it has been found to inhibit phosphodiesterase 3 (PDE3) at high concentrations, its positive inotropic effect is mostly due to its interaction with cTnC and not to an increase on intracellular Ca^{2+} [8, 9, 10]. Previous NMR studies have shown that in the presence of the cTnI regions that bind each domain of cTnC, levosimendan interacts only with the regulatory N-domain[11]. A three-dimensional structure or a precise binding site has not yet been localized due to the short lifetime of the cTnC·levosimendan complex. Using NMR chemical shift mapping, Sorsa and collaborators[11] found widespread chemical shift perturbations throughout the N-domain and could not determine a specific binding site. Using x-ray scattering experiments, they also found that the radius of gyration of cTnC is increased by levosimendan in a manner similar to cTnI. Because binding of cTnI to cTnC reduces the flexibility of the D/E linker between both domains of cTnC, the authors proposed that levosimendan binds close to the D/E linker and make it more rigid[12].

In addition, other studies have shown that C84 is essential for binding[13, 14]. Mutation of this residue to serine on cNTnC abolishes its interaction with levosimendan. Moreover, the reducing agent dithiothreitol (DTT) has been reported to react with levosimendan and prevent its binding to cNTnC[12, 14]. In addition, levosimendan contains two nitrile groups that can undergo nucleofilic addition in the presence of thiol groups. Because of these observations, we hypothesized that levosimendan may form a reversible covalent bond with C84 of cNTnC (Ian M. Robertson *et al*. 2015, in preparation).

There have been a number of studies of small molecules bound to cTnC that alter Ca^{2+}-sensitivity[15,16]. It is not always clear, however, whether it is the binding to cTnC that is directly responsible for the increase in contractility *in vivo*. For example, EMD57033 was initially shown to bind to cTnC as well as to increase the Ca^{2+}-sensitivity and force of contraction. However, after the structure of EMD57033 bound to cTnC was solved[17], it was shown that EMD57033 most likely enhances contractility by stabilizing actomyosin cross-bridges rather than through its interaction with cTnC. Likewise, levosimendan has been shown to bind to cTnC as well as to inhibit PDE3 — both of which can lead to an increase in contractility.

In order to unambiguously show that small molecule binding to cTnC can lead to such an increase in a muscle fiber, we designed a novel levosimendan analog (i9) that contains a reactive iodoacetamide group (Figure 7.1). We determined the NMR structure of i9 covalently bound to C84 of a

stable cNTnC·switch-cTnI hybrid protein (cChimera), and studied the effect of i9 attached to cTnC(C35S) on muscle fiber contractility. The results show that i9 binds to the hydrophobic cleft of cNTnC and is stabilized by switch-cTnI. When the covalent cTnC(C35S)-i9 complex was exchanged within cardiac muscle fibers there was an increase in the Ca^{2+}-sensitivity of muscle fiber contraction. These results indicate that i9 enhances muscle Ca^{2+}-sensitivity by binding to the hydrophobic pocket of cNTnC and stabilizing the open conformation.
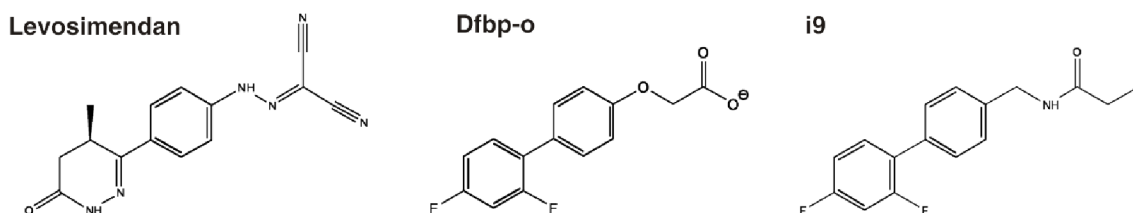
Figure 7.1. Design of the covalent levosimendan analogue i9.
The chemical structures of levosimendan, dfbp-o (a levosimendan analogue previously reported), and i9 (the covalent analogue reported here) are shown together for comparison.

Experimental procedures

Purification of troponin

Unlabeled cTnC(C35S), ^{13}C-^{15}N-cChimera, and ^{15}N-cChimera were expressed in *E. coli* as described elsewhere[18]. cChimera is a hybrid protein which contains a histidine tag, a thrombin cleavage site (GGLVPRGS), the N-domain of troponin C (residues 1-89), a TEV cleavage site (ENLYFQG), and switch-cTnI (residues 144-173). We have previously shown that cChimera resembles the cNTnC·switch-cTnI complex in the ~74% bound state[19]. Its improved solubility, 1:1 stoichiometry, and stability of the cNTnC-cTnI interaction allow for easy sample handling. Isotope labeling of cTnI makes it advantageous over the cNTnC•switch-cTnI complex which usually contains synthetic unlabeled cTnI. The cChimera proteins were purified by Ni-NTA affinity followed by gel filtration chromatography as previously reported[19]. The DNA from cTnC(C35S, C84S)[20] was used as a template for the preparation of cTnC(C35S) using a site-directed mutagenesis kit and cTnC(C35S) was purified as previously described[21]. The purity of the proteins was verified by reverse-phase HPLC and electrospray ionization Mass Spectrometry (ESI-MS). The synthetic cTnI peptide (residues 144-173) was obtained from GL Biochem Ltd. (Shanghai, China).

Levosimendan reactivity

A fresh solution of 2 mM levosimendan was prepared in DMSO-d_6. Small aliquots of a stock solution of 150 mM N-acetyl-cysteine (NAc-Cys) were titrated into the levosimendan solution. The titration was monitored by acquiring a ^{1}H NMR spectrum after each addition. The NAc-Cys:levosimendan ratio at each titration point was 0, 0.08, 0.15, 0.29, 0.56, and 2.07 as determined by spectral integration of levosimendan and NAc-Cys. The assignment of the levosimendan signals was as reported before[22].

Synthesis and purification of i9

Chloroacetyl chloride was obtained from Fluka Analytical (≥ 99% GC, 112.94 g/mol, 1.419 g/mL at 20°C), (2',4'-difluorobiphenyl-4-yl)methanamine (97%, 255.69 g/mol, compound **1**) from Amatek Chemical, and ethyldiisopropylamine (Hunig's Base, HB) was from Sigma-Aldrich (99.5%, 129.24 g/mol, 0.742 g/ml). In a glass vial 50 µmol of **1** and 170 µmol of HB were dissolved in 1.2 mL of acetonitrile. In a separate glass vial, 500 µmol of chloroacetyl chloride were dissolved in 40 µL acetonitrile and slowly added into the **1**/HB solution under the extraction hood. The reaction produced gas (HCl) and changed the color of the solution from clear to pale yellow. Then 6 mL of water were added to produce compound **2** as a white floating solid. Compound 2 was washed with water, recovered by centrifugation, and dried under vacuum. The dry product **2** was then dissolved in 1 mL of acetone, and an excess (270 mg) of NaI previously dried for 2h at 110°C was added. The halogen exchange reaction proceeded overnight at 37°C with the production of bubbles, color change to orange, and precipitation (NaCl). The whole reaction was passed to a separation funnel and 5 mL each of ethyl acetate and H_2O were added. The yellow organic phase was washed twice with water and once with 5% $Na_2S_2O_3$ which turned the solution clear. The clear organic phase was collected and dried with anhydrous Na_2SO_4 until no clumps were observed. The final solution was evaporated, the product redissolved in deuterated dimethyl formamide (DMF-d_7), aliquoted, and stored at -20°C wrapped in aluminum foil to protect from light.

Troponin labeling with i9

Full cTnC-C35S, cNTnC (residues 1-89), and ^{13}C,^{15}N-cChimera were labeled under denaturing conditions. In addition, cNTnC was labeled in aqueous buffer to assess the specificity of the reaction. The denaturing buffer contained 6 M urea, 150 mM KCl, 50 mM TRIS, and 1 mM EGTA. The aqueous buffer consisted of 100 mM KCl, and 10 mM imidazole at pH 8. The corresponding protein was dissolved in denaturing or aqueous buffer, 2 mM of fresh TCEP was added, and the solution incubated for 20 min to reduce all the cysteine residues. A stock solution of i9 in DMF-d_7 was added in small aliquots to the

protein solution under stirring and the pH was readjusted to 8. Although i9 is poorly soluble in water, the protein solution remained clear before the i9: protein ratio reached 1:1. After this point, the solution became turbid. The final drug:protein ratio was >2:1 for the reactions in urea and 1.2:1 for the reaction in aqueous buffer. The reaction proceeded in the dark with constant stirring at 27°C for 16 h. The reaction was stopped with four times excess DTT and spun down. The supernatant of the reaction in urea was applied to a size exclusion chromatography column to purify the labeled protein cTnC(C35S)-i9, cNTnC-i9, or cChimera-i9. The protein fraction was lyophilized and stored at 4°C.

NMR spectroscopy

The NMR samples consisted of 0.5-0.8 mM cTnC(C35S)-i9, cNTnC-i9, or cChimera-i9 in 500 or 600 μL of 100 mM KCl, 10 mM imidazole or imidazole-d_4, 2 mM $CaCl_2$, and 0.25 mM 2,2-dimethyl-2-silapentane-5-sulfonate-d_6 sodium salt (DSS-d_6) or trifluoroacetic acid (TFA) as internal reference, at pH 6.9. The NMR experiments were acquired in 500, 600, or 800 MHz Varian spectrometers at 30° C. All one-dimensional experiments were processed with VnmrJ v 3.2, all the multidimensional spectra were processed with NMRPipe[23] and analyzed with NMRViewJ[24]. The assignment of free i9 in DMSO was done based on examination of the ^{1}H NMR spectra acquired throughout the synthesis, and on previous assignment of the levosimendan analog dfbp-o[25]. The assignment of i9 in cChimera-i9 was achieved by a combination of two-dimensional ^{1}H and ^{19}F NMR spectra including ^{13}C, ^{15}N filtered noesy, ^{13}C, ^{15}N filtered tocsy, and ^{1}H, ^{19}F HMQC (Supplementary Figure 7.1 and Supplementary Table 7.1). Assignment of cChimera in cChimera-i9 was done by using typical 2d and 3d NMR experiments ^{1}H, ^{15}N- and ^{1}H, ^{13}C-HSQC, HNCACB, CBCA(CO)NH, HNHA, HCCONH, and CCONH detailed in Supplementary Table 7.1.

Structure determination

The structure of i9 bound to cChimera was determined using Xplor-NIH v. 2.35 with experimental backbone dihedral and distance restraints. Parameter and topology files for i9 covalently attached to cysteine were generated using the PRODRG server[26] (available at http://davapc1.bioch.dundee.ac.uk/cgi-bin/prodrg/). The backbone dihedral angles φ and ψ were predicted with the Talos+ server (available at http://spin.niddk.nih.gov/bax/nmrserver/talos/) based on the chemical shift of HN, N, CA, CB, and HA backbone atoms of cChimera-i9. Intramolecular distance restrains within the protein component of cChimera-i9 were obtained from noesyNhsqc and noesyChsqc NMR spectra, NOEs were calibrated using the bin method of NMRViewJ and classified as strong (1.8 -3 Å), medium (3 - 4.5 Å), and weak (4.5 - 6 Å). Intramolecular NOEs within i9 were obtained from the ^{13}C, ^{15}N filtered noesy spectrum in which signals from the ^{13}C, ^{15}N labeled protein moiety are filtered out to obtain NOEs from the unlabeled drug moiety only. Pseudo-intermolecular NOEs between cChimera and i9 were obtained from the three-dimensional noesyChsqc_CNfilt NMR

spectrum in which contacts between ^{13}C, ^{15}N labeled protein and unlabeled i9 are detected; all of these NOEs were classified as weak (1.8 – 6 Å). We used statistical torsion angle potential to improve the quality of backbone and side chain conformations; this is based on over a million residues from high quality crystal structures from the Protein Data Bank (PDB). We also used the gyration volume potential term to restraint the volume associated with the gyration tensor also based on values observed in the PDB. We used the anneal protocol of Xplor-NIH to generate 140 structures from which the lowest energy structure was used in the subsequent refine protocol. The final ensemble consists of the 20 lowest energy structures generated in the refinement step with no NOE violations greater than 0.4 Å or dihedral violation greater than 5°. This ensemble was validated with PROCHECK using the Protein Structure Validation Suite (PSVS 1.5) server (available at http://psvs-1_5-dev.nesg.org/).

Animals

Male Wistar rats (200–250 g) were stunned and killed by cervical dislocation (Schedule 1 procedure in accordance with UK Animal (Scientific Procedures) Act, 1986). The hearts were quickly removed and rinsed free of blood in Krebs solution (Sigma-Aldrich, K4002) containing: 118 mM NaCl, 24.8 mM NaHCO$_3$, 1.18 mMNa$_2$HPO$_4$, 1.18 mM MgSO$_4$, 4.75 mM KCl, 2.54 mM CaCl$_2$, 10 mM glucose, bubbled with 95% O$_2$–5% CO$_2$for 30-60 min; pH 7.4 at 20°C. Unbranched trabeculae (diameter <250 µm) were dissected from the right ventricle in Krebs solution containing 25 mm 2,3-butanedione-monoxime. The fibers were permeabilized in relaxing solution (see below) containing 1% Triton X-100 for 30 min, and stored in relaxing solution containing 50% (v/v) glycerol at −20°C for experiments. Fibers were used within 2 days of dissection.

Reconstitution of cTnC(C35S)-i9 into ventricular trabeculae

Native TnC was partially replaced by incubation of trabeculae in relaxing solution containing 30 µmol/L cTnC(C35S)for 30 minutes at 20-22°C. The fraction of TnC replaced by cTnC(C35S) was about 30% as estimated by ESI-MS of the fiber. Following incubation, the demembranated trabeculae were mounted via aluminum T-clips between a force transducer (AE801) and a fixed hook in a 60µl trough containing relaxing solution. The sarcomere length was set to 2.1 µm as indicated by a Helium-Neon laser (632.8 nm). The experimental temperature was 20-22°C.

Experimental solutions contained 25 mM imidazole, 5 mM Mg ATP, 1 mM free Mg^{2+}, 10 mM EGTA (except pre-activating solution), 0–10 mM total calcium, 1 mM dithiothreitol and 0.1% (v/v) protease inhibitor cocktail (P8340, Sigma). Ionic strength was adjusted to 200 mM with potassium propionate; pH was 7.1 at 20°C. The concentration of free Ca^{2+} was calculated using the program WinMAXC V2.5 (http://web.stanford.edu/~cpatton/maxc.html). The calculated free [Ca^{2+}] was in the range 1 nM (pCa

9) to 41 µM (pCa 4.39). In pre-activating solution, the concentration of EGTA was 0.2 mM and no calcium was added.

Results

Levosimendan reactivity

To assess the reactivity of levosimendan with cysteine residues we titrated N-acetyl cysteine into a solution of levosimendan (Figure 7.2). The results show the appearance of a new signal at 12.8 ppm attributed to protons H18 and H20 of the thioimidate product of the reaction. The reaction
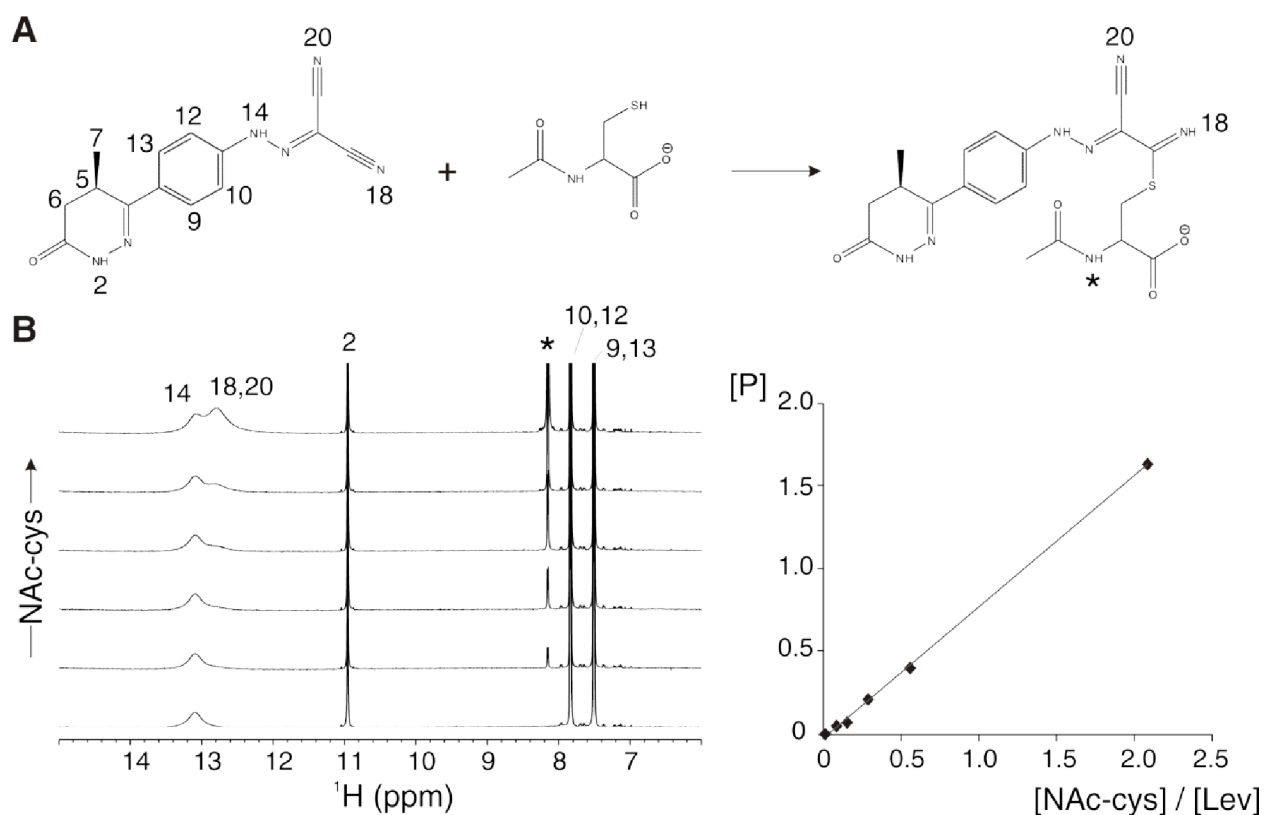
Figure 7.2. Reaction of levosimendan with NAc-Cys in DMSO-d$_6$.
A. Reaction scheme of levosimendan and NAc-Cys for one nitrile group. The other nitrile group is expected to follow the same scheme. B. Stack of the downfield region of the ^{1}H NMR spectra used to monitor the titration of NAc-Cys into levosimendan. Assignments of the levosimendan signals are as reported by Pollesello *et al*[22]. The * indicates the position of the NH proton of NAc-Cys. The graph on the right displays the correlation between the NAc-Cys/levosimendan ratio and the production of the thioimidate product ([P] on y-axis of plot).

continued passed the 1:1 molar ratio indicating that both nitrile groups of levosimendan react in the same manner. However; at 2:1 molar ratio the intensity of the H18/20 signal was only 1.6. This could be a result of exchange of protons H18/20 with the solvent. Although levosimendan was dissolved in DMSO-d_6, the NAc-Cys stock was prepared in water which results in broadening of the NH signals.

There was no change in signal intensities after 16 hours which indicates that the reaction product is stable (Figure 7.3). Addition of the thiol-free reducing agent TCEP resulted in decreased intensity of the H18/20 signals as well as the Hα and Hβ signals of oxidized NAc-Cys. In the other hand, signals corresponding to Hα and Hβ of reduced NAc-Cys showed increased intensity upon addition of TCEP which indicates that the reaction is reversible. Selective saturation of the water signal resulted in suppression of signals from protons H14 and H18/20 of the thioimidate product.
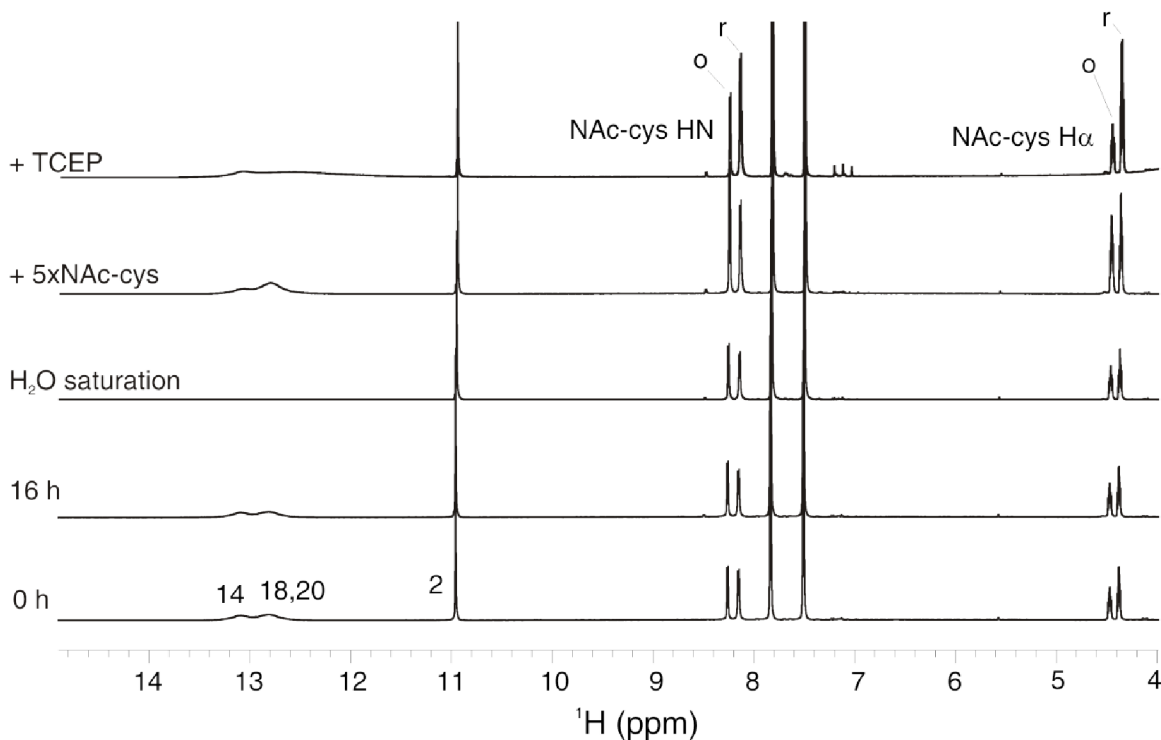
Figure 7.3. Stability and reversibility of the levosimendan reaction.

Stack of ^{1}H NMR spectra for the reaction of levosimendan with NAc-Cys in DMSO-d_6. Protons H2, H14, and H18,20 of levosimendan and its thioimidate derivative are labeled on the bottom spectrum. The HN and Hα protons of NAc-Cys are labeled on the top spectrum. Labels 'o' and 'r' indicate the oxidized and reduced forms, respectively.

The chemical structure of i9 was designed based on levosimendan and dfbp-o (Figure 7.1). They all contain a biphenyl group followed by a hetero-substituted tail. The biphenyl group of dfbp-o was chosen because it was shown to insert in the hydrophobic cleft of cNTnC and conserve the Ca^{2+} sensitization effect[25]. In addition, fluorine atoms are amenable for NMR studies. The hetero-substituted tail of i9 was designed based on the potential reactivity of the nitrile group of levosimendan with cysteine. A reactive acetamide group was incorporated such that the number of bonds separating the biphenyl moiety and the sulfur atom of reacted cysteine, was the same for reacted levosimendan and reacted i9. In contrast to dfbp-o, the covalent analogue i9 does not carry a formal charge and contains a planar center on the amide N which resembles more to levosimendan.
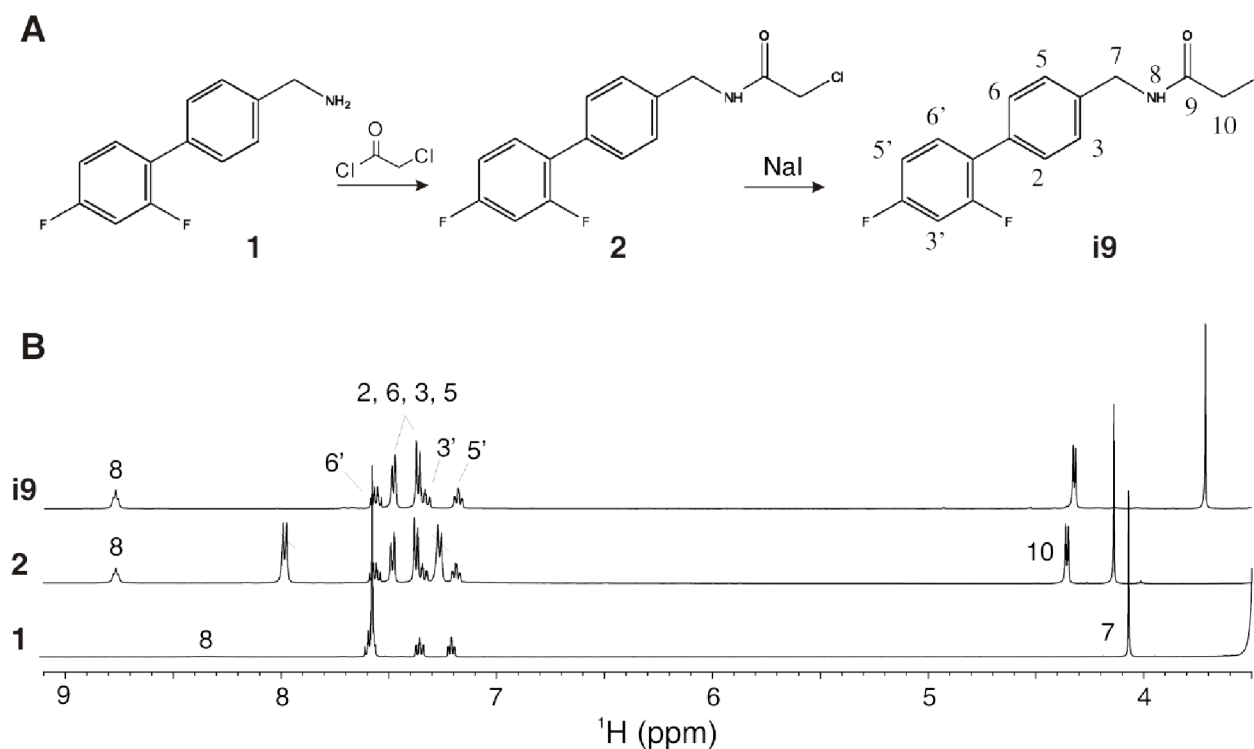
Figure 7.4. Synthesis of i9.
A. Synthetic route for the production of i9. B. Stack of ^1H NMR spectra in DMSO-d_6 corresponding to each compound on the synthesis shown in A.

Synthesis and purification of i9

To synthesize the levosimendan analog i9, we followed the route shown in Figure 7.4A. Compound **1** was reacted with chloroacetyl chloride in the presence of Hunig's base to produce

177

compound **2**. The following halogen exchange reaction of the chlorinated compound **2** with NaI in dry acetone produced i9. The identity and purity of compounds **1, 2**, and **i9** was verified by ^{1}H NMR spectroscopy and mass spectrometry. Figure 7.4B shows the ^{1}H NMR spectra of 1, 2, and i9. With the addition of the acetyl chloride moiety the signal corresponding to N8 is shifted downfield (from 8.36 to 8.75 ppm) as the result of deshielding by the newly attached carbonyl C9, also a new aliphatic signal at 4.35 ppm is observed corresponding to the new methylene protons at C10. The halogen exchange from Cl to I shifted the H10 singlet upfield (from 4.11 to 3.7 ppm) due to the less electronegative character of I compared to Cl. Both reactions had only small effects on the aromatic protons of the products which were assigned partly based on previous assignment of the levosimendan analog dfbp-o[25].

Troponin labeling with i9

Three proteins were independently labeled with the i9 compound: cTnC(C35S) for physiological characterization, cNTnC for assessment of reaction specificity, and [13]C-^{15}N-cChimera for structure determinaiton by NMR. The labeling reactions were performed in urea or NMR buffer and verified by ^{19}F NMR. Protein labeling is illustrated for cChimera in Figure 7.5A, where the ^{19}F NMR spectrum of i9 (spectrum a) shows two sharp signals at -36.2 and -39.3 ppm corresponding to the fluorine atoms F2' and F4'. After the reaction with cChimera (spectrum b) the two signals shift (to -36.4 and -37.1ppm) and broaden as a result of the change in molecular size and electronic environment, respectively, when i9 is bound to cChimera. To assess the completion of the reaction, 1 μL of 35 μM 3-bromo-1,1,1-trifluoroacetone was added to cChimera-i9 to react with any remaining free sulfhydryl group present (spectrum c). The presence of the unreacted trifluoro acetone only, as a sharp singlet at -8ppm, indicates that the reaction was complete and cChimera was 100% labeled. Spectrum d at the top shows the chemical shift of trifluoroacetone bound to cChimera in a different sample for comparison.

Figure 7.5B displays a summary of the ^{19}F spectra of all the reacted proteins. Full labeling of cNTnC with excess i9 in urea results in covalent binding at C35 and C84, but only the signals corresponding to C84-i9 sharpen in the presence of cTnI. The ^{19}F spectrum of cNTnC-i9 in the absence of cTnI (Figure 7.5B spectrum a) shows two sharper signals corresponding to F2' and F4' of C35-i9, and broader signals for C84-i9 that overlap to a large extent indicating multiple conformations of the drug molecule bound to C84. Addition of a 3:1 excess of switch-cTnI (residues 144-173), which binds to cNTnC, causes the fluorine signals of C84-i9 to sharpen and separate. In a similar way, the ^{19}F spectrum of cTnC(C35S)-i9 (spectrum b) shows the same change in line width for F2' and F4' of C84-i9 upon addition of cTnI. The reaction of i9 with cNTnC in aqueous NMR buffer using a small drug-to-protein excess resulted in preferential labeling on C84 as judged by the appearance of intense C84-i9 peaks and minuscule C35-i9 peaks (spectrum c). For cChimera-i9, which has cNTnC attached to switch-cTnI, the C84-i9 signals are very similar to those of cTnC(C35S)-i9 and cNTnC-i9 in the presence of switch-

cTnI (spectrum d). Comparable spectra indicate very similar electronic environments for i9 in all cases. Then the i9 molecule is expected to adopt the same conformation in all cNTnC·switch-cTnI systems which validates the use of cChimera for structural characterization of their interaction.
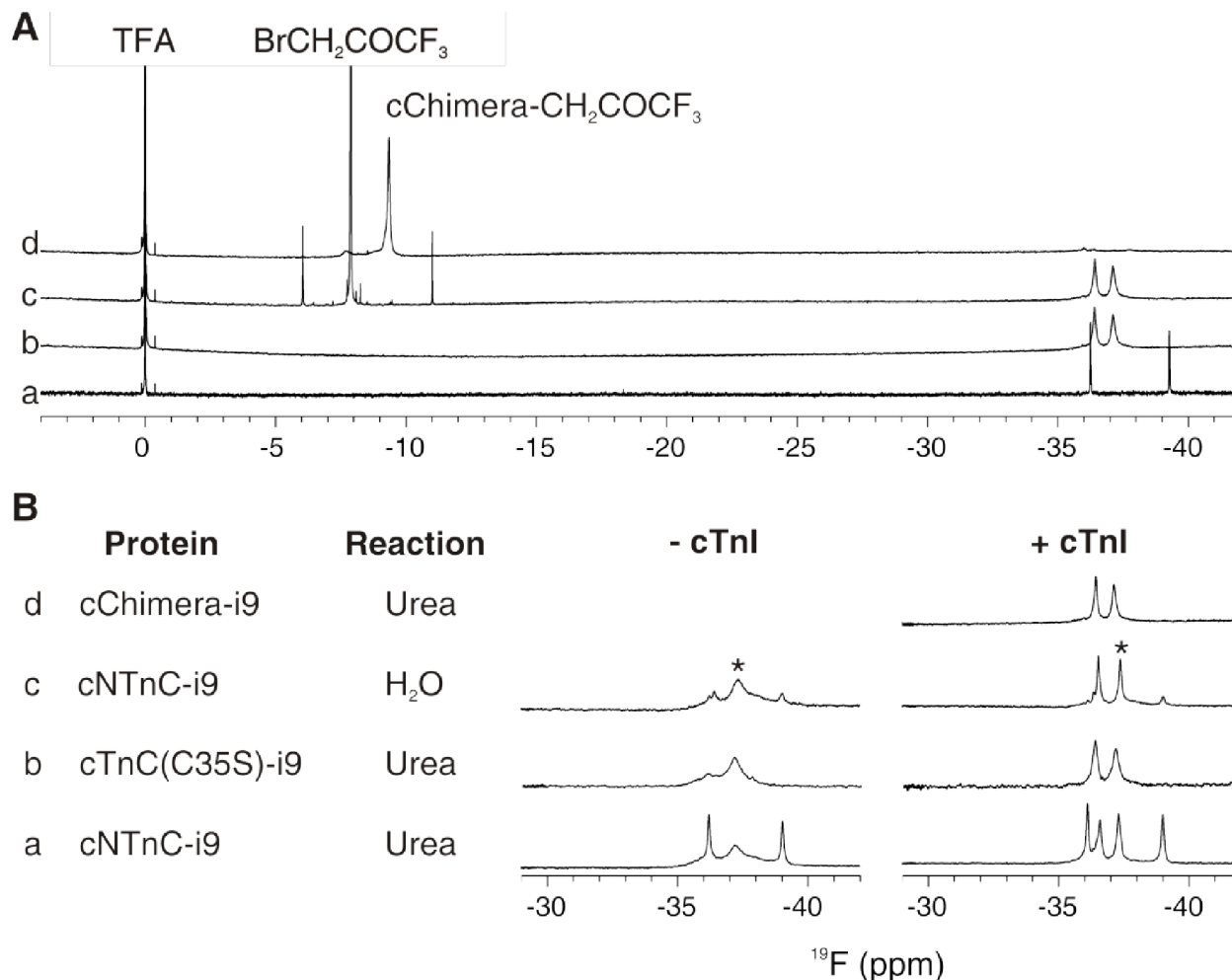
Figure 7.5. Troponin labeling with i9.
A. Stack of ¹⁹F spectra of i9 (1), cChimera-i9 (2), cChimera-i9 in the presence of 3-bromo-1,1,1-trifluoroacetone (3) showing complete reaction of cChimera with i9. Spectrum 4 shows the position of trifluoroacetone when bound to cChimera for reference. B. Stack of ¹⁹F spectra of cNTnC-i9, cTnC(C35S)-i9, and cChimera-i9 in the absence and presence of switch-cTnI. Matching signals across spectra are marked * only in c. The 'reaction' column specifies if labeling was done under denaturing conditions; however, all proteins were redissolved in NMR buffer.

Structure of cChimera-i9

cChimera contains the cNTnC (residues 1-89) attached to switch-cTnI (residues 144-173) through a flexible linker and represents the cNTnC•switch-cTnI complex[19]. This allows for structural assessment in the systolic state when switch-cTnI is bound to cNTnC. The present structure of cChimera-i9 (Figure 7.6A) is similar to the structure of cNTnC bound to the switch region of cTnI observed in other structures. Compared to the x-ray structure of the core domain of cTn[27], the rmsd of alpha carbons for all residues is 2.2 Å and for helical residues only the rmsd is 2.0 Å. Compared to the NMR structure of dfbp-o, another levosimendan analog, bound to cNTnC•switch-cTnI the rmsd of alpha carbons for all residues is 2.2 Å and for helical residues the rmsd is 2.1 Å. Structural statistics for the final ensemble are summarized in Supplementary Table 7.2.

Structure of cNTnC in cChimera-i9

The typical structural features of cNTnC in the Ca^{2+} and switch-TnI bound state are present in the structure of cChimera-i9. cNTnC in cChimera-i9 is in the open state accommodating i9 deep in the hydrophobic cleft and cTnI towards the surface. It contains five α-helices, N and A through D, and a small β-sheet involving the loops of each EF-hand. Compared to cNTnC in the crystal structure of the troponin core domain (1J1E) the rmsd of alpha carbons is 1.9 Å. Compared to the structure of dfbp-o bound to cNTnC and switch-cTnI (2L1R) the rmsd of alpha carbons is 1.9 Å (Figure 7.6). Helix N in cChimera-i9 is shifted slightly away from helix D and is extended by two residues on the N-terminal side (D2 and D3). Helix D is also extended by five residues towards the C-terminus (K86-E90). The stabilizing effect of the flexible linker in cChimera may be responsible for the extension of helices N and D. The apparent concentration of switch-cTnI in cChimera is increased by the presence of the linker[19]; as a result the interaction between cNTnC and switch-cTnI is stabilized and may promote consolidation of the secondary structural elements. However, the longer helices do not change the overall conformation of cNTnC or switch-cTnI.

Linker region in cChimera-i9

The linker region between cNTnC and cTnI in cChimera remains flexible. Three of the seven residues comprising the linker could not be assigned due to broadening of the signals beyond detection; this is probably related to NH exchange with the solvent not uncommon for solvent-exposed regions. We also confirmed the flexibility of the linker using the random coil index (RCI) analysis performed within TALOS+, which estimates values of the model-free order parameter S^2 based on the chemical shift of CA, CB, N, HA, and NH, backbone atoms[28]. The RCI indicates that residues 95 and 96 of the linker along with 144-147 of cTnI have $S^2 < 0.5$ and are classified as dynamic.
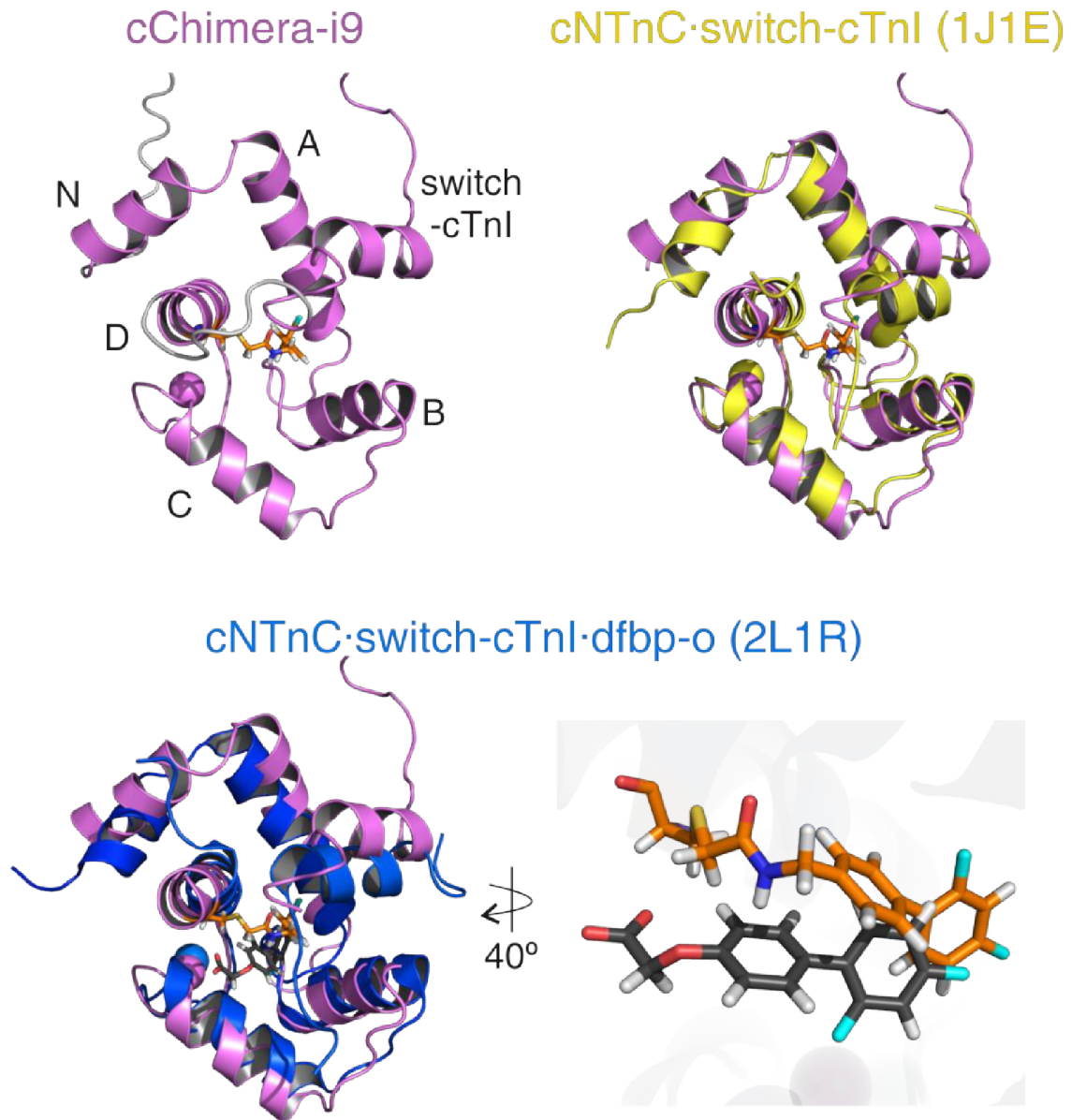
Figure 7.6. Structure of cChimera-i9.

The full structure of cChimera-i9 (pink) alone shows the linker region between cNTnC and cTnI in grey. Helices on cNTnC are labeled N and A through D, the switch region of cTnI is also labeled, i9 is in orange sticks, and the Ca^{2+} ion is shown as a sphere. The linker region is not shown in the structure overlaps for clarity. The structures of cNTnC•switch-cTnI (yellow) and cNTnC•switch-cTnI•dfbp-o (blue) were aligned to cChimera-i9 over the alpha carbons of all helical regions. The expansion shows the relative positions of i9 and dfbp-o in the hydrophobic pocket of cNTnC.

181

Structure of cTnI in cChimera-i9

Switch-cTnI in cChimera-i9 forms a helix that is shifted away from the core of the protein. The length and composition of the switch helix of TnI in cChimera-i9 is the same as that observed in the crystal structure of the troponin core domain (1J1E)[27], starting at residue A150 and continuing until residue L158 with the previous and following regions being flexible and unstructured. Although the switch helices of both structures are roughly parallel and localize between the A-B-D helices of cNTnC, the switch-helix of cChimera-i9 is moved away from the core of cNTnC. We compared the experimental NOEs observed between cTnI and cNTnC in cChimera with those reported previously for the NMR structure of the cNTnC·switch-cTnI complex[29] (1MXL). Although there are fewer NOEs observed for the present structure, there are common methyl-methyl inter-subunit contacts including M153 to M81 on helix D, L157 to M47 on helix B, and L158 to A22 on helix A. This indicates a similar binding site for cTnI in both structures. As a result, the switch helix of cTnI in cChimera-i9 also lies on the A-B-D interhelical space. Then the shift may be due to steric clash of i9 and A150 at the start of the switch-helix or/and M153 that faces the hydrophobic cleft of cNTnC (Supplementary Figure 7.2).

Structure of i9 in cChimera-i9

The covalently attached i9 molecule inserts deep in the hydrophobic pocket of cNTnC. A total of 14 experimental distance restraints define the position of i9 in the core of cChimera between helices B, C, and D, of cNTnC, and the switch helix of cTnI. The difluorophenyl ring of i9 contacts residues I61 and V64 on helix C, and I36 and V72 which form the ß-sheet of cNTnC; this is consistent with its position deep in the hydrophobic cleft. The middle phenyl ring of i9 contacts several residues on the middle region of the cleft such as L41, V44, and M45 on helix C and M80 on helix D. This ring also shows NOEs to M85 on helix D and V146 on switch-cTnI which are located towards the protein surface (Figure 7.7). The localization of i9 in cChimera-i9 is similar to that of the levosimendan analog dfbp-o in cNTnC in the presence of switch-cTnI[25] (Figure 7.6). The localization of the difluorophenyl rings of both compounds is very similar but i9 inserts deeper in the pocket than dfbp-o. The orientation of both compounds is also very similar such that they are parallel; however, i9 localizes closer to cTnI than dfbp-o, which is also related to the shift of cTnI.
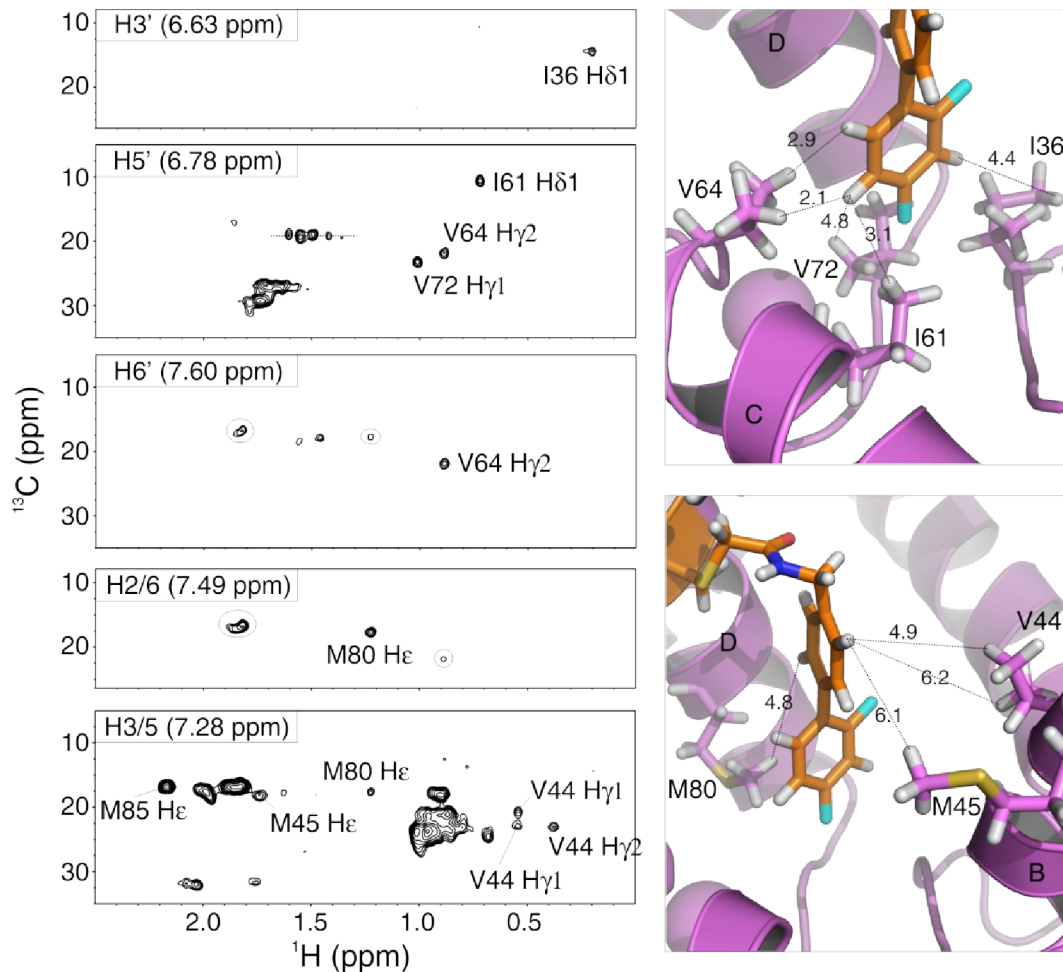
Figure 7.7. Molecular contacts between i9 and cChimera.

Planes from the three dimensional noesyChsqc_CNfilt NMR experiment corresponding to each aromatic proton of i9 in cChimera-i9. The name and chemical shift of the i9 protons are labeled in the upper left corner of each plane. The NOEs to protons on cChimera are also labeled and depicted in the panels on the right. In the panels, helices and residues of cNTnC (pink) are labeled, as well as the distances to i9 (orange) protons corresponding to the observed NOEs.

Physiologic effects of cTnC-i9

The structure of cChimera-i9 reveals that i9 inserts deep inside the hydrophobic pocket of cNTnC, much like dfbp-o[25]. We next investigated whether cTnC(C35S)-i9 caused an increase in Ca^{2+}-sensitivity in demembranated ventricular trabeculae. Following the exchange of cTnC(C35S)-i9 into ventricular trabeculae, we saw an increase in the Ca^{2+}-sensitivity (Figure 7.8). The pCa_{50} increased from 6.092 +/- 0.016 (SEM; n=4) to 6.218 +/- 0.018 (SEM; n=5) (P <0.05). Maximum Ca^{2+}-activated isometric force was 25.3 mN mm^{-2} +/- 1.7 (SEM; n=8) prior to cTnC(C35S)-i9 exchange into the muscle

fiber and 24.6 mM mm^{-2} +/- 2.7 (SEM; n=7) following the exchange with cTnC(C35S)-i9 into the fiber. Thus cTnC(C35S)-i9 did not affect maximum Ca^{2+}-activated force. This is consistent with studies investigating dfbp-o[25] or levosimendan. Interestingly, when we left cTnC(C35S)-i9 to exchange into the ventricular trabeculae overnight at 4°C or for greater than 30 min, we saw a gradual increase in the resting tension (data not shown). We hypothesize this is because i9 is irreversibly bound to cTnC and keeps it partly open. This would lead to some basal level of activity, even in the absence of Ca^{2+}.
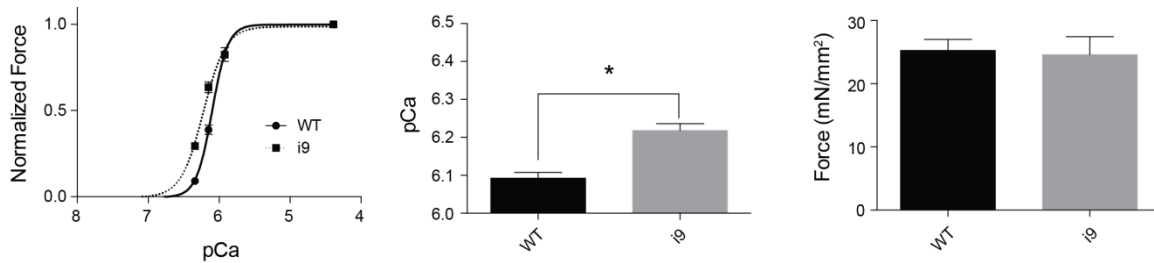
Figure 7.8. Effect of i9 on the force and pCa in muscle fibers.
Force-pCa relationship (left) of ventricular trabeculae containing wild type cTnC (WT) and containing cTnC(C35S)-i9 (i9) showing that i9 induces a significant increase in pCa (middle) without changing the maximum developed force (right).

Discussion

Based on previous studies and the analysis of the chemical nature of levosimendan, we previously hypothesized that levosimendan can react with the sulfhydryl group of C84 to form a reversible covalent bond (Ian M. Robertson *et al*. 2015, in preparation). Here we identified a new ^{1}H signal that corresponds to H18/H20 of the thioimidate product that verified the reaction of both nitrile groups of levosimendan with NAc-Cys. The product was found to be stable and the reaction reversible. This demonstrates the capacity of levosimendan to react with cysteine residues and provides a starting point for further characterization of the reaction in aqueous solution. A covalent interaction between levosimendan and C84 of cNTnC would be consistent with previous structural studies that determined that the binding site is in the N-domain[11, 12] and showed that this interaction occurs in the slow exchange limit[14]. It also agrees with studies showing that C84 is essential for binding and that DTT reacts with levosimendan and affects its stability and ability to bind to cNTnC[12, 14]. These data support the hypothesis of covalent binding of levosimendan and open a wider range of possibilities in the design of Ca^{2+} sensitizers that target cNTnC.

To better characterize the interaction between a covalent Ca^{2+} sensitizer and cTnC, we designed and synthesized the levosimendan analog i9. We determined the structure of cNTnC-i9 in the

presence of the switch region of cTnI. The structure shows i9 bound in the hydrophobic cleft of cNTnC, as is the case for other drugs that bind the N-domain of cTnC[17, 25, 30, 31]. Compared to dfbp-o, a similar levosimendan analog, i9 binds deeper in the pocket. This could be the result of reduced degrees of freedom on the drug that allow it to remain bound instead of in the typical on-off binding equilibrium. It also indicates that the distance between the biphenyl moiety of i9 and the reactive thiol of cNTnC (from C4 of i9 to Sγ of C84) is adequate to allow for deep binding (Figure 7.9). The spacer between them has one double and four single bonds, the same number and type as levosimendan would have when reacting with cysteine (from C11 of levosimendan to Sγ of C84). However, the planarity in the spacer region of both drugs is different. Whereas i9 contains only one sp^2 atom and one N amide atom with trigonal planar geometry, reacted levosimendan would contain three adjacent sp^2 atoms that would extend the planarity of the system. On this basis we suggest that levosimendan can potentially bind deep in the hydrophobic cleft of cNTnC but with an orientation of the spacer region different than that of i9.
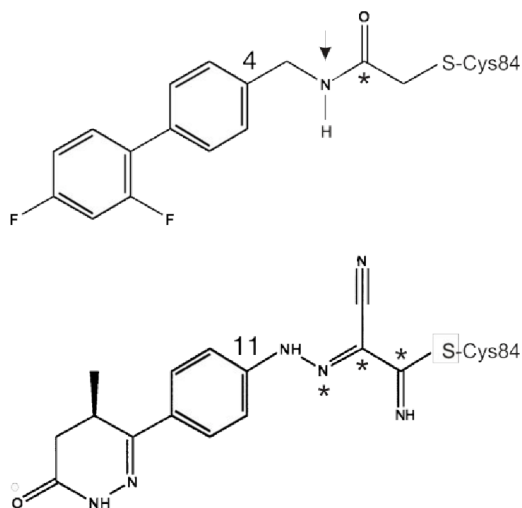
Figure 7.9. Structure of i9 and levosimendan reacted with C84.

Comparison between i9 and levosimendan covalently bound to Sγ of C84. Carbons 4 and 11 are labeled to mark the beginning of the spacer between the biphenyl moiety and C84. Atoms with sp^2 hibridization are marked with *. The arrow points to the additional planar center of the amide Nitrogen.

We showed that i9 reacts selectively with C84 of cNTnC. This is interpreted as the result of a two-step process, as in the case of other covalent inhibitors[32]. Initially, non-covalent binding to the protein target positions the reactive groups close in space. Then the complex undergoes bond formation. This is likely the case for i9, since the addition of a small excess of i9 into an aqueous solution of cNTnC (drug:protein ratio ~1.1:1) resulted in labeling mostly at C84. For an unspecific reaction, equal labeling of C35 and C84 would be expected. In addition, i9 is poorly soluble in water

but precipitates in an aqueous protein solution only after the drug-to-available SH ratio is over 1:1, which also suggests initial non-covalent binding of i9 to cNTnC. Selectivity is an important feature on the design of covalent drugs. However, in the specific case of cNTnC, a reversible covalent drug would be preferred in order to guarantee relaxation.

Our results indicate that switch-cTnI contributes to position and stabilize i9 in the hydrophobic cleft of cNTnC. In the absence of switch-cTnI, broad undistinguishable signals for the F2' and F4' atoms of C84-i9 indicated that i9 is in exchange between different conformations. Sharpening of the signals upon addition of switch-cTnI indicated that i9 was stabilized in one conformation. In contrast, cTnI has no effect on C35-i9, as the signals corresponding to its F2' and F4' atoms were sharper and unchanged in the absence and presence of switch-cTnI. In our structure of cChimera-i9, cNTnC is in the open state; therefore the ^{19}F signals of C84-i9 in cChimera-i9 also correspond to the open conformation. Close inspection of the ^{19}F spectra of cNTnC-i9 and cTnC(C35S)-i9 in the absence of cTnI reveals the presence of one signal corresponding to this conformation (* in Figure 7.5). This suggests that broadening is the result of exchange between a more populated open conformation and another less populated state. The other state may then correspond to the closed conformation of cNTnC with i9 outside the hydrophobic pocket. Along with the influence of cTnI on the position of C84-i9, the similarity of ^{19}F spectra of cChimera-i9 and cTnC(C35S)-i9 in the presence of switch-cTnI suggests that the orientation of i9 in cTnC(C35S)-i9 in muscle fibers is the same as in the present structure once switch-cTnI is bound.

We also showed that i9 increases the Ca^{2+} sensitivity of cardiac fibers by stabilizing the open conformation of cNTnC. Our results showed a shift to the left of 0.13 ± 0.03 pCa units in the force-pCa curve caused by cTnC(C35S)-i9. Since the i9 molecule is covalently attached to C84, the observed increase in Ca^{2+} sensitivity can be unequivocally attributed to the effect of i9 in cNTnC. This is in contrast to traditional experimental conditions in which drugs are perfused into muscle fibers and can reach other proteins or lipid membranes. Considering that the amount of cTnC(C35S)-i9 exchanged into the fibers was estimated to be 30%, we expect that higher ratios of protein exchange will result in a greater increase in Ca^{2+} sensitivity. In fact, longer incubation times for cTnC exchange resulted in increased resting tension in the absence of Ca^{2+}, which can be related to the stabilization of the open conformation of cNTnC by i9 as follows. In the mechanism of muscle contraction cNTnC, is in equilibrium between open and closed conformations. Ca^{2+} binding to cNTnC shifts the equilibrium toward the open state to allow the binding of switch-cTnI that triggers contraction. We propose that the mechanism of Ca^{2+} sensitization by i9 consists in a shift in the equilibrium to favor the open conformation. This explains our results regarding the tension development of fibers in the absence of Ca^{2+}, since i9 would have the same effect as Ca^{2+} to start contraction. It also agrees with the different conformations of C84-i9 observed in the absence of switch-cTnI corresponding to the change in

localization of i9 from inside to outside the hydrophobic cleft of cNTnC for which the open conformation is favored.

This work provides evidence for cNTnC opening as the major mechanism of action of Ca^{2+} sensitizers in muscle fibers. Although several Ca^{2+} sensitizing agents have been studied and characterized in the past, their mechanism of action is not fully understood. While dfbp-o increased the affinity of switch-cTnI for cNTnC[25], bepridil decreased it[30]. These effects were directly correlated with their structures. For cNTnC•switch-cTnI•dfbp-o the position of the cTnI peptide was not changed compared to the structure of cNTnC•switch-cTnI. In contrast, the NMR structure of cNTnC•switch-cTnI•bepridil shows switch-cTnI slightly away from cNTnC. Nevertheless both dfbp-o and bepridil induce Ca^{2+} sensitization in muscle fibers. Another contrasting case is W7, which also binds to cNTnC and, like bepridil, also shifts the switch-cTnI peptide[31] but causes Ca^{2+} desensitization in muscle fibers. Although W7 also binds to cNTnC, it does so with a low affinity (K_D ~ 0.5 mM) that may be too weak to stabilize the open conformation as the drug easily dissociates and cNTnC shifts back to a closed state. In contrast, bepridil binds tighter to either cNTnC (K_D = 23 μM) or cNTnC•switch-cTnI (K_D = 80 μM). As in the case of W7 and bepridil, our structure of cChimera-i9 shows switch-cTnI further from cNTnC to accommodate i9 in the hydrophobic pocket, yet it induces contraction independent of Ca^{2+} by promoting the occurrence of the open state of cNTnC. We conclude that this is the main mechanism by which other Ca^{2+} sensitizers induce contraction. Thus the ideal Ca^{2+} sensitizer should promote the open state of cNTnC for long enough by either tight binding to cNTnC (i9 and bepridil case) or stabilizing switch-cTnI binding (dfbp-o case) or an equilibrated combination of these. This knowledge may aid in the design of other therapies that target troponin to alleviate contractile failure.

In conclusion, this work unambiguously confirms that stabilization of the open state of cNTnC is the main mechanism of Ca^{2+} sensitization of contraction in muscle fibers. It also provides evidence of the reactive nature of levosimendan with thiol groups of cysteine residues. Moreover, we showed that i9, a covalent levosimendan analogue, can selectively react with C84 of cTnC to induce contraction of cardiac fibers independent of Ca^{2+}. This knowledge may lead the design of selective Ca^{2+} sensitizers that first bind to cNTnC and then exploit its reactivity to achieve an efficient inotropic effect on cardiac muscle.
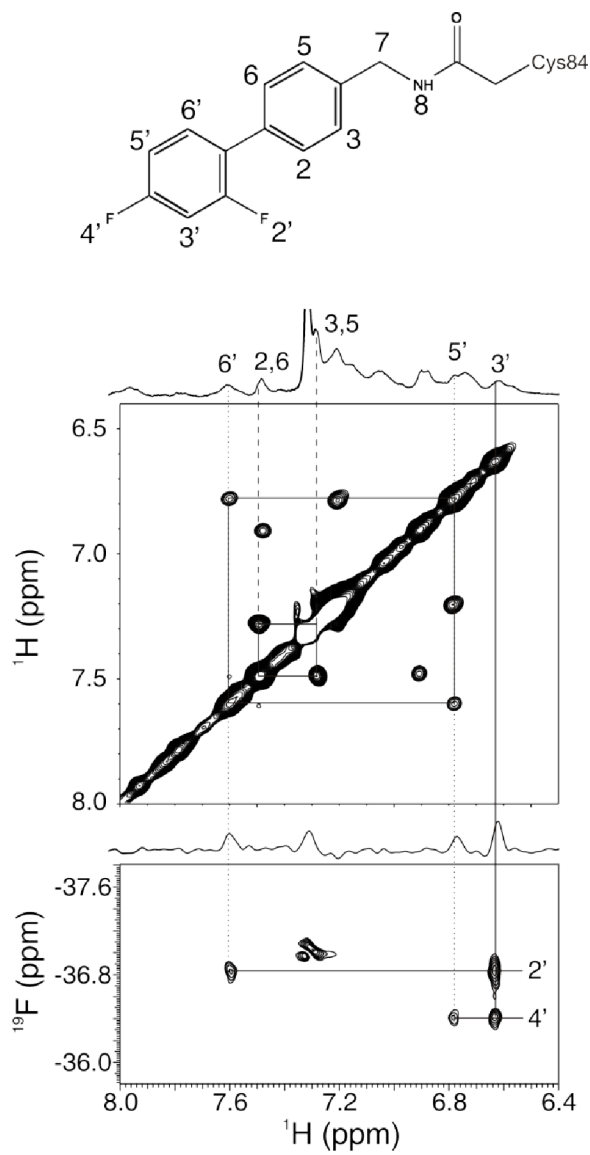
Supplementary Figure 7.1. Assignment of i9 in cChimera-i9.

^{13}C, ^{15}N filtered noesy and ^{19}F, ^{1}H HMQC used to assign the resonances of aromatic protons of i9 when bound to cChimera. The chemical structure of i9 is shown for reference.
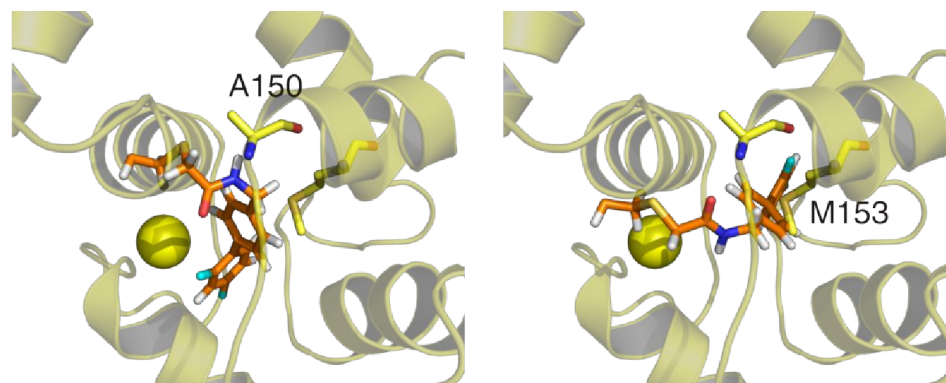
Supplementary Figure 7.2. Potential steric clash between i9 and cTnI.

The alpha carbons of cNTnC from the structure of cChimera-i9 and from the x-ray structure of the core domain of cTn (yellow) are aligned. From the structure of cChimera-i9 only the i9 molecule is shown for clarity (orange sticks). Two representative models from the final ensemble are depicted (lowest energy and closer to average). A150 and M153 from the x-ray structure are labeled and shown as yellow sticks.

Supplementary Table 7.1. Acquired NMR spectra for the study of cChimera-i9.

Experiment name (Varian)	Solvent	Nucleus in x/y/z dimension	^{1}H frequency (MHz)	nt[a]	x-points[b]	y-points[b]	z-points[b]	x-sw[c]	y-sw[c]	z-sw[c]	Mixing time (ms)
For assignment of i9 bound to cChimera											
CNfilnoesy	D$_2$O	^{1}H/^{1}H	600	64	4096	512		8398	8398		75
CNfiltocsy	D$_2$O	^{1}H/^{1}H	600	64	4096	256		8398	8398		43
HHMQC	D$_2$O	^{1}H/^{19}F	600	256	2048	56		8399	2500		
For assignment of cChimera bound to i9											
gNhsqc	H$_2$O	^{1}H/^{15}N	600	4	512	128		8398	2432		
gChsqc	H$_2$O	^{1}H/^{13}C	600	8	512	256		8398	10558		
ghn_cacb	H$_2$O	^{1}H/^{13}C/^{15}N	600	16	512	64	32	8398	12069	2432	
gcbca_co_nh	H$_2$O	^{1}H/^{13}C/^{15}N	600	16	512	64	32	8398	12069	2432	
ghnha	H$_2$O	^{1}H/^{1}H/^{15}N	600	8	512	128	32	8398	7198	1824	
ghc_co_nh	H$_2$O	^{1}H/^{1}H/^{15}N	600	16	512	72	40	8398	8398	2432	
gc_co_nh	H$_2$O	^{1}H/^{13}C/^{15}N	600	16	512	64	36	8398	12067	2432	
For structure determination											
gnoesyNhsqc	H$_2$O	^{1}H/^{1}H/^{15}N	600	8	512	128	48	8398	7198	1823	75
gnoesyChsqc	D$_2$O	^{1}H/^{1}H/^{13}C	600	16	512	64	64	8398	5999	4525	100
gnoesyChsqc_CNfilt	H$_2$O	^{1}H/^{1}H/^{13}C	800	16	820	64	48	9592	9596	16089	150

[a] Number of scans, [b] number of complex points, [c] spectral width (Hz).

Supplementary Table 7.2. Structural statistics for the final ensemble of 20 structures.

NOE restraints	
Total	1284
Intramolecular for cNTnC	1044
Short range ($\lvert i\text{-}j \rvert \leq 1$)	866
Medium range ($2 \leq \lvert i\text{-}j \rvert \leq 4$)	106
Long range ($\lvert i\text{-}j \rvert \geq 5$)	72
Intramolecular for cTnI	48
Intramolecular between cNTnC and cTnI	5
Intramolecular between cNTnC and i9	21
Intermolecular between cNTnC and Ca^{2+}	8
Dihedral restraints	
For cNTnC (+linker)	85 (+1)
For cTnI	13
PROCHECK validation	
RMSD from average (backbone atoms N, CA, C, O)	5.7 Å [a], 1.9 Å [b]
φ, ψ in allowed regions of Ramachandran plot	98.2 % [a], 100 % [b]
Z-score (all)	-0.35 [a], 2.60 [b]
Z-score[c] (φ, ψ)	0.63 [a], 3.74 [b]

[a] For all residues, [b] for ordered residues: 3-11, 14-27, 38-48, 54-64, 74-85, 150-157, [c] with respect to mean and standard deviation for a set of 252 x-ray structures < 500 residues, resolution ≤ 1.80 Å, R-factor ≤ 0.25, and R-free ≤ 0.28; a positive value indicates a "better" score.

References

1. Endoh, M. (2008) Cardiac Ca^{2+} signaling and Ca^{2+} sensitizers. *Circ. J. 72*, 1915-1925.

2. Robinson, J. M., Cheung, H. C., and Dong, W. (2008) The cardiac Ca^{2+}-sensitive regulatory switch, a system in dynamic equilibrium. *Biophys. J. 95*, 4772-4789.

3. Lindert, S., Kekenes-Huskey, P., Huber, G., Pierce, L., and McCammon, J. A. (2012) Dynamics and calcium association to the N-terminal regulatory domain of human cardiac troponin C: A multiscale computational study. *J Phys Chem B. 116*, 8449-8459.

4. Li, M., Wang, X., and Sykes, B. (2004) Structural based insights into the role of troponin in cardiac muscle pathophysiology. *J. Muscle Res. Cell Motil. 25*, 559-579.

5. Kobayashi, T., Jin, L., and de Tombe, P. (2008) Cardiac thin filament regulation. *Pflügers Arch. 457*, 37-46.

6. Pathak, A., Lebrin, M., Vaccaro, A., Senard, J. M., and Despas, F. (2013) Pharmacology of levosimendan: Inotropic, vasodilatory and cardioprotective effects. *J. Clin. Pharm. Ther. 38*, 341-349.

7. Pierrakos, C., Velissaris, D., Franchi, F., Muzzi, L., Karanikolas, M., and Scolletta, S. (2013) Levosimendan in critical illness: A literature review. *Journal of Clinical Medicine Research. 6*, 75-85.

8. Deschodt-Arsac, V., Calmettes, G., Raffard, G., Massot, P., Franconi, J., Pollesello, P., and Diolez, P. (2010) Absence of mitochondrial activation during levosimendan inotropic action in perfused paced guinea pig hearts as demonstrated by modular control analysis. *American Journal of Physiology - Regulatory, Integrative and Comparative Physiology. 299*, R786-R792.

9. Papp, Z., Csapó, K., Pollesello, P., Haikala, H., and Édes, I. (2005) Pharmacological mechanisms contributing to the clinical efficacy of levosimendan. *Cardiovasc. Drug Rev. 23*, 71-98.

10. Moreno, N., Tavares-Silva, M., Lourenco, A. P., Oliveira-Pinto, J., Henriques-Coelho, T., and Leite-Moreira, A. F. (2014) Levosimendan: The current situation and new prospects. *Rev. Port. Cardiol. 33*, 795-800.

11. Sorsa, T., Pollesello, P., Permi, P., Drakenberg, T., and Kilpeläinen, I. (2003) Interaction of levosimendan with cardiac troponin C in the presence of cardiac troponin I peptides. *J. Mol. Cell. Cardiol. 35*, 1055-1061.

12. Sorsa, T., Pollesello, P., and Solaro, R. J. (2004) The contractile apparatus as a target for drugs against heart failure: Interaction of levosimendan, a calcium sensitiser, with cardiac troponin c. *Molecular and Cellular Biochemistry. 266*, 87-107.

13. Levijoki, J., Pollesello, P., Kaivola, J., Tilgmann, C., Sorsa, T., Annila, A., Kilpeläinen, I., and Haikala, H. (2000) Further evidence for the cardiac troponin C mediated calcium sensitization by levosimendan: Structure-response and binding analysis with analogs of levosimendan. *J. Mol. Cell. Cardiol. 32*, 479-491.

14. Sorsa, T., Heikkinen, S., Abbott, M. B., Abusamhadneh, E., Laakso, T., Tilgmann, C., Serimaa, R., Annila, A., Rosevear, P. R., Drakenberg, T., Pollesello, P., and Kilpeläinen, I. (2001) Binding of levosimendan, a calcium sensitizer, to cardiac troponin C. *J. Biol. Chem. 276*, 9337-9343.

15. Li, M. X., Robertson, I. M., and Sykes, B. D. (2008) Interaction of cardiac troponin with cardiotonic drugs: A structural perspective. *Biochem. Biophys. Res. Commun. 369*, 88-99.

16. Hwang, P. M., and Sykes, B. D. (2015) Targeting the sarcomere to correct muscle function. *Nat. Rev. Drug Discov. 14*, 313-328.

17. Wang, X., Li, M. X., Spyracopoulos, L., Beier, N., Chandra, M., Solaro, R. J., and Sykes, B. D. (2001) Structure of the C-domain of human cardiac troponin C in complex with the Ca^{2+} sensitizing drug EMD 57033. *Journal of Biological Chemistry. 276*, 25456-25466.

18. Li, M., Saude, E., Wang, X., Pearlstone, J., Smillie, L., and Sykes, B. (2002) Kinetic studies of calcium and cardiac troponin I peptide binding to human cardiac troponin C using NMR spectroscopy. *E. B. J. 31*, 245-256.

19. Pineda-Sanabria, S., Julien, O., and Sykes, B. D. (2014) Versatile cardiac troponin chimera for muscle protein structural biology and drug discovery. *ACS Chem. Biol. 9*, 2121-2130.

20. Sun, Y. B., Lou, F., and Irving, M. (2009) Calcium- and myosin-dependent changes in troponin structure during activation of heart muscle. *J. Physiol. 587*, 155-163.

21. Ferguson, R. E., Sun, Y. B., Mercier, P., Brack, A. S., Sykes, B. D., Corrie, J. E., Trentham, D. R., and Irving, M. (2003) In situ orientations of protein domains: Troponin C in skeletal muscle fibers. *Mol. Cell. 11*, 865-874.

22. Pollesello, P., and Nore, P. (2003) Complete structure analysis of OR-1746, a complex product of cyclocondensation of arylhydrazomalononitriles containing clusters of protonated and unprotonated nitrogens, by pulsed-field-gradient heteronuclear NMR. *J. Pharm. Biomed. Anal. 31*, 125-131.

23. Delaglio, F., Grzesiek, S., Vuister, G. W., Zhu, G., Pfeifer, J., and Bax, A. (1995) NMRPipe: A multidimensional spectral processing system based on UNIX pipes. *Journal of Biomolecular NMR. 6*, 277-293.

24. Johnson, B. A., and Blevins, R. A. (1994) NMR view: A computer program for the visualization and analysis of NMR data. *Journal of Biomolecular NMR. 4*, 603-614.

25. Robertson, I. M., Sun, Y., Li, M. X., and Sykes, B. D. (2010) A structural and functional perspective into the mechanism of Ca^{2+}-sensitizers that target the cardiac troponin complex. *J. Mol. Cell. Cardiol. 49*, 1031-1041.

26. Schuttelkopf, A. W., and van Aalten, D. M. (2004) PRODRG: A tool for high-throughput crystallography of protein-ligand complexes. *Acta Crystallogr. D Biol. Crystallogr. 60*, 1355-1363.

27. Takeda, S., Yamashita, A., Maeda, K., and Maeda, Y. (2003) Structure of the core domain of human cardiac troponin in the Ca^{2+}-saturated form. *Nature. 424*, 35-41.

28. Berjanskii, M. V., and Wishart, D. S. (2005) A simple method to predict protein flexibility using secondary chemical shifts. *J. Am. Chem. Soc. 127*, 14970-14971.

29. Li, M. X., Spyracopoulos, L., and Sykes, B. D. (1999) Binding of cardiac troponin-I147-163 induces a structural opening in human cardiac troponin-C. *Biochemistry (N. Y.). 38*, 8289-8298.

30. Wang, X., Li, M. X., and Sykes, B. D. (2002) Structure of the regulatory N-domain of human cardiac troponin C in complex with human cardiac troponin I$_{147-163}$ and bepridil. *J. Biol. Chem. 277*, 31124-31133.

31. Oleszczuk, M., Robertson, I. M., Li, M. X., and Sykes, B. D. (2010) Solution structure of the regulatory domain of human cardiac troponin C in complex with the switch region of cardiac troponin I and W7: The basis of W7 as an inhibitor of cardiac muscle contraction. *J. Mol. Cell. Cardiol. 48*, 925-933.

32. Singh, J., Petter, R. C., Baillie, T. A., and Whitty, A. (2011) The resurgence of covalent drugs. *Nat Rev Drug Discov. 10*, 307-317.

CHAPTER 8

Structure of trans-resveratrol in complex with
the cardiac regulatory protein troponin C

Sandra E. Pineda-Sanabria[1], Ian M. Robertson[1], and Brian D. Sykes

Department of Biochemistry, School of Molecular and Systems Medicine, Faculty of Medicine and Dentistry, University of Alberta, Edmonton, Alberta, Canada T6G 2H7. [1]These authors contributed equally to this work.

This chapter describes the binding of a small molecule to the C-domain of troponin C. The compound under investigation, resveratrol, is a natural product found in red wine and other grape products. Its strong cardioprotective effects, including calcium sensitization, encouraged the investigation of its interaction with troponin. Although the C-domain is considered to have a mainly structural function, here the reader may appreciate its importance in the contractile machinery as a whole. A version of this chapter has been published previously: Pineda-Sanabria *et al.* (2011) *Biochemistry* 50:1309-1320.

Introduction

The physiological function of the heart is to pump blood throughout the body in order to fulfill the oxygen and nutrient demands of the organism. The thin filament in heart muscle is made up of actin, tropomyosin, and troponin. Troponin is a heterotrimeric protein complex formed by the Ca^{2+}-binding subunit, troponin C (TnC); the inhibitory subunit, troponin I (TnI); and the tropomyosin-binding subunit, troponin T (TnT). Cardiac TnC (cTnC) has four EF-hand metal binding sites (I-IV) – two in each of its terminal domains. The C-terminal (cCTnC) and N-terminal (cNTnC) domains are connected by a flexible linker, as shown by the NMR[1] and X-ray structures[2]. In cNTnC, site I is defunct and site II is a low-affinity Ca^{2+}-binding site; on the other hand, both site III and site IV in cCTnC are functional and can bind either Mg^{2+} or Ca^{2+}. During the contraction-relaxation cycle, cytosolic Ca^{2+} concentration dramatically oscillates: at high Ca^{2+} levels, cNTnC becomes Ca^{2+}-saturated, which primes cNTnC for binding with the "switch" region of cTnI ($cTnI_{147-163}$)[3],[4]; at low Ca^{2+} concentration, Ca^{2+} dissociates from cNTnC leading to the release of $cTnI_{147-163}$. Alternatively, cCTnC remains saturated with either Mg^{2+} or Ca^{2+} throughout the contraction cycle and is associated with the "anchoring" region of cTnI ($cTnI_{34-71}$); an interaction which may play both a structural and regulatory role[5]. Association of $cTnI_{147-163}$ with cNTnC drags the "inhibitory" region of cTnI ($cTnI_{128-147}$) off of actin, tropomyosin changes its orientation

on the thin-filament, the myosin binding site is exposed on actin, and myosin binding to actin leads to contraction (for reviews see [6],[7]).

The strength of heart muscle contraction is regulated by the amount of Ca^{2+} released from the sarcoplasmic reticulum into the cytosol and by the response of the myofilaments to Ca^{2+}. Many popular cardiotonic agents (such as digitalis or dobutamine) improve contraction in the failing heart by elevating intracellular Ca^{2+} concentration; however, intracellular Ca^{2+} modulation carries risks associated with Ca^{2+} overload such as cardiac arrhythmias, cell injury, or cell death. These limitations have shifted interest to a novel class of cardiotonic drugs: Ca^{2+}-sensitizers. Ca^{2+}-sensitizers induce a positive inotropic effect by modulating the myofilament's response to cytosolic Ca^{2+}, consequently circumventing the risks associated with altering Ca^{2+} homeostasis[8]. The essential role cTnC plays in regulation of contraction makes it a logical target for the development of Ca^{2+}-sensitizers. Several ligands that have been found to have a Ca^{2+}-sensitizing ability through direct interaction with cTnC include trifluoperazine (TFP)[9], bepridil[9,10], levosimendan[11-13], and EMD 57033[14-16]. While the majority of these compounds target cNTnC to elicit their Ca^{2+}-sensitizing effects, EMD 57033 functions by targeting cCTnC[15]. In addition, the natural tea polyphenol, epigallocatechin gallate (EGCg), modulates heart muscle contractility through an interaction with cCTnC[17,19]. These results suggest that both domains of cTnC represent targets for the development of Ca^{2+}-sensitizers to treat heart failure.

Cardiovascular diseases are the main cause of death worldwide. Interestingly, the mortality rate from heart disease is significantly lower in France than in other countries with comparable diets rich in fat and other risk factors. It has been suggested that this so called "French paradox" may be attributable to high wine consumption in France[20]. *Trans*-resveratrol (3,4',5-trihydroxystilbene) is produced in grapevines after fungal infection and exposure to ultraviolet light[21], and Siemann and Creasy proposed that it might be the biologically active ingredient of red wine[22]. *Trans*-resveratrol (resveratrol) has a variety of reported physiological effects including: antiplatelet aggregation, anti-inflammatory, and antioxidant activity linked to longevity[23,24] protective effects in skin photosensitivity[25]; neurodegenerative diseases[26]; cancer chemoprevention[27,28]; and cardioprotection[29]. Amongst its cardioprotective effects, it has been shown that resveratrol improves recovery of ventricular function including developed pressure in the face of ischemia reperfusion injury[30]. It was demonstrated that resveratrol directly affects the contractile function of guinea-pig myocytes, and it increased cell shortening in half the cells tested and decreased shortening in the other half. In the cells where it induced contraction, its relation with the Ca^{2+} transients was quantitatively determined indicating an increase in myofilament Ca^{2+}-sensitivity[31]. These findings indicate a direct relation between resveratrol and the Ca^{2+} regulated elements in myocytes; however, structural details of this interaction remain unclear.

The present study investigates the interaction between cTnC and resveratrol using the structural technique, NMR spectroscopy. There have been a number of research groups that describe the applications of relatively sparse NMR data for the determination of protein-ligand complexes[32-35] Recently, Hoffman and Sykes described a procedure to determine the structure of W7 bound with cNTnC using a previously determined structure of cNTnC as a template[36]. A similar protocol was followed here, and it was discovered that resveratrol binds to cCTnC in a similar manner as EGCg[19] and EMD 57033[14]. Several key hydrophobic interactions between cCTnC and resveratrol stabilize the binary structure. It also appears that resveratrol undergoes only a slight conformational change upon binding cCTnC. The solution structure provides clues into the cardioprotective mechanism of resveratrol, and molecular details of the interface between resveratrol and cCTnC may aid in the design of novel cCTnC-targeting drugs.

Experimental procedures

Sample preparation

Labeled ^{15}N- and ^{15}N,^{13}C-cCTnC and ^{15}N-cTnC were obtained from *E. coli* strains containing the expression vector as previously described[37,38]. *Trans*-resveratrol was purchased from Sigma-Aldrich Inc (99% purity as determined by gas chromatography). All NMR samples were 500 μL in volume and consisted of 100 mM KCl; 10 mM imidazole, or 8 mM imidazole-d_4 and 2 mM imidazole; and 0.5 mM DSS-d_6 as an NMR reference standard. Protein concentrations were ~0.2 mM for full length cTnC and ~0.5 mM for cCTnC with 20 mM or 10 mM CaCl$_2$ respectively. Sample pH was maintained at ~6.9 for all NMR experiments. Although resveratrol naturally exists in *cis* and *trans* isomeric forms, *trans*-resveratrol was used in this study due to its higher concentrations in red wine (0–15 μg/ml) in contrast with *cis*-resveratrol (0–5 μg/ml)[24]. Stock solutions of 20 mM *trans*-resveratrol (resveratrol) in a 100 mM tris(2-carboxyethyl)phosphine (TCEP) - DMSO-d_6 solution were prepared. TCEP was used to allay oxidation of resveratrol as done for EGCg and Ascorbic Acid[19,39]. The concentration ratio of resveratrol:cCTnC was ~4:1 for NMR experiments of the complex. All the stock solutions were prepared fresh prior to each experiment and were wrapped with aluminum foil to prevent photo-degradation.

NMR Spectroscopy and data processing

The NMR data used for this study was collected on Varian Inova 500-MHz and Unity 600-MHz spectrometers at 30 ˚C, or a Varian Inova 800-MHz spectrometer at 25 ˚C. All spectrometers have triple resonance probes with Z-pulsed field gradients. One-dimensional ^{1}H; and two-dimensional ^{1}H,^{1}H-NOESY and ^{1}H,^{1}H-ROESY experiments were acquired of resveratrol in D$_2$O with mixing times of 100 ms for the NOESY and 50, , 150, 200, and 300 ms mixing times for the ROESY experiments. Two-

dimensional ^{1}H,^{13}C-HSQC and ^{1}H,^{15}N-HSQC experiments were acquired to monitor the titration of resveratrol into ^{13}C,^{15}N- or ^{15}N-labeled cCTnC. Intramolecular NOEs of resveratrol when in complex with cCTnC were measured with the two-dimensional ^{13}C,^{15}N-filtered NOESY experiment with a mixing time of 100 ms[40,41]; intermolecular distance restraints between resveratrol and cCTnC were derived from two-dimensional ^{13}C-edited/filtered NOESY-HSQC (mixing times: 150, 200, 250 ms)[42] and three-dimensional ^{13}C-edited/filtered HMQC-NOESY (mixing times: 200, 250 ms)[43,44] experiments. In order to check whether the conformation of cCTnC was perturbed by the presence of resveratrol, a two-dimensional ^{1}H,^{1}H-NOESY was acquired of cCTnC•resveratrol in D_2O with a mixing time of 150 ms. VNMRJ (Varian Inc.) was used for the analysis of one-dimensional NMR spectra, all two-dimensional and three-dimensional NMR data were processed with NMRPipe[45] and analyzed with NMRView[46]. Chemical shifts of cCTnC were assigned using those deposited for cTnC1 and the methionine methyls were assigned from assignments previously determined by mutagenesis[47]. The interaction between resveratrol and cCTnC is in fast exchange, so the resonances from cCTnC could be followed throughout the titration of resveratrol and the assignments translated to the chemical shifts of the cCTnC•resveratrol complex.

Resveratrol assignment and assessment of stability

The proton chemical shifts of resveratrol were assigned in D_2O by the use of one-dimensional ^{1}H, two-dimensional ^{1}H,^{1}H-NOESY, and two-dimensional ^{1}H,^{1}H-ROESY NMR experiments. test the stability of resveratrol in aqueous solution, 500 μL samples of ~0.3 mM resveratrol were prepared in D_2O. ^{1}H NMR spectra were acquired at one-hour increments to test for oxidative degradation. Another sample of resveratrol was prepared with 10 mM TCEP and reassessed the sample stability. In both samples, the pD was ~7.0.

NMR structure and Ab initio calculations of resveratrol free in solution

The PRODRG web server[48] was used to create initial coordinates of resveratrol and XPLO-2D[49] was used to generate topology and parameter files for resveratrol. The structure of resveratrol was determined by ROE intensities of resveratrol at mixing time of 200 ms. XPLOR-NIH[50] was used to calculate the solution structure of resveratrol. Four NOEs contributed to the structure calculation, which were binned from strong (2.00-1.80 Å), medium (2.80-1.80 Å), and weak (3.60-1.80 Å). The simulated annealing comprised square-well potentials for inter-proton distances and a patch to keep the aromatic rings and olefin bond planar; the aromatic rings of resveratrol were allowed to freely rotate around the C1'-Cα' and C1-Cα bonds. 100 structures were calculated, and the lowest 10 in energy were kept. The lowest energy solution structure of free resveratrol was used as an input structure in Gaussian03[51] to calculate the total density and electrostatic potential (ESP). The energy calculation was performed in aqueous solvent with Becke's three-parameter Lee, Yang, Parr (B3LYP)

hybrid functional with a split-valence basis set and polarization d- and p-orbitals added (B3LYP/6-311++G(d, p)). Final contour surfaces were represented using GaussView 3.0.

Resveratrol titrations into cTnC and cCTnC

The 20 mM resveratrol stock solution was titrated into an NMR tube containing full length ^{15}N-labeled cTnC, [15]N-, and ^{15}N,[13]C-labeled cCTnC. Resveratrol additions were made to final concentrations of 62, 185, 367,665, 956, 1517 and 2050 μM for the titration with cTnC and to final concentrations of 43, 171, 379, 581, 975, 1346 and 1701 μM for the titration with cCTnC. One-dimensional ^{1}H and two-dimensional ^{1}H,^{15}N-HSQC spectra were acquired at each titration point. Additionally, ^{1}H,^{13}C-HSQC spectra were acquired throughout the titration of resveratrol into ^{13}C,[15]N-labeled cCTnC. At each titration point, the HSQC spectra were assigned, and residue specific chemical shift perturbations (CSPs) that were well resolved and underwent a large change were kept for the dissociation constant calculation. Chemical shift changes (Δδ) were calculated using the following equation:

$$\Delta\delta = \sqrt{(\Delta\delta_H)^2 + \frac{1}{25}(\Delta\delta_N)^2}$$

The dissociation constants (K_D) for resveratrol were calculated by using a global fitting approach with the program xcrvfit (www.bionmr.ualberta.ca/bds/software/xcrvfit), as described previously[52]. Briefly, the set of kept titration curves were fit using a fixed K_D range and a floating final shift value (since residues were perturbed to a varying extent). The sum of squared error (SSE) was minimized by optimizing the K_D, and thus a global K_D was calculated that best fit all the CSPs. The binding of resveratrol to cTnC and cCTnC was fit with a 1:1 stoichiometry:

$$troponin + resveratrol \leftrightarrow troponin \bullet resveratrol$$
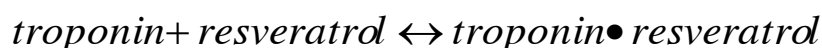
Concentrations of cTnC and cCTnC were calculated by integrating the one-dimensional-slice of the ^{1}H,^{15}N-HSQC spectrum, and comparing the spectral intensity with that of a sample with a protein concentration determined by amino acid analysis. The concentrations of the resveratrol stock solutions were determined by comparing the proton spectral intensity of resveratrol peaks with the DSS proton intensity. Concentrations of cTnC, cCTnC, and resveratrol were then corrected for dilution that occurred during the titrations. Since the addition of resveratrol slowly decreased the pH of the sample, the pH was adjusted to ~6.9 with 1M NaOH when necessary.

J-surface mapping

The program Jsurf was used to localize the binding site of resveratrol on cCTnC. Jsurf approximates the origin of the CSP as a single point-dipole in the center of an aromatic ring from a ligand[53]. With the coordinates of cTnC as input, Jsurf depicts the coordinates of a ligand ring as a dot based on the magnitude and sign of the CSPs. The region that shows the highest dot density is referred to as the j-surface, and is where the aromatic constituents of a ligand are most likely to reside. The chemical shifts in the ^{1}H,^{13}C-HSQC spectrum of the final point in the titration of cCTnC (CS_{PL}) with resveratrol were subtracted from the initial chemical shifts of cCTnC (CS_P).

$$CSP = CS_{PL} - CS_P$$

Only peaks that were well resolved and underwent a concentration-dependant CSP of ≥ 0.012 ppm in the proton dimension were used in the analysis; results were displayed in PyMOL.

Structure calculation of cCTnC•resveratrol

The structure of cCTnC•resveratrol was calculated using restraints for cCTnC from the complex of cCTnC•EGCg because the CSPs induced by both ligands are quite similar. A similar data-driven protocol has been used for the cNTnC•W7 complex[36]. Distance restraints for cCTnC were calibrated with CYANA[54] using an upper limit of 6 Å. Dihedral angle restraints from TALOS[55] were used as well as 12 distance restraints from X-ray crystallographic data of chelating oxygen atoms to the two Ca^{2+} ions. CYANA was used to calculate 100 structures of cCTnC, of which the 30 conformers with the lowest target function were used to further refine the structure with XPLOR-NIH. The restraints were converted from CYANA format into XPLOR-NIH format. The simulated annealing protocol of XPLOR-NIH, with 10 000 high temperature steps and 6000 cooling steps, was used in the structure calculation. The NOEs were averaged using the R-6 with a soft well potential. Spin-diffusion was a concern because the mixing times of 200 ms and 250 ms for the measurement of intermolecular NOEs were high. Therefore, only NOEs that had an NOE intensity≥μ-1/2σ were kept for the structure calculation, and all were calibrated with the same distance. A total of 23 intermolecular NOEs (6.0-1.8 Å) and four intramolecular NOEs (2.6-1.8 Å) were used in the structure calculation. 100 structures were calculated, from which the lowest 50 in energy were kept for refinement in explicit solvent with a water box edge length of 18.8 Å. It has been shown that refinement in explicit solvent including electrostatic potentials can improve the quality of structures[56]. Atomic charges calculated by Gaussian03 for resveratrol (see above) were included at this point in the structure calculation. The final ensemble is represented by the 20 lowest energy structures after water refinement and was validated by Procheck[57]

available with the online Protein Structure Validation Software (PSVS) suite (http://psvs-1_4-dev.nesg.org/); and the structural statistics are available in Supplementary Table 8.1.

Results

Stability of Resveratrol

NMR chemical shift assignments of *trans*-resveratrol (resveratrol), or *trans*-resveratrol derivatives have been previously reported in acetone[58], chloroform[59] , DMSO-d_6 [60], and in a DMSO-d_6/D_2O mixture[61]. Resveratrol (Figure 8.1) in D_2O was assigned by one-dimensional ^1H, two-dimensional ^1H,^1H-NOESY, and two-dimensional ^1H,^1H-ROESY NMR experiments. The aromatic protons were assigned using three and four bond couplings. H2'/H6' were distinguished from H3'/H5' by the acquisition of a two-dimensional NOESY and ROESY experiments; only the H2'/H6' made ROE contacts with the ethylene
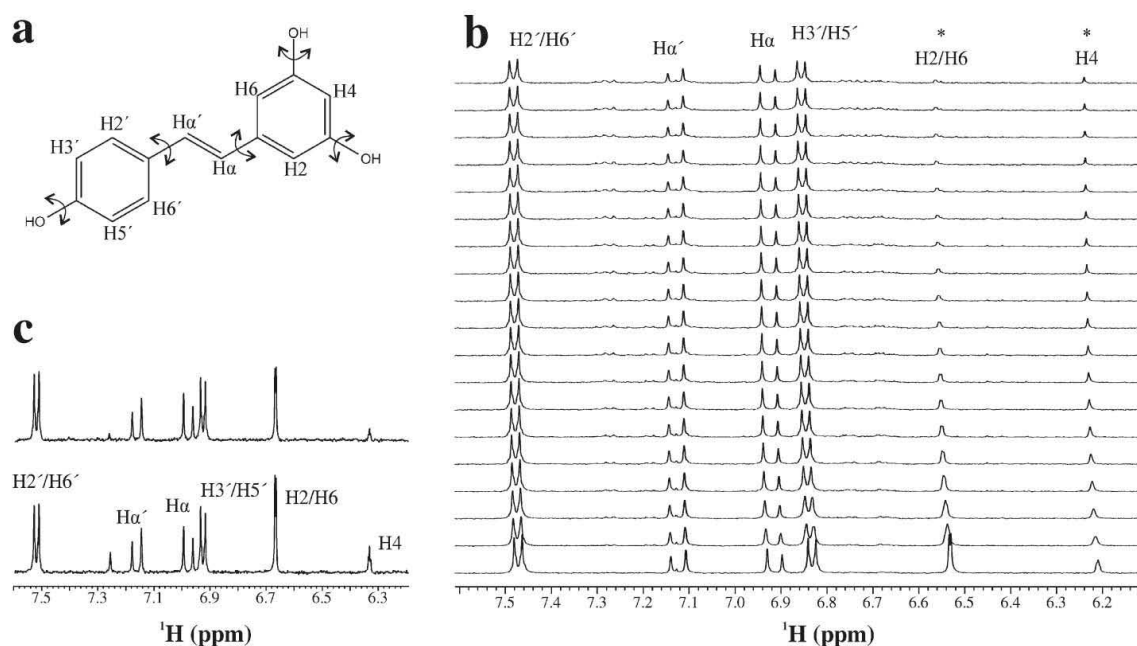
Figure 8.1. Stability of resveratrol.
a. Chemical structure of resveratrol. Torsion angles that were allowed to rotate during structure calculations are indicated. **b.** Degradation of resveratrol as a function of time. One-dimensional ^1H-NMR spectra acquired every 1 hour (bottom, first spectrum; top, last spectrum). **c.** The spectrum of resveratrol in the presence of 10 mM TCEP. Bottom spectrum is at time=0 and the top spectrum is of resveratrol after 24 hours. The unlabeled peak downfield from Hα' is from ^1H-imidazole which exchanged with D_2O over time.

protons (Hα and Hα'). The unambiguous assignments of Hα and Hα' were facilitated with previously published assignments for resveratrol[58-61]. The ethylene protons had a vicinal coupling constant of 16.4 Hz; consistent with a *trans*-ethylene bond[62].

The stability of resveratrol has been addressed previously[63]. The authors found that under acidic conditions, resveratrol was stable for at least 42 hours; while at pH 10, resveratrol had a half-life of 1.6 Hrs. Since three-dimensional NMR experiments require a stable sample for 2-3 days, and the samples are at neutral pH; the necessity of a reducing agent was investigated. The degradation of resveratrol was measured by acquiring one-dimensional ^{1}H-NMR spectra at one hour time points. Significant degradation of resveratrol was observed, primarily in the di-*meta*-hydroxyl (di-*m*-OH) ring (Figure 8.1b), and a half-life of 5-6 hours was estimated by monitoring the chemical shift change of the H2/H6 proton pair (Supplementary Figure 8.1). The sample also changed color from clear to brown over the course of the 24 hours. Next, 10 mM of TCEP was added to a sample of resveratrol and no significant degradation occurred after one day (Figure 8.1c). There was some decrease in peak intensities; however, there was no change in chemical shift or sample color; even after 72 hours.

Structure of Resveratrol in D$_2$O

In order to determine the structure of resveratrol in solution, two-dimensional ROESY spectra were acquired with different mixing times (50, 150, 200, and 300 ms); the ROE build-up curve is shown in Supplementary Figure 8.2. Two slices from the ROESY spectrum (mixing time = 200 ms) are shown in Figure 8.2a. The H2'/H6' protons make much stronger ROEs with the ethylene protons than the H2/H6 protons do (Table 8.1). The strong ROE between H2'/H6' and Hα is only consistent with a coplanar orientation of the *para*-hydroxyl (*p*-OH) ring and olefin. On the other hand, weak, approximately uniform ROEs between the ethylene protons and H2/H6 is indicative of roughly equal distance between H2/H6 and Hα and Hα'; consistent with a tilted and/or flexible di-*m*-OH ring. The ensemble of the 10 lowest energy structures is shown in Figure 8.2b. The torsion angles formed by Cα'-Cα-C1-C6 and Cα-Cα'-C1'-C6' can be used to describe the orientations of the two phenolic rings with respect to the olefin. In Table 8.2Table 8.1 the torsion angles for a number of structures of resveratrol are indicated. The *p*-OH ring is coplanar (0.5 ± 0.3°) with the olefin, whereas the di-*m*-OH ring is tilted by 43.9 ± 0.4°. The structure of free resveratrol has also been solved by NMR spectroscopy in DMSO[60] and by X-ray crystallography[64]; both structures revealed an overall planar structure. The X-ray structure of a trimethoxy-derivative of resveratrol was less planar; particularly in respect to the orientation of the di-*m*-O-CH$_3$ ring[65]. In the crystal structure of resveratrol, extensive hydrogen bonds contribute to the planarity of resveratrol, while the inability of 3,4',5-trimethoxystilbene to form intermolecular hydrogen bonds, resulted in a slight twist of the rings. It is possible that the presence of TCEP in the sample decreased the amount of intermolecular hydrogen-bonding of resveratrol by perturbing stacking

interactions, and may explain the somewhat tilted conformation of the di-*m*-OH ring. The lowest energy structure in the ensemble of resveratrol was used to calculate its electronic properties with the quantum chemistry program Gaussian03[51] (Figure 8.2c).
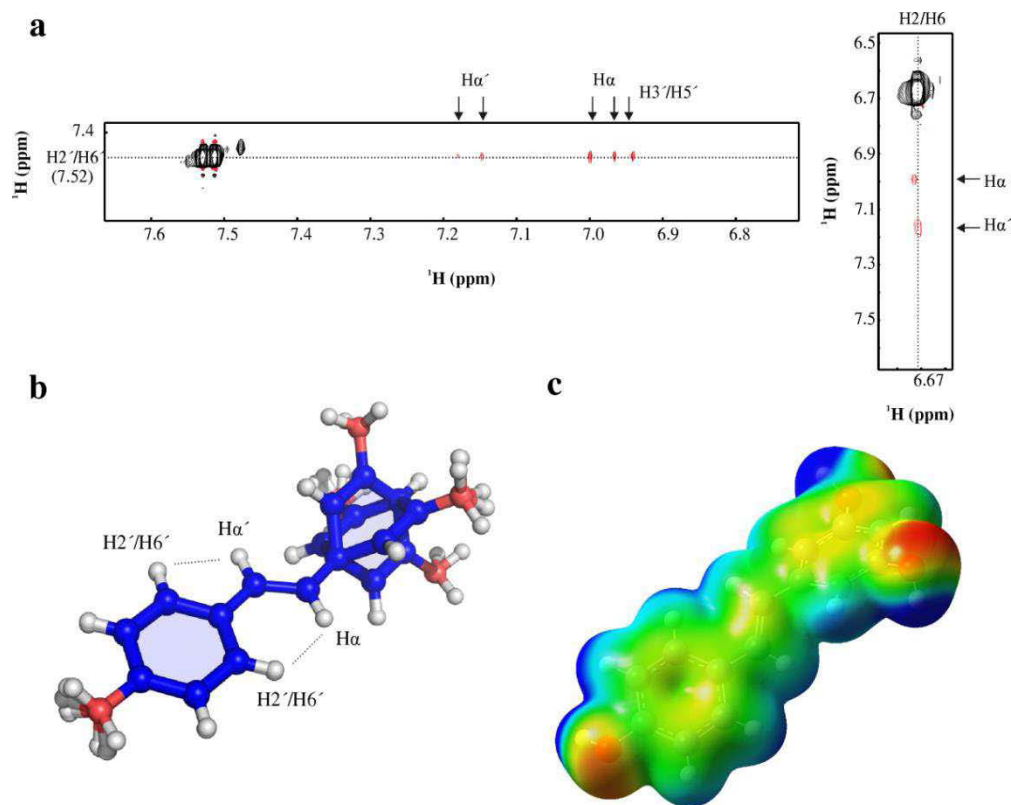
Figure 8.2. Structure of resveratrol

a. Two-dimensional-ROESY spectrum of resveratrol in D_2O. **b.** Ensemble of resveratrol aligned to the olefin atoms: Hα', Cα', Hα, and Cα. ROEs measured between H2'/H6' and Hα and Hα' are drawn on the structure to illustrate that the intensity of the ROE between H2'/H6' and Hα requires a planar orientation of phenol ring. **c.** Gaussian calculation from lowest energy structure of resveratrol. The electrostatic potential of resveratrol was mapped with an isovalue of 0.004 e/Å^3 (-7e^{-2} eV, red; 7e^{2+} eV, blue).

Table 8.1. Comparison of relative ROE or NOE intensities.

Contact	Free resveratrol[a]	Bound Resveratrol
H2'/H6' - Hα'	0.51	0.67
H2'/H6' - Hα	1.00	0.84
H2/H6 – Hα	0.17	0.71
H2/H6 – Hα'	0.16	1.00

[a]At mixing time of 200 ms.

Table 8.2. Comparison of resveratrol ring orientation with other structures.

Ring twist illustrates the orientation of the ring with comparison to the central olefin of resveratrol. The *p*-OH ring twist is the Cα-Cα'-C1'-C6' torsion angle; the di-*m*-OH ring twist is the Cα'-Cα-C1-C6 torsion angle. For the NMR structures, both positive and negative torsions were measured so they are reported in absolute degrees. Multiple values are given when more than one resveratrol is present in the X-ray structures.

Structure	*p*-OH ring twist (°)	di-*m*-OH ring twist (°)
X-ray structure of resveratrol[64]	8.02	-2.98
X-ray structure of 3,5,4'-Trimethoxystilbene[65]	3.53/-9.16	21.13/-16.32
NMR structure of resveratrol (D_2O) [a]	0.5 ± 0.3	43.9 ± 0.4
NMR structure of cCTnC [a]	20.7 ± 8.1	33.9 ± 9.4
X-ray structure of Chalcone Synthase (pdb: 1CGZ)[70]	-9.21	-32.00
X-ray structure of Transthyretin (pdb: 1DVS)[71]	0.7/1.06	0.55/1.13
X-ray structure of Quinone Reductase 2 (pdb: 1SG0)[73]	0.23/0.23	3.11/2.15
X-ray structure of mutant Chalcone Synthase (pdb: 1U0W)[72]	-0.16/-2.98	0.18/-1.49
X-ray structure of Stilbene Synthase (pdb: 1Z1F)[74]	62.92	-66.97
X-ray structure of Cytosolic Sulfotransferase (pdb: 3CKL)	19.84/20.51	5.80/19.16
X-ray structure of Leukotriene A4 Hydrolase (pdb: 3FTS)[76]	-27.28	-17.65
X-ray structure of F_1-ATPase (pdb: 1JIZ) [75] [b]	27.68/19.90/-35.06/42.25	-9.25/7.60/45.69/-21.39

[a] This study.

[b] The authors could not distinguish between two binding modes, and therefore concluded that resveratrol may bind to F_1-ATPase in multiple poses.

Resveratrol binding to cTnC

To characterize resveratrol's interaction with troponin it was titrated into a sample containing ^{15}N-labeled cTnC. ^{1}H,^{15}N-HSQC NMR spectra were acquired throughout the titration and most of the large chemical shift perturbations (CSPs) were of backbone amides in the C-domain of cTnC (Supplementary Figure 8.3). In addition, the residues that typically experience large perturbations upon cTnI or ligand binding to the N-domain[4,52] such as Gly34, Gly42, Glu66, and Asp73 remained relatively unperturbed. The linear nature of the CSPs is indicative of a 1:1 stoichiometry for resveratrol binding to cTnC. Multiple binding would lead to non-linear CSPs, as was observed for TFP and bepridil binding to cTnC[9]. Using the program xcrvfit, the CSPs of the backbone amides of Thr124, Gly125, Ile128, Thr129, Gly140, Gly159, and Glu161 were plotted as a function of resveratrol-to-cTnC concentration; a global dissociation constant (K_D) of 243 μM (SSE = 0.02) was determined (Supplementary Figure 8.3b).

Resveratrol binding to cCTnC

To test whether the interaction between resveratrol and cTnC was the same as in the isolated C-domain, resveratrol was titrated into cCTnC. Two-dimensional ^{1}H,^{13}C and ^{1}H,^{15}N HSQC experiments were used to monitor the titration of resveratrol into a sample containing cCTnC (Figure 8.3a and b). The ^{1}H,^{13}C-HSQC (without resveratrol) was assigned using chemical shift assignments deposited for cTnC[1]. Since resveratrol interacts with cCTnC in fast exchange, most assigned resonances could be easily followed throughout the titration. Global dissociation constants of 240 μM (SSE = 0.08); from the backbone amides, and 301 μM (SSE = 0.02); from the methyl groups of cCTnC were calculated (Figure 8.3). The residue specific CSPs are almost identical in both pattern and amplitude between the titrations of resveratrol to cCTnC and cTnC (Supplementary Figure 8.3c). The comparable dissociation constants and CSP patterns suggest that resveratrol interacts with cCTnC the same as it does with full-length cTnC.

Following determination of the affinity and stoichiometry of resveratrol binding to cCTnC, a j-surface mapping was executed to predict resveratrol's binding location on cCTnC. J-surface mapping works to predict a binding site by assuming that the ring current from an aromatic constituent of a ligand is the primary source of ligand-induced CSPs[53]. Typically, amide protons are used in the calculation; however, it is well-established that cTnC undergoes a large conformational change upon ligand binding. Thus, most of the backbone CSPs are indicative of a global change in its structure rather than direct contact with a given ligand[66]. In order to circumvent this difficulty, the CSPs of methyl protons were used in the j-surface calculation – as changes in these chemical shifts are more likely indicative of direct interactions with resveratrol. Methyl resonances used in the calculation were those

that underwent ≥ |0.012| ppm in the proton dimension. These included: Ile112, Met120, Leu121, Ala123, Ile128, Ile148, Met157, and Val160. The structure of cTnC (pdb: 1aj4)[1] was used in the j-surface calculation, and the results localize the binding of resveratrol to the cleft formed by the four helices of cCTnC (Figure 8.4). There appears to be two j-surfaces: one near the surface of cCTnC and the other deeper in the core. Because the j-surface calculation is unable to identify the specific pose resveratrol adopts when bound to cCTnC, NMR spectroscopy was used to identify intermolecular contacts between resveratrol and cCTnC.
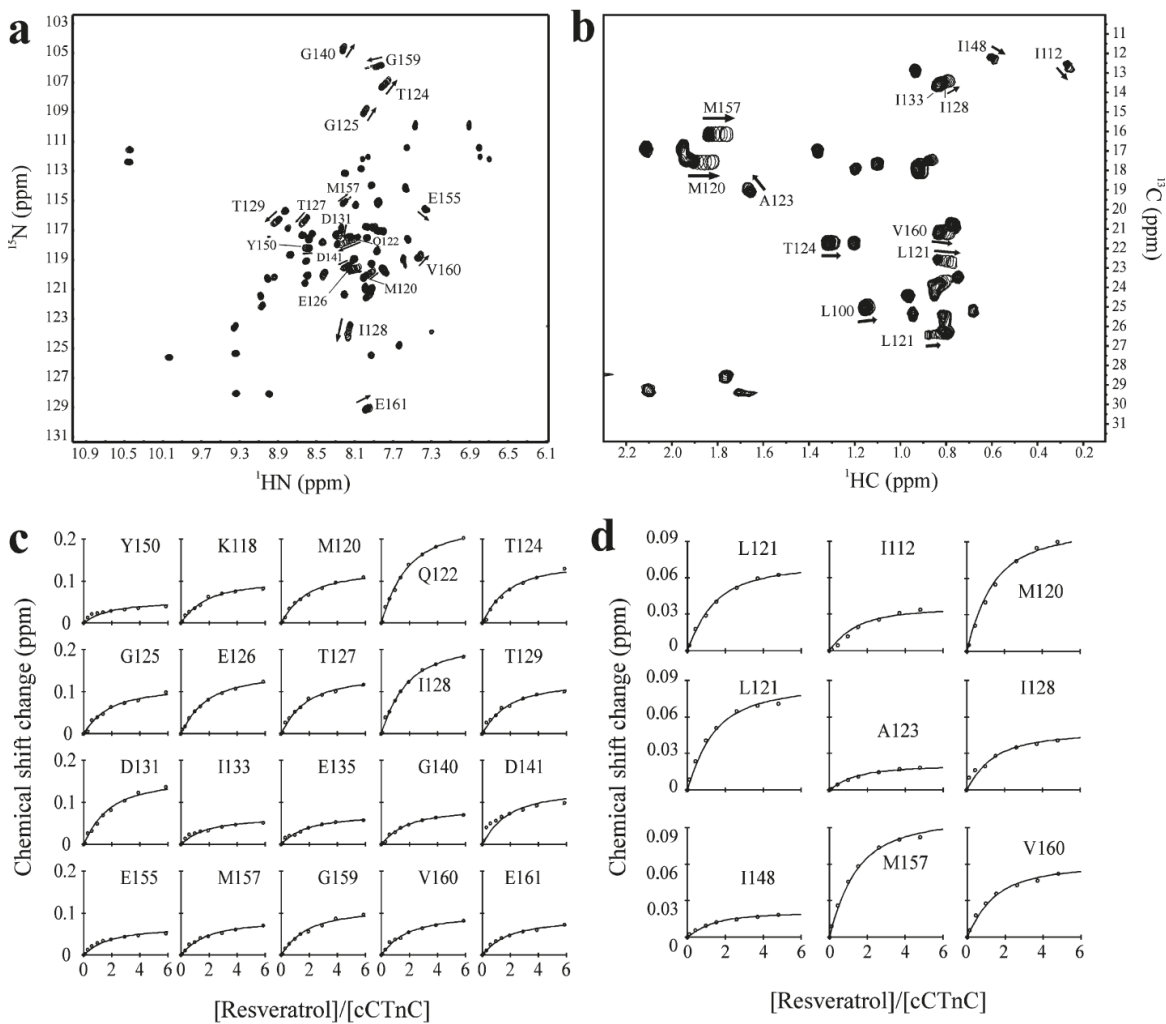
Figure 8.3. Binding of resveratrol to cCTnC

a. ^{1}H,^{15}N-HSQC and **b.** ^{1}H,^{13}C-HSQC (methyl-region) spectra of cCTnC acquired throughout the titration with resveratrol. The first point in the titration is represented with all 20 contours; whereas, each titration point with resveratrol is represented by a single contour. Direction of CSPs are indicated by arrows for several peaks. **c.** Fitting of ^{1}H,^{15}N-HSQC and **d.** ^{1}H,^{13}C-HSQC NMR data with xcrvfit to determine the dissociation constant.

206
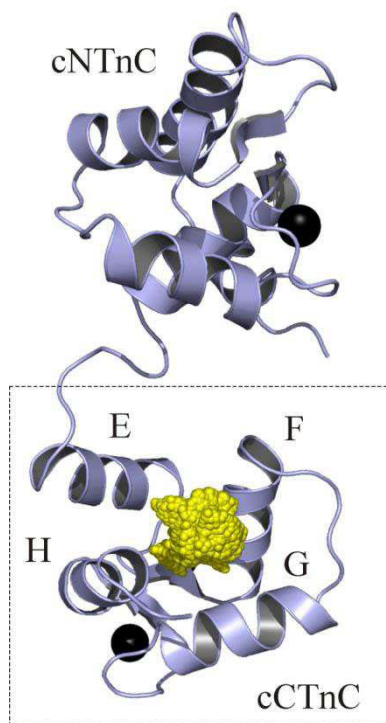
Figure 8.4. J-surface representation

Results are mapped on the structure of cTnC (pdb: 1aj4). The backbone atoms are depicted in cartoon representation (light blue), Ca^{2+} ions are represented by black spheres, and the j-surface dot density is depicted using yellow spheres. Residues used in the j-surface calculation were: Leu121, Val160, Ala123, Ile148, Ile128, Met157, Met120, and Ile112.

Structure of cCTnC•resveratrol complex

The structure of cCTnC free or in complex with a number of binding partners has been solved by both X-ray crystallography and NMR spectroscopy1[,2,14,19,67-69]. Instead of determining the structure of cCTnC again, a data-driven docking approach was pursued. The $^1H,^{15}N$-HSQC CSPs induced by resveratrol were compared with those induced by ligands that interact with cCTnC: cTnI[34-71], EMD 57033, and EGCg (Supplementary Figure 8.4). The CSPs are most similar between resveratrol and EGCg (in both magnitude and pattern); hence the intramolecular NOEs and dihedrals restraints of cCTnC used in the structure calculation were taken from the cCTnC•EGCg complex[19]. The only new restraints used in the structure calculation were those that defined the structure and pose of resveratrol in complex with cCTnC.

Intermolecular NOEs were measured between cCTnC and resveratrol with ^{13}C,^{15}N-edited/filtered NOESY experiments. These experiments measure solely NOEs between a ^{13}C/^{15}N-labeled molecule and an unlabeled molecule. Two-dimensional ^{13}C,^{15}N- filtered/edited NOESYHSQC[42] experiments were acquired with 150, 200, and 250 ms mixing times to establish the optimal mixing times to acquire the three-dimensional experiments. Since most of the intermolecular contacts observed were between methyl groups from cCTnC and the aromatic ring protons of resveratrol, the three-dimensional ^{13}C-edited/filtered HMQCNOESY experiment[43,44] was acquired. This NMR experiment is optimized for the identification of intermolecular NOEs involving ^{13}C-methyls[44]. Two three-dimensional ^{13}C-edited/filtered HMQCNOESY experiments were acquired: one with a mixing time of 250 ms and one with a mixing time of 200 ms. Intermolecular NOEs that had intensities ≥ 0.04 were included in the structure calculation. This is because of the long experimental mixing times of the intermolecular NOESY experiments and the tightly coupled nature of resveratrol increased the possibility of spin diffusion. When all NOEs were included in the structure run, many violations occurred, presumably because of spin diffusion. The intermolecular NOEs from a mixing time of 200 ms, used in the structure calculation are shown in Figure 8.5a. Initially, a structure calculation followed as was done for the EGCg calculation. The quality of the structure was subsequently improved by running a structure refinement in water; at this stage electrostatic potentials and atomic charges were included[56]. The 20 lowest energy structures of the complex are shown in Figure 8.5b and c. The structure indicates that, congruent with the prediction by j-surface mapping, resveratrol is localized to the hydrophobic pocket of cCTnC. The resveratrol-cCTnC interaction site is populated primarily by non-polar contacts. Resveratrol contacts the side chains of Leu100, Leu117, Leu121, Thr124, Leu136, Met157, and Val160 (Figure 8.5d). Weak NOEs between resveratrol and Ile148 and Ile112 (both β-sheet residues) – not used in the structure run because they did not meet the intensity cutoff criteria – were also consistent with the final structure. In addition to the methyl-resveratrol contacts, the structure indicates that arene-arene contacts made between resveratrol and Phe104, Phe153, and Phe156 contribute to the binding energy of resveratrol.

In addition to measuring intermolecular NOEs between resveratrol and cCTnC to determine their relative positions, the conformation of bound resveratrol was also determined. The intramolecular NOEs of resveratrol were measured with the ^{13}C,^{15}N-filtered NOESY experiment[40,41], which works by removing signals from a ^{13}C,^{15}N-labeled molecule, keeping only signals from an unlabeled molecule. All structure-defining intramolecular NOEs were close to the same intensity, with the strongest being the H2/H6-Hα' contact (see Table 8.1 and Supplementary Figure 8.5). This is in contrast with free resveratrol, where the strongest ROE was between H2'/H6' and Hα; and suggests that resveratrol undergoes a slight conformational change upon binding cCTnC. In order to limit biasing the structure of resveratrol during the calculation, one distance (2.6-1.8 Å) for the four intramolecular contacts was used; and the final structure was checked against the raw NOE data. Indeed, the results

Figure 8.5. Structure of the binary complex of cCTnC•resveratrol

a. Strip plots showing the NOEs between resveratrol and cCTnC. The resveratrol assignments are at the top of the spectrum; cCTnC assignments are indicated on the right. Peaks that are circled represent intramolecular cCTnC NOEs that were not adequately filtered. **b.** Ensemble of resveratrol from the binary complex. The carbon atoms are shown in yellow and the oxygen atoms in red. **c.** 20 lowest energy structures of the cCTnC•resveratrol complex with the backbone trace of cCTnC in light blue; helices E to H are labeled. **d.** Resveratrol's binding pocket on the lowest energy structure of cCTnC. Residues for which NOEs were measured are labeled and depicted in stick representation; resveratrol is shown in ball-and-stick representation (hydrogen atoms in white). Calcium ions are shown as black spheres.

209

are consistent with the relative NOE intensities: the closest proton pair was the H2/H6-Hα' proton pair (2.24 ± 0.13 Å). The other distances are: H2/H6-Hα; 2.55 ± 0.08 Å, H2'/H6'-Hα'; 2.29 ± 0.05 Å, and H2'/H6'-Hα; 2.33 ± 0.08 Å. The torsion angles were measured for resveratrol when in complex with cCTnC and were compared to those determined for free resveratrol. The *p*-OH ring is more twisted than what was observed for free resveratrol (from 0.5 ± 0.3° to 20.7 ± 8.1°), and the torsion angle of the di-*m*-OH ring is slightly smaller than it was for free resveratrol (from 43.9 ± 0.4° to 33.9 ± 9.4°).

There have been a number of crystal structures of resveratrol in complex with proteins solved, including: alfalfa chalcone synthase (CHS)[70], the fibril-forming transthyretin (TTR)[71], a variant of alfalfa CHS[72], quinone reductase 2 (QR2)[73], peanut stilbene synthase (STS)[74], bovine F1-ATPase[75], Leukotriene A4 hydrolase[76], and human cytosolic sulfotransferase (not published; but deposited in the PDB with the ID: 3ckl). In most of these structures resveratrol is planar or slightly distorted from a planar conformation with torsion angles no greater than 45°; the only exception is in the peanut STS-resveratrol complex, where both rings of resveratrol are twisted > 60° [74] (see Table 8.2). These results, in conjunction with the structures free resveratrol and resveratrol derivatives, point to a relatively rigid resveratrol framework. In accordance with the X-ray and NMR structures, Caruso *et al*. calculated single-point energy versus the torsion angle of the *p*-OH ring, and found the lowest energy structure is a planar conformation[64].

The structure of cCTnC in the cCTnC•resveratrol complex is not much different than that of cCTnC in other complexes. The Cα from residues in secondary structure elements of cCTnC•resveratrol were superimposed with cCTnC (pdb: 3ctn), cCTnC•EMD57033 (pdb: 1ih0), cCTnC•EGCg (pdb: 2kdh), and cCTnC•cTnI$_{34-71}$ (pdb: 1j2d) and rmsds of: 1.188 Å, 1.399 Å, 0.734 Å, and 1.336 Å were determined, respectively. These values indicate that resveratrol does not significantly perturb the structure of cCTnC. The E-helix of cCTnC•resveratrol is shifted away from the hydrophobic cleft, similar to the cCTnC•EMD5033 complex. The position of the F-helix of cCTnC•resveratrol is in almost an identical position as in the cCTnC•EGCg and cCTnC•cTnI$_{34-71}$ complexes; however, is shifted further away from the E-helix of cCTnC and not as far away as in the cCTnC•EMD57033 structure.

Discussion

The regulatory role of the interaction between cTnI$_{147-163}$ and cNTnC is well established, and has been the primary interaction site concentrated on for the development of Ca^{2+}-sensitizers[77,78]. Then again, there is mounting evidence that cCTnC also plays a part in the regulation of contraction, and therefore also is a potential target for the development of novel pharmaceuticals. The dilated cardiomyopathy mutation of cCTnC, Gly159Asp, decreases myofilament Ca^{2+}-sensitivity[79] *via* its modulation of the cTnI$_{34-71}$-cCTnC interaction[67]. The hypertrophic cardiomyopathy mutation,

Asp145Glu, increases Ca^{2+}-sensitivity[80], presumably by decreasing Ca^{2+} and cTnI binding to cCTnC[81]. The ablation of the Ca^{2+}-binding ability of the C-domain of cTnC increases the Ca^{2+}-sensitivity of muscle contraction[82]. There are two isoforms of TnC in insect flight muscle: the F1 isoform which regulates stretch-activated force, and the F2 isoform which is responsible for Ca^{2+}-activated contraction. Although it is not clear how F1 regulates stretch-activation, the interaction between the C-domain of F1 and TnH (an ortholog of cTnI) may play a role in regulation of stretch-activation[83]. Finally, as previously mentioned, the cardiotonic agents: EMD 57033[15,84] and EGCg[17,18] target cCTnC to modulate heart muscle contractility.

In this study, resveratrol was found to interact with the C-domain of cTnC, and the structure was determined by NMR spectroscopy. The *p*-OH group of resveratrol lies in the hydrophobic core of cCTnC, whereas the di-*m*-OH ring points towards the exterior of the protein. The stabilizing contacts between resveratrol and cCTnC are primarily hydrophobic: the nearest hydrogen bonding partners are the backbone carbonyl of Leu136 (4.42 ± 0.74 Å [Res-O – O-Leu136]) and the backbone amide of Gly140 (5.00 ± 0.56 Å [Res-O – HN-Gly140]) – too far to make hydrogen bonds with resveratrol. In the other resveratrol-protein structures, the binding site of resveratrol is also dominated by hydrophobic interactions; however, unlike the cCTnC•resveratrol structure, the structure is also stabilized by hydrogen bonds between the hydroxyls of resveratrol and the amino acids that line the binding pockets[70,76]. The design of resveratrol with the *p*-OH converted to a hydrophobic constituent may therefore increase its affinity for cCTnC; for example, converting the hydroxyl to a fluorine atom would increase the lipophilicity of resveratrol without dramatically decreasing its size[85,86]. On the other hand, removing the *p*-OH would undoubtedly reduce the antioxidant ability of resveratrol, especially given that the *p*-OH has been implicated as being the principal hydroxyl responsible for resveratrol's antioxidant nature[64,87].

The comparison of the cCTnC•resveratrol structure with the structures of cCTnC•EMD57033 and cCTnC•EGCg yields insights into several key functional groups. In the structure, the *p*-OH aromatic ring of resveratrol is positioned in a similar manner as the thiadiazinone ring of EMD 57033 – with the *para* hydroxyl pointed towards the cleft formed by helices G and H. The di-*m*-OH ring of resveratrol faces away from the hydrophobic cavity of cCTnC, leaving its hydroxyl moieties free to hydrogen bond with the surrounding aqueous milieu. The di-*m*-OH ring of resveratrol and the benzenediol of EGCg superimpose the best; consequently, resveratrol binds to cCTnC with features that uniquely resemble the EGCg and EMD 57033 bound structures. Resveratrol, EMD 57033, and EGCg all share their binding sites with the natural binding partner of cCTnC, $cTnI_{34-71}$ (Figure 8.6), and as a result, may have a common mode of action. The troponin dependant, Ca^{2+}-sensitizing ability of EMD 57033 has been suggested to involve a competition between EMD 57033 and $cTnI_{34-71}$ for cCTnC. The perturbation of the

cTnI$_{34-71}$-cCTnC interaction may lead to an increase in the affinity of cTnI$_{128-147}$ for cTnC and thus a decrease in contraction inhibition[90].
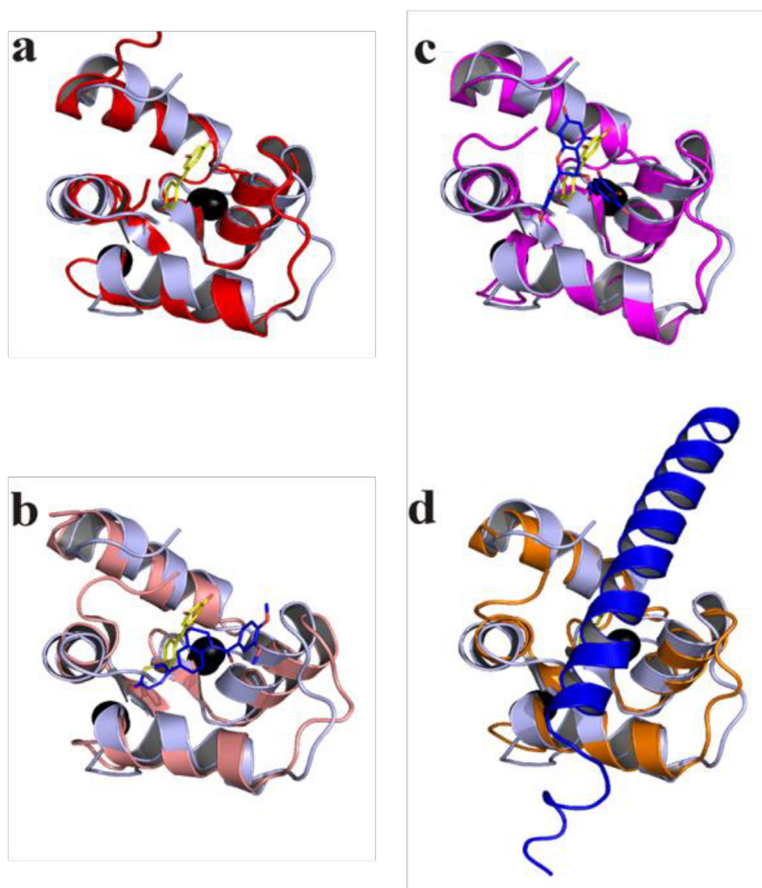
Figure 8.6. Structural comparisons

Superimposition between cCTnC•resveratrol (light blue) and **a.** cCTnC (red; pdb: 3ctn), **b.** cCTnC•EMD 57033 (pink; pdb: 1ih0), **c.** cCTnC•EGCg (magenta; pdb: 2kdh), and **d.** cCTnC•cTnI$_{34-71}$ (orange; pdb: 1j1d). The carbon atoms for resveratrol are colored in yellow, and the oxygen atoms are colored in red. For the other structures, ligand carbon atoms are colored in blue, oxygen atoms in red, nitrogen atoms in dark blue, and sulfur atoms in yellow. Ca^{2+} ions are shown as black spheres.

It was determined that resveratrol bound to cTnC and cCTnC with micromolar affinity. This relatively low affinity of resveratrol for cTnC was anticipated, since too high an affinity would lead to a marked increase in Ca^{2+}-sensitivity, which over the long-term would lead to negative effects, such as hypertrophic cardiomyopathy. On the other hand, it may be useful to optimize the resveratrol-cCTnC interaction for the development of drugs to treat acute heart failure. One method for the analysis of whether a small molecule represents a good lead molecule is to determine its ligand efficiency (LE)[91-93]. LE is described by the ratio of free energy of binding over the number of heavy atoms in a

compound, and is based on the premise that as a drug is optimized, it often increases in molecular weight; a trend fraught with problems including a decrease in bioavailability through insolubility and membrane permeability[94].

The free energy (ΔG) of binding and the ligand efficiency (binding energy per non-hydrogen atom) (LE) are:

$$\Delta G = -RT \ln K_D \qquad\qquad LE = \Delta G / N$$

For resveratrol binding to cCTnC; a K_D of 240 µM has a binding energy of 4.97 kcal/mol. Resveratrol has 17 non-hydrogen atoms (14 carbon atoms and 3 oxygen atoms), so its ligand efficiency is 0.29 kcal/mol. This ligand efficiency corresponds to a compound with 33 non-hydrogen atoms (approximately 2x the size of resveratrol: 450 MW) with a binding constant of 0.1 µM. The reasonable ligand efficiency of resveratrol, suggests that the substitution or addition of a few atoms that enhance its affinity for cCTnC may lead toward novel therapies for the treatment of heart failure.

Conclusion

Resveratrol is a natural product found in wine that modulates the Ca^{2+}-sensitivity of myofilaments[31]. In this study, the structure of resveratrol in complex with the cardiac regulatory protein troponin C was determined by NMR spectroscopy. Consistent with the small molecules EGCg and EMD 57033, resveratrol targeted the C-domain of troponin C. The binding of resveratrol is primarily stabilized by hydrophobic contacts such as methyl-arene and arene-arene interactions. In addition to providing clues into the cardioprotective nature of resveratrol, the structure highlights several functional groups that could be modified to optimize the binding efficacy of resveratrol. Recently, the polyphenol, propyl gallate, has also been identified to act as a Ca^{2+}-sensitizer[95], which alongside the functional and structural data for EGCg and resveratrol point toward a common mechanism by which these natural compounds target the thin filament to protect against heart failure.

Acknowledgements

Supplementary Figure 8.1. Oxidation rate or resveratrol.

The initial starting chemical shift of H2/H6 was normalized to one, and the chemical shift was measured at each time point. Since the H2/H6 is a doublet, the chemical shift from the further downfield peak of the doublet was measured.
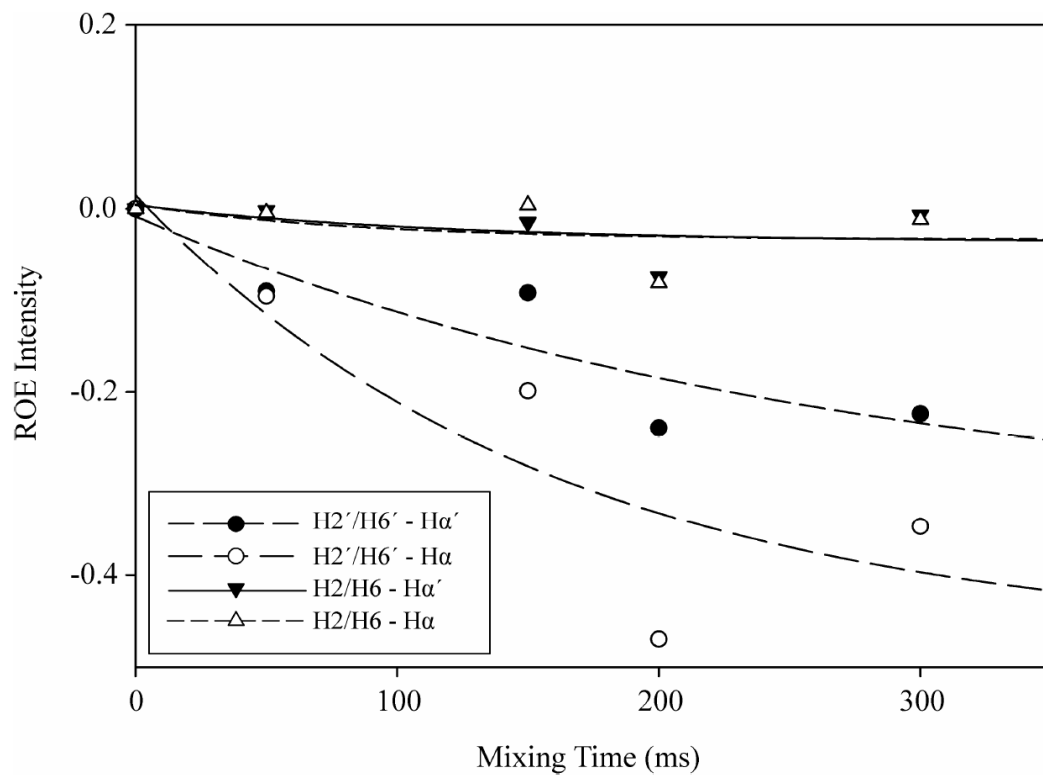
Supplementary Figure 8.2. ROEs measured at each mixing time.
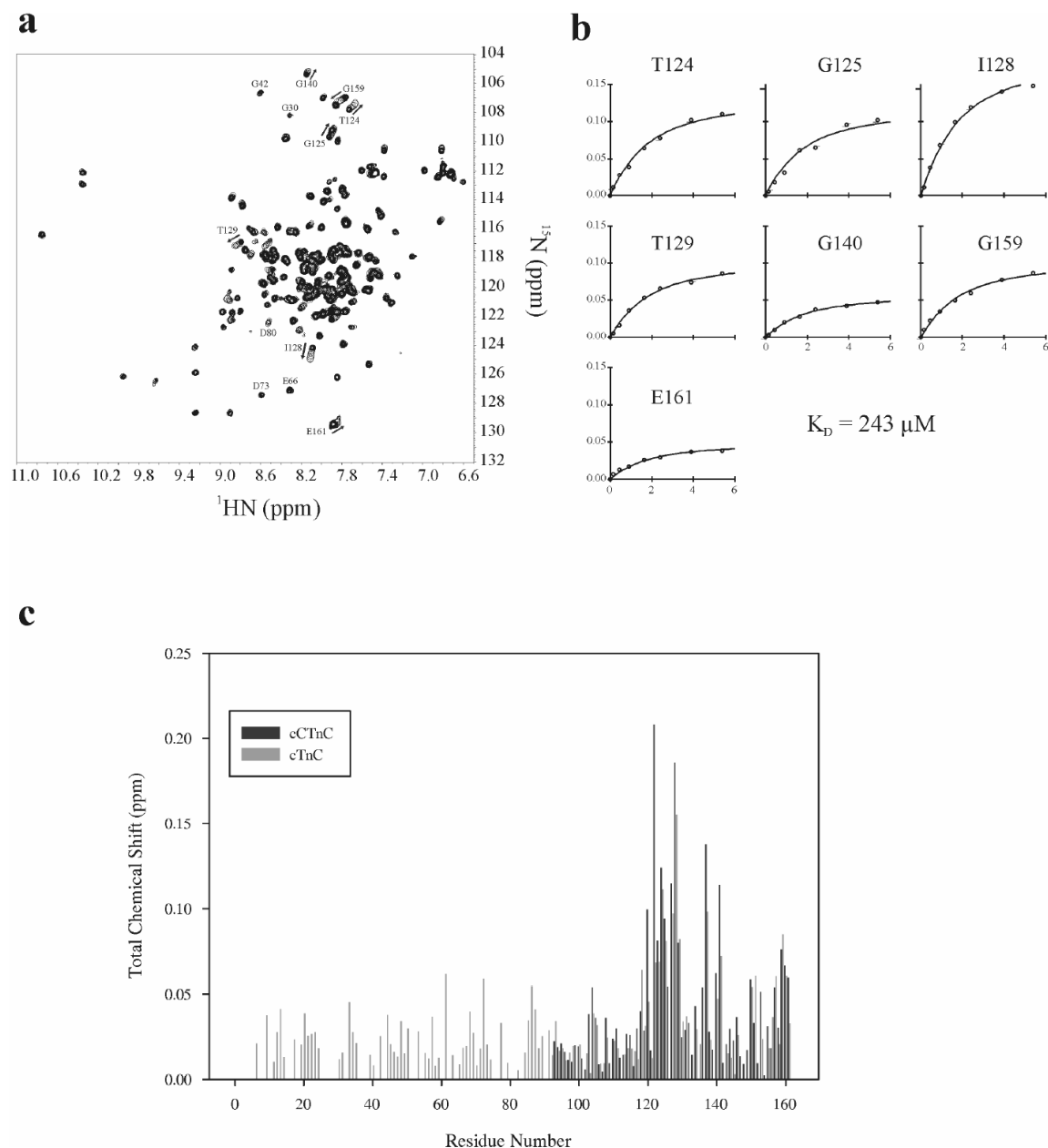
Supplementary Figure 8.3. Binding of resveratrol to cTnC.

a. ^{1}H,^{15}N-HSQC spectra of cCTnC acquired throughout the titration with resveratrol. The first point in the titration is represented with 20 contours; whereas, each titration point with resveratrol is represented by a single contour (O). Direction of CSPs are indicated by arrows for several peaks. b. fitting of ^{1}H,^{15}N-HSQC with xcrvfit to determine the dissociation constant. c. Bar graph of the total chemical shift change ($\Delta\delta = \sqrt{(\Delta\delta_H)^2 + \frac{1}{25}(\Delta\delta_N)^2}$) versus residue number for the titration of resveratrol into cTnC (light grey) and cCTnC (dark grey).
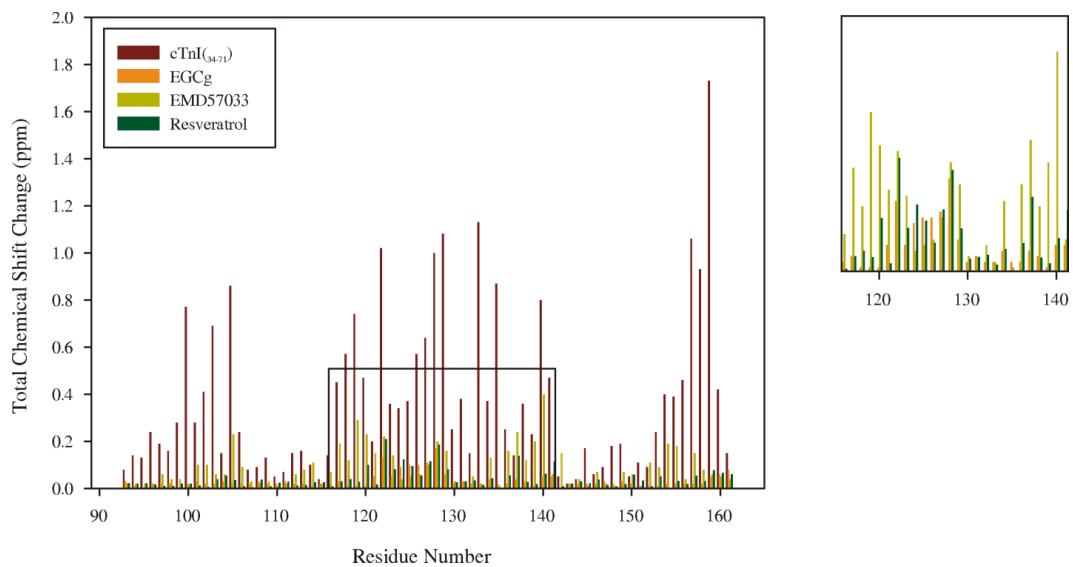
Supplementary Figure 8.4. Ligand-dependant chemical shift perturbations of cCTnC.

Bar graph of the total chemical shift change ($\Delta\delta = \sqrt{(\Delta\delta_H)^2 + \frac{1}{25}(\Delta\delta_N)^2}$) versus residue number for the titration of cTnI$_{34\text{-}71}$ (red), EGCg (orange), EMD 57033 (yellow), and resveratrol (green) into cCTnC. Chart on the right is an expansion of the bar chart; cTnI$_{34\text{-}71}$ CSPs have been removed for clarity.
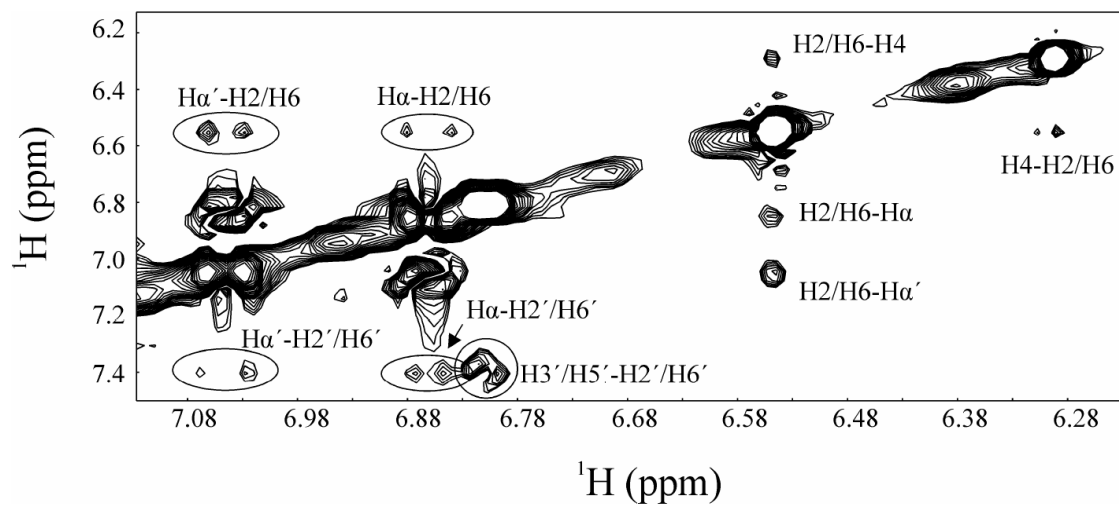
Supplementary Figure 8.5. Intramolecular NOEs of resveratrol in complex with cCTnC.

Supplementary Table 8.1. Structural statistics for 20 NMR structures of cCTnC•resveratrol.

	Backbone atoms	Heavy Atoms
R.m.s.d. from the average structure		
All residues (Å)	0.93 ± 0.14	1.42 ± 0.13
Ordered residues [a] (Å)	0.72 ± 0.11	1.21 ± 0.13
Total Distance Restraints	925	
Short range ($|i\text{-}j|$=1) NOEs	519	
Medium range (1<$|i\text{-}j|$<5) NOEs	201	
Long range ($|i\text{-}j|$≥5) NOEs	179	
Intermolecular NOEs	23	
Intramolecular NOEs	4	
Ca^{2+} distance restraints	12	
Dihedral restraints (ϕ/ψ)	106	
NOE violations per structure		
> 0.5 Å	0	
> 0.3 Å	0	
> 0.1 Å	2.15	
Dihedral Violations > 5º	0	
Ramachadran plot statistics [b]		
ϕ/ψ in most favored regions (%)	83.2 %	
ϕ/ψ in additionally allowed regions (%)	15.3 %	
ϕ/ψ generously allowed regions (%)	1.4 %	
ϕ/ψ in disallowed regions (%)	0.1 %	

[a] Residues 92-105, 111-124,and 131-158

[b] For all residues as determined by PROCHECK

References

1. Sia, S. K., Li, M. X., Spyracopoulos, L., Gagne, S. M., Liu, W., Putkey, J. A., and Sykes, B. D. (1997) Structure of cardiac muscle troponin C unexpectedly reveals a closed regulatory domain, *J. Biol. Chem. 272*, 18216-18221.

2. Takeda, S., Yamashita, A., Maeda, K., and Maeda, Y. (2003) Structure of the core domain of human cardiac troponin in the Ca(2+)-saturated form, *Nature 424*, 35-41.

3. Spyracopoulos, L., Li, M. X., Sia, S. K., Gagne, S. M., Chandra, M., Solaro, R. J., and Sykes, B. D. (1997) Calcium-induced structural transition in the regulatory domain of human cardiac troponin C, *Biochemistry 36*, 12138-12146.

4. Li, M. X., Spyracopoulos, L., and Sykes, B. D. (1999) Binding of cardiac troponin-I147-163 induces a structural opening in human cardiac troponin-C, *Biochemistry 38*, 8289-8298.

5. Tripet, B., Van Eyk, J. E., and Hodges, R. S. (1997) Mapping of a second actin-tropomyosin and a second troponin C binding site within the C terminus of troponin I, and their importance in the Ca2+-dependent regulation of muscle contraction, *J. Mol. Biol. 271*, 728-750.

6. Li, M. X., Wang, X., and Sykes, B. D. (2004) Structural based insights into the role of troponin in cardiac muscle pathophysiology, *J. Muscle Res. Cell Motil. 25*, 559-579.

7. Kobayashi, T., Jin, L., and de Tombe, P. P. (2008) Cardiac thin filament regulation, *Pflugers Archiv-European Journal of Physiology 457*, 37-46.

8. Endoh, M. (2001) Mechanism of action of Ca2+ sensitizers--update 2001, *Cardiovasc. Drugs Ther. 15*, 397-403.

9. Kleerekoper, Q., Liu, W., Choi, D., and Putkey, J. A. (1998) Identification of binding sites for bepridil and trifluoperazine on cardiac troponin C, *J. Biol. Chem. 273*, 8153-8160.

10. Li, Y., Love, M. L., Putkey, J. A., and Cohen, C. (2000) Bepridil opens the regulatory N-terminal lobe of cardiac troponin C, *Proc. Natl. Acad. Sci. U. S. A. 97*, 5140-5145.

11. Haikala, H., Kaivola, J., Nissinen, E., Wall, P., Levijoki, J., and Linden, I. B. (1995) Cardiac Troponin-C as a Target Protein for a Novel Calcium Sensitizing Drug, Levosimendan, *J. Mol. Cell. Cardiol. 27*, 1859-1866.

12. Haikala, H., Nissinen, E., Etemadzadeh, E., Levijoki, J., and Linden, I. B. (1995) Troponin C-Mediated Calcium Sensitization Induced by Levosimendan Does Not Impair Relaxation, *J. Cardiovasc. Pharmacol. 25*, 794-801.

13. Haikala, H., Nissinen, E., Etemadzadeh, E., Linden, I. B., and Pohto, P. (1992) Levosimendan Increases Calcium Sensitivity without Enhancing Myosin Atpase Activity and Impairing Relaxation, *J. Mol. Cell. Cardiol. 24*, S97-S97.

14. Wang, X., Li, M. X., Spyracopoulos, L., Beier, N., Chandra, M., Solaro, R. J., and Sykes, B. D. (2001) Structure of the C-domain of human cardiac troponin C in complex with the Ca2+ sensitizing drug EMD 57033, *J. Biol. Chem. 276*, 25456-25466.

15. Pan, B. S., and Johnson, R. G. (1996) Interaction of cardiotonic thiadiazinone derivatives with cardiac troponin C, *J. Biol. Chem. 271*, 817-823.

16. Kleerekoper, Q., and Putkey, J. A. (1999) Drug binding to cardiac troponin C, *J. Biol. Chem. 274*, 23932-23939.

17. Liou, Y. M., Kuo, S. C., and Hsieh, S. R. (2008) Differential effects of a green tea-derived polyphenol (-)-epigallocatechin-3-gallate on the acidosis-induced decrease in the Ca(2+) sensitivity of cardiac and skeletal muscle, *Pflugers Arch. 456*, 787-800.

18. Tadano, N., Du, C. K., Yumoto, F., Morimoto, S., Ohta, M., Xie, M. F., Nagata, K., Zhan, D. Y., Lu, Q. W., Miwa, Y., Takahashi-Yanaga, F., Tanokura, M., Ohtsuki, I., and Sasaguri, T. (2010) Biological actions of green tea catechins on cardiac troponin C, *Br. J. Pharmacol. 161*, 1034-1043.

19. Robertson, I. M., Li, M. X., and Sykes, B. D. (2009) Solution Structure of Human Cardiac Troponin C in Complex with the Green Tea Polyphenol, (-)-Epigallocatechin 3-Gallate, *J. Biol. Chem. 284*, 23012-23023.

20. Renaud, S., and Delorgeril, M. (1992) Wine, Alcohol, Platelets, and the French Paradox for Coronary Heart-Disease, *Lancet 339*, 1523-1526.

21. Langcake, P., and Pryce, R. J. (1976) Production of Resveratrol by Vitis-Vinifera and Other Members of Vitaceae as a Response to Infection or Injury, *Physiol. Plant Pathol. 9*, 77-86.

22. Siemann, E. H., and Creasy, L. L. (1992) Concentration of the Phytoalexin Resveratrol in Wine, *Am. J. Enol. Vitic. 43*, 49-52.

23. Das, D. K., Mukherjee, S., and Ray, D. (2010) Resveratrol and red wine, healthy heart and longevity, *Heart Failure Reviews 15*, 467-477.

24. Lekli, I., Ray, D., and Das, D. K. (2010) Longevity nutrients resveratrol, wines and grapes, *Genes and Nutrition 5*, 55-60.

25. Nichols, J. A., and Katiyar, S. K. (2010) Skin photoprotection by natural polyphenols: anti-inflammatory, antioxidant and DNA repair mechanisms, *Archives of Dermatological Research 302*, 71-83.

26. Sun, A. Y., Wang, Q., Simonyi, A., and Sun, G. Y. (2010) Resveratrol as a Therapeutic Agent for Neurodegenerative Diseases, *Molecular Neurobiology 41*, 375-383.

27. Jang, M. S., Cai, E. N., Udeani, G. O., Slowing, K. V., Thomas, C. F., Beecher, C. W. W., Fong, H. H. S., Farnsworth, N. R., Kinghorn, A. D., Mehta, R. G., Moon, R. C., and Pezzuto, J. M. (1997) Cancer chemopreventive activity of resveratrol, a natural product derived from grapes, *Science 275*, 218-220.

28. Holme, A. L., and Pervaiz, S. (2007) Resveratrol in cell fate decisions, *J. Bioenerg. Biomembr. 39*, 59-63.

29. Das, D. K., and Maulik, N. (2006) Red wine and heart: A cardioprotective journey from grape to resveratrol, *Alcoholism-Clinical and Experimental Research 30*, 84a-84a.

30. Ray, P. S., Maulik, G., Cordis, G. A., Bertelli, A. A. E., Bertelli, A., and Das, D. K. (1999) The red wine antioxidant resveratrol protects isolated rat hearts from ischemia reperfusion injury, *Free Radical Biology and Medicine 27*, 160-169.

31. Liew, R., Stagg, M. A., MacLeod, K. T., and Collins, P. (2005) The red wine polyphenol, resveratrol, exerts acute direct actions on guinea-pig ventricular myocytes, *Eur. J. Pharmacol. 519*, 1-8.

32. Bertini, I., Fragai, M., Giachetti, A., Luchinat, C., Maletta, M., Parigi, G., and Yeo, K. J. (2005) Combining in silico tools and NMR data to validate protein-ligand structural models: Application to matrix metalloproteinases, *J. Med. Chem. 48*, 7544-7559.

33. Cioffi, M., Hunter, C. A., Packer, M. J., and Spitaleri, A. (2008) Determination of protein-ligand binding modes using complexation-induced changes in H-1 NMR chemical shift, *J. Med. Chem. 51*, 2512-2517.

34. Krishnamoorthy, J., Yu, V. C. K., and Mok, Y. K. (2010) Auto-FACE: An NMR Based Binding Site Mapping Program for Fast Chemical Exchange Protein-Ligand Systems, *PLoS ONE 5*, -.

35. Pintacuda, G., John, M., Su, X. C., and Otting, G. (2007) NMR structure determination of protein-ligand complexes by lanthanide labeling, *Acc. Chem. Res. 40*, 206-212.

36. Hoffman, R. M. B., and Sykes, B. D. (2009) Structure of the Inhibitor W7 Bound to the Regulatory Domain of Cardiac Troponin C, *Biochemistry 48*, 5541-5552.

37. Chandra, M., Dong, W. J., Pan, B. S., Cheung, H. C., and Solaro, R. J. (1997) Effects of protein kinase A phosphorylation on signaling between cardiac troponin I and the N-terminal domain of cardiac troponin C, *Biochemistry 36*, 13305-13311.

38. Li, M. X., Gagne, S. M., Tsuda, S., Kay, C. M., Smillie, L. B., and Sykes, B. D. (1995) Calcium-Binding to the Regulatory N-Domain of Skeletal-Muscle Troponin-C Occurs in a Stepwise Manner, *Biochemistry 34*, 8330-8340.

39. Lykkesfeldt, J. (2000) Determination of ascorbic acid and dehydroascorbic acid in biological samples by high-performance liquid chromatography using subtraction methods: Reliable reduction with tris[2-carboxyethyl] phosphine hydrochloride, *Anal. Biochem. 282*, 89-93.

40. Gemmecker, G., Olejniczak, E. T., and Fesik, S. W. (1992) An Improved Method for Selectively Observing Protons Attached to C-12 in the Presence of H-1-C-13 Spin Pairs, *J. Magn. Reson. 96*, 199-204.

41. Ikura, M., and Bax, A. (1992) Isotope-Filtered 2d Nmr of a Protein Peptide Complex - Study of a Skeletal-Muscle Myosin Light Chain Kinase Fragment Bound to Calmodulin, *J. Am. Chem. Soc. 114*, 2433-2440.

42. Stuart, A. C., Borzilleri, K. A., Withka, J. M., and Palmer, A. G. (1999) Compensating for variations in H-1-C-13 scalar coupling constants in isotope-filtered NMR experiments, *J. Am. Chem. Soc. 121*, 5346-5347.

43. Lee, W., Revington, M. J., Arrowsmith, C., and Kay, L. E. (1994) A Pulsed-Field Gradient Isotope-Filtered 3d C-13 Hmqc-Noesy Experiment for Extracting Intermolecular Noe Contacts in Molecular-Complexes, *FEBS Lett. 350*, 87-90.

44. Robertson, I. M., Spyracopoulos, L., and Sykes, B. D. (2009) The Evaluation of Isotope Editing and Filtering for Protein-Ligand Interaction Elucidation by Nmr, *Biophysics and the Challenges of Emerging Threats*, 101-119.

45. Delaglio, F., Grzesiek, S., Vuister, G. W., Zhu, G., Pfeifer, J., and Bax, A. (1995) Nmrpipe - a Multidimensional Spectral Processing System Based on Unix Pipes, *J. Biomol. NMR 6*, 277-293.

46. Johnson, B. A., and Blevins, R. A. (1994) Nmr View - a Computer-Program for the Visualization and Analysis of Nmr Data, *J. Biomol. NMR 4*, 603-614.

47. Lin, X., Krudy, G. A., Howarth, J., Brito, R. M. M., Rosevear, P. R., and Putkey, J. A. (1994) Assignment and Calcium-Dependence of Methionyl Epsilon-C and Epsilon-H Resonances in Cardiac Troponin-C, *Biochemistry 33*, 14434-14442.

48. Schuttelkopf, A. W., and van Aalten, D. M. F. (2004) PRODRG: a tool for high-throughput crystallography of protein-ligand complexes, *Acta Crystallogr. Sect. D Biol. Crystallogr. 60*, 1355-1363.

49. Kleywegt, G. J., Zou, J.Y., Kjeldgaard, M., Jones, T.A., Around O. (2001) International Tables for Crystallography, Vol. F. Crystallography of Biological Macromolecules, (Rossmann, M. G., Arnold, E., Ed.), pp 353-356, 366-367, Dordrecht: Kluwer Academic Publishers, The Netherlands. .

50. Schwieters, C. D., Kuszewski, J. J., Tjandra, N., and Clore, G. M. (2003) The Xplor-NIH NMR molecular structure determination package, *J. Magn. Reson. 160*, 65-73.

51. M. J. Frisch, G. W. T., H. B. Schlegel, G. E. Scuseria, M. A. Robb, J. R. Cheeseman, J. A. Montgomery, Jr., T. Vreven, K. N. Kudin, J. C. Burant, J. M. Millam, S. S. Iyengar, J. Tomasi, V. Barone, B. Mennucci, M. Cossi, G. Scalmani, N. Rega, G. A. Petersson, H. Nakatsuji, M. Hada, M. Ehara, K. Toyota, R. Fukuda, J. Hasegawa, M. Ishida, T. Nakajima, Y. Honda, O. Kitao, H. Nakai, M. Klene, X. Li, J. E. Knox, H. P. Hratchian, J. B. Cross, V. Bakken, C. Adamo, J. Jaramillo, R. Gomperts, R. E. Stratmann, O. Yazyev, A. J. Austin, R. Cammi, C. Pomelli, J. W. Ochterski, P. Y. Ayala, K. Morokuma, G. A. Voth, P. Salvador, J. J. Dannenberg, V. G. Zakrzewski, S. Dapprich, A. D. Daniels, M. C. Strain, O. Farkas, D. K. Malick, A. D. Rabuck, K. Raghavachari, J. B. Foresman, J. V. Ortiz, Q. Cui, A. G. Baboul, S. Clifford, J. Cioslowski, B. B. Stefanov, G. Liu, A. Liashenko, P. Piskorz, I. Komaromi, R. L. Martin, D. J. Fox, T. Keith, M. A. Al-Laham, C. Y. Peng, A. Nanayakkara, M. Challacombe, P. M. W. Gill, B. Johnson, W. Chen, M. W. Wong, C. Gonzalez, and J. A. Pople. (2004) Gaussian 03, Gaussian 03 ed., Gaussian, Inc., Wallingford CT.

52. Hoffman, R. M. B., Li, M. X., and Sykes, B. D. (2005) The bindin of W7, an inhibitor of striated muscle contraction, to cardiac troponin C, *Biochemistry 44*, 15750-15759.

53. McCoy, M. A., and Wyss, D. F. (2002) Spatial localization of ligand binding sites from electron current density surfaces calculated from NMR chemical shift perturbations, *J. Am. Chem. Soc. 124*, 11758-11763.

54. Guntert, P. (2004) Automated NMR structure calculation with CYANA, *Methods Mol. Biol. 278*, 353-378.

55. Cornilescu, G., Delaglio, F., and Bax, A. (1999) Protein backbone angle restraints from searching a database for chemical shift and sequence homology, *J. Biomol. NMR 13*, 289-302.

56. Linge, J. P., Williams, M. A., Spronk, C. A. E. M., Bonvin, A. M. J. J., and Nilges, M. (2003) Refinement of protein structures in explicit solvent, *Proteins-Structure Function and Bioinformatics 50*, 496-506.

57. Laskowski, R. A., Rullmann, J. A. C., MacArthur, M. W., Kaptein, R., and Thornton, J. M. (1996) AQUA and PROCHECK-NMR: Programs for checking the quality of protein structures solved by NMR, *J. Biomol. NMR 8*, 477-486.

58. Jayatilake, G. S., Jayasuriya, H., Lee, E. S., Koonchanok, N. M., Geahlen, R. L., Ashendel, C. L., Mclaughlin, J. L., and Chang, C. J. (1993) Kinase Inhibitors from Polygonum-Cuspidatum, *J. Nat. Prod. 56*, 1805-1810.

59. Koh, D., Park, K. H., Jung, J., Yang, H., Mok, K. H., and Lim, Y. (2001) Complete assignment of the H-1 and C-13 NMR spectra of resveratrol derivatives, *Magn. Reson. Chem. 39*, 768-770.

60. Commodari, F., Khiat, A., Ibrahimi, S., Brizius, A. R., and Kalkstein, N. (2005) Comparison of the phytoestrogen trans-resveratrol (3,4 ',5-trihydroxystilbene) structures from x-ray diffraction and solution NMR, *Magn. Reson. Chem. 43*, 567-572.

61. Bonechi, C., Martini, S., Magnani, A., and Rossi, C. (2008) Stacking interaction study of trans-resveratrol (trans-3,5,4 '-trihydroxystilbene) in solution by nuclear magnetic resonance and Fourier transform infrared spectroscopy, *Magn. Reson. Chem. 46*, 625-629.

62. Karplus, M. (1959) Contact Electron-Spin Coupling of Nuclear Magnetic Moments, *J. Chem. Phys. 30*, 11-15.

63. Trela, B. C., and Waterhouse, A. L. (1996) Resveratrol: Isomeric molar absorptivities and stability, *J. Agric. Food Chem. 44*, 1253-1257.

64. Caruso, F., Tanski, J., Villegas-Estrada, A., and Rossi, M. (2004) Structural basis for antioxidant activity of trans-resveratrol: Ab initio calculations and crystal and molecular structure, *J. Agric. Food Chem. 52*, 7279-7285.

65. Yin, Q., Shi, Y. M., Liu, H. M., Li, C. B., and Zhang, W. Q. (2002) (E)-3,5,4 '-Trimethoxystilbene, *Acta Crystallographica Section E-Structure Reports Online 58*, O1180-O1181.

66. Robertson, I. M., Pineda-Sanabria, S., and Sykes, B. D. (In Press) Approaches to protein-ligand structure determination by NMR spectroscopy: applications in drug binding to the cardiac regulatory protein troponin C, *Biophysics and Structure to Counter Threats and Challenges*.

67. Baryshnikova, O. K., Robertson, I. M., Mercier, P., and Sykes, B. D. (2008) Dilated cardiomyopathy G159D mutation in cardiac troponin C weakens the anchoring interaction with troponin I, *Biochemistry 47*, 10950-10960.

68. Gasmi-Seabrook, G. M., Howarth, J. W., Finley, N., Abusamhadneh, E., Gaponenko, V., Brito, R. M., Solaro, R. J., and Rosevear, P. R. (1999) Solution structures of the C-terminal domain of cardiac troponin C free and bound to the N-terminal domain of cardiac troponin I, *Biochemistry 38*, 8313-8322.

69. Lindhout, D. A., and Sykes, B. D. (2003) Structure and dynamics of the C-domain of human cardiac troponin C in complex with the inhibitory region of human cardiac troponin I, *J. Biol. Chem. 278*, 27024-27034.

70. Ferrer, J. L., Jez, J. M., Bowman, M. E., Dixon, R. A., and Noel, J. P. (1999) Structure of chalcone synthase and the molecular basis of plant polyketide biosynthesis, *Nat. Struct. Biol. 6*, 775-784.

71. Klabunde, T., Petrassi, H. M., Oza, V. B., Raman, P., Kelly, J. W., and Sacchettini, J. C. (2000) Rational design of potent human transthyretin amyloid disease inhibitors, *Nat. Struct. Biol. 7*, 312-321.

72. Austin, M. B., Bowman, M. E., Ferrer, J. L., Schroder, J., and Noel, J. P. (2004) An aldol switch discovered in stilbene synthases mediates cyclization specificity of type III polyketide synthases, *Chem. Biol. 11*, 1179-1194.

73. Buryanovskyy, L., Fu, Y., Boyd, M., Ma, Y. L., Hsieh, T. C., Wu, J. M., and Zhang, Z. T. (2004) Crystal structure of quinone reductase 2 in complex with resveratrol, *Biochemistry 43*, 11417-11426.

74. Shomura, Y., Torayama, I., Suh, D. Y., Xiang, T., Kita, A., Sankawa, U., and Miki, K. (2005) Crystal structure of stilbene synthase from Arachis hypogaea, *Proteins-Structure Function and Bioinformatics 60*, 803-806.

75. Gledhill, J. R., Montgomery, M. G., Leslie, A. G. W., and Walker, J. E. (2007) Mechanism of inhibition of bovine F-1-ATPase by resveratrol and related polyphenols, *Proc. Natl. Acad. Sci. U. S. A. 104*, 13632-13637.

76. Davies, D. R., Mamat, B., Magnusson, O. T., Christensen, J., Haraldsson, M. H., Mishra, R., Pease, B., Hansen, E., Singh, J., Zembower, D., Kim, H., Kiselyov, A. S., Burgin, A. B., Gurney, M. E., and Stewart, L. J. (2010) Discovery of Leukotriene A4 Hydrolase Inhibitors Using Metabolomics Biased Fragment Crystallography (vol 52, pg 4694, 2009), *J. Med. Chem. 53*, 2330-2331.

77. Li, M. X., Robertson, I. M., and Sykes, B. D. (2008) Interaction of cardiac troponin with cardiotonic drugs: a structural perspective, *Biochem. Biophys. Res. Commun. 369*, 88-99.

78. Sorsa, T., Pollesello, P., and Solaro, R. J. (2004) The contractile apparatus as a target for drugs against heart failure: Interaction of levosimendan, a calcium sensitiser, with cardiac troponin c, *Mol. Cell. Biochem. 266*, 87-107.

79. Mirza, M., Marston, S., Willott, R., Ashley, C., Mogensen, J., McKenna, W., Robinson, P., Redwood, C., and Watkins, H. (2005) Dilated cardiomyopathy mutations in three thin filament regulatory proteins result in a common functional phenotype, *J. Biol. Chem. 280*, 28498-28506.

80. Landstrom, A. P., Parvatiyar, M. S., Pinto, J. R., Marquardt, M. L., Bos, J. M., Tester, D. J., Ornmen, S. R., Potter, J. D., and Ackerman, M. J. (2008) Molecular and functional characterization of novel hypertrophic cardiomyopathy susceptibility mutations in TNNC1-encoded troponin C, *J. Mol. Cell. Cardiol. 45*, 281-288.

81. Swindle, N., and Tikunova, S. B. (2010) Hypertrophic Cardiomyopathy-Linked Mutation D145E Drastically Alters Calcium Binding by the C-Domain of Cardiac Troponin C, *Biochemistry 49*, 4813-4820.

82. Szczesna, D., Guzman, G., Miller, T., Zhao, J. J., Farokhi, K., Ellemberger, H., and Potter, J. D. (1996) The role of the four Ca2+ binding sites of troponin C in the regulation of skeletal muscle contraction, *J. Biol. Chem. 271*, 8381-8386.

83. Agianian, B., Krzic, U., Qiu, F., Linke, W. A., Leonard, K., and Bullard, B. (2004) A troponin switch that regulates muscle contraction by stretch instead of calcium, *EMBO J. 23*, 772-779.

84. Solaro, R. J., Gambassi, G., Warshaw, D. M., Keller, M. R., Spurgeon, H. A., Beier, N., and Lakatta, E. G. (1993) Stereoselective Actions of Thiadiazinones on Canine Cardiac Myocytes and Myofilaments, *Circ. Res. 73*, 981-990.

85. Biffinger, J. C., Kim, H. W., and DiMagno, S. G. (2004) The polar hydrophobicity of fluorinated compounds, *Chembiochem 5*, 622-627.

86. Smart, B. E. (2001) Fluorine substituent effects (on bioactivity), *J. Fluorine Chem. 109*, 3-11.

87. Cao, H., Pan, X. L., Li, C., Zhou, C., Deng, F. Y., and Li, T. H. (2003) Density functional theory calculations for resveratrol, *Bioorg. Med. Chem. Lett. 13*, 1869-1871.

88. Del Nero, J., and De Melo, C. P. (2003) Investigation of the excited states of resveratrol and related molecules, *Int. J. Quantum Chem. 95*, 213-218.

89. Leopoldini, M., Marino, T., Russo, N., and Toscano, M. (2004) Antioxidant properties of phenolic compounds: H-atom versus electron transfer mechanism, *J. Phys. Chem. A 108*, 4916-4922.

90. Li, M. X., Spyracopoulos, L., Beier, N., Putkey, J. A., and Sykes, B. D. (2000) Interaction of cardiac troponin C with Ca2+ sensitizer EMD 57033 and cardiac troponin I inhibitory peptide, *Biochemistry 39*, 8782-8790.

91. Andrews, P. R., Craik, D. J., and Martin, J. L. (1984) Functional-Group Contributions to Drug Receptor Interactions, *J. Med. Chem. 27*, 1648-1657.

92. Hopkins, A. L., Groom, C. R., and Alex, A. (2004) Ligand efficiency: a useful metric for lead selection, *Drug Discov. Today 9*, 430-431.

93. Kuntz, I. D., Chen, K., Sharp, K. A., and Kollman, P. A. (1999) The maximal affinity of ligands, *Proc. Natl. Acad. Sci. U. S. A. 96*, 9997-10002.

94. Lipinski, C. A., Lombardo, F., Dominy, B. W., and Feeney, P. J. (1997) Experimental and computational approaches to estimate solubility and permeability in drug discovery and development settings, *Adv. Drug Delivery Rev. 23*, 3-25.

95. Tadano, N., Morimoto, S., Takahashi-Yanaga, F., Miwa, Y., Ohtsuki, I., and Sasaguri, T. (2009) Propyl Gallate, a Strong Antioxidant, Increases the Ca^{2+} Sensitivity of Cardiac Myofilament, *J. Pharmacol. Sci. 109*, 456-458.

CHAPTER 9

Approaches to protein-ligand structure determination by NMR spectroscopy: applications in drug binding to the cardiac regulatory protein troponin C

Ian M. Robertson, Sandra E. Pineda-Sanabria, and Brian D. Sykes

Department of Biochemistry, Faculty of Medicine & Dentistry,
University of Alberta, Edmonton, Alberta, Canada T6G 2H7.

This chapter explains the route we followed to determine the structure of resveratrol bound to troponin (detailed in Chapter 8) as a means to determine other protein-ligand structures using NMR spectroscopy. For our troponin-resveratrol structure we used an existing structure of troponin to find the binding pose of resveratrol based on the experimental data for their interaction. This method can accelerate the process for other protein-ligand systems since the structure of the target protein is not re-determined. However, the procedures described here are not applicable to all scenarios and caution should be used to ensure accurate results. This work has been previously published as a book chapter in: Robertson, I. M., Pineda-Sanabria, S. E., and Sykes, B. D. (2013). Approaches to protein-ligand structure determination by NMR spectroscopy: applications in drug binding to the cardiac regulatory protein troponin C. In Puglisi, J. D., and Margaris, M. V. (*Eds.*), *Biophysics and structure to counter threats and challenges* (pp. 121-134). Dordrecht, The Netherlands: Springer.

Introduction

A key element in rational drug design is the rapid determination of protein-ligand structures. X-ray crystallography and NMR Spectroscopy are the most commonly used techniques to determine high-resolution structures of protein-ligand complexes. While NMR spectroscopy has the advantage that different drugs can easily be titrated into the protein in solution, the determination of the full high resolution solution structure involves the assignment of thousands of nuclear Overhauser effect contacts (NOEs) and other data, which tends to be a time-consuming task. If the structure of a target protein is known and the NMR spectra of the $^{13}C,^{15}N$-labeled protein are assigned, the measurement of intermolecular NOEs between the ligand and the protein may be enough to faithfully localize the orientation of the ligand in the complex. This procedure can drastically reduce the overall time for determining the orientation of the ligand on its target, while still providing invaluable structural details about the important pharmacophores of a molecule. There are situations; however, when this method

is still too laborious (*e.g.* for high-throughput applications) or not possible (*e.g.* for a low affinity ligand, resulting in weak of NOEs).

NMR spectroscopy is unique from other screening and structural methods in that it can determine binding constants as well as identify the ligand binding site on a protein by monitoring residue specific changes in chemical shifts upon ligand binding. This approach is called chemical shift mapping; it is routinely used for rapidly identifying the binding site of a ligand on a protein and is a critical step in SAR-by-NMR[1]. Chemical shift mapping is most typically done by following the amide nuclei of a ^{15}N-labeled target molecule, and then highlighting the residues that are significantly shifted on the van der Waals surface of the target protein. These results can also be used as ambiguous distance restraints by docking programs, such as HADDOCK[2] or the mapped surface can be used for a binding-site centered docking with an automated docking program such as AutoDock[3]. Since chemical shift perturbations are a response to a change in the local chemical environment induced by ligand binding, it is possible to predict the location of the ligand rings from the magnitude and sign of the chemical shift changes if we assume these changes are caused predominantly by proximity to aromatic groups of a ligand. Finally, the use of a protein with a paramagnetic center can provide distance restraints between the ligand and the protein. A number of groups have investigated the efficacy of combining a variety of these methods to accurately and rapidly resolve protein-ligand structures[4-7]. In order to examine the usefulness of these techniques, we shall study their applications in regards to drug binding into the cardiac muscle contractile regulatory protein, troponin C (cTnC).

cTnC is a dumbbell shaped Ca^{2+}-binding protein that triggers contraction upon Ca^{2+}-binding its regulatory N-lobe (cNTnC). Ca^{2+} enters the cytosol of a muscle cell and binds to cNTnC, which induces a slight opening of cNTnC. Following Ca^{2+} association with cNTnC, the "switch region" of the protein troponin I (cTnI) binds to cNTnC, stabilizing the fully open conformation of cNTnC. The "inhibitory region" of cTnI is subsequently released from actin, which results in the contraction-dependant actin-myosin interaction. During relaxation, Ca^{2+} dissociates from cNTnC as it leaves the cytosol, cTnI translocates from cNTnC back to actin, which blocks the actin-myosin interface to inhibit contraction. The C-domain of cTnC (cCTnC) has two high-affinity metal binding sites that are occupied throughout the contraction-relaxation cycle. The binding partner of cCTnC is a different segment of cTnI, the "anchoring region". The primary role of the cCTnC-cTnI interaction is to tether cTnC to the thin filament, but recent insights into the structure and function of insect flight muscle troponin suggest this interaction may also play a role in regulation of contraction[8, 9]. For recent reviews into the molecular mechanism of contraction, see 10-12. Given both the C- and N-lobes of cTnC interact with cTnI to regulate contraction, the design of small molecules that bind cTnC and modulate its interaction with cTnI have therapeutic potential[13-15].

Intermolecular NOEs

The identification of NOEs between a protein and a ligand is a crucial step in solving the structure of the complex by NMR spectroscopy. Knowledge of the high-resolution structure of a protein-ligand complex can provide insights into the mechanism of a ligand as well as help in the design of new pharmaceuticals. The standard scheme of determining a protein-ligand structure by NMR spectroscopy begins by assigning the resonances of a ^{13}C,^{15}N- or ^{15}N-labeled protein. Following the resonance assignment, the structure of the protein is solved by assigning intramolecular NOEs to obtain distance restraints. Once the tertiary structure of the target is known, the unlabeled ligand is assigned when in complex with the protein using a variety of isotope filtered experiments[16-18]. Finally, NOE contacts between the unlabeled ligand and labeled target are measured to obtain distance restraints between the ligand and protein[19-21]. Frequently, the protein structure is not significantly altered upon binding to the ligand making the re-determination of the protein structure superfluous. In these cases, it may be sufficient to use only intermolecular NOEs to provide distance restraints between the labeled protein and unlabeled ligand. Unfortunately, the target molecule does often undergo structural changes when binding a ligand. If there has been a structure of the target molecule in complex with a related ligand, it may be possible to use intermolecular NOEs to localize the ligand onto the complex structure, with the homologous ligand removed. We have recently employed this technique to a complex with cNTnC and the small molecule, W7[22]. The structure of cNTnC was obtained from the NMR solution structure of cNTnC-cTnI[23], with cTnI removed prior to the docking of W7. The complex we will focus on in this report is cCTnC bound to the polyphenol, resveratrol (Figure 9.1).

Resveratrol is an antioxidant present at high concentrations in red wine and in the skins of grapes[24] and it has been studied intensely due to its benefits to cardiovascular health[25]. The low incidence of cardiovascular disease among Mediterranean populations despite a diet rich in fat, has prompted some researchers to suggest that the high consumption of red wine offers protection against heart disease, and has been dubbed, the "French paradox"[26, 27]. We have found that resveratrol targets cCTnC, and this interaction may impart some of its protective properties (*manuscript submitted*). The structure of cCTnC bound to the green tea polyphenol, epigallocatechin gallate (EGCg)[28], the anchoring region of cTnI (cTnI$_{34-71}$)[29, 30], and the cardiotonic drug EMD 57033[31] have been solved by either NMR spectroscopy or X-ray crystallography. Even though the ligands of cCTnC are chemically dissimilar, they all induce an analogous conformational change of cCTnC[28]. Instead of solving the structure of cCTnC again, we measured intermolecular NOEs between resveratrol and cCTnC and docked resveratrol onto the cCTnC-EGCg structure (figure 1b-d). In order to dock resveratrol, we repeated the simulated annealing procedure in Xplor-NIH[32, 33] using the intramolecular NOEs for cCTnC from the cCTnC-EGCg structure, and replaced the intermolecular NOEs from EGCg to cCTnC with restraints between resveratrol and cCTnC. We propose that this procedure is better than simply performing a rigid docking

since it allows for some flexibility of cCTnC. We chose the cCTnC-EGCg structure because both EGCg and resveratrol are polyphenols and thus may induce similar structural perturbations of cCTnC.
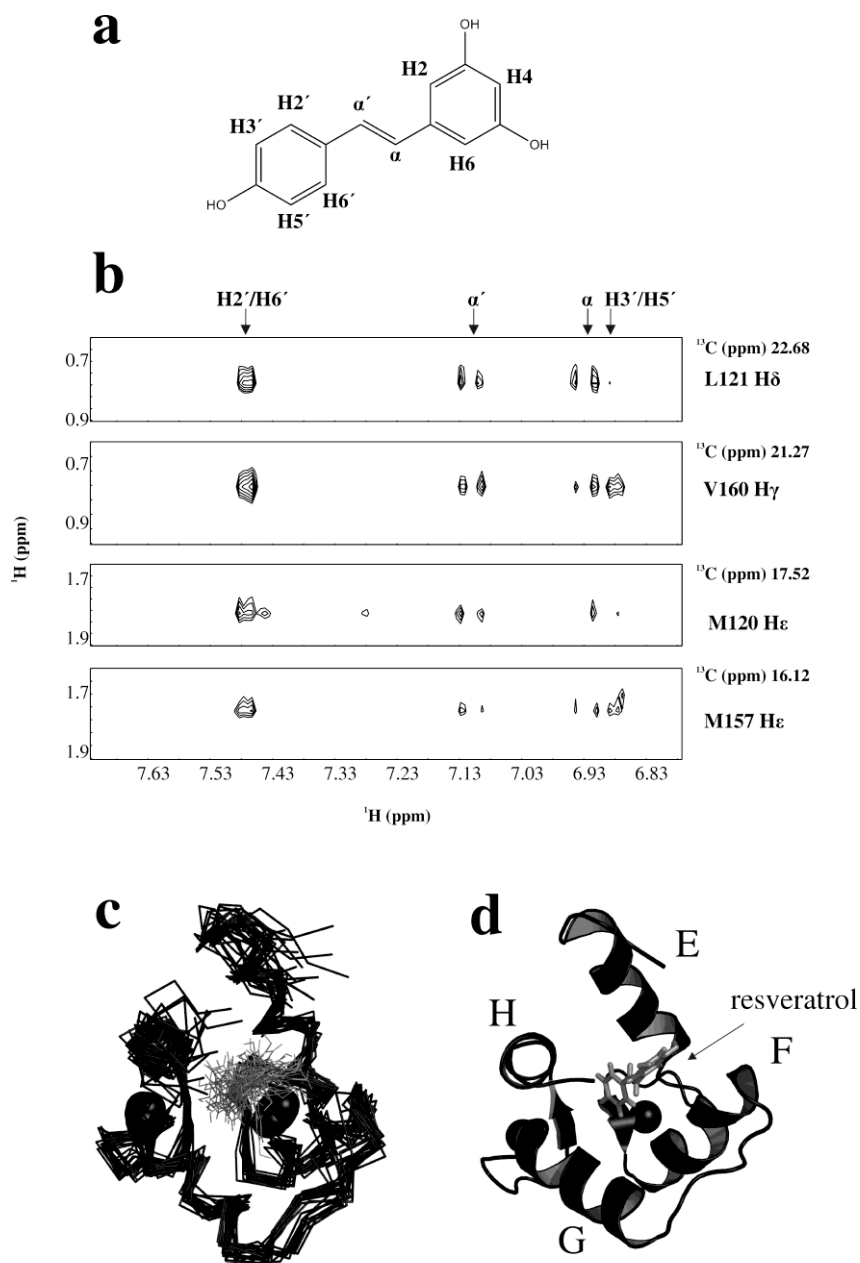
Figure 9.1. Structure of cCTnC in complex with resveratrol as determined by intermolecular NOEs.
a. Chemical structure of resveratrol. **b.** Strips from the ^{13}C-edited-filtered NOESY NMR experiment that identifies NOEs between an unlabeled ligand and a ^{13}C-labeled protein. **c.** Ensemble of the 20 lowest energy structures of cCTnC-resveratrol. **d.** The lowest energy structure from the ensemble. cCTnC is shown in black with the helices labeled and resveratrol is colored in grey. Black spheres represent Ca^{2+}.

Monitoring strong protein-ligand complexes can be a fruitful source of structural information. However, problems can arise when the unlabeled ligand is too large so that it contains an abundance of overlapping signals, or when the intermolecular NOEs are weak, making it difficult to distinguish noise from NOEs. Therefore, it is often necessary to make use of other methods to assist in the determination of protein-ligand structures. We will assess some of these approaches, by comparing the predictions from these methods with the cCTnC-resveratrol structure as determined with the NOE data.

Chemical shift mapping

Chemical shift mapping is a frequently used application of NMR spectroscopy which allows the estimation of a binding site of a ligand on a target molecule. Typically the perturbations of ^{15}N-amide chemical shifts are used, which can provide information on the binding location of the compound on the protein as well as its binding constant. While chemical shift mapping is a rapid method to estimate the binding surface on a protein, it has several pitfalls, including a lack of resolution, and is hampered by any allosteric effects induced by a ligand binding. This is because chemical shifts are perturbed in response to a change in local chemical environment, which may be due to proximity to a ligand or because of a conformational change induced by the ligand binding.

The use of amide chemical shift mapping with the interaction between cCTnC and resveratrol is shown in Figure 9.2a. While, perturbations seem to point towards the central groove as the binding site of resveratrol, the largest shifts are from residues residing in the F-G linker are not near to resveratrol in the structure (Figure 9.1c,d). By investigating the chemical shifts perturbed by resveratrol, and comparing to those induced by other ligands of cCTnC: EGCg, EMD 57033, and cTnI$_{34-71}$ we see that all these residues induce the same pattern of amide chemical shift change (Figure 9.2c). These ligands have unique structural features, and while they all bind in the core of the protein, the orientations they adopt are quite varied. Alternatively, the similar amide chemical shift perturbations are more likely from a similar conformational perturbation since all ligand bound forms of cCTnC in an open state (the F-G and E-H helix pairs are moved apart to accommodate the ligands). Although the amide shifts may they tell us very little about the specific binding site of resveratrol, they do give us some idea of the conformation of cCTnC.

Another way to map the binding surface of a ligand on a target molecule is to look at the ^{13}C-methyl chemical shift perturbations. Since most protein-ligand structures are stabilized via hydrophobic interactions, following methyl perturbations when a ligand binds to the protein may be more informative that using ^{15}N-amide chemical shifts. In Figure 9.2b we show mapped residues that underwent perturbations in the terminal methyls. Most of the perturbed residues, are on the E-, F-, and H-helices, as well as on the ß-sheet of cCTnC. These results are more consistent with the structure

we determined with intermolecular NOEs. In fact, many of the methyls that were perturbed during the titration were also involved in making NOEs with resveratrol. Chemical shift mapping of the methyls clearly do a better job than amide nuclei of identifying the binding site of resveratrol, but the predictions are still qualitative.
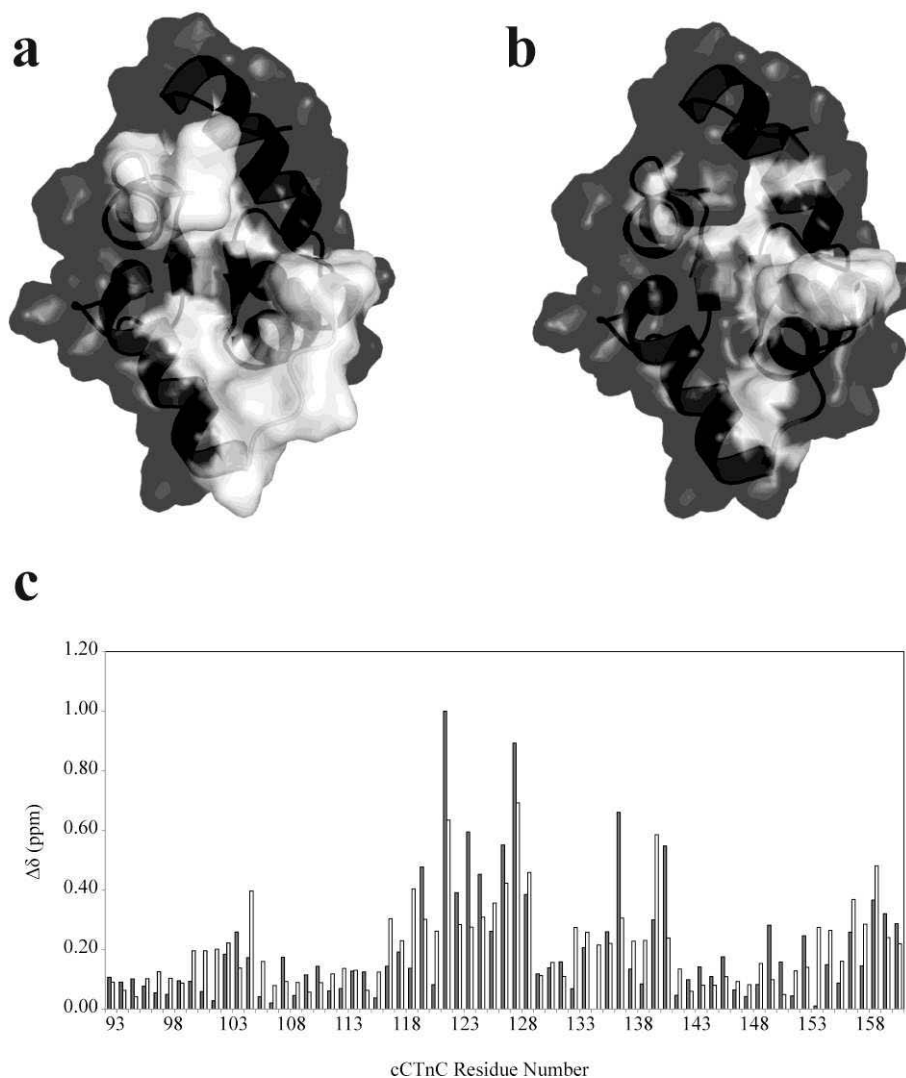
Figure 9.2. Chemical shift mapping of resveratrol induced shifts on cCTnC from the cCTnC-EGCg structure (2kdh.pdb).
a. ^{15}N-amide chemical shifts that were perturbed larger than the mean chemical shift perturbation. **b.** residues that were perturbed in the methyl region of the ^{1}H,^{13}C-HSQC spectrum. cCTnC is shown as a transparent surface (black), with the perturbed resonances highlighted in white. **c.** bar diagram that compares the total amide chemical shift (Δδ) pattern induced by resveratrol (black bars) and the average chemical shift perturbation induced by EMD 57033, cTnI$_{34-71}$, and EGCg (white bars). Δδ = $((\Delta\delta^1H)^2 + 1/25(\Delta\delta^{15}N)^2)^{1/2}$.

J-surface mapping

To supplement the qualitative chemical shift mapping, we mapped the J-surface of resveratrol on cCTnC. The ring current effect from aromatic ligands can induce chemical shift perturbations of nuclei proximal to the ligand. McCoy and Wyss described the application of this phenomenon to identify the binding surface of a ligand to the hepatitis C virus NS3 protease[34]. Caveats of using this method to identify the ligand binding site are that the ligand must contain an aromatic group and that the ring current effect from the ligand is the primary source of chemical shift perturbation. In order to localize the binding site of resveratrol on cCTnC we performed J-surface mapping with the program Jsurf using the amide and methyl chemical shift perturbation data (Figure 9.3). Jsurf approximates the origin of chemical shift perturbations as a single point-dipole at the center of the aromatic ring of a ligand[35]. The centre of the aromatic ring is then predicted based on the magnitude and sign of the proton perturbation. For each perturbed residue, the aromatic ring inducing the chemical shift change can be at any number of places and for each additional residue considered this location is narrowed down until finally a surface is identified where the ligand rings is likely to reside.
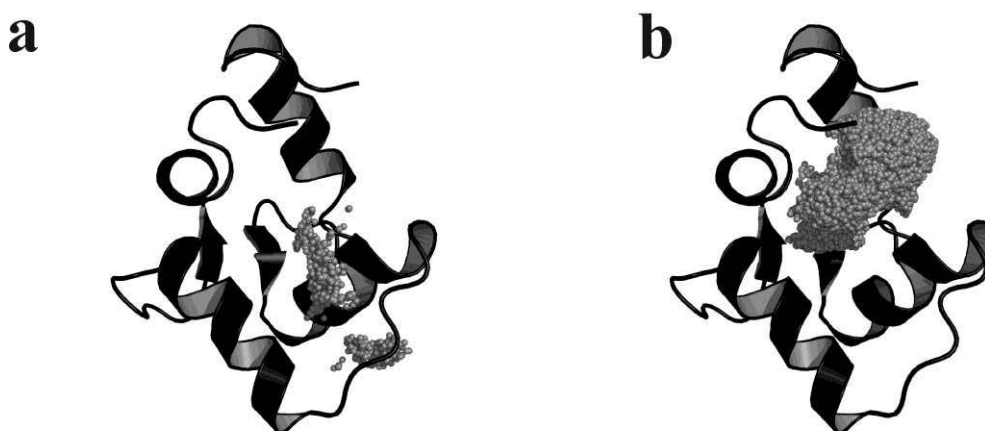
Figure 9.3. J-surface mapping on cCTnC structures.
The J-surface (grey spheres) from the amide (**a**) and methyl (**b**) chemical shift perturbations mapped on the structure of cCTnC (black cartoon) from the cCTnC-EGCg structure (2kdh.pdb)

We used the amide protons chemical shift perturbations to see if Jsurf could accurately predict the binding of resveratrol (Figure 9.3a). The predicted J-surface runs through the F and G helices, which is not consistent with the NOEs and for resveratrol to lie here would violate many van der Waals forces. While it is likely that some of the amide resonances perturbed in the presence of resveratrol are due to ring current effects, evidently many are caused not by direct contact with the ring, but

rather by an allosteric perturbation induced by resveratrol binding. We repeated the J-surface analysis using the methyl protons (Figure 9.3b). The result of using the methyl protons was a binding site localized to the hydrophobic pocket in a very similar location as calculate by the intermolecular NOEs. As an aside, Jsurf requires an input file that has atom numbers from the protein structure file (i.e. PDB file format) with the corresponding shift for that atom. In contrast to amide protons, there are three protons associated with each methyl. So the input file we used for Jsurf had three protons for each methyl perturbation included in the calculation.

Automated docking

While Jsurf does a reasonable job of predicting the binding site of resveratrol on cCTnC using the methyl proton perturbations, it does not predict the actual binding pose of resveratrol. In order to do this, we used AutoDock4.2 which predicts the conformations of a ligand bound to a macromolecular target of known structure as well as the free energy of binding. AutoDock4.2 allows flexibility for both the ligand and for a limited number of residues in the target protein indicated by the user, it also allows the user to select a region of the target molecule to perform the conformation searching (the grid volume)[36, 37]. AutoDock 4.2 with the AutoDockTools graphical interface was used to predict 150 binding conformations using a population size of 500 and 5000000 energy evaluations. The docking was guided by limiting the grid volume to encompass residues of cCTnC that the chemical shift and J-surface mappings predicted to be involved in binding resveratrol. Residues which showed chemical shifts greater than one standard deviation from the mean in the ^{1}H,^{13}C HSQC NMR experiment were defined as flexible residues.

A total of 15 clusters were predicted for resveratrol using an r.m.s.d. tolerance of 2.0 Å for each cluster. All 150 structures predict that resveratrol binds in the hydrophobic groove of cCTnC (Figure 9.4a). This is not surprising, considering the grid volume chosen from the experimental data encompassed primarily this region of cCTnC. In AutoDock identifying the lowest-energy cluster and the most populated cluster are two ways of choosing the best conformer[38, 39]. The ten lowest energy structures are shown in Figure 9.4b, and include two different conformations of resveratrol as having the lowest energy. The lowest energy conformer has resveratrol oriented parallel to the β-sheet of cCTnC, whereas the next lowest energy cluster predicts resveratrol binds in the hydrophobic pocket of cCTnC pointed towards the β-sheet. The buried structure of resveratrol more closely resembles the methyl-based Jsurf prediction and NOE data; however, the NOE data has the diphenol ring oriented away from the protein, not deep within the hydrophobic pocket as calculated by AutoDock.
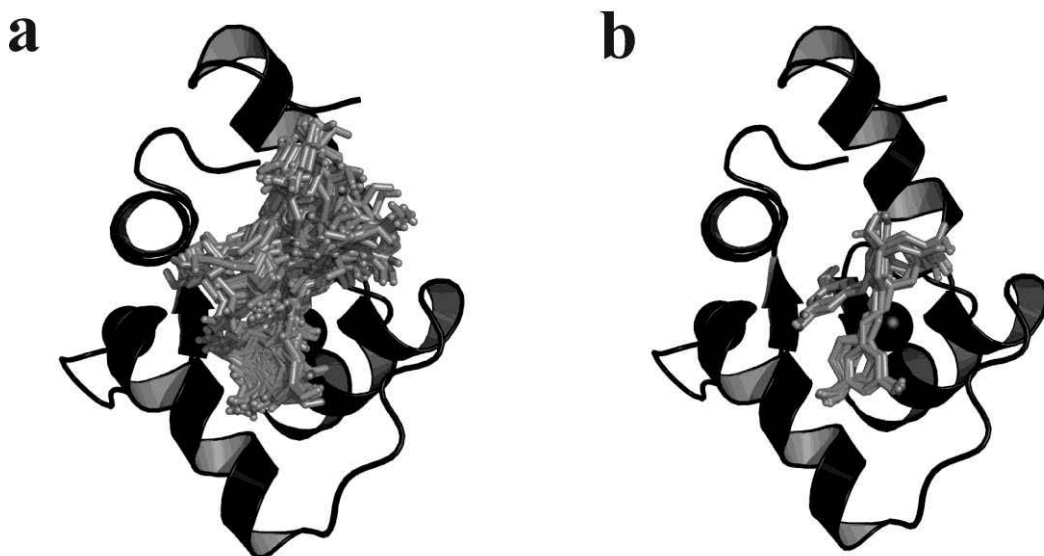
Figure 9.4. Binding pose of resveratrol predicted by AutoDock.

Overlay of the poses of resveratrol (grey sticks) on cCTnC (black cartoon) from the cCTnC-EGCg structure (2kdh.pdb). All 150 poses (**a**) and the ten lowest energy poses (**b**) generated using AutoDock.

Restraints derived from paramagnetic restraints

The prediction of the binding site of resveratrol on cCTnC by chemical shift mapping, J-surface mapping, and docking had some success; but, in the end it would be difficult to validate the results without less ambiguous data, such as NOEs. The use of paramagnetic relaxation enhancement (PRE) has been used extensively to aide in protein structure determination[40], in protein-protein structure determination[41], and in protein-ligand structure determination[42]. PRE is a phenomenon which arises when unpaired electrons from a paramagnetic center, such as a lanthanide ion, increase the relaxation of nuclei in a distance-dependant manner. Pseudocontact shifts (PCS) induced by paramagnetic lanthanide ions with anisotropic magnetic susceptibility tensors can also tell the user information about the orientation of the ligand with respect to the metal. The Otting group has recently employed PCS to determine the structure of a protein-drug complex[43]. On the other hand, the lanthanide gadolinium (Gd^{3+}) has an isotropic paramagnetic environment, so it does not yield information about the orientation between the nuclei and metal, but does provide distance information.

It has been shown that the trivalent lanthanides can substitute for calcium in troponin C[44, 45]. The C-terminal domain of troponin C binds two metal ions, and therefore it would be difficult to obtain structural restraints between resveratrol and both of these ions. Fortuitously, the cNTnC contains only one Ca^{2+} binding site. In a recent publication (*manuscript submitted*), we have used PRE to obtain

distance restraints between Gd^{3+} and the cardiotonic agent, 2',4'-difluoro(1,1'-biphenyl)-4-yloxy acetic acid (dfbp-o). In this type of experiment, free dfbp-o was titrated with Gd^{3+}-bound cNTnC-cTnI, and at each titration point we measured the transverse and longitudinal relaxation rates of ^{19}F and ^{1}H of dfbp-o. As the concentration of cNTnC-cTnI-Gd^{3+} increased, the relaxation rates of dfbp-o increased (see Figure 9.5 for signal broadening), and this increase in relaxation rates were used to calculate this distance between dfbp-o and Gd^{3+} as previously described[46]. We calculated the structure of the tertiary complex, cNTnC-cTnI-dfbp-o using only NOE restraints, and NOE and PRE restraints (Figure 9.6). The addition of the PRE restraints radically improved the resolution of dfbp-o in the structure, and illustrates the usefulness of this technique to aid in protein-ligand structure refinement.
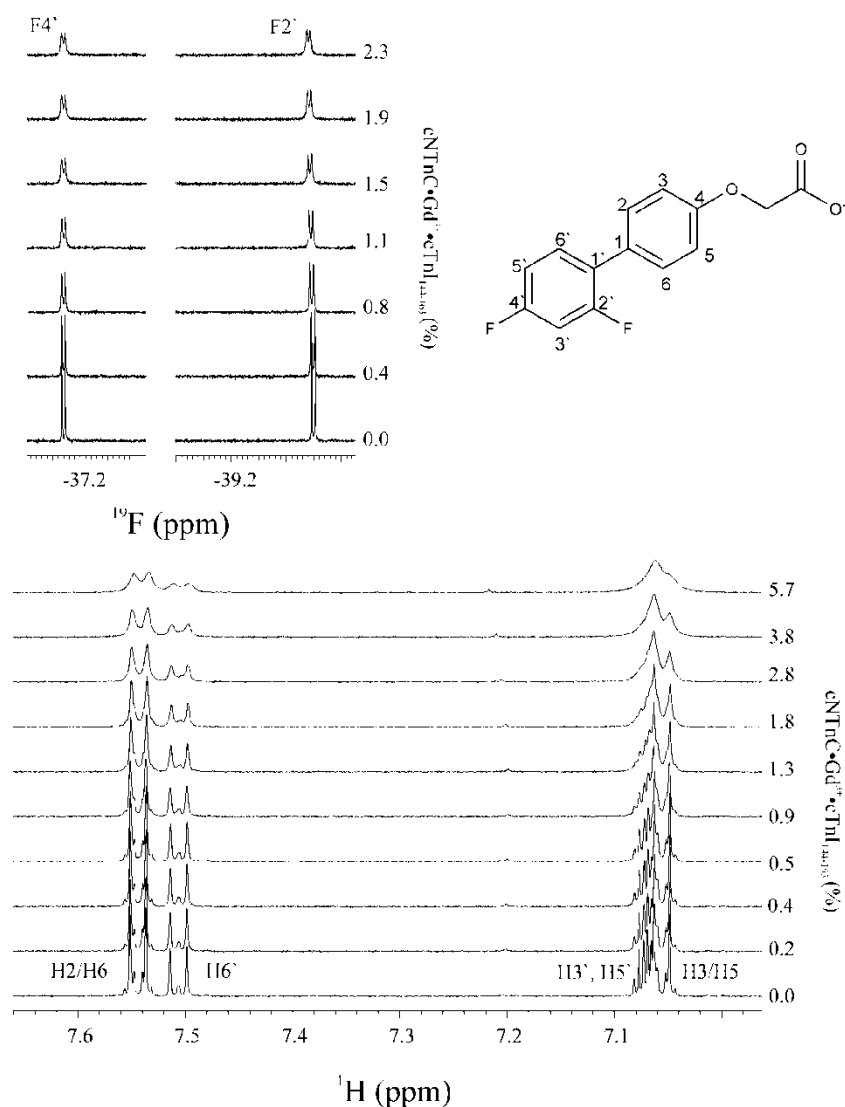
Figure 9.5. Paramagnetic relaxation enhancement of dfbp-o signals by Gd^{3+} bound to cNTnC-cTnI.

238

The stacked 1D ^{19}F spectrum of dfbp-o is shown in the upper left, and the stacked 1D ^{1}H spectrum of dfbp-o is shown at the bottom. Both stacked spectra are shown as a function of percentage dfbp-o bound to cNTnC•Gd^{3+}•cTnI. The numbering of dfbp-o is shown on its chemical structure as a reference.
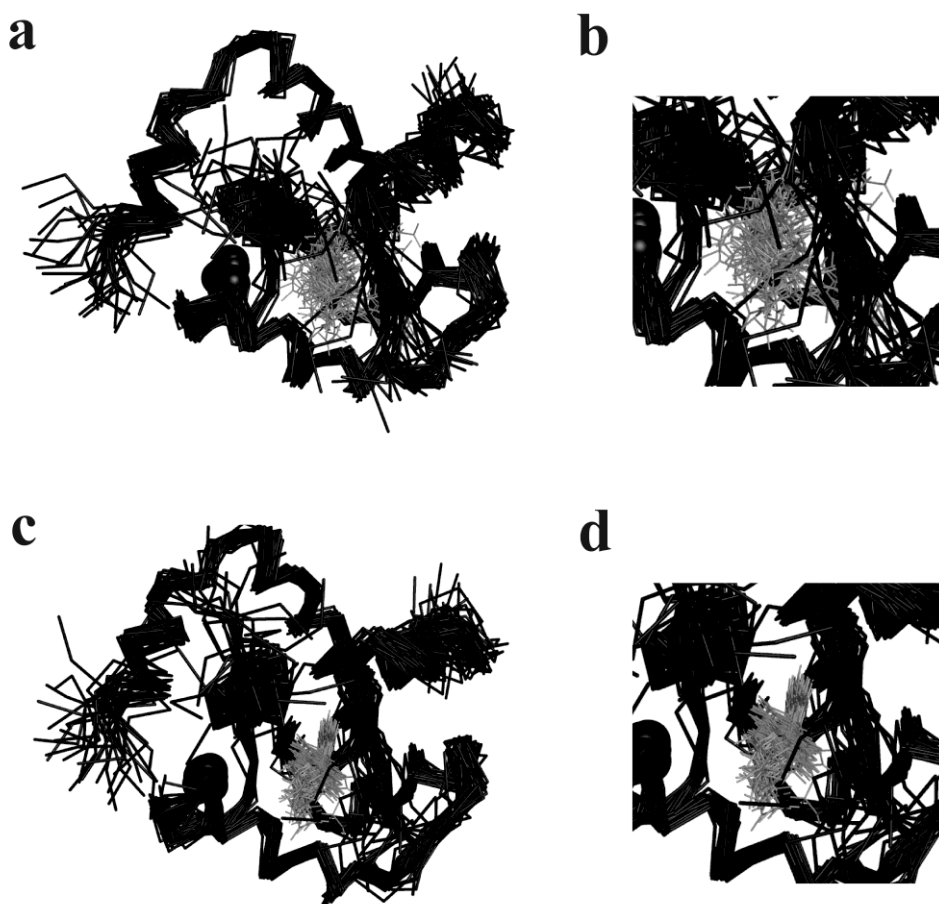
Figure 9.6. Structure of cNTnC·cTnI·dfbp-o determined with and without PRE restraints.
Ribbon diagram of cNTnC bound to cTnI (both in black) and dfbp-o (grey) in stick representation. (a) Refinement of the complex using only intermolecular NOEs. (b) close-up view of the binding site, highlighting the disorder of dfbp-o. (c) Refinement of the complex using intermolecular NOEs and PRE distance restraints. (d) close-up view of the binding site in (c).

Conclusion

The calculation of protein-ligand structures is an important step in the development of novel pharmaceuticals. The high resolution description of the binding site and pose of a ligand is a crucial step in the rationale design of novel drugs. In this review we have surveyed a few approaches available to scientists to help in the resolving of protein-ligand structures. Intermolecular NOEs are a crucial step in solving protein-ligand structures; however, they are not always attainable. Reasons for this include but are not limited to: time-constraints, no ^{13}C-labeled protein available, or a weak binding constant. There are other techniques that can validate structures solved with few NOEs, or substitute for NOEs when none exist. While ^{15}N-amide nuclei are the most used nucleus for estimating the binding site of a ligand, conformational changes in the protein upon ligand binding can be misleading. We show that the use of ^{13}C-methyl chemical shift mapping and J-surface prediction using methyl perturbations more accurately identify the binding site of a ligand. Identification of the binding pose of the ligand in the absence of NOE data can be done with AutoDock; however, it is difficult to choose the cluster that most closely resembles the real structure. Other experimentally derived restraints, such as PREs can significantly improve protein-ligand structures when either NOEs are not sufficient to define the binding pose of the ligand or when NOEs are not available.

References

1. Shuker, S. B., Hajduk, P. J., Meadows, R. P., and Fesik, S. W. (1996) Discovering high-affinity ligands for proteins: SAR by NMR, *Science 274*, 1531-1534.

2. Dominguez, C., Boelens, R., and Bonvin, A. M. J. J. (2003) HADDOCK: A protein-protein docking approach based on biochemical or biophysical information, *J. Am. Chem. Soc. 125*, 1731-1737.

3. Morris, G. M., Huey, R., Lindstrom, W., Sanner, M. F., Belew, R. K., Goodsell, D. S., and Olson, A. J. (2009) AutoDock4 and AutoDockTools4: Automated Docking with Selective Receptor Flexibility, *J. Comput. Chem. 30*, 2785-2791.

4. Bertini, I., Fragai, M., Giachetti, A., Luchinat, C., Maletta, M., Parigi, G., and Yeo, K. J. (2005) Combining in silico tools and NMR data to validate protein-ligand structural models: Application to matrix metalloproteinases, *J. Med. Chem. 48*, 7544-7559.

5. Cioffi, M., Hunter, C. A., Packer, M. J., Pandya, M. J., and Williamson, M. P. (2009) Use of quantitative H-1 NMR chemical shift changes for ligand docking into barnase, *J. Biomol. NMR 43*, 11-19.

6. Krishnamoorthy, J., Yu, V. C. K., and Mok, Y. K. (2010) Auto-FACE: An NMR Based Binding Site Mapping Program for Fast Chemical Exchange Protein-Ligand Systems, *PLoS ONE 5*, -.

7. Cioffi, M., Hunter, C. A., Packer, M. J., and Spitaleri, A. (2008) Determination of protein-ligand binding modes using complexation-induced changes in H-1 NMR chemical shift, *J. Med. Chem. 51*, 2512-2517.

8. Bullard, B., Agianian, B., Krzic, U., Linke, W. A., and Leonard, K. R. (2004) Independent regulation of insect flight muscle by two isoforms of troponin C, *Biophys. J. 86*, 215a-216a.

9. De Nicola, G., Burkart, C., Qiu, F., Agianian, B., Labeit, S., Martin, S., Bullard, B., and Pastore, A. (2007) The structure of Lethocerus troponin C: Insights into the mechanism of stretch activation in muscles, *Structure 15*, 813-824.

10. Gomes, A. V., Potter, J. D., and Szczesna-Cordary, D. (2002) The role of troponins in muscle contraction, *IUBMB Life 54*, 323-333.

11. Li, M. X., Wang, X., and Sykes, B. D. (2004) Structural based insights into the role of troponin in cardiac muscle pathophysiology, *J. Muscle Res. Cell Motil. 25*, 559-579.

12. Parmacek, M. S., and Solaro, R. J. (2004) Biology of the troponin complex in cardiac myocytes, *Prog. Cardiovasc. Dis. 47*, 159-176.

13. Kass, D. A., and Solaro, R. J. (2006) Mechanisms and use of calcium-sensitizing agents in the failing heart, *Circulation 113*, 305-315.

14. Li, M. X., Robertson, I. M., and Sykes, B. D. (2008) Interaction of cardiac troponin with cardiotonic drugs: a structural perspective, *Biochem. Biophys. Res. Commun. 369*, 88-99.

15. Sorsa, T., Pollesello, P., and Solaro, R. J. (2004) The contractile apparatus as a target for drugs against heart failure: Interaction of levosimendan, a calcium sensitiser, with cardiac troponin c, *Mol. Cell. Biochem. 266*, 87-107.

16. Gemmecker, G., Olejniczak, E. T., and Fesik, S. W. (1992) An Improved Method for Selectively Observing Protons Attached to C-12 in the Presence of H-1-C-13 Spin Pairs, *J. Magn. Reson. 96*, 199-204.

17. Ikura, M., and Bax, A. (1992) Isotope-Filtered 2d Nmr of a Protein Peptide Complex - Study of a Skeletal-Muscle Myosin Light Chain Kinase Fragment Bound to Calmodulin, *J. Am. Chem. Soc. 114*, 2433-2440.

18. Ogura, K., Terasawa, H., and Inagaki, F. (1996) An improved double-tuned and isotope-filtered pulse scheme based on a pulsed field gradient and a wide-band inversion shaped pulse, *J. Biomol. NMR 8*, 492-498.

19. Lee, W., Revington, M. J., Arrowsmith, C., and Kay, L. E. (1994) A Pulsed-Field Gradient Isotope-Filtered 3d C-13 Hmqc-Noesy Experiment for Extracting Intermolecular Noe Contacts in Molecular-Complexes, *FEBS Lett. 350*, 87-90.

20. Robertson, I. M., Spyracopoulos, L., and Sykes, B. D. (2009) The Evaluation of Isotope Editing and Filtering for Protein-Ligand Interaction Elucidation by Nmr, *Biophysics and the Challenges of Emerging Threats*, 101-119.

21. Stuart, A. C., Borzilleri, K. A., Withka, J. M., and Palmer, A. G. (1999) Compensating for variations in H-1-C-13 scalar coupling constants in isotope-filtered NMR experiments, *J. Am. Chem. Soc. 121*, 5346-5347.

22. Hoffman, R. M. B., and Sykes, B. D. (2009) Structure of the Inhibitor W7 Bound to the Regulatory Domain of Cardiac Troponin C, *Biochemistry 48*, 5541-5552.

23. Li, M. X., Spyracopoulos, L., and Sykes, B. D. (1999) Binding of cardiac troponin-I147-163 induces a structural opening in human cardiac troponin-C, *Biochemistry 38*, 8289-8298.

24. Jang, M. S., Cai, E. N., Udeani, G. O., Slowing, K. V., Thomas, C. F., Beecher, C. W. W., Fong, H. H. S., Farnsworth, N. R., Kinghorn, A. D., Mehta, R. G., Moon, R. C., and Pezzuto, J. M. (1997) Cancer chemopreventive activity of resveratrol, a natural product derived from grapes, *Science 275*, 218-220.

25. Corder, R., Douthwaite, J. A., Lees, D. M., Khan, N. Q., dos Santos, A. C. V., Wood, E. G., and Carrier, M. J. (2001) Endothelin-1 synthesis reduced by red wine - Red wines confer extra benefit when it comes to preventing coronary heart disease., *Nature 414*, 863-864.

26. Kopp, P. (1998) Resveratrol, a phytoestrogen found in red wine. A possible explanation for the conundrum of the 'French paradox'?, *Eur. J. Endocrinol. 138*, 619-620.

27. Goldberg, D. M., Hahn, S. E., and Parkes, J. G. (1995) Beyond Alcohol - Beverage Consumption and Cardiovascular Mortality, *Clin. Chim. Acta 237*, 155-187.

28. Robertson, I. M., Li, M. X., and Sykes, B. D. (2009) Solution Structure of Human Cardiac Troponin C in Complex with the Green Tea Polyphenol, (-)-Epigallocatechin 3-Gallate, *J. Biol. Chem. 284*, 23012-23023.

29. Takeda, S., Yamashita, A., Maeda, K., and Maeda, Y. (2003) Structure of the core domain of human cardiac troponin in the Ca(2+)-saturated form, *Nature 424*, 35-41.

30. Gasmi-Seabrook, G. M., Howarth, J. W., Finley, N., Abusamhadneh, E., Gaponenko, V., Brito, R. M., Solaro, R. J., and Rosevear, P. R. (1999) Solution structures of the C-terminal domain of cardiac troponin C free and bound to the N-terminal domain of cardiac troponin I, *Biochemistry 38*, 8313-8322.

31. Wang, X., Li, M. X., Spyracopoulos, L., Beier, N., Chandra, M., Solaro, R. J., and Sykes, B. D. (2001) Structure of the C-domain of human cardiac troponin C in complex with the Ca2+ sensitizing drug EMD 57033, *J. Biol. Chem. 276*, 25456-25466.

32. Schwieters, C. D., Kuszewski, J. J., and Clore, G. M. (2006) Using Xplor-NIH for NMR molecular structure determination, *Prog. Nucl. Magn. Reson. Spectrosc. 48*, 47-62.

33. Schwieters, C. D., Kuszewski, J. J., Tjandra, N., and Clore, G. M. (2003) The Xplor-NIH NMR molecular structure determination package, *J. Magn. Reson. 160*, 65-73.

34. McCoy, M. A., and Wyss, D. F. (2002) Spatial localization of ligand binding sites from electron current density surfaces calculated from NMR chemical shift perturbations, *J. Am. Chem. Soc. 124*, 11758-11763.

35. Moyna, G., Zauhar, R. J., Williams, H. J., Nachman, R. J., and Scott, A. I. (1998) Comparison of ring current methods for use in molecular modeling refinement of NMR derived three-dimensional structures, *J. Chem. Inf. Comput. Sci. 38*, 702-709.

36. Morris, G. M., Goodsell, D. S., Huey, R., and Olson, A. J. (1996) Distributed automated docking of flexible ligands to proteins: Parallel applications of AutoDock 2.4, *J. Comput. Aided Mol. Des. 10*, 293-304.

37. Huey, R., Morris, G. M., Olson, A. J., and Goodsell, D. S. (2007) A semiempirical free energy force field with charge-based desolvation, *Journal of Computational Chemistry 28*, 1145-1152.

38. Morris, G. M., Goodsell, D. S., Halliday, R. S., Huey, R., Hart, W. E., Belew, R. K., and Olson, A. J. (1998) Automated docking using a Lamarckian genetic algorithm and an empirical binding free energy function, *J. Comput. Chem. 19*, 1639-1662.

39. Rosenfeld, R. J., Goodsell, D. S., Musah, R. A., Morris, G. M., Goodin, D. B., and Olson, A. J. (2003) Automated docking of ligands to an artificial active site: augmenting crystallographic analysis with computer modeling, *J. Comput. Aided Mol. Des. 17*, 525-536.

40. Bertini, I., Donaire, A., Luchinat, C., and Rosato, A. (1997) Paramagnetic relaxation as a tool for solution structure determination: Clostridium pasteurianum ferredoxin as an example, *Proteins-Structure Function and Genetics 29*, 348-358.

41. Clore, G. M., and Iwahara, J. (2009) Theory, Practice, and Applications of Paramagnetic Relaxation Enhancement for the Characterization of Transient Low-Population States of Biological Macromolecules and Their Complexes, *Chem. Rev. 109*, 4108-4139.

42. Pintacuda, G., John, M., Su, X. C., and Otting, G. (2007) NMR structure determination of protein-ligand complexes by lanthanide labeling, *Acc. Chem. Res. 40*, 206-212.

43. John, M., Pintacuda, G., Park, A. Y., Dixon, N. E., and Otting, G. (2006) Structure determination of protein-ligand complexes by transferred paramagnetic shifts, *J. Am. Chem. Soc. 128*, 12910-12916.

44. Gay, G. L., Lindhout, D. A., and Sykes, B. D. (2004) Using lanthanide ions to align troponin complexes in solution: Order of lanthanide occupancy in cardiac troponin C, *Protein Sci. 13*, 640-651.

45. Wang, C. L. A., Leavis, P. C., Dehorrocks, W., and Gergely, J. (1981) Binding of Lanthanide Ions to Troponin-C, *Biochemistry 20*, 2439-2444.

46. Marsden, B. J., Hodges, R. S., and Sykes, B. D. (1988) H-1-Nmr Studies of Synthetic Peptide Analogs of Calcium-Binding Site-Iii of Rabbit Skeletal Troponin-C - Effect on the Lanthanum Affinity of the Interchange of Aspartic-Acid and Asparagine Residues at the Metal-Ion Coordinating Positions, *Biochemistry 27*, 4198-4206.

CHAPTER 10

Drug binding to the regulatory troponin C-troponin I complex

This last experimental chapter reports on a series of drug binding experiments conducted as part of the early drug screening efforts carried out in the laboratory. It starts with *in silico* methods to assess the amenability of troponin for docking studies. It follows an experimental section in which the main target is the cChimera protein described in Chapter 6 of this thesis. Although the work presented here has not yet been published, it provided initial proof of the applicability of cChimera as a target for the screening of drugs that bind the troponin C-troponin I interface. It also inspired the design of other troponin chimeras that are currently being used to continue NMR-based screening and structure determination. The reader will find here detailed titrations and analysis for three sets of compounds binding to cChimera or a troponin C-I complex; note, however, that the project is still in progress.

In silico identification of druggable sites in troponin

I used a fragment-based method *in silico*, FTMap[1], to find druggable sites in cNTnC. FTMap identifies druggable sites or 'hot-spots' by performing rigid docking of sixteen organic probe molecules into a protein target. It follows a round of energy minimization using the CHARMM force field, as well as two cycles of rmsd clustering and ranking, to identify the consensus sites (CS) of probe binding. This tool has been used to explore druggable space for Ras GTPase which was not considered a drug target before[2], for the ß1 and ß2 adrenergic receptors for which no structural data on allosteric ligand binding is available[3], and for DJ-1 and glucocerebrosidase which are targets for the development of therapeutics for Parkinson's and Gaucher's diseases, respectively[4]. Using all available structures of cNTnC in the open state and removing all ligands, FTMap predicted the canonical binding site found experimentally in cNTnC (Figure 10.1A). This validates the use of FTMap for druggable site prediction for cNTnC. Moreover, the agreement between bepridil and the FTMap probes predicted to bind to cNTnC (from 1J1E) is exceptional (Figure 10.1B). This suggests that bepridil and analogues are potentially accessible to analysis *in silico* prior to *in vitro*.

In a similar way, when the structure of the cNTnC bound to cTnI (residues 147-163, PDB ID: 1MXL) is used, the FTMap results suggest another hot-spot located between helices A (Q16, E19, A22, A23) and D (F77, M81, V82, M85) of cNTnC and cTnI (A150, M153, M154). In another prediction using all available structures of the cNTnC-cTnI switch peptide complex and removing the small molecule ligands, the same consensus site, formed by helices A (E15, Q16, E19, F20, A23) and D (M81, M85) of cNTnC and cTnI (A150, D151, M154), was identified. This site ranks one place below the canonical site for both sets of predictions (Figure 10.1C). It is interesting that this hot-spot is located where the

A162H substitution interacts with cNTnC and also involves E15 and E19. The previous results encourage the search of ligands that may bind a new site involving the surface formed by cNTnC and cTnI switch peptide.
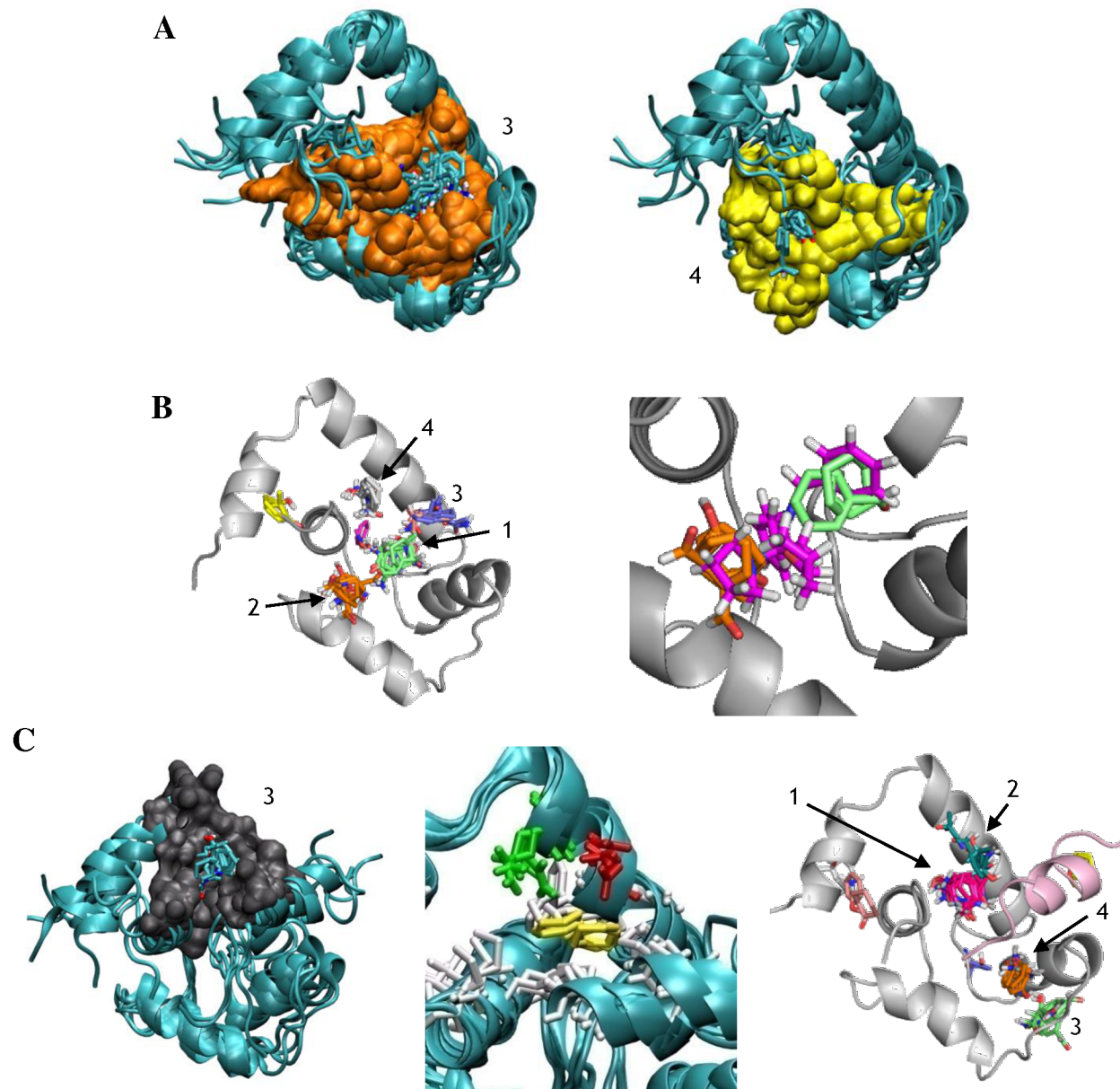
Figure 10.1. Localization of druggable sites on cNTnC predicted by FTMap.

A. Predicted druggable sites (orange and yellow) for representative conformations of all cNTnC (green) structures available. B. Probe binding sites for 1J1E predicted by FTMap. The expansion shows the structure of bepridil (pink) when bound to cNTnc (from 1LXF) superimposed to the FTMap results. Fewer probes are shown in the expansion for clarity. Numbers indicate the ranking of consensus sites identified.

The suggestion of another druggable site for cNTnC poses a question of the effect on switch-cTnI binding by small molecules binding the second site. Only the calcium sensitizer, dfbp-o, was shown to improve binding of the switch peptide to cNTnC, still its stabilization energy (-0.5 Kcal/mol) is much lower than the estimated for the A162H substitution (~2.2 Kcal/mol)[5, 6]. This deficiency could be overcome by binding small molecules in more than one site that involves contacts with cNTnC and cTnI. A possible method to search for small molecules that bind on a site different than the canonical, is to first block the canonical site. For this purpose the covalent ligand i9, described in detail in Chapter 7, can be used.

Compounds based on bepridil

Amongst the Ca^{2+} sensitizers for which a high resolution structure is available, bepridil stands out as a reasonable starting molecule for rational drug design (Figure 10.2). Bepridil binds to the regulatory N-domain of troponin C (cNTnC) in the presence of the switch region of troponin I (switch-cTnI). It has a low dissociation constant (K_D) of 23 μM and 80 μM when binding to cNTnC and cNTnC•switch-cTnI[7], respectively. Furthermore, docking experiments show that the benzyl and pyrrolidine groups of bepridil are in agreement with the localization of predicted druggable sites.

Despite such desirable characteristics, bepridil shows some disadvantages that may be overcome by modifications on its structure. Bepridil decreases the binding affinity of switch-cTnI for cNTnC by 3.5 fold[7]. This interference with switch-cTnI binding can be considered a main disadvantage since association of switch-cTnI to cNTnC is a crucial step on the mechanism of muscle contraction. Another inconvenience is its high hydrophobicity which makes it insoluble in aqueous physiological conditions. It has been suggested that the hydrophobic tail of bepridil clashes with the N-terminal region of switch-cTnI and is responsible for perturbing binding to cNTnC[7]. A plausible modification would be to remove or shorten such hydrophobic tail. To improve the solubility of bepridil, one can add hydrophilic groups especially on the face that is more exposed to the solvent once it is bound to cNTnC. However, a cautious method is needed to ensure that modifications do not impact the sensitizing properties of the starting compound.

- **Advantages**
  - Calcium sensitizer
  - Tight binding

- **Disadvantages**
  - Very hydrophobic
  - Decreases cTnI-cNTnC binding
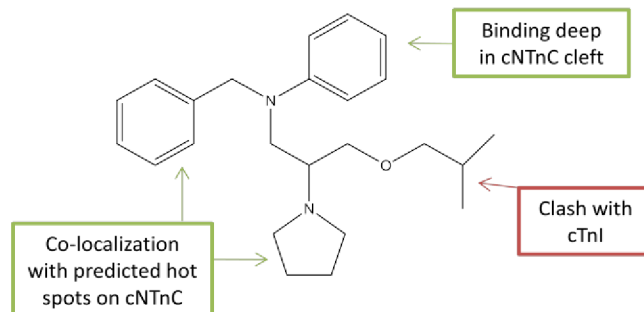
Figure 10.2. Overview of bepridil as lead molecule for drug design.

The advantages and disadvantages of bepridil binding to cNTnC are listed. The chemical structure of bepridil is shown on the right with positive and negative aspects labeled in green and red boxes, respectively.

Based on this rationale, five small molecules that resemble the core of bepridil (benzyl and phenyl rings) were titrated into cChimera: N-benzylaniline, diphenylamine, 3-methyl-diphenylamine (3m-DPA), 4-methyl-diphenylamine (4m-DPA), and ranolazine (Figure 10.3). A stock solution of each small molecule was prepared in DMSO-d_6 to a concentration of ~50 mM. Small aliquots were added to a sample containing 0.1 - 0.2 mM cChimera in 100 mM KCl, 10 mM imidazole, and 0.25 mM DSS-d_6 as internal reference. The titration was monitored by acquiring ^{1}H, ^{15}N HSQC NMR spectra after each addition. Chemical shift perturbations were plotted against the drug:protein ratio and fit to a hyperbolic binding curve to determine the K_D for the interaction.
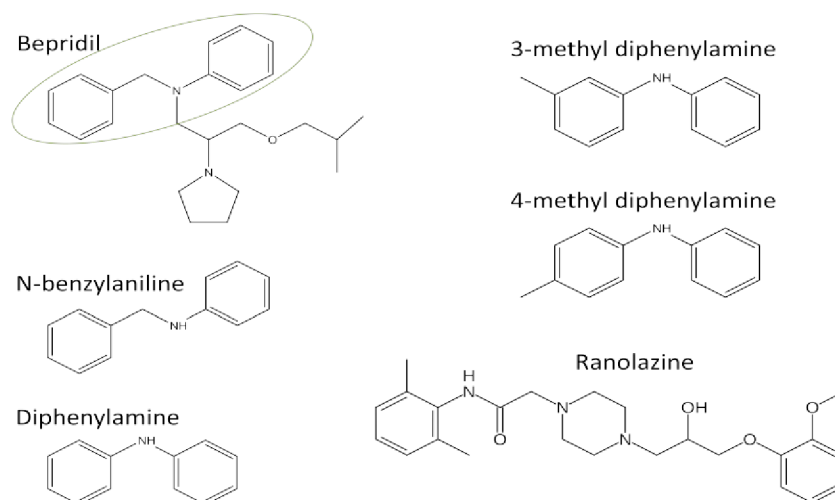
Figure 10.3. Bepridil and bepridil-like compounds tested.

Bepridil and the five compounds for which binding to cChimera was evaluated. The core of bepridil is circled in green.

The results are shown in Figure 10.4 to Figure 10.9, except for ranolazine which did not induce any chemical shift perturbation. Together, the results indicate that modifications of the bepridil core can improve binding to cNTnC in the presence of switch-cTnI. The N-benzylaniline compound represents the initial core of bepridil. Substitution of the benzyl ring for a phenyl group increased binding by over three-fold (from 58 ± 6 to 17 ± 7 µM). Subsequent addition of a methyl group at position 3 further improved binding by 23-fold (from 58 ± 6 to 2.5 ± 0.3 µM). The effects of these molecules on the Ca^{2+} sensitivity remains to be tested.
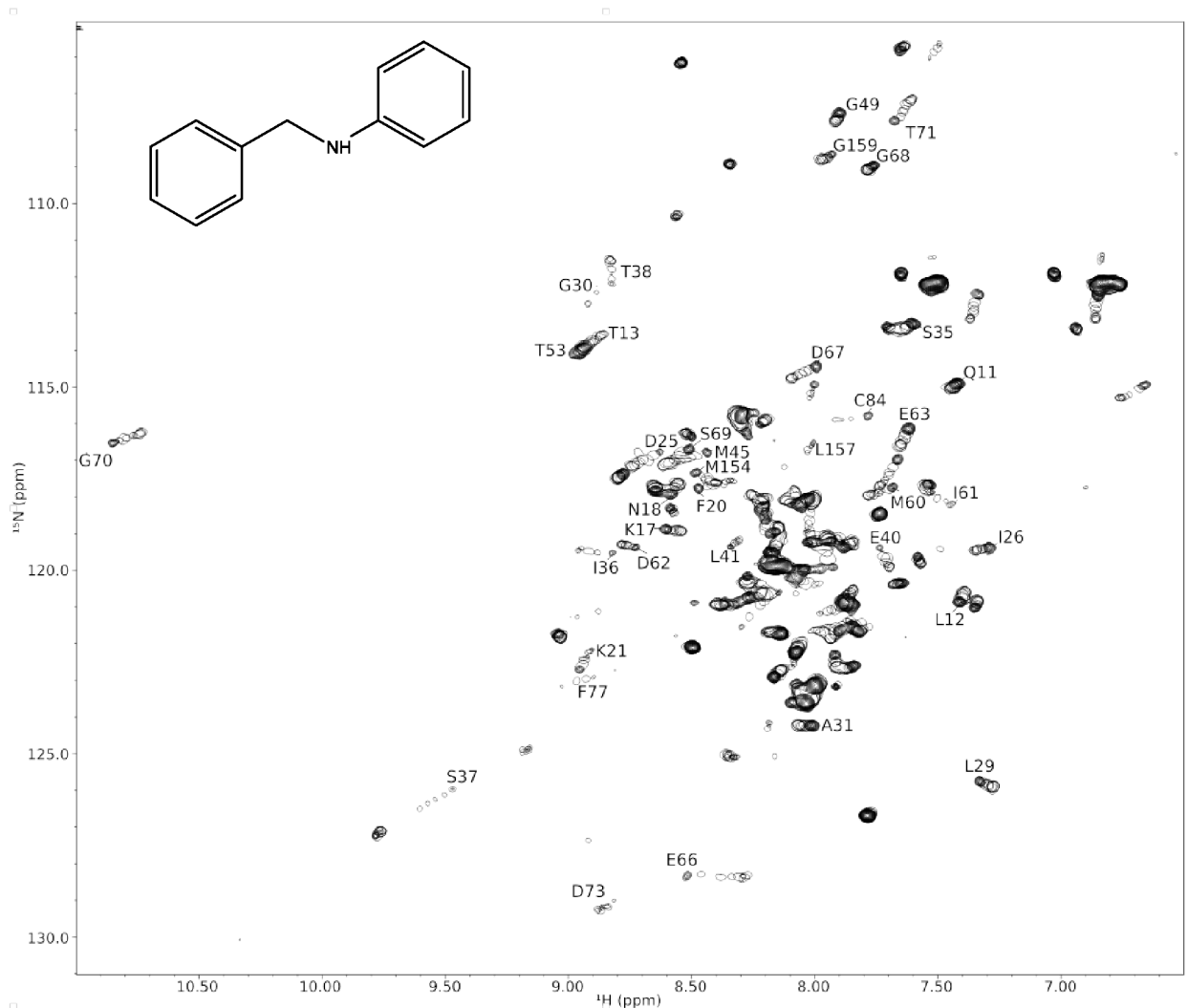
Figure 10.4. N-benzylaniline binding to cChimera.

^{1}H, ^{15}N HSQC spectral stack for the titration of N-benzylaniline into cChimera, the first point of the titration is represented in multiple contours. Residues experiencing large chemical shift perturbations are labeled.
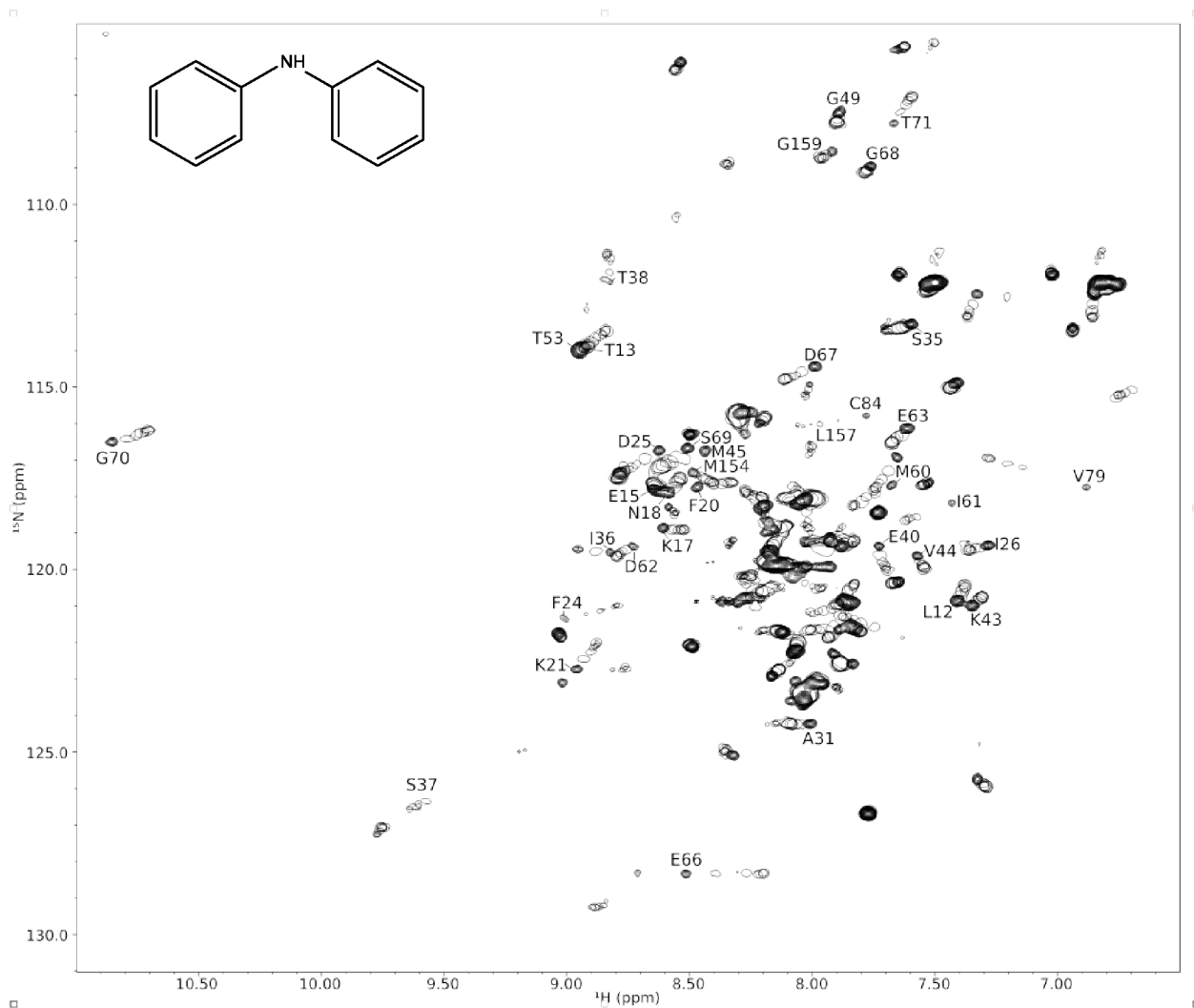
Figure 10.5. Diphenylamine binding to cChimera.

^{1}H, ^{15}N HSQC spectral stack for the titration of diphenyamine into cChimera, the first point of the titration is represented in multiple contours. Residues experiencing large chemical shift perturbations are labeled.

N-benzylaniline into cTEVChimera $K_D = 58 \pm 6$ μM
Diphenylamine into cTEVChimera $K_D = 17 \pm 7$ μM
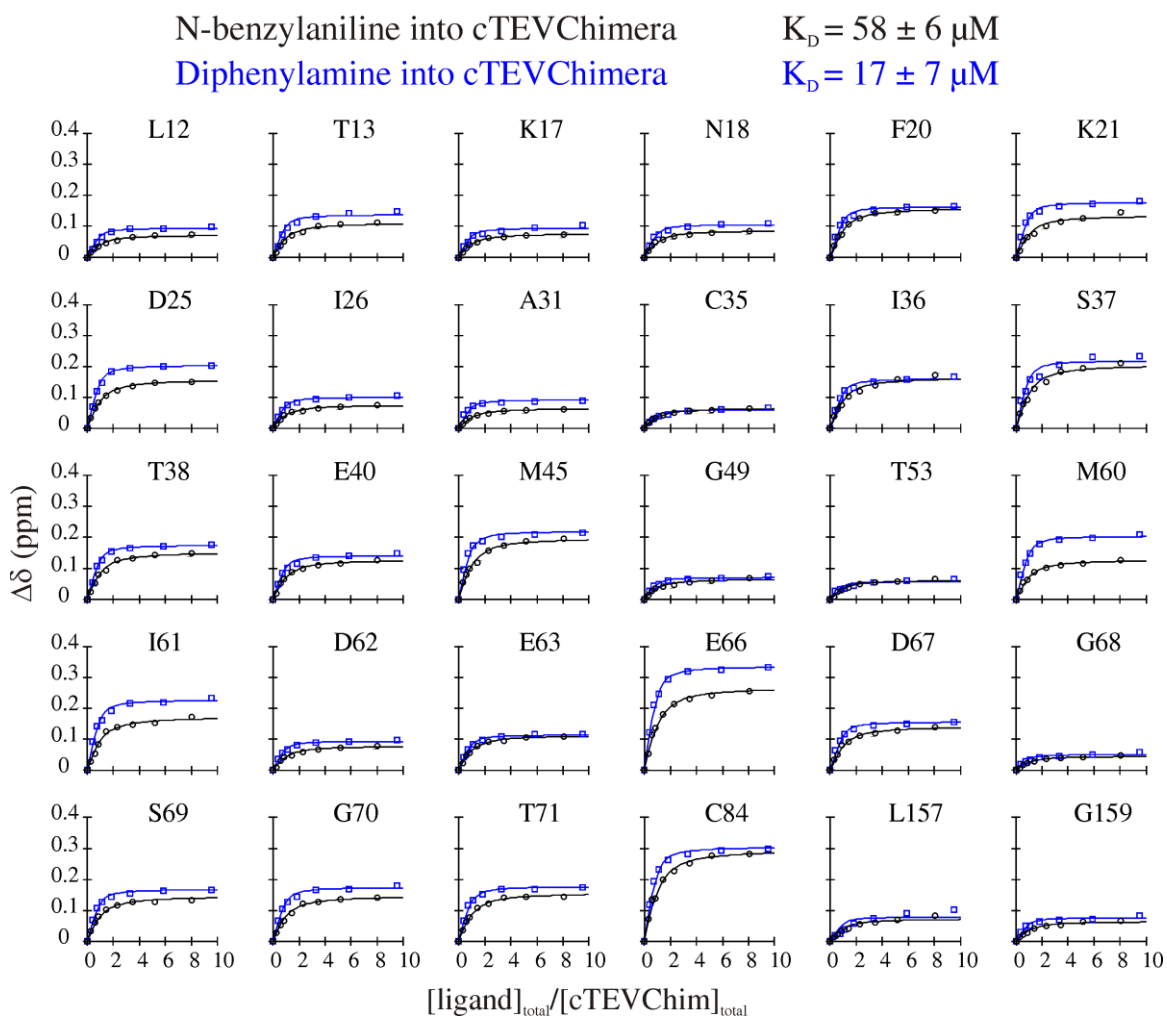
Figure 10.6. Global fit curves for the binding of N-benzylaniline and diphenylamine to cChimera.
Overlap of representative global fit curves for N-benzylaniline (black) and diphenylamine (blue) binding to cChimera. The global K_D of interaction is indicated for each compound at the top.
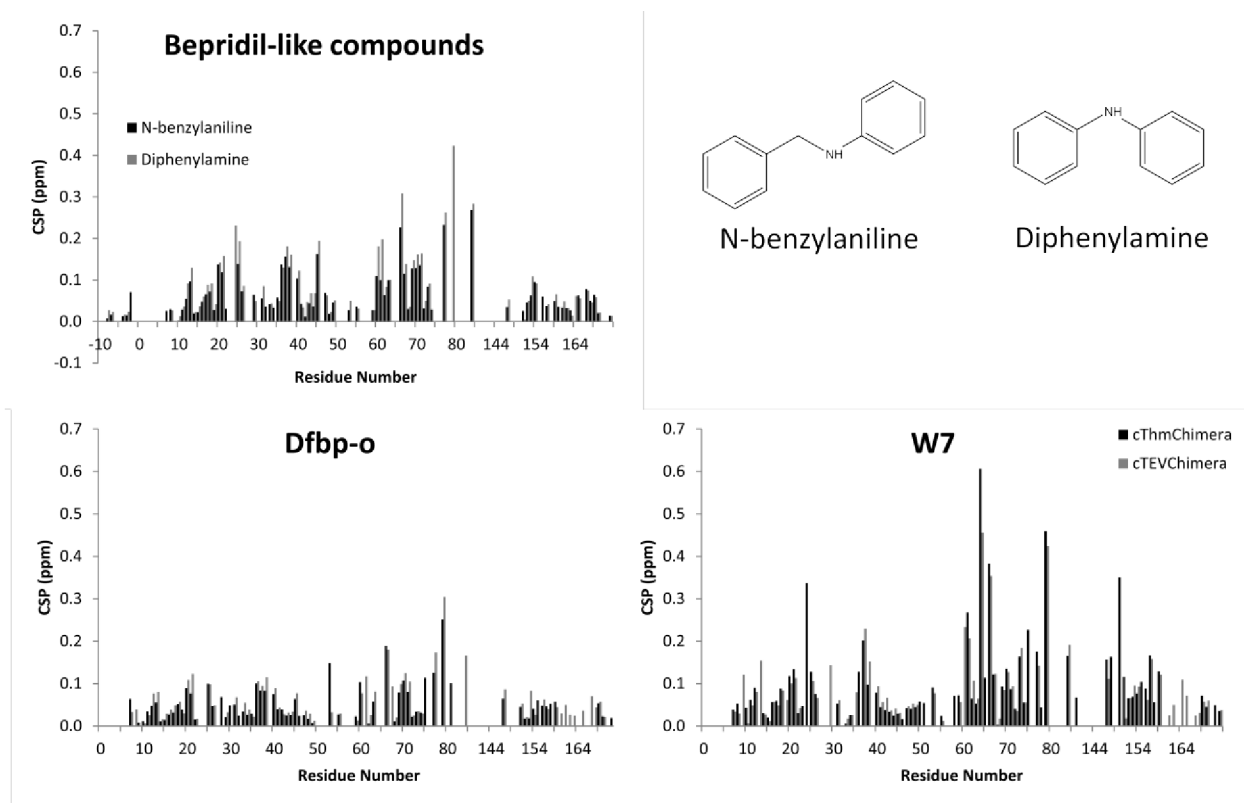
Figure 10.7. Comparison of chemical shift perturbations induced by small molecules on cChimera. The chemical shift perturbations induced by N-benzylaniline, diphenylamine, the Ca^{2+} sensitizer dfbp-o, and the Ca^{2+} desensitizer W7 are plotted against cChimera residue number. For dfbp-o and W7 two versions of cChimera were tested.
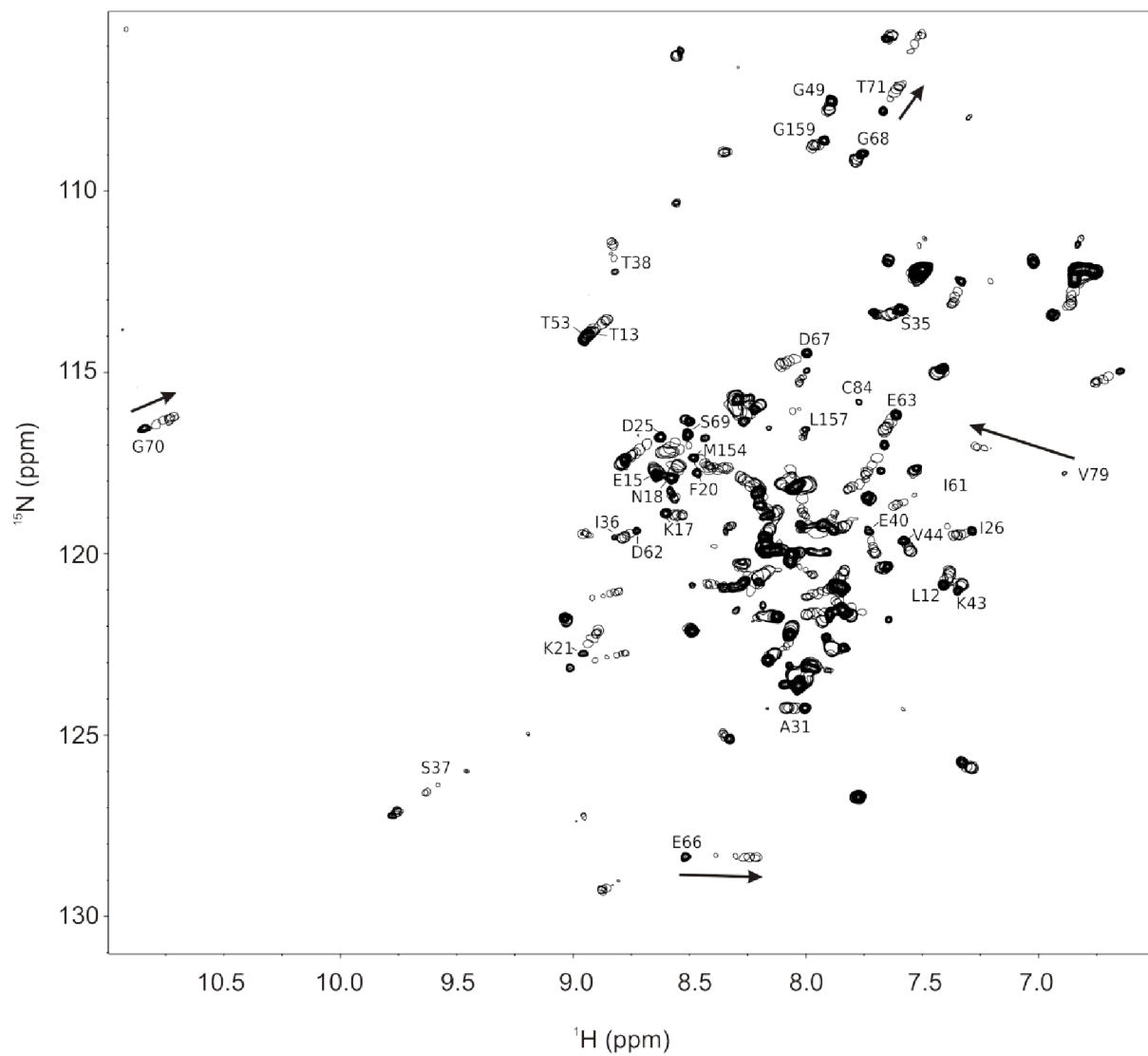
Figure 10.8. 3m-DPA binding to cChimera.

^{1}H, ^{15}N HSQC spectral stack for the titration of 3m-DPA into cChimera, the first point of the titration is represented in multiple contours. Residues experiencing large chemical shift perturbations are labeled.
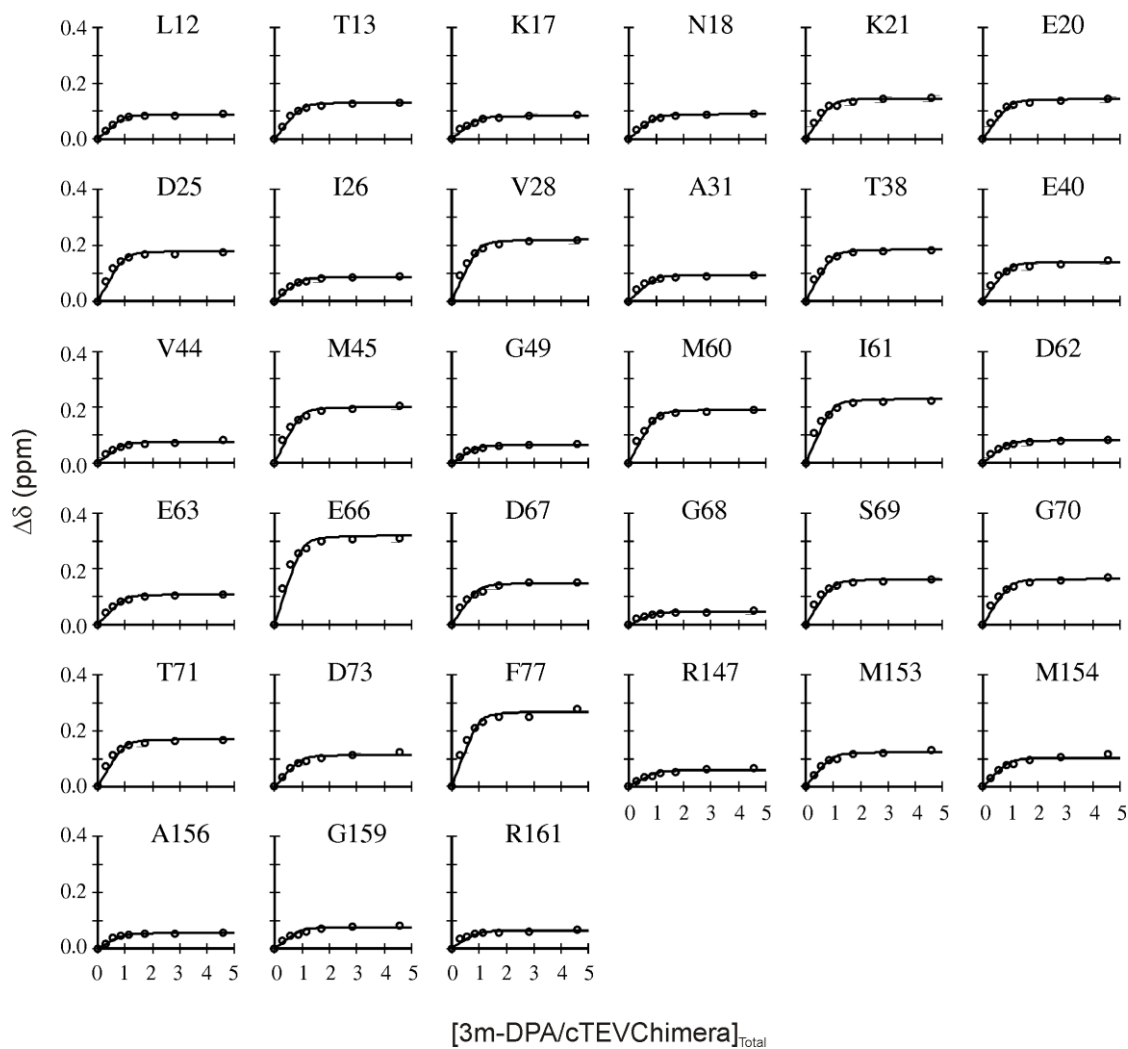
Figure 10.9. Global fit curves for the binding of 3m-DPA to cChimera.

Representative global fit curves for 3m-DPA binding to cChimera. The global K_D of interaction is indicated at the top.

Compounds from the National Cancer Institute

In addition, four compounds from the National Cancer Institute (NCI) were titrated into cChimera (Figure 10.10). These compounds were selected based on *in silico* screening of the NCI library. The titration procedure was the same as for the bepridil-based probes. Compounds NCI-88600 and NCI-93427 induced minor chemical shift perturbations of cChimera resonances and precipitated at drug:protein ratios much lower than 1:1. Compound NCI-91355 displayed mayor precipitation upon addition into the NMR sample and induced minor perturbations. Only compound NCI-147866 induced significant chemical shift perturbations (Figure 10.11) with small amounts of precipitation at drug:protein ratios higher than 1:1. The low solubility of these compounds was directly related to their estimated hydrophobicity determined with ChemDraw Ultra 11. The calculated CLogP corresponds to an estimation of the hydrophobic-to-hydrophilic ratio of the compound such that the lower the CLogP the higher the solubility in water. Compound NCI-147866 had the lowest value of CLogP (3.31) while compound NCI-91355 had the highest (4.36). Compounds NCI-88600 and NCI-93427 had intermediate CLogP values of 3.97 and 4.17, respectively. Then the predicted hydrophobicity agreed with the experimental observations.

NCI-88600   NCI-93427

NCI-147866   NCI-91355
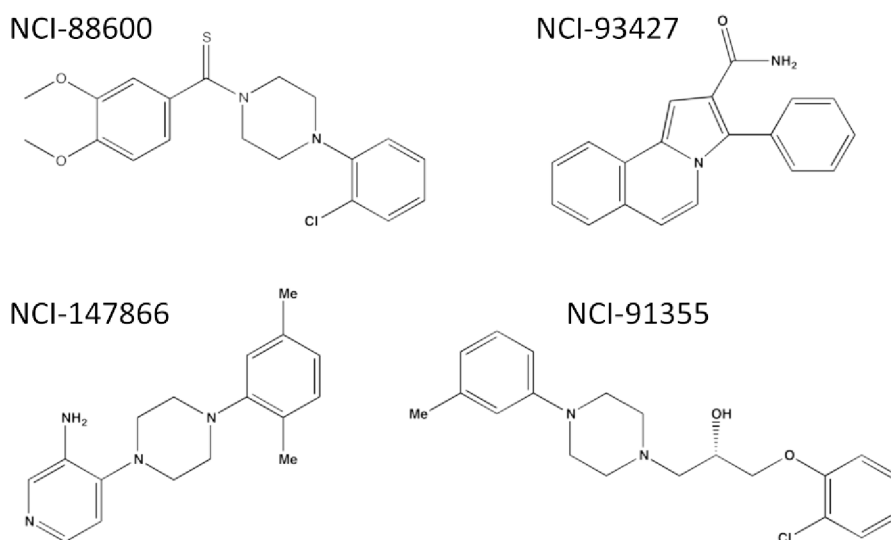
Figure 10.10. Chemical structure of NCI compounds tested.
Four compounds were selected based on their docking score on the binding to cNTnC.

The results shown in Figure 10.12 indicate that compound NCI-147866 binds weakly to cChimera (K_D = 610 ± 92 μM). Compared to previous studies of drug binding to cChimera (for a comprehensive analysis of drug binding to cChimera the reader is referred to Chapter 6) the chemical shift perturbations caused by NCI-147866 were small but similar in magnitude to those caused by the Ca^{2+}

sensitizer dfbp-o. However, chemical shift mapping revealed that the switch peptide region and its surroundings are largely perturbed by NCI-147866 as it is also observed for the Ca^{2+} desensitizer W7 (Figure 10.13). Therefore NCI-147866 is predicted to decrease the affinity of cTnI for cNTnC in a similar way as W7.
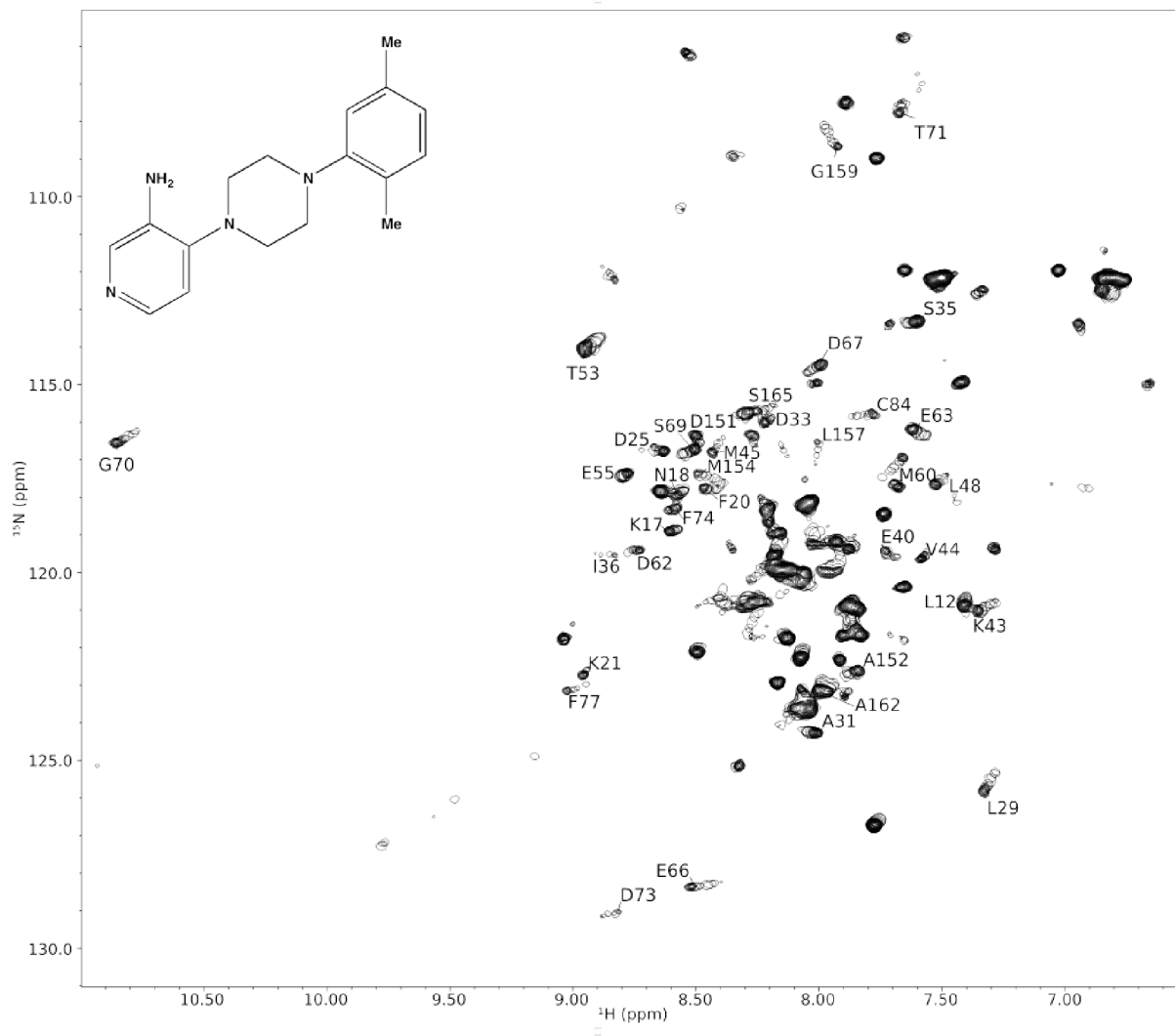
Figure 10.11. Binding of NCI-147866 to cChimera.

^1H, ^{15}N HSQC spectral stack for the titration of NCI-147866 into cChimera, the first point of the titration is represented in multiple contours. Residues experiencing large chemical shift perturbations are labeled.
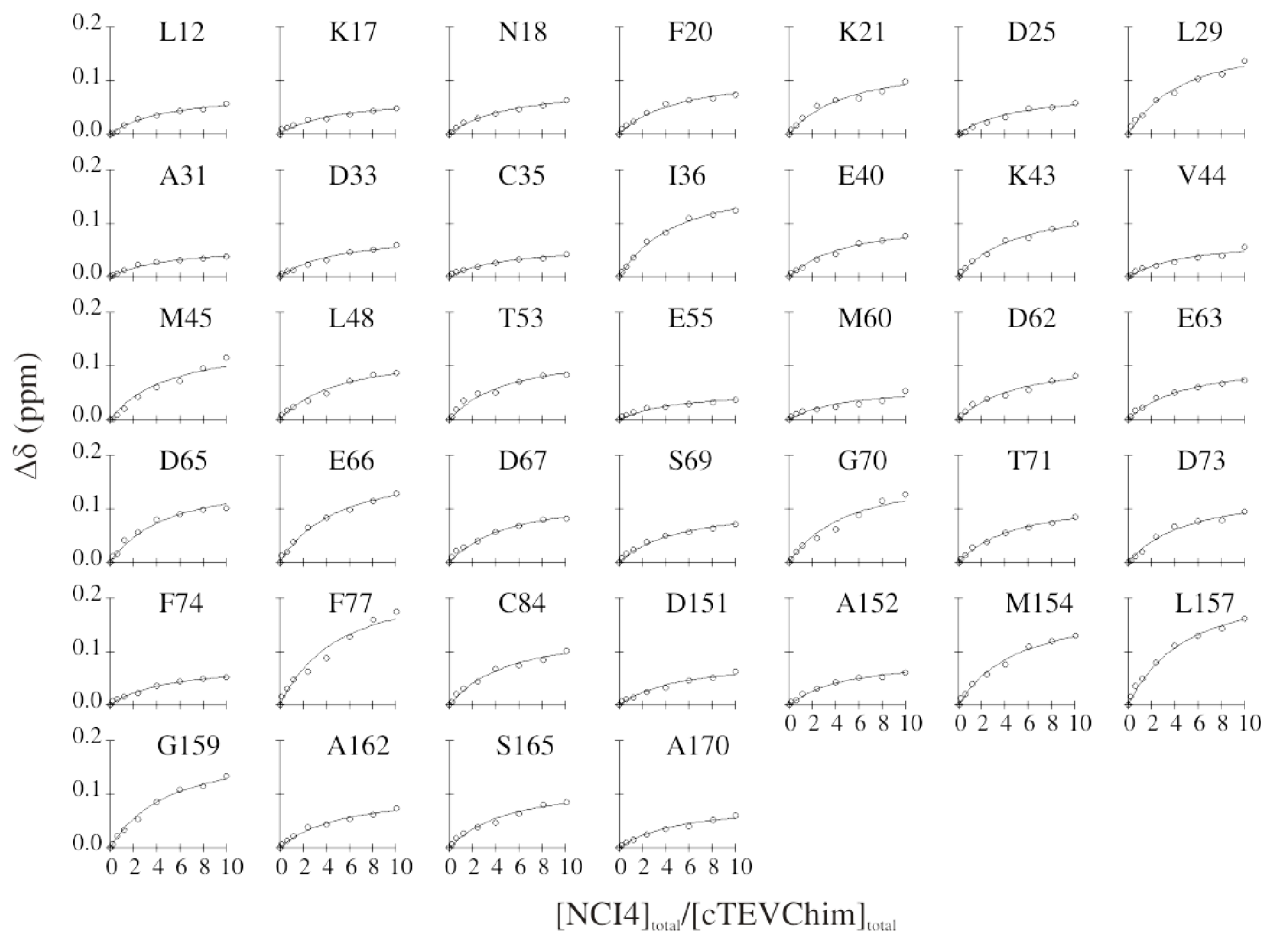
Figure 10.12. Global fit curves for the binding of NCI-147866 to cChimera.

Representative global fit curves for NCI-147866 binding to cChimera. The global K_D of interaction is indicated at the top.
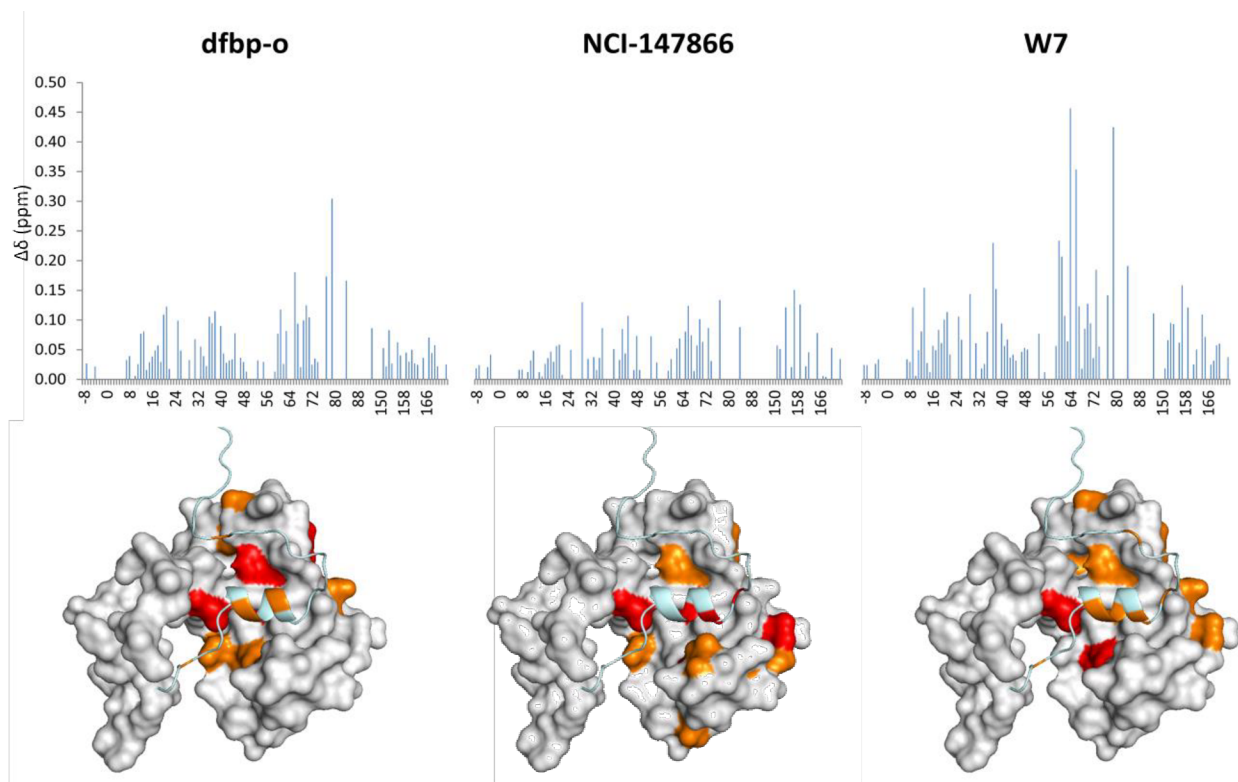
Figure 10.13. Mapping and comparison of chemical shift perturbations induced by NCI-147866.
The magnitude of chemical shift perturbation is plotted against residue number of cChimera for the binding of the Ca^{2+} sensitizer dfbp-o (left), NCI-147866, and the Ca^{2+} desensitizer W7 for comparison. The changes were mapped onto a model of Chimera in which cNTnC is in the surface representation and cTnI is in the cartoon representation. Perturbations higher than the average are shown in orange, and those higher than the average plus one standard deviation are shown in red.

Compounds from the Sanford-Burnham Medical Research Institute

A library of 480 compounds was tested for binding to cNTnC in complex with switch-cTnI (residues 144-170). Four hit compounds were identified (Figure 10.14). Binding of compound 95F5 was further characterized by NMR spectroscopy. Although the ^{1}H NMR spectrum of 95F5 showed the presence of impurities (Figure 10.15), these were considered to be too little to prevent further characterization. The target protein was cNTnC in the presence and absence of switch-cTnI (residues 144-170) containing the A162H substitution. Each titration was repeated at two pH values of 6 and 7. The drug titrations were performed as previously described (see 'Compounds based on bepridil' section).
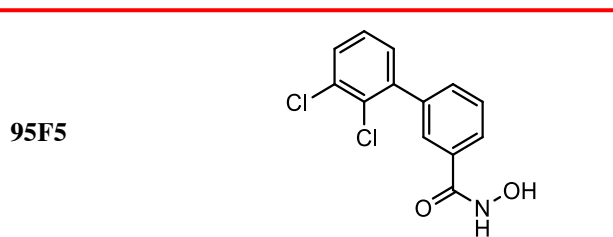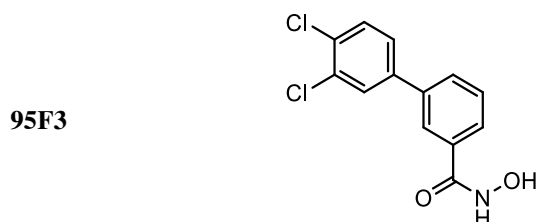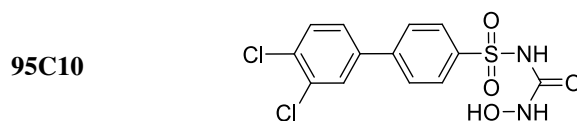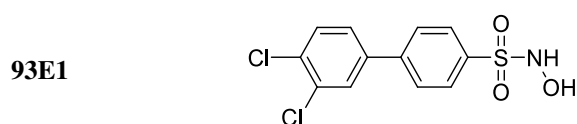
Figure 10.14. Chemical structure of hit compounds.

The structure of the four compounds identified as hits for binding to cNTnC·switch-cTnI is shown. Binding of compound 95F5 (red box) was further characterized by NMR spectroscopy.
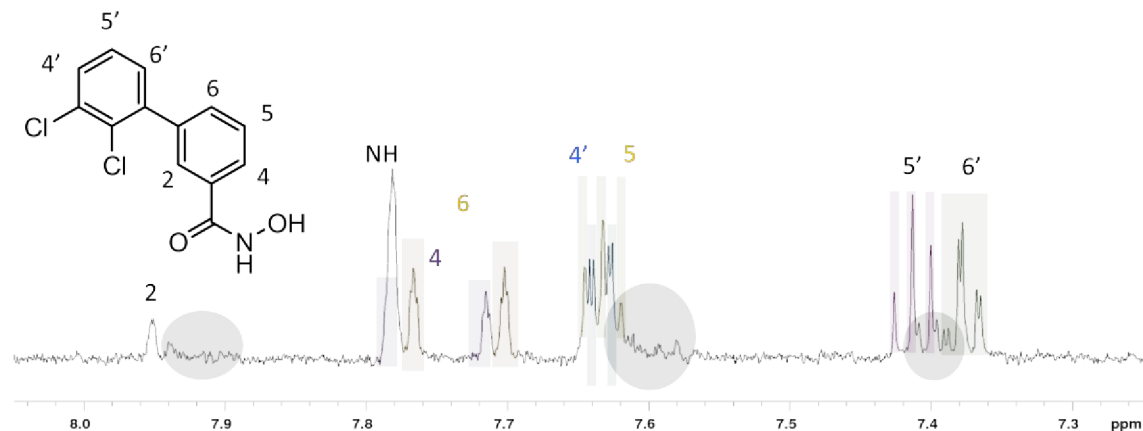
Figure 10.15. ^{1}H NMR spectrum of 95F5.
The spectrum of 95F5 showing the potential assignment based on prediction of ^{1}H signals with ChemDraw Ultra. The signals shown in grey were attributed to impurities in the sample.

The results of 95F5 binding to cNTnC or cNTnC·switch-cTnI are shown in Figure 10.16 to Figure 10.20 for two different pH values. The majority of chemical shift perturbations observed were in the fast exchange limit. However, for the titration of 95F5 into cNTnC (Figure 10.16 blue/right) some residues experienced intermediate to slow exchange. For this titration, the K_D was determined by line shape analysis (Figure 10.17 right). In addition, in the same titration a few residues displayed changes in the direction of the chemical shift perturbation. This was probably caused by binding of two molecules of 95F5 to cNTnC in the absence of cTnI. Multiple binding was not observed in the presence of switch-cTnI at any pH value tested (Figure 10.18 and

Figure 10.19) indicating that switch-cTnI may occupy the binding site of the second molecule of 95F5 preventing its association. To assess the effect of 95F5 on the binding of switch-cTnI we also titrated the saturated cNTnC·95F5 complex with switch-cTnI(A162H). The global fit of the resulting binding curves are compared in Figure 10.21.

The results showed that switch-cTnI(A162H) enhances the binding of 95F5 at both pH 7 and pH 6. The effect is more pronounced at acidic conditions with a four-fold increase in affinity (K_D from 250 to 57 µM) compared to a two-fold increase at pH 7 (K_D from 187 to 96 µM). Compared to the binding of switch-cTnI(A162H) to cNTnC[6] (Chapter 2, page 28), 95F5 caused a minor improvement on binding at pH 7 (from 40 to 35 µM) but a two-fold decrease in affinity at pH 6 (from 10 to 21 µM).

Figure 10.16. Binding of 95F5 into Ca^{2+} saturated cNTnC.

Stack of ^{1}H, ^{15}N HSQC NMR spectra for the titration of 95F5 into cNTnC·Ca^{2+} at pH 7 (left, black) and pH 6 (right, blue). The arrows indicate the direction of chemical shift perturbations. The first point of the titration is represented in multiple contours. Residues experiencing large chemical shift perturbations are labeled. Green arrows indicate residues undergoing intermediate exchange.
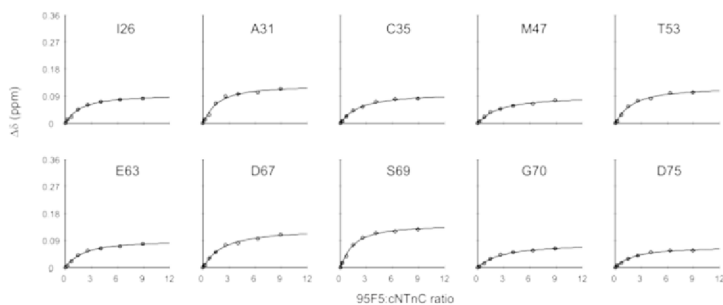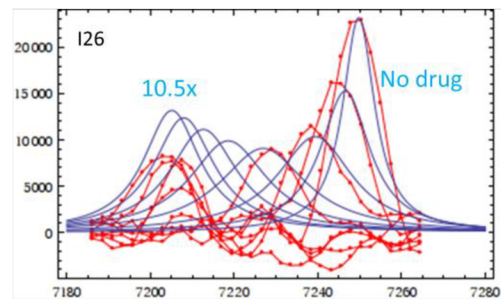
Figure 10.17. Determination of K$_D$ for the binding of 95F5 to cNTnC·Ca^{2+}.

Left: representative global fit curves for binding at pH 7. Right: line shape analysis for a representative residue (I26) undergoing intermediate exchange for the binding of 95F5 to cNTnC·Ca^{2+} at pH 6.
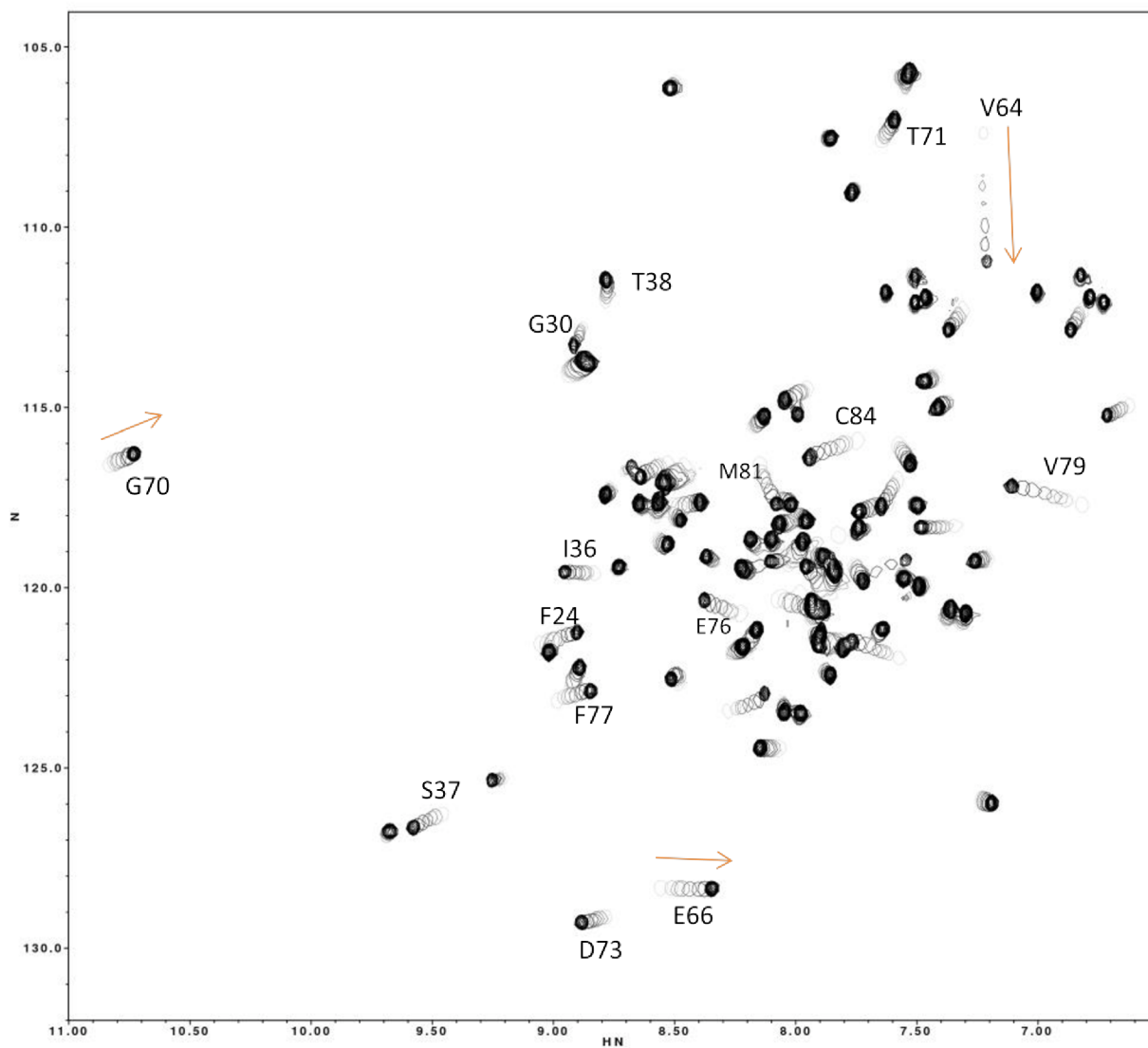
Figure 10.18. Binding of 95F5 to Ca^{2+} saturated cNTnC·switch-cTnI A162H at pH 7.

Stack of ^{1}H, ^{15}N HSQC NMR spectra for the titration of 95F5 into cNTnC·switch-cTnI A162H at pH 7. The arrows indicate the direction of chemical shift perturbations. The first point of the titration is represented in multiple contours. Residues experiencing large chemical shift perturbations are labeled.
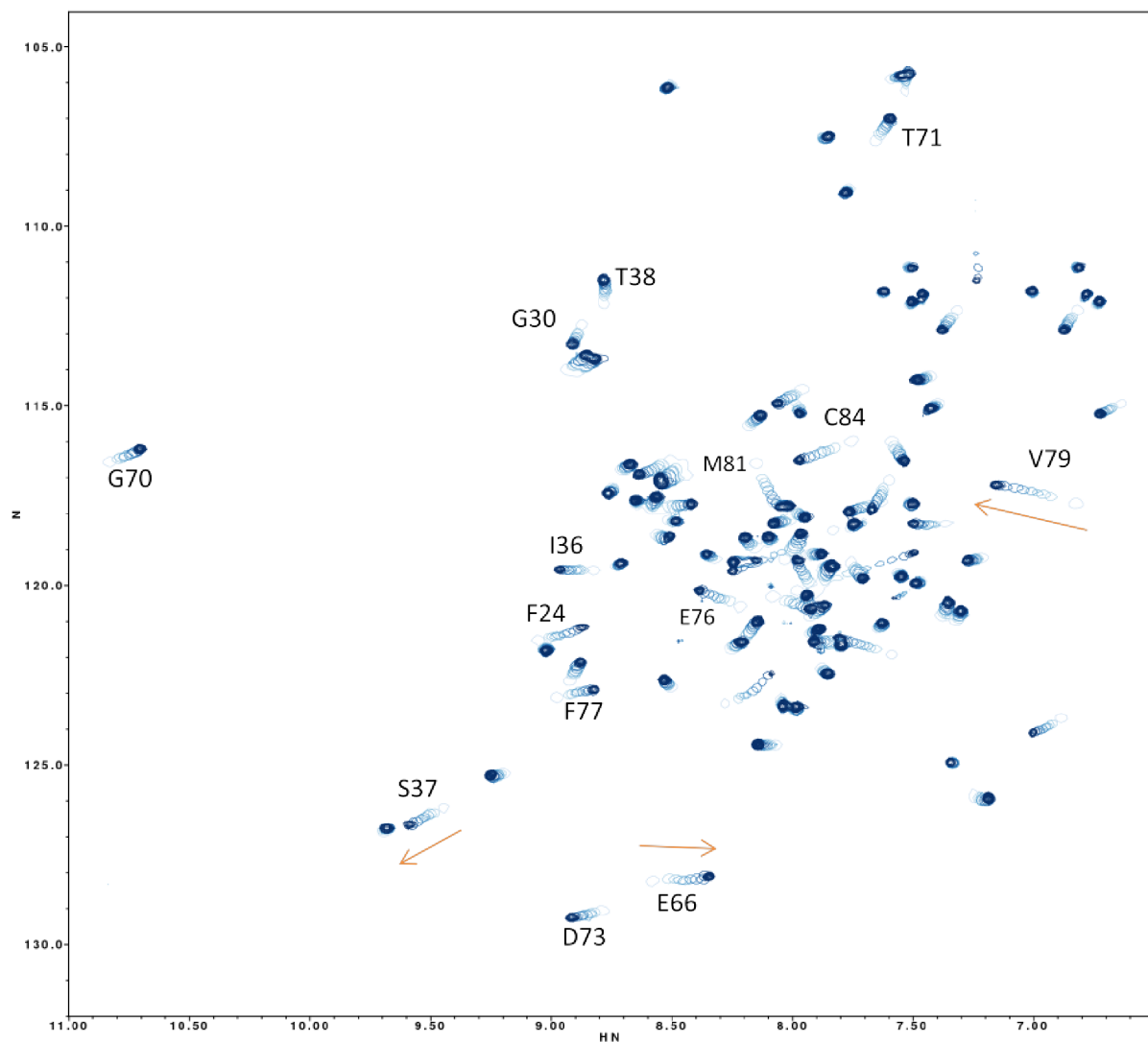
Figure 10.19. Binding of 95F5 to Ca^{2+} saturated cNTnC·switch-cTnI A162H at pH 6.

Stack of ^{1}H, ^{15}N HSQC NMR spectra for the titration of 95F5 into cNTnC·switch-cTnI A162H at pH 6. The arrows indicate the direction of chemical shift perturbations. The first point of the titration is represented in multiple contours. Residues experiencing large chemical shift perturbations are labeled.

95F5 titration into cNTnC•cTnI$_{144-170}$A162H

K_D 57 μM at pH 6 (blue crosses)
96 μM at pH 7 (black circles)
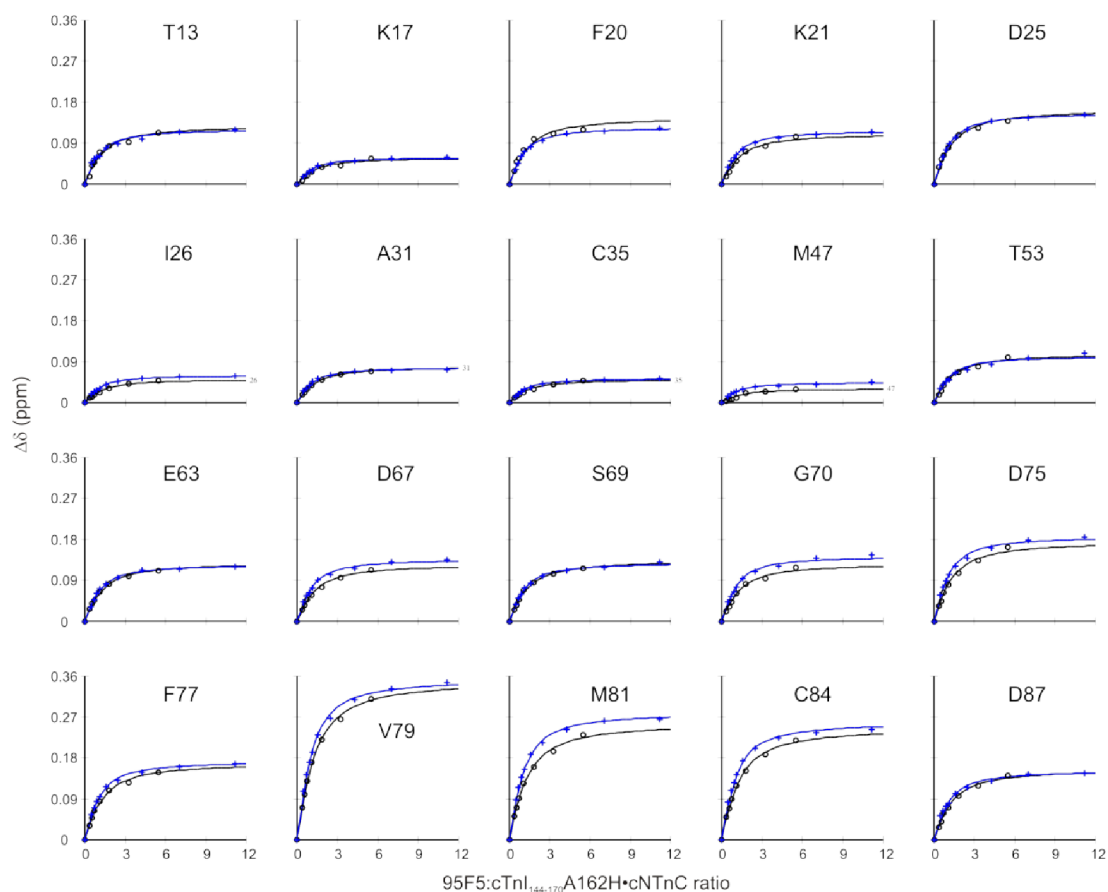
Figure 10.20. Global fit curves for the binding of 95F5 to cNTnC·switch-cTnI A162H at different pH values.

Overlap of global fit binding curves for 95F5 binding to cNTnC·switch-cTnI A162H at pH 7 (black circles) and at pH 6 (blue crosses). The global K_D is indicated on the top right for each set of curves.
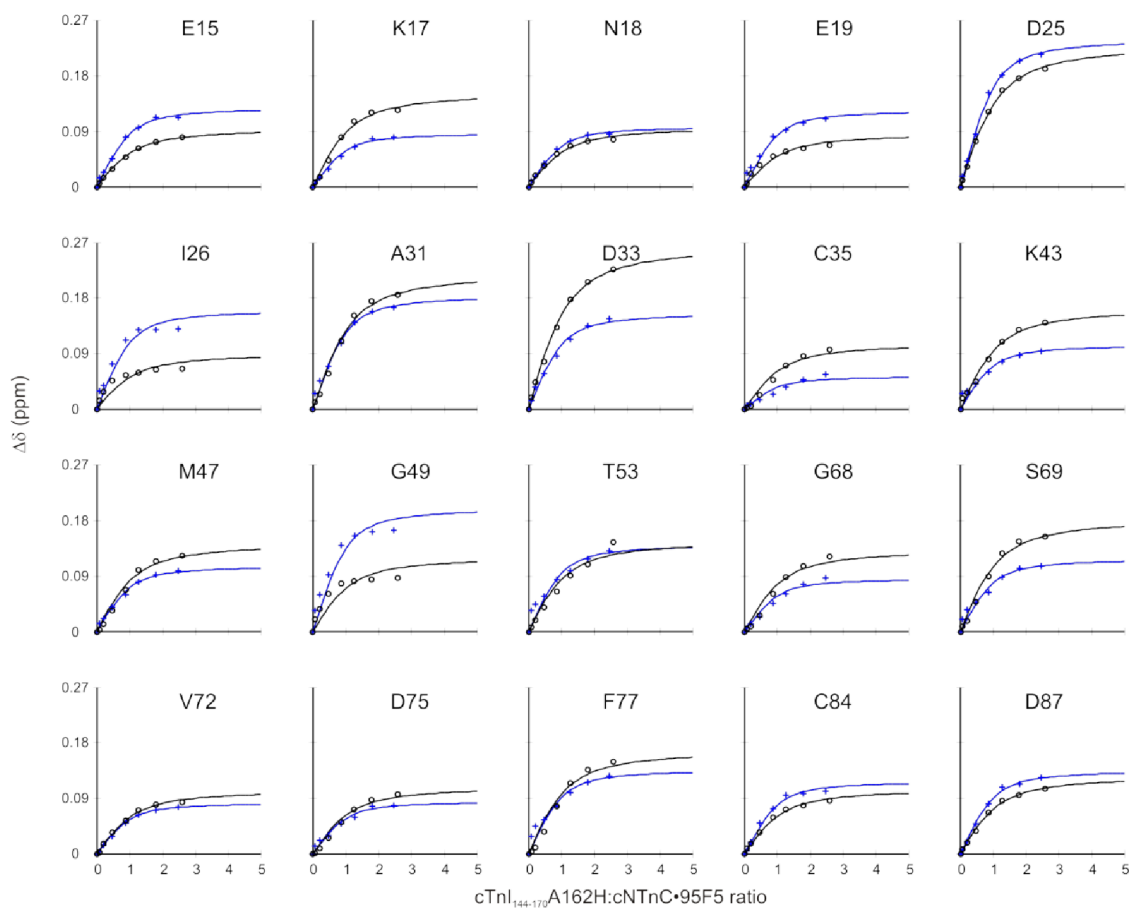
Figure 10.21. Global fit curves for the binding of switch-cTnI A162H to cNTnC·95F5 at different pH values.

Overlap of global fit binding curves for binding at pH 7 (black circles) and at pH 6 (blue crosses). The global K_D is indicated on the top right for each set of curves.

Acknowledgments

References

1. Brenke, R., Kozakov, D., Chuang, G. Y., Beglov, D., Hall, D., Landon, M. R., Mattos, C., and Vajda, S. (2009) Fragment-based identification of druggable 'hot spots' of proteins using fourier domain correlation techniques. *Bioinformatics. 25*, 621-627.

2. Buhrman, G., O'Connor, C., Zerbe, B., Kearney, B. M., Napoleon, R., Kovrigina, E. A., Vajda, S., Kozakov, D., Kovrigin, E. L., and Mattos, C. (2011) Analysis of binding site hot spots on the surface of ras GTPase. *J. Mol. Biol. 413*, 773-789.

3. Ivetac, A., and Andrew McCammon, J. (2010) Mapping the druggable allosteric space of G-protein coupled receptors: A fragment-based molecular dynamics approach. *Chemical Biology & Drug Design. 76*, 201-217.

4. Landon, M. R., Lieberman, R. L., Hoang, Q. Q., Ju, S., Caaveiro, J. M., Orwig, S. D., Kozakov, D., Brenke, R., Chuang, G., Beglov, D., Vajda, S., Petsko, G. A., and Ringe, D. (2009) Detection of ligand binding hot spots on protein surfaces via fragment-based methods: Application to DJ-1 and glucocerebrosidase. *Journal of Computer Aided-Molecular Design. 23*, 491-500.

5. Palpant, N. J., Houang, E. M., Delport, W., Hastings, K. E. M., Onufriev, A. V., Sham, Y. Y., and Metzger, J. M. (2010) Pathogenic peptide deviations support a model of adaptive evolution of chordate cardiac performance by troponin mutations. *Physiological Genomics. 42*, 287-299.

6. Pineda-Sanabria, S. E., Robertson, I. M., Li, M. X., and Sykes, B. D. (2013) Interaction between the regulatory domain of cardiac troponin C and the acidosis-resistant cardiac troponin I A162H. *Cardiovasc. Res. 97*, 481-489.

7. Wang, X., Li, M. X., and Sykes, B. D. (2002) Structure of the regulatory N-domain of human cardiac troponin C in complex with human cardiac troponin I$_{147-163}$ and bepridil. *J. Biol. Chem. 277*, 31124-31133.

CHAPTER 11
Conclusions

Based on the preceding chapters, which reflect more than five and a half years of scientific study, we come to a conclusion. In the following pages I correlate the final answers of all chapters to respond both of my initial research objectives. I start with Chapter 2 to Chapter 5, which together unravel the mechanism underlying the effects of the A162H mutant of troponin. The discussion then turns to the effect of Ca^{2+} sensitizers on troponin, which encompasses Chapter 6 to Chapter 10. Finally findings from both parts of this project come together to bring the open conformation of cNTnC to the center of our efforts to help alleviate contractile dysfunction.

To address the first query, in Chapter 2 to Chapter 5 we investigated the molecular details of the interaction between cTnI A162H, and the homologous skeletal isoform sTnI, with cNTnC[1, 2]. Previously Dargis et al.[3] hypothesized that the more positively charged histidine at low pH may stabilize the cNTnC-cTnI interface by interacting with glutamate or aspartate residues in cNTnC. We provided evidence of the electrostatic interaction between A162H and E19 and E15 of cNTnC by investigating their acid dissociation constants. In a similar fashion, we also proved the formation of a salt bridge between H130 and E20 in the all-skeletal system. We observed that the binding affinity of cTnI A162H for cNTnC was improved by reducing the pH to promote the charged state of H162. A similar improvement was observed for sTnI binding to sNTnC. We concluded that the extra electrostatic attraction contributed by the charged histidine of sTnI or cTnI A162H accounts for their increased affinity for sTnC or cNTnC, respectively, and compensates the reduction in Ca^{2+} sensitivity at low pH. Recall here that the association of cTnI to cNTnC causes the release of inhibition of myosin ATPase to allow contraction. Thus, a first effect of A162H to improve contraction is to increase the affinity of cTnI for cNTnC via electrostatic interactions under acidic conditions. In addition, Day et al.[4] suggested that this positive charge could weaken interactions with actin, but because this interaction was not addressed by our study, this theory remains a possibility.

The previous findings showed that the skeletal and A162H cardiac systems are very similar; in Chapter 4 and Chapter 5 we determined that their structures are no exception. Previous structures show the conformation of cTnI in the troponin complex as extended[5, 6], whereas the conformation of sTnI is bent and brings H130 close to E20 of sNTnC[7]. We showed that the bent conformation and location of sTnI bound to cNTnC are the same as in the sTnI·sTnC complex. This confirmed that the conformation of TnI is independent of the TnC isoform. We also found that the conformation of cTnI A162H was the same as that of sTnI. This revealed that histidine alone determines the conformation of TnI. Based on these deductions, we suggested the way in which a conformational change in TnI can regulate contraction. We

proposed that a bent conformation of the switch region of TnI (in sTnI and cTnI A162H) positions the C-terminal region away from actin[8]. This relative position favors contraction since the interaction of C-terminal TnI with actin is necessary to inhibit the myosin ATPase[9, 10]. Thus a conformational change of cTnI is also a way in which A162H maintains cardiac contraction during ischemic challenge.

Although the structures of cTnI A162H and sTnI bound to cNTnC are similar, we revealed that these carry subtle but important differences. cTnI A162H adopts the same conformation as sTnI when bound to cNTnC, but it localizes further away from cNTnC[11]. The change in location was rationalized as the result of a negative electrostatic potential induced by E164 that shifts the position of the pH-sensitive region away from E19 via a repulsive effect. The homologous residue in sTnI is V132, which is hydrophobic and could not repel E19. Previously Westfall *et al.* suggested a partial role for V132 of sTnI in modulating the pH sensitivity at acidic conditions since the V132E mutation produced a hybrid cardiac-skeletal phenotype[12]. In contrast, we propose that E164 is crucial to ensure proper relaxation in the presence of A162H. This is consistent with previous studies showing that cTnI A162H does not impair relaxation *in vivo*[4] but sTnI does[13]. Moreover, it has been shown that proper diastole in mice expressing cTnI A162H is not a result of phosphorylation of the N-terminal extension of cTnI[14]. It is also possible that E164 prevents electrostatic interactions of R161 and K163 with cNTnC to ensure relaxation in wild type cardiac muscle.

Based on these findings, we proposed a model of gradient stabilization of TnI in which the extent of positive potential of the pH-sensitive region facing cNTnC dictates the state of the contraction-relaxation equilibrium[11]. In this model the more positive the potential, the more favored is the bent conformation of TnI that promotes electrostatic attraction between cTnI and cNTnC. With this model we were able to explain and predict the impact of charge substitutions on pH-sensitivity in a variety of mutants. Nevertheless, it raised a question of specificity of location of the positive potential; i.e. if the positive charge were located at a position other than 162 would it still induce the bent conformation? It is likely that it would, as long as the positive potential is on the side that faces cNTnC and remains in the vicinity of 162. Position 164 seems to meet these conditions such that an E164H or E164R mutant may also induce resistance to acidosis. However, such mutants have not been characterized.

Together, these findings add to the evidence of a favored relaxed state for the cardiac muscle. It is known that phosphorylation of the N-terminal extension of cTnI decreases Ca^{2+} sensitivity[15, 16] and this is only present in the cardiac isoform. In addition, here we showed how two residues of cTnI also promote relaxation: A162, by promoting an extended conformation of cTnI, and E164, by preventing potential electrostatic interactions between switch-cTnI and cNTnC. Interestingly, in the evolutionary variation of cTnI[17] both residues were replaced (from H162 and V164, respectively) around the same time. The change from V164 to E164 could have been more direct than that from H162 to A162, for which a P162 evolutionary intermediate has been proposed[17]. In any case, the change of two residues inclined

to relaxation seems redundant. But together with phosphorylation of the N-terminal extension these highlight the importance of the relaxed state for the heart muscle.

It seems that the natural efforts incline the scale toward relaxation to finely regulate and maintain heartbeat dynamics. Yet enhancing cardiac contraction is a reasonable choice to pursue in the treatment of heart failure. This is why the second part of this work aims to provide insight into the mechanism of Ca^{2+} sensitization by small molecules that bind to troponin. To better study this interaction we designed cChimera to represent the cNTnC·switch-cTnI complex in the saturated state[18]. A major methodological contribution of this tool was the chance to isotope label the switch region. In the past this region was usually synthetic and unlabeled[5, 11, 19, 20, 21]. Now with isotope labeled cChimera we could assign the switch-cTnI resonances using the same experiments as for the cNTnC region, which saves time. We could use the backbone Cα and Cβ resonances to predict φ and ψ dihedral angles for structure determination. Previously in the Sykes laboratory, Wang and Oleszczuk observed displacement of switch-cTnI after they determined the structure of a cNTnC·switch-cTnI·drug complex[19,21]. By monitoring amide NH chemical shift perturbations for the first time in switch-cTnI of labeled cChimera, we could determine to what extent a drug molecule disturbs this region prior to structure determination. This turned out to be very important as we showed that the larger the perturbations on switch-cTnI, the more likely is the drug to displace it, worsen its binding, and be a desensitizer. As detailed in Chapter 10, this tool also allowed to start drug screening efforts carried out in collaboration with Dr. Peter Hwang at the University of Alberta, Dr. Maurizio Pellecchia at the Sanford-Burnham Medical Research Insitute, and Dr. Andrew McCammon at the University of California San Diego.

Despite the structural characterization of diverse cTnC·drug complexes, it remains a possibility that that these drugs bind non-specifically to other proteins or lipid membranes in the body. In Chapter 7 we provided conclusive evidence to confirm that small molecule binding to cNTnC is indeed responsible for Ca^{2+} sensitization in muscle tissue (unpublished). Therein we looked at i9, a covalent Ca^{2+} sensitizer designed based on levosimendan. We observed that incomplete exchange of cTnC-i9 into cardiac trabeculae increased Ca^{2+} dependent tension. Further exchange resulted in tension development independent of Ca^{2+}. By correlating these with the structure of cChimera-i9 we explained this powerful effect on contraction as the result of stabilization of the open conformation of cNTnC by i9. This represents a major contribution to the elucidation of the mechanism of Ca^{2+} sensitization.

We may now bring these and earlier studies together to propose that the shift to the open conformation of cNTnC is the major mechanism of Ca^{2+} sensitization by small molecules that bind cNTnC. cNTnC exists in an equilibrium between open and closed conformations. Binding of Ca^{2+} increases the population of the open conformation enough for cTnI to bind and stabilize it[22, 23]. In 2002, Wang proposed that an ideal Ca^{2+} sensitizer should "enhance the cTnC-cTnI interaction" referring to an increase in the

affinity of binding[19]. With cChimera we added that the best Ca^{2+} sensitizers should perturb switch-cTnI the least[18]. Looking back to our discussion of the A162H substitution we learned that enhancing cTnI affinity for cNTnC is one way for this mutation to enhance contraction[11]. Thus, all evidence indicates that indeed improved cTnI binding is an important effect that a contraction enhancer should have. However, with the study of i9 covalently bound to cChimera we showed that i9 promotes the open conformation to which cTnI can bind and initiate contraction independent of Ca^{2+}. This is consistent with our former hypothesis in that Ca^{2+} binds preferentially to the open conformation of cNTnC stabilized by cTnI in cChimera[18]. Thus promoting the open state of cNTnC is the main effect we should look for in a contraction enhancer prior to improving cTnI binding.

This is in agreement with the fact that some Ca^{2+} sensitizers (bepridil[19] and even i9) cause a shift in the position of swtich-cTnI away from cNTnC but still are able to enhance tension development. Although bepridil worsens the binding of cTnI by ~3.5 fold, it binds to cNTnC tight enough to keep a high population of open cNTnC to which cTnI can readily bind even if it does so with a lower affinity. For the cNTnC-i9 complex, the affinity of cTnI has not been assessed. Based on the structure of cChimera-i9 it is not impossible that i9 also worsens the binding of cTnI. Nevertheless, it has a profound effect on muscle contraction. In the case of the Ca^{2+} desensitizer W7, its low affinity for cNTnC impede the stabilization of the open conformation as the drug dissociates much more rapidly. In addition, it also decreases cTnI binding but by much more than bepridil (~13-fold). Then stronger binding of switch-cTnI to cNTnC can be considered as a secondary characteristic of contraction enhancers that target cNTnC. The fine equilibrium between the stabilization of the open state of cNTnC and cTnI binding may determine the efficacy of sensitization.

In the design of effective sensitizers I propose to finely optimize the substituents of a reversible version of i9 or bepridil to achieve stabilization of the open state of cNTnC and attraction of switch-cTnI simultaneously (see also Appendix B). One approach for this purpose is to include hydrogen-bond acceptors and donors on opposite sides of the pyrrolidine ring of bepridil or the tail of i9 to interact with cTnI and cNTnC, respectively. Another approach is to search for small molecules that bind on a second site on cNTnC. The hits can then be linked to the i9- or bepridil-like molecule to cover a larger area that may keep cNTnC open and interact with cTnI. The use of pH sensitive groups can be specific for ischemic heart disease as we have seen the importance of electrostatic interactions in cTn interactions. The task is still challenging, but research can certainly narrow down the choices of paths to follow.

And here ends our journey, in which we have tried to understand how to improve the contraction of the heart. I conclude this project optimistic that the knowledge contained here can be applied further in the development of positive inotropes that bring a real benefit to patients. For this, it is crucial to keep in mind how cardiac performance requires the finest contraction-relaxation equilibrium to

guarantee efficient work. Therefore, the scale needs to incline just enough to compensate for what the diseased heart has lost without posing a risk of outweighing the other side. I hope that like me, the reader can appreciate how balance is a delicate but crucial need at the center of proper heart functioning just as it is in life.

References

1. Pineda-Sanabria, S. E., Robertson, I. M., Li, M. X., and Sykes, B. D. (2013) Interaction between the regulatory domain of cardiac troponin C and the acidosis-resistant cardiac troponin I A162H. *Cardiovasc. Res. 97*, 481-489.

2. Robertson, I. M., Holmes, P. C., Li, M. X., Pineda-Sanabria, S. E., Baryshnikova, O. K., and Sykes, B. D. (2012) Elucidation of isoform-dependent pH sensitivity of troponin I by NMR spectroscopy. *J. Biol. Chem. 287*, 4996-5007.

3. Dargis, R., Pearlstone, J. R., Barrette-Ng, I., Edwards, H., and Smillie, L. B. (2002) Single mutation (A162H) in human cardiac troponin I corrects acid pH sensitivity of Ca^{2+}-regulated actomyosin S1 ATPase. *J. Biol. Chem. 277*, 34662-34665.

4. Day, S. M., Westfall, M. V., Fomicheva, E. V., Hoyer, K., Yasuda, S., Cross, N. C. L., D'Alecy, L.,G., Ingwall, J. S., and Metzger, J. M. (2006) Histidine button engineered into cardiac troponin I protects the ischemic and failing heart. *Nat. Med. 12*, 181-189.

5. Li, M. X., Spyracopoulos, L., and Sykes, B. D. (1999) Binding of cardiac troponin-I147-163 induces a structural opening in human cardiac troponin-C. *Biochemistry (N. Y.). 38*, 8289-8298.

6. Takeda, S., Yamashita, A., Maeda, K., and Maeda, Y. (2003) Structure of the core domain of human cardiac troponin in the Ca^{2+}-saturated form. *Nature. 424*, 35-41.

7. Vinogradova, M. V., Stone, D. B., Malanina, G. G., Karatzaferi, C., Cooke, R., Mendelson, R. A., and Fletterick, R. J. (2005) Ca^{2+}-regulated structural changes in troponin. *Proceedings of the National Academy of Sciences of the United States of America. 102*, 5038-5043.

8. Robertson, I. M., Pineda-Sanabria, S. E., Holmes, P. C., and Sykes, B. D. (2014) Conformation of the critical pH sensitive region of troponin depends upon a single residue in troponin I. *Arch. Biochem. Biophys. 552-553*, 40-49.

9. Tripet, B., Van Eyk, J. E., and Hodges, R. S. (1997) Mapping of a second actin-tropomyosin and a second troponin C binding site within the C terminus of troponin I, and their importance in the Ca^{2+}-dependent regulation of muscle contraction1. *J. Mol. Biol. 271*, 728-750.

10. Ramos, C. H. I. (1999) Mapping subdomains in the C-terminal region of troponin I involved in its binding to troponin C and to thin filament. *Journal of Biological Chemistry. 274*, 18189-18195.

11. Pineda-Sanabria, S., Robertson, I. M., and Sykes, B. D. (2015) Structure and dynamics of the acidosis-resistant A162H mutant of the switch region of troponin I bound to the regulatory domain of troponin C. *Biochemistry (N. Y.). 54*, 3583-3593.

12. Westfall, M. V., and Metzger, J. M. (2007) Single amino acid substitutions define isoform-specific effects of troponin I on myofilament Ca^{2+} and pH sensitivity. *J. Mol. Cell. Cardiol. 43*, 107-118.

13. Fentzke, R. C., Buck, S. H., Patel, J. R., Lin, H., Wolska, B. M., Stojanovic, M. O., Martin, A. F., Solaro, R. J., Moss, R. L., and Leiden, J. M. (1999) Impaired cardiomyocyte relaxation and diastolic

function in transgenic mice expressing slow skeletal troponin I in the heart. *J. Physiol. (Lond.). 517*, 143-157.

14. Palpant, N. J., D'Alecy, L. G., and Metzger, J. M. (2009) Single histidine button in cardiac troponin I sustains heart performance in response to severe hypercapnic respiratory acidosis in vivo. *The FASEB Journal. 23*, 1529-1540.

15. Solaro, R. J., Moir, A. J., and Perry, S. V. (1976) Phosphorylation of troponin I and the inotropic effect of adrenaline in the perfused rabbit heart. *Nature. 262*, 615-617.

16. Robertson, S. P., Johnson, J. D., Holroyde, M. J., Kranias, E. G., Potter, J. D., and Solaro, R. J. (1982) The effect of troponin I phosphorylation on the Ca^{2+}-binding properties of the Ca^{2+}-regulatory site of bovine cardiac troponin. *Journal of Biological Chemistry. 257*, 260-263.

17. Palpant, N. J., Houang, E. M., Delport, W., Hastings, K. E. M., Onufriev, A. V., Sham, Y. Y., and Metzger, J. M. (2010) Pathogenic peptide deviations support a model of adaptive evolution of chordate cardiac performance by troponin mutations. *Physiological Genomics. 42*, 287-299.

18. Pineda-Sanabria, S., Julien, O., and Sykes, B. D. (2014) Versatile cardiac troponin chimera for muscle protein structural biology and drug discovery. *ACS Chem. Biol. 9*, 2121-2130.

19. Wang, X., Li, M. X., and Sykes, B. D. (2002) Structure of the regulatory N-domain of human cardiac troponin C in complex with human cardiac troponin $I_{147-163}$ and bepridil. *J. Biol. Chem. 277*, 31124-31133.

20. Robertson, I. M., Sun, Y., Li, M. X., and Sykes, B. D. (2010) A structural and functional perspective into the mechanism of Ca^{2+}-sensitizers that target the cardiac troponin complex. *J. Mol. Cell. Cardiol. 49*, 1031-1041.

21. Oleszczuk, M., Robertson, I. M., Li, M. X., and Sykes, B. D. (2010) Solution structure of the regulatory domain of human cardiac troponin C in complex with the switch region of cardiac troponin I and W7: The basis of W7 as an inhibitor of cardiac muscle contraction. *J. Mol. Cell. Cardiol. 48*, 925-933.

22. Robinson, J. M., Cheung, H. C., and Dong, W. (2008) The cardiac Ca^{2+}-sensitive regulatory switch, a system in dynamic equilibrium. *Biophys. J. 95*, 4772-4789.

23. Lindert, S., Kekenes-Huskey, P., Huber, G., Pierce, L., and McCammon, J. A. (2012) Dynamics and calcium association to the N-terminal regulatory domain of human cardiac troponin C: A multiscale computational study. *J Phys Chem B. 116*, 8449-8459.

Bibliography

Abbott, M. B., Dong, W., Dvoretsky, A., DaGue, B., Caprioli, R. M., Cheung, H. C., and Rosevear, P. R. (2001) Modulation of cardiac troponin C-cardiac troponin I regulatory interactions by the amino-terminus of cardiac troponin I. *Biochemistry (N. Y.). 40*, 5992-6001.

Abusamhadneh, E., Abbott, M. B., Dvoretsky, A., Finley, N., Sasi, S., and Rosevear, P. R. (2001) Interaction of bepridil with the cardiac troponin C/troponin I complex. *FEBS Lett. 506*, 51-54.

Adhikari, B. B., and Wang, K. (2003) Interplay of troponin- and myosin-based pathways of calcium activation in skeletal and cardiac muscle: The use of W7 as an inhibitor of thin filament activation. *Biophys. J. 86*, 359-370.

Agianian, B., Krzic, U., Qiu, F., Linke, W. A., Leonard, K., and Bullard, B. (2004) A troponin switch that regulates muscle contraction by stretch instead of calcium, *EMBO J. 23*, 772-779.

Allen, D. G., and Orchard, C. H. (1987) Myocardial contractile function during ischemia and hypoxia. *Circ. Res.* 60, 153–168

Anandakrishnan, R., Aguilar, B., and Onufriev, A. V. (2012) H++3.0: automating pK prediction and the preparation of biomolecular structures for atomistic molecular modeling and simulations, *Nucleic Acids Res.40*, W537-W541.

Andrews, P. R., Craik, D. J., and Martin, J. L. (1984) Functional-Group Contributions to Drug Receptor Interactions, *J. Med. Chem. 27*, 1648-1657.

Arad M *et al.* (2005) Gene mutations in apical hypertrophic cardiomyopathy. *Circulation* 112, 2805–2811.

Austin, M. B., Bowman, M. E., Ferrer, J. L., Schroder, J., and Noel, J. P. (2004) An aldol switch discovered in stilbene synthases mediates cyclization specificity of type III polyketide synthases, *Chem. Biol. 11*, 1179-1194.

Barile, E., and Pellecchia, M. (2014) NMR-based approaches for the identification and optimization of inhibitors of protein-protein interactions. *Chem. Rev. 114*, 4749-4763.

Baryshnikova OK, Li MX, Sykes BD (2008) Modulation of cardiac troponin C function by the cardiac-specific N-terminus of troponin I: influence of PKA phosphorylation and involvement in cardiomyopathies. *J Mol Biol* 375, 735–751.

Baryshnikova, O. K. Cardiomyopathy mutations in cardiac troponin C: Functional and structural consequences. Edmonton, Alberta: University of Alberta. 2008 (Thesis).

Baryshnikova, O. K., Robertson, I. M., Mercier, P., and Sykes, B. D. (2008) Dilated cardiomyopathy G159D mutation in cardiac troponin C weakens the anchoring interaction with troponin I, *Biochemistry 47*, 10950-10960.

Baryshnikova, O. K., Williams, T. C., and Sykes, B. D. (2008) Internal pH indicators for biomolecular NMR, *J. Biomol. NMR 41*, 5-7.

Berjanskii, M. V., and Wishart, D. S. (2005) A simple method to predict protein flexibility using secondary chemical shifts. *J. Am. Chem. Soc. 127*, 14970-14971.

Bermejo, G. A., Clore, G. M., and Schwieters, C. D. (2012) Smooth statistical torsion angle potential derived from a large conformational database via adaptive kernel density estimation improves the quality of NMR protein structures. *Protein Science. 21*, 1824-1836.

Bertini, I., Donaire, A., Luchinat, C., and Rosato, A. (1997) Paramagnetic relaxation as a tool for solution structure determination: Clostridium pasteurianum ferredoxin as an example, *Proteins-Structure Function and Genetics 29*, 348-358.

Bertini, I., Fragai, M., Giachetti, A., Luchinat, C., Maletta, M., Parigi, G., and Yeo, K. J. (2005) Combining in silico tools and NMR data to validate protein-ligand structural models: Application to matrix metalloproteinases, *J. Med. Chem. 48*, 7544-7559.

Biesiadecki BJ *et al*. (2010) Removal of the cardiac troponin I N-terminal extension improves cardiac function in aged mice. *J Biol Chem* 285, 19688–19698.

Biffinger, J. C., Kim, H. W., and DiMagno, S. G. (2004) The polar hydrophobicity of fluorinated compounds, *Chembiochem 5*, 622-627.

Bjornson, M. E., Corson, D. C., and Sykes, B. D. (1985) 13Cand 113Cd NMR studies of the chelation of metal ions by the calcium-binding protein parvalbumin. *J. Inorg. Biochem*. 25, 141–149

Blanchard, E. M., and Solaro, R. J. (1984) Inhibition of the activation and troponin calcium binding of dog cardiac myofibrils by acidic pH. *Circ. Res*. 55, 382–391

Blumenschein, T. M. A., Stone, D. B., Fletterick, R. J., Mendelson, R. A., and Sykes, B. D. (2006) Dynamics of the C-terminal region of TnI in the troponin complex in solution. *Biophys. J. 90*, 2436–2444.

Blumenschein, T. M. A., Stone, D. B., Fletterick, R. J., Mendelson, R. A., and Sykes, B. D. (2005) Calcium-dependent changes in the flexibility of the regulatory domain of troponin C in the troponin complex. *J. Biol. Chem. 280*, 21924–21932.

Bonechi, C., Martini, S., Magnani, A., and Rossi, C. (2008) Stacking interaction study of trans-resveratrol (trans-3,5,4 '-trihydroxystilbene) in solution by nuclear magnetic resonance and Fourier transform infrared spectroscopy, *Magn. Reson. Chem. 46*, 625-629.

Boucher W, Laue ED, Campbell-Burk S, Domaille PJ (1992) Four-dimensional heteronuclear triple resonance NMR methods for the assignment of backbone nuclei in proteins. *J Am Chem Soc* 114, 2262–2264.

Bozoky Z *et al*. (2013) Regulatory R region of the CFTR chloride channel is a dynamic integrator of phospho-dependent intra- and intermolecular interactions. *Proc Natl Acad Sci U S A* 110, E4427–E4436.

Brenke, R., Kozakov, D., Chuang, G. Y., Beglov, D., Hall, D., Landon, M. R., Mattos, C., and Vajda, S. (2009) Fragment-based identification of druggable 'hot spots' of proteins using fourier domain correlation techniques. *Bioinformatics. 25*, 621-627.

Brown, L. J., Sale, K. L., Hills, R., Rouviere, C., Song, L., Zhang, X., and Fajer, P. G. (2002) Structure of the inhibitory region of troponin by site directed spin labeling electron paramagnetic resonance. *Proceedings of the National Academy of Sciences. 99*, 12765-12770.

Buhrman, G., O'Connor, C., Zerbe, B., Kearney, B. M., Napoleon, R., Kovrigina, E. A., Vajda, S., Kozakov, D., Kovrigin, E. L., and Mattos, C. (2011) Analysis of binding site hot spots on the surface of ras GTPase. *J. Mol. Biol. 413*, 773-789.

Bullard, B., Agianian, B., Krzic, U., Linke, W. A., and Leonard, K. R. (2004) Independent regulation of insect flight muscle by two isoforms of troponin C, *Biophys. J. 86*, 215a-216a.

Bundi, A., and Wüthrich, K. (1979) Use of amide ^{1}H-NMR titration shifts for studies of polypeptide conformation. *Biopolymers* 18, 299-311.

Bundi, A., and Wuthrich, K. (1979) H-1-NMR parameters of the common amino-acid residues measured in aqueous-solutions of the linear tetrapeptides H-Gly-Gly-X-L-Ala-OH. *Biopolymers* 18, 285–297

Buryanovskyy, L., Fu, Y., Boyd, M., Ma, Y. L., Hsieh, T. C., Wu, J. M., and Zhang, Z. T. (2004) Crystal structure of quinone reductase 2 in complex with resveratrol, *Biochemistry 43*, 11417-11426.

Camilloni C, De Simone A, Vranken WF, Vendruscolo M (2012) Determination of secondary structure populations in disordered states of proteins using nuclear magnetic resonance chemical shifts. *Biochemistry* 51, 2224–2231.

Campbell, A. P., and Sykes, B. D. (1991) Interaction of troponin I and troponin C: Use of the two-dimensional nuclear magnetic resonance transferred nuclear Overhauser effect to determine the structure of the inhibitory troponin I peptide when bound to skeletal troponin C. *J. Mol. Biol. 222*, 405-421.

Campbell, A. P., Van Eyk, J. E., Hodges, R. S., and Sykes, B. D. (1992) Interaction of troponin I and troponin C: Use of the two-dimensional transferred nuclear overhauser effect to determine the structure of a gly-110 inhibitory troponin I peptide analog when bound to cardiac troponin C. *Biochim. Biophys. Acta. 1160*, 35-54.

Cao, H., Pan, X. L., Li, C., Zhou, C., Deng, F. Y., and Li, T. H. (2003) Density functional theory calculations for resveratrol, *Bioorg. Med. Chem. Lett. 13*, 1869-1871.

Carballo S *et al*. (2009) Identification and functional characterization of cardiac troponin I as a novel disease gene in autosomal dominant dilated cardiomyopathy. *Circ Res* 105, 375–382.

Caruso, F., Tanski, J., Villegas-Estrada, A., and Rossi, M. (2004) Structural basis for antioxidant activity of trans-resveratrol: Ab initio calculations and crystal and molecular structure, *J. Agric. Food Chem. 52*, 7279-7285.

Causes of death 2008, World Health Organization, Geneva, http://www.who.int/healthinfo/ global_burden_disease/ cod_2008_sources_methods.pdf.

Cederholm, M. T., Stuckey, J. A., Doscher, M. S., and Lee, L. (1991) Histidine p*Ka* shifts accompanying the inactivating Asp-121. Asn substitution in a semisynthetic bovine pancreatic ribonuclease. *Proc. Natl. Acad. Sci. U.S.A.* 88, 8116–8120

Chandra, M., Dong, W. J., Pan, B. S., Cheung, H. C., and Solaro, R. J. (1997) Effects of protein kinase A phosphorylation on signaling between cardiac troponin I and the N-terminal domain of cardiac troponin C, *Biochemistry 36*, 13305-13311.

Cheung MS, Maguire ML, Stevens TJ, Broadhurst RW (2010) DANGLE: A Bayesian inferential method for predicting protein backbone dihedral angles and secondary structure. *J Magn Reson* 202, 223–233.

Cioffi, M., Hunter, C. A., Packer, M. J., and Spitaleri, A. (2008) Determination of protein-ligand binding modes using complexation-induced changes in H-1 NMR chemical shift, *J. Med. Chem. 51*, 2512-2517.

Cioffi, M., Hunter, C. A., Packer, M. J., Pandya, M. J., and Williamson, M. P. (2009) Use of quantitative H-1 NMR chemical shift changes for ligand docking into barnase, *J. Biomol. NMR 43*, 11-19.

Clore, G. M. (2000) Accurate and rapid docking of protein-protein complexes on the basis of intermolecular nuclear Overhauser enhancement data and dipolar couplings by rigid body minimization, *Proc. Natl. Acad. Sci. U. S. A.97*, 9021-9025.

Clore, G. M., and Iwahara, J. (2009) Theory, Practice, and Applications of Paramagnetic Relaxation Enhancement for the Characterization of Transient Low-Population States of Biological Macromolecules and Their Complexes, *Chem. Rev. 109*, 4108-4139.

Cohen, P., Griffin, J. H., Camier, M., Caizergues, M., Fromageot, P., and Cohen, J. S. (1972) Hormonal interactions at the molecular level. A high resolution proton magnetic resonance study of bovine neurophysins and their interactions with oxytocin. *FEBS Lett*. 25, 282–286

Commodari, F., Khiat, A., Ibrahimi, S., Brizius, A. R., and Kalkstein, N. (2005) Comparison of the phytoestrogen trans-resveratrol (3,4 ',5-trihydroxystilbene) structures from x-ray diffraction and solution NMR, *Magn. Reson. Chem. 43*, 567-572.

Corder, R., Douthwaite, J. A., Lees, D. M., Khan, N. Q., dos Santos, A. C. V., Wood, E. G., and Carrier, M. J. (2001) Endothelin-1 synthesis reduced by red wine - Red wines confer extra benefit when it comes to preventing coronary heart disease., *Nature 414*, 863-864.

Cornilescu, G., Delaglio, F., and Bax, A. (1999) Protein backbone angle restraints from searching a database for chemical shift and sequence homology, *J. Biomol. NMR 13*, 289-302.

Cumming, D. V. E., Seymour, A. M. L., Rix, L. K., Kellett, R., Dhoo, G. K., Yacoub, M. H. *et al*. (1995) Troponin I and T protein expression in experimental cardiac hyperthophy. *Cardioscience* 6, 65-70.

Dargis, R., Pearlstone, J. R., Barrette-Ng, I., Edwards, H., and Smillie, L. B. (2002) Single mutation (A162H) in human cardiac troponin I corrects acid pH sensitivity of Ca^{2+}-regulated actomyosin S1 ATPase. *J Biol Chem* 277, 34662-34665.

Das, D. K., and Maulik, N. (2006) Red wine and heart: A cardioprotective journey from grape to resveratrol, *Alcoholism-Clinical and Experimental Research 30*, 84a-84a.

Das, D. K., Mukherjee, S., and Ray, D. (2010) Resveratrol and red wine, healthy heart and longevity, *Heart Failure Reviews 15*, 467-477.

Davies, D. R., Mamat, B., Magnusson, O. T., Christensen, J., Haraldsson, M. H., Mishra, R., Pease, B., Hansen, E., Singh, J., Zembower, D., Kim, H., Kiselyov, A. S., Burgin, A. B., Gurney, M. E., and Stewart, L. J. (2010) Discovery of Leukotriene A4 Hydrolase Inhibitors Using Metabolomics Biased Fragment Crystallography (vol 52, pg 4694, 2009), *J. Med. Chem. 53*, 2330-2331.

Davis, J. P., Norman, C., Kobayashi, T., Solaro, R. J., Swartz, D. R., and Tikunova, S. B. (2007) Effects of thin and thick filament proteins on calcium binding and exchange with cardiac troponin C. *Biophys. J. 92*, 3195–3206.

Day, S. M., Westfall, M. V., Fomicheva, E. V., Hoyer, K., Yasuda, S., Cross, N. C. L., D'Alecy, L.,G., Ingwall, J. S., and Metzger, J. M. (2006) Histidine button engineered into cardiac troponin I protects the ischemic and failing heart. *Nat. Med. 12*, 181-189.

Day, S., Westfall, M., and Metzger, J. (2007) Tuning cardiac performance in ischemic heart disease and failure by modulating myofilament function. *J Mol Med* 85, 911-921.

De Nicola, G., Burkart, C., Qiu, F., Agianian, B., Labeit, S., Martin, S., Bullard, B., and Pastore, A. (2007) The structure of Lethocerus troponin C: Insights into the mechanism of stretch activation in muscles, *Structure 15*, 813-824.

Del Nero, J., and De Melo, C. P. (2003) Investigation of the excited states of resveratrol and related molecules, *Int. J. Quantum Chem. 95*, 213-218.

Delaglio, F., Grzesiek, S., Vuister, G. W., Zhu, G., Pfeifer, J., and Bax, A. (1995) NMRPipe: A multidimensional spectral processing system based on UNIX pipes. *J. Biomol. NMR 6*, 277–293.

Deschodt-Arsac, V., Calmettes, G., Raffard, G., Massot, P., Franconi, J., Pollesello, P., and Diolez, P. (2010) Absence of mitochondrial activation during levosimendan inotropic action in perfused paced guinea pig hearts as demonstrated by modular control analysis. *American Journal of Physiology - Regulatory, Integrative and Comparative Physiology. 299*, R786-R792.

Dominguez, C., Boelens, R., and Bonvin, A. M. J. J. (2003) HADDOCK: A protein-protein docking approach based on biochemical or biophysical information, *J. Am. Chem. Soc. 125*, 1731-1737.

Donaldson, S. K., Hermansen, L., and Bolles, L. (1978) Differential, direct effects of H^+ on Ca^{2+} activated force of skinned fibers from the soleus, cardiac, and adductor magnus muscles of rabbits. *Pflugers Arch. 376*, 55-65

Eichmuller C, Skrynnikov NR (2005) A new amide proton R1rho experiment permits accurate characterization of microsecond time-scale conformational exchange. *J Biomol NMR* 32, 281–293.

el-Saleh, S. C., and Solaro, R. J. (1988) Troponin I enhances acidic pH induced depression of Ca2_ binding to the regulatory sites in skeletal troponin C. *J. Biol. Chem.* 263, 3274–3278

Endoh, M. (2001) Mechanism of action of Ca^{2+} sensitizers--update 2001, *Cardiovasc. Drugs Ther. 15*, 397-403.

Endoh, M. (2008) Cardiac Ca^{2+} signaling and Ca^{2+} sensitizers. *Circ. J. 72*, 1915-1925.

Fabiato, A., and Fabiato, F. (1978) Effects of pH on the myofilaments and the sarcoplasmic reticulum of skinned cells from cardiac and skeletal muscles. *J. Physiol.* 276, 233–255

Farah, C. S., Miyamoto, C. A., Ramos, C. H. I., Dasilva, A. C. R., Quaggio, R. B., Fujimori, K., Smillie, L. B., and Reinach, F. C. (1994) Structural and Regulatory Functions of the Nh2- and Cooh-Terminal Regions of Skeletal-Muscle Troponin-I, *J. Biol. Chem.269*, 5230-5240.

Farman GP *et al*. (2011) Myosin head orientation: a structural determinant for the Frank-Starling relationship. *Am J Physiol Heart Circ Physiol* 300, H2155–H2160.

Farrell, D., Miranda, E. S., Webb, H., Georgi, N., Crowley, P. B., McIntosh, L. P., and Nielsen, J. E. (2010) Titration_DB. Storage and analysis of NMR monitored protein pH titration curves. *Proteins* 78, 843–857

Fentzke, R. C., Buck, S. H., Patel, J. R., Lin, H., Wolska, B. M., Stojanovic, M. O., Martin, A. F., Solaro, R. J., Moss, R. L., and Leiden, J. M. (1999) Impaired cardiomyocyte relaxation and diastolic function in transgenic mice expressing slow skeletal troponin I in the heart. *J. Physiol. (Lond.). 517*, 143-157.

Ferguson, R. E., Sun, Y. B., Mercier, P., Brack, A. S., Sykes, B. D., Corrie, J. E., Trentham, D. R., and Irving, M. (2003) In situ orientations of protein domains: Troponin C in skeletal muscle fibers. *Mol. Cell. 11*, 865-874.

Ferrer, J. L., Jez, J. M., Bowman, M. E., Dixon, R. A., and Noel, J. P. (1999) Structure of chalcone synthase and the molecular basis of plant polyketide biosynthesis, *Nat. Struct. Biol. 6*, 775-784.

Ferrieres G. *et al*. (2000) Systematic mapping of regions of human cardiac troponin I involved in binding to cardiac troponin C: N- and C-terminal low affinity contributing regions. *FEBS Lett* 479, 99–105.

Fielding, L. (2007) NMR methods for the determination of protein-ligand dissociation constants. *Prog. Nucl. Magn. Reson. Spectrosc. 51*, 219-242.

Finley, N., Abbott, M. B., Abusamhadneh, E., Gaponenko, V., Dong, W. J., Gasmi-Seabrook, G., Howarth, J. W., Rance, M., Solaro, R. J., Cheung, H. C., and Rosevear, P. R. (1999) NMR analysis of cardiac troponin C-troponin I complexes: effects of phosphorylation, *FEBS Lett. 453*, 107-112.

Forsyth, W. R., Antosiewicz, J. M., and Robertson, A. D. (2002) Empirical relationships between protein structure and carboxyl p*Ka* values in proteins. *Proteins Struct. Funct. Genet*. 48, 388–403

Fuxreiter M (2012) Fuzziness: linking regulation to protein dynamics. *Mol Biosyst* 8, 168–177.

Gagné, S. M., Tsuda, S., Li, M. X., Smillie, L. B., and Sykes, B. D. (1995) Structures of the troponin C regulatory domains in the apo and calcium-saturated states. *Nat. Struct. Biol. 2*, 784-789.

Galinska, A., Hatch, V., Craig, R., Murphy, A. M., Van Eyk, J. E., Wang, C. L. A., Lehman, W., and Foster, D. B. (2010) The C Terminus of Cardiac Troponin I Stabilizes the Ca^{2+}-Activated State of Tropomyosin on Actin Filaments, *Circ. Res.106*, 705-U148.

Gaponenko V *et al*. (1999) Effects of troponin I phosphorylation on conformational exchange in the regulatory domain of cardiac troponin C. *J Biol Chem* 274, 16681–16684.

Gasmi-Seabrook, G. M., Howarth, J. W., Finley, N., Abusamhadneh, E., Gaponenko, V., Brito, R. M., Solaro, R. J., and Rosevear, P. R. (1999) Solution structures of the C-terminal domain of cardiac troponin C free and bound to the N-terminal domain of cardiac troponin I, *Biochemistry 38*, 8313-8322.

Gay, G. L., Lindhout, D. A., and Sykes, B. D. (2004) Using lanthanide ions to align troponin complexes in solution: Order of lanthanide occupancy in cardiac troponin C, *Protein Sci. 13*, 640-651.

Gemmecker, G., Olejniczak, E. T., and Fesik, S. W. (1992) An Improved Method for Selectively Observing Protons Attached to C-12 in the Presence of H-1-C-13 Spin Pairs, *J. Magn. Reson. 96*, 199-204.

Gledhill, J. R., Montgomery, M. G., Leslie, A. G. W., and Walker, J. E. (2007) Mechanism of inhibition of bovine F-1-ATPase by resveratrol and related polyphenols, *Proc. Natl. Acad. Sci. U. S. A. 104*, 13632-13637.

Goldberg, D. M., Hahn, S. E., and Parkes, J. G. (1995) Beyond Alcohol - Beverage Consumption and Cardiovascular Mortality, *Clin. Chim. Acta 237*, 155-187.

Goldhaber, J. I., and Hamilton, M. A. (2010) Role of inotropic agents in the treatment of heart failure. *Circulation. 121*, 1655-1660.

Gomes A. V., Harada K., Potter J. D. (2005) A mutation in the N-terminus of troponin I that is associated with hypertrophic cardiomyopathy affects the Ca($2+$)-sensitivity, phosphorylation kinetics and proteolytic susceptibility of troponin. *J Mol Cell Cardiol* 39, 754–765.

Gomes, A. V., Potter, J. D., and Szczesna-Cordary, D. (2002) The role of troponins in muscle contraction, *IUBMB Life 54*, 323-333.

Gonzalez-Ruiz, D., and Gohlke, H. (2006) Targeting protein-protein interactions with small molecules: Challenges and perspectives for computational binding epitope detection and ligand finding. *Curr. Med. Chem. 13*, 2607–2625.

Gordon, A. M., Homsher, E., and Regnier, M. (2000) Regulation of contraction in striated muscle. *Physiol. Rev. 80*, 853-924.

Guntert, P. (2004) Automated NMR structure calculation with CYANA, *Methods Mol. Biol. 278*, 353-378.

Hagen, R., and Roberts, J. D. (1969) Nuclear magnetic resonance spectroscopy–13C spectra of aliphatic carboxylic acids and carboxylate anions. *J. Am. Chem. Soc.* 91, 4504–4506

Haikala, H., Kaivola, J., Nissinen, E., Wall, P., Levijoki, J., and Linden, I. B. (1995) Cardiac Troponin-C as a Target Protein for a Novel Calcium Sensitizing Drug, Levosimendan, *J. Mol. Cell. Cardiol. 27*, 1859-1866.

Haikala, H., Nissinen, E., Etemadzadeh, E., Levijoki, J., and Linden, I. B. (1995) Troponin C-Mediated Calcium Sensitization Induced by Levosimendan Does Not Impair Relaxation, *J. Cardiovasc. Pharmacol. 25*, 794-801.

Haikala, H., Nissinen, E., Etemadzadeh, E., Linden, I. B., and Pohto, P. (1992) Levosimendan Increases Calcium Sensitivity without Enhancing Myosin Atpase Activity and Impairing Relaxation, *J. Mol. Cell. Cardiol. 24*, S97-S97.

Hamdani N *et al*. (2009) Distinct myocardial effects of beta-blocker therapy in heart failure with normal and reduced left ventricular ejection fraction. *Eur Heart J* 30, 1863–1872.

Hanft LM, Biesiadecki BJ, McDonald KS (2013) Length dependence of striated muscle force generation is controlled by phosphorylation of cTnI at serines 23/24. *J Physiol* 591, 4535–4547.

Henze M *et al*. (2013) New insights into the functional significance of the acidic region of the unique N-terminal extension of cardiac troponin I. *Biochim Biophys Acta* 1833, 823–832.

Hernández, G., Blumenthal, D. K., Kennedy, M. A., Unkefer, C. J., and Trewhella, J. (1999) Troponin I inhibitory peptide (96-115) has an extended conformation when bound to skeletal muscle troponin C. *Biochemistry (N. Y.)*. *38*, 6911-6917.

Herzberg, O., and James, M. N. (1988) Refined crystal structure of troponin C from turkey skeletal muscle at 2.0 A resolution. *J. Mol. Biol*. *203*, 761-779.

Herzberg, O., and James, M. N. G. (1985) Structure of the Calcium Regulatory Muscle Protein Troponin-C at 2.8-a Resolution, *Nature 313*, 653-659.

Hidaka, H., Yamaki, T., Naka, M., Tanaka, T., Hayashi, H., and Kobayashi, R. (1980) Calcium-regulated modulator protein interacting agents inhibit smooth muscle calcium-stimulated protein kinase and ATPase. *Mol. Pharmacol*. *17*, 66-72.

Hinken AC *et al*. (2012) Protein kinase C depresses cardiac myocyte power output and attenuates myofilament responses induced by protein kinase A. *J Muscle Res Cell Motil* 33, 439–448.

Hoffman, R. M. B., and Sykes, B. D. (2009) Structure of the Inhibitor W7 Bound to the Regulatory Domain of Cardiac Troponin C, *Biochemistry 48*, 5541-5552.

Hoffman, R. M. B., Li, M. X., and Sykes, B. D. (2005) The binding of W7, an inhibitor of striated muscle contraction, to cardiac troponin C. *Biochemistry 44*, 15750–15759.

Hoffman, R. M., Blumenschein, T. M., and Sykes, B. D. (2006) An interplay between protein disorder and structure confers the Ca^{2+} regulation of striated muscle, *J. Mol. Biol.361*, 625-633.

Hoffman, R. M., Li, M. X., and Sykes, B. D. (2005) The binding of W7, an inhibitor of striated muscle contraction, to cardiac troponin C. *Biochemistry 44*, 15750–15759

Holme, A. L., and Pervaiz, S. (2007) Resveratrol in cell fate decisions, *J. Bioenerg. Biomembr*. *39*, 59-63.

Holmes, K. C., Angert, I., Kull, F. J., Jahn, W., and Schroder, R. R. (2003) Electron cryo-microscopy shows how strong binding of myosin to actin releases nucleotide, *Nature425*, 423-427.

Hopkins, A. L., Groom, C. R., and Alex, A. (2004) Ligand efficiency: a useful metric for lead selection, *Drug Discov. Today 9*, 430-431.

Horsley, W. J., and Sternlicht, H. (1968) Carbon-13 magnetic resonance studies of amino acids and peptides. *J. Am. Chem. Soc*. 90, 3738–3748

Houdusse, A., Love, M. L., Dominguez, R., Grabarek, Z., and Cohen, C. (1997) Structures of four Ca^{2+}-bound troponin C at 2.0 A resolution: Further insights into the Ca^{2+}-switch in the calmodulin superfamily. *Structure*. *5*, 1695-1711.

Howarth, J. W., Meller, J., Solaro, R. J., Trewhella, J., and Rosevear, P. R. (2007) Phosphorylation-dependent conformational transition of the cardiac specific N-extension of troponin I in cardiac troponin. *J. Mol. Biol*. *373*, 706-722.

Huang, X., Lee, K. J., Beth, R., Zhang, C., Lemanski, L. F., and Walker, J. W. (2000) Thyroid hormone regulates slow skeletal troponin I gene inactivation in cardiac troponin I null mouse hearts. *J Mol Cell Cardiol* 32, 2221-2228.

Huey, R., Morris, G. M., Olson, A. J., and Goodsell, D. S. (2007) A semiempirical free energy force field with charge-based desolvation, *Journal of Computational Chemistry 28*, 1145-1152.

Hwang PM, Pan JS, Sykes BD (2012) A PagP fusion protein system for the expression of intrinsically disordered proteins in Escherichia coli. *Protein Expr Purif* 85, 148–151.

Hwang, P. M., and Sykes, B. D. (2015) Targeting the sarcomere to correct muscle function. *Nat. Rev. Drug Discov. 14*, 313-328.

Hwang, P. M., Cai, F., Pineda-Sanabria, S. E., Corson, D. C., and Sykes, B. D. (2014) The cardiac-specific N-terminal region of troponin I positions the regulatory domain of troponin C. *Proceedings of the National Academy of Sciences. 111*, 14412-14417.

Iakoucheva LM *et al.* (2004) The importance of intrinsic disorder for protein phosphorylation. *Nucleic Acids Res* 32, 1037–1049.

Ikura, M., and Bax, A. (1992) Isotope-Filtered 2d Nmr of a Protein Peptide Complex - Study of a Skeletal-Muscle Myosin Light Chain Kinase Fragment Bound to Calmodulin, *J. Am. Chem. Soc.114*, 2433-2440.

Ivetac, A., and Andrew McCammon, J. (2010) Mapping the druggable allosteric space of G-protein coupled receptors: A fragment-based molecular dynamics approach. *Chemical Biology & Drug Design. 76*, 201-217.

Jackson, S. E., and Fersht, A. R. (1993) Contribution of long range electrostatic interactions to the stabilization of the catalytic transition state of the serine protease subtilisin BPN. *Biochemistry* 32, 13909–13916

Jang, M. S., Cai, E. N., Udeani, G. O., Slowing, K. V., Thomas, C. F., Beecher, C. W. W., Fong, H. H. S., Farnsworth, N. R., Kinghorn, A. D., Mehta, R. G., Moon, R. C., and Pezzuto, J. M. (1997) Cancer chemopreventive activity of resveratrol, a natural product derived from grapes, *Science 275*, 218-220.

Jayatilake, G. S., Jayasuriya, H., Lee, E. S., Koonchanok, N. M., Geahlen, R. L., Ashendel, C. L., Mclaughlin, J. L., and Chang, C. J. (1993) Kinase Inhibitors from Polygonum-Cuspidatum, *J. Nat. Prod. 56*, 1805-1810.

Jennings, R., and Reimer, K. (1991) The cell biology of acute myocardial-ischemia. *Annu. Rev. Med. 42*, 225-246.

John, M., Pintacuda, G., Park, A. Y., Dixon, N. E., and Otting, G. (2006) Structure determination of protein-ligand complexes by transferred paramagnetic shifts, *J. Am. Chem. Soc. 128*, 12910-12916.

Johnson, B. A., and Blevins, R. A. (1994) NMR view: A computer program for the visualization and analysis of NMR data. *J. Biomol. NMR 4*, 603–614.

Julien, O., Mercier, P., Allen, C. N., Fisette, O., Ramos, C. H., Lague, P., Blumenschein, T. M., and Sykes, B. D. (2011) Is there nascent structure in the intrinsically disordered region of troponin I? *Proteins Struct. Funct. Bioinformatics* 79, 1240–1250

Karplus, M. (1959) Contact Electron-Spin Coupling of Nuclear Magnetic Moments, *J. Chem. Phys. 30*, 11-15.

Kass, D. A., and Solaro, R. J. (2006) Mechanisms and use of calcium-sensitizing agents in the failing heart, *Circulation 113*, 305-315.

Kirkpatrick, K. P., Robertson, A. S., Klaiman, J. M., and Gillis, T. E. (2011) The influence of trout cardiac troponin I and PKA phosphorylation on the Ca^{2+} affinity of the cardiac troponin complex, *J. Exp. Biol.214*, 1981-1988.

Kischel, P., Bastide, B., Potter, J. D., and Mounier, Y. (2000) The role of the $Ca(^{2+})$ regulatory sites of skeletal troponin C in modulating muscle fibre reactivity to the $Ca(^{2+})$ sensitizer bepridil. *Br. J. Pharmacol. 131*, 1496–1502.

Klabunde, T., Petrassi, H. M., Oza, V. B., Raman, P., Kelly, J. W., and Sacchettini, J. C. (2000) Rational design of potent human transthyretin amyloid disease inhibitors, *Nat. Struct. Biol. 7*, 312-321.

Kleerekoper, Q., and Putkey, J. A. (1999) Drug binding to cardiac troponin C, *J. Biol. Chem. 274*, 23932-23939.

Kleerekoper, Q., Liu, W., Choi, D., and Putkey, J. A. (1998) Identification of binding sites for bepridil and trifluoperazine on cardiac troponin C, *J. Biol. Chem. 273*, 8153-8160.

Kleywegt, G. J., Zou, J.Y., Kjeldgaard, M., Jones, T.A., Around O. (2001) International Tables for Crystallography, Vol. F. Crystallography of Biological Macromolecules, (Rossmann, M. G., Arnold, E., Ed.), pp 353-356, 366-367, Dordrecht: Kluwer Academic Publishers, The Netherlands. .

Knowles, A. C., Irving, M., and Sun, Y. (2012) Conformation of the troponin core complex in the thin filaments of skeletal muscle during relaxation and active contraction. *J. Mol. Biol. 421*, 125-137.

Kobayashi, T., and Solaro, R. J. (2005) Calcium, thin filaments, and the integrative biology of cardiac contractility. *Annu. Rev. Physiol. 67*, 39-67.

Kobayashi, T., Jin, L., and de Tombe, P. (2008) Cardiac thin filament regulation. *Pflügers Arch. 457*, 37-46.

Koh, D., Park, K. H., Jung, J., Yang, H., Mok, K. H., and Lim, Y. (2001) Complete assignment of the H-1 and C-13 NMR spectra of resveratrol derivatives, *Magn. Reson. Chem. 39*, 768-770.

Kopp, P. (1998) Resveratrol, a phytoestrogen found in red wine. A possible explanation for the conundrum of the 'French paradox'?, *Eur. J. Endocrinol. 138*, 619-620.

Krishnamoorthy, J., Yu, V. C. K., and Mok, Y. K. (2010) Auto-FACE: An NMR Based Binding Site Mapping Program for Fast Chemical Exchange Protein-Ligand Systems, *PLoS ONE 5*, -.

Kuntz, I. D., Chen, K., Sharp, K. A., and Kollman, P. A. (1999) The maximal affinity of ligands, *Proc. Natl. Acad. Sci. U. S. A. 96*, 9997-10002.

Kuszewski, J., Gronenborn, A. M., and Clore, G. M. (1997) Improvements and extensions in the conformational database potential for the refinement of NMR and X-ray structures of proteins and nucleic acids, *J. Magn. Reson.125*, 171-177.

Kuszewski, J., Gronenborn, A. M., and Clore, G. M. (1999) Improving the packing and accuracy of NMR structures with a pseudopotential for the radius of gyration, *J. Am. Chem. Soc.121*, 2337-2338.

Kuwahara, K., Nishikimi, T., and Nakao, K. (2012) Transcriptional regulation of the fetal cardiac gene program. *J Pharmacol Sci* 119, 198-203.

Landon, M. R., Lieberman, R. L., Hoang, Q. Q., Ju, S., Caaveiro, J. M., Orwig, S. D., Kozakov, D., Brenke, R., Chuang, G., Beglov, D., Vajda, S., Petsko, G. A., and Ringe, D. (2009) Detection of ligand binding hot spots on protein surfaces via fragment-based methods: Application to DJ-1 and glucocerebrosidase. *Journal of Computer Aided-Molecular Design. 23*, 491-500.

Landstrom, A. P., Parvatiyar, M. S., Pinto, J. R., Marquardt, M. L., Bos, J. M., Tester, D. J., Ornmen, S. R., Potter, J. D., and Ackerman, M. J. (2008) Molecular and functional characterization of novel hypertrophic cardiomyopathy susceptibility mutations in TNNC1-encoded troponin C, *J. Mol. Cell. Cardiol. 45*, 281-288.

Langcake, P., and Pryce, R. J. (1976) Production of Resveratrol by Vitis-Vinifera and Other Members of Vitaceae as a Response to Infection or Injury, *Physiol. Plant Pathol. 9*, 77-86.

Laskowski, R. A., Rullmann, J. A. C., MacArthur, M. W., Kaptein, R., and Thornton, J. M. (1996) AQUA and PROCHECK-NMR: Programs for checking the quality of protein structures solved by NMR, *J. Biomol. NMR 8*, 477-486.

Lassalle, M. W. (2010) Defective dynamic properties of human cardiac troponin mutations. *Biosci. Biotechnol. Biochem. 74*, 82–91.

Lee, J. A., and Allen, D. G. (1991) Mechanisms of acute ischemic contractile failure of the heart. Role of intracellular calcium. *J Clin Invest. 88*, 361-367.

Lee, W., Revington, M. J., Arrowsmith, C., and Kay, L. E. (1994) A Pulsed-Field Gradient Isotope-Filtered 3d C-13 Hmqc-Noesy Experiment for Extracting Intermolecular Noe Contacts in Molecular-Complexes, *FEBS Lett. 350*, 87-90.

Lekli, I., Ray, D., and Das, D. K. (2010) Longevity nutrients resveratrol, wines and grapes, *Genes and Nutrition 5*, 55-60.

Leopoldini, M., Marino, T., Russo, N., and Toscano, M. (2004) Antioxidant properties of phenolic compounds: H-atom versus electron transfer mechanism, *J. Phys. Chem. A 108*, 4916-4922.

Levijoki, J., Pollesello, P., Kaivola, J., Tilgmann, C., Sorsa, T., Annila, A., Kilpeläinen, I., and Haikala, H. (2000) Further evidence for the cardiac troponin C mediated calcium sensitization by levosimendan: Structure-response and binding analysis with analogs of levosimendan. *J. Mol. Cell. Cardiol. 32*, 479-491.

Li, G., Martin, A. F., and Solaro, J. R. (2001) Localization of regions of troponin I important in deactivation of cardiac myofilaments by acidic pH. *J. Mol. Cell. Cardiol. 33*, 1309-1320.

Li, M. X., Gagné, S. M., Spyracopoulos, L., Kloks, C. P. A. M., Audette, G., Chandra, M., Solaro, R. J., Smillie, L. B., and Sykes, B. D. (1997) NMR studies of Ca^{2+} binding to the regulatory domains of cardiac and E41A skeletal muscle troponin C reveal the importance of site I to energetics of the induced structural changes. Biochemistry 36, 12519–12525.

Li, M. X., Gagné, S. M., Tsuda, S., Kay, C. M., Smillie, L. B., and Sykes, B. D. (1995) Calcium binding to the regulatory N-domain of skeletal muscle troponin C occurs in a stepwise manner. *Biochemistry. 34*, 8330–8340.

Li, M. X., Hoffman, R. M. B., and Sykes, B. D. (2006) Interaction of cardiac troponin C and troponin I with W7 in the presence of three functional regions of cardiac troponin I. *Biochemistry 45*, 9833–9840.

Li, M. X., Robertson, I. M., and Sykes, B. D. (2008) Interaction of cardiac troponin with cardiotonic drugs: A structural perspective. *Biochem. Biophys. Res. Commun. 369*, 88-99.

Li, M. X., Saude, E. J., Wang, X., Pearlstone, J. R., Smillie, L. B., and Sykes, B. D. (2002) Kinetic studies of calcium and cardiac troponin I peptide binding to human cardiac troponin C using NMR spectroscopy. *Eur. Biophys. J. 31*, 245–256

Li, M. X., Spyracopoulos, L., and Sykes, B. D. (1999) Binding of cardiac troponin-I$_{147-163}$ induces a structural opening in human cardiac troponin-C. *Biochemistry 38*, 8289-8298.

Li, M. X., Spyracopoulos, L., Beier, N., Putkey, J. A., and Sykes, B. D. (2000) Interaction of cardiac troponin C with Ca^{2+} sensitizer EMD 57033 and cardiac troponin I inhibitory peptide. *Biochemistry 39*, 8782-8790.

Li, M. X., Wang, X., and Sykes, B. D. (2004) Structural based insights into the role of troponin in cardiac muscle pathophysiology, *J. Muscle Res. Cell Motil. 25*, 559-579.

Li, S., and Hong, M. (2011) Protonation, tautomerization, and rotameric structure of histidine: A comprehensive study by magic-angle-spinning solid-state NMR. *JACS* 133, 1534-1544.

Li, Y., Love, M. L., Putkey, J. A., and Cohen, C. (2000) Bepridil opens the regulatory N-terminal lobe of cardiac troponin C, *Proc. Natl. Acad. Sci. U. S. A.97*, 5140-5145.

Liew, R., Stagg, M. A., MacLeod, K. T., and Collins, P. (2005) The red wine polyphenol, resveratrol, exerts acute direct actions on guinea-pig ventricular myocytes, *Eur. J. Pharmacol. 519*, 1-8.

Lin, X., Krudy, G. A., Howarth, J., Brito, R. M. M., Rosevear, P. R., and Putkey, J. A. (1994) Assignment and Calcium-Dependence of Methionyl Epsilon-C and Epsilon-H Resonances in Cardiac Troponin-C, *Biochemistry 33*, 14434-14442.

Lindert, S., Kekenes-Huskey, P., Huber, G., Pierce, L., and McCammon, J. A. (2012) Dynamics and calcium association to the N-terminal regulatory domain of human cardiac troponin C: A multiscale computational study. *J Phys Chem B. 116*, 8449-8459.

Lindhout, D. A., and Sykes, B. D. (2003) Structure and dynamics of the C-domain of human cardiac troponin C in complex with the inhibitory region of human cardiac troponin I, *J. Biol. Chem. 278*, 27024-27034.

Linge, J. P., Williams, M. A., Spronk, C. A. E. M., Bonvin, A. M. J. J., and Nilges, M. (2003) Refinement of protein structures in explicit solvent, *Proteins-Structure Function and Bioinformatics 50*, 496-506.

Linse, S., Helmersson, A., and Forsén, S. (1991) Calcium binding to calmodulin and its globular domains. *J. Biol. Chem. 266*, 8050–8054.

Liou, Y. M., and Chang, J. C. (2004) Differential pH effect on calciuminduced conformational changes of cardiac troponin C complexed with cardiac and fast skeletal isoforms of troponin I and troponin T. *J. Biochem*. 136, 683–692

Liou, Y. M., Kuo, S. C., and Hsieh, S. R. (2008) Differential effects of a green tea-derived polyphenol (-)-epigallocatechin-3-gallate on the acidosis-induced decrease in the Ca^{2+} sensitivity of cardiac and skeletal muscle, *Pflugers Arch. 456*, 787-800.

Lipari G, Szabo A (1982) Model-free approach to the interpretation of nuclear macnetic resonance relaxation in macromolecules. 1. Theory and range of validity. *J Am Chem Soc* 104, 4546–4559.

Lipinski, C. A., Lombardo, F., Dominy, B. W., and Feeney, P. J. (1997) Experimental and computational approaches to estimate solubility and permeability in drug discovery and development settings, *Adv. Drug Delivery Rev. 23*, 3-25.

Lykkesfeldt, J. (2000) Determination of ascorbic acid and dehydroascorbic acid in biological samples by high-performance liquid chromatography using subtraction methods: Reliable reduction with tris[2-carboxyethyl] phosphine hydrochloride, *Anal. Biochem. 282*, 89-93.

M. J. Frisch, G. W. T., H. B. Schlegel, G. E. Scuseria, M. A. Robb, J. R. Cheeseman, J. A. Montgomery, Jr., T. Vreven, K. N. Kudin, J. C. Burant, J. M. Millam, S. S. Iyengar, J. Tomasi, V. Barone, B. Mennucci, M. Cossi, G. Scalmani, N. Rega, G. A. Petersson, H. Nakatsuji, M. Hada, M. Ehara, K. Toyota, R. Fukuda, J. Hasegawa, M. Ishida, T. Nakajima, Y. Honda, O. Kitao, H. Nakai, M. Klene, X. Li, J. E. Knox, H. P. Hratchian, J. B. Cross, V. Bakken, C. Adamo, J. Jaramillo, R. Gomperts, R. E. Stratmann, O. Yazyev, A. J. Austin, R. Cammi, C. Pomelli, J. W. Ochterski, P. Y. Ayala, K. Morokuma, G. A. Voth, P. Salvador, J. J. Dannenberg, V. G. Zakrzewski, S. Dapprich, A. D. Daniels, M. C. Strain, O. Farkas, D. K. Malick, A. D. Rabuck, K. Raghavachari, J. B. Foresman, J. V. Ortiz, Q. Cui, A. G. Baboul, S. Clifford, J. Cioslowski, B. B. Stefanov, G. Liu, A. Liashenko, P. Piskorz, I. Komaromi, R. L. Martin, D. J. Fox, T. Keith, M. A. Al-Laham, C. Y. Peng, A. Nanayakkara, M. Challacombe, P. M. W. Gill, B. Johnson, W. Chen, M. W. Wong, C. Gonzalez, and J. A. Pople. (2004) Gaussian 03: Gaussian 03 ed., Gaussian, Inc., Wallingford CT.

Maciel, G. E., and Natterstad, J. J. (1965) Carbon-13 chemical shifts of carbonyl group. III. Solvent effects. *J. Chem. Phys.* 42, 2752–2759

Maciel, G. E., and Traficante, D. D. (1966) Carbon-13 chemical shifts of carbonyl group. IV. Dilution curves for acetic acid in representative solvents. *J. Am. Chem. Soc*. 88, 220–223

Macomber, R. S. (1992) An introduction to NMR titration for studying rapid reversible complexation. *J. Chem. Educ. 69*, 375.

Makinde, A. O., Kantor, P. F., and Lopaschuk, G. D. (1998) Maturation of fatty acid and carbohydrate metabolism in the newborn heart, *Mol. Cell. Biochem.188*, 49-56.

Markley, J. L. (1975) Observation of histidine residues in proteins by means of nuclear magnetic-resonance spectroscopy. *Acc. Chem. Res*. 8, 70-80

Markley, J. L., Williams, M. N., and Jardetzky, O. (1970) Nuclear magnetic resonance studies of the structure and binding sites of enzymes. XII. A conformational equilibrium in staphylococcal nuclease involving a histidine residue. *Proc. Natl. Acad. Sci. U.S.A.* 65, 645–651

Marsden, B. J., Hodges, R. S., and Sykes, B. D. (1988) H-1-Nmr Studies of Synthetic Peptide Analogs of Calcium-Binding Site-Iii of Rabbit Skeletal Troponin-C - Effect on the Lanthanum Affinity of the Interchange of Aspartic-Acid and Asparagine Residues at the Metal-Ion Coordinating Positions, *Biochemistry 27*, 4198-4206.

Martin, S. R., Biekofsky, R. R., Skinner, M. A., Guerrini, R., Salvadori, S., Feeney, J., and Bayley, P. M. (2004) Interaction of calmodulin with the phosphofructokinase target sequence. *FEBS Lett*. 577, 284–288

Marti-Renom, M. A., Stuart, A. C., Fiser, A., Sanchez, R., Melo, F., and Sali, A. (2000) Comparative protein structure modeling of genes and genomes. Annu. Rev. Biophys. Biomol. Struct. 29, 291–325.

Mateja RD, de Tombe PP (2012) Myofilament length-dependent activation develops within 5 ms in guinea-pig myocardium. *Biophys J* 103, L13–L15.

Mayer, R., Lancelot, G., and Spach, G. (1979) Side chain-backbone hydrogen bonds in peptides containing glutamic acid residues. *Biopolymers* 18, 1293-1296.

McCann, P., and Hauptman, P. J. (2012) Inotropic therapy: An important role in the treatment of advanced symptomatic heart failure. *Med. Clin. North Am. 96*, 943-954.

McCoy, M. A., and Wyss, D. F. (2002) Spatial localization of ligand binding sites from electron current density surfaces calculated from NMR chemical shift perturbations, *J. Am. Chem. Soc. 124*, 11758-11763.

McKay, R. T., Tripet, B. P., Pearlstone, J. R., Smillie, L. B., and Sykes, B. D. (1999) Defining the region of troponin-I that binds to troponin-C. *Biochemistry 38*, 5478–5489

McMurray, J. J. V., Packer, M., Desai, A. S., Gong, M. P. H., Lefkowitz, M. P., Rizkala, A. R., …, Zile, M. R. (2014) Angiotensin-neprilysin inhibition versus enalapril in heart failure. *N Engl J Med*. 371, 993-1004.

Memo M *et al*. (2013) Familial dilated cardiomyopathy mutations uncouple troponin I phosphorylation from changes in myofibrillar Ca(2)(+) sensitivity. *Cardiovasc Res* 99, 65–73.

Mercier, P., Ferguson, R. E., Irving, M., Corrie, J. E. T., Trentham, D. R., and Sykes, B. D. (2003) NMR structure of a bifunctional rhodamine labeled N-domain of troponin C complexed with the regulatory "switch" peptide from troponin I: Implications for in situ fluorescence studies in muscle fibers, *Biochemistry42*, 4333-4348.

Metra, M., Bettari, L., Carubelli, V., and Cas, L. D. (2011) Old and new intravenous inotropic agents in the treatment of advanced heart failure. *Prog. Cardiovasc. Dis. 54*, 97-106.

Metra, M., Bettari, L., Carubelli, V., Bugatti, S., Dei Cas, A., Del Magro, F., Lazzarini, V., Lombardi, C., and Dei Cas, L. (2011) Use of inotropic agents in patients with advanced heart failure. *Drugs. 71*, 515-525.

Metzger, J. M., and Westfall, M. V. (2004) Covalent and noncovalent modification of thin filament action. *Circulation Research. 94*, 146-158.

Mirza, M., Marston, S., Willott, R., Ashley, C., Mogensen, J., McKenna, W., Robinson, P., Redwood, C., and Watkins, H. (2005) Dilated cardiomyopathy mutations in three thin filament regulatory proteins result in a common functional phenotype, *J. Biol. Chem. 280*, 28498-28506.

Mittag T *et al.* (2008) Dynamic equilibrium engagement of a polyvalent ligand with a single-site receptor. *Proc Natl Acad Sci U S A* 105, 17772–17777.

Morelli, X., Bourgeas, R., and Roche, P. (2011) Chemical and structural lessons from recent successes in protein–protein interaction inhibition (2P2I). *Curr. Opin. Chem. Biol. 15*, 475–481.

Moreno, N., Tavares-Silva, M., Lourenco, A. P., Oliveira-Pinto, J., Henriques-Coelho, T., and Leite-Moreira, A. F. (2014) Levosimendan: The current situation and new prospects. *Rev. Port. Cardiol. 33*, 795-800.

Morris, G. M., Goodsell, D. S., Halliday, R. S., Huey, R., Hart, W. E., Belew, R. K., and Olson, A. J. (1998) Automated docking using a Lamarckian genetic algorithm and an empirical binding free energy function, *J. Comput. Chem. 19*, 1639-1662.

Morris, G. M., Goodsell, D. S., Huey, R., and Olson, A. J. (1996) Distributed automated docking of flexible ligands to proteins: Parallel applications of AutoDock 2.4, *J. Comput. Aided Mol. Des. 10*, 293-304.

Morris, G. M., Huey, R., Lindstrom, W., Sanner, M. F., Belew, R. K., Goodsell, D. S., and Olson, A. J. (2009) AutoDock4 and AutoDockTools4: Automated Docking with Selective Receptor Flexibility, *J. Comput. Chem. 30*, 2785-2791.

Moyna, G., Zauhar, R. J., Williams, H. J., Nachman, R. J., and Scott, A. I. (1998) Comparison of ring current methods for use in molecular modeling refinement of NMR derived three-dimensional structures, *J. Chem. Inf. Comput. Sci. 38*, 702-709.

Nelson, D. J., Theoharides, A. D., Nieburgs, A. C., Murray, R. K., GonzalezFernandez, F., and Brenner, D. S. (1979) C-13 magnetic-resonance study of lanthanide-substituted muscle calcium-binding parvalbumins. *Int. J. Quantum Chem.* 16, 159–174

Nichols, J. A., and Katiyar, S. K. (2010) Skin photoprotection by natural polyphenols: anti-inflammatory, antioxidant and DNA repair mechanisms, *Archives of Dermatological Research 302*, 71-83.

Niwano, S., and Tojo, T. (2010) Systemic acidosis in acute myocardial ischemia; – cause or result of life-threatening ventricular arrhythmia? –. *Circulation Journal. 74*, 1794-1795.

Oda, Y., Yamazaki, T., Nagayama, K., Kanaya, S., Kuroda, Y., and Nakamura, H. (1994) Individual ionization constants of all the carboxyl groups in ribonuclease HI from *Escherichia coli* determined by NMR. *Biochemistry* 33, 5275–5284

Ogura, K., Terasawa, H., and Inagaki, F. (1996) An improved double-tuned and isotope-filtered pulse scheme based on a pulsed field gradient and a wide-band inversion shaped pulse, *J. Biomol. NMR 8*, 492-498.

Ohtsuki, I. (2007) Troponin: Structure, Function and Dysfunction, in (S. Ebashi, and I. Ohtsuki, Eds.) pp 21-36, Springer Japan.

Oleszczuk, M., Robertson, I. M., Li, M. X., and Sykes, B. D. (2010) Solution structure of the regulatory domain of human cardiac troponin C in complex with the switch region of cardiac troponin I and W7: The basis of W7 as an inhibitor of cardiac muscle contraction. *J. Mol. Cell. Cardiol. 48*, 925-933.

Overington, J. P., Al-Lazikani, B., and Hopkins, A. L. (2006) How many drug targets are there? *Nat Rev Drug Discov. 5*, 993–996.

Palpant, N. J., D'Alecy, L. G., and Metzger, J. M. (2009) Single histidine button in cardiac troponin I sustains heart performance in response to severe hypercapnic respiratory acidosis in vivo. *The FASEB Journal. 23*, 1529-1540.

Palpant, N. J., Day, S. M., Herron, T. J., Converso, K. L., and Metzger, J. M. (2008) Single histidine-substituted cardiac troponin I confers protection from age-related systolic and diastolic dysfunction. Cardiovasc. Res. 80, 209-218

Palpant, N. J., Houang, E. M., Delport, W., Hastings, K. E. M., Onufriev, A. V., Sham, Y. Y. *et al*. (2010) Pathogenic peptide deviations support a model of adaptive evolution of chordate cardiac performance by troponin mutations. *Physiol Genomics 42*, 287-299.

Palpant, N. J., Houang, E. M., Sham, Y. Y., and Metzger, J. M. (2012) pH-responsive titratable inotropic performance of histidine-modified cardiac troponin I, *Biophys. J.102*, 1570-1579.

Pan, B. S., and Johnson, R. G. (1996) Interaction of cardiotonic thiadiazinone derivatives with cardiac troponin C, *J. Biol. Chem. 271*, 817-823.

Pan, B. S., and Solaro, R. J. (1987) Calcium-binding properties of troponin C in detergent-skinned heart muscle fibers. *J. Biol. Chem. 262*, 7839–7849.

Papp, Z., Csapó, K., Pollesello, P., Haikala, H., and Édes, I. (2005) Pharmacological mechanisms contributing to the clinical efficacy of levosimendan. *Cardiovasc. Drug Rev. 23*, 71-98.

Papp, Z., Édes, I., Fruhwald, S., De Hert, S. G., Salmenperä, M., Leppikangas, H., Mebazaa, A., Landoni, G., Grossini, E., Caimmi, P., Morelli, A., Guarracino, F., Schwinger, R. H. G., Meyer, S., Algotsson, L., Wikström, B. G., Jörgensen, K., Filippatos, G., Parissis, J. T., González, M. J. G., Parkhomenko, A., Yilmaz, M. B., Kivikko, M., Pollesello, P., and Follath, F. (2012) Levosimendan: Molecular mechanisms and clinical implications: Consensus of experts on the mechanisms of action of levosimendan. *Int. J. Cardiol. 159*, 82–87.

Parmacek, M. S., and Solaro, R. J. (2004) Biology of the troponin complex in cardiac myocytes, *Prog. Cardiovasc. Dis. 47*, 159-176.

Parsons, B., Szczesna, D., Zhao, J., Van Slooten, G., Kerrick, W. G., Putkey, J. A., and Potter, J. D. (1997) The effect of pH on the Ca2_ affinity of the Ca2_ regulatory sites of skeletal and cardiac troponin C in skinned muscle fibers. *J. Muscle Res. Cell Motil*. 18, 599–609

Pathak, A., Lebrin, M., Vaccaro, A., Senard, J. M., and Despas, F. (2013) Pharmacology of levosimendan: Inotropic, vasodilatory and cardioprotective effects. *J. Clin. Pharm. Ther. 38*, 341-349.

Pierrakos, C., Velissaris, D., Franchi, F., Muzzi, L., Karanikolas, M., and Scolletta, S. (2013) Levosimendan in critical illness: A literature review. *Journal of Clinical Medicine Research. 6*, 75-85.

Pierson, E. S., Miller, D. D., Callaham, D. A., Shipley, A. M., Rivers, B. A., Cresti, M., and Hepler, P. K. (1994) Pollen tube growth is coupled to the extracellular calcium ion flux and the intracellular calcium gradient: Effect of BAPTA-type buffers and hypertonic media. *Plant Cell. 6*, 1815–1828.

Pineda-Sanabria, S. E., Robertson, I. M., Li, M. X., and Sykes, B. D. (2013) Interaction between the regulatory domain of cardiac troponin C and the acidosis-resistant cardiac troponin I A162H, *Cardiovasc. Res.97*, 481-489.

Pineda-Sanabria, S., Julien, O., and Sykes, B. D. (2014) Versatile cardiac troponin chimera for muscle protein structural biology and drug discovery. *ACS Chem. Biol. 9*, 2121-2130.

Pineda-Sanabria, S., Robertson, I. M., and Sykes, B. D. (2015) Structure and dynamics of the acidosis-resistant A162H mutant of the switch region of troponin I bound to the regulatory domain of troponin C. *Biochemistry (N. Y.). 54*, 3583-3593.

Pintacuda, G., John, M., Su, X. C., and Otting, G. (2007) NMR structure determination of protein-ligand complexes by lanthanide labeling, *Acc. Chem. Res. 40*, 206-212.

Pirani, A., Vinogradova, M. V., Curmi, P. M., King, W. A., Fletterick, R. J., Craig, R., Tobacman, L. S., Xu, C., Hatch, V., and Lehman, W. (2006) An atomic model of the thin filament in the relaxed and Ca^{2+}-activated states, *J. Mol. Biol.357*, 707-717.

Pollesello, P., and Nore, P. (2003) Complete structure analysis of OR-1746, a complex product of cyclocondensation of arylhydrazomalononitriles containing clusters of protonated and unprotonated nitrogens, by pulsed-field-gradient heteronuclear NMR. *J. Pharm. Biomed. Anal. 31*, 125-131.

Porumb, T., Yau, P., Harvey, T. S., and Ikura, M. (1994) A calmodulin-target peptide hybrid molecule with unique calcium-binding properties. *Protein Eng. 7*, 109-115.

Ramos, C. H. I. (1999) Mapping subdomains in the C-terminal region of troponin I involved in its binding to troponin C and to thin filament, *J. Biol. Chem. 274*, 18189-18195.

Rarick, H. M., Tu, X. H., Solaro, R. J., and Martin, A. F. (1997) The C terminus of cardiac troponin I is essential for full inhibitory activity and Ca^{2+} sensitivity of rat myofibrils, *J. Biol. Chem. 272*, 26887-26892.

Ray, P. S., Maulik, G., Cordis, G. A., Bertelli, A. A. E., Bertelli, A., and Das, D. K. (1999) The red wine antioxidant resveratrol protects isolated rat hearts from ischemia reperfusion injury, *Free Radical Biology and Medicine 27*, 160-169.

Rees, D. C. (1980) Experimental evaluation of the effective dielectric constant of proteins. *J. Mol. Biol. 141*, 323-326

Reiser, P. J., Westfall, M. V., Schiaffino, S., and Solaro, R. J. (1994) Tension production and thin-filament protein isoforms in developing rat myocardium. *American Journal of Physiology - Heart and Circulatory Physiology. 267*, H1589-H1596.

Renaud, S., and Delorgeril, M. (1992) Wine, Alcohol, Platelets, and the French Paradox for Coronary Heart-Disease, *Lancet 339*, 1523-1526.

Rezvanpour, A., Phillips, J. M., and Shaw, G. S. (2009) Design of high-affinity S100-target hybrid proteins. *Protein Sci. 18*, 2528–2536.

Robertson, I. M., Baryshnikova, O. K., Li, M. X., and Sykes, B. D. (2008) Defining the binding site of levosimendan and its analogues in a regulatory cardiac troponin C-troponin I complex. *Biochemistry 47*, 7485-7495.

Robertson, I. M., Boyko, R. F., and Sykes, B. D. (2011) Visualizing the principal component of (1)H, (1)N-HSQC NMR spectral changes that reflect protein structural or functional properties: application to troponin C, *J. Biomol. NMR 51*, 115-122.

Robertson, I. M., Holmes, P. C., Li, M. X., Pineda-Sanabria, S. E., Baryshnikova, O. K., and Sykes, B. D. (2012) Elucidation of isoform-dependent pH sensitivity of troponin I by NMR spectroscopy. *J Biol Chem 287*, 4996-5007.

Robertson, I. M., Li, M. X., and Sykes, B. D. (2009) Solution Structure of Human Cardiac Troponin C in Complex with the Green Tea Polyphenol, (-)-Epigallocatechin 3-Gallate, *J. Biol. Chem. 284*, 23012-23023.

Robertson, I. M., Pineda-Sanabria, S. E., Holmes, P. C., and Sykes, B. D. (2014) Conformation of the critical pH sensitive region of troponin depends upon a single residue in troponin I. *Arch. Biochem. Biophys. 552-553*, 40-49.

Robertson, I. M., Pineda-Sanabria, S., and Sykes, B. D. (In Press) Approaches to protein-ligand structure determination by NMR spectroscopy: applications in drug binding to the cardiac regulatory protein troponin C, *Biophysics and Structure to Counter Threats and Challenges*.

Robertson, I. M., Spyracopoulos, L., and Sykes, B. D. (2009) *Biophysics and the Challenges of Emerging Threats*, NATO Science for Peace and Security Series B: Physics and Biophysics (Puglisi, J. D., ed) pp. 101–119, IOS Press, Amsterdam

Robertson, I. M., Sun, Y., Li, M. X., and Sykes, B. D. (2010) A structural and functional perspective into the mechanism of Ca^{2+}-sensitizers that target the cardiac troponin complex. *J. Mol. Cell. Cardiol. 49*, 1031-1041.

Robertson, S. P., Johnson, J. D., Holroyde, M. J., Kranias, E. G., Potter, J. D., and Solaro, R. J. (1982) The effect of troponin I phosphorylation on the Ca^{2+}-binding properties of the Ca^{2+}-regulatory site of bovine cardiac troponin. *J. Biol. Chem. 257*, 260-263.

Robinson, J. M., Cheung, H. C., and Dong, W. (2008) The cardiac Ca^{2+}-sensitive regulatory switch, a system in dynamic equilibrium. *Biophys. J. 95*, 4772-4789.

Rosenfeld, R. J., Goodsell, D. S., Musah, R. A., Morris, G. M., Goodin, D. B., and Olson, A. J. (2003) Automated docking of ligands to an artificial active site: augmenting crystallographic analysis with computer modeling, *J. Comput. Aided Mol. Des. 17*, 525-536.

Russell, A. J., Thomas, P. G., and Fersht, A. R. (1987) Electrostatic effects on modification of charged groups in the active site cleft of subtilisin by protein engineering. *J. Mol. Biol.* 193, 803–813

Russell, S. T., and Warshel, A. (1985) Calculations of electrostatic energies in proteins. The energetics of ionized groups in bovine pancreatic trypsin inhibitor. *J. Mol. Biol.* 185, 389–404

Sarkar, S., Witham, S., Zhang, J., Zhenirovskyy, M., Rocchia, W., and Alexov, E. (2012) DelPhi web server: A comprehensive online suite for electrostatic calculations of biological macromolecules and their complexes. *Communications in computational physics. 13*, 269-284.

Sasse, S., Brand, N. J., Kyprianou, P., Dhoot, G. K., Wade, R. Arai, M. *et al.* (1993) Troponin I gene expression during human cardiac development and in end-stage heart failure. *Circ Res* 72, 932-938.

Satyshur, K. A., Rao, S. T., Pyzalska, D., Drendel, W., Greaser, M., and Sundaralingam, M. (1988) Refined structure of chicken skeletal muscle troponin C in the two-calcium state at 2-A resolution. *J. Biol. Chem. 263*, 1628-1647.

Schuttelkopf, A. W., and van Aalten, D. M. (2004) PRODRG: A tool for high-throughput crystallography of protein-ligand complexes. *Acta Crystallogr. D Biol. Crystallogr. 60*, 1355-1363.

Schwieters, C. D., Kuszewski, J. J., and Clore, G. M. (2006) Using Xplor-NIH for NMR molecular structure determination, *Prog. Nucl. Magn. Reson. Spectrosc. 48*, 47-62.

Schwieters, C. D., Kuszewski, J. J., Tjandra, N., and Clore, G. M. (2003) The Xplor-NIH NMR molecular structure determination package, *J. Magn. Reson. 160*, 65-73.

Senzaki, H., Isoda, T., Paolocci, N., Ekelund, U., Hare, J. M., and Kass, D. A. (2000) Improved mechanoenergetics and cardiac rest and reserve function of in vivo failing heart by calcium sensitizer EMD-57033. *Circulation. 101*, 1040-1048.

Shaffer, J. F., and Gillis, T. E. (2010) Evolution of the regulatory control of vertebrate striated muscle: the roles of troponin I and myosin binding protein-C, *Physiol. Genomics42*, 406-419.

Sharma K, Kass DA (2014) Heart Failure With Preserved Ejection Fraction: Mechanisms, Clinical Features, and Therapies. *Circ Res* 115(1), 79–96.

Sheehan, K. A., Arteaga, G. M., Hinken, A. C., Dias, F. A., Ribeiro, C., Wieczorek, D. F., Solaro, R. J., and Wolska, B. M. (2011) Functional effects of a tropomyosin mutation linked to FHC contribute to maladaptation during acidosis. *J. Mol. Cell. Cardiol.* 50, 442–450

Shen Y, Bax A (2012) Identification of helix capping and b-turn motifs from NMR chemical shifts. *J Biomol NMR* 52, 211–232.

Shen, Y., Delaglio, F., Cornilescu, G., and Bax, A. (2009) TALOS+: A hybrid method for predicting protein backbone torsion angles from NMR chemical shifts. *J. Biomol. NMR. 44*, 213-223.

Shomura, Y., Torayama, I., Suh, D. Y., Xiang, T., Kita, A., Sankawa, U., and Miki, K. (2005) Crystal structure of stilbene synthase from Arachis hypogaea, *Proteins-Structure Function and Bioinformatics 60*, 803-806.

Shuker, S. B., Hajduk, P. J., Meadows, R. P., and Fesik, S. W. (1996) Discovering high-affinity ligands for proteins: SAR by NMR, *Science 274*, 1531-1534.

Sia, S. K., Li, M. X., Spyracopoulos, L., Gagné, S. M., Liu, W., Putkey, J. A., and Sykes, B. D. (1997) Structure of cardiac muscle troponin C unexpectedly reveals a closed regulatory domain, *J. Biol. Chem. 272*, 18216-18221.

Siemann, E. H., and Creasy, L. L. (1992) Concentration of the Phytoalexin Resveratrol in Wine, *Am. J. Enol. Vitic. 43*, 49-52.

Singh, J., Petter, R. C., Baillie, T. A., and Whitty, A. (2011) The resurgence of covalent drugs. *Nat Rev Drug Discov. 10*, 307-317.

Slupsky, C. M., Boyko, R. F., Booth, V. K., and Sykes, B. D. (2003) Smart-Notebook. A semi-automated approach to protein sequential NMR resonance assignments. *J. Biomol. NMR* 27, 313–321

Slupsky, C. M., Reinach, F. C., Smillie, L. B., and Sykes, B. D. (1995) Solution secondary structure of calcium-saturated troponin C monomer determined by multidimensional heteronuclear NMR spectroscopy. *Protein Sci. 4*, 1279-1290.

Smart, B. E. (2001) Fluorine substituent effects (on bioactivity), *J. Fluorine Chem. 109*, 3-11.

Smith, N., Witham, S., Sarkar, S., Zhang, J., Li, L., Li, C., and Alexov, E. (2012) DelPhi web server v2: Incorporating atomic-style geometrical figures into the computational protocol. *Bioinformatics. 28*, 1655-1657.

Solaro RJ, Henze M, Kobayashi T (2013) Integration of troponin I phosphorylation with cardiac regulatory networks. *Circ Res* 112, 355–366.

Solaro RJ, Moir AJ, Perry SV (1976) Phosphorylation of troponin I and the inotropic effect of adrenaline in the perfused rabbit heart. *Nature* 262, 615–617.

Solaro RJ, van der Velden J (2010) Why does troponin I have so many phosphorylation sites? Fact and fancy. *J Mol Cell Cardiol* 48, 810–816.

Solaro, R. J., and Kobayashi, T. (2011) Protein phosphorylation and signal transduction in cardiac thin filaments, *J. Biol. Chem.286*, 9935-9940.

Solaro, R. J., Bousquet, P., and Johnson, J. D. (1986) Stimulation of cardiac myofilament force, ATPase activity and troponin C ca++ binding by bepridil. *Journal of Pharmacology and Experimental Therapeutics. 238*, 502-507.

Solaro, R. J., Gambassi, G., Warshaw, D. M., Keller, M. R., Spurgeon, H. A., Beier, N., and Lakatta, E. G. (1993) Stereoselective actions of thiadiazinones on canine cardiac myocytes and myofilaments. *Circ Res. 73*, 981-990.

Solaro, R. J., Henze, M., and Kobayashi, T. (2013) Integration of troponin I phosphorylation with cardiac regulatory networks. *Circulation Research. 112*, 355-366.

Solaro, R. J., Kumar, P., Blanchard, E. M., and Martin, A. F. (1986) Differential effects of pH on calcium activation of myofilaments of adult and perinatal dog hearts. Evidence for developmental differences in thin filament regulation. *Circ. Res. 58*, 721-729.

Solaro, R. J., Lee, J. A., Kentish, J. C., and Allen, D. G. (1988) Effects of acidosis on ventricular muscle from adult and neonatal rats. *Circ. Res. 63*, 779–787 11.

Solaro, R. J., Moir, A. J., and Perry, S. V. (1976) Phosphorylation of troponin I and the inotropic effect of adrenaline in the perfused rabbit heart. *Nature*. *262*, 615-617.

Solaro, R. J., Rosevear, P., and Kobayashi, T. (2008) The unique functions of cardiac troponin I in the control of cardiac muscle contraction and relaxation. *Biochem. Biophys. Res. Commun. 369*, 82-87.

Sorsa, T., Heikkinen, S., Abbott, M. B., Abusamhadneh, E., Laakso, T., Tilgmann, C., Serimaa, R., Annila, A., Rosevear, P. R., Drakenberg, T., Pollesello, P., and Kilpeläinen, I. (2001) Binding of levosimendan, a calcium sensitizer, to cardiac troponin C. *J. Biol. Chem. 276*, 9337-9343.

Sorsa, T., Pollesello, P., and Solaro, R. J. (2004) The contractile apparatus as a target for drugs against heart failure: Interaction of levosimendan, a calcium sensitiser, with cardiac troponin C. *Mol. Cell. Biochem. 266*, 87-107.

Sorsa, T., Pollesello, P., Permi, P., Drakenberg, T., and Kilpeläinen, I. (2003) Interaction of levosimendan with cardiac troponin C in the presence of cardiac troponin I peptides. *J. Mol. Cell. Cardiol. 35*, 1055-1061.

Spyracopoulos, L., Gagné, S. M., Li, M. X., and Sykes, B. D. (1998) Dynamics and thermodynamics of the regulatory domain of human cardiac troponin C in the apo- and calcium-saturated states. *Biochemistry. 37*, 18032-18044.

Spyracopoulos, L., Li, M. X., Sia, S. K., Gagné, S. M., Chandra, M., Solaro, R. J., and Sykes, B. D. (1997) Calcium-induced structural transition in the regulatory domain of human cardiac troponin C. *Biochemistry 36*, 12138–12146.

Sternberg, M. J., Hayes, F. R., Russell, A. J., Thomas, P. G., and Fersht, A. R. (1987) Prediction of electrostatic effects of engineering of protein charges. *Nature* 330, 86–88

Stuart, A. C., Borzilleri, K. A., Withka, J. M., and Palmer, A. G. (1999) Compensating for variations in H-1-C-13 scalar coupling constants in isotope-filtered NMR experiments, *J. Am. Chem. Soc. 121*, 5346-5347.

Stuart, A. C., Borzilleri, K. A., Withka, J. M., and Palmer, A. G. (1999) Compensating for variations in H-1-C-13 scalar coupling constants in isotope-filtered NMR experiments, *J. Am. Chem. Soc. 121*, 5346-5347.

Sun, A. Y., Wang, Q., Simonyi, A., and Sun, G. Y. (2010) Resveratrol as a Therapeutic Agent for Neurodegenerative Diseases, *Molecular Neurobiology 41*, 375-383.

Sun, Y. B., Lou, F., and Irving, M. (2009) Calcium- and myosin-dependent changes in troponin structure during activation of heart muscle. *J. Physiol. 587*, 155-163.

Swindle, N., and Tikunova, S. B. (2010) Hypertrophic Cardiomyopathy-Linked Mutation D145E Drastically Alters Calcium Binding by the C-Domain of Cardiac Troponin C, *Biochemistry 49*, 4813-4820.

Szaka´cs, Z., Kraszni, M., and Nosza´l, B. (2004) Determination of microscopic acid-base parameters from NMR-pH titrations. *Anal. Bioanal. Chem*. 378, 1428–1448

Szczesna, D., Guzman, G., Miller, T., Zhao, J. J., Farokhi, K., Ellemberger, H., and Potter, J. D. (1996) The role of the four Ca^{2+} binding sites of troponin C in the regulation of skeletal muscle contraction, *J. Biol. Chem. 271,* 8381-8386.

Tadano, N., Du, C. K., Yumoto, F., Morimoto, S., Ohta, M., Xie, M. F., Nagata, K., Zhan, D. Y., Lu, Q. W., Miwa, Y., Takahashi-Yanaga, F., Tanokura, M., Ohtsuki, I., and Sasaguri, T. (2010) Biological actions of green tea catechins on cardiac troponin C, *Br. J. Pharmacol. 161,* 1034-1043.

Tadano, N., Morimoto, S., Takahashi-Yanaga, F., Miwa, Y., Ohtsuki, I., and Sasaguri, T. (2009) Propyl Gallate, a Strong Antioxidant, Increases the Ca^{2+} Sensitivity of Cardiac Myofilament, *J. Pharmacol. Sci. 109,* 456-458.

Takeda, S., Yamashita, A., Maeda, K., and Maeda, Y. (2003) Structure of the core domain of human cardiac troponin in the Ca^{2+}-saturated form. *Nature 424,* 35-41.

Tanford, C. (1961) *Physical Chemistry of Macromolecules,* John Wiley, New York.

Tang X *et al.* (2012) Composite low affinity interactions dictate recognition of the cyclin-dependent kinase inhibitor Sic1 by the SCFCdc4 ubiquitin ligase. *Proc Natl Acad Sci U S A* 109, 3287–3292.

Thompson, B., Houang, E., Sham, Y., and Metzger, J. (2014) Molecular determinants of cardiac myocyte performance as conferred by isoform-specific TnI residues. *Biophys. J.* 106, 2105-2114.

Tran, K., Smith, N. P., Loiselle, D. S., and Crampin, E. J. (2010) A metabolite-sensitive, thermodynamically constrained model of cardiac crossbridge cycling. Implications for force development during ischemia. *Biophys. J.* 98, 267–276

Trela, B. C., and Waterhouse, A. L. (1996) Resveratrol: Isomeric molar absorptivities and stability, *J. Agric. Food Chem. 44,* 1253-1257.

Tripet, B., Van Eyk, J. E., and Hodges, R. S. (1997) Mapping of a second actin-tropomyosin and a second troponin C binding site within the C terminus of troponin I, and their importance in the Ca^{2+}-dependent regulation of muscle contraction1. *J. Mol. Biol. 271,* 728-750.

Tung, C. S., Wall, M. E., Gallagher, S. C., and Trewhella, J. (2000) A model of troponin-I in complex with troponin-C using hybrid experimental data: The inhibitory region is a beta-hairpin. *Protein Sci. 9,* 1312-1326.

van der Velden J (2011) Diastolic myofilament dysfunction in the failing human heart. *Pflugers Arch* 462, 155–163.

van der Velden J *et al.* (2006) Functional effects of protein kinase C-mediated myofilament phosphorylation in human myocardium. *Cardiovasc Res* 69, 876–887.

Vassylyev, D. G., Takeda, S., Wakatsuki, S., Maeda, K., and Maeda, Y. (1998) Crystal structure of troponin C in complex with troponin I fragment at 2.3-angstrom resolution, *Proc. Natl. Acad. Sci. U. S. A.95,* 4847-4852.

Vinogradova, M. V., Stone, D. B., Malanina, G. G., Karatzaferi, C., Cooke, R., Mendelson, R. A., and Fletterick, R. J. (2005) $Ca(^{2+})$-regulated structural changes in troponin, *Proc. Natl. Acad. Sci. U. S. A.102,* 5038-5043.

Voet, A., Banwell, E. F., Sahu, K. K., Heddle, J. G., and Zhang, K. Y. (2013) Protein interface pharmacophore mapping tools for small molecule protein: Protein interaction inhibitor discovery. *Curr. Top. Med. Chem*. *13*, 989–1001.

Wang X, Mercier P, Letourneau PJ, Sykes BD (2005) Effects of Phe-to-Trp mutation and fluorotryptophan incorporation on the solution structure of cardiac troponin C, and analysis of its suitability as a potential probe for in situ NMR studies. *Protein Sci* 14, 2447–2460.

Wang Y *et al*. (2012) Generation and functional characterization of knock-in mice harboring the cardiac troponin I-R21C mutation associated with hypertrophic cardiomyopathy. *J Biol Chem* 287, 2156–2167.

Wang, C. L. A., Leavis, P. C., Dehorrocks, W., and Gergely, J. (1981) Binding of Lanthanide Ions to Troponin-C, *Biochemistry 20*, 2439-2444.

Wang, X., Li, M. X., and Sykes, B. D. (2002) Structure of the regulatory N-domain of human cardiac troponin C in complex with human cardiac troponin I$_{147-163}$ and bepridil. *J. Biol. Chem. 277*, 31124-31133.

Wang, X., Li, M. X., Spyracopoulos, L., Beier, N., Chandra, M., Solaro, R. J., and Sykes, B. D. (2001) Structure of the C-domain of human cardiac troponin C in complex with the Ca^{2+} sensitizing drug EMD 57033, *J. Biol. Chem. 276*, 25456-25466.

Wang, Y. P., and Fuchs, F. (1994) Length, force, and Ca($^{2+}$)-troponin C affinity in cardiac and slow skeletal muscle. *Am. J. Physiol. 266*, C1077–82.

Ward DG *et al*. (2004) NMR and mutagenesis studies on the phosphorylation region of human cardiac troponin I. *Biochemistry* 43, 5772–5781.

Ward DG, Cornes MP, Trayer IP (2002) Structural consequences of cardiac troponin I phosphorylation. *J Biol Chem* 277, 41795–41801.

Ward, D. G., Brewer, S. M., Calvert, M. J., Gallon, C. E., Gao, Y., and Trayer, I. P. (2004) Characterization of the interaction between the N-terminal extension of human cardiac troponin I and troponin C, *Biochemistry 43*, 4020-4027.

Ward, D. G., Brewer, S. M., Comes, M. P., and Trayer, I. P. (2003) A cross-linking study of the N-terminal extension of human cardiac troponin I, *Biochemistry 42*, 10324-10332.

Warren, C. M., Kobayashi, T., and Solaro, R. J. (2009) Sites of Intra- and Intermolecular Cross-linking of the N-terminal Extension of Troponin I in Human Cardiac Whole Troponin Complex, *J. Biol. Chem.284*, 14258-14266.

Wattanapermpool J, Guo X, Solaro RJ (1995) The unique amino-terminal peptide of cardiac troponin I regulates myofibrillar activity only when it is phosphorylated. *J Mol Cell Cardiol* 27, 1383–1391.

Westfall, M. V., Albayya, F. P., Turner, I. I., and Metzger, J. M. (2000) Chimera analysis of troponin I domains that influence Ca^{2+}-activated myofilament tension in adult cardiac myocytes. *Circ. Res. 86*, 470-477.

Westfall, M. V., and Metzger, J. M. (2001) Troponin I isoforms and chimeras: Tuning the molecular switch of cardiac contraction. *Physiology. 16,* 278–281.

Westfall, M. V., and Metzger, J. M. (2007) Single amino acid substitutions define isoform-specific effects of troponin I on myofilament Ca^{2+} and pH sensitivity. *J. Mol. Cell. Cardiol. 43*, 107-118.

Westfall, M. V., Rust, E. M., and Metzger, J. M. (1997) Slow skeletal troponin I gene transfer, expression, and myofilament incorporation enhances adult cardiac myocyte contractile function. *Proc. Natl. Acad. Sci. U.S.A. 94*, 5444-5449

Whitby, F. G., and Phillips, G. N., Jr. (2000) Crystal structure of tropomyosin at 7 Angstroms resolution, *Proteins38*, 49-59.

Wijnker PJ *et al.* (2014) Length-dependent activation is modulated by cardiac troponin I bisphosphorylation at Ser23 and Ser24 but not by Thr143 phosphorylation. *Am J Physiol Heart Circ Physiol* 306, H1171–H1181.

Wijnker PJ *et al.* (2014) Phosphorylation of protein kinase C sites Ser42/44 decreases Ca(2+)-sensitivity and blunts enhanced length-dependent activation in response to protein kinase A in human cardiomyocytes. *Arch Biochem Biophys* 554, 11–21.

Wishart, D. S., and Sykes, B. D. (1994) Chemical-Shifts as a Tool for Structure Determination, *Method Enzymol239*, 363-392.

Wishart, D. S., Sykes, B. D., and Richards, F. M. (1991) Relationship between Nuclear-Magnetic-Resonance Chemical-Shift and Protein Secondary Structure, *J. Mol. Biol.222*, 311-333.

Wishart, D. S., Sykes, B. D., and Richards, F. M. (1992) The Chemical-Shift Index - a Fast and Simple Method for the Assignment of Protein Secondary Structure through Nmr-Spectroscopy, *Biochemistry 31*, 1647-1651.

Wolska, B. M., Keller, R. S., Evans, C. C., Palmiter, K. A., Phillips, R. M., Muthuchamy, M., Oehlenschlager, J., Wieczorek, D. F., de Tombe, P. P., and Solaro, R. J. (1999) Correlation between myofilament response to Ca^{2+} and altered dynamics of contraction and relaxation in transgenic cardiac cells that express ß-tropomyosin. *Circ. Res. 84*, 745–751.

Wolska, B. M., Vijayan, K., Arteaga, G. M., Konhilas, J. P., Phillips, R. M., Kim, R., Naya, T., Leiden, J. M., Martin, A. F., de Tombe, P. P., and Solaro, R. J. (2001) Expression of slow skeletal troponin I in adult transgenic mouse heart muscle reduces the force decline observed during acidic conditions, *J Physiol 536*, 863-870.

World Health Organization 2012 www.who.int/mediacentre/factsheets/fs310/en/

Wüthrich, K. NMR of Proteins and Nucleic Acids. USA, Wiley Interscience, 1986.

Yamazaki, T., Yoshida, M., and Nagayama, K. (1993) Complete assignments of magnetic resonances of ribonuclease H from *Escherichia* coli by double- and triple-resonance 2D and 3D NMR spectroscopies. *Biochemistry 32*, 5656-5669.

Yin, Q., Shi, Y. M., Liu, H. M., Li, C. B., and Zhang, W. Q. (2002) (E)-3,5,4 '-Trimethoxystilbene, *Acta Crystallographica Section E-Structure Reports Online 58*, O1180-O1181.

Zhang J *et al.* (2011) Top-down quantitative proteomics identified phosphorylation of cardiac troponin I as a candidate biomarker for chronic heart failure. *J Proteome Res* 10, 4054–4065.

Zheng, L., Baumann, U., and Reymond, J. (2004) An efficient one-step site-directed and site-saturation mutagenesis protocol. *Nucleic Acids Research. 32*, e115-e115.

Zhou, H. (2001) The affinity-enhancing roles of flexible linkers in two-domain DNA-binding proteins. *Biochemistry 40*, 15069–15073.

Zhou, H. (2006) Quantitative relation between intermolecular and intramolecular binding of pro-rich peptides to SH3 domains. *Biophys. J. 91*, 3170–3181.

Zhou, H., and Gilson, M. K. (2009) Theory of free energy and entropy in noncovalent binding. *Chem. Rev. 109*, 4092–4107.

Zhou, Z., Li, K., Rieck, D., Ouyang, Y., Chandra, M., and Dong, W. (2012) Structural dynamics of C-domain of cardiac troponin I protein in reconstituted thin filament. *J. Biol. Chem. 287*, 7661-7674.

Appendix A

This appendix contains previously published material to which I have made a modest contribution. It reports the structural characterization of the N-terminal extension of cardiac troponin I bound to troponin C by NMR spectroscopy. No high resolution structure is available for this region. The present study revealed an unstructured N-terminal extension that interacts with the N-domain of troponin C through electrostatics. Domain positioning is proposed as the mode of regulating Ca^{2+} affinity by this cardiac specific extension of troponin I. Hwang *et al.* (2014) *Proc. Natl. Acad. Sci.* 40:14412-14417.

The intrinsically disordered cardiac-specific N-terminal region of troponin I positions the regulatory domain of troponin C

Peter M. Hwang[1,2], Fangze Cai[2], Sandra E. Pineda-Sanabria[2], David C. Corson[2], and Brian D. Sykes[2]

[1] Division of General Internal Medicine, Department of Medicine, [2] Department of Biochemistry, Faculty of Medicine and Dentistry, University of Alberta, Edmonton, Alberta, Canada

Introduction

The balance between contraction and relaxation must be carefully regulated in the heart. Impaired relaxation can lead to diastolic heart failure, while systolic failure is characterized by insufficient contractility. Despite having different etiologies, both forms of heart failure are similar in terms of prevalence, symptoms, and mortality (1). Of all the signaling pathways that regulate contractile function, the best studied is sympathetic β_1-adrenergic stimulation (2), which leads to cardiomyocyte cAMP production and activation of protein kinase A (PKA). Downstream phosphorylation of L-type calcium channels and phospholamban increases calcium fluxes, while phosphorylation of sarcomeric proteins, cardiac troponin I (cTnI), cardiac myosin binding protein-C, and titin(3), regulates the calcium-induced mechanical response.

In human cTnI, Ser22 and Ser23 are the residues most consistently phosphorylated (4, 5) (there are some numbering inconsistencies in the literature, and we will refer to Ser22/23 instead of Ser23/24 to account for physiologic removal of the N-terminal methionine residue). Originally identified as PKA targets, Ser22/23 are now known to be phosphorylated by other kinases, including PKG, PKCβ, PKCδ,

and PKD1(6), showing it to be an important locus at which multiple signaling pathways converge. Phosphorylation at cTnI Ser22/23 decreases the calcium sensitivity of the cardiac sarcomere(7). High levels of phosphorylation are seen in healthy individuals, but decreased phosphorylation levels occur in a number of pathologic states, including heart failure with reduced ejection fraction (HFrEF), heart failure with preserved ejection fraction (HFpEF), dilated cardiomyopathy, and hypertrophic cardiomyopathy(5, 8). While dephosphorylation is likely a compensatory mechanism in many cases, it may be a disease-driving dysregulation in others.

Other regulatory mechanisms are strongly influenced by the phosphorylation state of Ser22/23. The Frank-Starling law of the heart, also known as length dependent activation or stretch activation, is more pronounced when Ser22/23 are phosphorylated (9)(10). In contrast Ser6 (11) or Ser43/45 (12)(13) phosphorylation has more of an impact when Ser22/23 are unphosphorylated. Finally, some mutations that cause familial dilated cardiomyopathy have been shown to mitigate the effect of Ser22/23 phosphorylation (14). Despite the physiologic importance of cTnI[1-31] in regulating cardiac calcium sensitivity, the extent of its modulatory capacity has remained elusive.

Ser22/23 lie within the cardiac-specific N-terminal region, cTnI[1-31], not present in the skeletal muscle isoforms. cTnI[1-209] forms long stretches of helical structure along a winding course that binds to troponin C, troponin T, and actin-tropomyosin. The X-ray structure of the cardiac troponin complex(15) did not include cTnI[1-34], so the structure of this region has not been determined, though there have been some preliminary investigations (16, 17). It is known that cTnI[1-31] interacts with cTnC in its unphosphorylated state(18), but phosphorylation abolishes this interaction, having an effect similar to truncation or removal of cTnI[1-31](19). Our present study provides a detailed analysis of the structure and dynamics of cTnI[1-73] in complex with cTnC usingsolution NMR spectroscopy, highlighting its unique mechanism of action and physiologic implications.

Results

Chemical shift assignment and secondary structure of cTnI[1-73] free and in complex with cTnC

NMR chemical shift assignment of protein backbone atoms, $^1H\alpha$, $^{13}C\alpha$, $^{13}C\beta$, ^{13}CO, ^1HN, and ^{15}N, provides information about secondary structure on a per-residue basis. For example, α-helical residues have downfield $^{13}C\alpha$ chemical shifts compared to random coil values, while residues with extended structure appear upfield. In free cTnI[1-73], residues 42-67 possess downfield $^{13}C\alpha$ shifts indicative of nascent helical structure (see

Figure A.1). The chemical shift analysis program δ2D (20) indicates overall <25% helical content for this region and random coil for the rest of the protein (See Supplementary Figure A.1). There is no suggestion of a stable helix from residues 19-31, as had been suggested by a previous NMR analysis (16) that did not have the benefit of ^{13}C chemical shift data.
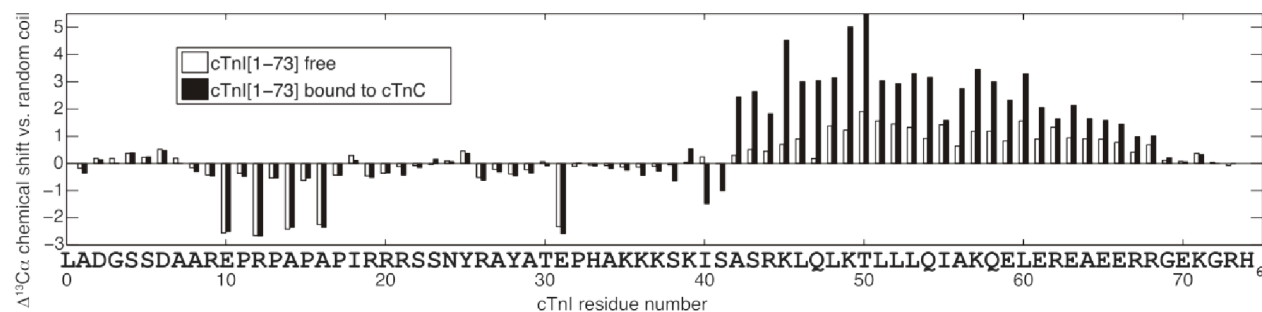
Figure A.1. Chemical shift analysis of cTnI[1-73].

Deviation from random coil chemical shifts for backbone ^{13}Cα chemical shifts in free cTnI[1-73] (open bars) and cTnI[1-73] in complex with cTnC (black bars).

Large deviations from random coil chemical shifts are observed in residues preceding proline (see Figure A.1), which are almost always in an extended conformation. (Prolines themselves can adopt either turn-like or extended conformations.)The chemical shift analysis program, DANGLE, analyzes glycine, proline, and pre-proline residues separately from other amino acid residues because of their unique conformational preferences (21). DANGLE predicted an extended conformation for the proline-rich region spanning residues 10-18 (containing P11, P13, P15, P17), though it does not specify a percentage, like δ2D, which predicted a random coil conformation with a small degree of extended conformation (see Supplementary Figure A.1). NOE assignments showed that all prolines in cTnI[1-73] preferred the trans conformation, although there is evidence of some minor peaks corresponding to cis forms.

Addition of wildtype- or C35S,C84S-cTnC to cTnI[1-73] causes pronounced chemical shift changes in cTnI residues 42-68 suggestive of increased helical content (see Figure A.1 and Supplementary Figure A.1), with Ser41 acting as the N-terminal helix cap residue (22). Helical structure is induced by binding of cTnI[39-60] to the large hydrophobic patch of the cTnC C-domain (cCTnC), forming a very tight complex with a nanomolar range dissociation constant(18) that effectively anchors cCTnC to the troponin IT arm at all physiologic calcium concentrations.

Negligible chemical shift changes occur in cTnI residues 1-34 upon addition of cTnC (see Figure A.1), despite a wealth of biochemical data documenting an interaction between this region and the N-

domain of cTnC (cNTnC) (for example, see ref. (23),(24)). Using chemical shift data alone, there is no evidence of helix formation or other induced conformational preference anywhere along cTnI[1-34] as a result of the interaction (see Supplementary Figure A.1). There are examples in the literature of "fuzzy complexes" (25), some of which involve intrinsically disordered regions (IDRs) that show minimal chemical shift changes upon binding, like the phosphorylated Sic1-Cdc4 complex(26) and CFTR R domain complexes(27). Evidence of an interaction can still be found through ^{1}H-^{1}H NOEs, signal broadening, or relaxation measurements, as turns out to be the case for cTnI[19-37]-cNTnC (see below).

Reciprocal chemical shift changes in cTnC are also observed when cTnI[1-73] is added. The hydrophobic binding of cTnI[39-60] induces large chemical shift changes in cCTnC, but the interaction with cNTnC produced only minimal chemical shift changes (see Figure A.2). It has previously been suggested that the interaction between cTnI[1-31] and cNTnC shifts the equilibrium of cNTnC towards the "open" state(28). The dominant conformation of calcium-bound cNTnC is in fact closed(29), with the open conformation sampled less than 20% of the time (30). The equilibrium is shifted to the open conformation when cNTnC binds hydrophobically to the helical switch region, cTnI[148-158](31), the critical step that releases the flanking inhibitory segments of cTnI and triggers muscle contraction. The shift involves a sizeable conformational change that manifests in large NMR chemical shift changes, particularly in loops I and II (see Figure A.2). Stabilization of the calcium bound open conformation also markedly increases the calcium affinity of cNTnC (32). Since no conformational change is observed when cNTnC interacts with cTnI[1-73], the cardiac-specific cTnI[1-31] must exert its calcium sensitizing effect through a different mechanism than stabilization of the open conformation.

In summary, the interaction between cTnI[1-31] and cNTnC has no observable effect on the secondary structure of cTnI[1-31] or the closed-open equilibrium of cNTnC.
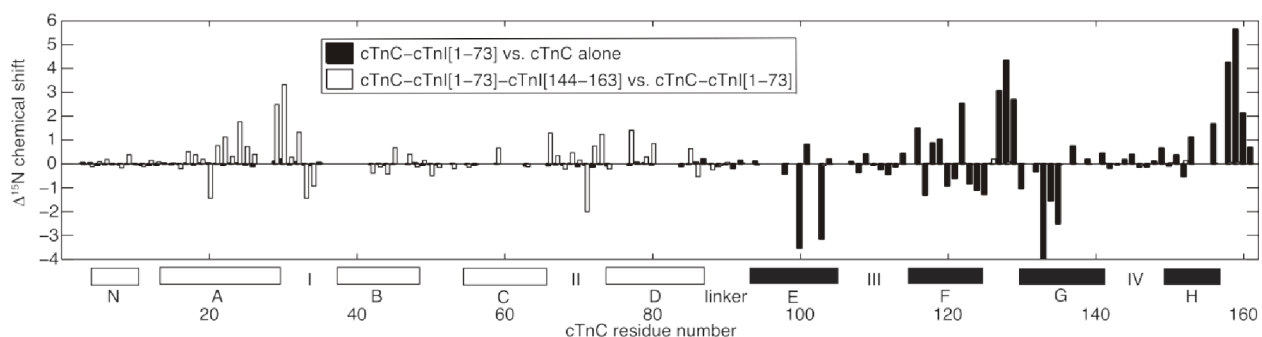
**Figure A.2. Structural changes in C35S,C84S-cTnC induced by binding of cTnI.**
Binding-induced structural changes in C35S,C84S-cTnC are highlighted by backbone amide ^{15}N chemical shift changes. The black bars denote changes that occur when cTnC binds to cTnI[1-73]. The largest

changes occur in cCTnC (see helices E-H along the *x*-axis), while negligible changes are observed in cNTnC (helices N, A-D). This is because of the extensive hydrophobic interface between cTnI[39-60] and cCTnC, as opposed to the more superficial electrostatic interactions between cTnI[19-37] and cNTnC. In contrast, the open bars highlight the structural changes that occur when cTnI[144-163] binds cNTnC hydrophobically, driving a closed-to-open conformational transition in cNTnC. In this case the predominant structural changes occur in cNTnC and not cCTnC. Stretches of missing assignments due to conformational exchange include residues 36-41, 60-62, 81-83, and 95-97.

¹H-¹H NOE analysis of the cTnC-cTnI[1-73] complex

Homonuclear ¹H-¹H NOEs can be observed between any two ¹H atoms within ~6 Å, critical for any NMR-based structure determination. The vast majority of intermolecular ¹H-¹H NOEs occur between cTnI[39-60] and cCTnC, consistent with extensive hydrophobic binding. There are few intermolecular NOEs observed between cNTnC and cTnI[1-73], but the most critical NOEs are between cNTnC Ala7 and cTnI Ala42/Ser43. The importance of this contact is underscored by the fact that a double Ser41/43 mutation to aspartate (mimicking phosphorylation) markedly decreases the troponin calcium affinity (33). Since cTnI Ala42/Ser43 are part of a rigid alpha helix bound to cCTnC, and Ala7 is part of cNTnC helix N, the interaction fixes the position of cNTnC relative to cCTnC. This contact is actually present in the X-ray crystal structure (see Figure A.3), suggesting that the true inter-domain orientation in solution is in fact very similar. This single contact point is alone insufficient to stably fix the domains in solution, stabilized by crystal packing contacts in the X-ray structure. In solution, the orientation is bolstered by additional electrostatic interactions from the disordered N-terminal tail of cTnI (see below).
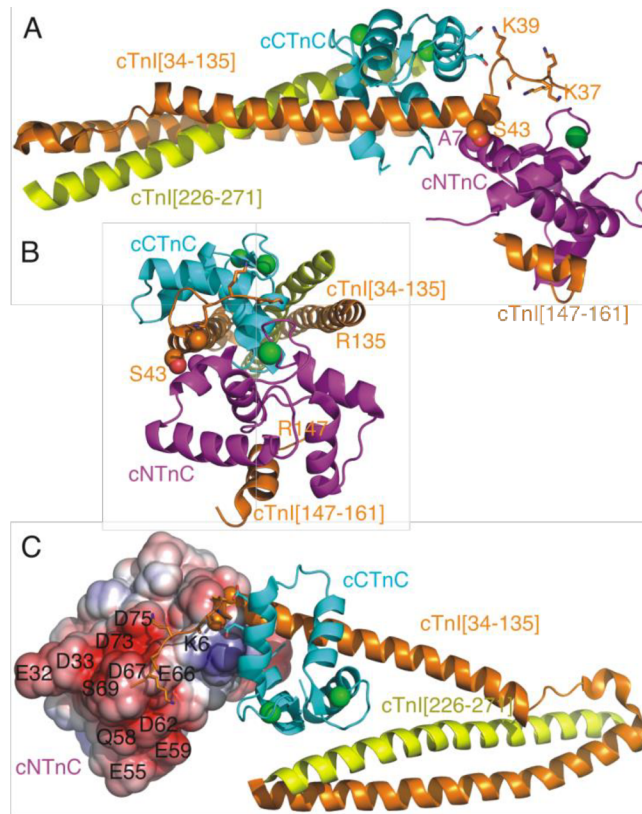
Figure A.3. Localization of NOEs between cTnC and cTnI[1-73].

Ribbon diagrams of the troponin complex drawn by PyMol and derived from reference (15). cNTnC is shown in magenta, while cCTnC is shown in cyan. Calcium ions are shown as green spheres. Troponin T, residues 226-271, is shown in yellow. cTnI, residues 34-135 and 147-161, is shown in orange. A) and B) The key contact that fixes the position of cNTnC relative to cCTnC is between A7 of cNTnC and A42/S43 of cTnI, shown as space-filling spheres. The sidechains of cTnI[35-39] are also shown in stick figures, with K39 of cTnI contacting D131 and E135of cCTnC (shown in sticks) and K35-S38 hovering over cNTnC. C) Electrostatic surface representation of cNTnC showing the negatively charged surface that interacts with cTnI[19-37].

cTnI Ser41 is the N-terminal helix cap residue, but it is also part of a type VIII turn based on Ser38-Lys39-Ile40-Ser41 backbone chemical shifts, according to the MICS Protein Structural Motif Prediction program (22). Lys39 shows NOE contacts with Asp131 and Glu135 of helix G in cCTnC, while Ser38 has intermolecular NOEs to a lysine residue consistent with cNTnC Lys6 in the crystal structure (see Figure A.3). This brings Lys35-Lys36-Lys37 into contact with a prominent negatively charged surface that includes EF-hand loop II, the all-important calcium-binding loop (see Figure A.3). cTnI Lys35-37 display NOEs to residues with Asp- and Glu-like chemical shifts, but these could not be unambiguously separated from each other. In the crystal structure, there are two troponin complexes

per asymmetric unit. In one complex, Lys35-37 are invisible, but in the other, they are modeled hovering over EF-hand loop II, with Lys37 closest to Asp75 of cNTnC. Finally, cTnI Arg21 and Arg26 also make weak NOEs to cTnC residues with Glu-like chemical shifts (see Supplementary Figure A.2), but these could not be unambiguously assigned either.

The considerable chemical shift overlap for charged Lys, Arg, Asp, and Glu sidechains make unambiguous intermolecular NOE assignment near impossible. Nevertheless, these NOEs demonstrate specific and stable electrostatic interactions involving cTnI Arg21, Arg26, and part of Lys35-37. This is in marked contrast to the lack of NOEs involving hydrophobic residues, which are usually critical for defining intermolecular contacts. cTnI Pro17, Ile18, Tyr25, Ala27, Tyr28, and Ala29 showed no intermolecular NOEs (see Supplementary Figure A.2 for an example).

Classically, protein-protein interactions are dominated by hydrophobic interactions, which require close packing, exclusion of water, and a rigid structuring of the backbone, as exemplified by the interaction between cTnI[39-60] and cCTnC. In contrast, the electrostatic interactions involving cTnI[19-37] occur in a solvated environment that does not require as much rigidification of the backbone. It does require many positive charges, with as many as eight potentially involved (if His33 is included). Notably, Lys35 has been strongly implicated in autosomal dominant dilated cardiomyopathy (K36Q by the alternate numbering scheme), decreasing the calcium sensitivity of reconstituted thin filaments by 0.3-0.6 pCa units(14)(34).

15N relaxation of cTnI[1-73] free and in complex with cTnC

^{15}N relaxation rates provide a window into nanosecond to picosecond (10^{-9} to 10^{-12} s) timescale conformational fluctuations in a protein. Structured proteins tumble with a global rotational correlation time, τ_c, on the order of several nanoseconds for a small domain, with τ_c scaling roughly proportionally to molecular weight. In rigidly structured regions, the overall motion is approximated by the global correlation time. As structural flexibility increases, for example, towards the N- or C-terminus, faster internal motions begin to dominate NMR relaxation behavior. Binding causes a decrease in internal motions that can be detected via changes in relaxation.

^{15}N backbone relaxation studies were obtained for cTnI[1-73] both free and bound to C35S,C84S-cTnC (Figure A.4). The transverse relaxation rate, R_2, is roughly proportional to the weighted average correlation time (including global tumbling and internal motions) at each backbone amide site. R_1 relaxation is most effectively induced by motions with a timescale near 2-3 nanoseconds (^{15}N nucleus on a 600 MHz spectrometer). A negative ^{1}H-^{15}N heteronuclear NOE is most effectively induced by motions with a timescale near 0.2-0.3 nanoseconds.

305
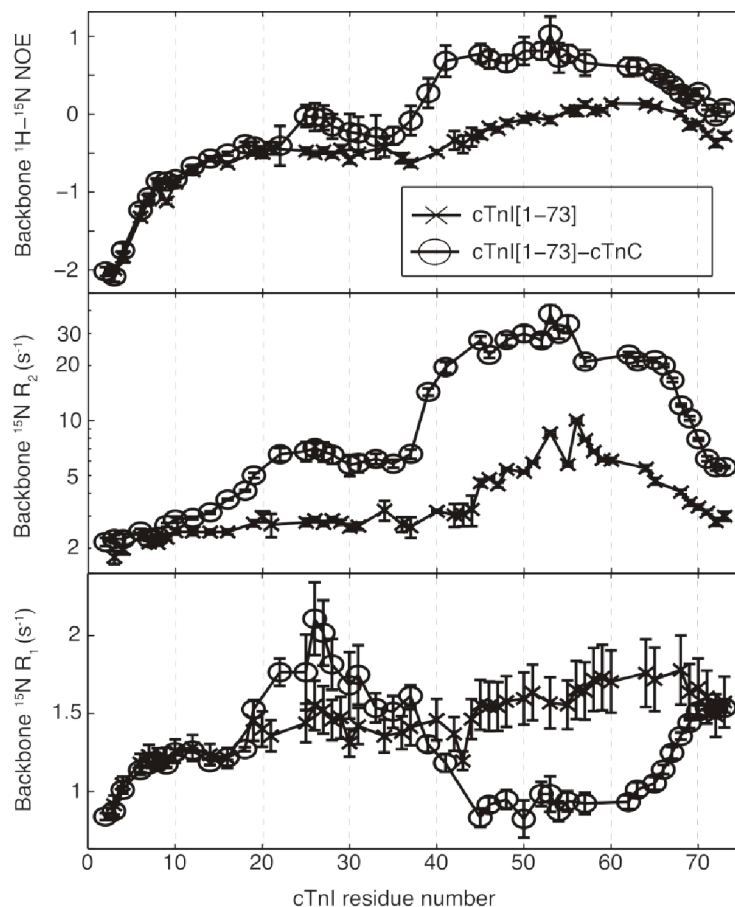
Figure A.4. ^{15}N backbone relaxation data for cTnI[1-73].

'x' denotes free and 'o' denotes bound to C35S,C84S-cTnC.

Looking at the plots of R_1, R_2, and heteronuclear NOEs in free cTnI[1-73], it becomes evident that residues 45-67 are the most rigid in all of cTnI[1-73], with the highest R_1, R_2, and least negative heteronuclear NOE values, consistent with nascent helix formation. When this region binds to cTnC, it appears more massive and tumbles with a correlation time of about 15 ns (calculated using a model-free analysis, $R_2 \sim 29$ s^{-1}, $R_1 \sim 0.9$ s^{-1}, NOE ~ 0.8). The 15 ns correlation time is consistent with a 28 kDa protein. This suggests that not only is cTnI[1-73] tightly bound to the C-domain of cTnC, but the N-domain of cTnC is immobilized as well, with the whole complex tumbling as a single 28 kDa unit.

R_2 values for cTnI[1-73] are consistent with those measured by Rosevear *et al.*, for cTnC bound to cTnI[1-80] (35). In the absence of cTnI[1-80] the two domains of cTnC tumbled independently (like two smaller proteins) (mean R_2 13 s^{-1}). Upon addition of cTnI[1-80], the two domains became rigidly fixed and tumble as a single unit (mean R_2 31 s^{-1}). Pseudophosphorylation of cTnI Ser22/Ser23 by mutation to aspartate caused the two domains of cTnC to tumble as two separate proteins (mean R_2 15

s[-1]). This work, along with the present study, show that interaction with the cardiac-specific N-terminal extension of cTnI fixes the position of the cNTnC regulatory domain relative to the rest of the troponin complex, while phosphorylation of cTnI Ser22/Ser23 abolishes this.

The relaxation data for cTnI[19-37]are quite informative. Upon addition of cTnC the most striking change is the plateau of increased R_2 values in this region (see Figure A.4). This indicates that, although cTnI[19-37] is intrinsically disordered with no secondary structure preference, there is a substantial restriction of mobility. This would be expected if Arg19-21, Arg26, and Lys35-37 are electrostatically tethered, but there is likely transient structuring occurring in the intervening segments as well. Faint intermediate-range (*i,i+3* and *i,i+4*) intramolecular ^{1}H-^{1}H NOEs are scattered throughout residues 18-32, indicating transient helix- or turn-like structure, though chemical shift analysis indicates no net helical preference. Interestingly, the MICS Protein Structural Motif Prediction program indicates some potential turn structure at residues 22-25 and 31-34. The increased R_2 values in cTnI[19-37] could result from fast conformational exchange (microsecond to millisecond timescale) and/or conformational restriction on the nanosecond timescale. Support for the latter comes from accompanying changes in R_1 and heteronuclear NOE values. Note that the R_1 values for cTnI[19-37] are the highest in all of cTnI, and these could not arise from an equilibrium between a strongly bound structured state (which would have a correlation time of 15 ns and $R_1 <$ 1 s^{-1}) and a free state (with $R_1 <$ 1.5 s^{-1} from Figure A.4). If this were the case, the R_1 values would be an average of these two states and significantly lower (so long as the exchange time constants were significantly longer than the nanosecond timescale correlation times). Instead, the high R_1 values (up to 2 s^{-1}) suggest a single partially structured state (or ensemble of very rapidly interconverting partially structured states).

Residues 2-18 of cTnI appear to be very mobile with considerable subnanosecond timescale motions and increasing mobility towards the N-terminus. Upon addition of cTnC, there is no change in the rapid motions (followed by R_1 and NOEs) in this region, suggesting that it is not tethered in the same way as cTnI[19-37].

Calcium titration of cTnI[1-73]-cTnC

The calcium binding affinity of IAANS-Cys84 conjugate of C35S-cTnC was studied using fluorescence, in complex with either cTnI[1-73] or cTnI[34-71] (see Supplementary Figure A.3). cTnI[1-73]-cTnC had a calcium pCa_{50} of 6.04 ± 0.03, and cTnI[34-71]-cTnC, 6.04 ± 0.04. Thus, there was no measurable difference between the calcium affinities of the complexes. Thus, the electrostatic interaction between cTnI[19-37] and cNTnC does not exert a direct effect on the calcium binding affinity of cNTnC.

Discussion

The unphosphorylated cardiac-specific N-terminal extension of cTnI interacts with cNTnC while remaining in a mobile, disordered state. Intrinsically disordered regions (IDRs) are believed to make up a large proportion of protein sequences in eukaryotic proteomes. Due to their high solvent accessibility, they are readily available for post-translational modifications like proteolysis and phosphorylation(36). IDRs can be regulated by multiple weak electrostatic interactions, and multiple phosphorylations are an effective means to add to or overcome these. A good example of the former is the increasing binding affinity between Sic-1 and Cdc4 as Sic-1 is increasingly phosphorylated (26, 37). In contrast, phosphorylation of both Ser22 and Ser23in cTnI has been shown to abolish the interaction with cNTnC(23)(38)(35), with the two phosphate groups neutralizing the +4 positive charge locally contributed by Arg19, Arg20, Arg21, and Arg26. The physiologic effect of arginine mutation or PKA phosphorylation is to reduce the calcium sensitivity of troponin(24)(38). On the other hand, the R21C (R20C by our numbering) mutation disrupts the PKA consensus phosphorylation sequence, RRXS, causing increased calcium sensitivity and hypertrophic cardiomyopathy in humans (39) and animal models(40, 41).

The direct consequence of the interaction between cTnC and unphosphorylated cTnI[1-37] is that the orientation of cNTnC becomes fixed relative to the rest of the troponin complex. Any post-translational modification or mutation within the troponin complex that disrupts the delicate positioning of the cNTnC domain would then be expected to have an effect similar to cTnI Ser22/23 phosphorylation, releasing cNTnC and allowing it to gyrate independently of the troponin complex. This may explain why many of these modifications abolish the effect of Ser22/23 phosphorylation or have a greater influence on the unphosphorylated state (see Introduction).

The positioning of cNTnC is critically important because it binds to the switch region, cTnI[148-158], to initiate cardiac contraction. The switch region is flanked by the inhibitory and regulatory regions, cTnI[136-147] and cTnI[161-209], that are anchored to actin during diastole(42). During calcium-activated systole, hydrophobic binding of "opened" cNTnC induces helix formation in cTnI[148-158] and sequesters the inhibitory and regulatory segments from their respective binding sites on actin. The positioning of cTnI[148-158] in the context of the thin filament is currently unknown, but it is quite possible that, while cTnI is unphosphorylated, cNTnC is well positioned to bind cTnI[148-158] as soon as calcium becomes available during systole. This would increase the effective concentration of the cTnI[148-158] switch peptide, driving the cNTnC equilibrium toward the calcium-stabilized open state and thereby enhancing the calcium sensitivity of the cardiac thin filament.

Optimal positioning of the cNTnC domain may also explain the steeper length dependence curve of the Frank-Starling law of the heart when cTnI is phosphorylated(9, 10). The Frank-Starling law is caused by an unknown structural change that brings myosin heads into closer proximity of actin (43, 44), increasing duty ratio, the proportion of myosin heads strongly bound to actin. This change displaces tropomyosin and the inhibitory segments of cTnI from their diastolic actin binding sites, making the switch region, cTnI[148-158], more readily available for cNTnC binding and thereby increasing the calcium affinity of cNTnC. The effective concentration of free cTnI[148-158] may be a more important factor when cNTnC is unrestrained and must randomly "search" for its binding partner. Alternatively, downstream structural changes resulting from the actin-myosin interaction may lead to a positioning of cNTnC (through an as of yet uncharacterized interaction) that is redundant to that set up by unphosphorylated cTnI[1-37].

One limitation of the current study is that not all of the troponin complex components are present. While it seems unlikely that cTnI[1-73] binds to the IT arm on the opposite face of cCTnC, it is quite possible that the large volume of space accessible to the mobile cTnI[1-37] segment intersects with that of cTnI[136-147], cTnI[161-209], and cTnT[272-288], highly charged IDRs invisible in the crystal structure but known to interact with actin. Indeed, a major consequence of fixing the orientation of cNTnC via the cTnI[1-37] IDR could be that potentially non-productive interactions with other IDRs are prevented. The extent to which all of these IDRs interact with each other and with charged surfaces on troponin, tropomyosin, or actin remains to be clarified by future NMR studies.

In conclusion, our findings contradict an earlier model that proposed a rigid structure for cTnI[1-37] that stabilizes the open state of cNTnC to directly increase its calcium affinity (16). We did not observe evidence for a rigid structure in any way, nor a direct increase in calcium affinity. In our proposed model, the cardiac-specific N-terminal extension of cTnI remains largely disordered while it interacts electrostatically with cNTnC. This interaction does not affect the closed-open equilibrium of cNTnC, but indirectly increases calcium affinity by optimally positioning cNTnC to bind cTnI switch peptide. Phosphorylation at cTnI Ser22/23 disrupts this delicate arrangement, which we predict will be impacted by other regulatory mechanisms as well.

Materials and methods

Protein production and purification

Wildtype- or C35S,C84S-cTnC was expressed in *E. coli* using a pET3a-derivedexpression vector(45) and purified according to previously published protocols(46). In brief, purification involved three chromatographic steps: anion exchange, hydrophobic, and gel filtration chromatography. cTnI[1-

73] with a C-terminal His-tag was expressed in a modified pET31b vector altered to fuse cTnI[1-73] to the C-terminus of the β-barrel membrane protein, PagP, as previously described(47). cTnI[1-73] was separated from PagP via cyanogen bromide cleavage in 0.1 M HCl, 6 M Gdn-HCl and purified using nickel affinity chromatography under denaturing conditions. cTnI[144-163] a and cTnI[34-71] peptides were synthesized and purified by GL Biochem (Shanghai, China).

The cTnI[1-73] protein purified from the PagP-fusion construct was stable over the course of NMR experiments. However, after addition of cTnC, it was not uncommon for cTnI[1-73] to be slowly degraded, with proteolytic cleavage occurring N-terminal to Tyr25 or Tyr28, similar to what was observed from cTnI from human heart tissue(5). The change could be monitored by following the disappearance of NMR peaks corresponding to Tyr25-Ala29. Alternatively, it could be detected in cTnC by measuring ^{15}N R_2 relaxation rates, which would show that the two domains of cTnC were no longer tethered together by cTnI[1-73].

NMR spectroscopy sample preparation

For spectral simplicity, only one component of the protein complexes was isotopically labeled at a time. Enough labeled (^{15}N- or $^2H,^{15}N$- or $^{13}C,^{15}N$-enriched) lyophilized protein to make a 0.5-1.0 mM sample was dissolved in 450 μL of buffer, consisting of 100 mM KCl, 10 mM imidazole, 10 mM CaCl$_2$, 0.5 mM DSS, CalBiochem Protease Inhibitor Cocktail Set I, and 5% D$_2$O. When wildtype-cTnC was used, the buffer was further supplemented with 20 mM DTT. The pH was corrected to about 6.2 and monitored using 1D-^1H NMR by measuring the pH-sensitive downfield imidazole H2 peak(48). A $^1H,^{15}N$-HSQC spectrum of the initial sample was obtained at 40°C, and a 5 mM solution of the unlabeled binding partner was titrated in 10-15 μL aliquots. The titration was followed by serial $^1H,^{15}N$-HSQC spectra. The binding equilibrium was in the slow exchange regime, so the titration was continued until the peaks corresponding to the unbound form disappeared completely. A ternary complex was also made by adding an excess (2 mg) of unlabeled cTnI[144-163] switch peptide.

NMR spectroscopy and data analysis

Three-dimensional backbone assignment spectra were recorded on a Varian Inova 600 spectrometer. All experiments were from Agilent BioPack (VnmrJ 3.2D) unless otherwise specified. The experiments used for backbone assignment were HNCA, HN(CO)CA, HN(CA)CO, and HNCO. The molecular weight of the cTnC-cTnI[1-73] complex was 28 kDa, and sensitivity was further limited by exchange broadening. Additional experiments were used to assign the flexible regions of cTnI[1-73]: HNCACB, H(CCO)NH-TOCSY, and (H)C(CO)NH-TOCSY. To obtain the complete assignments of cTnC, HN(CA)HA and HA(CACO)NH (49)experiments were recorded, in-house modified from the BioPack

HNCACB and CBCA(CO)NH experiments, respectively. ^{15}N-edited NOESY-HSQC spectra were also used for backbone assignment. Enhanced sensitivity and gradient selection was utilized in the backbone assignment triple resonance experiments, but TROSYwas not used for the ^{15}N and ^{1}H dimensions.

Three-dimensional NOESY spectra were acquired on a Varian Inova 800 spectrometer equipped with cryoprobe. ^{13}C-edited HMQC-NOESY spectra were run on ^{13}C,[15]N-labeled samples in H_2O, though the majority of intramolecular NOE data were obtained from ^{13}C-edited NOESY-HSQC spectra acquired in D_2O, and intermolecular NOEs were obtained from ^{12}C-filtered, ^{13}C-edited NOESY-HSQC spectra in D_2O. NMR data were processed using NMRPipe (50)software and visualized and analyzed with NMRViewJ(51).

[15]N T_1, T_2, and [1]H-^{15}N NOE experiments were conducted using ^{2}H,[15]N- labeled cTnI[1,73] with unlabeled aCys-cTnC. TROSY was utilized in the ^{1}H and ^{15}N dimensions. A 6-second saturation time or recycle delay was used in the NOE experiments. For T_1 and T_2, curves were fit using a monoexponential decay function using the simplex minimization algorithm in MATLAB®. The variance for each timepoint was estimated from the sum of the squares of the residuals divided by (N-2), where N is the number of data points for each curve and 2 is the number of fitting parameters. A Monte Carlo method was then applied to obtain error estimates for R_1 and R_2. For [1]H-^{15}N NOE, the error estimate was based on the ratio of spectral noise to signal intensity in the reference spectrum, multiplied by a factor of $\sqrt{2}$ to reflect the fact that the [1]H-^{15}N NOE is a ratio.[15]N R_1, R_2, and [1]H-^{15}N NOE data were further analyzed using either a model-free analysis of internal motions(52).

Fluorescence spectroscopy

2-(4'- (iodoacetamido)anilino)naphthalene-6-sulfonic acid (IAANS) reacted with C35S cTnC Cys84 in labeling buffer (in 50mM Tris, 150mM KCl, 1mM EGTA, and 6M urea, pH 7.0) for 4 h at 4°C(32). The labeling reaction was stopped by addition of 2 mM DTT, and the labeled protein was exhaustively dialyzed against refolding buffer (600mM MOPS, 150mM KCl, and 2mM EGTA, pH7.0) to remove unreacted label.

All steady-state fluorescence measurements were performed at 22 °C. IAANS fluorescence was excited at 325 nm and monitored at 450 nm. Microliter amounts of $CaCl_2$ were titrated into a 2 mL solution containing cTnC-cTnI[1-73] or cTnC-cTnI[34-71] (0.2 μM), 200mM MOPS, pH 7.0, 150mM KCl, 2mM EGTA, 1 mM DTT, and 3 mM $MgCl_2$.An excess of cTnI peptide was used for the complexes ([cTnI]/[cTnC] =1.3), with protein concentrations quantitated by amino acid analysis following acid hydrolysis. Free [Ca^{2+}] was calculated with the program Maxchelator developed by Chris Patton and

available at *http://maxchelator.stanford.edu/CaMgATPEGTA-NIST.htm*. Fluorescence experiments were performed in triplicate to determine error ranges for individual measurements as well as pCa.

Acknowledgments
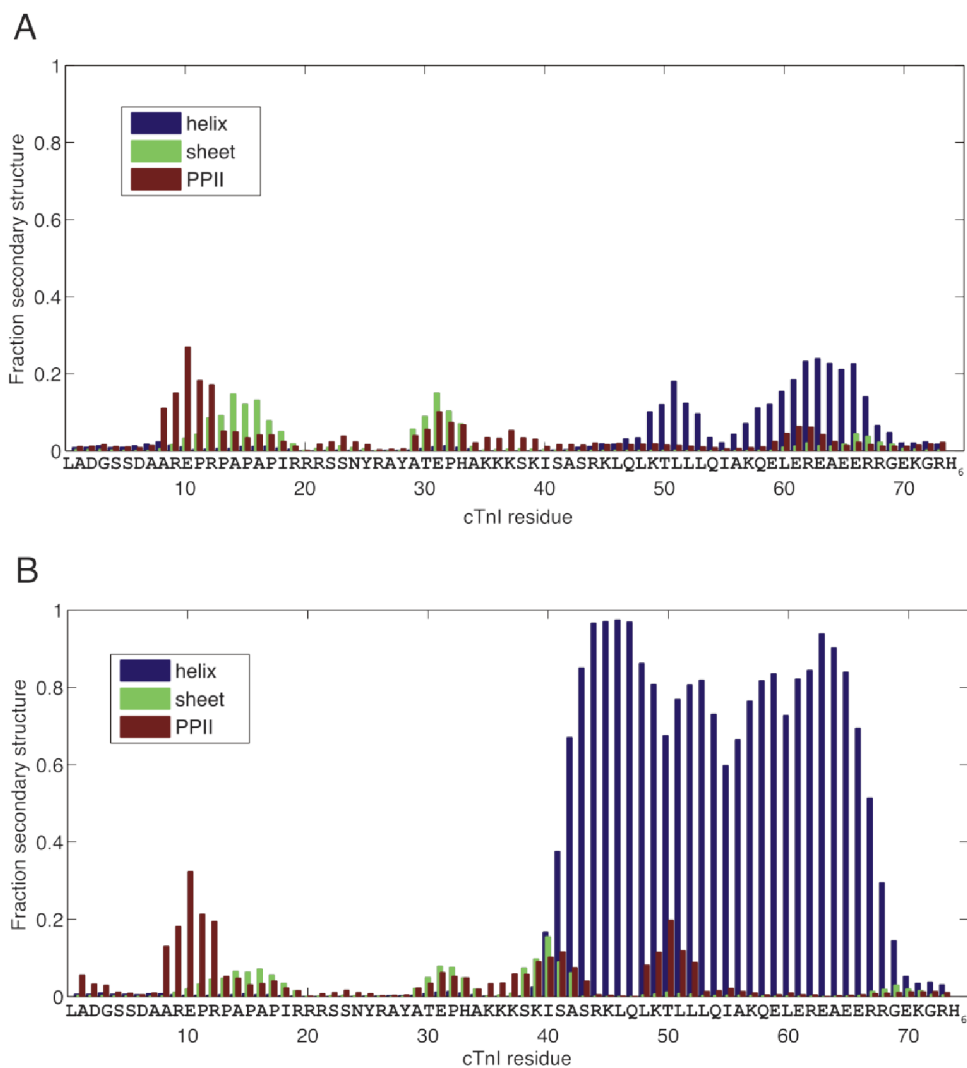
Supplementary Figure A.1. Predicted secondary structure for cTnI[1-73].

Predicted fraction secondary structure calculated from backbone chemical shift data using the program, δ2D (see main text for details). A) Free cTnI[1-73]. B) cTnI[1-73] in complex with cTnC. Note that the fractions of helix, sheet, polyproline type II helix, and random coil, add up to one (the remainder is all random coil.)
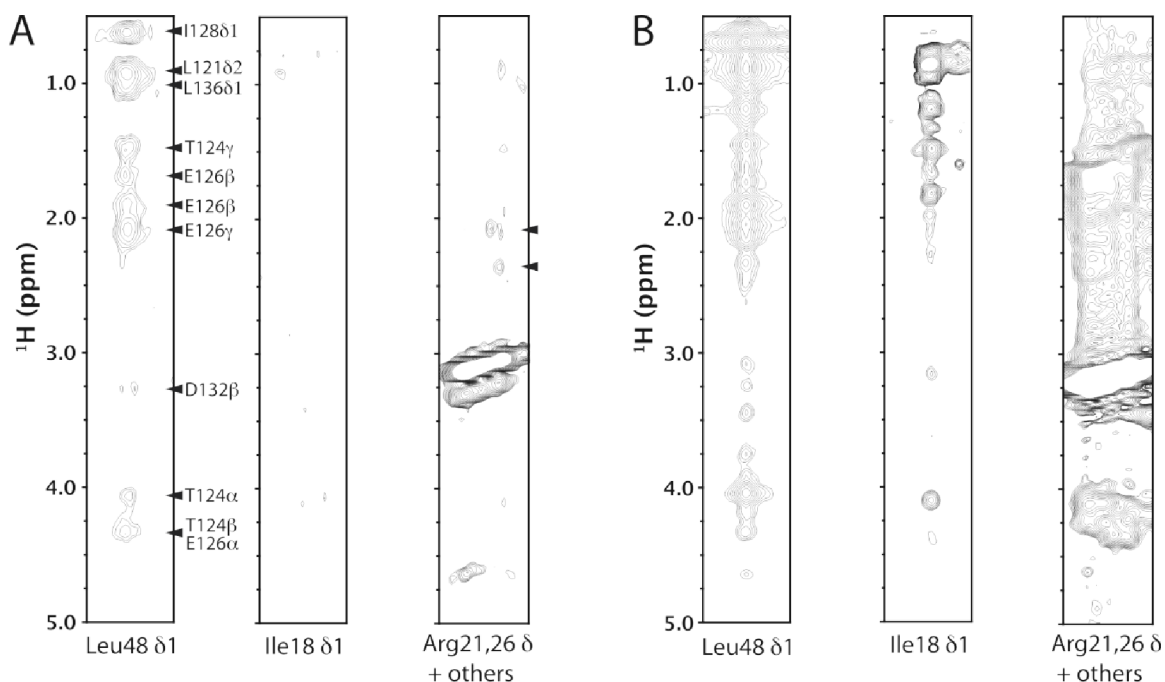
**Supplementary Figure A.2. Intermolecular ^{1}H-^{1}H NOEs from unlabeled cTnC to ^{13}C-labeled cTnI[1-73].**

A) Strip plots taken from the ^{12}C-filtered, ^{13}C-edited NOESY-HSQC spectrum, designed to select for intermolecular ^{1}H-^{1}H NOEs from unlabeled cTnC to ^{13}C-labeled cTnI[1-73]. From left to right, a cTnI Leu48 δ1-methyl group shows multiple intermolecular NOEs to cTnC, consistent with tight hydrophobic binding between cTnI[39-60] and cCTnC. In contrast, the cTnI Ile18 δ-methyl group shows no intermolecular NOEs, as with all other hydrophobic residues in cTnI[1-37]. Weak intermolecular NOEs can be observed between Arg26H δ (3.13 ppm) and a Glu-like residue in cTnC with chemical shifts at 2.11 and 2.35 ppm (unlabeled arrows). An NOE can also be observed between Arg21H δ (3.15 ppm) and an unassigned signal at 2.09 ppm. These NOEs are suggestive of weak electrostatic interactions between cTnI[19-37] and cNTnC. (Note that the strong peaks around 3.2 ppm are diagonal artifacts due to incomplete filtering.) B) Corresponding strip plots for Leu48, Ile18, and arginine residues from the unfiltered ^{13}C-edited NOESY-HSQC spectrum, which contains both inter- and intramolecular NOEs (dominated by short-range intra-residue NOEs).Note that the signal from Ile18 is much more intense than that from Leu48, because it is part of an intrinsically disordered region with slower signal decay due to R_2 relaxation.
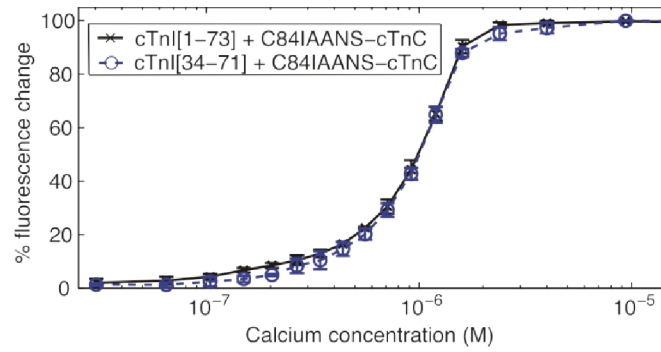
Supplementary Figure A.3. Ca²⁺ binding to C35S-cTnC bound to either cTnI[1-73] or cTnI[34-71].
Calcium titrations of IAANS-labeled C35S-cTnC bound to either cTnI[1-73] or cTnI[34-71] (N=3, error bars show SD). The total percentage fluorescence change is plotted against calcium concentration.

References

1. Sharma K, Kass DA (2014) Heart Failure With Preserved Ejection Fraction: Mechanisms, Clinical Features, and Therapies. *Circ Res* 115(1), 79–96.

2. Solaro RJ, Moir AJ, Perry SV (1976) Phosphorylation of troponin I and the inotropic effect of adrenaline in the perfused rabbit heart. *Nature* 262, 615-617.

3. van der Velden J (2011) Diastolic myofilament dysfunction in the failing human heart. *Pflugers Arch* 462, 155–163.

4. Solaro RJ, van der Velden J (2010) Why does troponin I have so many phosphorylation sites? Fact and fancy. *J Mol Cell Cardiol* 48, 810-816.

5. Zhang J *et al*. (2011) Top-down quantitative proteomics identified phosphorylation of cardiac troponin I as a candidate biomarker for chronic heart failure. *J Proteome Res* 10, 4054–4065.

6. Solaro RJ, Henze M, Kobayashi T (2013) Integration of troponin I phosphorylation with cardiac regulatory networks. *Circ Res* 112, 355–366.

7. Wattanapermpool J, Guo X, Solaro RJ (1995) The unique amino-terminal peptide of cardiac troponin I regulates myofibrillar activity only when it is phosphorylated. *J Mol Cell Cardiol* 27, 1383-1391.

8. Hamdani N *et al*. (2009) Distinct myocardial effects of beta-blocker therapy in heart failure with normal and reduced left ventricular ejection fraction. *Eur Heart J* 30, 1863–1872.

9. Hanft LM, Biesiadecki BJ, McDonald KS (2013) Length dependence of striated muscle force generation is controlled by phosphorylation of cTnI at serines 23/24. *J Physiol* 591, 4535-4547.

10. Wijnker PJ *et al*. (2014) Length-dependent activation is modulated by cardiac troponin I bisphosphorylation at Ser23 and Ser24 but not by Thr143 phosphorylation. *Am J Physiol Heart Circ Physiol* 306, H1171–H1181.

11. Henze M *et al*. (2013) New insights into the functional significance of the acidic region of the unique N-terminal extension of cardiac troponin I. *Biochim Biophys Acta* 1833, 823–832.

12. Hinken AC *et al*. (2012) Protein kinase C depresses cardiac myocyte power output and attenuates myofilament responses induced by protein kinase A. *J Muscle Res Cell Motil* 33, 439–448.

13. van der Velden J *et al*. (2006) Functional effects of protein kinase C-mediated myofilament phosphorylation in human myocardium. *Cardiovasc Res* 69, 876–887.

14. Memo M *et al*. (2013) Familial dilated cardiomyopathy mutations uncouple troponin I phosphorylation from changes in myofibrillar Ca(2)(+) sensitivity. *Cardiovasc Res* 99, 65–73.

15. Takeda S, Yamashita A, Maeda K, Maeda Y (2003) Structure of the core domain of human cardiac troponin in the Ca(2+)-saturated form. *Nature* 424, 35-41.

16. Howarth JW, Meller J, Solaro RJ, Trewhella J, Rosevear PR (2007) Phosphorylation-dependent conformational transition of the cardiac specific N-extension of troponin I in cardiac troponin. *J Mol Biol* 373, 706-722.

17. Ward DG *et al*. (2004) Characterization of the interaction between the N-terminal extension of human cardiac troponin I and troponin C. *Biochemistry* 43, 4020-4027.

18. Ferrieres G *et al*. (2000) Systematic mapping of regions of human cardiac troponin I involved in binding to cardiac troponin C, N- and C-terminal low affinity contributing regions. *FEBS Lett* 479, 99–105.

19. Biesiadecki BJ *et al*. (2010) Removal of the cardiac troponin I N-terminal extension improves cardiac function in aged mice. *J Biol Chem* 285, 19688–19698.

20. Camilloni C, De Simone A, Vranken WF, Vendruscolo M (2012) Determination of secondary structure populations in disordered states of proteins using nuclear magnetic resonance chemical shifts. *Biochemistry* 51, 2224-2231.

21. Cheung MS, Maguire ML, Stevens TJ, Broadhurst RW (2010) DANGLE, A Bayesian inferential method for predicting protein backbone dihedral angles and secondary structure. *J Magn Reson* 202, 223–233.

22. Shen Y, Bax A (2012) Identification of helix capping and b-turn motifs from NMR chemical shifts. *J Biomol NMR* 52, 211–232.

23. Baryshnikova OK, Li MX, Sykes BD (2008) Modulation of cardiac troponin C function by the cardiac-specific N-terminus of troponin I: influence of PKA phosphorylation and involvement in cardiomyopathies. *J Mol Biol* 375, 735-751.

24. Ward DG, Cornes MP, Trayer IP (2002) Structural consequences of cardiac troponin I phosphorylation. *J Biol Chem* 277, 41795–41801.

25. Fuxreiter M (2012) Fuzziness: linking regulation to protein dynamics. *Mol Biosyst* 8, 168–177.

26. Mittag T *et al*. (2008) Dynamic equilibrium engagement of a polyvalent ligand with a single-site receptor. *Proc Natl Acad Sci U S A* 105, 17772–17777.

27. Bozoky Z *et al*. (2013) Regulatory R region of the CFTR chloride channel is a dynamic integrator of phospho-dependent intra- and intermolecular interactions. *Proc Natl Acad Sci U S A* 110, E4427–E4436.

28. Finley N *et al*. (1999) NMR analysis of cardiac troponin C-troponin I complexes: effects of phosphorylation. *FEBS Lett* 453, 107–112.

29. Sia SK *et al*. (1997) Structure of cardiac muscle troponin C unexpectedly reveals a closed regulatory domain. *J Biol Chem* 272, 18216-18221.

30. Eichmuller C, Skrynnikov NR (2005) A new amide proton R1rho experiment permits accurate characterization of microsecond time-scale conformational exchange. *J Biomol NMR* 32, 281–293.

31. Li MX, Spyracopoulos L, Sykes BD (1999) Binding of cardiac troponin-I147-163 induces a structural opening in human cardiac troponin-C. *Biochemistry* 38, 8289–8298.

32. Davis JP *et al*. (2007) Effects of thin and thick filament proteins on calcium binding and exchange with cardiac troponin C. *Biophys J* 92, 3195–3206.

33. Wijnker PJ *et al*. (2014) Phosphorylation of protein kinase C sites Ser42/44 decreases Ca(2+)-sensitivity and blunts enhanced length-dependent activation in response to protein kinase A in human cardiomyocytes. *Arch Biochem Biophys* 554, 11–21.

34. Carballo S *et al*. (2009) Identification and functional characterization of cardiac troponin I as a novel disease gene in autosomal dominant dilated cardiomyopathy. *Circ Res* 105, 375–382.

35. Gaponenko V *et al*. (1999) Effects of troponin I phosphorylation on conformational exchange in the regulatory domain of cardiac troponin C. *J Biol Chem* 274, 16681–16684.

36. Iakoucheva LM *et al*. (2004) The importance of intrinsic disorder for protein phosphorylation. *Nucleic Acids Res* 32, 1037-1049.

37. Tang X *et al*. (2012) Composite low affinity interactions dictate recognition of the cyclin-dependent kinase inhibitor Sic1 by the SCFCdc4 ubiquitin ligase. *Proc Natl Acad Sci U S A* 109, 3287–3292.

38. Ward DG *et al*. (2004) NMR and mutagenesis studies on the phosphorylation region of human cardiac troponin I. *Biochemistry* 43, 5772–5781.

39. Arad M *et al*. (2005) Gene mutations in apical hypertrophic cardiomyopathy. *Circulation* 112, 2805–2811.

40. Gomes AV, Harada K, Potter JD (2005) A mutation in the N-terminus of troponin I that is associated with hypertrophic cardiomyopathy affects the Ca(2+)-sensitivity, phosphorylation kinetics and proteolytic susceptibility of troponin. *J Mol Cell Cardiol* 39, 754-765.

41. Wang Y *et al*. (2012) Generation and functional characterization of knock-in mice harboring the cardiac troponin I-R21C mutation associated with hypertrophic cardiomyopathy. *J Biol Chem* 287, 2156–2167.

42. Tripet B, Van Eyk JE, Hodges RS (1997) Mapping of a second actin-tropomyosin and a second troponin C binding site within the C terminus of troponin I, and their importance in the Ca2+-dependent regulation of muscle contraction. *J Mol Biol* 271, 728–750.

43. Farman GP *et al*. (2011) Myosin head orientation: a structural determinant for the Frank-Starling relationship. *Am J Physiol Heart Circ Physiol* 300, H2155–H2160.

44. Mateja RD, de Tombe PP (2012) Myofilament length-dependent activation develops within 5 ms in guinea-pig myocardium. *Biophys J* 103, L13-L15.

45. Li MX *et al*. (2002) Kinetic studies of calcium and cardiac troponin I peptide binding to human cardiac troponin C using NMR spectroscopy. *Eur Biophys J* 31, 245–256.

46. Wang X, Mercier P, Letourneau PJ, Sykes BD (2005) Effects of Phe-to-Trp mutation and fluorotryptophan incorporation on the solution structure of cardiac troponin C, and analysis of its suitability as a potential probe for in situ NMR studies. *Protein Sci* 14, 2447-2460.

47. Hwang PM, Pan JS, Sykes BD (2012) A PagP fusion protein system for the expression of intrinsically disordered proteins in Escherichia coli. *Protein Expr Purif* 85, 148–151.

48. Baryshnikova OK, Williams TC, Sykes BD (2008) Internal pH indicators for biomolecular NMR. *J Biomol NMR* 41, 5-7.

49. Boucher W, Laue ED, Campbell-Burk S, Domaille PJ (1992) Four-dimensional heteronuclear triple resonance NMR methods for the assignment of backbone nuclei in proteins. *J Am Chem Soc* 114, 2262–2264.

50. Delaglio F *et al*. (1995) NMRPipe: a multidimensional spectral processing system based on UNIX pipes. *J Biomol NMR* 6, 277–293.

51. Johnson BA, Blevins RA (1994) NMR View: A computer program for the visualization and analysis of NMR data. *J Biomol NMR* 4, 603–614.

52. Lipari G, Szabo A (1982) Model-free approach to the interpretation of nuclear macnetic resonance relaxation in macromolecules. 1. Theory and range of validity. *J Am Chem Soc* 104, 4546–4559.

Appendix B
Future Directions

This appendix contains my original ideas regarding specific modifications to the structure of bepridil to explore in the future based on the content of this thesis. It also contains suggestions for additional experiments to follow the work reported in previous chapters.

In the design of better Ca^{2+} sensitizers we aim for two main effects. First the stabilization of the open conformation of cNTnC. To accomplish this first and primary feature, we learned that binding of small molecules in the hydropobic core of cNTnC in the low micromolar range can be sufficient, as in the case of bepridil. In Chapter 10, we showed that the affinity of the core of bepridil could be improved. Thus a starting point could be 3-methyl-diphenylamine (3m-DPA), as it showed the lowest dissociation constant when binding to cChimera. A next logical step would be to improve the rest of the original bepridil structural susbtituents, i.e. the pyrrolidine ring and the hydrophobic tail (Figure B.1). Modifications to these groups can be directed to meet the secondary but desirable effect of increasing switch-cTnI binding to cNTnC. For this purpose I propose to remove the hydrophic tail and modify the pyrrolidine group to favor interactions with cNTnC and switch-cTnI simultaneously.

It was proposed earlier that the hydrophobic tail of bepridil may clash with the N-terminal region of switch-TnI[1]. In addition, the lack of NOEs between cNTnC and both the hydrophobic tail and the pyrrolidine groups of bepridil prevented an exact localization of these groups in the NMR structure of cNTnC·switch-cTnI·bepridil. Nonetheless, the lowest energy structure shows the pyrrolidine ring in the same site as in the crystal structure of cTnC·3bepridil[2]. In addition, the same site is predicted for probe binding by FTMap *in silico*. Thus, removing the tail while keeping the pyrrolidine ring seems a logical step in the optimization of bepridil.

Substituents in the original pyrrolidine ring of bepridil may enhance interactions of the small molecule with switch-cTnI. A stretch of positive arginine residues is present in the N-terminal side of switch-cTnI (RRVR residues 144-147) close to the binding site of the pyrrolidine ring. This can be used to induce interactions with the small molecule once bound to cNTnC. For this purpose, groups that can function as hydrogen-bond acceptors can be incorporated on the pyrrolidine ring to interact with arginine as the hydrogen-bond donor. Negatively charged groups can also be incorporated to promote electrostatic interactions with the RRVR motif of cTnI.
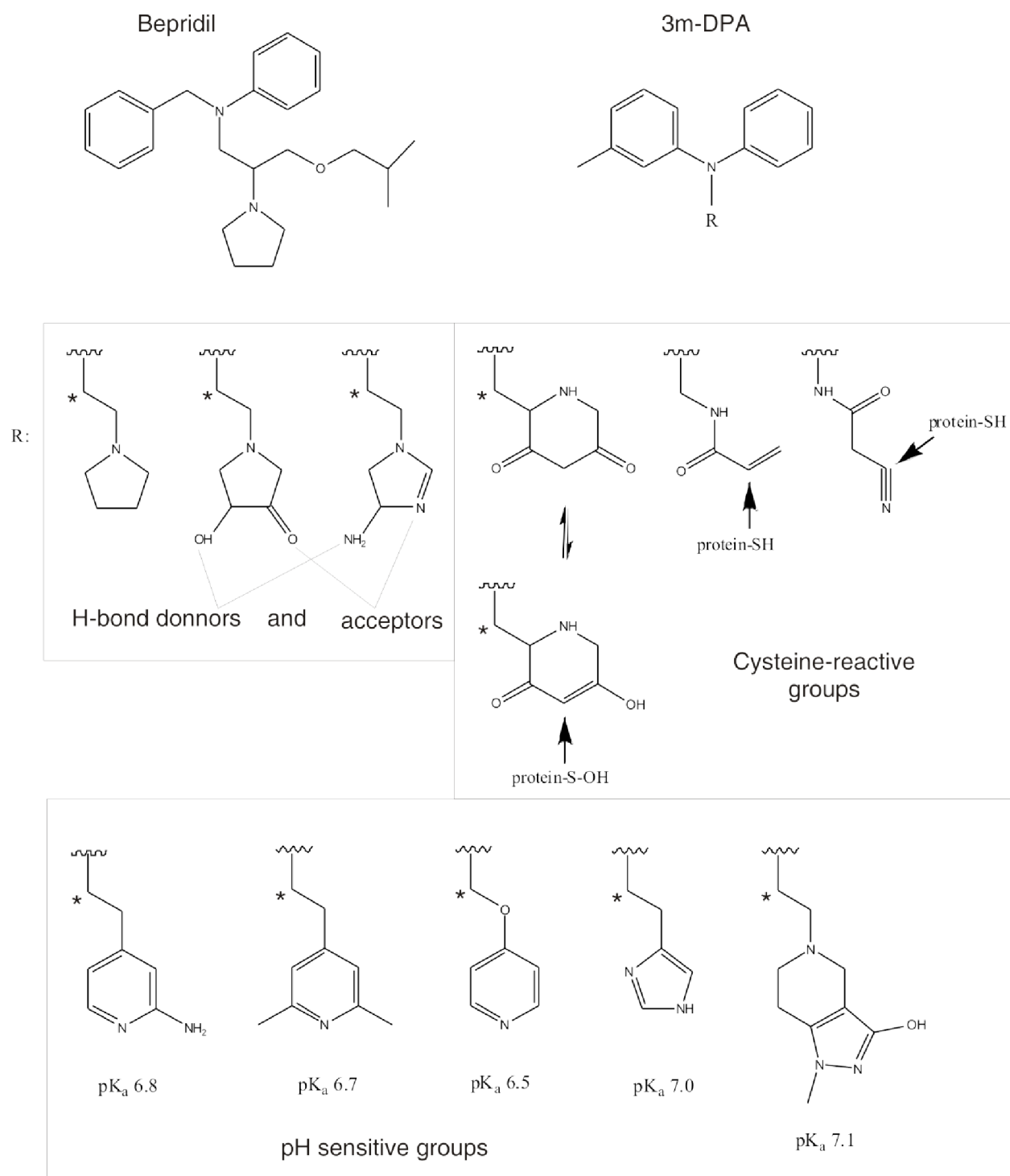
Figure B.1. Summary of structural modifications proposed for the optimization of Ca²⁺ sensitizers. The chemical structure of bepridil and the optimized berpidil core (3m-DPA) are shown. Modifications are organized in three groups according to their desired effect on cNTnC or switch-cTnI. The * indicates the regions available for addition of solubilizing functional groups or for change in chain length.

In the vicinity of the pyrrolidine binding site is the glutamate residue E63 on helix C of cNTnC which may be advantageous to enhance the interaction of the drug molecule with cNTnC. In a similar manner, the formation of hydrogen-bonds can be induced by incorporating donors in the small molecule. Another possibility to enhance interactions with E63 is the incorporation of positively charged groups. We already learned the importance of electrostatic interactions between the Tn subunits. In the design of pH sensitive drugs for ischemic heart disease it is necessary that the pK_a of these groups is within the range of pH change observed during ischemia. Above pH ~6.5 and below the physiological pH of 7.4 would be ideal to enhance interactions under acidic conditions in the diseased heart.

The previous modifications could also be applied to a different core molecule such as i9 or dfbp-o which bind deep in the hydrophobic cleft of cNTnC. Alternatively, the reactive group of i9 could be modified to favor reversible covalent binding to allow the conversion to the relaxed state of in the cardiac muscle. Yet another variant is to incorporate cysteine-reactive groups in the 3m-DPA molecule.

In Chapter 7, I reported the selective reaction of i9, a covalent Ca^{2+} sensitizer, with C84 of cNTnC. This was proposed to be the result of a two-step process in which the first event is non-covalent binding of i9 in the hydrophobic cleft of cNTnC. To corroborate this theory, I suggest to assess the binding of a non-reactive analogue of i9. By reacting (2',4'-difluorobiphenyl-4-yl)-methanamine (See compound **1** in Figure 7.4 on page 177) with 2-hydroxyacetyl-chloride, an OH group is incorporated instead of I of i9. This compound can be used to assess the non-covalent binding step. Also, to assess the effect of i9 on the binding of switch-cTnI I suggest to perform a titration of the cTnI peptide into cNTnC reacted with i9.

References

1. Wang, X., Li, M. X., and Sykes, B. D. (2002) Structure of the regulatory N-domain of human cardiac troponin C in complex with human cardiac troponin I$_{147-163}$ and bepridil. *J. Biol. Chem. 277*, 31124-31133.
2. Li, Y., Love, M. L., Putkey, J. A., and Cohen, C. (2000) Bepridil opens the regulatory N-terminal lobe of cardiac troponin C. *Proceedings of the National Academy of Sciences. 97*, 5140-5145.